

CYPRUS VOLCANOGENIC SULPHIDE DEPOSITS
IN RELATION TO
THEIR ENVIRONMENT OF FORMATION

By

N. G. Adamides B. Sc. (Hons).



Thesis submitted for the degree of
Doctor of Philosophy
at the
Department of Geology
University of Leicester, 1984.

Dedicated to my wife, Soula

Declaration

I hereby declare that all the work recorded in this thesis is original unless otherwise acknowledged in the text or by references. None of the work has been submitted for another degree in this or any other university.

ABSTRACT

The present thesis is concerned with the volcanogenic sulphide deposits associated with the Troodos ophiolite, Cyprus.

Extensive petrological, chemical and field data are presented and these suggest that the ophiolite has formed on a spreading axis which was located above a subduction zone. This tectonic regime was responsible for the enrichment of the Troodos primary magma in silica and the large ion lithophile elements. Formation of the Sheeted Complex and Lower Pillow Lavas is envisaged to have taken place close to the axis of spreading. The lavas are extrusive products of subaxial chambers which exhibited both open and closed system fractionation. The Upper Pillow Lavas are considered to be derived from the same primary magma as the other members of the ophiolite but exhibit only limited fractionation. The difference between the two suites is attributed to extrusion of the Upper Pillow Lavas on the flanks of the spreading axis, from diapirically rising magma chambers.

A detailed geochemical study of the hydrothermal metamorphism of the ophiolite suggests extensive mobility of components in the Sheeted Complex. All geochemical changes are in agreement with experimental and field evidence of seawater-rock interaction; they suggest enrichment of the rocks in magnesium and sodium and extensive leaching of calcium, silica, barium and zinc. Strontium is locally leached and concentrated in secondary minerals. Calculations of element fluxes during hydrothermal metamorphism suggest that the amounts leached from the Sheeted Complex can account for the amounts deposited in the sulphide

deposits and metalliferous sediments (umbers). A hydrothermal model is proposed according to which seawater trapped within the Sheeted Complex is heated under the influence of the geothermal gradient, enriched in metallic and other elements by breakdown of primary silicates and finally driven off by the intrusion of magma chambers at high levels in the crust. These chambers are deduced to be those which formed the Upper Pillow Lavas, as inferred from the association of sulphide deposits with the initial stages of eruption of these lavas.

Examination of the field occurrence of several sulphide deposits suggests that these are most often localised by faults which were inherited from the tensional regime of the spreading axis. Localisation at sites of structural intersections is also described. The size of the deposits is determined to a great extent by the structural disturbance in the area in which they occur, smaller deposits being favoured at strongly tectonised areas. In the absence of tectonism ore localisation may take place within the lava pile. It is concluded that the presence of a heat source is more important than structural disturbance in the formation of deposits. The results suggest, also, that there was only one period of sulphide-producing hydrothermal activity and this is temporally placed at the early stages of extrusion of the Upper Pillow Lavas.

The mineralogical characteristics of deposits are described, with emphasis on the behaviour of the hydrothermal fluids at discharge sites. The main conclusions suggest that extensive interaction of the fluids with the wall rocks and

seawater takes place and this determines the final mineralogical character of the deposits and the formation of copper-rich and copper-poor orebodies. The extent of interaction is determined to a large extent by the structure and results to the formation of extensive alteration zones in deposits which formed deep within the lavas. Exchange between the fluids and wall rocks is mainly characterised by enrichment of the surrounding lavas in magnesium and sodium, depletion in calcium and strong enrichment in barium and potassium. The mineralized lavas are depleted in alkalies and enriched in magnesium.

The implications of the above conclusions on future exploration are briefly discussed, with emphasis on the application of geochemical methods in the search for sulphide deposits.

Acknowledgements

I am deeply grateful to my wife, Soula, who, for long years, has graciously accepted the isolation this work has forced her to endure. Our children Andreas, Frosoula and George, with a maturity beyond their age, accepted without complaint my constant absence from their midst. I am thankful for that and hope to compensate them in the years to come with more attention and love than they had had hitherto.

Thanks and gratitude are expressed to my supervisor at the University of Leicester, Dr M. J. Le Bas, for his interest and advice throughout the project.

Sincere thanks are also expressed to the following:

From Hellenic Mining Company:

Mr P. Paschalides, Chairman, for permission to make free use of all data collected during my employment and for a donation towards expenses.

Academician L. Mousoulos, advisor to Hellenic Mining Company, for his untiring discussions of all our ideas through the years.

Dr G. Maliotis, chief geologist, for continuous interest and encouragement; Mr J. Christoforou and Dr A. Michaelides, geologists, for discussions on various aspects of the work.

Mr G. Constantinides and Mr A. Evtychiou, technical assistants, for their invaluable help in the field and in the office. Particular thanks are due to Mr J. Vouniotis for the expert drafting of some of the diagrams.

From Limni Mines:

The late General Manager, Mr R. H. S. Ewins for permission to use all data collected during my employment at Limni.

Mr T. O. Trennery, Mine Manager, Mr G. Papadopoulos, chief surveyor, and many other colleagues with whom I collaborated from time to time.

From the Geological Survey Department:

Dr G. Constantinou, Director, for permission to use of some of the facilities of the department. Dr C. Xenophontos and Dr A. Panayiotou, senior geologists, for discussions on various aspects of the work.

Mr J. Markides for the preparation of some of the thin sections and Mr K. Nikolaou for the expert preparation of a number of plates. Mrs M. Economidou, librarian, for her help in the continuous search for new references.

From Leicester University:

Mr N. G. Marsh for the XRF analyses. Mr R. N. Wilson and Mr C. J. Cunningham for invaluable assistance with the electron microprobe. Mr J. Preston, Mr P. Ayto and Mr P. Matkovits for the preparation of thin and polished sections. Miss P. Turner for invaluable assistance in the laboratory. Finally grateful thanks are expressed to Mr W. Teasdale, chief technician, for making freely available the facilities of the laboratory, sometimes at inconveniently short notice.

From Clausthal University, W. Germany:

Professor H. Krause and Dr G. Pedall for the preparation of numerous polished sections of ores.

From Aachen University, W. Germany:

Professor G. Friedrich for comments on mineralogical aspects. Mr P. Herzig and Mr S. Keyssner for the preparation of numerous photocopies of papers.

From the Cyprus Crustal Study Project:

Professor P. T. Robinson for constant discussions on various aspects and for permission to make use of the project's word processor for the preparation of this thesis. Professor J. R. Cann for invaluable discussions and expert advice freely given. Professor J. M. Hall for his great interest and useful discussions. Dr C. Stillman for numerous suggestions on geochemical aspects which completely modified earlier drafts. Dr W. R. Baragar for suggestions and advice on petrological aspects. Dr J. Lydon for detailed revision of the chapters on ore deposits, for sharing with me his great knowledge of hydrothermal systems and for numerous references. Dr J. Malpas and Professor F. J. Vine for discussions.

Last but not least:

Sincere thanks are expressed to all the individual scientists who expressed interest in the work and provided assistance either in the form of discussions, or references on various aspects. In particular Professor D. Watkinson, who provided some of the excellent colour plates of ores, Prof. F. M. Vokes for valuable comments on ore textures, Dr. R. A. Koski and Prof. F. Coucky for lengthy discussions on various aspects of the work, Dr R. Haymon for a copy of her excellent thesis.

The help of all the above people is by no means

compensated by the simple mention of their names in these pages. It is, however, the least that could be done in grateful appreciation of the assistance so selflessly provided.

TABLE OF CONTENTS

	Page
Abstract.....	
Acknowledgements.....	
Table of contents.....	i
List of figures.....	viii
List of tables.....	xv
List of plates.....	xviii
List of publications.....	xxi

Preface

Description of contents.....	1
Methods and techniques used.....	3

PART 1.

CHAPTER 1.

General Geology of Cyprus

1.1.	General.....	5
1.2.	The geology of the Troodos Massif.....	7
1.2.1.	The sedimentary rocks.....	7
1.2.2.	The igneous rocks.....	10
1.2.2.1.	Definition of ophiolite.....	10
1.2.2.2.	The Troodos Igneous Complex.....	12
1.2.2.2a.	The Plutonic Complex.....	12
1.2.2.2b.	The Sheeted Complex.....	14
1.2.2.2c.	The Pillow Lava Series.....	16
1.3.	Structure of the Massif.....	17

	Page
1.4. Mineral deposits.....	18
1.4.1. Sulphides.....	18
1.4.2. Chromite.....	19
1.4.3. Asbestos.....	20
1.5. Previous studies on the Troodos Massif.....	20

CHAPTER 2.

The tectonic environment of formation of the ophiolite

2.1. Introduction.....	25
2.2. Petrography and mineral chemistry.....	26
2.2.1. The Gabbros.....	26
2.2.2. The Sheeted Complex.....	27
2.2.3. The Lower Pillow Lavas.....	30
2.2.4. The EMS lavas.....	30
2.2.5. The Upper Pillow Lavas.....	32
2.2.6. Overall variations in pyroxene chemistry.....	35
2.2.7. The clinopyroxene discriminant diagrams.....	35
2.3. Geochemistry.....	38
2.3.1. Introduction.....	38
2.3.2. Normative calculations.....	41
2.3.3. Discriminant diagrams.....	44
2.3.4. Trace element geochemistry.....	49
2.3.5. Geochemical patterns.....	58
2.4. Summary of conclusions.....	64
2.5. Discussion of evidence and proposed model.....	65

CHAPTER 3.

Hydrothermal processes in the Troodos ophiolite

3.1.	Introduction.....	71
3.2.	Review of field and experimental evidence on seawater-rock interaction.....	72
3.2.1.	Field evidence.....	72
3.2.2.	Experimental studies.....	74
3.3.	Salient features of alteration in the Troodos ophiolite.....	75
3.3.1.	Field evidence.....	75
3.3.2.	Petrographic evidence.....	77
3.4.	Elemental mobilities during alteration and metamorphism.....	82
3.4.1.	General.....	82
3.4.2.	Collection of samples and analytical techniques.....	83
3.4.3.	Presentation of data.....	84
3.4.3.1.	Magnesium.....	90
3.4.3.2.	Calcium.....	91
3.4.3.3.	Sodium.....	95
3.4.3.4.	Silica.....	102
3.4.3.5.	Zinc.....	105
3.4.3.6.	Strontium.....	105
3.4.3.7.	Barium.....	109
3.5.	Petrological calculations.....	114
3.6.	Numerical calculations and elemental fluxes.....	117
3.7.	Discussion and proposed hydrothermal model.....	125

PART 2.

CHAPTER 4.

The volcanogenic sulphide deposits

General introduction and previous studies

4.1.	Introduction.....	135
4.2.	General features of the sulphide deposits.....	137
4.3.	Previous studies on the sulphide deposits and umbers.....	140

CHAPTER 5.

Field and stratigraphic aspects

of the sulphide deposits.

5.1.	The Limni mining district.....	146
5.1.1.	Introduction and general information.....	146
5.1.2.	Geological framework.....	147
5.1.3.	The tectonic situation.....	152
5.1.4.	The sulphide deposits.....	155
5.1.4.1.	The Limni orebody.....	155
5.1.4.2.	The Evloimeni orebody.....	160
5.1.4.3.	The Kinousa and Uncle Charles deposits.....	162
5.1.5.	Stratigraphic position of the orebodies of the Limni mining district.....	164
5.1.6.	Conclusions from the study of the Limni deposits.....	166
5.2.	The Kalavassos mining district.....	167
5.2.1.	Introduction.....	167
5.2.2.	Geological framework.....	168

5.2.3.	The tectonic situation.....	177
5.2.4.	The sulphide deposits.....	179
5.2.4.1.	The Petra orebody.....	180
5.2.4.2.	The Mavridia group.....	183
5.2.4.2.1.	'A' orebody.....	183
5.2.4.2.2.	The Mousoulos and 'B' orebodies.....	186
5.2.4.3.	The Landaria and Mavri Sykia deposits.....	188
5.2.5.	Stratigraphic position of the orebodies.....	189
5.2.6.	The Kalavastos deposits in relation to their setting.....	191
5.2.7.	Conclusions from the study of the Kalavastos deposits.....	195
5.3.	The Mangaleni orebody, Parekklishia area: An unusual Cyprus deposit.....	196
5.3.1.	Introduction.....	196
5.3.2.	Geological framework.....	197
5.3.3.	Structure of the area.....	200
5.3.4.	Mode of occurrence of the Mangaleni mineralization.....	201
5.4.	Skouriotissa and Phoenix.....	206
5.5.	The deposits of the Tamasos area.....	211
5.5.1.	Agrokipia.....	211
5.5.2.	Kokkinopezoula.....	215
5.6.	West Apliki.....	219
5.7.	Summary of conclusions.....	221

CHAPTER 6. .

Mineralogical and chemical

characteristics of the sulphide deposits

6.1	Introduction.....	223
6.2.	Descriptive mineralogy.....	224
6.2.1.	The Limni orebody.....	224
6.2.2.	The mineralogy of the Mangaleni ore.....	229
6.2.2.1.	The massive sulphide.....	230
6.2.2.2.	The hard sulphide blocks.....	232
6.2.2.3.	The effects of tectonism on the ores.....	234
6.2.2.4.	Discussion of the lamellar intergrowth in chalcopyrite.....	235
6.2.2.5.	Sphalerite compositions and their implications.....	239
6.2.3.	Petrography of mineralized lavas.....	243
6.2.4.	Paragenetic relationships.....	244
6.3.	The transition between mineralized and unmineralized ground.....	248
6.3.1.	Field and mineralogical evidence.....	248
6.3.1.1.	Skouriotissa.....	248
6.3.1.2.	Limni.....	249
6.3.1.3.	Kokkinopezoula.....	250
6.3.1.4.	Memi-Alestos zone.....	253
6.3.2.	Chemical exchange during mineralization.....	256
6.4.	Metal zonations.....	263
6.5.	Discussion of the mineralogical characteristics of the sulphide deposits.....	273

CHAPTER 7.

Summary and conclusions

7.1.	Summary and conclusions.....	291
7.2.	Remarks on future work.....	300
List of references.....		306
Appendix 1: X-ray fluorescence analyses of samples collected along traverses.....		325
Appendix 2: X-ray fluorescence analyses of samples from Evloimeni and Mavri Sykia.....		356
Appendix 3: Location of samples collected from the region of ore zones.....		366
Appendix 4: Electron microprobe (EDS) analyses of pyroxenes from Troodos.....		369

LIST OF FIGURES.

CHAPTER 1.

- Fig. 1.1. Geological map of Cyprus showing location
of deposits described in text.....
- Fig. 1.2. The stratigraphy of the Troodos
autochthonous sedimentary sequence.....
- Fig. 1.3. Stratigraphy of the Troodos Igneous Complex.....
- Fig. 1.4. Interpretive section of the Troodos Ophiolite.....

CHAPTER 2.

- Fig. 2.1. Plot of chrome spinel compositions
from olivine basalt.....
- Fig. 2.2. Overall compositional variations of
clinopyroxenes from various members
of the ophiolite.....
- Fig. 2.3. Composition of clinopyroxene microphenocrysts.....
- Fig. 2.4. The Ca-Mg-Fe clinopyroxene
discriminant diagram.....
- Fig. 2.5. The Al_2O_3 - TiO_2 clinopyroxene
discriminant diagram.....
- Fig. 2.6. The SiO_2 - Al_2O_3 clinopyroxene
discriminant diagram.....
- Fig. 2.7. Normative mineralogy vs Zr content for the
Gabbros and Lower Pillow Lavas.....
- Fig. 2.8. TiO_2 - Zr co-variation diagram for
various members of the ophiolite.....

Fig. 2.9.	The SiO_2 vs $\text{FeO}t:\text{MgO}$ discriminant diagram.....
Fig. 2.10.	The $\text{FeO}t$ vs $\text{FeO}t:\text{MgO}$ discriminant diagram.....
Fig. 2.11.	The SiO_2 vs $\text{Zr}:\text{TiO}_2$ discriminant diagram.....
Fig. 2.12.	The $\text{Al}_2\text{O}_3:\text{TiO}_2$ vs TiO_2 discriminant diagram.....
Fig. 2.13.	Ti- Zr co-variations for the EMS and Lower Pillow Lavas.....
Fig. 2.14.	Zr- Y co-variations.....
Fig. 2.15.	Zr- Nb co-variations.....
Fig. 2.16.	Ba- Zr co-variations.....
Fig. 2.17.	Geochemical patterns for transitional and enriched MORB.....
Fig. 2.18.	Geochemical patterns for basalts from the West Mariana Ridge.....
Fig. 2.19.	Geochemical patterns for selected samples from the Troodos ophiolite.....
Fig. 2.20.	Diagram illustrating the tectonic environment of formation of the ophiolite:.....

CHAPTER 3.

Fig. 3.1.	Geological map showing location of traverses and sample points.....
Fig. 3.2..	MgO - Zr co-variations.....

- Fig. 3.3. Areal distribution of magnesium
enrichments and depletions.....
- Fig. 3.4. Relationship of magnesium variations
to igneous stratigraphy.....
- Fig. 3.5. CaO- Zr co-variations.....
- Fig. 3.6. Areal distribution of calcium
enrichments and depletions.....
- Fig. 3.7. Relationship of calcium variations
to igneous stratigraphy.....
- Fig. 3.8. Na₂O- Zr co-variations.....
- Fig. 3.9. Areal distribution of sodium
enrichments and depletions.....
- Fig. 3.10. Relationship of sodium variations
to igneous stratigraphy.....
- Fig. 3.11 SiO₂- Zr co-variations.....
- Fig. 3.12 Relationship of silica variations
to igneous stratigraphy.....
- Fig. 3.13. Zn- Zr co-variations.....
- Fig. 3.14. Areal distribution of zinc
enrichments and depletions.....
- Fig. 3.15. Relationship of zinc variations
to igneous stratigraphy.....
- Fig. 3.16. Sr- Zr co-variations.....
- Fig. 3.17 Relationship of strontium variations
to igneous stratigraphy.....
- Fig. 3.18. Ba- Zr co-variations.....
- Fig. 3.19 Relationship of barium variations

to igneous stratigraphy.....

Fig. 3.20. Proposed model for the generation
of hydrothermal fluids in the ophiolite.....

Chapter 4.

Fig. 4.1. Diagram illustrating the typical form
of a Cyprus sulphide deposit.....

CHAPTER 5.

Fig. 5.1. Geological map of the Limni mining district.....

Fig. 5.2. The stratigraphy of the Limni mining district.....

Fig. 5.3. Geological map of the Limni opencast mine.....

Fig. 5.4. Series of sections illustrating
the structure of Limni orebody.....

Fig. 5.5. Geological section through Evloimeni.....

Fig. 5.6. Isometric projection of Kinousa
and Uncle Charles deposits.....

Fig. 5.7. Map showing location of Kalavassos area
with relation to the Arakapas fault belt.....

Fig. 5.8. The stratigraphy of the Kalavassos
mining district.....

Fig. 5.9. Geological map of the Kalavassos mining district.....

Fig. 5.10. Detailed section of the intervalcanic sediments.....

Fig. 5.11. Diagram illustrating the disposition of deposits
in the Kalavassos area.....

Fig. 5.12. Isometric projection of the Petra orebody.....

Fig. 5.13. Longitudinal section through 'A' orebody.....

Fig. 5.14. Geological map of the Mavridia opencast mine.....	
Fig. 5.15. Transverse section through 'A' and Mousoulos orebodies.....	
Fig. 5.16. Longitudinal section through Mousoulos and 'B' orebodies.....	
Fig. 5.17. Diagrammatic illustration of the environment of formation of the Kalavasos deposits.....	
Fig. 5.18. The stratigraphic sequence of the Parekklisia area.....	
Fig. 5.19. Geological map of the Mangaleni opencast mine.....	
Fig. 5.20. Geological section through the Mangaleni mineralization.....	
Fig. 5.21. Geological map of Skouriotissa area.....	
Fig. 5.22. Detailed geology of Skouriotissa and Phoenix orebodies.....	
Fig. 5.23. Isometric projection of the Agrokipia deposits.....	
Fig. 5.24. Geological section through Agrokipia 'A' and 'B' orebodies.....	
Fig. 5.25. Geological map of Kokkinopezoula.....	
Fig. 5.26. Geological section through Kokkinopezoula orebody.....	
Fig. 5.27. Geological map of West Apliki.....	
Chapter 6	
Fig. 6.1. Plot of cuprian sphalerite on the Cu-Zn-S diagram.....	

- Fig. 6.2. Plot of compositions of brown and grey alterations on the Cu- Fe- Zn- S diagram.....
- Fig. 6.3. Plot of compositions of lamellar and ridged chalcopyrite on the Cu- Fe- S diagram.....
- Fig. 6.4. Plot of sphalerites from various environments on the Zn- Fe- S diagram.....
- Fig. 6.5. The paragenetic sequence of the Limni orebody.....
- Fig. 6.6. X-ray diffraction data for three boreholes from the Limni ore zone.....
- Fig. 6.7. Geological map of Memi opencast.....
- Fig. 6.8. Chemical variations within and around the Evloimeni ore zone.....
- Fig. 6.9. Chemical changes within and around the Mavri Sykia ore zone.....
- Fig. 6.10. Barium and potassium variations within and around the Evloimeni ore zone.....
- Fig. 6.11. Barium and potassium variations within and around the Mavri Sykia ore zone.....
- Fig. 6.12. Al₂O₃- MgO- Alkalies diagram for mineralized and unmineralized lavas from Evloimeni.....
- Fig. 6.13. Al₂O₃- MgO- Alkalies diagram for mineralized and unmineralized lavas of Mavri Sykia.....
- Fig. 6.14. Distribution of copper in the third floor of Kinousa orebody.....

- Fig. 6.15. Distribution of zinc in
the third floor of Kinousa orebody.....
- Fig. 6.16. Distribution of copper in
the sixth floor of Kinousa orebody.....
- Fig. 6.17. Distribution of zinc in
the sixth floor of Kinousa orebody.....
- Fig. 6.18. Variation of Cu/ Cu+Zn ratio
in the third floor of Kinousa orebody.....
- Fig. 6.19. Variation of Cu/ Cu+Zn ratio
in the sixth floor of Kinousa orebody.....
- Fig. 6.20. Section showing variation of Cu/Cu+Zn
ratio in the Kinousa orebody.....
- Fig. 6.21. Areal distribution of S/Cu (atomic) ratio
in the Kinousa- Uncle Charles ore zone.....
- Fig. 6.22. Distribution of sulphur and S/Cu ratio
along Kinousa- Uncle Charles ore zone.....
- Fig. 6.23 Log fS_2 - Temperature diagram.....
- Fig. 6.24. Log fO_2 - Temperature diagram.....
- Fig. 6.25. Diagram illustrating mixing trends
for some Cyprus deposits.....

LIST OF TABLES.

CHAPTER 2.

Table 2.1.	Petrography and mineral chemistry of selected gabbroic rocks.....
Table 2.2.	Petrography and mineral chemistry of selected samples from the Sheeted Complex.....
Table 2.3.	Petrography and mineral chemistry of selected samples of Lower Pillow Lavas.....
Table 2.4.	The main petrographic features of the Upper Pillow Lavas.....
Table 2.5.	Chemical analyses of clinopyroxenes and co-existing chrome spinels in olivine basalt.....
Table 2.6.	Chemical analyses and CIPW norms of gabbroic rocks.....
Table 2.7.	Chemical analyses and CIPW norms of samples of Lower Pillow Lavas.....

CHAPTER 3.

Table 3.1.	Electron probe analyses of secondary minerals from the Sheeted Complex.....
Table 3.2.	X-ray diffraction data for various members of the ophiolite.....
Table 3.3.	Representative major and trace element analyses of gabbroic rocks.....

Table 3.4.	Representative major and trace element analyses of samples of Lower Pillow Lavas.....
Table 3.5.	Representative major and trace element analyses of samples from the Sheeted Complex.....
Table 3.6.	Compositions of rocks and minerals used in petrological calculations.....
Table 3.7	Correlation coefficients and regression equations for gabbroic rocks.....
Table 3.8.	Correlation coefficients and regression equations for Lower Pillow Lavas.....
Table 3.9.	Chemical composition of umbers.....

CHAPTER 4.

Table 4.1.	Composite sample of Skouriotissa massive ore.....
Table 4.2.	The range of sizes of Cyprus deposits.....

CHAPTER 5.

Table 5.1.	Production data for the mines of the Kalavassos..... mining district.....
------------	--

CHAPTER 6.

Table 6.1.	Electron microprobe analyses of pyrites from Limni mine.....
Table 6.2.	Electron microprobe analyses of chalcopyrite from Limni mine.....
Table 6.3.	Electron microprobe analyses of cuprian sphalerite from Limni mine.....

Table 6.4.	Electron microprobe analyses of brown and grey alterations of chalcopyrite.....
Table 6.5.	Electron microprobe analyses of lamellar and ridged chalcopyrite.....
Table 6.6.	Electron microprobe analyses of unaltered chalcopyrite.....
Table 6.7.	Electron microprobe analyses of sphalerites from Parekklisia and the East Pacific Rise.....
Table 6.8.	Electron microprobe analyses of sphalerites from Mathiatis (Mitsero) and Agrokipia 'B'.....
Table 6.9.	The composition of chlorites from Limni, compared to chlorites from Agrokipia 'B'.....
Table 6.10.	X-ray diffraction data for various assemblages from Limni mine.....
Table 6.11.	Representative analyses of mineralized and unmineralized lavas from Evloimeni.....
Table 6.12.	Representative analyses of mineralized and unmineralized lavas from Mavri Sykia.....
Table 6.13.	Statistical data for three floors of Kinousa underground deposit.....

LIST OF PLATES

CHAPTER 2.

- Plate 2.1. Photomicrograph of gabbro.....
- Plate 2.2. Photomicrograph of diabase.....
- Plate 2.3. Photomicrograph of Lower Pillow Lava.....
- Plate 2.4. Photomicrograph of Lower Pillow Lava showing
plagioclase as phenocryst phase.....
- Plate 2.5. Photomicrograph of EMS lava.....
- Plate 2.6. Photomicrograph of olivine basalt.....

CHAPTER 3.

- Plate 3.1. Chalcedonic silica vein in silicic lava.....
- Plate 3.2. Celadonite- fibrous zeolite association.....
- Plate 3.3. Laumontite concentrations in Lower Pillow Lavas...
- Plate 3.4. Association of calcite and epidote in cavities....
- Plate 3.5. Initial stage of pervasive action of hydrothermal
fluids.....
- Plate 3.6. Photomicrograph of smectite.....
- Plate 3.7. Detail of the transformation of clinopyroxene to
actinolite.....

CHAPTER 5.

- Plate 5.1. Limburgitic flows and hyaloclastites
exposed in the Double Seven area.....
- Plate 5.2. Exposure of EMS lavas at Evloimeni mine.....

- Plate 5.3. Infilling of faults by calcite in the
Double Seven area.....
- Plate 5.4. Detail of the intervalcanic sediments.
- Plate 5.5. Low angle fault at Kalavassos.....
- Plate 5.6. View of Mavridia opencast looking north.....
- Plate 5.7. Pillowed flows in Basal Group.....
- Plate 5.8. The deformation of umbers in the
Mangaleni opencast.....
- Plate 5.9. Massive pyrite resting on
unaltered pillow lavas at Skouriotissa.....
- Plate 5.10. Massive pyrite overlain by umber.....
- Plate 5.11. The mineralized-unmineralized lava
transition at Kokkinopezoula.....
- Plate 5.12. The mineralized-unmineralized lava
transition at Kokkinopezoula.....
- CHAPTER 6.
- Plate 6.1. Photomicrograph of partial rimming of pyrite
by quartz.....
- Plate 6.2. Photomicrograph of hematite enclosed in pyrite....
- Plate 6.3. Photomicrograph of alteration of chalcopyrite
to bornite.....
- Plate 6.4. Photomicrograph of cuprian sphalerite.....
- Plate 6.5. Photomicrograph of skeletal iron sulphide
in the Parekklishia massive ore.....
- Plate 6.6. Detail of brown alteration of chalcopyrite.....
- Plate 6.7. Detail of the alteration of chalcopyrite

	to bornite and covellite.....
Plate 6.8.	Replacement of chalcopyrite by sphalerite.....
Plate 6.9.	Dendritic crystals involving chalcopyrite and sphalerite.....
Plate 6.10.	Epitaxial growth of pyrite on chalcopyrite.....
Plate 6.11.	Formation of marcasite by tectonism.....
Plate 6.12.	Detail of the lamellar intergrowth in chalcopyrite.....
Plate 6.13.	Detail of the ridged pattern in chalcopyrite.....
Plate 6.14.	Deformation of chalcopyrite lamellae.....
Plate 6.15.	Photomicrograph of chlorite- quartz association in vesicles.....
Plate 6.16	Replacement of pyrite by quartz.....
Plate 6.17.	Euhedral quartz coating fracture in mineralized lava.....
Plate 6.18.	Association of hematitic jasper and pyrite.....
Plate 6.19.	Vesicle-filling minerals at Kokkinopezoula.....
Plate 6.20.	General view of Memi-Alestos area.....
Plate 6.21.	Hematite-quartz assemblage in vesicles.....
Plate 6.22.	Hematite- epidote-quartz assemblage.....
Plate 6.23.	Chloritic alteration of pillows at the Memi opencast.....
Plate 6.24.	Mineralized-unmineralized lava transition at Memi opencast.....

LIST OF PUBLICATIONS.

Adamides, N. G., Geological history of the Limni concession, Cyprus, in the light of the plate tectonics hypothesis. Trans. Inst. Min. Metall., 84, 17-23, 1975.

Adamides N. G., Kalavassos mining district. Intern. Ophiolite Sympos., Cyprus, field excursion guidebook, 80-93, 1979.

Adamides, N. G., The form and environment of formation of the Kalavassos ore deposits- Cyprus. Proc. Intern. Ophiol. Sympos., Cyprus, 117- 128, 1980.

Adamides, N. G., Diverse modes of occurrence of Cyprus sulphide deposits and comparison with recent analogues. GAC/MAC/CGU joint annual meeting, Victoria, 1983 (In press).

Preface

1. Description of contents

The volcanogenic sulphide deposits of Cyprus have recently become the focus of multidisciplinary research as a result of the discovery of their supposed genetic equivalents in modern oceanic spreading centres. Formulation of hypotheses on the mode of formation of these deposits, such as the proposed seawater circulation hypothesis (Spooner and Fyfe, 1973), have shed new light on rock relationships and have caused a revision of previous ideas. Support for the hypothesis is provided by experimental studies on seawater-rock interaction; the composition of hydrothermal fluids as derived from study of fluid inclusions; the evidence of interrelationship between metamorphism in ophiolite terrains and the ore deposits associated with such terrains as obtained from isotope studies. All these suggest that volcanic and hydrothermal processes are closely interrelated. It is therefore expected that the ore-forming processes will leave their imprint on the intrusive and extrusive section in the same way that the latter, in their genesis, were the cause for hydrothermal circulation.

The purpose of this work is to examine whether the mode of occurrence of the sulphide deposits, the controls of their localisation, their mineralogical character and associated alteration and their stratigraphic relationships are in support of the hypothesis of seawater circulation.

The thesis is essentially divisible into two independent parts, the first being concerned with regional aspects touching on

the regime of formation of the ophiolite and the generation of hydrothermal fluids; the second dealing with aspects relevant to the behaviour of those same fluids as they reach higher levels and are finally discharged on the sea floor.

Part 1

Chapter 1 describes in detail the geology of Cyprus, with emphasis on the Troodos ophiolite, and summarises previous work. It provides the general background onto which this work is based and to which it endeavours to add.

Chapter 2 is concerned with regional petrological and geochemical aspects of the ophiolite. Particular emphasis is placed on the definition of the tectonic environment of its formation and the resolution of genetic relationships between volcanic suites.

Chapter 3 examines the field, petrographic and geochemical evidence for element mobility during hydrothermal metamorphism. A model is proposed for the generation of hydrothermal fluids by interaction of seawater with oceanic crust at spreading regimes.

Having established how and where the fluids responsible for the sulphide deposits and metalliferous sediments were generated, their subsequent behaviour is examined in part 2 of this work.

Part 2

Chapter 4 provides a general introduction to the sulphide deposits and summarises previous work.

Chapter 5 examines the mode of occurrence of a number of deposits in various mining districts. The Limni, Kalavassos and Parekklishia areas are described in detail and the study is supplemented by brief description of other deposits distributed throughout the island. Particular emphasis is placed on structural controls of ore deposition, the influence of faulting in the final form of the resultant orebodies and the stratigraphic horizon of the mineralization. The last named has a direct bearing on the timing of the hydrothermal event.

Chapter 6 is concerned with mineralogical and chemical aspects of the deposits and the light these shed on the original and final nature of the hydrothermal fluids. Special aspects include:

1. The nature of the chemical exchange between the fluids and the wall rocks;
2. The causes for the mineralogical diversity of the precipitates as reflected in the formation of copper-rich and copper-poor orebodies;
3. The influence of structure and depth of ore formation on the nature of wall rock alteration.

The conclusions derived from the whole of the thesis are summarised and, briefly, discussed in chapter 7 and the implications on exploration outlined.

2. Methods and techniques used

This study is based to a great extent on the results of field mapping of mineralized occurrences carried out while the

author was employed by the Cyprus Sulphur and Copper Company (1971-1975) and Hellenic Mining Company (1975- present). With the exception of the Kalavassos mining district, which was mapped by tape and compass on a scale 1:2500, mapping of the other areas was carried out on 1:5000 scale by pace and compass methods. Mines were mapped at detailed scales 1:500 or 1:1000, using topographic maps supplied by the above mentioned companies.

In addition to field work, the following methods were used:

The petrography of the various members of the ophiolite was examined by use of numerous thin sections and supported by limited electron probe (energy dispersive) examination of the chemistry of primary igneous phases. Petrographic and X-ray diffraction methods were also used in the study of wall rock alteration in sulphide deposits.

The mineralogy of sulphide ores from selected deposits was examined by ore microscopic techniques for the determination of dominant phases and textures. The investigations were supported by extensive electron probe (energy dispersive) analyses aimed at examining phase variations.

The geochemistry of the ophiolite and chemical changes associated with the metamorphism and mineralization were examined by X-ray fluorescence analyses of over 200 samples for major and trace elements. Details on the location of samples and analytical techniques used are given in chapter 3.

PART 1

CHAPTER 1.

General Geology of Cyprus.

1.1. General.

The island of Cyprus (Fig. 1.1), 9200 sq.km. in area and with a mixed, mainly Greek, population of 640 000, lies in the northeastern corner of the Mediterranean Sea.

It is tectonically divided into four, arcuate, easterly-trending belts which, from north to south, are:

a. The Kyrenia range, comprising allochthonous slices of recrystallised limestones associated with autochthonous clays and intercalated volcanic rocks. The allochthonous rocks are considered to have been thrust over Cyprus by the orogenic movements which culminated in the construction of the Taurodinaric belt. The presence of lavas with strong calc-alkaline character led Baroz (1980) to suggest that the range marks a continent-island arc collisional event.

b. The Mesaoria Plain. This is made up of a series of autochthonous sediments, ranging in age from Upper Cretaceous to Recent. These comprise radiolarian marls, chalks, cherts, calcareous marls and local evaporites, mainly gypsum. They are unconformably overlain by a sequence of coarse conglomeratic beds, the result of the rapid erosion of the Troodos Massif which followed its uplift in Recent times.

c. The Troodos Massif consists of a centrally located mass of plutonic rocks, centred at Mt. Olympus (Elev.1951

metres). These vary from harzburgite through dunite into pyroxenite and gabbro. They pass outwards into a sheeted dyke complex and finally into pillow lavas.

d. The Mamonia Complex, best developed in the Paphos district, comprises rocks of diverse origins, including autochthonous sandstones and siltstones (the Kannaviou formation) and clays (the Moni Melange) and allochthonous serpentinites, quartzose sandstones, schists, marbles and lavas. The relationship of this formation to Troodos is still controversial but prevailing theories associate the Moni Melange with trench sedimentation. Robertson (1977) considers the exotic blocks incorporated in the melange as deposited by gravity sliding following tectonic disruption of a continental margin. This margin was originally located to the northwest, presently found in southwestern Cyprus (Moores and Vine, 1971) as a result of the anticlockwise rotation of the island in the last 10 million years (Shelton and Gass, 1980).

1.2. The geology of the Troodos Massif.

1.2.1. The sedimentary rocks.

The stratigraphy of the autochthonous sedimentary sequence is shown in fig. 1.2.

The Fanglomerate Series unconformably overlies all older formations and has been formed as a consequence of the rapid uplift of Troodos in Pleistocene to Recent times. It consists of poorly sorted boulder beds predominantly consisting of diabase and gabbro but locally interdigitates with shallow water marine


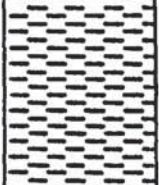
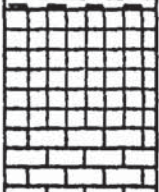
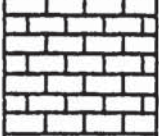

<u>LITHOLOGY</u>	<u>FORMATION</u>	<u>AGE</u>
	FANGLOMERATE	Pleistocene
	MESAORIA GROUP	Pliocene
	PAKHNA FORMATION	Miocene
	LEFKARA GROUP	Miocene to Upper Cretaceous
	PERAPEDHI FORMATION	Upper Cretaceous

FIG. 1.2. The stratigraphy of the Troodos autochthonous sedimentary sequence. (After data of Geological Survey Department).

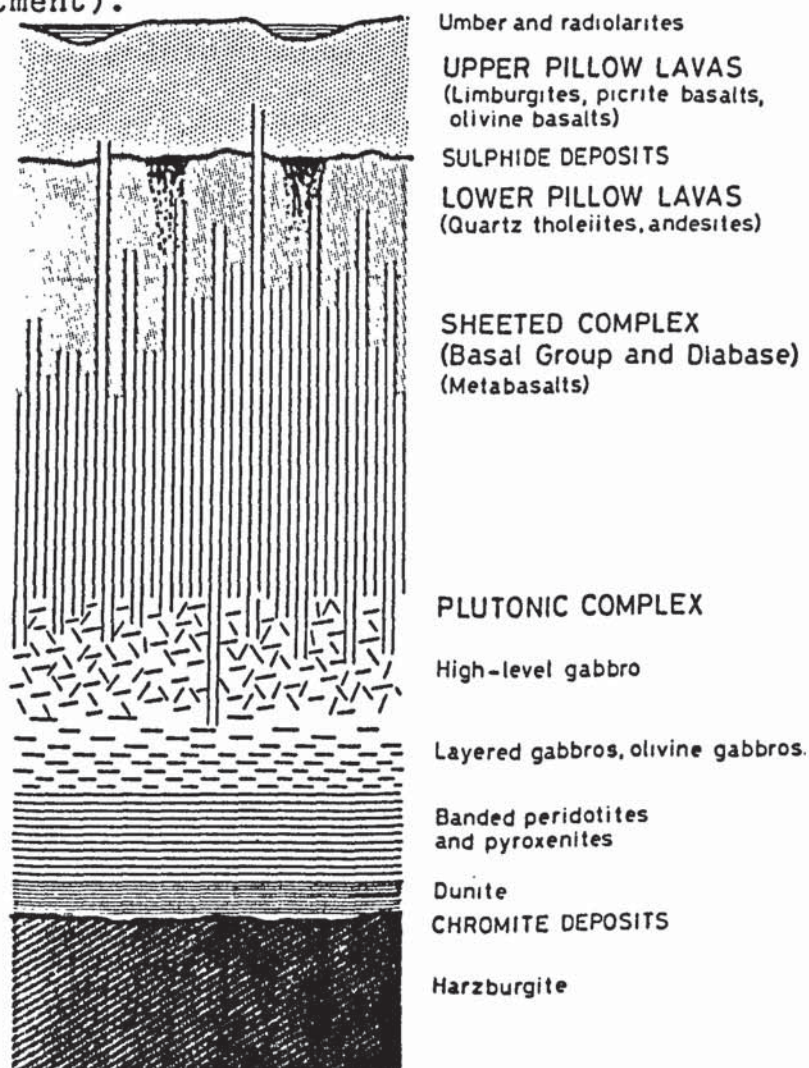


FIG. 1.3. The stratigraphy of the Troodos Igneous Complex. (Redrawn from Allen, 1975).

sediments (Wilson, 1959, Bear, 1963).

The Pliocene Marl predominantly comprises buff-coloured marls and darker grey silty clays with local thin limestone bands. The formation locally attains a great thickness and rests, sometimes, unconformably on pillow lavas. Elsewhere a sandstone facies develops, probably the lateral equivalent of the silty clays (Carr and Bear, 1960).

The Pakhna Formation is represented by a sequence of well-bedded marls, chalks, and calcarenites with locally developed reef limestone (the Koronia limestone) and massive beds of selenite gypsum. Minor celestite is associated with gypsum, gypsiferous marls and reef limestone but its extent and significance are as yet undetermined.

The Koronia limestone is, at the type locality of Koronia hill, represented by a karsted, cavernous and highly brecciated coral-bearing limestone but elsewhere well bedded facies may occur. The reef limestone is quarried for the production of lime and crashed aggregates.

The Lefkara group is characterised by pure, well-bedded chalks and interbedded cherty bands, particularly in the lower parts. The formation is equivalent to the Lapithos Formation, developed in the region of the Kyrenia range, but is much better developed in the southern part of Cyprus. In the Lapithos region it is intercalated with volcanic rocks, presumably a reflection of contemporaneous vulcanicity related to incipient island arc development (Baroz, 1980).

The Moni Formation is a clayey, locally highly tectonised

sequence , well developed in the region of southern Cyprus and particularly in the area of Moni village from which it derives its name. The name Moni Melange (Pantazis, 1967) has been given to the formation as a result of the chaotic nature and incorporation of blocks of exotic lithology. The formation thins out against the Troodos Massif but attains a great thickness to the south, in the region of Limassol.

The Perapedhi Formation rests on the Upper Pillow Lavas and starts at the base with massive, dark brown, fine grained umber, normally passing in higher levels into well bedded and delicately banded umbers. Hues generally vary from orange brown to dark brown and are interpreted as resulting from variations in manganese: iron ratio or the oxidation state of the component minerals. In higher levels well-bedded pink-coloured radiolarites are developed.

Compositionally the umber is a mixture of goethite and poorly crystalline manganese oxides (Elderfield et al., 1972) with small amounts of quartz. Interbedded highly silicified umbers are widespread and in alternation with non-silicified beds suggesting chemical variations during deposition. Relative to the overlying sediments the umbers are strongly enriched in many trace elements such as Ba, Co, Cu, Ni, Pb, V, Zn and Zr (Robertson, 1975).

1.2.2. The igneous rocks

1.2.2.1. Definition of ophiolite.

In order to understand why Troodos has come to be regarded as one of the best developed ophiolite complexes on

earth, it is pertinent to site the definition of a complete ophiolite as provided by the participants of the Penrose field conference (Geotimes, 1972). This definition may then be compared with the detailed description of the Troodos igneous sequence which is presented in later paragraphs.

Ophiolite refers to a distinctive assemblage of mafic to ultramafic rocks. It should not be used as a rock name or as a lithologic unit in mapping. In a completely developed ophiolite the rock types occur in the following sequence, starting from the bottom and working up:

Ultramafic complex, consisting of variable proportions of harzburgite and dunite, usually with a metamorphic tectonic fabric (more or less serpent-inised).

Gabbroic complex, ordinarily with cumulus textures commonly containing cumulus peridotites and pyroxenites and usually less deformed than the ultramafic complex.

Mafic sheeted dyke complex.

Mafic volcanic complex, commonly pillowed.

Associated rock types include (1) an overlying sedimentary section typically including ribbon cherts, thin shale interbeds, and minor limestones; (2) podiform bodies of chromite generally associated with dunite; (3) sodic felsic intrusive and extrusive rocks.

Faulted contacts between mappable units are common. Whole sections may be missing. An ophiolite may be incomplete, dismembered, or metamorphosed in which case it should be called a partial, dismembered or metamorphosed ophiolite. Although ophiolite is interpreted to be oceanic crust and upper mantle the use of the term should be independent of its supposed origin.

1.2.2.2. The Troodos Igneous Complex.

The stratigraphic sequence as established from studies by numerous workers is shown in fig. 1.3.

The Complex is traditionally subdivided into a lowermost Plutonic Complex, the Sheeted Complex and the Pillow Lava Series. As a result of recent uplift centred on Mt. Olympus the three subdivisions are exposed in a complete section rendering Troodos easily accessible to detailed study.

1.2.2.2a. The Plutonic Complex

The harzburgite forms the central core of the Plutonic Complex and is a coarse grained rock remarkably uniform in chemical and modal composition, averaging 80 % olivine, partly serpentinised, 20 % orthopyroxene and traces of chrome spinel and clinopyroxene (Allen, 1975).

Petrofabric studies (George, 1978), coupled with the homogeneity of chemical composition, suggest that the harzburgite is not a product of cumulation but the refractory residuum of partial fusion. Inclusions of plagioclase lherzolite within the harzburgite

gite are interpreted as representatives of primordial mantle (Menzies and Allen, 1974).

The contacts of the harzburgite with the overlying dunite, marked by the disappearance of orthopyroxene, are irregular and defined by a zone of transition of one to the other (Michaelides, 1983). Chromite concentrations appear to be closely related to this zone but have also been located within the harzburgite.

Dunite, considered a metacumulate, overlies the harzburgite and tectonite fabrics suggest that it has suffered the same deformation history as the harzburgite. The dunite is a pure olivine rock, partially serpentinitised and containing accessory chromite whose proportion steadily decreases from 4 % close to the chromite deposits to 1-2 % at the level of first appearance of clinopyroxene (Allen, 1975).

The transition from dunite metacumulate to gabbroic cumulates is marked by cyclic units of harzburgite containing 60-70 % olivine, the remainder comprising diopside and enstatite in a 3:1 ratio (Wilson, 1959).

The gabbros may be essentially subdivided into a lower sequence of layered gabbros and an upper sequence of massive, unlayered, frequently uralitised gabbro. Layering is caused by rhythmic variations in abundance of mafic and light minerals.

The melagabbros, marking the first appearance of cumulus plagioclase, predominantly comprise olivine and clinopyroxene with lesser amounts of orthopyroxene and plagioclase. They are followed in higher levels by olivine gabbros and the rock type is con-

sidered intermediate between wehrlite and olivine-gabbro (Wilson, 1959).

The pyroxene gabbros, essentially composed of hypersthene, augite and calcic plagioclase, are typically massive to poorly banded and may grade in higher levels to quartz gabbros close to the gabbro/diabase boundary.

The contacts of the gabbros with the overlying Sheeted Complex are frequently marked by the discontinuous development of leucocratic rocks, the plagiogranite (Coleman and Peterman, 1975). Petrologically these vary from hornblende-trondhjemite through epidote-trondhjemite to quartz granulite. The unit has been much affected by post-magmatic metamorphism resulting to the complete destruction of primary mineralogy. According to Allen (1975) it was originally continuously developed between gabbro and Diabase but Wilson (1959) describes interdigitation between the two units in the southeastern margin of the plutonic rocks.

1.2.2.2b. The Sheeted Complex.

This is subdivided into an intrusive lower unit, composed of 100 % dykes with gabbro screens (the Diabase) and an extrusive upper unit, the Basal Group, the contact essentially being marked by the first appearance of pillowed flows as screens between dykes.

The lower part of the Diabase is characterised by abundant intervening screens of fine grained gabbro between the dykes, but the underlying plagiogranites, considered the roof zone of the plutonic rocks, are remarkably free of diabase dykes. These

gabbroic screens are thought to be the dismembered root zones of earlier dykes in a spreading environment where roof zone nucleation produces fine grained gabbro which forms a sandwich zone between plagiogranite and Diabase (Allen, 1975). The thickness of this horizon is estimated at 50-75 metres, in higher levels the proportion of fine grained gabbro screens rapidly decreasing.

The Diabase, in its most typical appearance, is represented by a swarm of parallel, predominantly north-south trending mafic dykes generally metamorphosed to the greenschist facies, veined by a quartz-epidote assemblage, and frequently weakly iron stained as a result of their involvement in the ore forming processes. Signs of important mineralization are, however, rare and represented by the occasional development of small concentrations of sulphides along zones of shattering and brecciation.

The upper contact of the Diabase with the Basal Group is arbitrarily placed on the evidence of first appearance of pillows, representing the contribution of an extrusive component.

The lower parts of the Basal Group merge into the Diabase proper but in higher levels marked differences in alteration are apparent while the proportion of hostrock to intrusives steadily increases from 1:20 at the base to 1:10 at the top of the sequence (Bear, 1963).

Metamorphic gradation of the Basal Group into the overlying pillow lavas has been described by Gass and Smewing (1973).

1.2.2.2c. The Pillow Lava Series.

The Pillow Lava Series is traditionally subdivided into the Lower Pillow Lavas and the Upper Pillow Lavas on the basis of a petrological discontinuity, differences in degree of alteration and, in some cases, an unconformable relationship. Recent studies suggest that the boundary, as presently defined, does not coincide with a chemical break (Smewing et al., 1975, Robinson et al., 1983).

The Lower Pillow Lavas are characterised in the field by abundant non-pillowed flows and sills, frequently columnar-jointed, with dykes being particularly abundant in the lower parts where the formation merges into the underlying Sheeted Complex. Pillows are abundant and on the average may constitute 50 % of the outcrop (Bear, 1963) and are in many cases strongly vesicular.

Alteration is evident in the formation of abundant celadonite, staining joint planes in dykes and flows and also occurring in the massive form in the interspaces of pillows. Stilbite, heulandite and chalcedonic silica are the most common cavity-filling minerals.

Mineralization is particularly evident in the rocks of this formation by the development of intense gossans which provided the first guide to the presence of sulphide deposits.

In contrast to the Lower Pillow Lavas the rocks of the Upper Pillow Lavas show some petrographic diversity mainly as a result of variations in abundance of olivine which is considered a characteristic mineral of this formation.

The base of the formation is locally made of a sequence of glassy rocks, the limburgites. These are essentially composed of

abundant glass with enclosed quenched clinopyroxene and rare fresh olivine and chrome spinel. Plagioclase is completely absent. Overlying the limburgites are olivine basalts which vary considerably in abundance of contained olivine from essentially olivine-free to extremely olivine-phyric. Development of picrite basalts is sporadically observed, as e.g. in the Kalavassos region, where such picritic flows are well developed in the higher levels of the sequence, at the contact between the limburgites and the olivine basalts.

The Upper Pillow Lavas are characterised by abundance of pillowed flows and a scarcity of dykes which, however, may reach some density in the lower parts of the formation. A lighter grey colour of the pillows, as opposed to the darker grey Lower Pillow Lavas, and a pinkish surface colouration attributed to the alteration of volcanic glass to chlorophaeite have been sited as guides in the field differentiation between the two formations.

1.3. Structure of the Massif.

Recent uplift, centred over the plutonic core, has resulted to a broadly domal structure. This uplift has been associated with underthrusting of Troodos by African continental crust (Gass and Masson-Smith, 1963) and is considered responsible for the annular outcrop of pillow lavas fringing the sheeted dyke complex and for the continuing elevation of Troodos as a result of isostatic re-adjustment.

South of Troodos a major east-west trending fault zone, called the Arakapas fault belt (Fig. 1.1), is associated with

coarse and fine clastic intervolcanic sediments and very primitive vulcanicity. This is considered a fossil transform fault (Moore and Vine, 1971; Simonian, 1975).

The predominant fault pattern in the pillow lavas and Sheeted Complex is one of normal faulting. Thrusting is predominantly confined to the southern part of Troodos and particularly in the region of the Limassol Forest Plutonic Complex where serpentinite has been recognised in thrust relationships with pillow lavas and sediments (Panayiotou, 1977).

1.4. Mineral deposits.

1.4.1. Sulphides.

Details of the sulphide deposits, which are the main concern of this work, are presented in chapter 4. It is, however, pertinent to describe here their broad characteristics since they are inseparably related to the stratigraphy and history of the volcanic rocks.

The sulphide deposits are predominantly located within the Lower Pillow Lavas and comprise, in the idealised situation, an upper stratiform zone of massive pyrite passing in lower levels through a thin zone of siliceous pyrite and thence into fracture and cavity fillings of sulphide within altered, silicified and chloritised country rocks. In still deeper levels the proportion of rock to total sulphide increases and the mineralization occurs in the form of veins and disseminations in altered lavas.

Mineralogically they are characterised by pyrite as the

main iron sulphide, marcasite being generally rare and probably in all cases secondary. Chalcopyrite is second in abundance and sphalerite may occur in significant amounts in some deposits but is generally rare.

The size of individual deposits is extremely variable, the largest known deposit being Mavrovouni which amounted to 15 million tons of massive pyrite. The smallest do not exceed a few thousand tons. Between the two extremes, deposits in the range of 1-2 million tons may be considered normal.

1.4.2. Chromite.

Deposits of chromite are developed within the dunite or at the transition zone between dunite and harzburgite. Deposits within harzburgite are also known but rather rare. The Kannoures mine is such an example (Maliotis and Michaelides, 1979).

Chromite deposits typically occur as pods and lenses, concordant with the foliation of the surrounding tectonites but pinching and swelling unpredictably (Ingham, 1959). Dimensions of individual pods vary from less than one metre to over 25 metres and are typically surrounded by a thin zone of discolouration in dunite.

The largest chromite deposit in the Troodos complex is Kokkinorotsos with total ore extracted being 600 000 tons and remaining reserves estimated at 200 000 tons (Maliotis and Michaelides, 1979).

1.4.3. Asbestos.

Chrysotile asbestos of the cross-fibre type is mined in one area within the harzburgite and is related to intense serpentinisation and shattering, the best values being found where smashing is most severe (Bear, 1963). The Amiandos mine represents the only producer on the island. Mining began in 1904 and remaining reserves are expected to last for over 50 more years at a yearly production of 5 million tons.

1.5. Previous studies on the Troodos Massif.

The detailed character of the Massif emerged through the efforts of officers of the Geological Survey Department resulting to the production of maps in a scale 1:31680 (2 inches to one mile). The results of these studies were incorporated in a series of memoirs (1-8). Particular mention is made of the work of Wilson (1959) who recognised the evidence of crustal extension provided by the diabase and outlined the relationships between the plutonic rocks and the overlying intrusive and extrusive components of the ophiolite.

Although recognition of Troodos as a probable fragment of oceanic crust was originally made by Gass (1968), detailed evaluation of evidence and the significance of individual members was made by Moores and Vine (1971) who proposed a model according to which the harzburgite and dunite represent depleted mantle, the olivine pyroxenite and gabbro represent intrusive or cumulate magmatic material and the high-level gabbro and Diabase are equivalent to layer 3 of oceanic crust. The Basal Group, Lower

Pillow Lavas and Upper Pillow Lavas are considered to represent layer 2.

Greenbaum (1972), although accepting the general relationships between igneous suites as outlined by Moores and Vine (1971), considered the harzburgite as the depleted mantle, the dunite being included with the cumulates. This latter view is also supported by the petrological work of Allen (1975) which suggests formation of the dunite by adcumulate processes, pointing to the absence of other silicate phases. Evidence in support of the harzburgite as refractory residuum after partial melting is mainly based on the uniformity of composition and its great thickness which would require an impossibly large magma chamber to account for its formation as a cumulate. George (1978), on the basis of petrofabric studies, interpreted the strong foliation and layering in the harzburgite as the result of penetrative deformation at temperatures close to or above peridotite solidus, a conclusion in support of the residual character of this rock type.

A single large magma chamber was postulated by Greenbaum (1972) to account for the plutonic and volcanic rocks in a spreading axis environment, in contrast to Moores and Vine (1971) who envisaged crystallisation in multiple chambers. The existence of independent magma cells is also supported by the petrological studies of Allen (1975) which suggest a complex history as the primary magmas are separated from their source until they are finally intruded or extruded at an accreting plate margin.

An interpretive diagram, based on the above deductions is

shown in fig. 1.4.

A study of the extrusive section of the ophiolite was carried out by Smewing (1975) who postulated a spreading axis origin for the Sheeted Complex and Lower Pillow Lavas and formation of the Upper Pillow Lavas by off-axis activity. The author postulated in addition a zonation of zeolitic assemblages and associated this with a distinct facies of metamorphism, the zeolite facies, passing in deeper levels into the greenschist facies.

The configuration of the spreading axis was studied by Kidd and Cann (1974) who, based on evidence of one-way chilling of the predominantly north-south trending dykes in the diabase, suggested that the spreading axis responsible for the formation of the ophiolite lay in the present west of Cyprus. A spreading rate of 0.5-1.2 cm/year was postulated by Nisbet and Pearce (1973) on the basis of TiO_2 abundances in the Troodos basalts.

The tectonic environment of formation of the ophiolite was investigated by Pearce and Cann (1973) and Pearce (1975) using immobile elements (Ti, Zr, Y, Nb). They suggested a spreading origin in an interarc basin, with the Lower Pillow Lavas and Sheeted Complex showing ocean floor characteristics and the Upper Pillow Lavas exhibiting typical island arc affinities. An island arc origin for the ophiolite in general was suggested by Miyashiro (1973) on the basis of major element evidence but this suggestion was debated on the grounds of mobility of such elements during alteration and metamorphism (Hynes, 1975; Moores, 1975; Church and

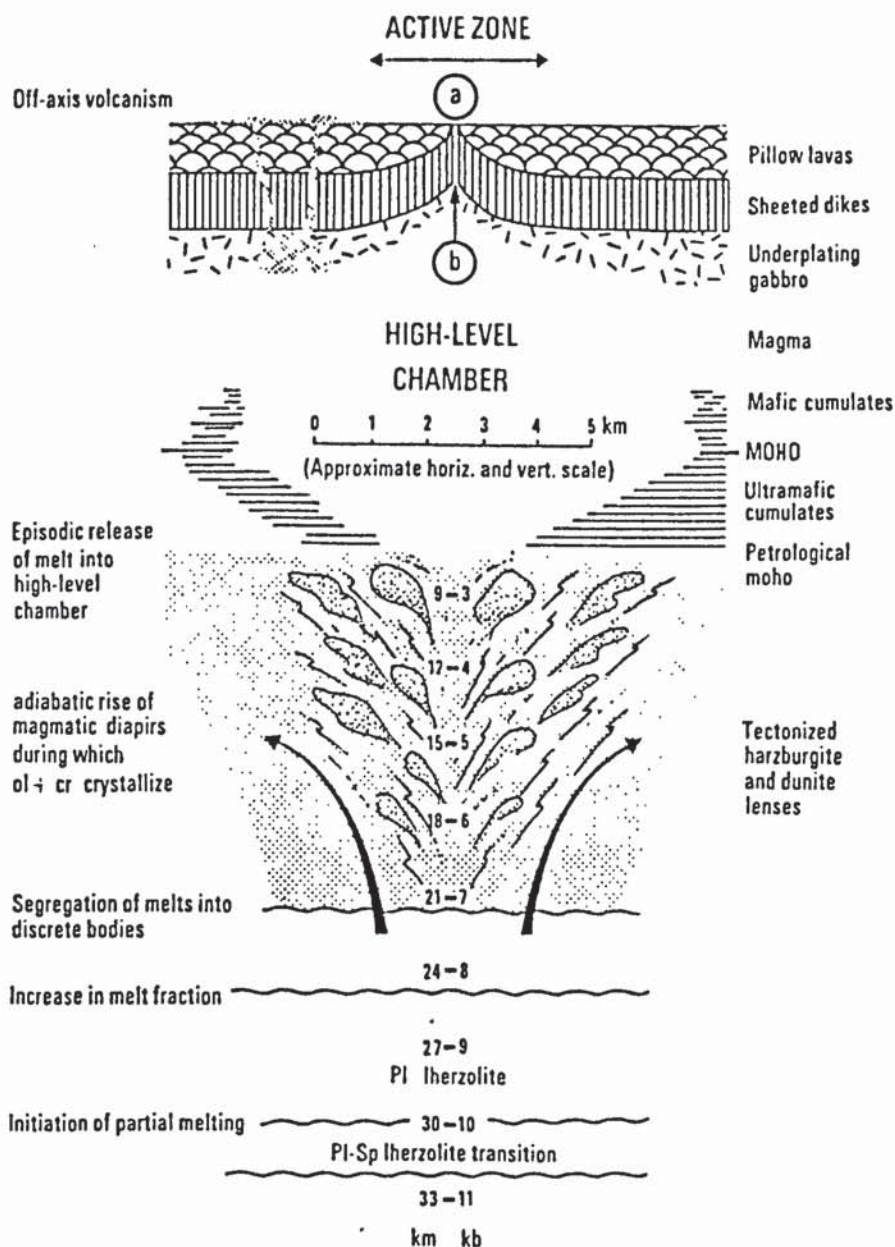


FIG. 1.4. Interpretive diagram illustrating relationships in the Troodos ophiolite. (From Gass, 1980).

Coish, 1976). Major element evidence was also used by Pantazis (1980) in support of an island arc origin for Troodos. Formation of the Lower Pillow Lavas in the axial parts of a ridge with the Upper Pillow Lavas being extruded slightly off-axis from discrete yet contemporaneous magma chambers was suggested by Smewing et al. (1975). A similar environment is suggested by Pearce (1980) who related the Troodos ophiolite to mantle which had first been depleted in incompatible elements and then enriched by aqueous fluids driven off subducted oceanic crust. Spreading is postulated to have taken place above a shallow dipping subduction zone. Petrological studies of glassy basalts from the Upper Pillow Lavas (Jorgensen and Brooks, 1981) were interpreted as evidence for a back-arc environment for these rocks. Robinson et al. (1983) used the compositions of volcanic glasses to suggest that part of the Lower Pillow Lavas exhibit primitive chemistry indistinguishable from the Upper Pillow Lavas. The authors place the environment of extrusion of all Troodos lavas in an early island arc locale and compare the Troodos pillow lavas with assemblages from the Mariana-Bonin arc.

CHAPTER 2.

Tectonic environment of formation of the Troodos ophiolite.

2.1. Introduction.

The Troodos ophiolite has been generally associated with a mid-ocean ridge environment (Moore and Vine, 1971, Gass and Smewing, 1973, Greenbaum, 1972) mainly in view of the spectacular development of a sheeted dyke complex and the Troodos rocks were compared to typical mid-ocean ridge basalts (MORB). The associated sulphide deposits have thus been linked to hydrothermal activity at such an environment. Miyashiro's postulate that the environment of formation of the ophiolite was probably an island arc (Miyashiro, 1973) was initially rejected in a series of heated exchanges (Hynes, 1975; Miyashiro, 1975; Moore, 1975; Miyashiro, 1975a). It led, however, to a review of evidence and later workers (Pearce, 1975; Smewing and Potts, 1976; Kay and Senechal, 1976; Pantazis, 1980) generally noted an island arc imprint on the Troodos assemblages, and associated the ophiolite with either a marginal basin environment or an island arc.

It has recently become increasingly evident, mainly as a result of extensive drilling in present day ocean basins and the accumulation of abundant data from diverse environments, that many complications exist in the processes taking place even at typical mid-oceanic ridges. These result to a variety of extrusive products bearing the signature of complex interplay between partial melting and fractional crystallisation and the additional problem of source heterogeneities. In the place of normal MORB

which were considered the representatives of all basalts extruded at a spreading axis, transitional and enriched (T and E-type) MORB have been recognised (Wood et al., 1980).

The processes taking place at mid-oceanic ridges are relatively simple compared to processes at marginal basin environments which bear additional complications relating to an underlying or nearby Benioff zone and, in the case of basins formed by arc-splitting, (Karig, 1970, Tarney et al., 1981) the formation of assemblages bearing characteristics of both MORB and island arc volcanics.

The main objective of this chapter is the clarification of the tectonic environment of formation of the ophiolite, based on petrological and chemical evidence. Such knowledge is essential in the formulation of models of hydrothermal ore genesis, the clarification of relationships between lava suites and the search for ore deposits on present day oceanic environments. Extensive use will be made of the wealth of information obtained in recent years, particularly through the deep drilling project (DSDP), in establishing how Troodos compares with modern oceanic crust.

2.2. Petrography and mineral chemistry.

2.2.1. The gabbros.

Textures in the gabbros vary from automorphic granular to allotriomorphic. Primary mineralogy comprises clinopyroxene and plagioclase (Plate 2.1). Olivine and orthopyroxene become important constituents in mafic members of the sequence.

The petrography and mineral chemistry of selected samples

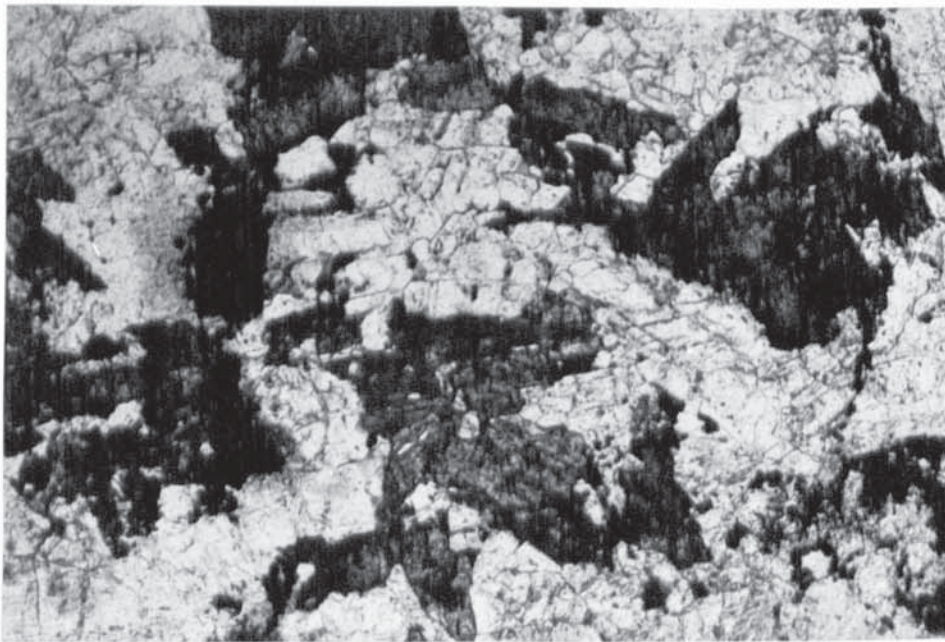


PLATE 2.1. Fresh to slightly uralitised hypidiomorphic clinopyroxene and fresh allotriomorphic plagioclase in gabbro. Parallel polars, X25

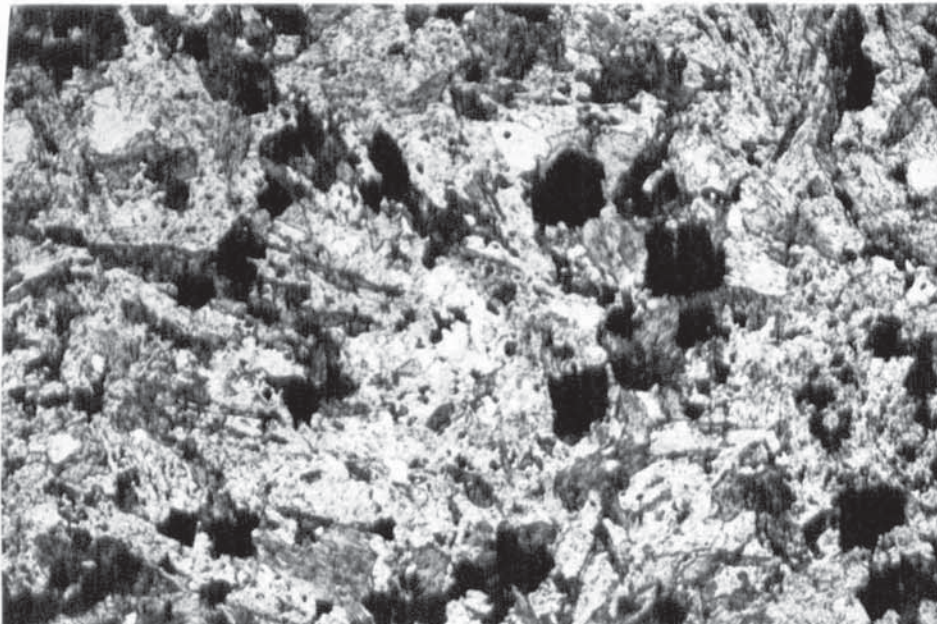


PLATE 2.2. Pervasively altered diabase dyke. Clinopyroxene converted to actinolite and chlorite, plagioclase albitised. Euhedral, slightly corroded pyrite in matrix. Parallel polars, X25.

from the gabbros is summarised in Table 2.1. Compositional variations are observed in all phases. Orthopyroxene shows strong iron enrichment, reaching Fs34 and therefore entering the field of inverted pigeonites. Clinopyroxene shows similar iron enrichment, reaching Fs22 and plagioclase varies from An91 to An55. Complicated crystallisation history is also suggested by the presence of plagioclase poikilitically enclosed in olivine and followed by simultaneous crystallisation of plagioclase and clinopyroxene. Such features are consistent with repeated injections of unfractionated magma and mixing with more fractionated melt.

2.2.2. The Sheeted Complex.

Hydrothermal metamorphism has affected this formation resulting in many cases to the destruction of primary mineralogy. Relict igneous phases are, however, commonly preserved and so are original textures in many cases. The latter are typically diabasic (Plate 2.2) but vary from microcrystalline to holocrystalline microporphyritic.

Assemblages from the Sheeted Complex are summarised in Table 2.2. Clinopyroxene and plagioclase are the commonest phenocryst and groundmass assemblages, but plagioclase is most commonly confined to the groundmass. The presence of primary quartz may be discerned in some instances.

The composition of clinopyroxenes shows strong variation from primitive (Ca40Mg52Fe8) to evolved (Ca37Mg39Fe24), corresponding to a change in Mg/Mg+Fe ratio from 0.87 to 0.62.

TABLE 2.1. Petrography and mineral chemistry of selected gabbroic rocks.

Rock type	:	Massive coarse melanocratic gabbro (TR6-1).
Texture	:	Hypidiomorphic granular.
Mineralogy	:	Euhedral cumulus plagioclase, early euhedral orthopyroxene, anhedral intercumulus clinopyroxene.
Mineral chemistry	:	Orthopyroxene: $\text{Ca}_4\text{Mg}_{73}\text{Fe}_{23}$ to $\text{Ca}_4\text{Mg}_{62}\text{Fe}_{34}$. Clinopyroxene: $\text{Ca}_4\text{Mg}_{45}\text{Fe}_{13}$ to $\text{Ca}_4\text{Mg}_{40}\text{Fe}_{14}$. Plagioclase : $\text{An}_{91}\text{Ab}_9$ to $\text{An}_{88}\text{Ab}_{12}$.
Rock type	:	High level gabbro (TR5-3).
Texture	:	Equigranular allotriomorphic.
Mineralogy	:	Subhedral clinopyroxene, abundant, fresh anhedral plagioclase.
Mineral chemistry	:	Orthopyroxene : $\text{Ca}_5\text{Mg}_{74}\text{Fe}_{21}$ to $\text{Ca}_4\text{Mg}_{74}\text{Fe}_{22}$. Clinopyroxene: $\text{Ca}_4\text{Mg}_{46}\text{Fe}_{11}$ to $\text{Ca}_4\text{Mg}_{46}\text{Fe}_{10}$. Plagioclase : $\text{An}_{91}\text{Ab}_9$.
Rock type	:	Coarse melanocratic gabbro (TR4-11)
Texture:	:	Automorphic granular
Mineralogy	:	Early clinopyroxene, followed by strongly zoned plagioclase.
Mineral chemistry	:	Clinopyroxene: $\text{Ca}_4\text{Mg}_{39}\text{Fe}_{17}$ to $\text{Ca}_4\text{Mg}_{34}\text{Fe}_{21}$. Plagioclase : $\text{An}_{88}\text{Ab}_{12}$ to $\text{An}_{71}\text{Ab}_{29}$.

TABLE 2.2. Petrography and mineral chemistry
of selected samples from the Sheeted Complex.

Rock type :	Diabase dyke (TR7-11)
Texture :	Diabasic to sparsely microporphyritic.
Mineralogy :	Rare plagioclase and pyroxene microphenocrysts in a matrix of plagioclase and pyroxene.
Alteration:	Pyroxene microphenocrysts converted partly to actinolite, groundmass clinopyroxene thoroughly. Plagioclase thoroughly albitised. Association of chlorite and smectite in alteration products.
Mineral chemistry :	Clinopyroxene: $\text{Ca}_{40}\text{Mg}_{52}\text{Fe}_8$ to $\text{Ca}_{44}\text{Mg}_{49}\text{Fe}_7$.
Rock type:	Diabase dyke (TR9-4).
Texture:	Holocrystalline microporphyritic.
Mineralogy :	Rare pyroxene and plagioclase microphenocrysts. Groundmass of plagioclase and clinopyroxene.
Alteration :	Pyroxene completely fresh, plagioclase thoroughly albitised. Alteration products comprise calcite, chlorite and quartz.
Mineral chemistry :	Pyroxene microphenocrysts: $\text{Ca}_{42}\text{Mg}_{48}\text{Fe}_{10}$ to $\text{Ca}_{31}\text{Mg}_{50}\text{Fe}_{19}$. Groundmass clinopyroxene : $\text{Ca}_{44}\text{Mg}_{45}\text{Fe}_{11}$.
Rock type :	Medium grained diabase dyke (TR9-16).
Texture:	Holocrystalline diabasic.
Mineralogy :	Pyroxene in microphenocrysts, groundmass plagioclase poikilitically encloses pyroxene.
Alteration :	Plagioclase completely albitised, pyroxene completely fresh. Chlorite- smectite association in groundmass.
Mineral chemistry :	Clinopyroxene microphenocrysts: $\text{Ca}_{44}\text{Mg}_{47}\text{Fe}_9$ to $\text{Ca}_{37}\text{Mg}_{49}\text{Fe}_{14}$.

The modifications on mineralogy as a result of the hydrothermal metamorphism will be described in chapter 3.

2.2.3. The Lower Pillow Lavas.

Textures of these lavas show considerable variability as a result of their extrusive nature. They range from intersertal in the marginal parts of flows, through hyalopilitic, to holocrystalline hypidiomorphic in central parts of dykes. The lavas are commonly strongly vesicular.

The petrographic features of selected samples are described in Table 2.3. Prevailing mineral assemblages comprise clinopyroxene and plagioclase (Plate 2.3). Quartz is present in significant amounts in the evolved members. Plagioclase may be in some cases the only microphenocryst phase present (Plate 2.4).

The composition of clinopyroxenes spans a considerable range ($\text{Ca}_{42}\text{Mg}_{49}\text{Fe}_9$ to $\text{Ca}_{39}\text{Mg}_{41}\text{Fe}_{20}$, with a corresponding change in Mg/Mg+Fe ratio from 0.84 to 0.67. Compositions of co-existing plagioclases vary from An₇₈ to An₅₂.

2.2.4. The EMS lavas.

The presence of very primitive lavas within the Lower Pillow Lavas was suggested from petrographic examination of samples from Evloimeni, in the Limni mining district and Mavri Sykia, in the Kalavassos mining district (chapter 5). These lavas stratigraphically underlie the limburgites (basal member of the Upper Pillow Lavas) and exhibit alteration assemblages characteristic of the Lower Pillow Lavas. As a result, however, of

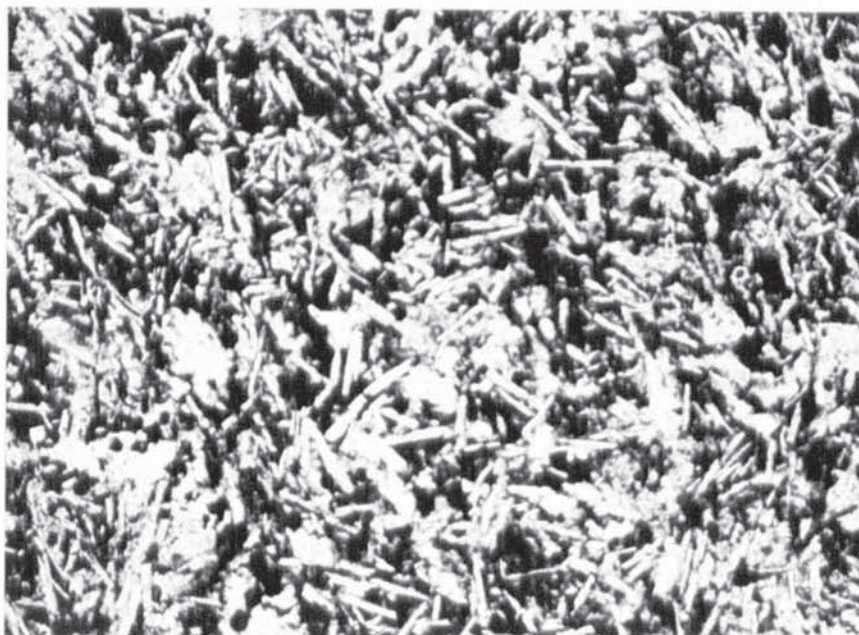


PLATE 2.3. Lower Pillow Lava. Fresh clinopyroxene and plagioclase in slightly altered glass.

Crossed polars, X25.

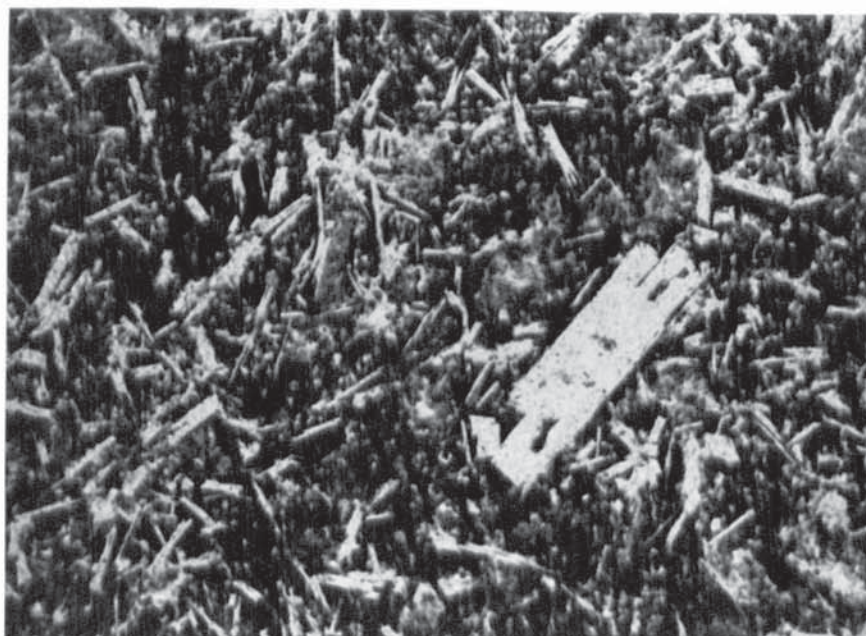


PLATE 2.4. Plagioclase microphenocryst in intersertal to trachytic groundmass comprising skeletal plagioclase and partly altered glass. Clinopyroxene is completely absent.

Crossed polars, X25.

TABLE 2.3. Petrography and mineral chemistry
of selected samples from the Lower Pillow Lavas.

Rock type :	Central parts of non-pillowed flow (TR1-2).
Texture :	Microcrystalline microporphyritic.
Mineralogy :	Pyroxene and plagioclase in interstitial glass. Small pyroxenes poikilitically enclosed in plagioclase.
Mineral chemistry:	Clinopyroxene microphenocrysts: $\text{Ca}_{42}\text{Mg}_{49}\text{Fe}_9$ to $\text{Ca}_{33}\text{Mg}_{54}\text{Fe}_{13}$. Plagioclase: $\text{An}_{76}\text{Ab}_{24}$ to $\text{An}_{79}\text{Ab}_{21}$.
Rock type :	Celadonite-stained dyke (TR1-3).
Texture :	Hyalopilitic.
Mineralogy :	Fresh plagioclase, fresh sub-ophitic clinopyroxene, in slightly altered glass.
Mineral chemistry :	Clinopyroxene: $\text{Ca}_{39}\text{Mg}_{46}\text{Fe}_{15}$ to $\text{Ca}_{41}\text{Mg}_{43}\text{Fe}_{16}$. Plagioclase : $\text{An}_{71}\text{Ab}_{29}$ to $\text{An}_{52}\text{Ab}_{48}$.
Rock type :	Columnar flow (TR1-4).
Texture :	Andesitic to hyalopilitic.
Mineralogy :	Abundant plagioclase, clinopyroxene and glass. Plagioclase fresh, zoned, andesine to labradorite. Sub-ophitic relationship of plagioclase and clinopyroxene.
Mineral chemistry :	Clinopyroxene $\text{Ca}_{42}\text{Mg}_{43}\text{Fe}_{15}$.

their primitive petrography and chemistry, they are described as a separate member. In abbreviation of 'Evloimeni' and 'Mavri Sykia' they will, heretofore, be referred to as the EMS lavas.

The groundmass of the EMS lavas is microcrystalline and the texture microporphyritic. Phenocryst assemblages comprise orthopyroxene, in the examined situations being replaced by zeolites, and clinopyroxene. The groundmass is characterised by abundant clinopyroxene and rarer plagioclase (Plate 2.5). The mineral chemistry of these lavas was not examined.

2.2.5. The Upper Pillow Lavas.

The main petrographic features of the various members of the Upper Pillow Lavas are described in Table 2.4. Study of their mineral chemistry was confined to the examination by electron microprobe of chrome spinels and associated clinopyroxenes from one olivine-phyric pillow collected from the region of Limni mine.

Sample LI-18R is characterised by porphyritic texture (Plate 2.6), with first generation euhedral olivine, altered to hematite and calcite. Second generation clinopyroxene is present in abundance and the groundmass, fine grained, is characterised by clinopyroxene and plagioclase microlites in altered smectitised glass.

Clinopyroxene microphenocrysts shows very high Mg/Mg+Fe ratios (maximum 0.89) and average composition is $\text{Ca}_{38}\text{Mg}_{53}\text{Fe}_9$ with greatest variation shown by calcium (34-42). Chemical analyses of clinopyroxenes and co-existing chrome spinels are shown in Table 2.5.

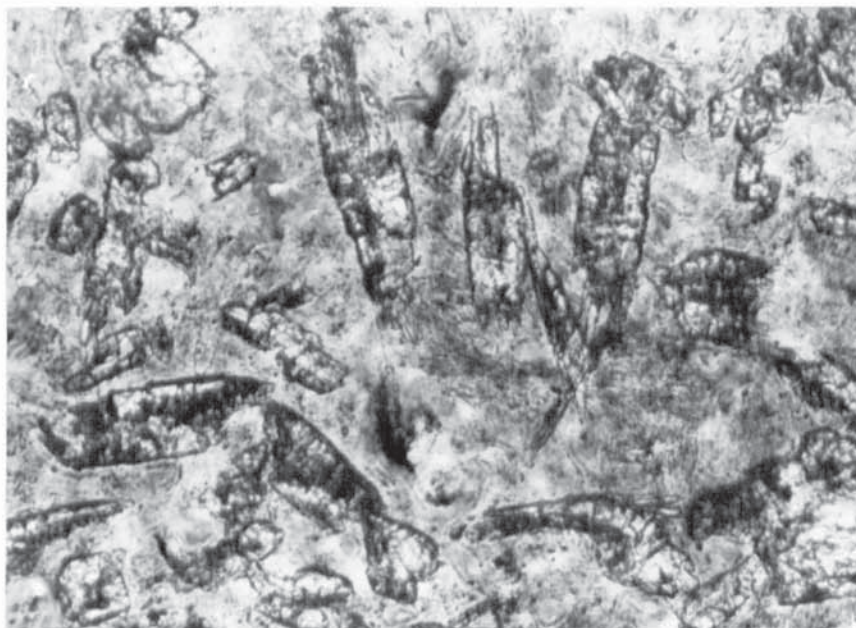


PLATE 2.5. Groundmass of EMS lava. Finely crystalline clinopyroxene embedded in altered glass.
Parallel polars, X100

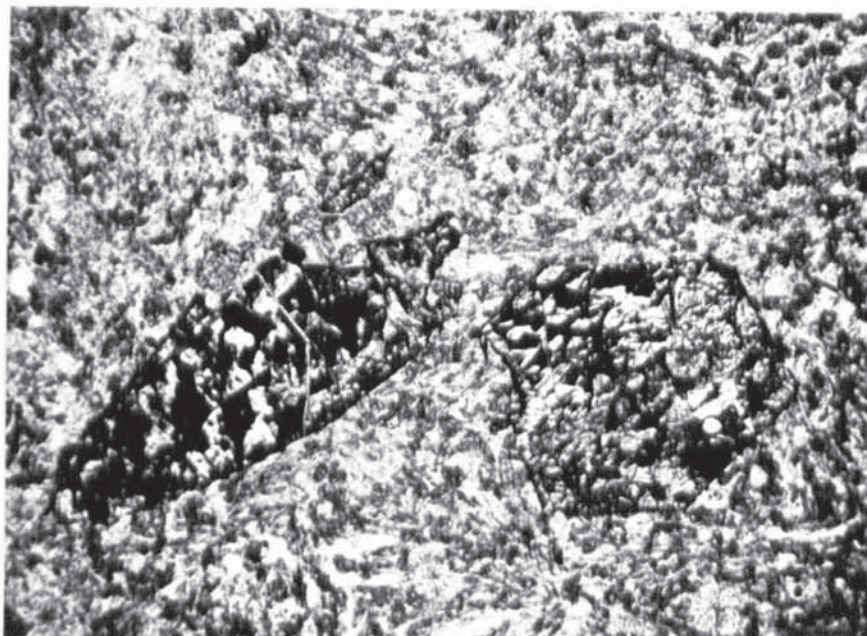


PLATE 2.6. Olivine basalt. Large euhedral olivines, altered to hematite and calcite, in a fine groundmass of clinopyroxene micro-lites in altered glass.
Parallel polars, X25.

TABLE 2.4. The main petrographic features of representative samples of Upper Pillow Lavas.

Rock type	:	Limburgite pillow margin (PA-11R).
Texture	:	Intersertal to sparsely microporphyritic.
Mineralogy	:	Fresh euhedral olivine microphenocrysts, clinopyroxene microlites, quenched, densely packed in matrix of very slightly devitrified glass. Plagioclase absent.
Rock type	:	Olivine basalt, pillow margin (LI-18R).
Texture	:	Microporphyritic to vitrophyric.
Mineralogy	:	Large, first generation olivines, replaced by hematite and calcite, smaller, similarly altered olivines. Third generation clinopyroxenes, completely fresh, in a fine matrix of incipiently devitrified glass and plagioclase microlites.
Rock type	:	Picrite basalt flow (KA-6e).
Texture	:	Hypidiomorphic granular.
Mineralogy	:	Euhedral to partly igneous-corroded olivine, extensively altered to serpentine and magnetite. Anhedral clinopyroxene, fresh, infills interstices between olivine crystals. Minute chromite euhedra enclosed in olivine or its alteration products. Groundmass altered to complex mixture of clay minerals.

Spinel from the olivine basalt sample, plotted on the Cr/Cr+Al, Mg/Mg+Fe diagram (Fig. 2.1), are chemically identical to those from the plutonic complex. It is inferred that limited fractionation in spinel composition has occurred since the melts were separated from their source. The chemistry of these spinels differs greatly from spinels of MORB and shows similarities to spinels from marginal basin environments (Cameron et al., 1980).

2.2.6. Overall variations in pyroxene chemistry.

The compositional variations of clinopyroxenes from the various members of the ophiolite are summarised in fig. 2.2. A similar trend towards iron enrichment is evident in all members and a superimposed trend from more calcic to less calcic assemblages is apparent from the gabbros to the extrusive members.

The compositions of clinopyroxene microphenocrysts from the intrusive-extrusive section of the ophiolite are plotted on the Ca:Mg:Fe diagram (fig. 2.3). These compositions are considerably evolved relative to pyroxenes of MORB and follow a trend of parallel to the Skaergaard augites. They strongly contrast the trend of pyroxenes of abyssal tholeiites, which generally vary from salites to augites, and show similarities to pyroxenes from the Shikoku basin (Dick et al., 1977) but appear more fractionated than pyroxenes from the latter lavas.

2.2.7. The clinopyroxene discriminant diagrams.

Kushiro (1960) and Le Bas (1962) concluded that the composition of clinopyroxenes varies as a function of the

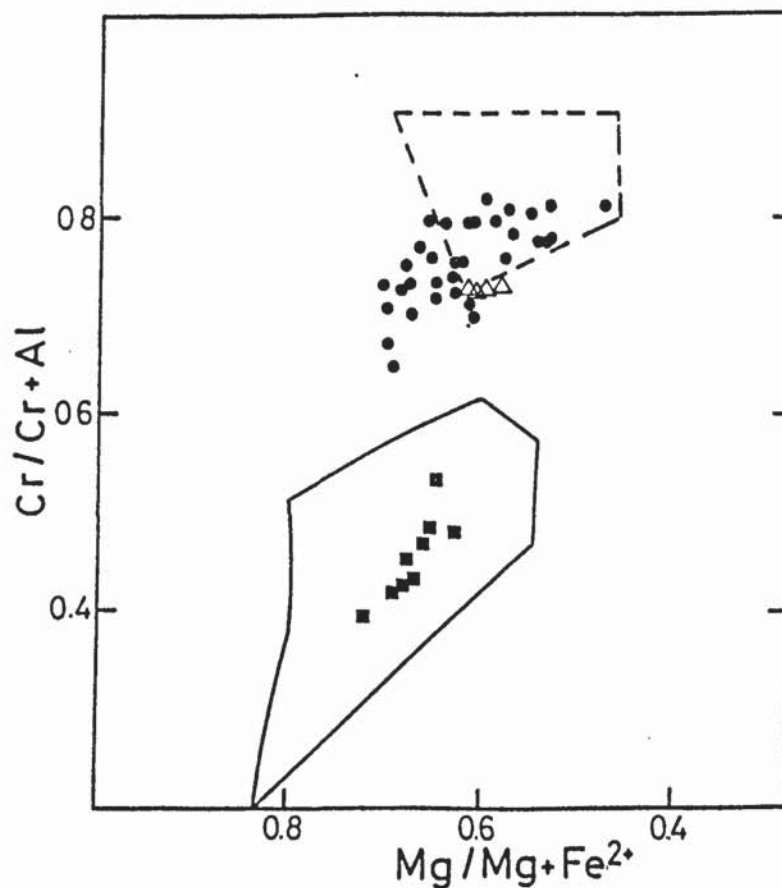


FIG. 3.1. Plot of chrome spinels from olivine basalt sample LI-18R on the $\text{Cr}/\text{Cr}+\text{Al}$, $\text{Mg}/\text{Mg}+\text{Fe}$ face of the spinel prism.

Open triangles: Spinel from LI-18R.

Filled circles: Spinel from the Troodos chromite deposits (After Michaelides, 1982).

Filled squares: Spinel from the W. Philippine basin, hole 447A (After Matthey et al., 1980).

The fields of spinels from the Mid-Atlantic ridge (solid outline) and from the Western Pacific and Cape Vogel (dashed outline) are from Cameron et al., 1980.

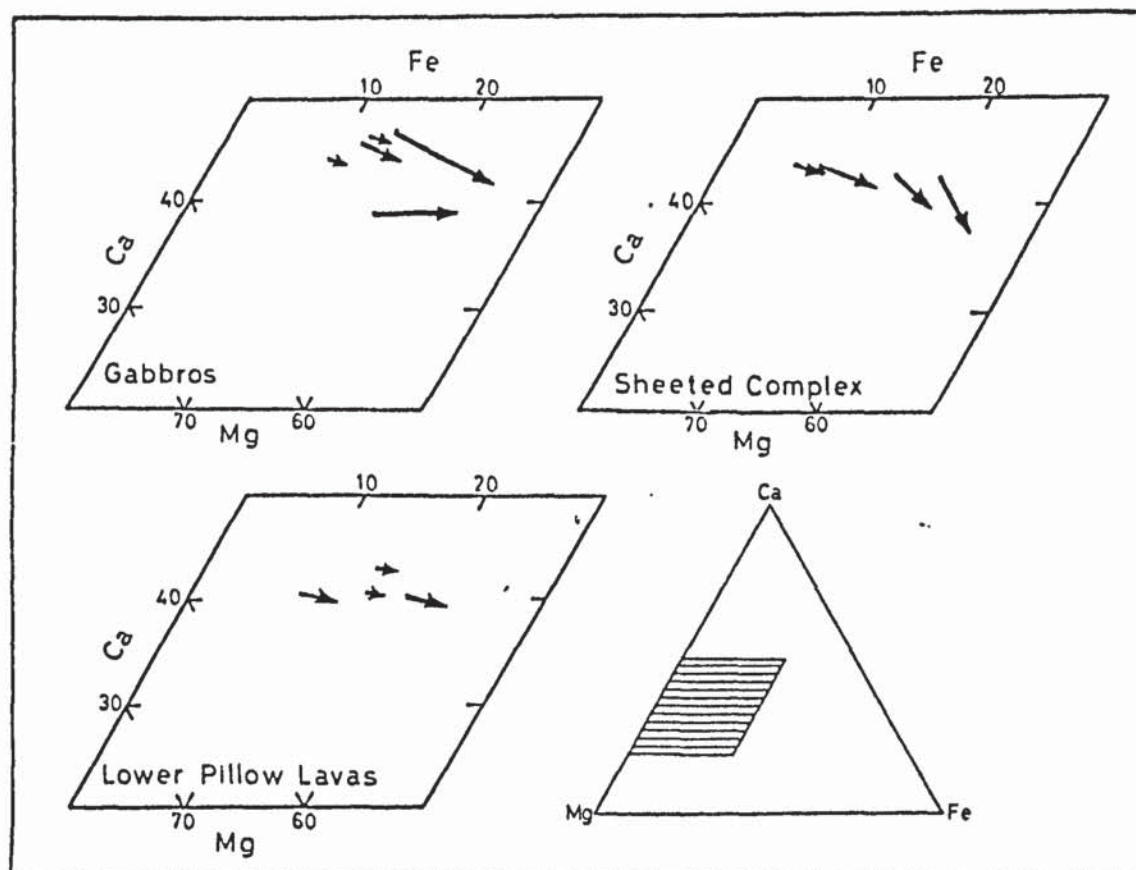


Fig. 2.2. Overall compositional variations in clinopyroxenes from the various members of the Troodos ophiolite.

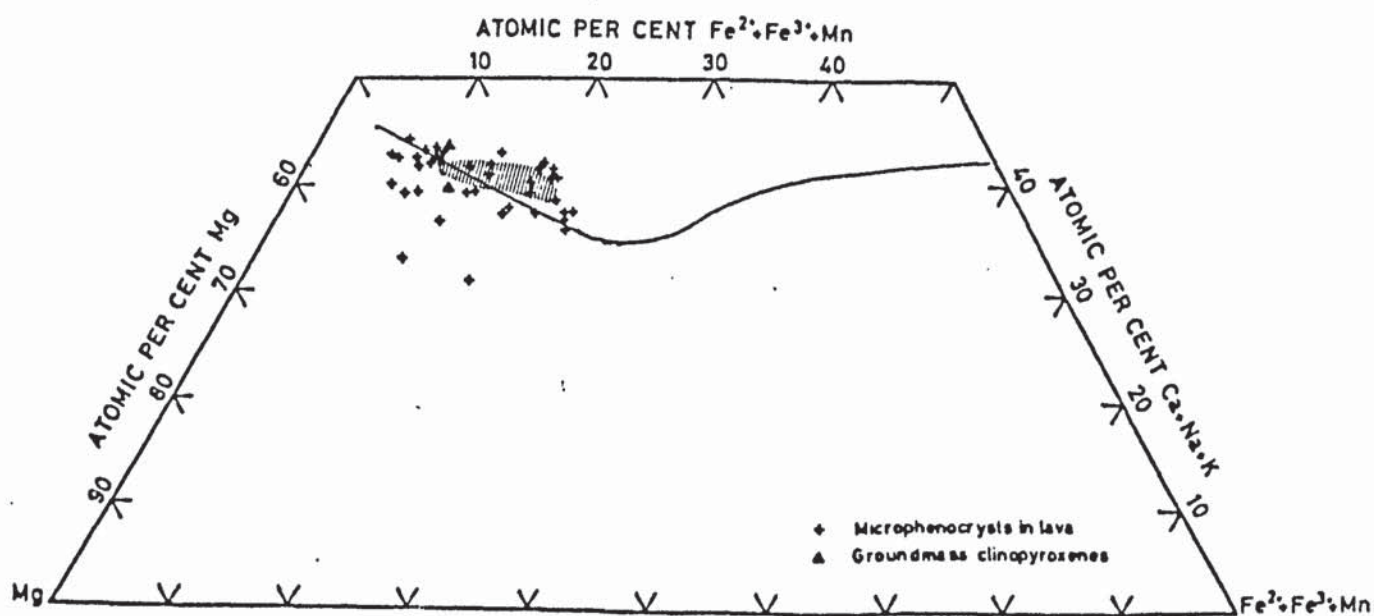


Fig. 2.3. Compositional variations of clinopyroxene microphenocrysts and from the igneous groundmass. The augite-ferroaugite trend of iron enrichment is superimposed for reference (From Brown, 1967). Shaded field represents clinopyroxenes from the Shikoku basin (after Dick et al., 1979).

alkalinity of the parental magma. Discriminant diagrams based on pyroxene compositions from diverse terrains were derived and these were used in the identification of the various magma types. Such diagrams were primarily based on the antipathetic relationship which exists between silica and alumina resulting to higher aluminium entering the pyroxene structure in silica-deficient magmas. The factor Alz ($Alz = Al^{iv} \times 100 : z$ where z is taken as 2) is used as a measure of the silica deficiency in the magma from which the pyroxenes crystallised (Kushiro, 1960).

Utilisation of clinopyroxene composition as an indicator of magmatic parentage is particularly useful in terrains where the major element geochemistry is modified by secondary processes (see e.g. Hynes, 1976).

Based on the principles outlined above all the analysed pyroxenes from Troodos were plotted on the discriminant diagrams of Le Bas (1962) (Figs 2.4- 2.6). All analysed clinopyroxenes plot in the nonalkaline fields of the discriminant diagrams, suggestive of silica-oversaturated nature of the Troodos parental magma.

2.3. Geochemistry.

2.3.1. Introduction.

In the characterisation of the tectonic environment of formation of ophiolites, particular attention should be directed to the effects of alteration and metamorphism which would modify initial elemental abundances. At the Mid-Atlantic Ridge, e.g., extensive migration of CaO and SiO_2 accompanies metamorphism to

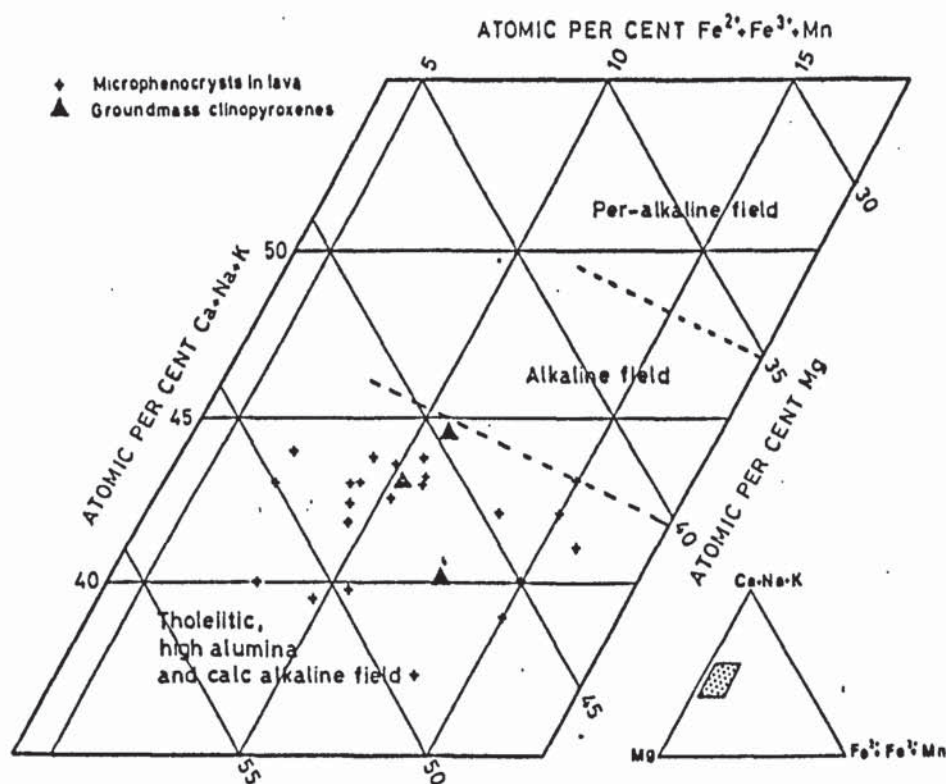


Fig. 2.4. Plot of compositions of clinopyroxene microphenocrysts and clinopyroxenes from the igneous groundmass on the Ca*-Mg-Fe* discriminant diagram of Le Bas (1962).

Ca* = Ca+Na+K. Fe* = Fe²⁺+Fe³⁺+Mn.

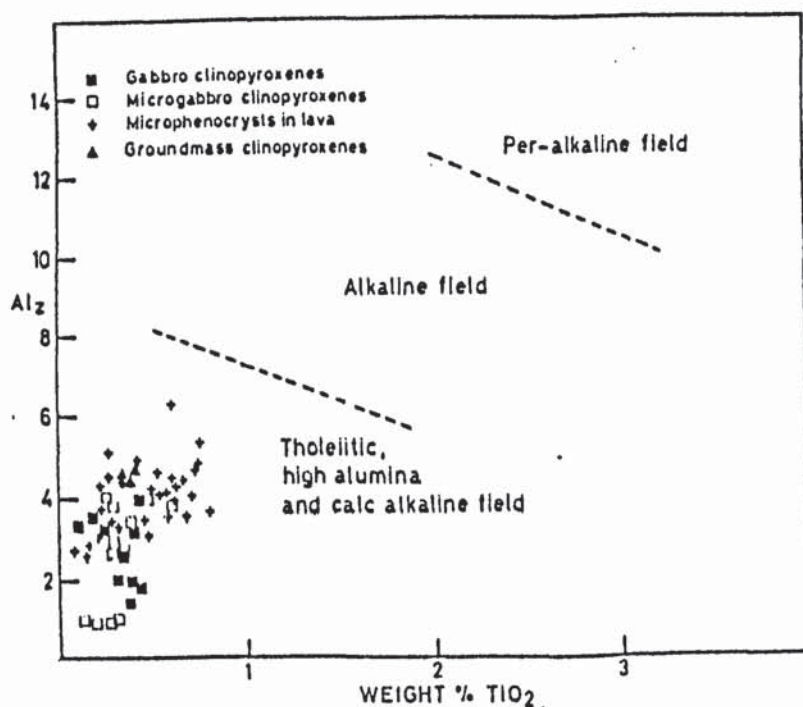


Fig. 2.5. Plot of clinopyroxenes from various members of the ophiolite on the Al₂ vs TiO₂ discriminant diagram of Le Bas (1962).

Clinopyroxenes from Gabbros and microgabbros also plot in the nonalkaline field, although the diagram is only used as discriminant for groundmass clinopyroxenes in lavas.

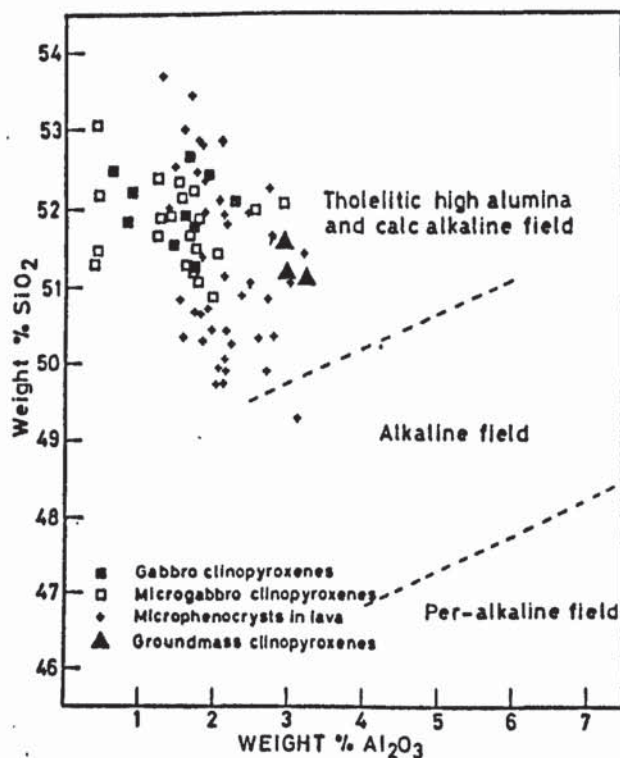


FIG. 2.6. Clinopyroxenes from various members of the ophiolite plotted on the Al_2O_3 - SiO_2 discriminant diagram of Le Bas (1962).

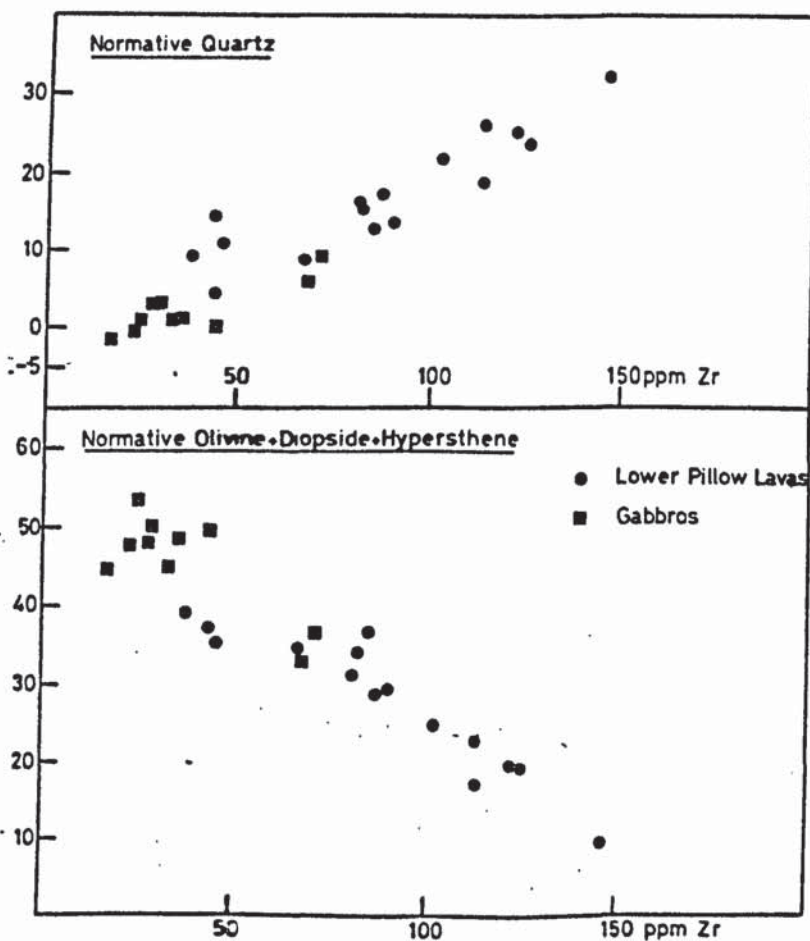


FIG. 2.7. Variation of normative mineralogy against zirconium as differentiation index for selected samples of gabbros and Lower Pillow Lavas.

greenschist facies (Miyashiro, 1971) and results in the extreme situation to the formation of pure chlorite rocks. Mobility of major and trace elements under zeolite facies conditions has been also inferred (Wood et al., 1976).

The petrographic characteristics of the Sheeted Complex suggest that major chemical modifications have taken place. On the other hand, the preservation of original mineralogy in the Lower Pillow Lavas and gabbros may be taken as evidence of similar preservation of initial elemental abundances. These conclusions will be further elaborated and chemical changes quantitatively assessed in chapter 3.

It has been shown by the work of Cann (1970) that some elements (Ti, Zr, Y, Nb) are relatively immobile under conditions of severe alteration and metamorphism. These are also incompatible, being enriched in residual liquids and provide evidence on the extent of igneous differentiation. Much of the work described in later paragraphs will make ample use of these facts.

2.3.2. Normative calculations.

Selected chemical analyses and CIPW norms for some samples from the Lower Pillow Lavas and gabbros are shown in Tables 2.6 and 2.7. The samples were chosen so as to provide a complete range of compositions. Means and standard deviations are also shown on the tables.

All the rocks are characterised by normative quartz and hypersthene with complete absence of both olivine and nepheline.

MORB-type basalts are characterised by silica contents in

TABLE 2.6. Chemical analyses and CIPW norms of selected gabbroic rocks.*

Ox. %	1	2	3	4	5	6
SiO ₂	48.40	49.20	50.70	51.70	53.55	55.10
TiO ₂	0.12	0.13	0.32	0.45	0.48	1.33
Al ₂ O ₃	22.20	19.30	13.80	15.40	14.30	15.53
FeO	4.47	4.43	7.08	8.02	7.83	8.51
Fe ₂ O ₃	0.67	0.66	1.06	1.20	1.17	1.27
MnO	0.11	0.11	0.15	0.16	0.16	0.18
MgO	8.00	8.90	9.95	8.50	10.90	7.20
CaO	15.80	18.40	11.91	10.95	9.38	6.59
Na ₂ O	0.96	0.70	1.39	2.26	2.18	3.19
K ₂ O	0.02	0.00	0.08	0.21	0.53	0.52
P ₂ O ₅	0.02	0.02	0.04	0.04	0.04	0.19
Total	100.77	101.85	96.48	98.89	100.52	99.61
CIPW NORMS						
Q	----	---	2.67	0.60	0.74	5.50
Or	0.11	---	0.45	1.22	3.12	3.06
Ab	8.13	5.93	11.75	19.14	18.46	27.01
An	56.20	49.52	31.19	31.24	27.68	26.57
Ne	-----	-----	-----	-----	-----	-----
Di	17.76	33.42	22.34	18.59	15.03	4.03
Hy	12.90	6.68	25.84	25.40	32.80	28.67
Ol	4.43	5.07	-----	-----	-----	-----
Mt	0.97	0.95	1.53	1.74	1.69	1.85
Ilm	0.23	0.24	0.61	0.85	0.91	2.43
Ap	0.03	0.03	0.10	0.10	0.10	0.44
1= TR5-3, 2= TR5-1, 3= TR1-17, 4= TR5-5, 5= TR3-10, 6= TR4-11.						

* Refer to appendix 1 (pages 325-355) for description of samples.

the range 48-51% SiO_2 and predominantly normative olivine (Tarney et al., 1978). Compared to MORB, the Troodos Lower Pillow Lavas are enriched in silica and resemble island arc tholeiites, as e.g. those of the Palau Kyushu ridge (Mattey et al., 1980).

The crucial question arises whether the high silica of the Troodos lavas is inherent in the rocks or a result of secondary introduction as previously suggested (Smewing, 1975). This is resolved by plotting normative mineralogy against a known immobile and incompatible element, such as Zr. This is shown in fig. 2.7, and suggests that the Troodos Lower Pillow Lavas and gabbros have crystallised from magma which was enriched in silica relative to MORB magma.

2.3.3. Discriminant diagrams.

The TiO_2 vs Zr discriminant diagram.

Miyashiro and Shido (1975) postulated that the variations of some elements, in particular FeO^* (Total iron expressed as FeO), TiO_2 and V provides clues in the distinction between the tholeiitic and calc-alkaline series. In the typical tholeiitic series these parameters first increase during the differentiation of the magma and, after reaching a maximum, decrease in the later fractionation products as a result of the control imposed by crystallisation of magnetite. In the calc-alkaline series all three decrease monotonically and rapidly with advancing fractionation.

The variation of TiO_2 with Zr as fractionation index is

shown in fig. 2.8. TiO_2 was chosen in view of its immobile nature (Cann, 1970) permitting the inclusion in the diagram of the rocks of the Sheeted Complex, and its strong partitioning in magnetite (Pearce and Norry, 1979), in contrast to FeO which may be modified by variable abundance of mafic silicates. The diagram shows a steady increase in TiO_2 with increasing Zr up to a Zr content of approximately 100 ppm, followed by a steady decrease in later differentiates. Spurious results in the Sheeted Complex may be correlated with the complete breakdown of the pyroxene to actinolite and chlorite, resulting to some release of the titanium, probably accompanied by breakdown of magnetite.

A significant feature of the TiO_2 -Zr diagram, apart from defining a tholeiitic trend, is the strong coherence of the pattern shown for all samples from the gabbros to the intrusive-extrusive members. This suggests that all members are related by a process of fractional crystallisation of magma which, at least as far as these elements are concerned, did not vary.

FeO' vs FeO:MgO variations.

It has been suggested by Miyashiro (1973) that the variation of FeO' (total iron expressed as FeO) and SiO_2 using the ratio FeO:MgO as fractionation index, may effectively distinguish between tholeiitic and calc-alkalic parentage for lava suites. The author (Miyashiro, 1973), examined assemblages from the Sheeted Complex and Lower Pillow Lavas and deduced the presence of calc-alkalic rocks at Troodos. The postulation of an environment of formation of the Troodos ophiolite in an island arc

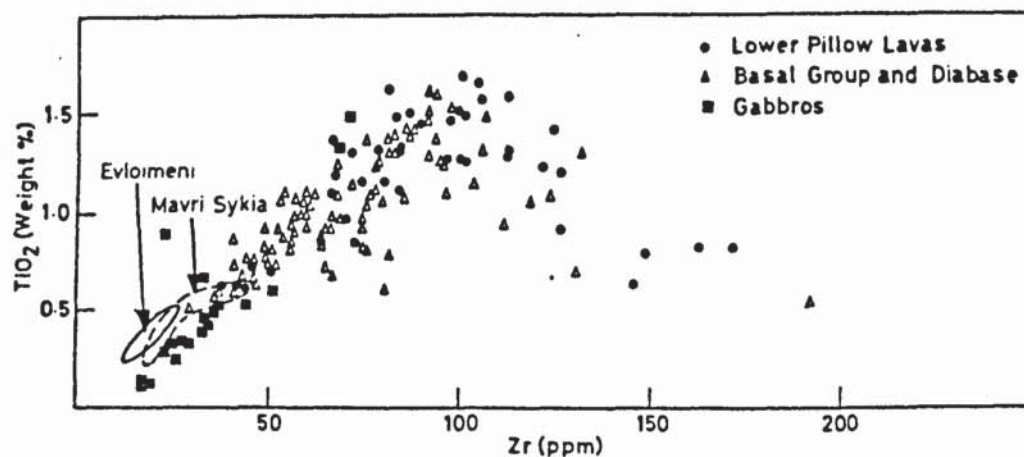


FIG. 2.8. TiO_2 -Zr covariation for various members of the ophiolite. The compositional range of lavas from Evloimeni and Mavri Sykia also outlined.

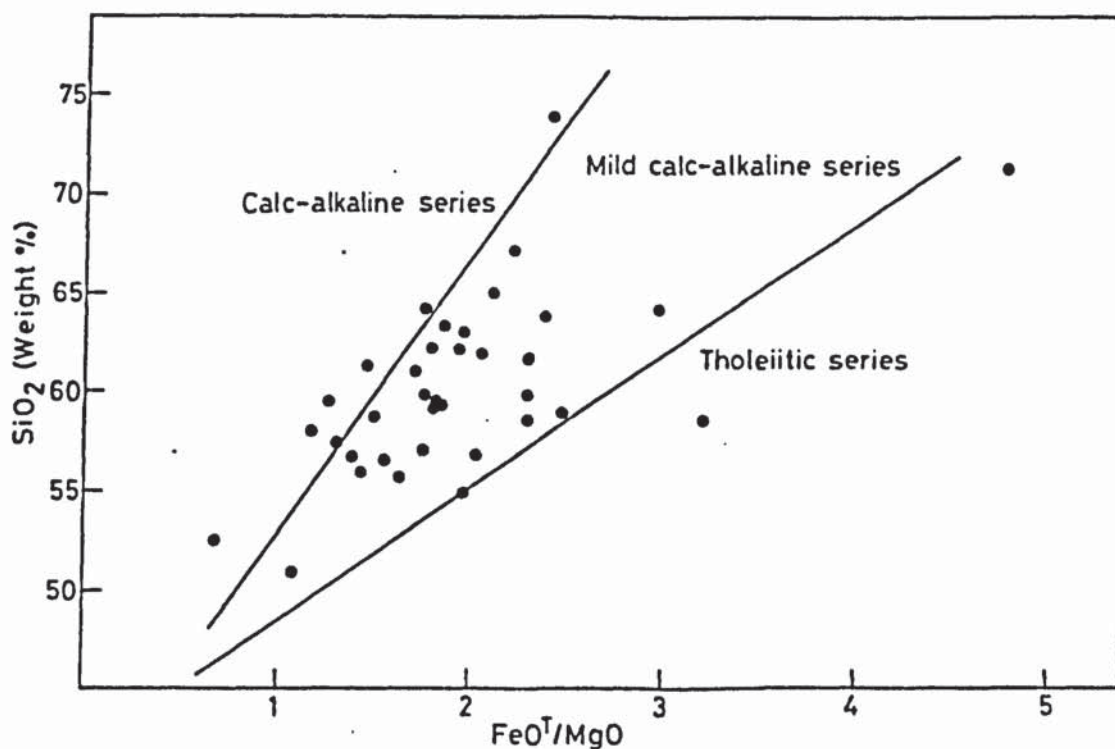


FIG. 2.9. Plot of samples of Lower Pillow Lavas on the SiO_2 vs FeO^t/MgO diagram of Miyashiro (1973). FeO^t : Total iron as FeO .

was debated on the basis of extensive mobility of components used by the metamorphism of the rocks of the Sheeted Complex. In this study use of the discriminant diagrams will be limited to the Lower Pillow Lavas.

The plot of the data from the Lower Pillow Lavas on the discriminant diagrams of Miyashiro (1973) suggest that these lavas show characteristics intermediate between the tholeiitic and calc-alkaline series. The SiO_2 discriminant diagram (Fig. 2.9) indicates mild calc-alkalic affinities for the majority of the samples. The FeO discriminant (Fig. 2.10) suggests a character intermediate between tholeiitic and calc-alkaline.

The SiO_2 vs $\text{Zr}:\text{TiO}_2$ discriminant diagram.

Winchester and Floyd (1976), utilising elements which are mostly unaffected by secondary processes, devised diagrams which may be used in the characterisation of the fractionation trends exhibited by a variety of volcanic suites.

Silica is expected to be relatively stable in the alteration regime of the Lower Pillow Lavas, as suggested by petrography. It is, therefore, used as an index of fractionation in the SiO_2 - $\text{Zr}:\text{TiO}_2$ diagram in preference to other diagrams utilising only trace element ratios.

The Lower Pillow Lavas and the low-Ti lavas of Evloimeni and Mavri Sykia (EMS) as plotted on the SiO_2 - $\text{Zr}:\text{TiO}_2$ discriminant diagram of Winchester and Floyd (1976) are shown in fig. 2.11. A regular trend is suggested from the diagram between the two lava types from the primitive EMS lavas to the fractionated rocks of

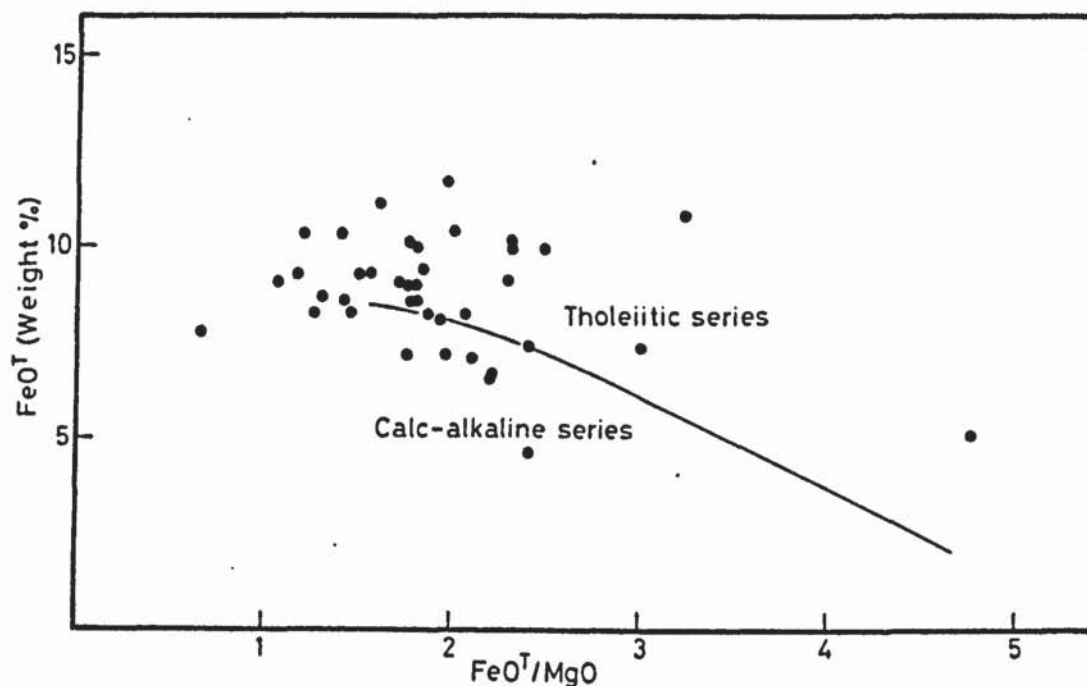


FIG. 2.10. Plot of analyses of Lower Pillow Lavas on the FeO^t vs FeO^t/MgO discriminant diagram of Miyashiro (1973).

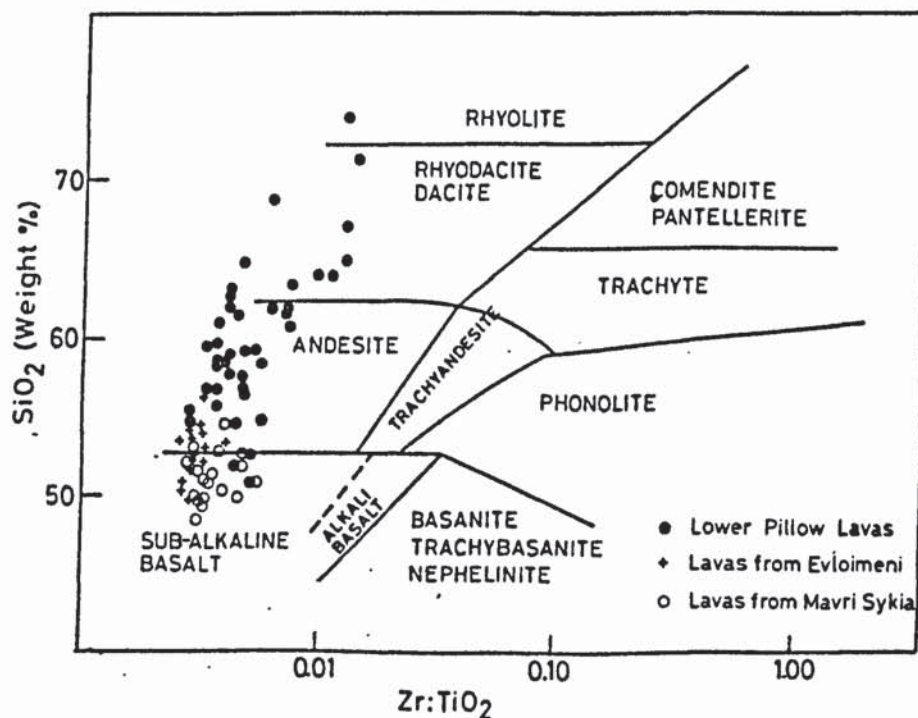


FIG. 2.11. Plot of samples of Lower Pillow Lavas and the EMS lavas on the SiO_2 vs Zr:TiO_2 discriminant of Winchester and Floyd (1976). Note the continuous trend exhibited between the two lava suites.

the Lower Pillow Lavas, probably suggestive of derivation from the same parental magma.

The $\text{Al}_2\text{O}_3 : \text{TiO}_2$ discriminant diagram.

Sun and Nesbitt (1978) postulated that low-Ti basalts are not the products of mid-oceanic ridges but of a spreading centre close to a subduction zone, such as occurs in interarc basins or incipient island arcs. The remelting of a refractory source in such environments is facilitated by introduction of water from subducted oceanic crust. Partial melting of such a depleted source would explain the high $\text{Al}_2\text{O}_3 : \text{TiO}_2$ and $\text{CaO} : \text{TiO}_2$ ratios characteristic of low-Ti lavas.

Fig. 2.12 shows the plot of the samples from the Troodos ophiolite on the discriminant diagram of Sun and Nesbitt (1978). The Lower Pillow Lavas and Sheeted Complex are characterised by low $\text{Al}_2\text{O}_3 : \text{TiO}_2$ ratios and plot in the field of MORB as defined by Sun and Nesbitt (1978). The EMS lavas show much higher ratios and they plot in the field of Upper Pillow Lavas as defined from the data of Smewing (1975).

The continuous field indicated on the diagram between the rocks of the Sheeted Complex and Lower Pillow Lavas and the low-Ti EMS lavas probably implies that all these are genetically related.

2.3.4. Trace element geochemistry.

The use of particular trace elements in the identification of tectonic environments mainly rests on their

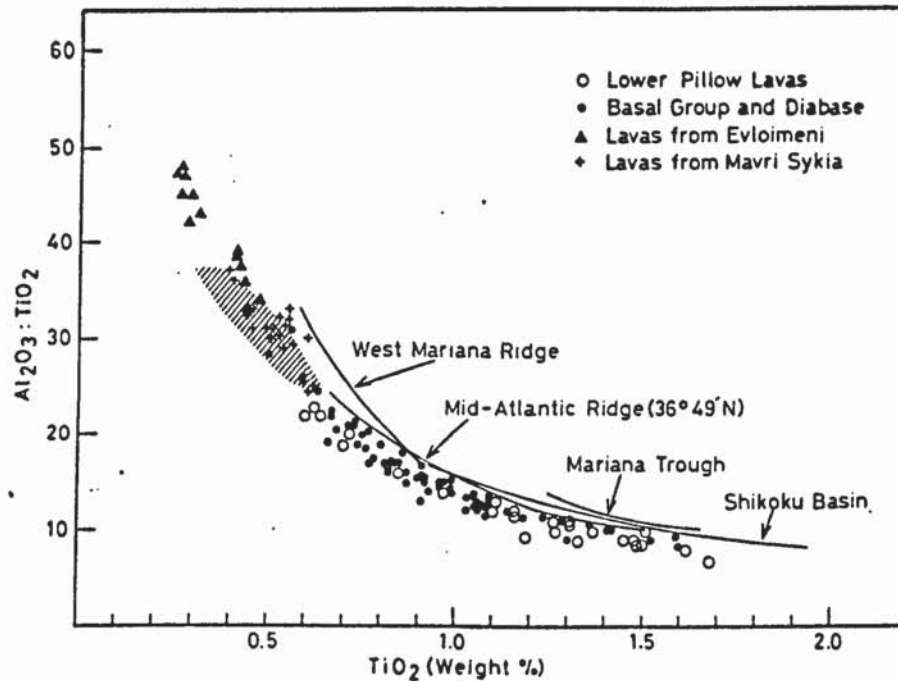


FIG. 2.12. Plot of assemblages from the Troodos ophiolite on the Al_2O_3 - TiO_2 discriminant diagram (Sun and Nesbitt, 1978).

Data for the West Mariana Ridge after Matthey et al. (1980); for the Shikoku Basin, after Wood et al., (1980) and Marsh et al. (1980); for the Mariana Trough after Hart et al. (1972) and for the Mid-Atlantic Ridge after Bryan and Moore (1977). Shaded field encloses compositions of Upper Pillow Lavas after Smewing (1975).

incompatibility, resulting to strong enrichment in later differentiates, and their lack of mobility in the regime of moderate alteration processes. Few elements fulfil these requirements, the most important being Ti, P, Zr, Nb, Y and the REE (Cann, 1970; Saunders et al., 1980).

The strongly coherent behaviour of such elements whose absolute abundance is dependent on mantle processes (O' Hara, 1977) and variation in that abundance provided by fractional crystallisation, provides a powerful tool in the characterisation of the combination of factors influencing the final product as expressed in the lavas in ophiolite terrains.

In the following paragraphs the evidence provided by the distribution of such elements in the Troodos ophiolite will be presented and compared with similar evidence from known settings.

Titanium and Ti:Zr ratios.

Titanium behaves as an incompatible element, being enriched in residual liquids, until magnetite becomes a liquidus phase. Thereafter it decreases in acidic melts due to magnetite precipitation. As a consequence, the Ti:Zr ratio is relatively uniform in primitive melts but decreases sharply in evolved acid compositions. The abrupt drop in Ti:Zr ratio is often used for the separation of primitive and evolved members in volcanic suites (Pearce, 1980).

Primitive members of the Lower Pillow Lavas and samples of the low- Ti EMS lavas are plotted on fig. 2.13. The field of Upper Pillow Lavas, as outlined from the data of Smewing (1975) is

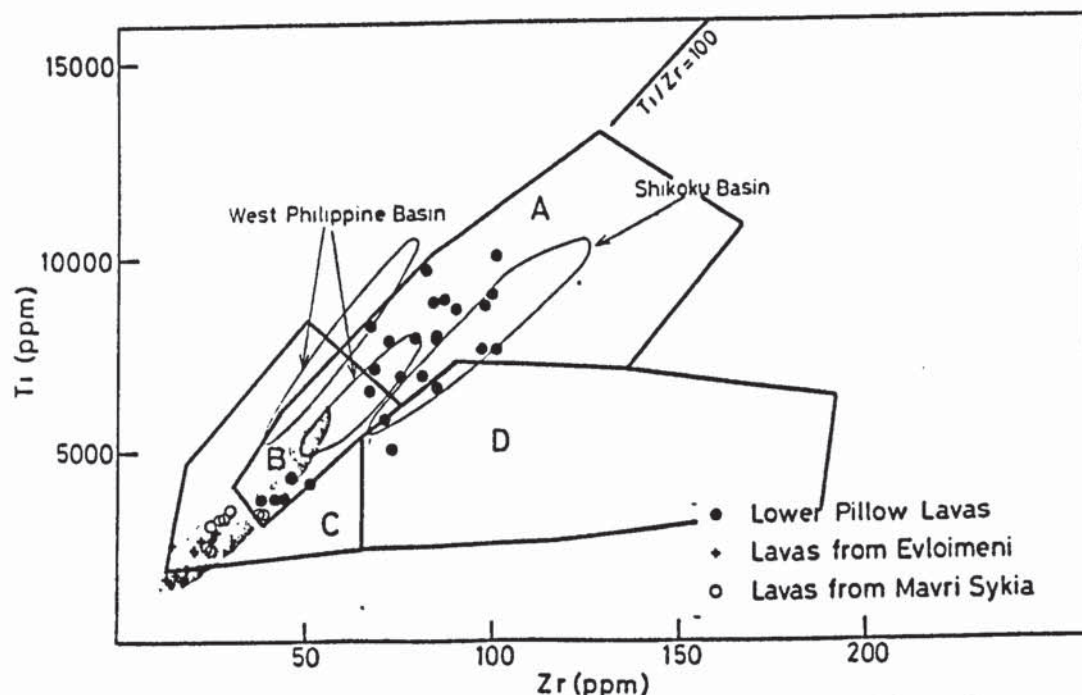


FIG. 2.13. Primitive members of the Lower Pillow Lavas ($Zr < 100$ ppm) and samples of EMS lavas plotted on the Ti-Zr discriminant diagram of Pearce and Cann (1973).

Fields B and D, ocean ridge basalts; A and B, island arc tholeiites; B and C, calc alkaline basalts.

Assemblages from the West Philippine Basin after Matthey et al. (1980); from the Shikoku Basin after Marsh et al. (1980).

Shaded field encloses compositions of Upper Pillow Lavas (Smewing, 1975).

coincident with the field of the EMS lavas. A continuous trend is implied from the diagram from the EMS lavas to the Lower Pillow Lavas, with average Ti:Zr ratio of 100. Diversions from this ratio in the EMS lavas are interpreted as the result of pyroxene cumulation. The presence of pyroxene microphenocrysts, suggested from petrography, would lead to increase in the ratio due to the larger distribution coefficient for Ti relative to Zr (Pearce and Norry, 1979).

Ti:Zr ratios of 100 are typical of ocean floor tholeiites but the average Ti and Zr contents are lower in Troodos than in the latter rocks which average 9000 ppm Ti and 90 ppm Zr respectively (Smewing et al., 1975). Ti:Zr ratios, however, similar to Troodos, are also found in diverse environments such as the West Philippine basin and the Shikoku basin (Mattey et al., 1980, Marsh et al., 1980) although with generally higher Ti and Zr contents suggestive of a less depleted source, or smaller degrees of partial melting in the latter environments.

Yttrium and Zr:Y variations.

The variation of yttrium with zirconium is shown in fig. 2.14. A strongly coherent variation is obtained as a result of their immobile nature and the strong geochemical similarities between the two elements (Goldschmidt, 1954; Pearce and Norry, 1979; Wood et al., 1976).

The trends of fractional crystallisation and partial melting (after Tarney et al., 1978) are superimposed for reference.

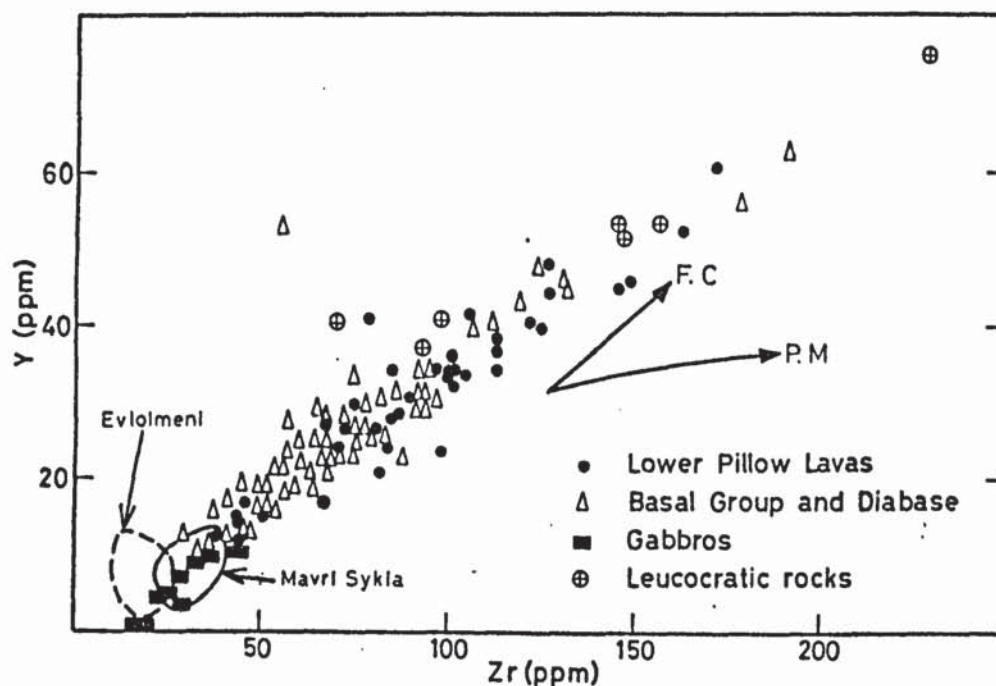


FIG. 2.14. Zr-Y variations for various s assemblages of the ophiolite. Trends of partial melting (P.M) and fractional crystallisation (F.C) are from Tarney et al. (1978).

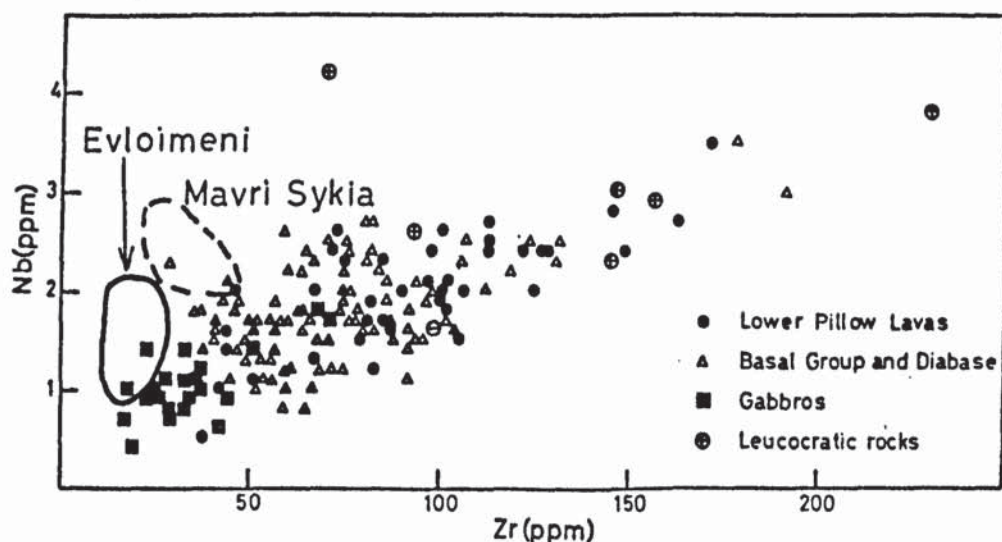


FIG. 2.15. Zr-Nb variations for various assemblages of the ophiolite. Fields of EMS lavas also outlined.

The inference is made from the diagram that fractional crystallisation has played a dominant role in the evolution of these assemblages, resulting to the regular increase in abundance with fractionation.

The EMS lavas are interpreted as more primitive equivalents of the evolved Sheeted Complex and Lower Pillow Lavas and have been derived from the same parental magma.

Niobium and Zr:Nb variations.

Niobium partitions much more strongly in orthopyroxene and clinopyroxene than in plagioclase in the rocks of basaltic composition and the distribution coefficients for the two minerals follow similar and parallel trends in the more primitive melts (Pearce and Norry, 1979). On the other hand, Zr partitions more strongly in clinopyroxene than in orthopyroxene through the same range of compositions. Hence, partial melting of a source whose major component is orthopyroxene, as e.g. harzburgite, will contribute relatively more niobium than zirconium with resultant lower Zr:Nb ratios.

The variation of niobium with zirconium for all the samples from the Troodos ophiolite is shown in fig. 2.15. A linear relationship is obtained and the average Zr:Nb ratio is approximately 50 although varying broadly from 30-70. Rocks of basaltic composition show mean Nb contents up to 1.7 ppm. Typical MORB show slightly higher Nb (3 ppm) but comparable Zr:Nb ratios (averaging 37) while basalts from the mid-Atlantic ridge 45° N average 10 ppm Nb and show much lower ratios (8) (Erlank and

Kable, 1976). This implies that the source for the Troodos basalts was more depleted in incompatible elements than the source for MORB and considerably more than the source for 45° N basalts. Basalts from marginal basins show Zr:Nb ratios comparable to Troodos but Nb contents normally extend to higher values (reaching 10 ppm) (Saunders et al., 1980) again implying a less depleted source for these basalts.

The low-Ti EMS basalts show much lower Zr:Nb ratios, averaging 15, the variable ratios being clearly the result of Nb variability in the samples, a feature correlated with the presence of orthopyroxene microphenocrysts in these lavas.

Barium and Ba:Zr variations.

Barium belongs to the hygromagmatophile (incompatible) elements but, together with K and Sr, is relatively mobile under conditions of moderate alteration (Kay and Senechal, 1976, Wood et al., 1980). Its use in the identification of volcanic environments is, therefore, limited to rocks which have not been severely metamorphosed.

The variation of barium with zirconium in the Lower Pillow Lavas is shown in fig. 2.16. It suggests that abundances have not been severely modified by alteration in these lavas. The regular increase in Ba with Zr also suggests that the trend reflects fractional crystallisation processes. Mean barium content is thrice the content of typical MORB (Wood et al., 1980) suggesting that the Troodos magma has been enriched in this element. Similarly the Ba:Zr ratio (averaging 0.5) is much higher

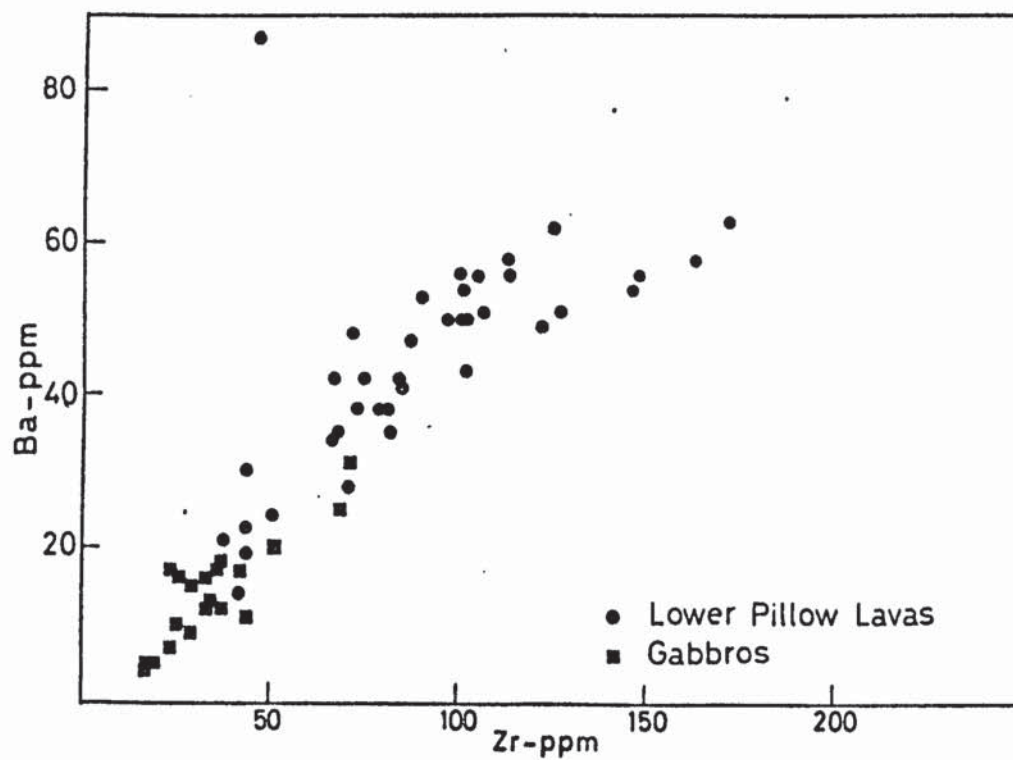


FIG. 2.16. Ba-Zr variations for gabbros and Lower Pillow Lavas.

that typical MORB ratio of 0.07. Ba:Zr ratios comparable to Troodos obtain in the Shikoku basin (Saunders et al., 1980).

The EMS lavas are not depicted on the diagram due to extreme enrichment in barium by proximity to mineralization (chapter 6). Similarly, extreme mobility of barium in the Sheeted Complex is proved in chapter 3. Rocks from this formation are also excluded.

2.3.5. Geochemical patterns.

The elemental co-variations described in the preceding paragraphs lead to the inference that all Troodos assemblages are related by a process of fractional crystallisation of the same parental magma. The ratios between selected, mostly immobile, elements have been compared with ratios from other tectonic environments. Such comparisons, however, are hindered by the fact that elemental abundances are not taken into account. A common way of bypassing this problem is to compare the ratios of abundances of selected elements against a common parameter. Typical (N-type) MORB is frequently used for this purpose.

Prior, however, to describing geochemical patterns for the Troodos lavas, it would be in place to discuss the characteristics of basalts from modern tectonic environments.

The products of extrusion of mid-oceanic ridges are chemically diverse. This diversity has been ascribed to the degree of partial melting, to source heterogeneities or to fractional crystallisation after the separation of the melts from their source region. Differences in the degree of partial melting are

reflected in variations in abundance of incompatible elements in basalts of comparable major element composition. Variations in ratios between incompatible elements are generally interpreted as implying different source regions (O'Hara, 1977).

Pristine mantle is thought to have the composition of plagioclase lherzolite (Menzies and Allen, 1974). Small degrees of partial melting of such mantle results to melts strongly enriched in incompatible elements and the production of alkaline magmas (Kay and Hubbard, 1978). Such alkalic melts may also be produced by veining of N-type MORB source by undersaturated basic melts (Wood et al., 1979). Basalts enriched in incompatible trace elements (E-type MORB), are erupted at hot spots and exemplified by the Azores thermal plume (Wood et al., 1980).

Typical (N-type) MORB are considered to be the products of partial melting of mantle which had been depleted in incompatible elements by previous episodes of magma extraction.

Between the two extremes typified by N- and E-type MORB, transitional (T-type) MORB have been recognised. These may be exemplified by the eruptive products of Reykjanes (Iceland) (Wood et al., 1980).

The lavas erupted at back-arc basins are compositionally as varied as those produced at normal spreading ridges. A contribution from the down-going slab is evident in such environments, with hydrous melting being responsible for low concentrations of REE and other immobile elements and enrichment in the large ion lithophile elements (K, Rb, Ba, Sr) relative to Nb, Ta, Zr, Hf and Ti (Tarney et al., 1981).

Typical geochemical patterns of E- and T- type MORB are shown in fig. 2.17. On fig. 2.18 is shown the pattern obtained for the West Mariana Ridge. This shows a distinctive pattern, characterised by enrichment in the l.i.l. elements relative to MORB, and depletion in the less hygromagmatophile elements (Ti, Zr, Y).

Typical patterns obtaining at Troodos are shown in fig. 2.19. The most striking feature is the extreme depletion in incompatible trace elements, particularly Y, Ti, Zr, P and Ce relative to N-type MORB and the enrichment in Ba, K and Sr relative to the other incompatible elements, as exemplified by the low-Ti EMS lavas, represented by sample MS-15CHR. These lavas may be interpreted as products of partial melting of a source more depleted in incompatible elements than N-type MORB source, followed or accompanied by enrichment in the l.i.l. elements. The pattern obtained for the EMS lavas shows great similarities to the geochemical pattern of basalts from the West Mariana Ridge, suggesting similar genetic processes.

The patterns of a basaltic lava from the Sheeted Complex and an evolved lava from the Lower Pillow Lavas are also plotted on fig. 2.19. Abundances of Sr, Ba and K in the sample from the Sheeted Complex have been calculated since these abundances have been modified by metamorphism. Such calculation is justified by the strong coherence exhibited by more immobile elements such as Ce, Y, and Ti and also from deductions made in chapter 3 on the mobilities of Sr, Ba and K under greenschist facies conditions.

The similarities in the patterns obtained in all these

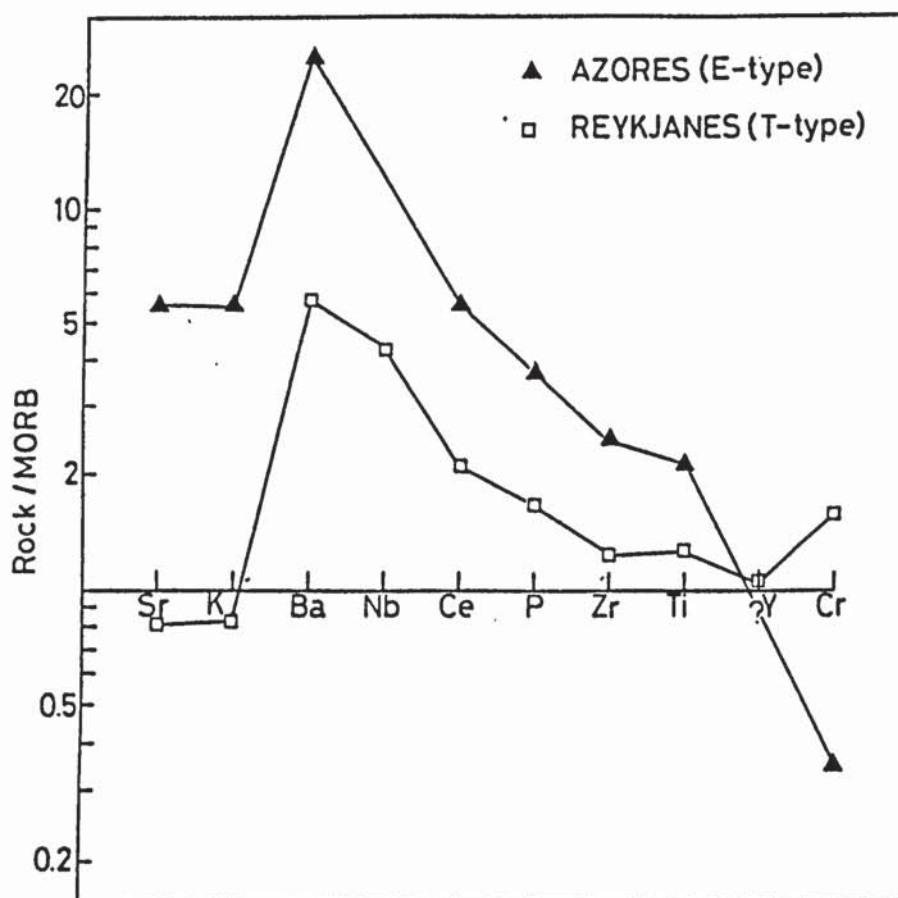


FIG. 2.17 Geochemical patterns for transitional (T-type) and enriched (E-type) basalts from the Mid-Atlantic Ridge, normalised against N-type MORB. Normalising factors are: Sr= 124 ppm, K_2O = 0.22%, Ba= 12 ppm, Nb= 3 ppm, Ce= 9 ppm, P_2O_5 = 0.13 %, Zr= 90 ppm, TiO_2 = 1.37 %, Y= 33 ppm, Cr= 200 ppm. All analyses are from Wood et al., 1980.

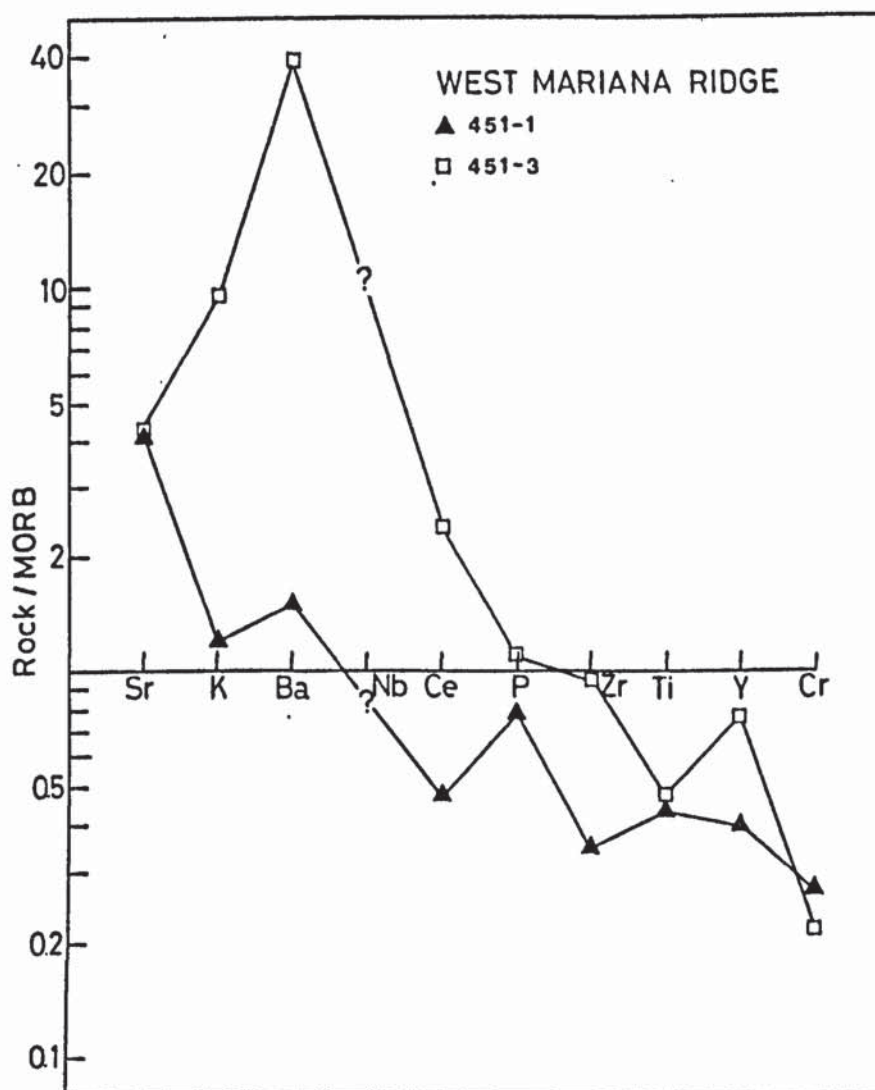


FIG. 2.18 Geochemical patterns for basalts from the West Mariana Ridge, normalised against N-type MORB. Refer to fig.2.17 for normalising factors. On this diagram, note the strong enrichment in the large ion lithophile elements relative to Zr, Ti and Y.

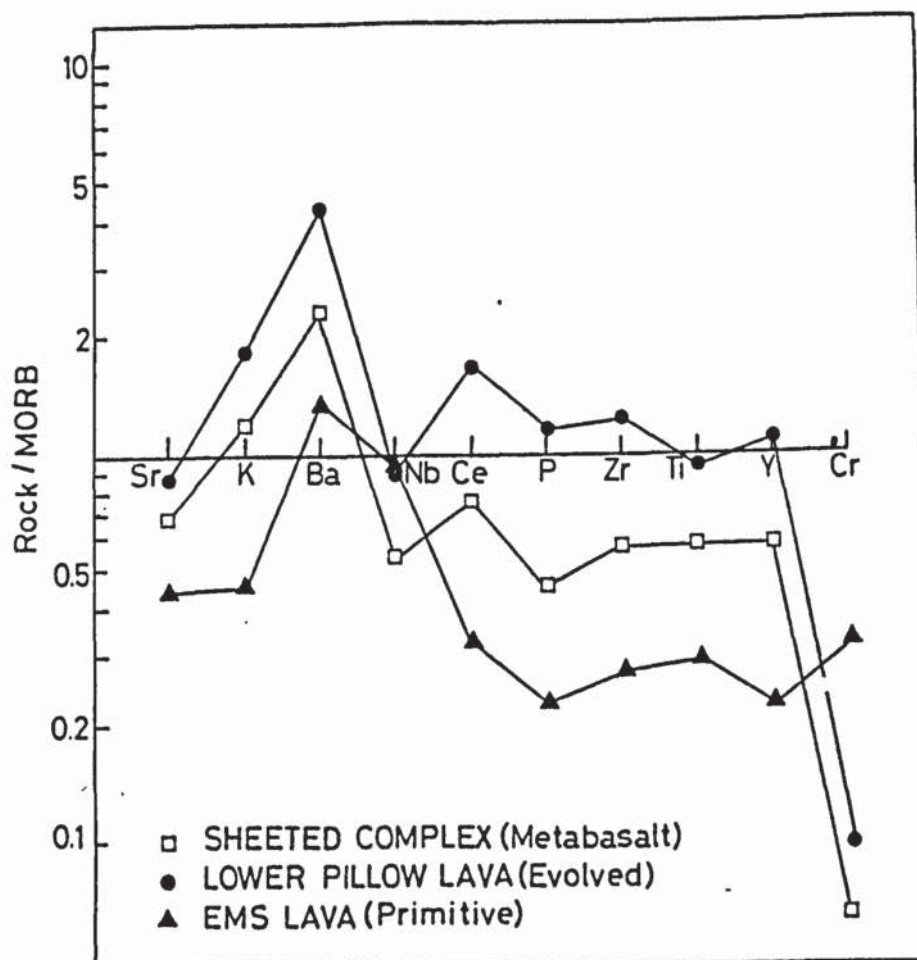


FIG. 2.19. Geochemical patterns for selected samples from the Lower Pillow Lavas (TR4-1), the Sheeted Complex (TR2-14) and the EMS lavas (MS-15CHR), normalised against N-type MORB. Normalising factors in fig.2.17. Account has been taken of mobilities of Ba, Sr and K and values for these elements have been calculated by use of diagrams of variation with Zr (see chapter 3). This diagram highlights the strong similarities in geochemical patterns for all assemblages, as well as the similarities to the pattern of the West Mariana Ridge (Fig. 2.18).

assemblages point towards direct genetic relationships. The EMS lavas may be considered as representing the closest approximation to the parental magma for all Troodos assemblages.

2.4. Summary of conclusions.

Petrography and mineral chemistry suggest that the Troodos assemblages differ from MORB in the common presence of modal quartz and the fractionated nature of the associated clinopyroxenes. The EMS lavas and the genetically related olivine-phyric basalts show very primitive mineral chemistry, exemplified by the associated chrome spinels, and may be considered as mantle-derived melts with limited fractional crystallisation.

The composition of clinopyroxenes from the various members of the ophiolite testify to nonalkaline parentage for all assemblages.

In contrast to MORB, the Troodos magma was enriched in silica, resulting to the Troodos basalts being quartz-normative. The regular variation in normative silica with Zr content suggests that the high silica is not a result of later metasomatic introduction.

Trace element data, especially involving the immobile elements fully support the contention that extensive fractional crystallisation was associated with the formation of the Sheeted Complex and Lower Pillow Lavas. They further suggest that the EMS lavas could have been derived from the same primary magma as the other members but with much more limited pre-eruption

fractionation.

A final conclusion, based on geochemical patterns, is that the Troodos primary magma was the product of partial melting of mantle more depleted than source mantle from which MORB or marginal basin basalts were derived. The similarities in geochemical patterns for the EMS lavas and the basalts of the West Mariana Ridge suggest that genetic processes were similar.

2.5. Discussion of evidence and proposed model

The association between tholeiites and olivine tholeiites in ophiolites has been interpreted as the result of the fractional crystallisation of the same magma, the alternation between the two attributed to growth and waning of the magma chamber by periodic replenishment (Laurent et al., 1980). This view is contrasted to that expressed by Stern and de Wit (1980) who suggested that in a spreading environment open and closed system fractionation may take place from magma chambers which are arranged in a gaussian distribution around the spreading axis. The chambers in the central parts behave as nearly open systems with frequent magma mixing while the ones at the flanks behave as closed systems and give rise to more fractionated lavas.

Zoning of extrusive products of spreading ridges has been described from the mid-Atlantic Ridge 36° 49' N (Hekinian et al., 1976). A zoned central chamber is invoked, giving rise to primitive magmas in the axial valley and fractionated lavas in the marginal parts.

Evidence presented in the preceding paragraphs supports

zonation of extrusive products: The Sheeted Complex is characterised by more primitive chemistry than the Lower Pillow Lavas, as indicated by their lower contents in incompatible elements. The Sheeted Complex has been in the past associated with the crestal parts of a spreading axis (Moore and Vine, 1971, Gass and Smewing, 1973), the Lower Pillow Lavas having been extruded farther away. It may therefore be envisaged that closed system fractionation may have played a major role in the derivation of the assemblages of Lower Pillow Lavas as contrasted to the dykes and lavas of the Sheeted Complex.

The presence of discrete magma chambers has been inferred from recent studies at Troodos, by cross-cutting relationships between layered gabbros and massive static gabbros in the higher levels of the plutonic rocks, close to the sheeted dykes (Allen, 1975, Malpas, pers.com.1982). Such chambers may have provided, by closed system fractional crystallisation and extrusion, the magma responsible for the more fractionated members of the Lower Pillow Lavas.

Primitive basalts, chemically similar to the low-Ti EMS lavas, have been correlated with more extensive partial melting than basalts of normal oceanic settings. Extensive partial melting of upper mantle pyrolite, e.g., was invoked by Gale (1973) for the petrogenesis of some basalts from northeastern Newfoundland. These rocks were termed basaltic komatiites and are depleted in incompatible elements, particularly Zr and Y. A similar conclusion was reached by Sun and Nesbitt (1978) who postulated that such low-Ti basalts are not characteristic of mid-oceanic ridges but of

spreading centres close to zones of subduction. Remelting of the refractory source mantle is facilitated by introduction of water by dehydration of subducted crust.

Basalts chemically similar to the EMS, but differing mineralogically in the presence of hydrous minerals, have also been described from the Mariana trench (Sharanskin et al., 1980). They were again interpreted as the result of intense partial melting under hydrous conditions, the water being derived from a subducting plate.

A similar mode of formation of the chemically primitive lavas of Troodos has been proposed in a recent study of volcanic glass compositions and supported by the high water content of these glasses (Robinson et al., 1983). These authors suggested formation of Troodos in a tectonic environment comparable to the Mariana-Bonin arc.

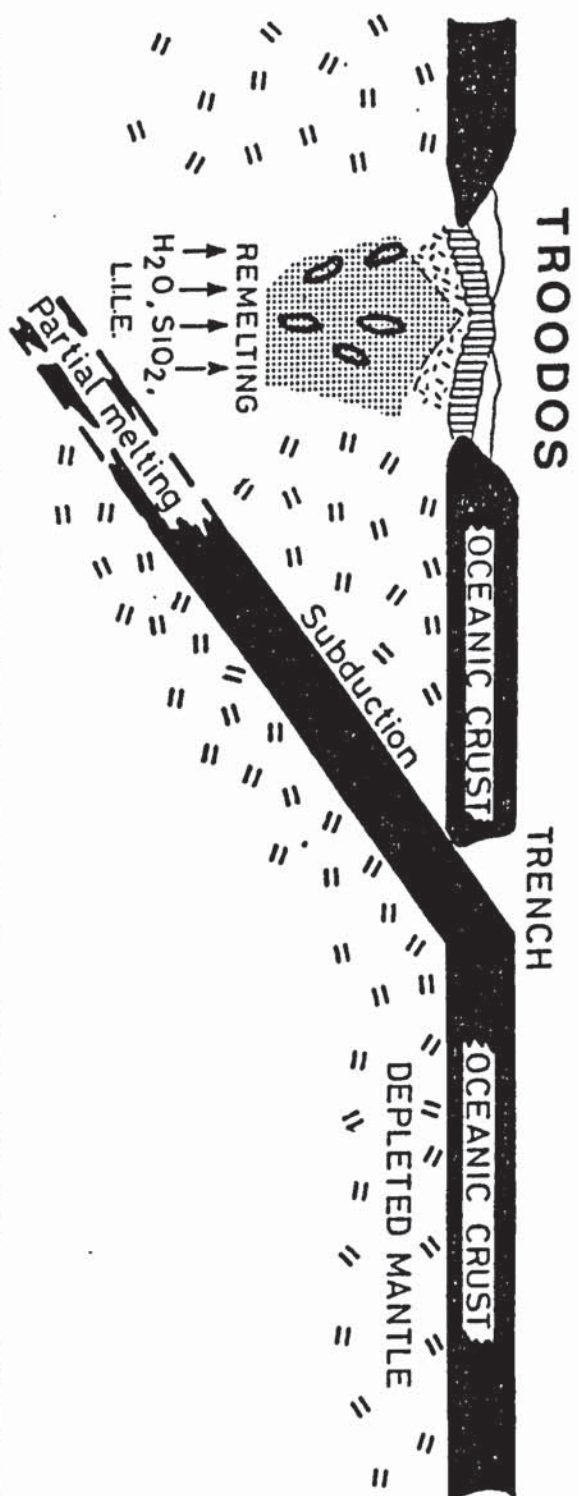
The chemical differences between the Upper Pillow Lavas and the evolved members of the ophiolite were interpreted (Langdon, 1982) as resultant from second stage melting of the same source.

The available data do not permit the estimation of the role played by extra melting in the derivation of the parental magma for the EMS lavas and related Upper Pillow Lavas as contrasted to the lavas of the Sheeted Complex and Lower Pillow Lavas. The chemical continuity between EMS lavas and the older members of the ophiolite, demonstrated by use of immobile elements, suggests that fractional crystallisation, as opposed to different degrees of partial melting, was probably the determining

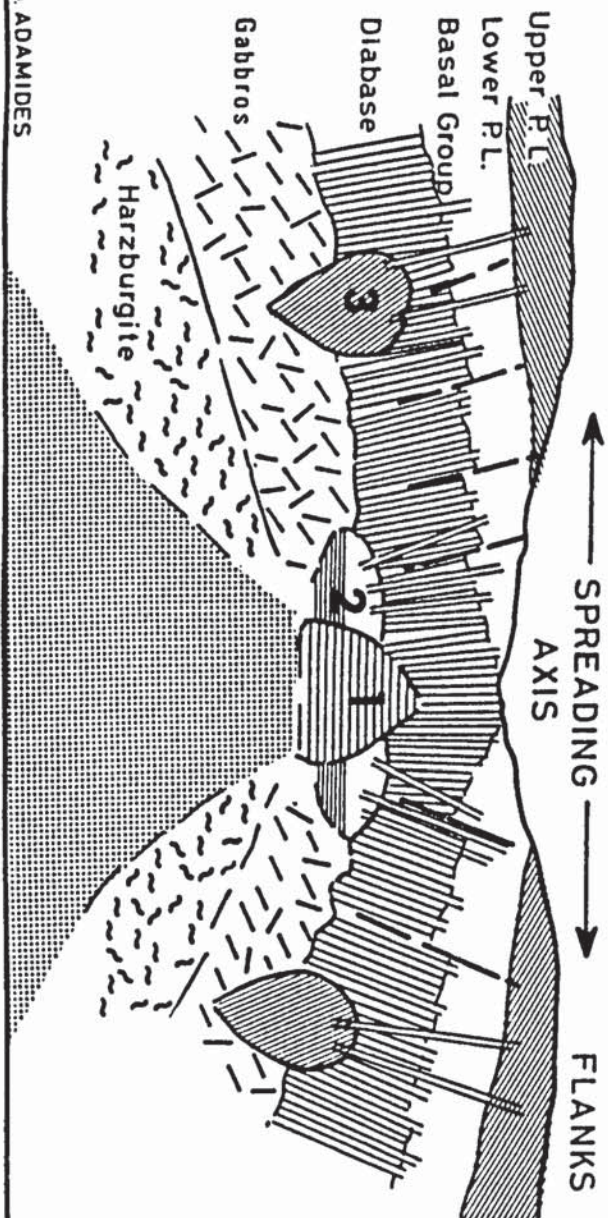
FIG. 2.20. Proposed model for the genesis of the ophiolite. Remelting of depleted mantle is initiated by ingress of seawater along the subduction zone and by dehydration of subducted slab of oceanic crust. This results to enrichment of primary magma in silica and the large ion lithophile elements. The rising asthenoliths split the oceanic crust and initiate spreading above the subduction zone (a).

In (b) the situation at the spreading axis is shown in detail. Asthenoliths at the central parts of the axis (1) are commonly replenished and behave as open systems, being responsible for the greater part of the Sheeted Complex. Adjacent chambers (2) are infrequently tapped and behave as closed systems. These are responsible for strongly fractionated lavas (mainly Lower Pillow Lavas). Generation of the Upper Pillow Lavas is envisaged to take place at the flanks of the spreading axis from diapirically rising chambers (3) which suffered very limited fractionation.(ol- cr)

The model incorporates ideas of Gass (1980), Stern and de Wit (1980), Karig (1971) and Malpas (pers. com. 1982).



d



b

factor in the evolution of the Troodos lavas.

The relationships envisaged between the various lava units are compatible with the formation of the Sheeted Complex at a spreading axis and under conditions of open system fractional crystallisation and periodic replenishment; extrusion of the Lower Pillow Lavas also in an axial environment but with closed system fractionation playing a significant role; and extrusion of the EMS and Upper Pillow Lavas, in flanking parts of the spreading axis and probably under diapiric conditions, as the relatively unfractionated equivalents of the same parental magma.

The enrichment of the Troodos primary magma in silica and the large ion lithophile elements may have been induced by spreading above a subducting oceanic plate in processes comparable to those operative in present day marginal basins (Karig, 1970, Malpas, pers. com. 1982).

Based on the above deductions, the tectonic environment of formation of the ophiolite is diagrammatically illustrated in fig. 2.20.

CHAPTER 3

Hydrothermal processes in the Troodos ophiolite.

3.1. Introduction.

The hypothesis of seawater circulation through oceanic crust as the process responsible for the formation of some volcanogenic sulphide deposits and metalliferous sediments (Elder, 1965, Spooner and Fyfe, 1973) has been gaining ground in recent years. According to the hypothesis, seawater enters oceanic crust in the vicinity of spreading centres from delocalised sites of recharge and, after being heated and chemically modified, exits at focussed discharge sites as a metal-laden hydrothermal fluid. The exit sites mark the location of sulphide deposits. The metals are supposedly leached from the basalts by interaction with heated seawater.

The Troodos sulphide deposits have been considered as typical representatives of such a mode of formation and support was provided by a variety of evidence. Fluid inclusion studies (Spooner and Bray, 1977) suggest that the ore fluid is of seawater salinity. Isotope studies (Heaton and Sheppard, 1977, Chapman and Spooner, 1977) indicate that the fluid responsible for the metamorphism of the ophiolite and formation of the sulphide deposits was seawater.

The purpose of this chapter is to examine the field, petrographic and geochemical features of the ophiolite directly relevant to the hypothesis of seawater-basalt interaction and to discuss a model for the generation of hydrothermal fluids through

interaction of seawater with the ophiolite. Particular emphasis will be placed on mobility of components since, if seawater-basalt interaction is responsible for the formation of the sulphide deposits, evidence of leaching of those elements which are enriched in the deposits should be present in the deeper parts of the sequence.

3.2. Review of field and experimental evidence on seawater-rock interaction.

3.2.1. Field evidence.

Typical assemblages described from the ocean floor indicate that the first product of alteration of volcanic glass is smectite with basal spacings around 14 \AA , followed by carbonate and phillipsite. Alteration involves oxidation, hydration and the growth of secondary minerals at temperatures close to that of seawater. Pyrite and other opaque minerals follow smectite and are often associated with calcite. Other carbonates found include aragonite, magnesite and dolomite (Robinson et al., 1977).

Zoned veins are common, with smectite on the walls, followed by Fe-Mn oxides, phillipsite and calcite (Bohlke et al., 1980).

Olivine is pseudomorphed by calcite or smectite (Dick et al., 1979) or by hydrous Fe-oxides. Other primary minerals are unaffected by alteration. Only plagioclase may be exceptionally, and then only partly, replaced by smectites and calcite (Honnorez et al., 1978).

Secondary mineral assemblages and chemical changes produced by hydrothermal alteration of basalts were described by Miyashiro (1971). Metagabbros dredged from the Mid-Atlantic Ridge are metamorphosed to the greenschist-amphibolite facies but some are retrogressively altered to the zeolite facies, the commonest zeolites being natrolite, analcite, chabazite, laumontite and stilbite. Severe chemical migration of components is postulated (Miyashiro, op.cit), resulting in increase in Na_2O during zeolitisation and decrease in CaO , increase in H_2O^+ and erratic behaviour of SiO_2 during greenschist facies metamorphism. The author suggested that aqueous fluids could be responsible for these geochemical changes.

Alteration assemblages related to sulphide precipitation were described from fracture zones in the Mid-Atlantic Ridge (Bonatti et al., 1976). These involve the presence of sulphide veins associated with chlorite, quartz, epidote and calcite. The clinopyroxene microphenocrysts were generally preserved, while the plagioclase microlites were only partly replaced by albite. Both the alteration of the basalts and the deposition of the sulphides are postulated to be the result of interaction of basalt with seawater which leached the ore metals from deeper levels of the crust.

The mineral assemblages outlined above are suggestive of significant mobility of components and chemical exchange between basalt and seawater, either at temperatures near ambient, in the formation of the calcite-phillipsite assemblages directly on the sea floor, or, at elevated temperatures, for the formation of the

chlorite-epidote assemblages. Cold hydration was found to result to leaching of silica, calcium and magnesium and the enrichment of the basalts in potassium, rubidium, iron, titanium, manganese, sodium and phosphorus (Hart, 1970, Cann, 1970). Hydrothermal alteration results to extensive leaching of calcium and strontium, leaching of copper and local precipitation as chalcopyrite, and mobilisation of Fe, B, Li, Ba, Mn, Ni and Co (Humphris and Thompson, 1978).

Perhaps the best evidence of seawater-basalt interaction in the formation of alteration assemblages is provided by the study of active geothermal areas, since both the alteration minerals and the altering fluids may be readily sampled and analysed. One such area is the Reykjanes geothermal field (Tomasson and Kristmannsdottir, 1972). Alteration minerals include zeolites (particularly mordenite, stilbite, mesolite and analcite), opal, which is replaced by quartz at deeper levels, calcite, prehnite, epidote and anhydrite. The main clay minerals are montmorillonite, chlorite and mixed-layer chlorite-montmorillonite. The altering fluid is seawater and this is completely depleted of contained sulphate by anhydrite precipitation.

3.2.2. Experimental studies.

Interaction of basalt with seawater at low temperatures (70°C) results to slight but continuous loss of Mg, Na, and K and enrichment of Ca and SiO_2 in seawater. At higher temperatures Mg and SO_4 are quickly removed from seawater, while Ca, SiO_2 , Na, K,

Fe, Mn and Ba are added (Seyfried and Bischoff, 1979). Mg is lost early in the experiments and so is Ca due to precipitation of smectite and anhydrite but Ca later increases due to uptake from the rocks. Removal of Mg from seawater is balanced by leaching of Ca from basalt, while transfer of Na was similarly balanced by Ca removal (Mottl and Holland, 1978).

The heavy elements Fe, Mn, Cu and Ni are 2-3 orders of magnitude enriched over normal seawater (Bischoff and Dickson, 1975). Barium, boron and carbon dioxide are also enriched in the reacted seawater (Mottl and Holland, 1978).

Reaction of seawater with basalt changes the fluid from an oxygenated to a reducing solution with anomalous Fe, Mn, Cu and Si concentrations. Aluminium remains low in seawater at all temperatures.

Minerals forming during interaction are smectite, giving way to tremolite at higher temperatures, phillipsite, analcite, albite and anhydrite (Hawkins and Roy, 1963). The absence of chlorite from the assemblages is attributed to kinetic reasons. Minerals directly relevant to the sulphide deposits, such as chalcopyrite, pyrrhotite and hematite were also among the products of interaction (Hajash, 1975).

3.3. Salient features of alteration in the Troodos ophiolite.

3.3.1. Field evidence

Alteration minerals are abundantly present in the lava sequence and the Sheeted Complex as veins and cavity fillings.

These have been ascribed a stratigraphic connotation (Smewing, 1975). However, as will be evident in chapter 5, the origin of zeolites is associated with diverse causes related to both ascending, heated fluids and descending seawater. The following descriptions, therefore, based on the results of extensive field mapping, are only considered as generalizations.

Analcite and calcite, sometimes associated with gmelinite, are predominantly found in the upper levels of the pillow lava sequence; natrolite is common in deeper parts of the Upper Pillow Lavas and in the higher levels of the Lower Pillow Lavas.

Chalcedonic silica is widespread within the Lower Pillow Lavas and its formation appears to be partly controlled by the lithology (Plate 3.1). Heulandite and stilbite are predominantly present in the Lower Pillow Lavas but also found within deeper parts of the Upper Pillow Lavas.

Celadonite (Plate 3.2), a mineral which was originally considered to characterise only the Lower Pillow Lavas is found to extend into the lower parts of the Upper Pillow Lavas and green staining, akin to celadonite, is frequently present through most of the Upper Pillow Lavas, particularly associated with joint planes in dykes.

Laumontite is mainly confined to deeper levels of the Lower Pillow Lavas and particularly close to the contact with the Sheeted Complex (Plate 3.3). There, it may be found in association with epidote, decreasing in abundance as epidote increases.

The commonest occurrence of the zeolites is in the form



PLATE 3.1. Chalcedonic silica vein, generated in silicic hyaloclastites (lower half of photograph), thins out and disappears in basic flow.

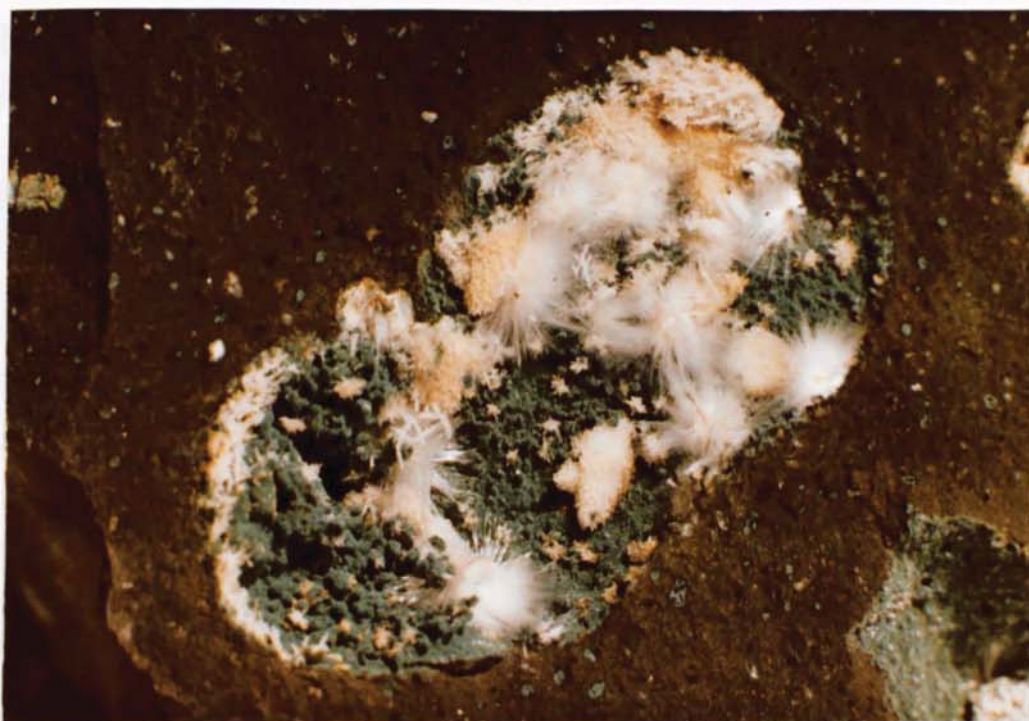


PLATE 3.2. Celadonite (dark green) in association with calcite (creamy) and fibrous zeolite, infills vesicle in Lower Pillow Lava. Length of vesicle is 6 cm.



PLATE 3.3. Laumontite infilling vesicles and fractures in Lower Pillow Lavas.

Length of field of view is 10 cm.



PLATE 3.4. Association of calcite and epidote in vesicles. Basal Group/Lower Pillow Lava interface.



PLATE 3.5. Initial stages of pervasive action of hydrothermal fluids. Strongly chloritised inter-flow material (top of hammer), weakly altered to fresh pillow interiors (upper part of photograph).



PLATE 3.6. Photomicrograph illustrating the transformation of glassy matrix of lava to smectite.

Crossed polars, X128.

of open space fillings, veins, vesicle fillings and in interpillow spaces. No zeolitisation of the crystalline matrix has been observed.

Within the Sheeted Complex, vein and vesicle filling minerals are mostly represented by quartz and epidote, commonly associated with calcite (Plate 3.4).

In contrast to alteration in the higher levels of the volcanic sequence, where the original character of the rocks is retained, alteration in the Sheeted Complex is a pervasive process. In the field the transition is indicated by a change in colour of the rocks from dark grey in the pillow lavas to bluish-green in the sheeted complex. The contact between pervasive and non-pervasive alteration is in many cases gradational, initial stages being suggested by zones of intense alteration particularly around pillows and in the interspace between lava flows (Plate 3.5).

3.3.2. Petrographic evidence.

Alteration in the lavas is first suggested by devitrification of the volcanic glass with the development of a microcrystalline texture without, however, formation of any discrete minerals. Smectitisation proceeds from the margins and, in advanced stages of alteration, the whole of the glassy matrix may be transformed to smectite (Plate 3.6).

Of the silicates, olivine is most susceptible to alteration, being almost universally replaced by hematite and calcite (Plate 2.6), or, more rarely, smectite or serpentine.

Clinopyroxene and plagioclase generally survive alteration although replacement of clinopyroxene by smectite and saussuritisation of plagioclase, in association with the formation of secondary quartz were noted in rare situations, probably reflecting proximity to mineralization.

Chloritisation of the glassy mesostasis and clinopyroxenes, albitisation of plagioclase and the common formation of secondary quartz are the main modes of alteration in the higher levels of the Sheeted Complex. At deeper levels actinolite becomes an important phase, sometimes to the complete exclusion of chlorite.

Chlorite occurs as an alteration product of the glass; associated with smectite in an apparently stable relationship; less commonly in the form of veins, associated with alteration of plagioclase, or, with epidote, in cavities. The commonest occurrence of this mineral, however, is in association with actinolite as alteration products of the pyroxenes. In the last mode of occurrence a retrograde relationship is commonly suggested, with chlorite replacing actinolite after clinopyroxene along cleavages. Stable co-existence of the two minerals is also noted with actinolite replacing clinopyroxene and chlorite occurring alone as the product of alteration of the glass.

Albitisation is the commonest form of alteration of the plagioclase. Initial alteration is petrographically suggested by the clouding of plagioclase crystals and partial destruction of twin lamellae (saussuritisation). At a later stage, the whole crystal may be transformed to albite.

In stratigraphically deeper levels of the Sheeted Complex, oligoclase is the stable phase co-existing with actinolite.

Electron microprobe analyses of secondary minerals from the Sheeted Complex are presented in Table 3.1.

Alteration in the gabbros is, in all examined cases, limited to the partial or complete transformation of the pyroxenes into actinolite (uralitisation). The plagioclase remains generally free of alteration. The process of uralitisation is guided by fractures and cleavage traces (Plate 3.7) and may result to the complete replacement of the pyroxene by actinolite.

The petrographic studies were corroborated by X-ray diffraction examination of samples from all stratigraphic levels aimed at investigating predominant assemblages in the various units. The results are presented in Table 3.2.

Smectites from the Upper Pillow Lavas show dominant basal spacings around 14 \AA , normally with a very minor reflection at 3 \AA . The broad nature of the basal peak ($12.6\text{--}14.7^\circ$) is suggestive of poor crystallinity. The smectite belongs to the saponite group and is optically and crystallographically similar to smectites from the ocean floor (Robinson et al., 1977).

Better crystallinity is suggested for the smectites of the Lower Pillow Lavas by the narrower span of the basal peaks. In addition to smectite, other phases identified by X-ray diffraction in varying amounts in the Lower Pillow Lavas include calcite, analcite, quartz and celadonite.

Chlorite and actinolite are the dominant phases in the Sheeted Complex, invariably occurring with varying amounts of



PLATE 3.7. Transformation of clinopyroxene to actinolite in gabbro, guided by cleavage. Parallel polars, X100

TABLE 3.1. Electron probe analyses of amphibole and coexisting plagioclase in Diabase.

Ox. %	1	2	3	4
SiO ₂	47.42	51.56	51.69	52.49
TiO ₂	0.22	0.14	0.04	0.00
Al ₂ O ₃	7.41	3.92	29.57	29.31
FeO	13.75	13.44	0.78	0.68
Cr ₂ O ₃	0.00	0.00	0.00	0.00
MnO	0.35	0.41	0.07	0.05
MgO	16.69	15.21	0.23	0.29
CaO	8.02	10.72	14.02	11.95
Na ₂ O	0.41	0.29	3.67	3.82
K ₂ O	0.34	0.14	0.07	0.92
Total	94.61	95.83	100.14	99.51
Si	7.075	7.584	9.429	9.601
Aliv	0.925	0.416	6.359	6.320
Alvi	0.378	0.263	-----	-----
Ti	0.024	0.016	0.006	0.000
Fe	1.716	1.653	0.119	0.105
Cr	0.000	0.000	0.000	0.000
Mg	3.712	3.335	0.063	0.080
Mn	0.044	0.051	0.012	0.007
Ca	1.283	1.689	2.740	2.342
Na	0.118	0.082	1.299	1.354
K	0.065	0.026	0.017	0.214
			Ab:32	Ab:35
			An:68	An:60
			Or: 0	Or: 5
1, 2 = Amphibole, TR8-14				
3, 4 = Plagioclase, TR8-14				

UPPER PILLOW LAVAS									
	SMECTITE				CHL. ACT.	QZ	CEL.	CAL.	AN.
	12Å	14Å	16Å	18Å					
PA11R		+	■						
PA-5R	■	■							
PA-1R		■							
PE-12	■								
PA-14R			■	□					
PA13R			■						
PA-12R	■								
LOWER PILLOW LAVAS									
PE-14		■					□		
PA-16R		■					□		
PA-15R		■						■	
PA-7R		■							■
PA-6R		■				■			
PA-3R			■						
PA-4R			■						
PA-2R					■		□		
PE-18		■				■			
PE-17		■							
PE-16		■					■		
PE-15-2			■					■	■
PE-13		■							
7C		■							
4C		■						■	
3C		■							
KA1R		■				■			
SHEETED COMPLEX									
ANG-1R	■				■				
PA-10R					■				
PA-9R	■	■			■				
ANG-5R			■		■	■			
ANG-4R			■		■	□	■		
ANG-3R		■			■	■			
ANG-2R		■		□	■				
PE-11		□		□	■	■			
PE-9					■	□			
PE-8		■				■	■		
PE-7		□			■	■	■		
PE-6						■			

TABLE 3.2. Summary of X-ray diffraction data for various members of the intrusive-extrusive sequence.

Large filled squares: Phase present in abundance.
 Small filled squares: Phase present in significant amounts. Small empty squares: Trace.

CHL: Chlorite, ACT: Actinolite, QZ: Quartz,
 CEL: Celadonite, CAL: Calcite, AN: Analcite.
 Horizontal lines indicate peak breadth.

smectites. The presence of the latter is commonly noted by the enhancement of the 14 \AA chlorite peak, suggestive of saponite. Montmorillonites with basal spacings of 13.6 \AA (sodium rich?) and 12.1 \AA were detected in rarer situations.

3.4. Elemental mobilities during alteration and metamorphism.

3.4.1. General.

The primary problem in the quantitative determination of additions and subtractions of components is the lack of knowledge of the original composition of the unaltered rocks. Primary (magmatic) processes relating to fractional crystallisation, in addition to secondary alteration and metamorphism, lead to strong modifications in major and trace element abundances. The use of 'average' compositions as measures of additions or subtractions of components do not give unequivocal conclusions.

It has been indicated in chapter 2 that the Gabbros, Sheeted Complex and Lower Pillow Lavas are derived from the same parental magma and as such are chemically related by a process of fractional crystallisation. Silica, however, which could provide a measure of element variation, is significantly mobile, particularly in the Sheeted Complex, as suggested by the common occurrence of vein quartz. The linear increase of Zr with differentiation, resultant upon its incompatible nature and its immobility under conditions of severe alteration and metamorphism (Cann, 1970; Wood et al., 1976; Humphris and Thompson, 1978), make

it ideal for plotting element variations and as such it has been used in the past (Coish, 1977).

The purpose of this section is the study of element mobilities during alteration and metamorphism, based on the principles outlined above, and the correlation of the derived conclusions with experimental and field evidence of seawater-basalt interaction.

3.4.2. Collection of samples and analytical techniques.

Samples were collected along nine traverses over the greater part of northern Troodos (Fig. 3.1) and included rocks of the Lower Pillow Lavas, the Sheeted Complex and upper Gabbros. The Upper Pillow Lavas and the lower members of the gabbroic sequence were not included in the sampling due to absence of evidence on their participation in the processes of ore deposition.

Samples were preferentially collected from the inner parts of intrusives and massive flows. Pillows were mostly excluded due to greater susceptibility to chemical modification by weathering and alteration unrelated to pervasive action of fluids which forms primarily the concern of this study. A limited number of samples from chilled margins of flows were collected for comparison purposes.

Chemical analyses for major and trace elements were carried out at the University of Leicester by Mr N. G. Marsh. A pressed pellet technique was used, methods and standards being identical to those employed at the University of Birmingham and described by Tarney et al.(1978).

Representative chemical analyses of some of the rocks sampled are presented in Tables 3.3-3.5. A full table of analyses of all the rocks sampled is presented in Appendix 1.

3.4.3. Presentation of data.

In the following paragraphs three types of diagrams will be presented and discussed:

1. A set of diagrams illustrating the variation of a number of elements against zirconium. Lower Pillow Lavas and gabbros are used in the definition of the compositional fields of the relatively unaltered rocks. The defined fields are overlain on the diagrams showing element- zirconium variations for the rocks of the Sheeted Complex and chemical changes quantitatively estimated.

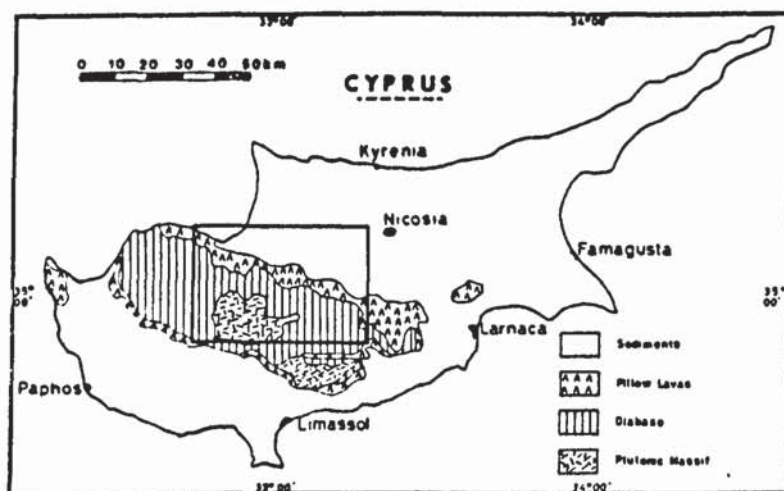
2. The determined element enrichments and depletions in some selected elements are plotted on a plan of northern Troodos and contoured, so that the distribution of chemical changes with respect to the geology is depicted.

3. The final set of diagrams was constructed by projecting all samples onto a single plane making the following assumptions:


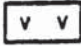
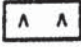


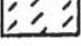


- a. The various formations were taken as being of constant thickness;

- b. All samples were projected onto a single plane;

- c. The position of a sample on the section was determined by estimation of the relative distance of the sample from the underlying and overlying formation as measured in the



L E G E N D

-  Sediments
-  Upper Pillow Lavas
-  Lower Pillow Lavas
-  Basal Group
-  Diabase
-  Gabbro and Granophyre
-  Ultramafic rocks
-  Sulphide deposits

Location map of the area geochemically examined and legend of maps showing geochemical variations.

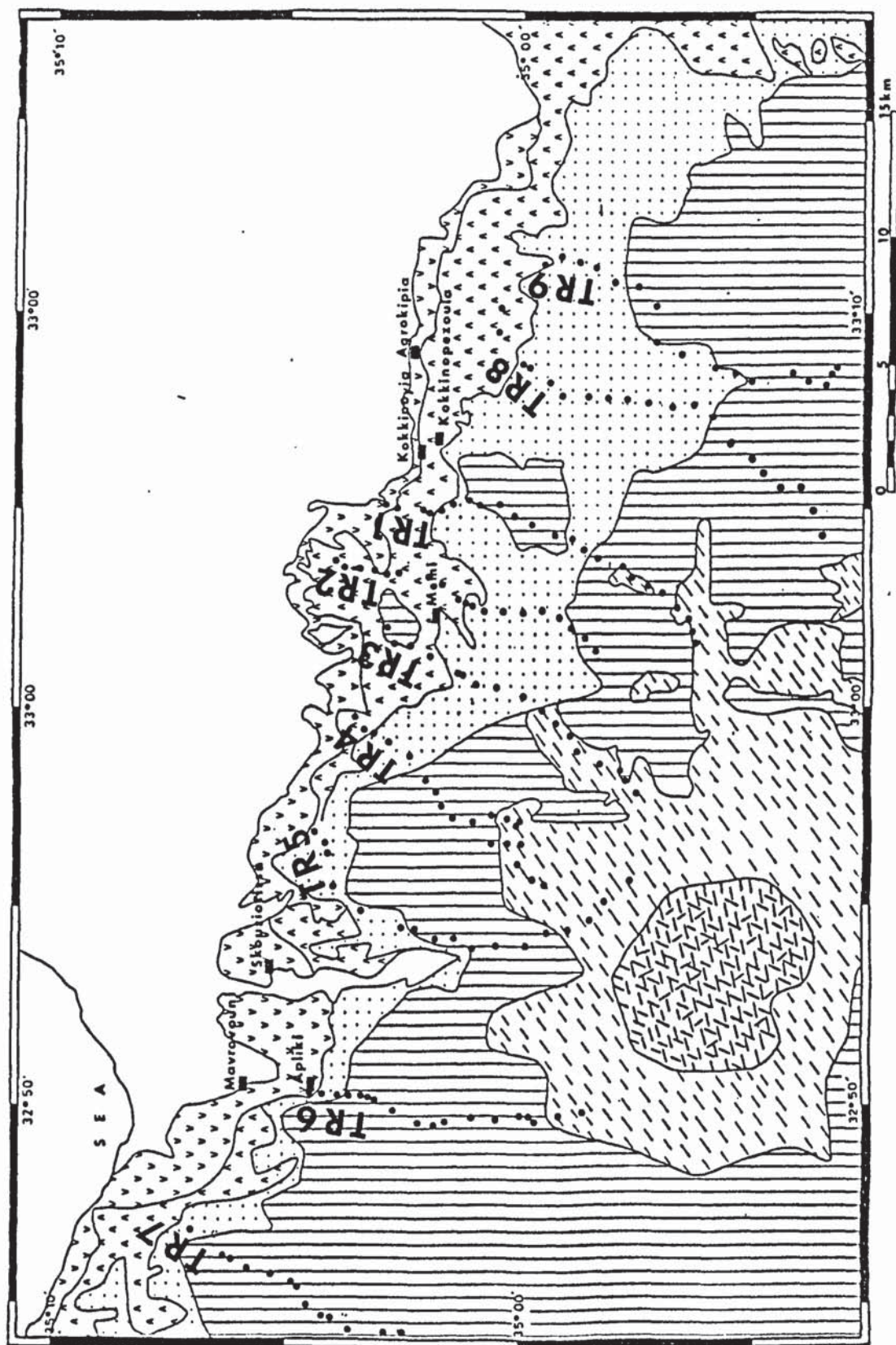


FIG. 3.1. Geological map of area examined (Redrawn from maps in Memoirs of the Geological Survey), showing location of geochemical traverses and sample points.

horizontal direction.

The aim of the latter set of diagrams is to depict the predominant pattern of alteration with relation to the stratigraphy of the ophiolite and the position of the sulphide orebodies.

Not all samples were used in the derivation of the alteration patterns. Since the distance between traverses was in the region of 10 km, the inclusion of an anomalous sample in the contoured results would give rise to false anomalies far greater in size than the area of influence of the sample. Such anomalous samples include mineralized rocks collected from local shear zones and also samples representing extreme fractionation such as leucocratic dykes and plagiogranite bodies in the gabbros. Finally, samples whose incompatible element pattern indicates marked chemical differences from the surrounding rocks were also removed so that a regular pattern of variation was obtained.

Enrichments and depletions in particular elements were estimated by the use of the plots of variation against zirconium. A sample is considered enriched by 0.5 % CaO, e.g., when it plots at a point 0.5 % CaO above the upper limit of the background zone as shaded in these figures. It is similarly depleted in CaO by the same amount when it plots 0.5 % CaO below the lower limit of the shaded zone for the given Zr content. The samples plotting in the shaded field were considered as background.

3.4.3.1. Magnesium

The behaviour of magnesium with fractionation (Fig. 3.2)

is consistent with its strong enrichment in early products of differentiation. With the exception of samples with cumulate ferromagnesian minerals, showing strong enrichment and falling outside the shaded field, a well defined trend of variation is evident (Fig. 3.2a). This suggests that original abundance has not been ^{greatly} modified by alteration. In contrast, the rocks of the Sheeted Complex are characterised by a dominantly enriched pattern (Fig. 3.2b).

The areal and stratigraphic distribution of magnesium variations (Figs 3.3 and 3.4) suggest that:

a. Magnesium enrichment characterises the Basal Group, with the Diabase showing background values or depletions.

b. Depleted values in magnesium are preferentially concentrated in the Diabase stratigraphically underlying the sulphide deposits. This feature is particularly evident in the Mavrovouni-Apliki-Skouriotissa (MAS) group of deposits and to a lesser extent in the Kokkinoyia-Agrokipia-Kokkinopezoula (KAK) group.

The above features suggest that active deposition of magnesium, incorporated in chlorite, takes place in the higher levels of the Sheeted Complex by downward percolating fluids, while leaching of magnesium accompanies the upward movement of the heated, magnesium-depleted fluids which resulted to the formation of the sulphide deposits.

3.4.3.2. Calcium

A logarithmic decrease in calcium with fractionation is

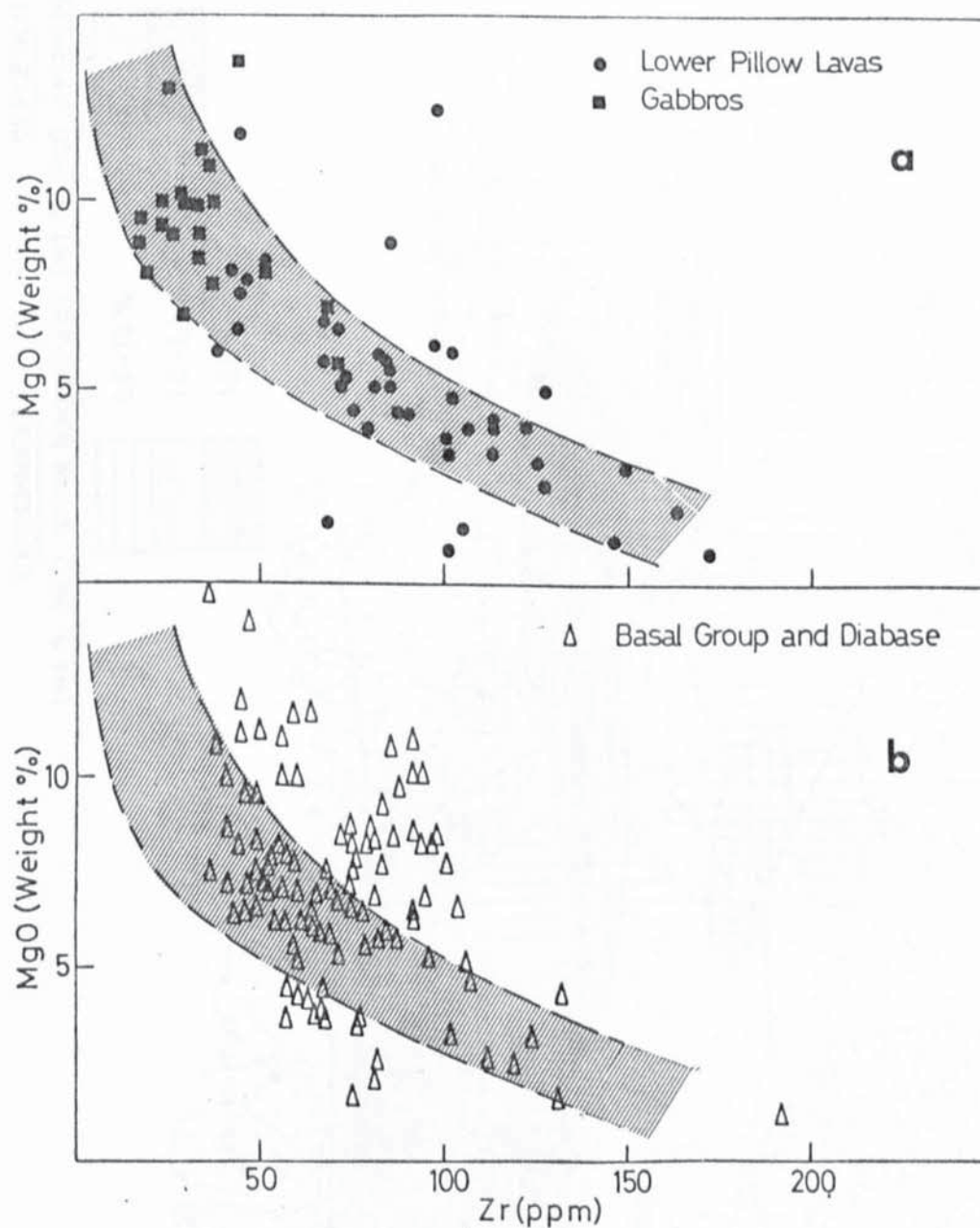


FIG. 3.2. MgO-Zr variation for the Lower Pillow Lavas and gabbros (a) and for the Sheeted Complex (b). The diagram suggests coherence of magnesium during alteration in (a) and strong mobility, dominated by enrichment, in (b).

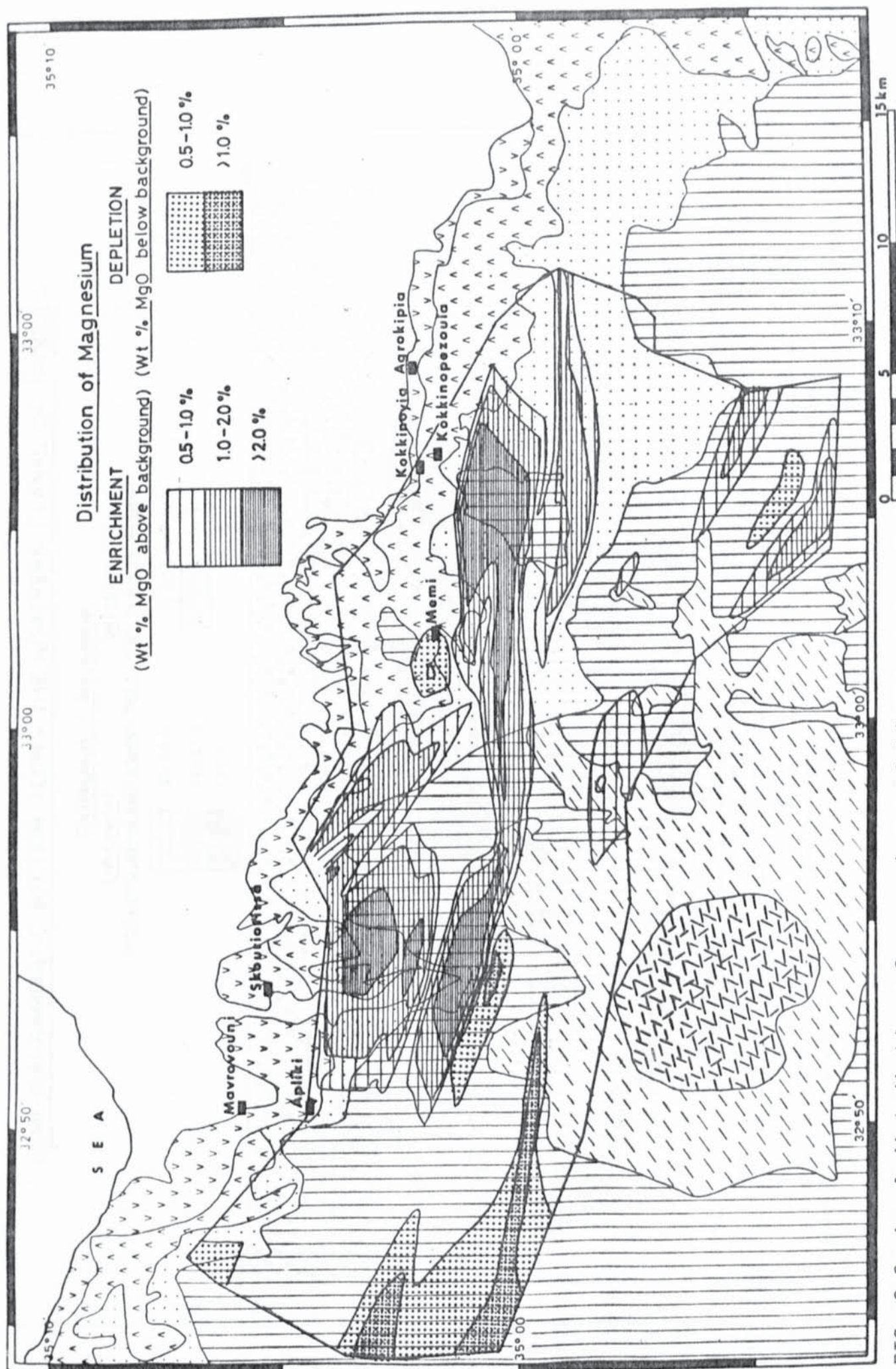


FIG. 3.3. Areal distribution of magnesium variations.
Refer to p.88 for key to geological symbols.

SEMI-DIAGRAMMATIC SECTION ALONG THE NORTHERN FLANKS OF TROODOS

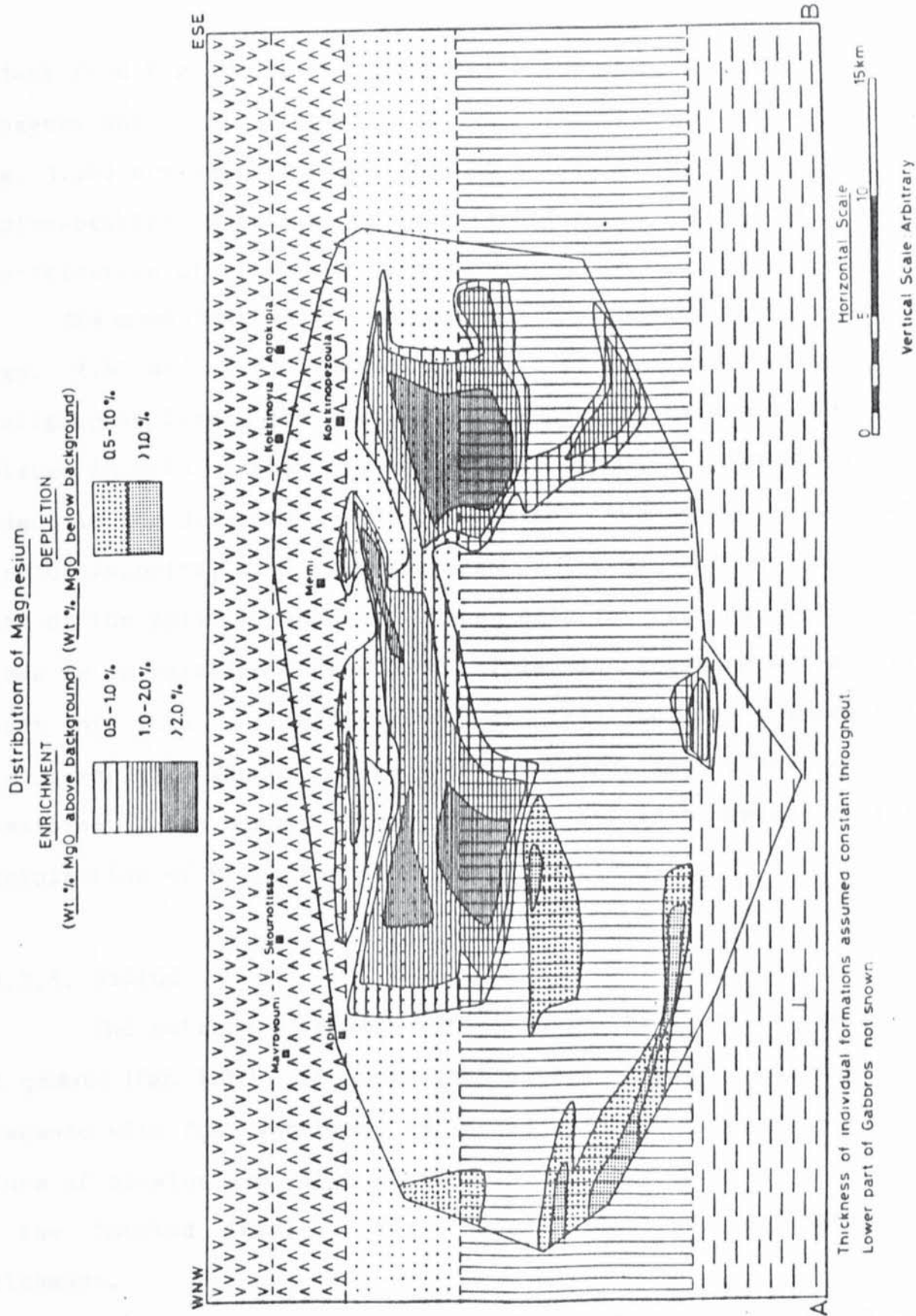


FIG. 3.4. Magnesium variations with relation to igneous stratigraphy. See p 88 for key to geological symbols.

evident from Fig. 3.5a, associated with the early precipitation of pyroxenes and calcic plagioclase. The rocks of the Sheeted Complex (Fig. 3.5b) are leached of calcium as a result of the breakdown of calcium-bearing minerals by albitisation of plagioclase and chloritisation of glass and pyroxenes.

The areal distribution of calcium enrichments and depletions (Figs. 3.6 and 3.7) does not suggest any relationship to stratigraphic level, although the Diabase appears to be more depleted in calcium than the Basal Group. No clear relationship is evident in the distribution of calcium and the position of the sulphide deposits, with the exception of the MAS group, directly south of the Apliki deposit, where calcium retains background values or is relatively enriched. This is interpreted as the result of local precipitation of calcite by ascending, calcium-enriched fluids, as they moved towards the sites of ore deposition in the higher levels of the volcanic sequence (Cf. precipitation of calcite and epidote in plate 3.4).

3.4.3.3. Sodium

The pattern of sodium variation in the Lower Pillow Lavas and gabbros (Fig. 3.8a) is consistent with a gradual increase in abundance with fractionation, reflected in the increasingly sodic nature of plagioclase. This pattern is strongly upset in the rocks of the Sheeted Complex (Fig. 3.8b) which are dominated by enrichment.

The areal distribution of sodium (Figs. 3.9 and 3.10) strongly reflects the position of the major mining districts: A

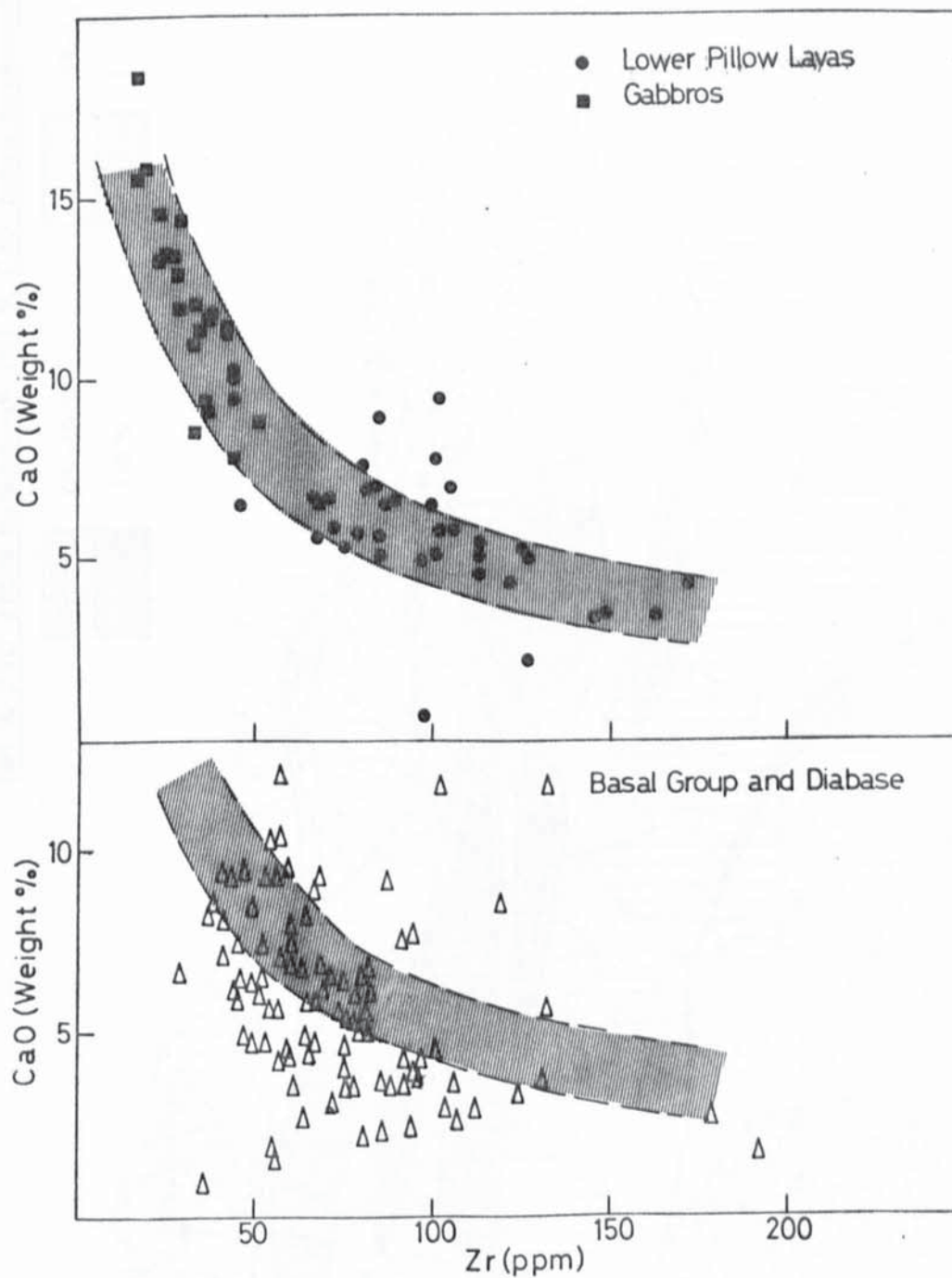


FIG. 3.5. Variation of calcium using zirconium as index of differentiation. The diagram suggests coherence of calcium in the gabbros and Lower Pillow Lavas (a) and strong mobility, dominated by leaching, in the Sheeted Complex (b).

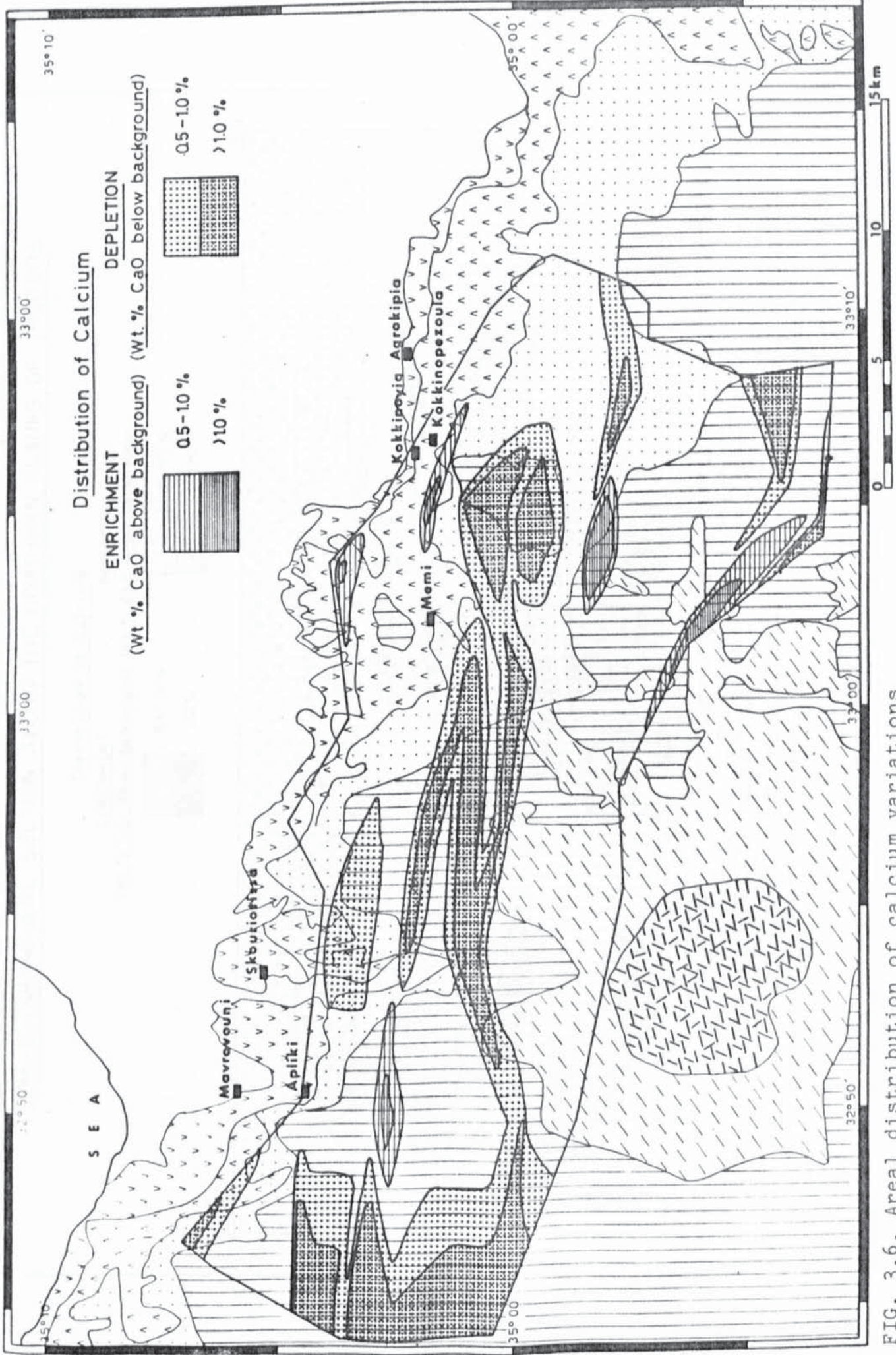


FIG. 3.6. Areal distribution of calcium variations. Refer to page 88 for key to geological symbols.

SEMI-DIAGRAMMATIC SECTION ALONG THE NORTHERN FLANKS OF TROODOS

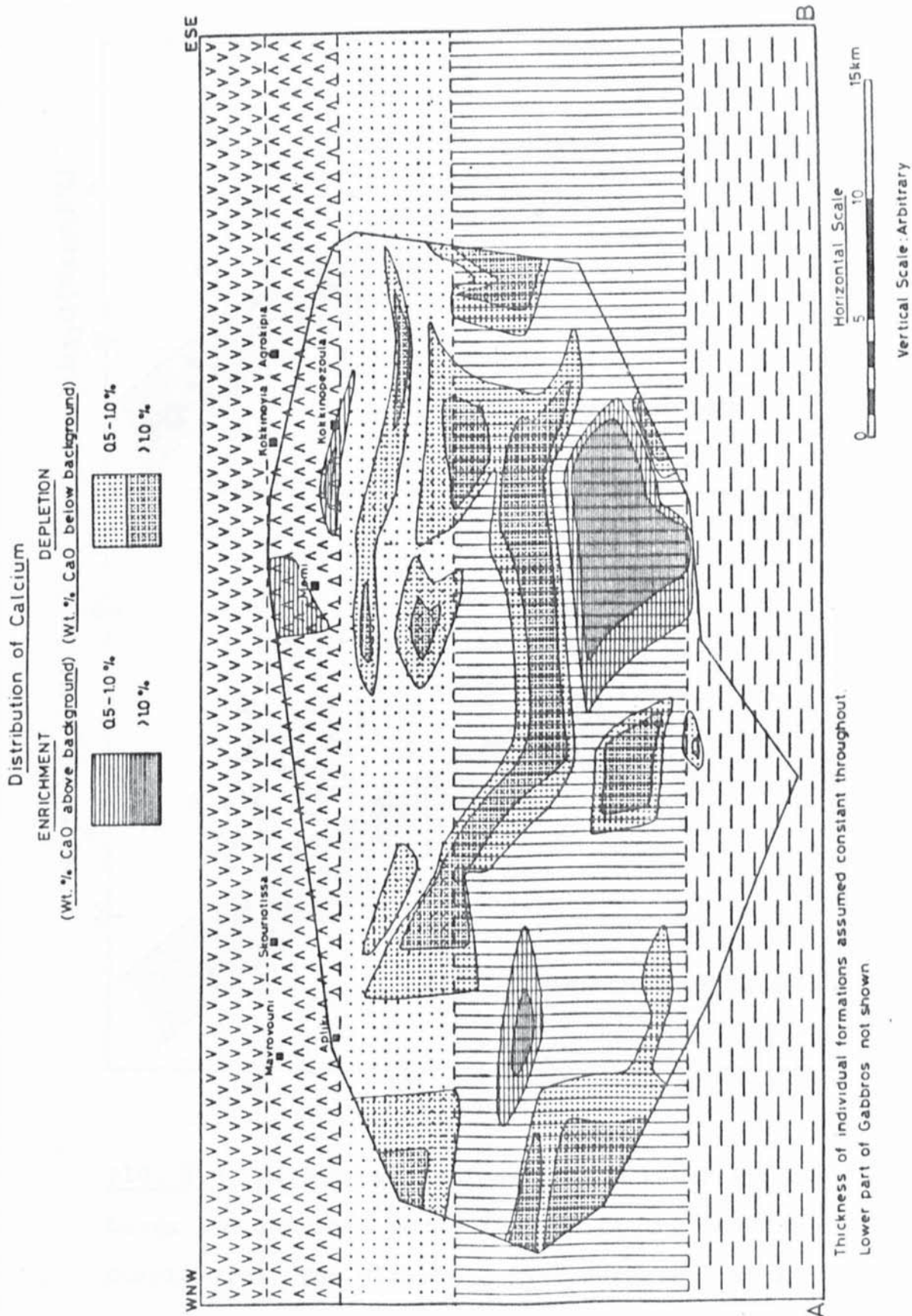


FIG. 3.7. Calcium variations with relation to igneous stratigraphy.

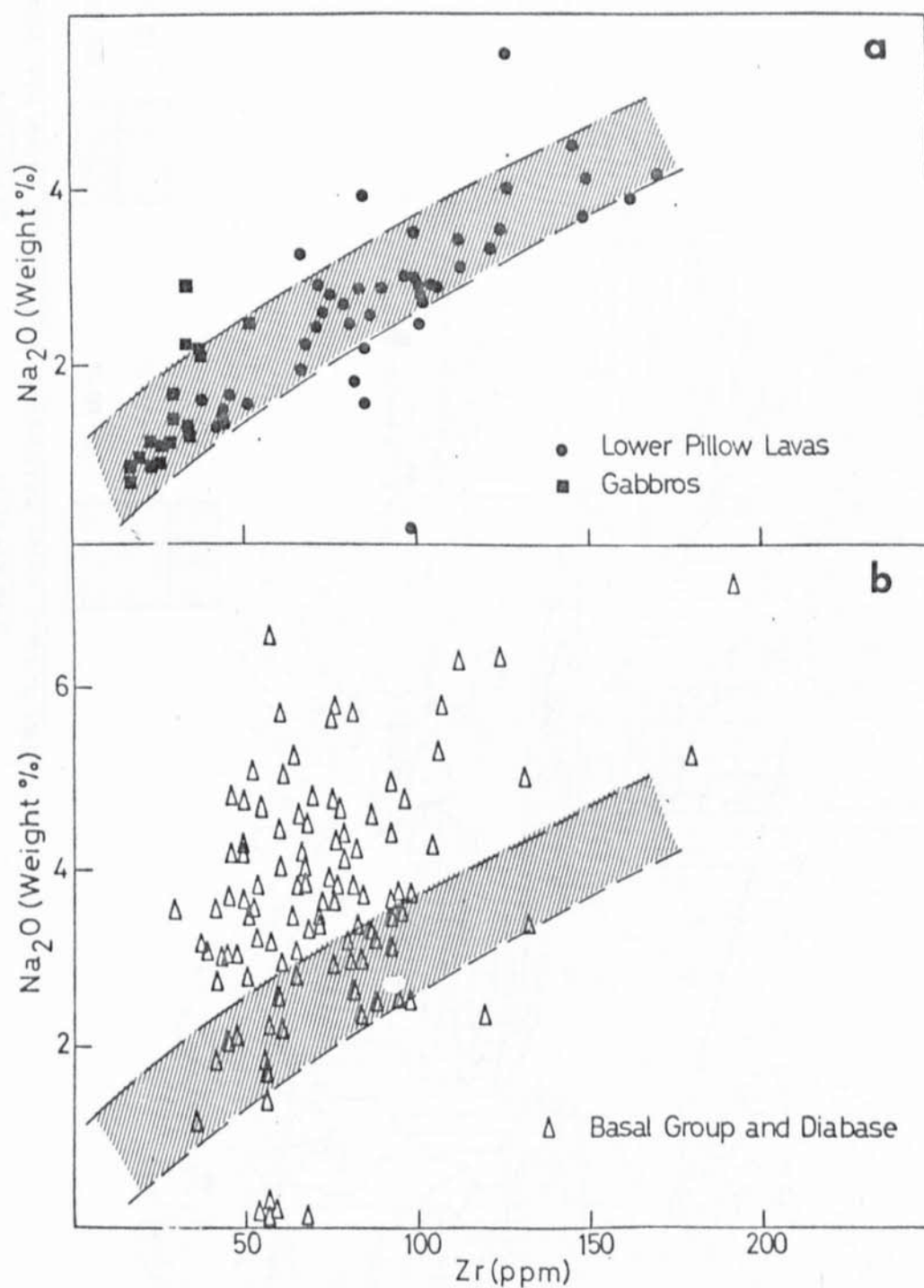


FIG. 3.8. Na_2O -Zr variations in the Lower Pillow Lavas and gabbroic rocks (a) and in the Sheeted Complex (b). The diagram suggests enrichment in sodium of the Sheeted Complex during hydrothermal metamorphism.

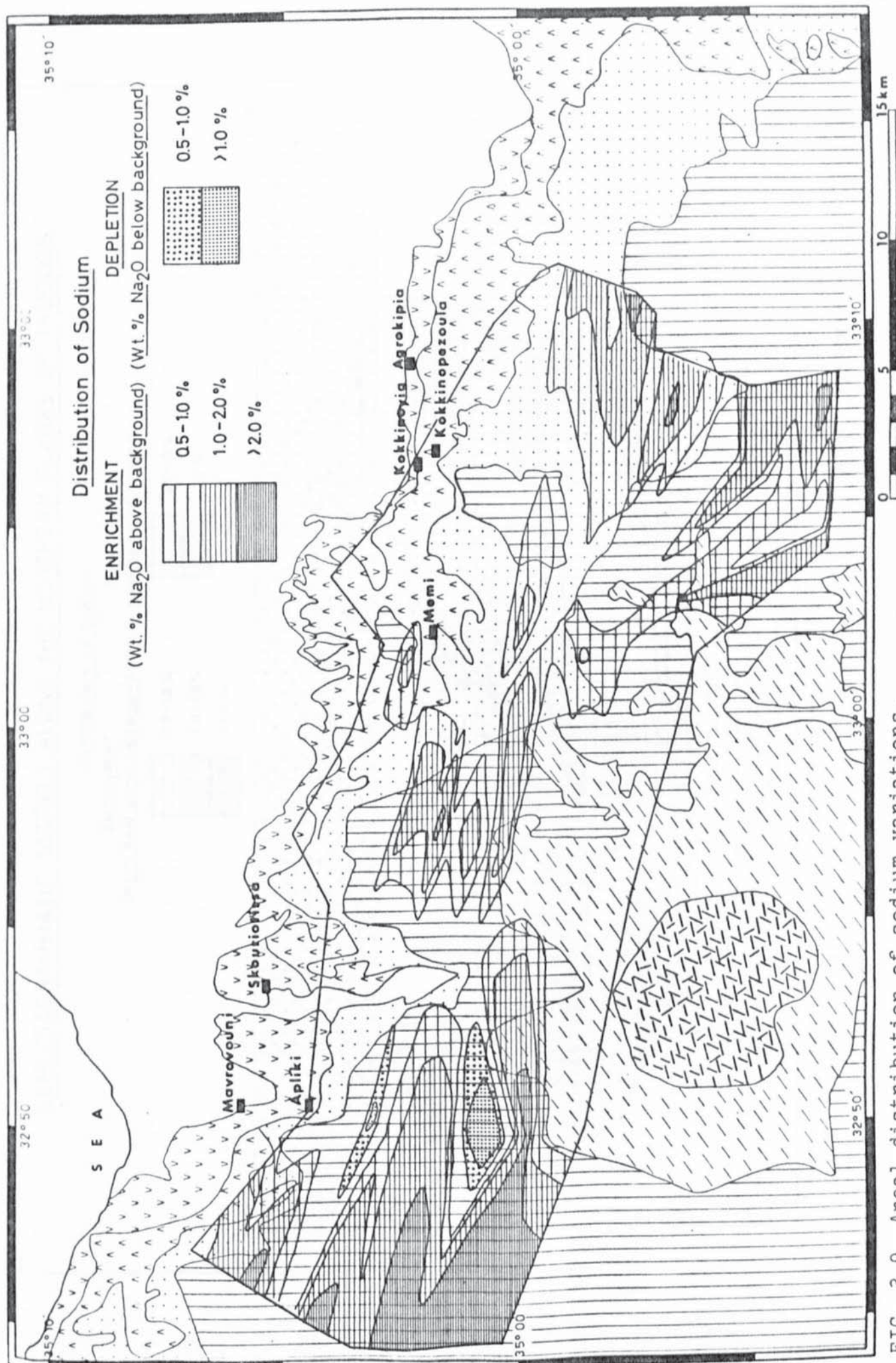


FIG. 3.9. Areal distribution of sodium variations.
Refer to p.88 for key to geological symbols.

SEMI-DIAGRAMMATIC SECTION ALONG THE NORTHERN FLANKS OF TROODOS

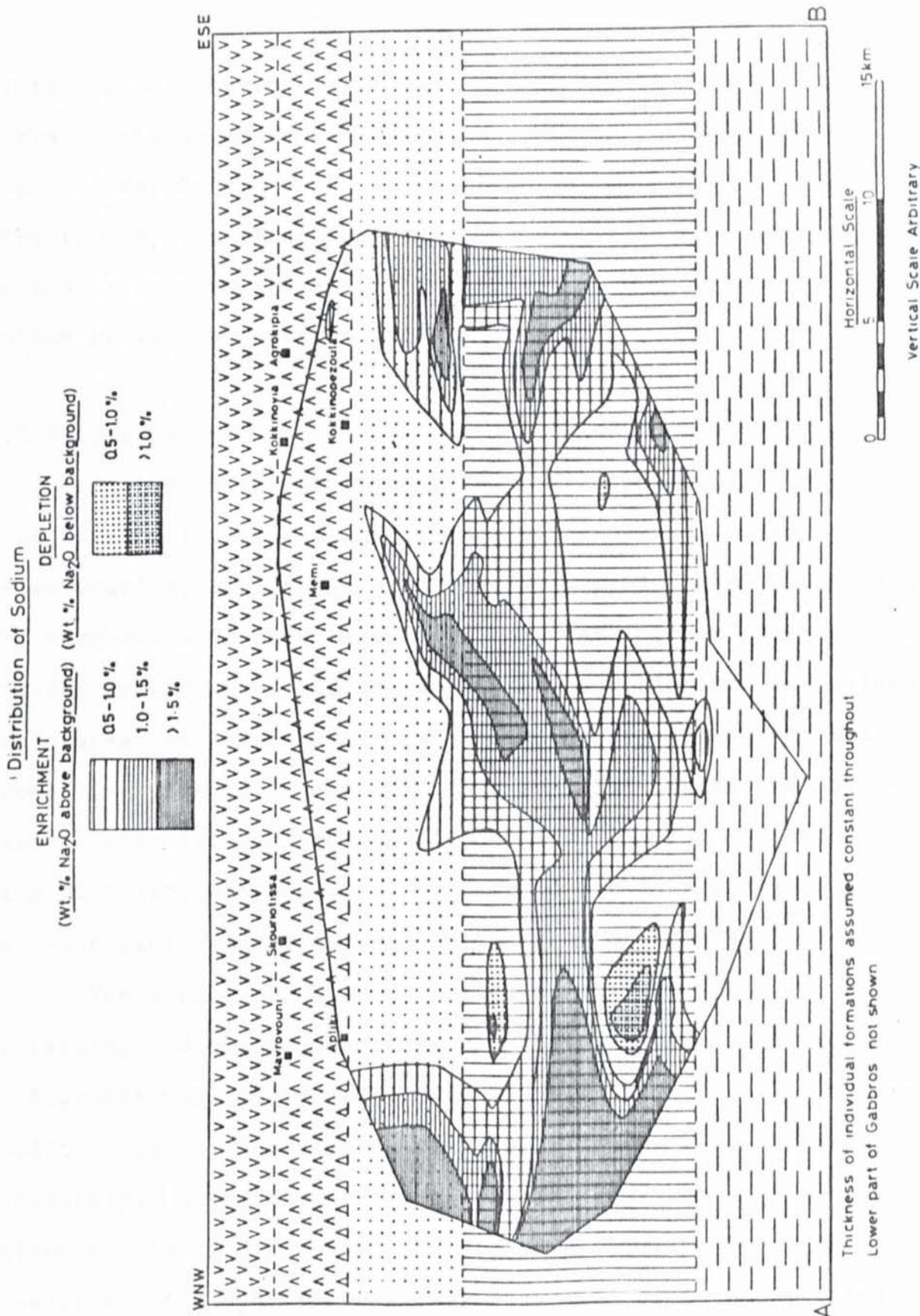


FIG. 3.10. Sodium variations with relation to igneous stratigraphy.

depleted pattern (relative to the areas remote from orebodies) appears to characterise the region underlying both the MAS and KAK group of deposits. This is suggestive of active feldspar destruction by the ascending hydrothermal fluids and leaching of alkalis, a process which is demonstrated in detail at sites of sulphide precipitation (chapter 5).

3.4.3.4. Silica

Silica increases linearly with fractionation (Fig. 3.11) in the Lower Pillow Lavas and gabbros but appears mobile in the Sheeted Complex. The pattern of stratigraphic variation (Fig. 3.12) suggests a leached pattern in the Basal Group between the two major groups of orebodies. A direct correlation is evident between areas enriched in magnesium and those leached of silica, by comparing figs 3.12 and 3.4. This is also suggested by the numerical calculations reported in section 3.5. The regions of the mining districts are enriched relative to the intermediate areas, this being particularly evident in the case of the MAS cell.

The direct decrease in silica solubility with decreasing temperature, and its independence of other dissolved components in the hydrothermal fluid (Holland, 1967) suggest that silica deposition may be correlated with decreasing temperature. The relationship, therefore, between silica enrichment and the location of mining districts is consistent with ascending and gradually cooling hydrothermal fluids as they rise to the sites of sulphide deposition.

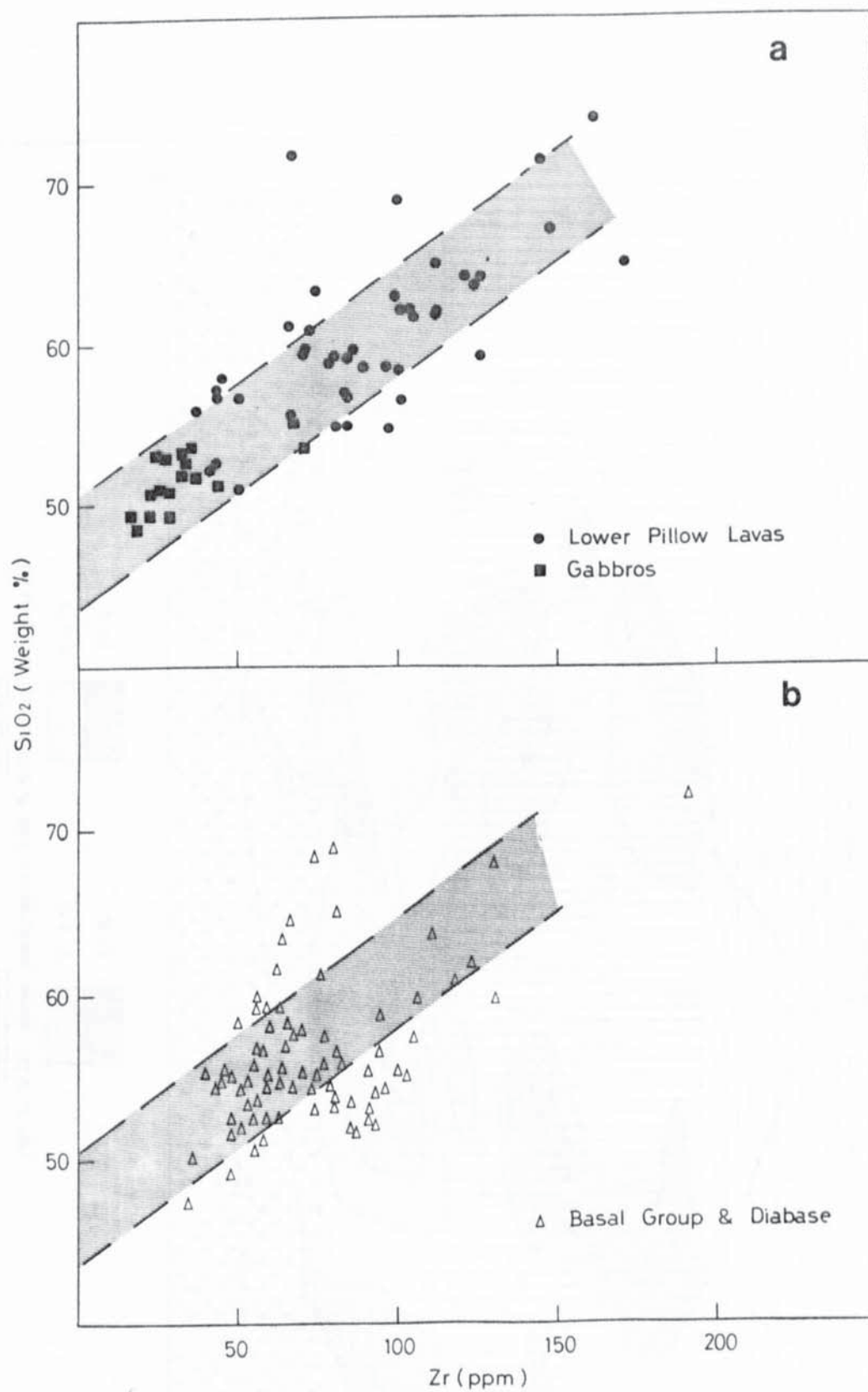


FIG. 3.11. SiO₂- Zr diagram for the Lower Pillow Lavas and gabbros (a) and the Sheeted Complex (b).

SEMI-DIAGRAMMATIC SECTION ALONG THE NORTHERN FLANKS OF TROODOS

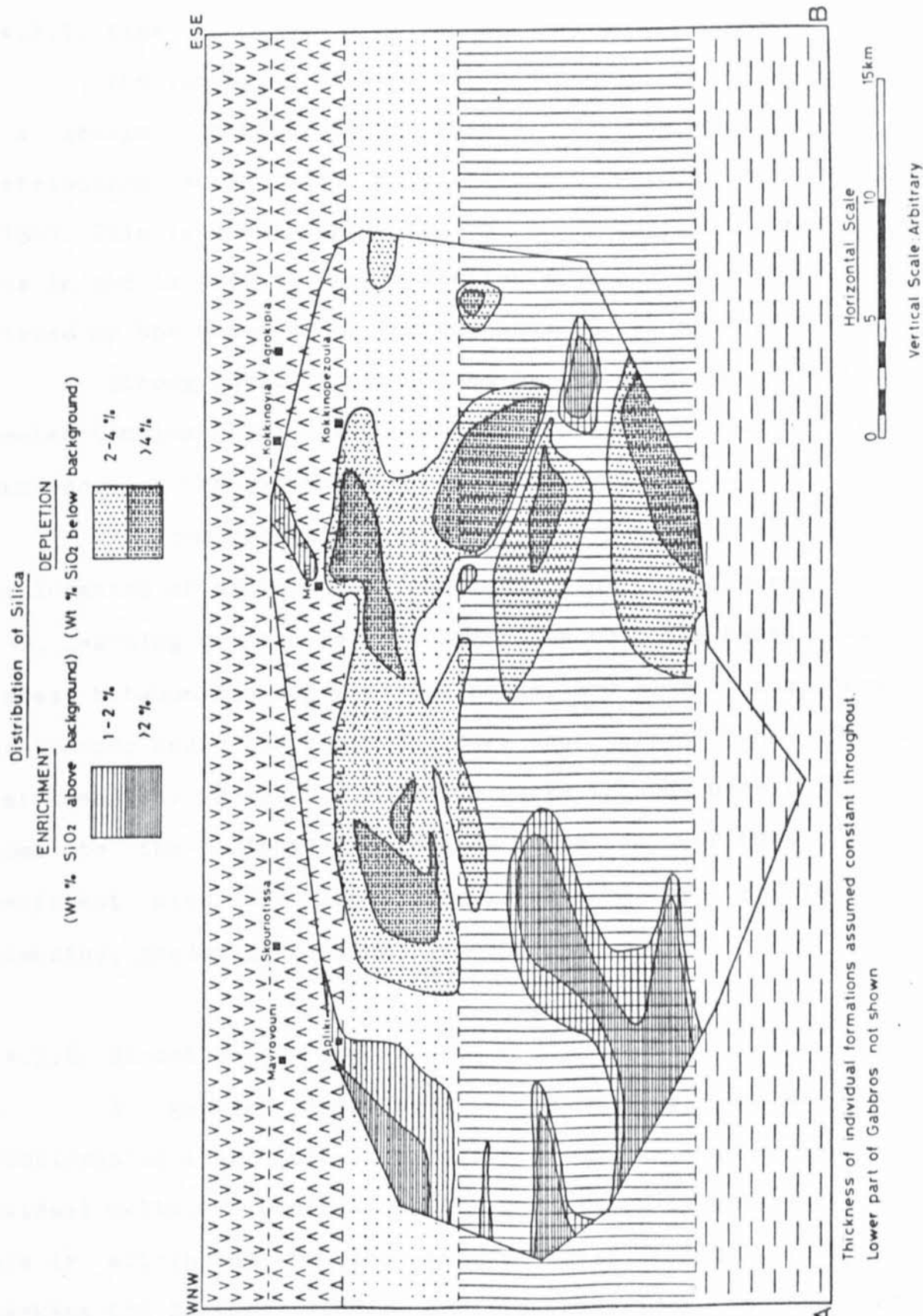


FIG. 3.12. Silica variations with relation to igneous stratigraphy.

3.4.3.5. Zinc

The variation of zinc with fractionation is characterised by a gentle increase in abundance, and a levelling of the distribution curve with more advanced crystallisation (Fig. 3.13a). This is consistent with the preferential entry of zinc ions in the lattice of ferromagnesian minerals only after this is dilated by the presence of ferrous ions (Goldschmidt, 1954).

Strong mobility, dominated by leaching, characterises the Sheeted Complex (Fig. 3.13b), in contrast to retention of original abundances in the gabbros and Lower Pillow Lavas.

A close relationship between areas of zinc enrichment and the location of mining districts is evident from figures 3.14 and 3.15. Leaching of zinc is most severe in both the Basal Group and Diabase between the major mining areas, and also at deep levels in the Diabase under the deposits: More than half of the originally contained zinc is leached from the rocks in some cases. The areas close to the sulphide orebodies show an enriched pattern, consistent with the local precipitation of sphalerite by ascending, gradually cooling hydrothermal fluids.

3.4.3.6. Strontium

A gentle increase in strontium abundance with fractionation (Fig. 3.16a) is consistent with its enrichment in residual melts, in contrast to the geochemically related calcium. This is attributed to the larger ionic radius of strontium (Rankama and Sahama, 1949). Erratic behaviour in the Sheeted Complex (Fig. 3.16b) is thought to be the result of breakdown of

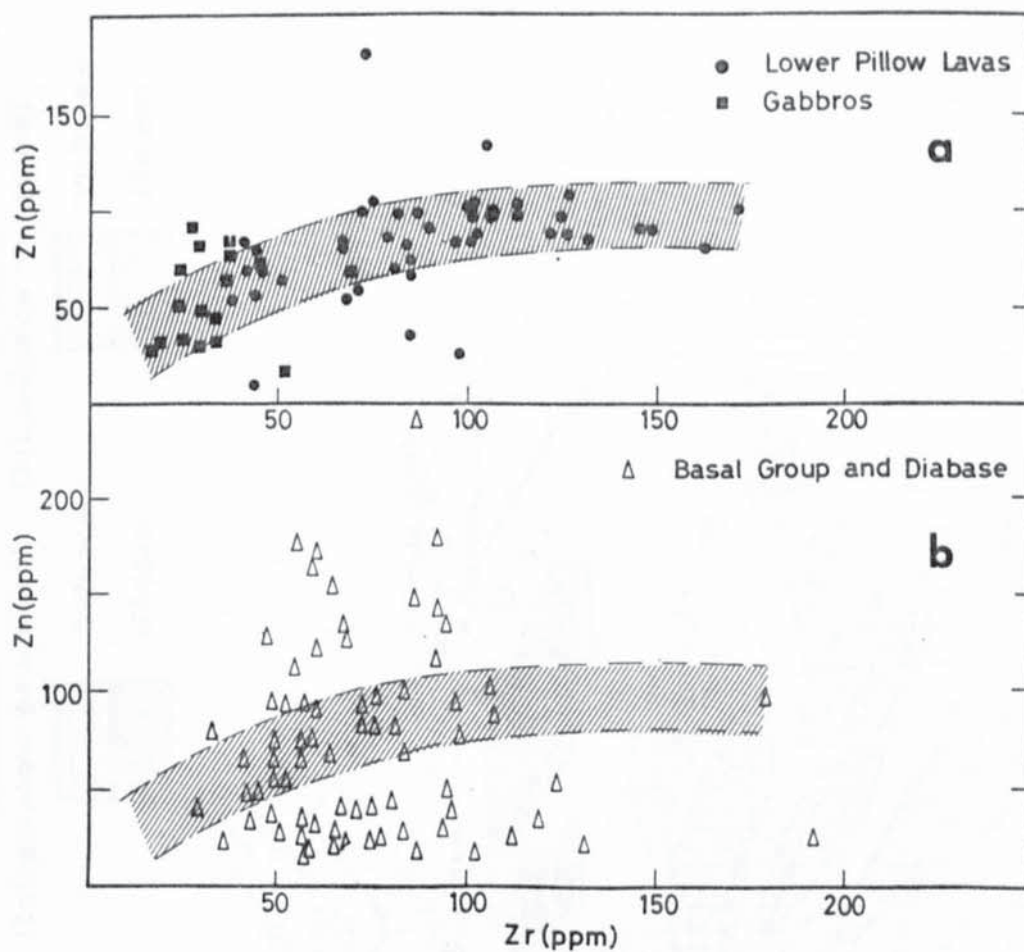


FIG. 3.13. Zn-Zr variations for the Lower Pillow Lavas and gabbros (a) and the Sheeted Complex (b). Note extreme mobility of zinc in the Sheeted Complex, mainly characterised by depleted pattern.



FIG. 3.14. Areal distribution of zinc variations.
Refer to p.88 for key to geological symbols.

SEMI-DIAGRAMMATIC SECTION ALONG THE NORTHERN FLANKS OF TROODOS

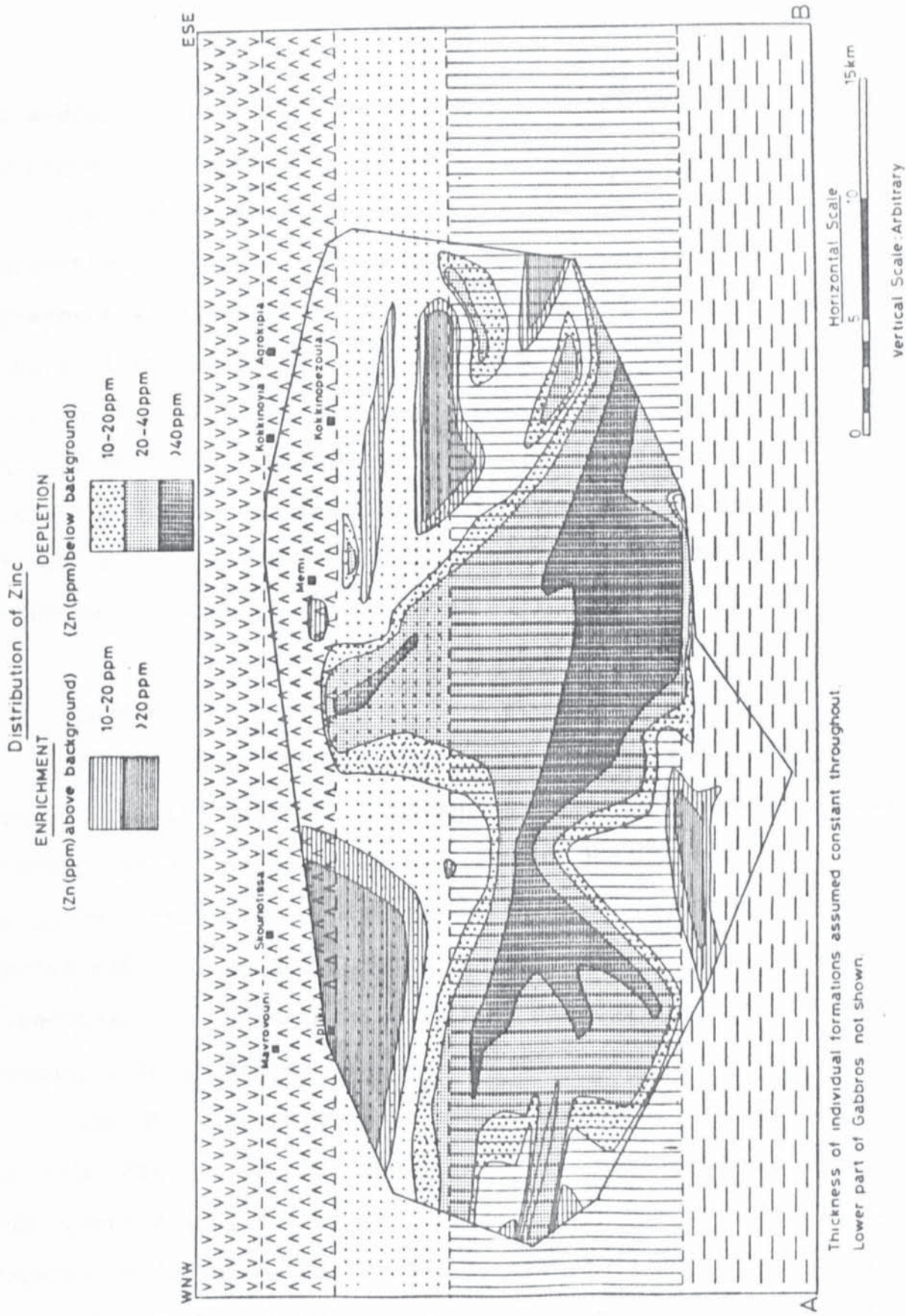


FIG. 3.15. Zinc variations with relation to igneous stratigraphy.

calcium-bearing minerals and liberation of strontium during hydrothermal metamorphism.

Strontium variation with stratigraphic level (Fig. 3.17) is suggestive of erratic behaviour, particularly in the Diabase, in agreement with the ready incorporation of this element in secondary minerals, particularly epidote. Its behaviour is most erratic in the region of the major mining areas, particularly the KAK group, which is dominated by a leached pattern. This probably reflects the action of ascending hydrothermal fluids, leaching strontium from the rocks, with local deposition along the hydrothermal conduits.

3.4.3.7. Barium

The feldspar structure is the most important habitat of barium and its liberation is dependent on feldspar-destructive reactions. Strong coherence in the gabbros and Lower Pillow Lavas (Fig. 3.18a) reflects retention of original abundance, while extensive mobility in the Sheeted Complex (Fig. 3.18b), dominated by leaching, is a reflection of plagioclase-transformative reactions, mainly related to albitisation.

The stratigraphic distribution of barium enrichments and depletions (Fig. 3.19) is suggestive of strong dependence of barium leaching and, therefore, extensive destruction of primary feldspars, on depth in the intrusive-extrusive section: The Basal Group in most part retains original abundance, or shows local enrichment, in contrast to the Diabase which is dominated by a leached pattern. No direct relationship between barium

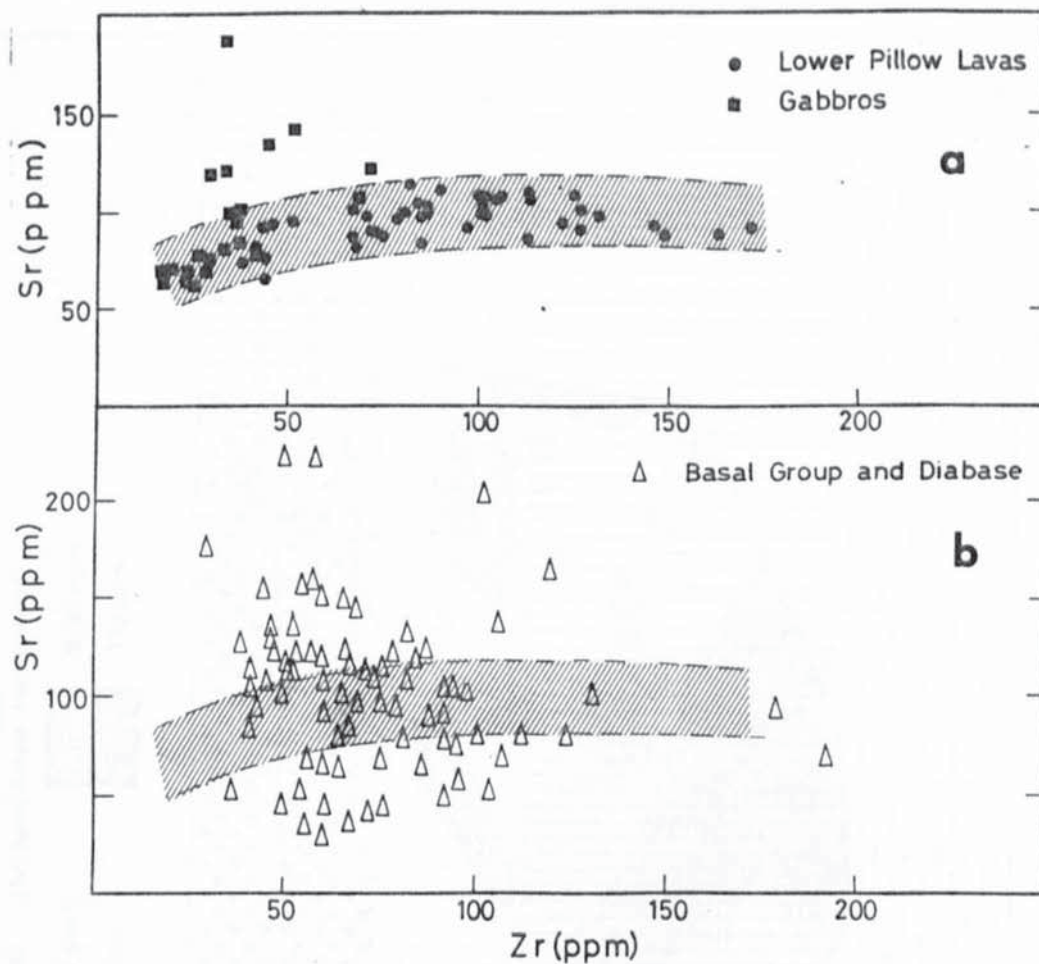


FIG. 3.16. Variation of strontium with zirconium as fractionation index. The diagram suggests retention of original abundance in the Lower Pillow Lavas and gabbros and extreme mobility in the Sheeted Complex.

SEMI-DIAGRAMMATIC SECTION ALONG THE NORTHERN FLANKS OF TROODOS

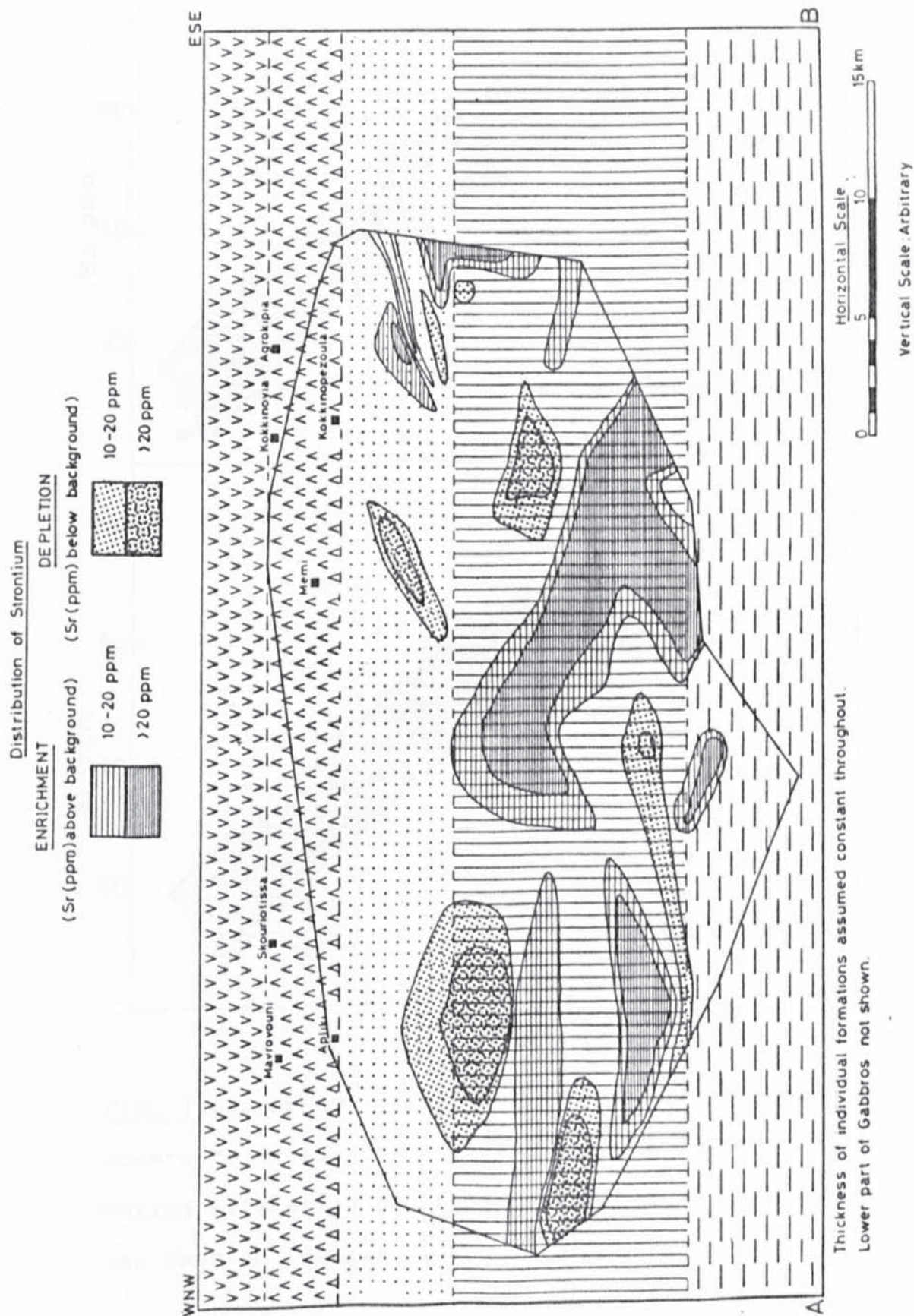


FIG. 3.17. Strontium variations with relation to igneous stratigraphy.

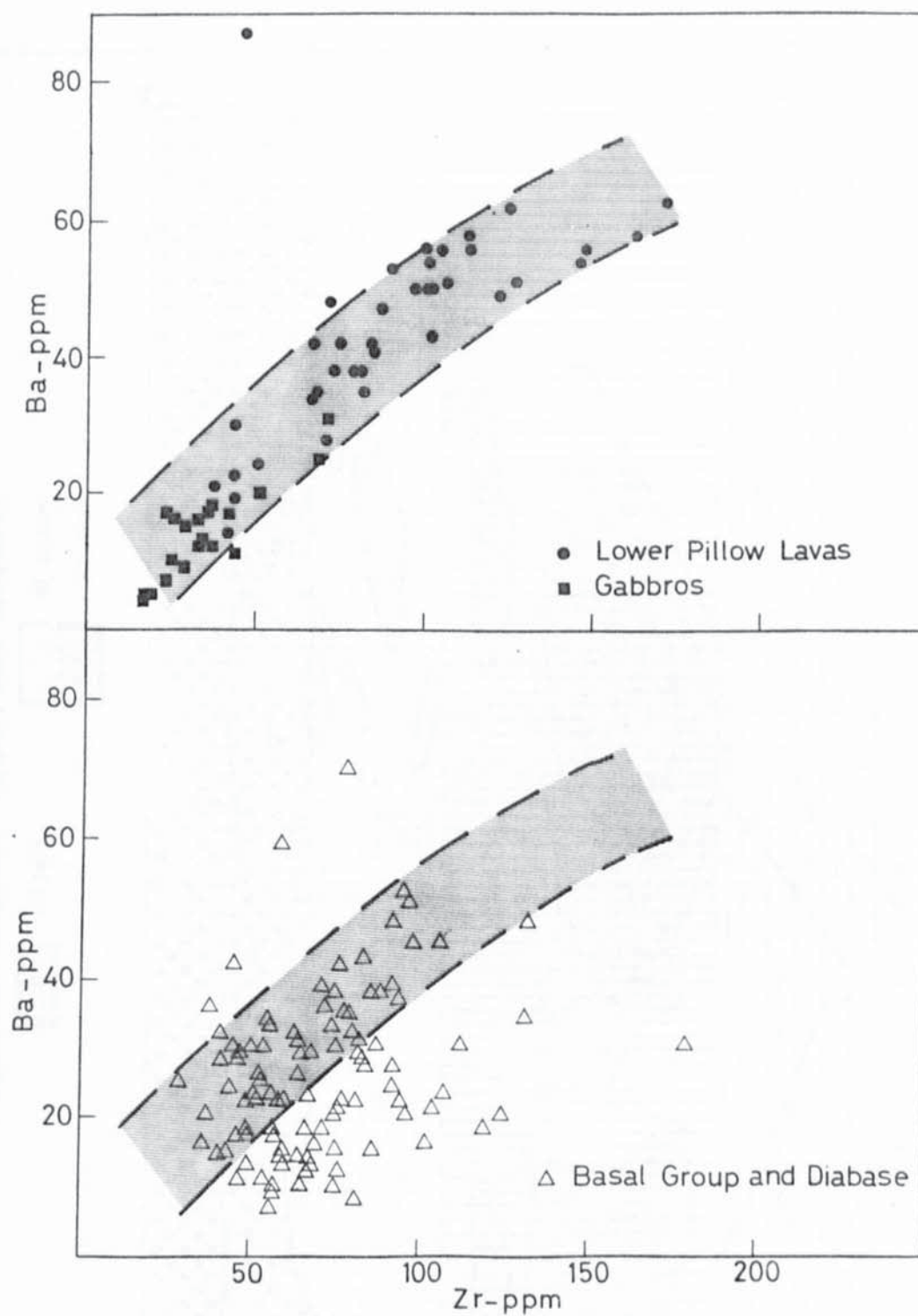


FIG. 3.18. Barium- zirconium variation. Strong coherence in the Lower Pillow Lavas and gabbros (a) during alteration contrasts with leached pattern in the Sheeted Complex (b).

SEMI-DIAGRAMMATIC SECTION ALONG THE NORTHERN FLANKS OF TROODOS

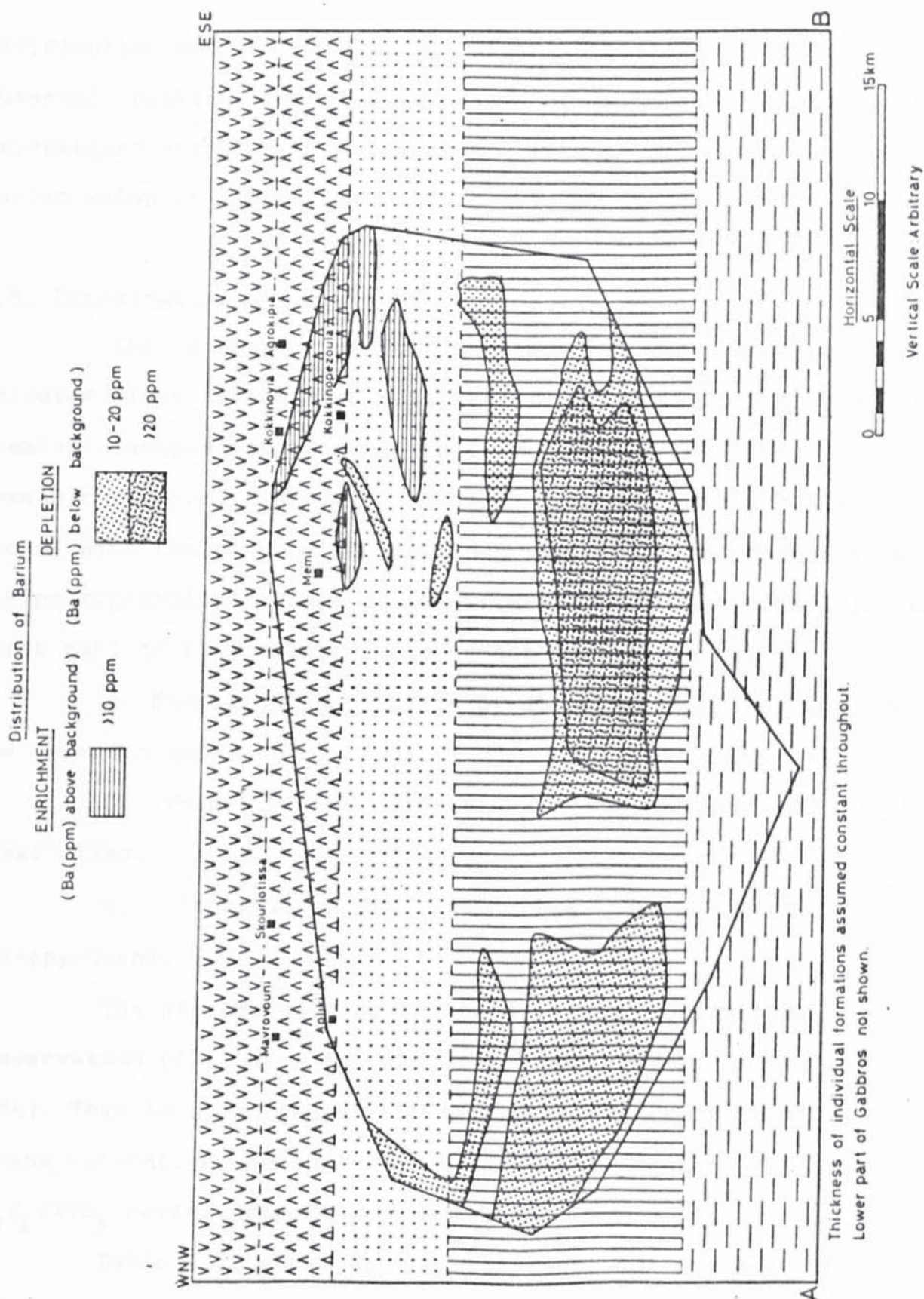


FIG. 3.19. Barium variations with relation to igneous stratigraphy.

distribution and the position of mining districts is apparent, the observed pattern being suggestive of generally limited and delocalised enrichment of the upper levels of the sequence by barium which is leached from lower levels.

3.5. Petrological calculations

The distribution of enrichments and depletions in selected elements has been described in preceding paragraphs. The chemical changes are examined in this section in the light of possible chemical reactions between seawater and the volcanic rocks, with the constraint that such reactions are consistent with the petrographic features of the alteration as described in the first part of this chapter. Such reactions relate to:

- a. Formation of chlorite by alteration of clinopyroxene and volcanic glass.
- b. Formation of albite by destruction of calcic plagioclase.
- c. Formation of actinolite by alteration of clinopyroxene.

The procedure to be followed in the calculations assumes preservation of alumina in the reactions (Lydon and Jamieson, 1984). This is supported by the strong coherence of this element during alteration, as suggested e.g. by the regular variation of $\text{Al}_2\text{O}_3/\text{TiO}_2$ ratios (Fig.2.12, Chapter 2).

Table 3.6. shows the compositions and sources of rocks and minerals used for the calculations. Based on these compositions the following reactions may be suggested:

TABLE 3.6. Compositions of minerals used in petrological calculations.

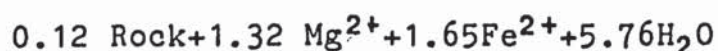
Actinolite composition in sample TR8-14: Si 7.584 Al 0.679
Mg 3.335 Fe 1.653 Ca 1.689 O 24 H 2.

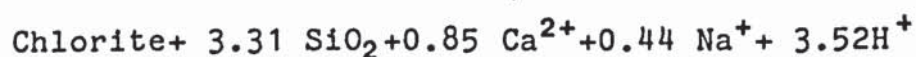
Clinopyroxene (Mean of several electron probe (EDS) analyses).
Si 1.914 Al 0.099 Fe 0.325 Mg 0.828 Ca 0.811 O 6.

Plagioclase composition (Mean of several electron probe
(EDS)analyses): Ca 2.0 Na 1.91 Al 5.69 Si 10.07.

Chlorite composition (After Lydon and Jamieson, 1984):
Mg 2.5 Fe 2.5 Al 2.0 Si 3.0 O 18 H 8.

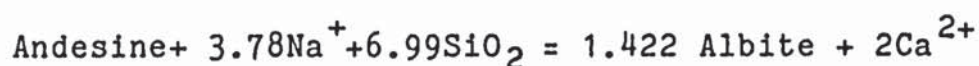
Average glass composition (Based on XRF results in appendix 1):
Si 53.5 Al 16.96 Mg 10.00 Fe 7.21 Na 3.69 O 160.



$$=$$


The above reaction suggests that chloritisation of the volcanic glass will result to the uptake of magnesium and iron and release of silica, calcium and sodium into the altering fluids, accompanied by a drop in pH. Enrichment of magnesium in the Basal Group, therefore, associated with depletion in silica and calcium, is concluded to be the result of chlorite and/or interlayered chlorite-smectite formation.

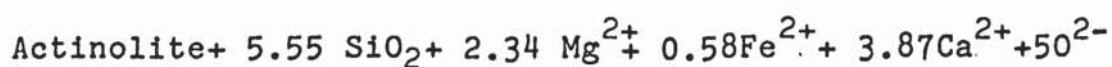
The conversion of plagioclase to albite may be expressed by the reaction:



The reaction is favoured by the presence of sodium and silica in the altering fluids and results to the release of calcium ions. High silica activity is, therefore, a pre-requisite, and this suggests that albitisation will preferentially take place by the action of fluids which had been enriched in silica, e.g. by chloritisation.

Formation of actinolite may be related to hydrolysis of clinopyroxene, as suggested from the reaction:



$$=$$


Formation of actinolite from clinopyroxene, therefore, results to the release of silica, magnesium, iron and calcium and increase in $f\text{O}_2$. It may be speculated that magnesium and iron are

used in the formation of further chlorite by alteration of glass, while silica and calcium are released into the altering fluids.

3.6. Numerical calculations and elemental fluxes

In addition to the graphical technique for the quantitative estimation of chemical changes, correlation coefficients and regression equations were determined for pairs of elements in the Gabbros and Lower Pillow Lavas for the purpose of establishing net element fluxes in the rocks of the Sheeted Complex. The results are shown in Tables 3.7. and 3.8.

Strong correlations with zirconium are obtained for SiO_2 , MgO , CaO and Na_2O and the derived linear regression equations were directly applied in the establishment of enrichments and depletions in the Sheeted Complex. A marked absence of linear relationship is apparent in strontium and zinc variations, which contrasts with their evident variation with differentiation. Equations for these elements were determined graphically.

For strontium the equation which accurately fits the distribution curve is: $\text{Sr} = 30.61 \text{ LogZr} + 30$. For zinc, the respective equation is: $\text{Zn} = -0.00527\text{Zr}^2 + 1.3433\text{Zr} + 14$.

Utilising the derived equations, the chemical changes in the Sheeted Complex were determined:

Silica shows net depletion of 2.04 %,

Magnesium shows net enrichment of 1.04 %,

Calcium shows a net depletion of 1.96 %,

Sodium shows a net enrichment of 1.25 %,

Strontium shows a net enrichment of 12.48 ppm,

Zinc shows a net depletion of 11.43 ppm,
Barium shows a net depletion of 9.69 ppm.

Based on the above calculations, the net chemical changes in the Sheeted Complex were estimated per cubic kilometer of altered rock (2.5×10^9 tons). It is estimated that the combined thickness of the Basal Group and Diabase is in the range of 1.5 km, whereas the total length of the examined section of northern Troodos is approximately 50 km. It is further assumed that formation of the deposits enclosed within the section and any that have been removed or are concealed beneath post-ore lavas and sediments is the result of intrusion of high level magma chambers which were oriented parallel to the axis and whose length was in the range of 10 km. Both these assumptions are based on the distribution of chemical changes, in association with the dominant northerly trend of the diabase dykes. The volume of rock represented by the above parameters is 750 cubic km, and the components added or removed from this volume are:

38.2×10^9 tons SiO_2 leached from the rocks,
 19.5×10^9 tons MgO added,
 36.8×10^9 tons CaO leached,
 23.5×10^9 tons Na_2O added,
 23.4×10^6 tons Sr added,
 21.4×10^6 tons Zn leached,
 18.2×10^6 tons Ba leached.

If the zinc content of the lavas is considered to be of

TABLE 3.7. Correlation coefficients and regression equations for gabbroic rocks.*

Element pair	A	B	R
SiO ₂ -Zr	47.946	0.108	0.761
Al ₂ O ₃ -Zr	19.132	-0.079	-0.522
TiO ₂ -Zr	-0.246	0.022	0.882
Fe ₂ O ₃ -Zr	6.815	0.065	0.503
MnO-Zr	0.145	-0.000	-0.053
MgO-Zr	11.045	-0.055	-0.490
CaO-Zr	17.430	-0.149	-0.823
Na ₂ O-Zr	0.220	0.038	0.853
K ₂ O-Zr	-0.044	0.005	0.599
P ₂ O ₅	-0.032	0.002	0.894
Sr-Zr	50.479	1.089	0.687
Rb-Zr	0.532	0.035	0.503
Zn-Zr	49.925	-0.069	-0.047
Ba-Zr	-4.563	0.573	0.897
* A and B represent the constants in the linear regression equation $Y = A + Bx$. R is the correlation coefficient.			

TABLE 3.8. Correlation coefficients and regression equations for the Lower Pillow Lavas.*

Element pair	A	B	R
SiO ₂ -Zr	0.822	49.955	0.110
TiO ₂ -Zr	0.265	0.886	0.003
Al ₂ O ₃ -Zr	-0.407	14.305	-0.008
Fe ₂ O ₃ -Zr	-0.562	12.094	-0.026
MnO-Zr	-0.175	0.164	0.000
MgO-Zr	-0.836	9.730	-0.052
CaO-Zr	-0.786	11.653	-0.057
Na ₂ O-Zr	0.842	0.697	0.023
K ₂ O-Zr	-0.212	0.751	-0.002
P ₂ O ₅ -Zr	0.866	0.021	0.001
CaO-MgO	0.668	2.560	0.780
CaO-SiO ₂	-0.762	31.056	-0.410
MgO-SiO ₂	-0.818	27.598	-0.377
Sr-Zr	0.368	83.361	0.118
Rb-Zr	-0.298	20.313	-0.102
Zn-Zr	0.376	61.935	0.273
Ba-Zr	0.615	21.475	0.254

*R is the correlation coefficient.

A and B represent the constants in the linear regression equation $Y = A + Bx$.

the same order of magnitude as the copper content, a calculation of the tonnages and grades of the deposits enclosed in the examined area suggests that less than one million tons of copper metal is contained in the orebodies, out of the 20 million tons which were leached from the rocks. If the same amount of metal is contained in the much more extensive, but poorer, stockwork zones which underlie the deposits, only 7 % of the copper removed from the rocks is enough to account for it. The remaining 93 % was either dissipated into seawater or partly used in the formation of further orebodies.

The zinc content of the Cyprus orebodies, with rare exceptions (cf. Kinousa orebody, chapter 5) is generally low and erratic. The calculations cited above suggest that this low content is attributable to non precipitation at the discharge sites than to absence of zinc from the hydrothermal fluids.

Particularly noteworthy, with reference to the above calculations, is the fact that barium, depleted from the rocks by the same amount as zinc, is completely absent from the sulphide deposits, although barytes has been identified in small amounts as a vein-filling mineral in the unmineralized lavas surrounding orebodies, as e.g. at Memi mine (chapter 6).

Quartz is a universal gangue mineral in the sulphide deposits, and hematitic jaspers are commonly found in the lava sequence, particularly close to the orebodies. However, the amount of silica estimated to have been leached from the Sheeted Complex is several orders of magnitude larger than that contained in the stockwork zones of the orebodies. Similar arguments apply for

calcium which is, additionally, removed from the ore zones.

A full discussion of the chemical changes accompanying rock-hydrothermal fluid interaction at discharge sites will be presented in chapter 6. The implications of the data as presented in the preceding paragraphs are:

1. An amount of zinc metal far greater than that deposited within the ore zones is dispersed into seawater at discharge sites.

2. The discharge sites are major sources of silica, calcium and barium.

3. Strontium, magnesium and sodium are enriched in the rocks by the circulating fluids. The amount of magnesium and sodium added is of the same order of magnitude as the amount of calcium and silica removed.

All the above inferences are directly comparable to observations on elemental fluxes at the proximity of spreading axes. These suggest that oceanic ridges, as e.g. the Galapagos spreading axis (Edmond et al., 1979) are major sources of calcium, silica, barium and rubidium and major sinks of magnesium. The behaviour of strontium is inconclusive (Edmond et al., op. cit.), since its content in exiting fluids is indistinguishable from ambient seawater.

It may be speculated that the enrichment of the umbers and the overlying radiolarites in metallic and other elements (Robertson, 1977) is related to the same period of hydrothermal activity which resulted to the formation of the sulphide deposits. Typical chemical compositions of these precipitates are presented

in Table 3.9. Their thickness is highly variable from 0-30 metres (Robertson and Hudson, 1974) and an average thickness of 2 metres may be considered reasonable. Based on these data, and assuming that the area examined was completely covered by these sediments (500 sq. km), the following amounts of elements were deposited:

1.5x10⁹ tons silica,
1.27x10⁶ tons barium,
1.14x10⁶ tons zinc,
2.60x10⁶ tons copper,
15x10⁶ tons calcium oxide.

These order of magnitude calculations are close to the amounts leached from the Sheeted Complex, despite the numerous inponderables associated. In particular, fixation of barium in the rocks surrounding the sulphide deposits, the dissipation of elements to much greater distances than the narrow regime of hydrothermal exhalation and the partition into seawater. Relevant to the last factor is the fact that zinc is contained in the radiolarites in almost equal amounts as in the umbers, suggesting long retention into seawater, in contrast to the rapid deposition of copper.

Iron and manganese are the two notable absentees from the above calculations. Examination of these elements was hampered by the analytical technique used (XRF) which did not permit the estimation of exact contents of the three dominant iron phases (FeO, Fe₂O₃, FeS₂) and hence quantitative variations in abundance. Manganese was similarly found to be too mobile, even in the unaltered lavas for the definition of original compositional

TABLE 3.9. Chemical analyses of umbers and radiolarites¹.

Wt. %	1	2	3	4	5	6	7
SiO ₂	25.09	8.93	20.73	30.89	57.13	65.46	82.64
TiO ₂	0.23	0.20	0.26	0.32	0.12	0.12	0.11
Al ₂ O ₃	4.19	2.69	5.75	5.43	1.30	1.43	0.90
Fe ₂ O ₃	51.92	56.16	43.53	43.56	23.23	20.31	10.12
FeO	0.00	0.00	0.00	0.00	0.00	0.00	0.00
MnO ₂	0.43	17.04	9.79	1.40	8.22	4.90	2.80
MgO	1.61	1.51	1.60	1.91	0.29	0.43	0.09
CaO	0.74	0.80	1.37	0.50	0.97	0.76	0.13
Na ₂ O	0.08	0.32	0.57	0.23	0.16	0.13	0.11
K ₂ O	0.26	0.42	0.52	1.31	0.19	0.17	0.05
P ₂ O ₅	0.43	0.67	0.37	0.64	0.25	0.57	0.09
H ₂ O ⁺	8.68	7.94	8.70	7.29	5.77	4.70	2.35
H ₂ O ⁻	4.75	2.78	5.87	5.28	2.50	1.79	0.80
CO ₂	0.45	0.59	0.29	0.10	0.55	0.10	0.54
Averages of partial chemical analyses of umbers and radiolarites ² .							
	Ba		Cu		Zn		
Umbur	427		897		235		
Radiolarite	80		142		222		

¹ Analyses 1-6 represent umbers from various parts of the island.
Analysis 7 is a black radiolarite. All analyses from Pantazis (1973).
² After Robertson and Hudson (1974)

range. It may be inferred, however, from the evidence of mobility of other components, that enrichment of Fe and Mn in the hydrothermal fluids takes place. The total iron content, however, is probably buffered by saturation with respect to an iron bearing mineral such as pyrite. This is suggested from the abundant presence of pyritic disseminations in the Sheeted Complex and further supported from the low iron content of hydrothermal fluids in similar environments (Lydon, 1983). The absence of manganese minerals in the Sheeted Complex, on the other hand, suggests that manganese is not precipitated during ascent and is finally liberated into seawater. By comparison with modern day analogues (Haymon, 1982) it may be inferred that precipitation at sites of sulphide deposition is prohibited by the sluggishness of oxidation of Mn^{2+} to Mn^{4+} .

Another exception in the calculation of elemental fluxes is calcium. The amount leached by the hydrothermal fluids is comparable to the amount of silica, while amount deposited in the umbers and radiolarites is 2500 times less. The low CaO content of these precipitates is interpreted as due to retention in solution, umber deposition probably having taken place below carbonate compensation depths (Robertson and Hudson, 1974).

3.7. Discussion and proposed hydrothermal model

A review of field and experimental evidence on seawater-rock interaction and comparison with the chemical and mineralogical characteristics of the alteration in the Troodos ophiolite suggest that the postulation of a model of seawater

circulation in the genesis of the sulphide deposits is well founded. Established fluxes for several elements are sufficient to account for the metal content of the deposits as well as for dispersion into seawater at discharge sites. Order of magnitude calculations suggest that, even in the case that the amount of zinc contained in the sulphide deposits was comparable to the copper content, less than 10 % of the zinc leached from the Sheeted Complex is precipitated at discharge sites. The amount of silica and calcium removed is more than 1000 times greater and comparable amounts of sodium and magnesium are added during hydrothermal alteration.

The deduced patterns of distribution of enrichments and depletions are also compatible with a model of large scale hydrothermal circulation and mass transfer. This is mainly inferred from the direct relationships of alteration patterns and the location of major mining districts, and suggests that the clusters of deposits within these districts are contemporaneous and not the result of a specific cell of hydrothermal circulation for each individual deposit as previously argued (Spooner, 1977).

Magma chambers intruded at high levels in the crust have been invoked as the promoters of hydrothermal circulation in the formation of the sulphide deposits of Oman ophiolite (Alabaster, 1982). These chambers may be traced from the distribution of cone sheets and specific chambers for individual deposits outlined. A comparable situation to the rhyolite domes associated with the Japanese Kuroko deposits (Franklin et al., 1981) may be envisaged. By comparison, large scale chambers, or groups of smaller

chambers, of the order of 10-15 km in length are probably responsible for the formation of the MAS and KAK groups of deposits. Evidence for the presence of such large scale chambers is now sought in the ophiolite (Stillman, pers. com., 1983). The distribution of geochemical anomalies, in correlation with the northerly trend of the dykes in the Sheeted Complex suggest that these will be dominantly oriented in a north-south direction.

The essential features of a hydrothermal system, as reviewed in the literature (Gibson et al, 1983) are:

1. Heat source for the promotion of circulation,
2. Aquifer to transfer solution,
3. An overlying impermeable caprock,
4. Channelways for recharge and discharge.

The heat source is determined from the above discussion to be high level chambers. A potential aquifer for the storing of hydrothermal solution is the Sheeted Complex. This is concluded from the major chemical and mineralogical changes which accompany hydrothermal metamorphism of this formation, as contrasted to the lack of pervasive alteration in either the Gabbros or the Lower Pillow Lavas. Conditions within the aquifer, prior to the intrusion of high level chambers, may be speculated by observation of the chemical changes with stratigraphic level as suggested by the area between the two mining districts:

a. Magnesium is dominantly enriched in the higher parts of the aquifer by processes of intense chloritisation. Silica, calcium and zinc are depleted.

b. Barium leaching is characteristic of the lower levels

of the aquifer, related to feldspar destruction by albite-oligoclase formation.

3. Zinc is more strongly leached at lower than at higher levels of the aquifer: More than 50 % of contained zinc is removed from the base of the sheeted dykes in some cases.

The above suggest a zonal arrangement of the alteration within the aquifer, with chloritisation dominating higher levels and feldspar transformation reactions being particularly effective at lower levels. The absence of evidence for magnesium enrichment in the deeper levels is compatible with alteration by waters which had been depleted of contained magnesium, and therefore of deep penetration of "reacted" waters to low levels in the Sheeted Complex.

The significance of water:rock ratio (i.e. the ratio of the volume of water reacting with the rocks over the volume of altered rock) in the alteration assemblages has been treated by Seyfried et al. (1978) with the conclusion that high ratios favour the formation of abundant chlorite and smectite and low ratios favour formation of albite and actinolite. It may be speculated that alteration at high levels in the Sheeted Complex was characterised by the ingress of large amounts of seawater, as a result of the high porosity of this pillow-dominated sequence, with the aquifer finally sealed by the formation of secondary minerals, so that alteration at deeper levels proceeded at low W:R ratios. These ratios may be estimated based on the assumption that all magnesium contained in seawater is removed by reaction with the rocks (Mottl, 1983), and the further assumption that no

significant uptake of magnesium takes place prior to the pervasive interaction in the Sheeted Complex. The net enrichment in magnesium (1.04 % MgO) is approximately 5 times the content of seawater (0.22 % MgO), suggesting that a minimum W:R ratio of 5:1 is associated with the hydrothermal metamorphism of the Sheeted Complex. These ratios, however, vary strongly with stratigraphic level. The Basal group shows enrichment of almost 6 % MgO in some cases, corresponding to ratios of 30:1 in the dykes of the sequence, with probably much higher ratios in pillows, which were not sampled. The Diabase, showing background values and local depletions, is altered under much lower ratios, probably less than 1.

Alteration under low W:R ratios is probably a necessary pre-requisite for the concentration of metals in solution (Lydon, 1983). The metals are contained in the rocks as diadochic substitutions for essential elements. They are only released into solution by breakdown of the original host into its alteration products. Equilibrium, therefore, between the fluids and the alteration minerals must first be attained before significant metal can enter solution. This can best be effected in a stagnant reservoir which allows the heating of the fluids in response to the geothermal gradient.

Whether the components entering the solution by the alteration reactions will finally be removed at discharge sites depends on the behaviour of these elements to changing physicochemical parameters and, also, on the partition coefficient between the leachate and the secondary minerals (Lydon, op. cit.).

The overall strontium enrichment in the Sheeted Complex, e.g., suggests that partitioning of strontium into secondary minerals, such as epidote, is greater than into the altering fluids. By contrast, barium is universally depleted since the solubility of barytes is strongly dependent on the concentration of sulphate in solution (Holland, 1967). The reducing conditions within the Sheeted Complex, indicated by the dominance of pyrite, prohibit the precipitation of barytes within the reservoir zone.

Following the above discussion, a hydrothermal model may be proposed for the generation of ore solutions by interaction of heated seawater with the rocks of the Sheeted Complex (Fig. 3.20).

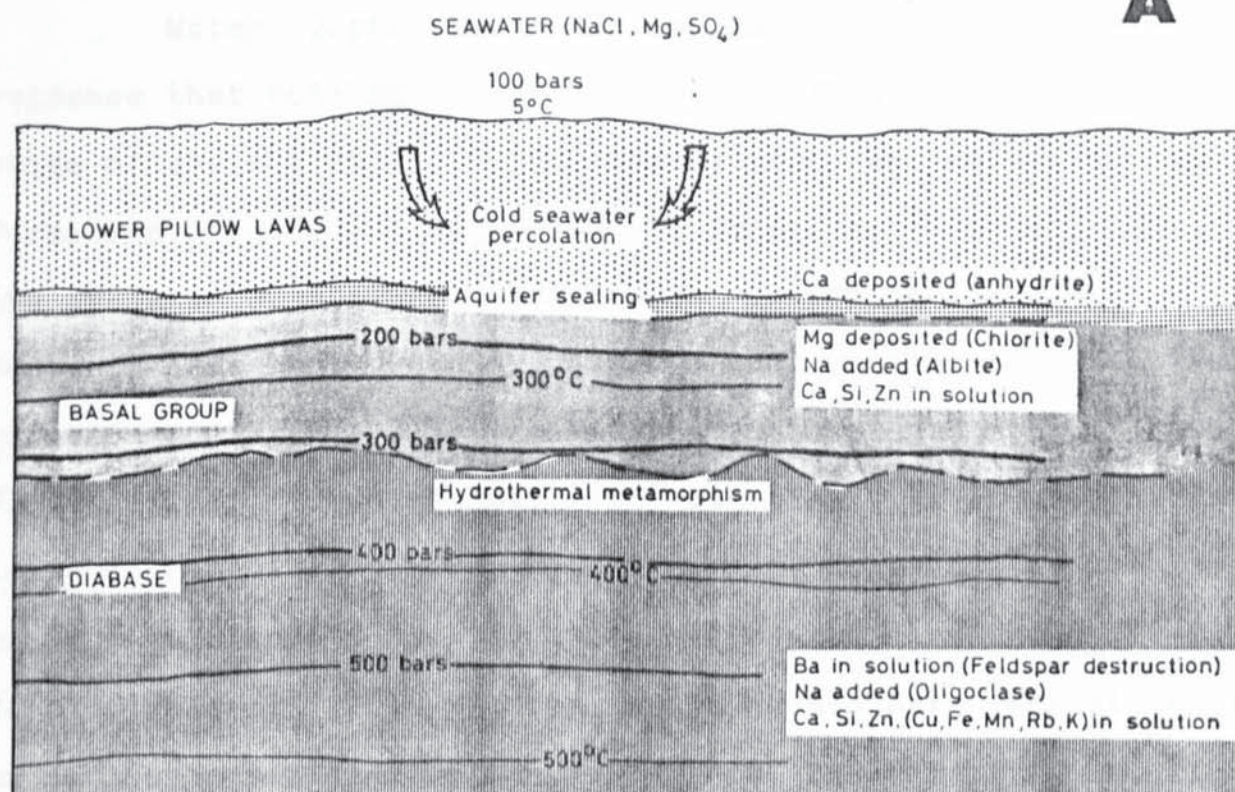
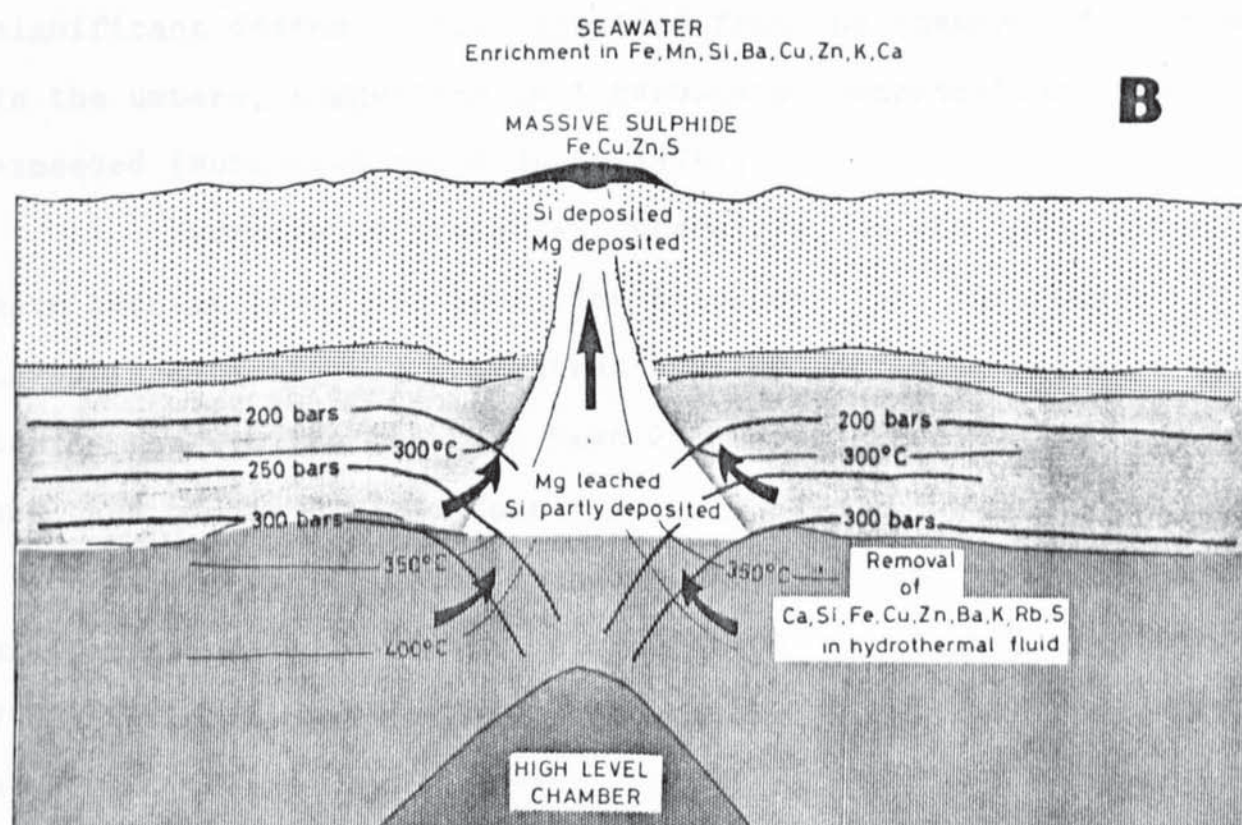
Low temperature alteration of the lavas by cold seawater is believed to start directly after extrusion. Such alteration, associated with the formation of smectites and zeolites in fractures and open spaces, probably prohibits the development of marked geothermal gradients in the region of the spreading axis (Mottl, 1983), as suggested from the lack of pervasive alteration in drill holes on the ocean floor (Cann, 1979) and from the similar lack of pervasive alteration in the Troodos pillow lavas.

It has been concluded in chapter 2 that formation of the Sheeted Complex and Lower Pillow Lavas was completed within the narrow regime of the spreading axis, while extrusion of the Upper Pillow Lavas is considered to have taken place at the flanks of the axis. Sealing of the system, therefore, by formation of secondary minerals, took place as the newly formed oceanic crust was moving towards the flanks. This resulted to the development of lithostatic pressure gradients in a closed system, which also

FIG. 3.20. Proposed model of hydrothermal metamorphism and mineralization in the ophiolite.

Percolation of seawater through fractures and open spaces (A) as the crust moves from the axis towards the flanks results to formation of zeolites, smectite and anhydrite. Sealing of the system by secondary minerals allows heating of the rocks under the influence of geothermal gradients. The inter-pore fluids become enriched in metallic and other elements which are leached from the rocks by destruction of primary igneous minerals.

Intrusion of magma to high levels (B) creates a high temperature, low pressure regime and causes the movement of the metal-enriched fluids to higher levels. These fluids are responsible for the formation of massive sulphide deposits on the sea floor and enrichment of seawater in various elements which are later incorporated in the umbers. The latter are not shown on the diagram, nor are the Upper Pillow Lavas which are thought to be the extrusive products of these high level magma chambers.

A**B**

Drawn by N. G. Adamides

permitted the heating of the fluids.

Water depths may be estimated from the absence of evidence that boiling of the hydrothermal fluids occurred at any stage of their history. Such evidence would be reflected in the formation of abundant salt with the sulphides (Ridge, 1973) and the presence of abnormal salinities in fluid inclusions. Such features have not been recorded, and fluids from inclusions (Spooner and Bray, 1977) exhibit salinities identical to seawater. Fluid inclusion studies have, in addition, given estimates of temperatures of formation of the sulphide deposits in the region of 300° C. Based on this evidence, it may be estimated from the data of Haas (1971) that water depths should have been at least 1 km for suppression of boiling at 300° C, and almost 2 km if the fluids exited with temperatures of 350° C. Indirect evidence for significant depths is also provided from the absence of carbonate in the umbers, suggesting that carbonate compensation depth was exceeded (Robertson and Hudson, 1974).

Hydrostatic pressures, therefore, on the sea floor may have been at least 100 bars. The thickness of the Lower Pillow Lavas is estimated at 500 metres and the confining pressure at the top of the aquifer may have been 250 bars, reaching 700 bars at the base of the Sheeted Complex.

The formation of abundant chlorite at the top of the aquifer suggests temperatures of $250-300^{\circ}$ C (Stakes and O'Neal, 1982) while the base of the Sheeted Complex may have been altered at 450° C (Heaton and Sheppard, 1977).

Based on the above estimates, the confined aquifer and

the compositions of inter pore fluids are shown in fig. 3.20a.

The intrusion of magma at high levels and into the originally stagnant reservoir (Fig. 3.20b) creates a high-temperature, low-pressure region resulting to the removal of the metal-enriched fluids and their transportation to higher levels in the ophiolite. The creation of low pressures above the chamber was probably aided by the re-opening of old zones of weakness by the intrusive pressure, or the development of new fractures and the change from originally lithostatic to hydrostatic conditions.

PART 2

CHAPTER 4

The volcanogenic sulphide deposits

General introduction and previous studies.

4.1. Introduction

The first part of this work was concerned with petrological, chemical and hydrothermal processes in the ophiolite in general. The main conclusions derived may be summarised as follows:

1. Formation of the whole ophiolite at a spreading regime located above a subduction zone by the intense partial melting of mantle which was depleted by previous episodes of magma extraction.

2. Formation of the Sheeted Complex and the lower part of the Lower Pillow Lavas directly at, or close to, the spreading axis.

3. Extrusion of the higher members of the Lower Pillow Lavas and all of the Upper Pillow Lavas at the flanks of the spreading axis.

4. The petrological contrast between the lower, chemically evolved members of the ophiolite and the upper, primitive members, is attributed to fractional crystallisation processes consequent upon the two contrasting tectonic regimes, i.e. the axial and flanking parts of the spreading axis.

The hydrothermal metamorphism of the ophiolite was examined in chapter 3 with particular emphasis on the evidence of

mobilisation of components by processes of water- rock interaction. It was concluded that patterns of geochemical changes for a number of elements are directly comparable with experimental evidence. Derived fluxes are qualitatively identical to those observed at present day spreading centres, as at Galapagos (Edmond, 1982), and they can account for the metal content of the sulphide deposits and metalliferous sediments.

The purpose of the second part of this work is to examine the behaviour of the hydrothermal fluids as they reach higher levels in the ophiolite and deposit their content either within the lavas, or at the lava- seawater interface. This is achieved by:

1. The description of the field occurrence of a number of deposits from various mining districts with particular emphasis on the structural controls of the mineralization and their stratigraphic location. Such studies shed light on the behaviour of the hydrothermal fluids at different tectonic regimes and the relative role played by structure in the channeling of the hydrothermal fluids; and, also, on the relationships of hydrothermal activity to lava stratigraphy and the interrelationships between volcanic and hydrothermal processes.

2. The examination of mineralogical characteristics of the deposits and the nature of wall rock alteration. Study of these aspects is essential in the understanding of the behaviour of hydrothermal fluids at discharge sites, the composition of the fluids, the nature of their interaction with the wall rocks and the causes of mineral deposition or selective suppression of

precipitation.

The author feels obliged to emphasise at this stage that, unless otherwise stated, all data presented in the following chapters are based on his own field work and mineralogical studies. In an area as well studied as Cyprus and its associated sulphide deposits have been in recent years, almost no aspect is left untouched. Since the data are derived from the study of a large number of deposits in various mining districts, it is not possible to summarise all previous work in each section. Reference to past works is, therefore, mostly confined to situations where no first hand information could be obtained, as when discussing worked, presently inaccessible, deposits or when the interpretation given by the author is in conflict with previous interpretations.

It is further emphasised that, for the same reasons as above outlined, detailed descriptions of rock relationships and general geology of individual areas is not given. Such descriptions are limited only to selected areas, such as the Limni and Kalavassos districts, which are treated in detail in the text. Information on other areas is contained in geological reports submitted to Hellenic Mining Company and these may be accessed on request.

4.2. General features of the sulphide deposits

The details of the deposits emerged through a series of detailed geological and mineralogical studies by numerous workers.

Such studies revealed features common in most deposits, in particular a morphological and mineralogical pattern, generally simple, and applicable, with little variation, in most orebodies. This pattern indicates that the sulphide deposits are generally characterised by a lenticular upper zone of massive sulphide, composed mainly of pyrite with little chalcopyrite, passing in lower levels through a zone composed of silica and pyrite into chloritic lavas impregnated by sulphides. These relationships are illustrated in fig. 4.1 and may be recognised in the majority of the sulphide deposits.

Consensus of opinion rests on associating the zone of massive sulphide precipitation with the original surface of the lavas, the ore fluids having been exhaled on the sea floor through the fractured, sulphide impregnated zone represented by the stockworks. This inference is supported by the concordance with the overlying unaltered lavas, the high purity of the sulphide ore (Table 4.1) and the absence of titanium in the pyrite of the massive ore as contrasted with pyrites from the stockwork zone (Hutchinson and Searle, 1971; Constantinou, 1972).

In addition to the simple paragenesis of pyrite and chalcopyrite, sphalerite is a common constituent of both the massive ore and the stockwork zones but, with rare exceptions, does not exceed minor amounts (Bear, 1963; Constantinou and Govett, 1973). Paragenetic relationships suggest early precipitation of pyrite, followed by the copper and, finally, the zinc sulphide.

Wall rock alteration associated with the action of the

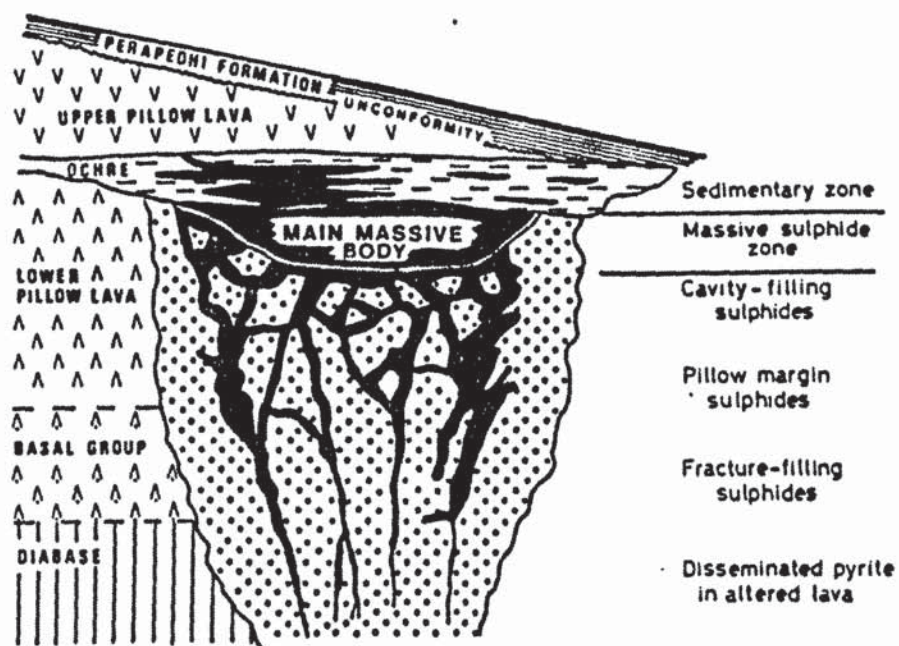


FIG. 4.1. Idealised form of a Cyprus sulphide deposit (After Hutchinson and Searle, 1971).

TABLE 4.1. Composite sample of Skouriotissa ore (After Cullis and Edge, 1927)

Fe	44.47 %
S	50.90 %
Cu	1.36 %
SiO ₂	0.81 %
Al ₂ O ₃	0.71 %
CaO	0.22 %
MgO	0.16 %
Mn	0.01 %
As	0.02 %
Pb	Trace
Zn	Trace
Cd	Nil
Undetermined	1.342 %

hydrothermal fluids, and considered contemporaneous with the mineralization, is mainly represented by chloritisation and silicification. The term 'propylitisation' has been used as a field term in describing hydrothermally altered rocks. Since, however, the essential constituents of propylitic alteration include, apart from chlorite, also albite, epidote and carbonates (Meyer and Hemley, 1967), the term is a misnomer. Usage, however, still persists and this term will also be used in this work for the description of the nature of the alteration by the mineralizing fluids.

Overlying the massive sulphide, in some deposits, there occurs a thin zone of laminated iron hydroxides and intercalated clastic pyritic bands. This oxidic facies has been termed ochre and was variously interpreted as the product of submarine weathering of the massive sulphide prior to burial (Constantinou, 1972), or the result of oscillating redox conditions at the final stages of hydrothermal activity (Hutchinson and Searle, 1971; Johnson, 1972).

The size of the deposits varies widely (Table 4.2) from large bodies measuring millions of tons, to sliver-like concentrations of a few thousand tons. The grades are similarly variable, from copper-rich to copper-poor deposits. Zinc is generally absent, with Kinousa underground (chapter 5) being one of the notable exceptions.

4.3. Previous studies on the sulphide deposits and umbers

A volcanic exhalative origin for the sulphide deposits

Table 4.2 : The size and grade of some economic orebodies.

Orebody	Tonnage	S	Cu	Zn

Mavrovouni	15 000 000	47	4.0	0.5
Skouriotissa	6 000 000	48	2.2	---
Limni	16 000 000	14	1.0	X
Apliki	1 650 000	36	1.8	---
North Mathiatis	2 800 000	33	0.2	---
Kinousa Underground	300 000	44	2.4	3.4
Kinousa Opencast	220 000	47	2.2	---
Memi	1 500 000	26	---	---
Sha	350 000	25	1.0	---
Ambelikou	16 000	45	1.0	---
Klirou East	420 000	23	1.1	1.4
Klirou West	77 000	21	0.5	0.5
Phoenix	15 000 000	3	0.5	---

X:Denotes presence in trace amounts.

was invoked by Hutchinson (1965). Formation of the stockworks by penetration of sulphides into cracks and connected openings in the underlying and adjacent flows is suggested, with the fluids responsible for the deposits envisaged as sulphur-rich metallic melts generated by volcanic differentiation.

The significance of the stockwork zones underlying the massive pyrite as the passageways for ascending ore fluids rather than descending masses was first recognised by Suffel (1965). He envisaged highly reactive gaseous fluids which caused widespread brecciation of the rocks in their uprise from deeper levels. The author further recognised that it is not essential that all deposits have an associated exhalative component and some may form within the lava pile while others could be essentially magmatic.

The suggestion for generally upward-moving ore fluids is also accepted by Vokes (1965) who envisaged, in addition, genetic relationships between the deposits and the enclosing lavas, suggesting that copper-rich deposits are located within the Upper Pillow Lavas and copper-poor deposits within the Lower Pillow Lavas.

The origin of the pyrite deposits was the subject of a Ph.D. thesis by Johnson (1970). The author postulated close genetic relationships between the sulphide deposits and the umbers and a sedimentary exhalative origin for the massive pyrite. Deposits within the lavas are interpreted as the result of cavity filling.

The geology, geochemistry and origin of the sulphide deposits have been described in detail by Constantinou (1972) and

Constantinou and Govett (1973). The main conclusions suggest that ore deposition took place at the contact between the Upper and Lower Pillow Lavas. The conglomeratic texture of the massive pyrite was produced by secondary leaching of the compact ore, the sandy matrix representing the extreme effects of dissolution. The locale of formation of the deposits is envisaged as sea floor depressions formed by caldera collapse at the end of a volcanic cycle. The high concentration of copper and zinc occurring in the upper parts of the orebodies are considered to be the result of submarine secondary enrichment consequent upon the leaching of pyrite.

The problem of the position of the sulphide deposits in the volcanic stratigraphy has been discussed by Cullis and Edge (1927). Based mainly on evidence provided by Skouriotissa orebody, the authors concluded that mineralization was post-volcanic in age and related to late stage solfataric activity which followed the deposition of the marls. The latter sediments were presumed to have acted as an impervious mantle onto which the ore fluids impounded and, being thus dammed, deposited their burden, forming the massive sulphide lenses. As a result of the action of the fluids, the marls were converted to umbers. Although the hypothesis was rejected by some workers (Ingham, 1959), a post-umber age is accepted by Bear (1963), Mousoulos (1957) and Gordon-Smith (1961).

An intervalcanic rather than post-volcanic age for the mineralization is suggested by Hutchinson (1965) who placed the principal phase at the waning stages of Lower Pillow Lava

vulcanicity. Constantinou (1972) also places the period of mineralization at the interval between extrusion of Lower and Upper Pillow Lavas but suggests that some massive orebodies, such as Kokkinopezoula, in the Tamasos district, were formed at the contact between the Basal Group and the Lower Pillow Lavas.

Comparison of the deposits of Cyprus with Canadian examples was made by Hutchinson and Searle (1971). A synvolcanic exhalative origin is inferred and close analogies suggested, partly upset by the metamorphism of the Canadian deposits. Clark (1971) concluded that formation of the deposits took place by submarine exhalative processes in sea floor depressions, fluid flow being sufficient to maintain a locally reducing environment amenable for the precipitation of massive pyrite. Conditions of strong disequilibrium are suggested by the gel-like nature of the original precipitate, while in deeper parts, where crystalline pyrite is deposited, equilibrium conditions were approached. The timing of the mineralization is placed at the last stages of extrusion of the Lower Pillow Lavas.

The circulation of seawater through oceanic crust as the process responsible for the formation of the sulphide deposits and ferromanganese precipitates of Cyprus and other ophiolites was suggested by Spooner and Fyfe (1973). According to the proposed model, seawater enters oceanic crust in the vicinity of spreading centres through delocalised areas of recharge and, after being heated and chemically modified by reaction with the rocks, is exhaled as a metal-laden ore fluid in localised discharge sites identified as the sulphide deposits. Subsequent studies using

strontium isotopes (Spooner et al., 1977) suggest that penetration of seawater reaches to the level of the gabbros. Fluid inclusion studies (Spooner and Bray, 1977) show salinities corresponding to seawater, while O^{18} enrichment of the Sheeted Complex is interpreted as the result of massive interaction of seawater with basalt, with interaction and greater enrichments in the Sheeted Complex reflecting increasing temperatures.

The origin of the umbers has been controversial and the controversy has not yet been resolved. Cullis and Edge (1927) considered them as hydrothermal alteration products of the marls produced by iron and manganese-rich emanations related to the final stages of volcanicity. Wilson (1959) postulated that umbers may be either a primary precipitate or a replacement product of volcanic ash. Bear (1963) favoured a lagoonal environment of deposition. Constantinou (1972) suggested a marine origin, the umber constituents having been derived from the Troodos pillow lavas. The exact process is not discussed. Johnson (1972) included the umbers with the sulphide deposits in the Perapedhi formation and postulated a single process for their genesis involving sulphur-bearing exhalations related to subaqueous fumarolic activity resulting to the formation of the sulphides with the umbers representing the unsulphidised portion of the original precipitate. Robertson (1975) compared the umbers with metalliferous sediments from spreading axes and concluded that they represent hydrothermal precipitates which were released into the more oxidising environment of the elevated flanks of the ridge.

CHAPTER 5

Field and stratigraphic aspects of the sulphide deposits

5.1. The Limni Mining District.

5.1.1. Introduction and general information.

The Limni mining district is situated in western Cyprus (Fig. 1.1) and is the first area to attract the attention of recent prospectors, exploration having started as early as 1882, concentrated on the spectacular evidence of mineralization suggested by major gossans in the region of Limni mine. A depression, forming a lake, remnant of an ancient attempt at opencasting, gave the mine its present name (Limni is the Greek word for lake).

The early phase of exploration was occupied in the opening of numerous adits, initially for the draining of the lake and later for exploratory purposes. No record of the earlier operations remains with the exception of detailed assay plans of the underground workings carried out by W. Y. Westervelt in 1910 which disclosed the presence of a considerable tonnage of cupriferous sulphides. Serious exploration did not start, however, until 1947 and mining by opencast methods began in 1959. Detailed accounts of all phases of the early exploratory work are presented by Cullis and Edge (1927) and Gordon-Smith (1959).

Kinousa orebody was discovered in 1956 under a cover of sediments and discovery of Uncle Charles deposit (Kinousa opencast) followed shortly after by drilling of a major self

potential anomaly.

Drilling in the Evloimeni area was initiated in 1954 and the detected low grade sulphides were intermittently exploited in association with mining of the Limni ore.

A small body of ore was discovered by drilling in early 1959 in the Double Seven area, amounting to 100 000 tons (30 % S, 1.0 % Cu) and this is still unexploited.

The location of all the above mines is shown in fig. 5.1.

All mining operations at Limni ceased in 1979 as a result of exhaustion of reserves.

The author was employed as exploration geologist in 1971-1975, during which period most of the field data were collected. Some of the results of this work were published (Adamides, 1975). The field data were supported by additional sampling and examination of assay plans during the period of this study (1978-1983). Prior to the author's work, Gordon-Smith (1959) and Searle (1964) reported on the Limni orebody, while a report by Taylor and Sons (1956) on the whole of the mining district exists.

5.1.2. Geological framework.

A simplified geological map of the area is shown in fig. 5.1. A detailed map is enclosed in pocket (Map 1).

The stratigraphic sequence exposed in the area beneath the Pleistocene and Recent deposits is shown in fig. 5.2

The Koronia limestone occupies the higher ground around the villages of Kinousa and Pelathousa (Fig. 5.1) and rests unconformably either directly on pillow lavas, on clays of the

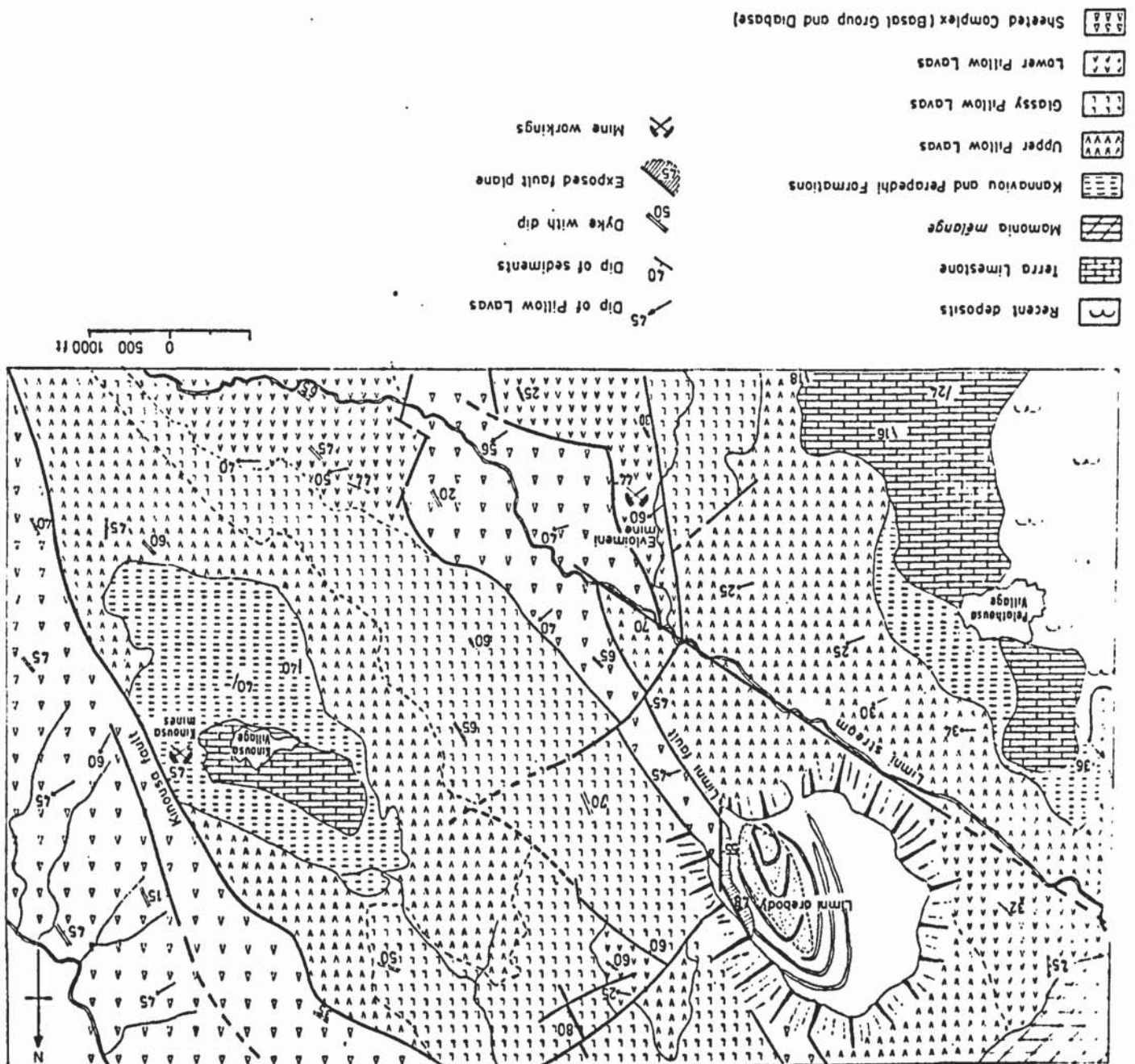


FIG. 5.1. Geological map of the Lmt mining district. (After Adamides, 1975).

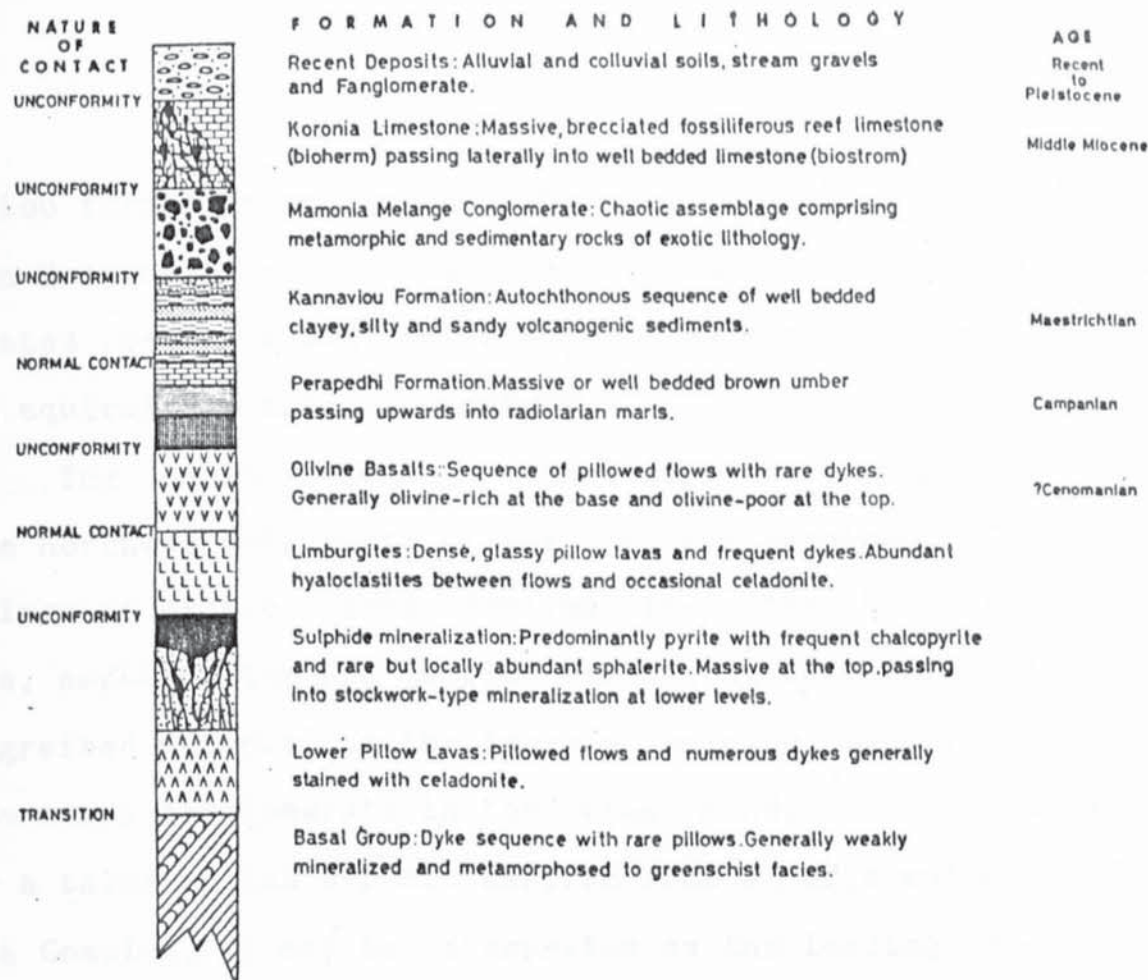


FIG. 5.2. The stratigraphy of the Limni mining district.

Kannaviou formation or, in the extreme northwest, on the Mamonia Melange Conglomerate. It is a massive, unbedded and frequently brecciated fossiliferous reef limestone in the most part, but well-bedded equivalents are also present.

The Mamonia Melange Conglomerate is exposed in the extreme northwesterly parts of the area and consists of a mixed assemblage of exotic blocks derived from the Mamonia Complex. Schists, amphibolites and marbles are haphazardly intermixed, with finer-grained material as the loosely welding medium. The rock type is not a conglomerate in the true sense of the word but rather a talus or fan deposit derived from an adjacent area of the Mamonia Complex. It may be interpreted as the leading edge of that complex whose main development may be observed in the region of Akamas peninsula. The formation rests either on pillow lavas or on the clays of the Kannaviou Formation and is locally unconformably overlain by the Koronia limestone. Therefore the time of its emplacement may be accurately fixed. It is comparatively thin in the mapped area but it rapidly attains a great thickness westwards and more than 200 metres were penetrated in a borehole sited at the coast without reaching its lower contact.

The Kannaviou Formation is best developed in the region of Kinousa village where it is unconformably overlain by the Koronia limestone. Stratigraphically downwards it passes transitionally into the radiolarites of the Perapedhi Formation. It comprises a lower thinly laminated, and very well-bedded marly to clayey facies, passing upwards into fine-grained silty sands with occasional hard sandstone bands and interlaminated shaly beds. The

formation is the lateral equivalent of the Moni clays described in the Kalavassos region and, similarly to the latter area, it is autochthonous and completely free of exotic blocks.

The Perapedhi Formation, directly underlying the Kannaviou Formation, comprises the normal sequence of thinly-bedded radiolarites passing in the lower parts into massive or bedded umber.

The Upper Pillow Lavas exhibit the normal sequence of well pillowed olivine-rich and olivine-poor basalts with a few tortuous dykes that are hard to distinguish from the surrounding pillow lavas. They occupy a large tract of ground in the region of Kinousa village, their outcrop being roughly parallel to the major fault which bounds the later volcanics and sediments from the Sheeted Complex. A second major outcrop of these lavas is also found in a belt from Evloimeni to Limni mine and to the west of this area.

The contact of the olivine basalts with the limburgites, which comprise the lower part of the Upper Pillow Lavas, is generally only marked by the difference between the pink stained or grey finely crystalline pillows of the olivine basalts and the glassy, dark grey, hyaloclastite-rich limburgitic lavas (Plate 5.1). No sedimentary deposition is observed in any part of the contact or within the volcanic formations nor are picritic intrusives and sills evident in any part of the area. Similarly the contact of the limburgites with the Lower Pillow Lavas is defined by the change in lithological character from the glassy, friable limburgitic lavas to the hard, blocky pillows of the Lower



PLATE 5.1. Limburgitic pillow lavas, transected by rare dykes, as exposed in the Double Seven area.



PLATE 5.2. Pillowed flow of the Lower Pillow Lavas (EMS) in the region of Evloimeni mine. Note the abundant presence of celadonite in pillow inter-spaces.
Length of field of view 20 metres.

Pillow Lavas (Plate 5.2). The latter lavas are only erratically exposed through the cover of later flows and the exposures are mainly characteristic of the upper parts of the formation, with abundant pillows associated with considerable hyaloclastic material.

The contact of the Lower Pillow Lavas with the Sheeted Complex is generally faulted throughout the area, while an overlap relationship between the latter and the limburgites is indicated in the northeastern side of the Athkiatjia ridge resulting in the limburgites resting directly on the Sheeted Complex along most of the length of the ridge.

The Basal Group occupies a large part of the northeastern corner of the area and represents a portion of the main massif which extends almost uninterrupted towards the plutonic core of Troodos. A second, smaller, outcrop extends in the form of a fault-dissected ridge from the region of Limni mine towards Evloimeni and beyond. This outcrop area is typical of the middle parts of the Sheeted Complex, consisting essentially of diabase dykes with frequent pillow screens, pervasively chloritised, silicified and epidotised and with widespread evidence of mineralization throughout.

5.1.3. The tectonic situation.

The structure of the area is essentially simple, although a multitude of minor faults result to an apparently complicated pattern.

The reef limestone rests almost horizontally on the older

rocks. This is also the case with the Kannaviou Formation, although local high dips are frequently observed in the latter formation as a result of the incompetent behaviour of the clays. The regional dip of the pillow lavas is shallow northeasterly (25° - 30°) with steeper dips related to local structural factors and the position of individual pillows within a lava flow. Similarly the dykes both in the Basal Group and the pillow lavas are generally steeply dipping to the southwest (50° - 60°) although modifications as a result of structural factors are locally observed.

The Limni region is dominated by two major faults, both trending in a northwesterly (330°) direction and dipping at 50° towards the southwest. Both faults are parallel to the dykes in the Basal Group and played a determining role in ore deposition and lava extrusion. The first structure, termed the 'Kinousa fault' (Adamides, 1975), forms the boundary between the Basal Group in the footwall side and the younger pillow lavas and sediments in the hanging wall side. It is a major structure and continues well outside the mapped area. Its normal vertical movement, which has apparently been continuous since the early stages of volcanic activity, resulted to the accumulation of thick lavas in the hanging wall side with the footwall side remaining free of lavas younger than the Sheeted Complex.

The second fault, termed 'the Limni fault', in view of its importance in the deposition of the Limni orebody, is also normal in nature and defines the southwesterly contact of the Basal Group with the younger lavas. It may be traced along the

ridge extending from the region of Limni mine towards Evloimeni (Fig. 5.1).

A second family of faults trends in a north-south direction and its main representatives are well exposed at Limni mine. They appear to have a strong transcurrent component of movement and have played a decisive role in the final disposition of the mineralization.

A strike-slip displacement is also envisaged for the fault which trends in a direction of 290° parallel to the Limni stream (Fig. 5.1). This fault dislocates the continuation of the Limni fault close to the region of Evloimeni and a translation of approximately 200 metres is inferred from observations on either side of the structure.

An additional direction of faulting is oriented northeast-southwest and such faults displace the Kinousa fault in the region of the mines, while in the Double Seven area such structures, infilled by crystalline calcite, stand out as positive features due to differential weathering of the lavas (Plate 5.3). The amount of displacement of these faults appears, at least in the Double Seven area, to be minimal as indicated by the correlation of dykes on either side of the structures.

It may be concluded that by far the 330° direction of faulting is the main structural direction in the area and the alignment both the dykes of the Basal Group and the dykes in the later pillow lavas parallel to this indicates that it has been active in the early stages of volcanic history.

In general the tectonic situation at the Limni area may



PLATE 5.3. Minor fault (right hand side of photograph) infilled by crystalline calcite. Double Seven area.

be summarised as follows:

Extrusion of the pillow lavas and intrusion of the dykes in the underlying Sheeted Complex has been mostly governed by structures which are at present aligned parallel to the northwesterly (330°) direction. Major faults of this direction, with their continuous downthrowing movements during volcanism, resulted to the development of a thick pile of pillow lavas in the hanging wall side with the footwall side remaining comparatively free of thick accumulations. Fractures sub-parallel to this direction became passageways through which lavas were extruded to give the younger flows. Later periods of movements along these old lines of weakness controlled also to some extent the deposition of the sediments as indicated by the disposition of the Kinousa sedimentary basin.

5.1.4. The sulphide deposits.

5.1.4.1. The Limni orebody.

The orebody was developed in the obtuse angle between two major faults which also form the northeasterly and easterly footwalls of the mineralization (Fig. 5.3). The ore was wholly of the stockwork type, only isolated pockets of massive ore having formed locally, and was characterised by unusually high copper, the final tonnage mined running to 16 million tons assaying 14 % S and 1.0 % Cu.

The eastern footwall of the mineralization, called the Eastern Boundary fault has long been considered as the structure

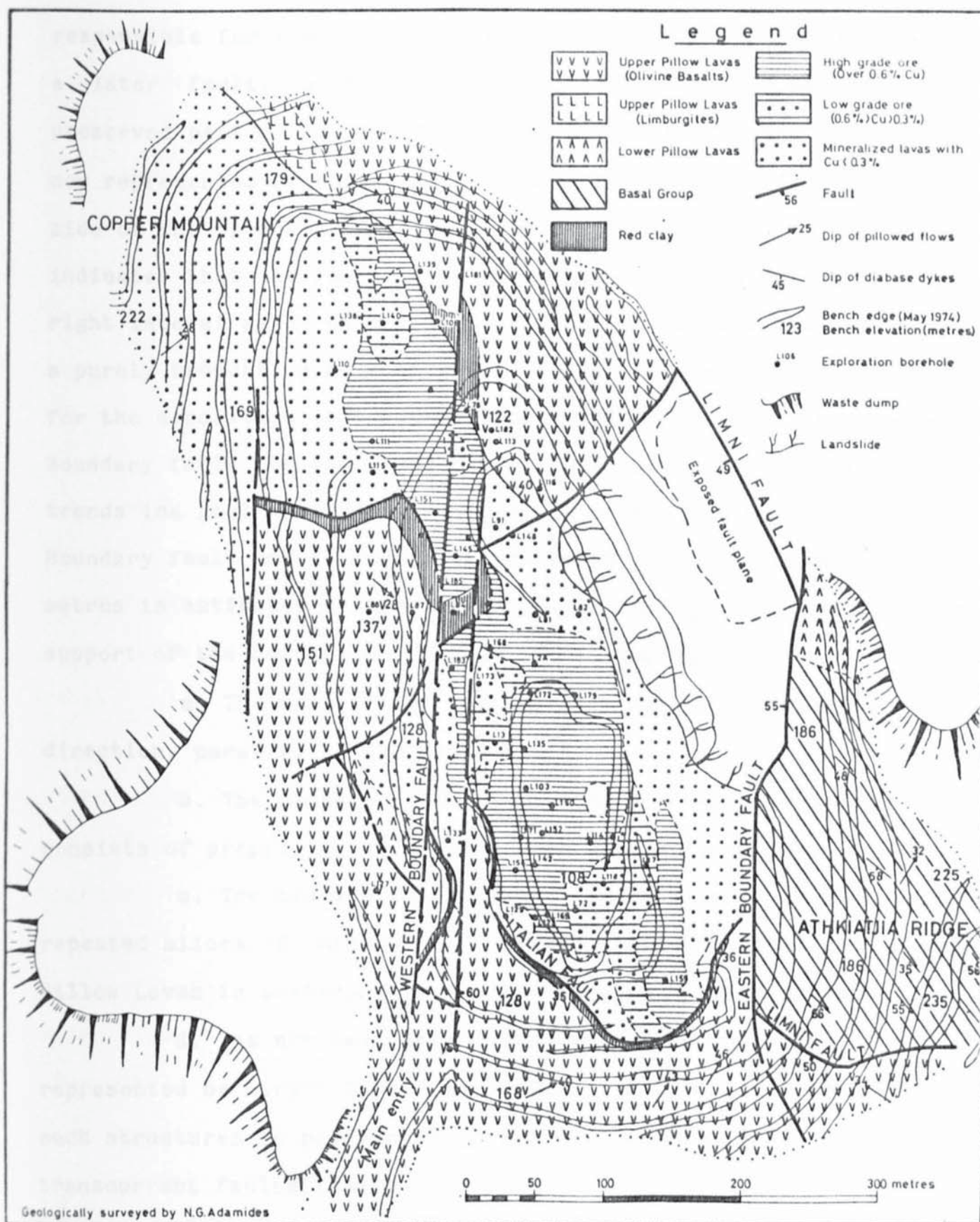


FIG. 5.3. Geological map of the Limni opencast mine.

responsible for the deposition of ore (Gordon-Smith, 1961), or as a later fault, normal in nature, which has downthrown and preserved part of the original orebody, the rest being eroded and now represented by the ridge of Basal Group exposed in the eastern side of the opencast (Searle, 1964). The present investigation indicates that the fault is mainly transcurrent in nature with a right lateral sense of movement, is post-ore in age and has played a purely truncating role on the orebody. The controlling structure for the deposition of the mineralization is not the Eastern Boundary fault but the Limni fault. This latter structure, which trends in a northwesterly direction, is affected by the Eastern Boundary fault and a lateral displacement in the range of 200 metres is estimated to have taken place along it. Evidence in support of the conclusion lies in the following:

a. The axis of the orebody trends in a northwesterly direction, parallel to the Limni fault.

b. The plane of the Limni fault is mineralized and consists of propylitic alteration impregnated by pyrite.

c. The plane of the Eastern Boundary fault is made up of repeated slices of mineralized ground and unmineralized Upper Pillow Lavas in testimony of its post-mineralization movements.

d. The northwesterly direction has been proved to be represented by normal faults and deposition of ore is favoured by such structures in preference to the closed structures produced by transcurrent faults (Badgley, 1965).

It may be concluded from the above that deposition of the mineralization at Limni has taken place under the controlling

influence of a major normal fault, the downthrowing movements of which, coupled with the effects of the mineralizing solutions, fractured the rocks and deposited ore in its hanging wall side. The Athkijatja ridge of Basal Group is visualised as a positive feature even at the time of mineralization and, in view of its location on the footwall side of the controlling structure, it could not be expected to have been the site of deposition of rich ore, although it has been severely affected by the ore fluids as the abundant signs of mineralization suggest.

The host rocks for the deposition of the Limni orebody are clearly the Lower Pillow Lavas. Representatives of these, in the unmineralized state, are present in limited outcrops in the lateral extensions of the orebody where they are frequently observed to pass laterally as well as downwards into mineralized lavas.

A series of sections illustrating the geological features of the deposit are shown in fig. 5.4. The orebody was covered to a large extent by unmineralized olivine-rich basalts characteristic of the higher levels of the Upper Pillow Lavas. Their contact with the mineralization was marked by a zone of red hematitic alteration and intense satin spar veining. Previous workers (Searle, 1964) considered this zone as the contact aureole of the deposit which was therefore considered as post-Upper Pillow Lava in age. The present work indicates that the red clay, which locally coincides with a shallow dipping structure termed 'the Italian fault', elsewhere continues to form a complete capping over the mineralization (Fig. 5.4) . In that sense it is

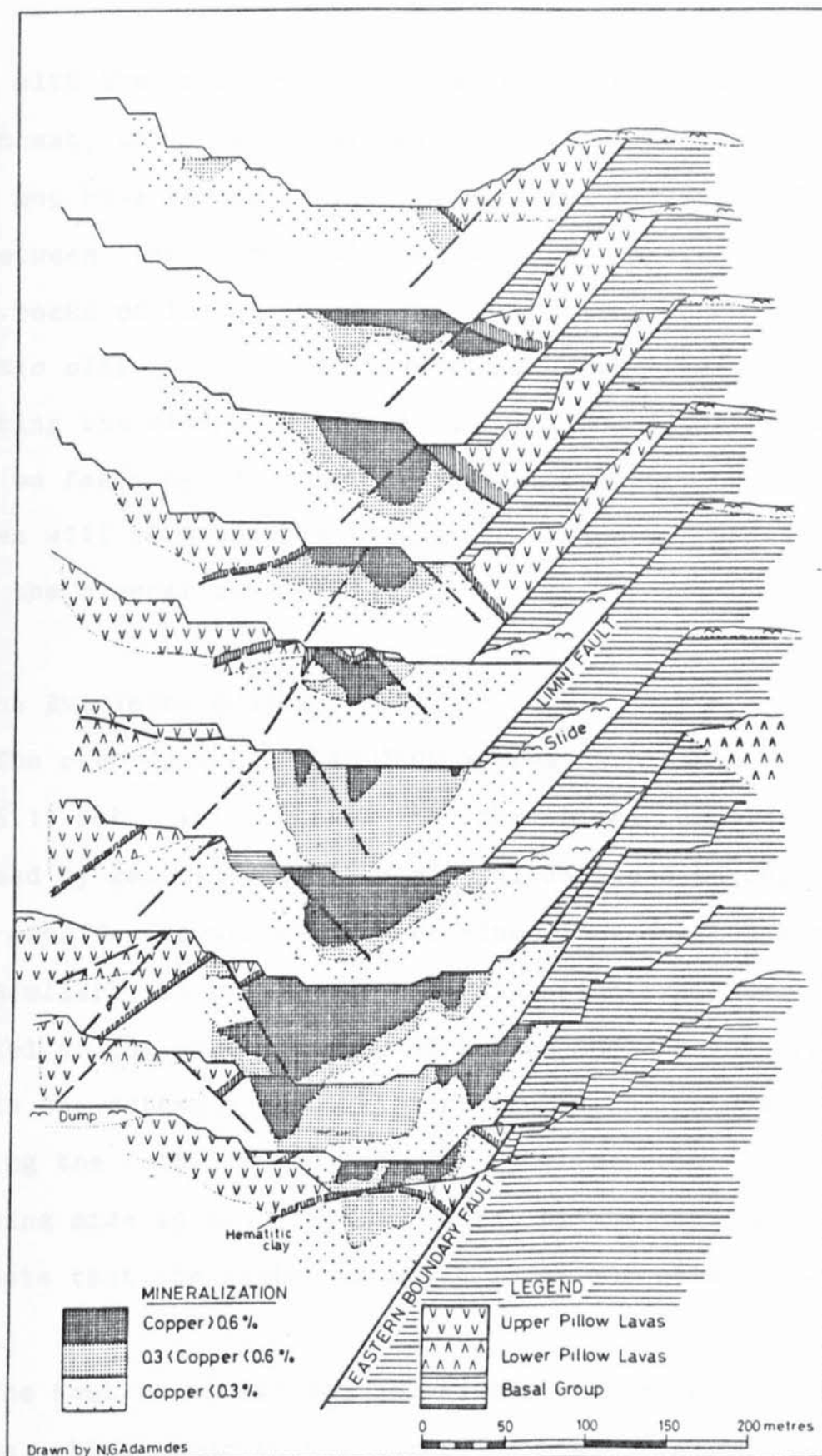


FIG. 5.4. Series of sections through the Limni ore-body showing structural relationships and distribution of grades.

concordant with the unmineralized lavas in the northeasterly parts of the opencast, while being strongly discordant to the southwest. As such it may have formed by the differential movements along the contact between the unmineralized olivine basalts and the silicified rocks of the ore zone. The more intense development of the hematitic clay at the intersections with the north-south faults cutting the mineralization is a further indication of the dependence on faulting for its formation. A further treatment of this problem will be presented in the discussion of stratigraphic horizon of the mineralization.

5.1.4.2. The Evloimeni orebody.

The orebody is located 1500 metres southeast of Limni mine (Fig.5.1) but, in contrast to the Limni orebody it is characterised by generally pyritic mineralisation with only local pockets of cupriferous ore which were mined in a small opencast.

Similarly to Limni, the mineralization exhibits a long axis parallel to the northwesterly direction and the controlling structure is the extension of the Limni fault. The nature of the fault forming the footwall boundary of the deposit is exactly similar, being made up of propylite with pyrite disseminations, which suggests that the fault has acted as a channelway for the ore fluids.

The host rocks for the deposition of ore are the Lower Pillow Lavas, which occur in the unaltered state in the western parts of the opencast (Plate 5.2), and pass in a gradational manner into mineralized lavas towards the northeast. A geological

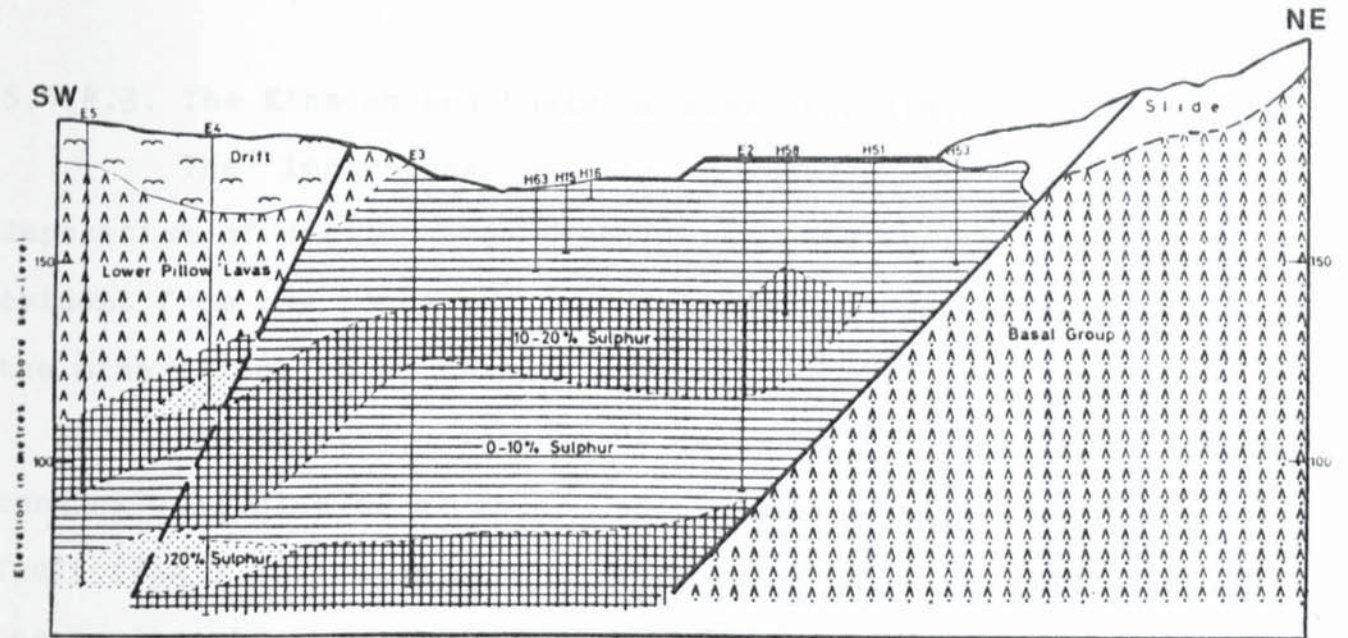


FIG. 5.5. Geological section through the Eyloimeni orebody.

section transverse to the controlling structure (Fig.5.5), shows the disposition of the mineralization with relation to the rock types and also the generally poor grade of the ore.

5.1.4.3. The Kinousa and Uncle Charles deposits.

The importance of the northwesterly faults in the deposition of ore in the Limni mining district, already made evident from the foregoing descriptions, is further emphasised by the mineralization at Kinousa.

The Kinousa underground deposit was developed in the hanging wall side of a major northwesterly fault, the Kinousa fault (Fig 5.1), which forms the footwall of the mineralization to the northeast. In contrast to the Limni orebody, which did not have any associated massive pyrite, the Kinousa orebody is a typical Cyprus type deposit with a massive upper zone passing downwards into stockwork-type mineralization in altered country rocks, the pyrite content falling gradually with depth.

The orebody was located directly beneath the sediments (Fig. 5.6) and, although Upper Pillow Lavas occur in faulted relationship with the mineralization, none covered it. A small fragment of drag ore, left behind during the downthrowing movements of the Kinousa fault, was oxidised into a strong gossan and this provided the only indication of mineralization in the area.

The Uncle Charles deposit, otherwise called the Kinousa opencast, was located 250 metres to the southeast of Kinousa and the two orebodies were localised by the same structure and linked

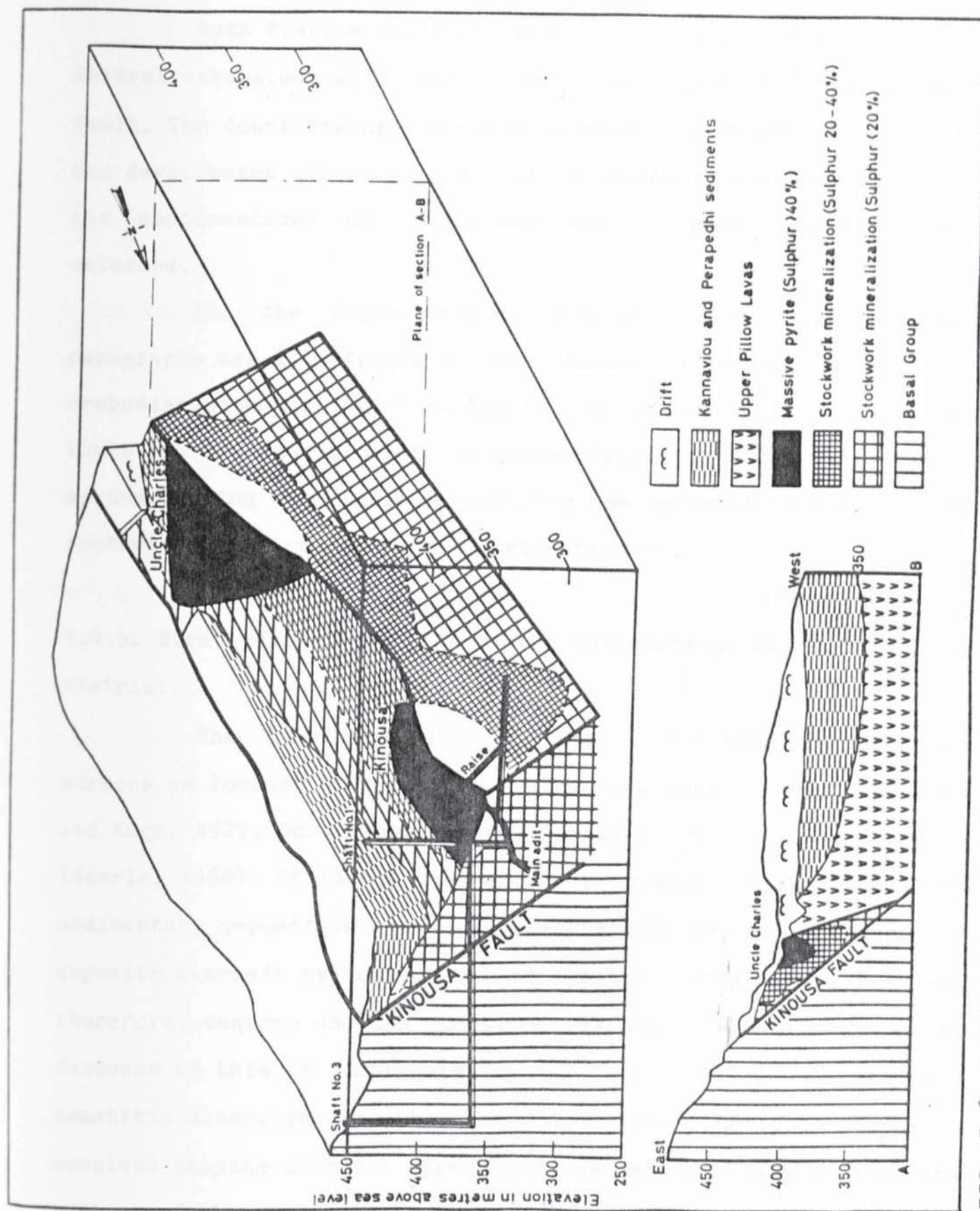


FIG. 5.6. Isometric projection and geological section through the Kinoussa orebodies.

by a continuous zone of poorer mineralization.

Both Kinousa and Uncle Charles are dislocated in their lateral extensions by a structure sub-parallel to the Kinousa fault. The downthrowing movements of this structure resulted to the development of thick lavas and sediments in that direction and the continuations of the mineralization have not yet been detected.

All the relationships described in the previous paragraphs are illustrated in the isometric projection of the orebodies shown in fig. 5.6. The strong influence of the Kinousa fault in the deposition of the mineralization and the role played by the hanging wall fault in limiting the mineralization in the southwesterly direction are clearly apparent.

5.1.5. Stratigraphic position of the orebodies of the Limni mining district.

The Limni orebody has been considered by previous workers as located at the Upper Pillow Lava-umber contact (Cullis and Edge, 1927, Gordon-Smith, 1959) or within the olivine basalts (Searle, 1964). It is now apparent that mineralization pre-dated sedimentary deposition. This is suggested from the presence of deposits overlain by unmineralized pillow lavas. The problem, therefore, centres on its position within the volcanic pile. Evidence on this is complicated by the relationship of the red hematitic alteration to the deposit. This alteration forms a complete capping over the mineralization and generally defines the contact of the orebody with the unmineralized olivine basalts.

Locally it coincides with the Italian fault (Fig. 5.3) but in the northern part of the opencast it shows a dip in the opposite direction so that, in that area, it is conformable with the similarly dipping pillow lavas. Searle (1964) considered the red clay as defining the contact aureole of the orebody and concluded that the deposit was formed by replacement of the olivine basalts.

The red clay shows great similarities to the hematitic gouge frequently observed in faults and may, therefore, be related more to faulting than to any other factor such as contact effects of the mineralization on the surrounding lavas. The fact that development of this clay is more intense in the region of the north-south faults is relevant to the issue. Furthermore, if this red clay was the product of contact metamorphism, it should not be present in areas where unmineralized lavas come in faulted contact and yet, in the southwestern part of the opencast, such situations are frequently observed. On the other hand the clay is best developed in the interspace between the north-south faults, within mineralized ground and away from ore-host rock contacts. A final piece of evidence is provided by the gradational contacts between the mineralization and the unmineralized Lower Pillow Lavas which are present in the lateral termination of the ore zone and which are devoid of any sign of such clay.

It is apparent from the above evidence that the red clay shows much closer association with the structure of the deposit than with any contact metamorphic effects. Its peculiar mode of occurrence in the form of an envelop surrounding the orebody could conceivably be produced if the orebody was originally covered by a

pile of post-ore Upper Pillow Lavas. Later downthrowing movements along the Limni fault in association with slip movements along the contact between the mineralized ground and the unmineralized lavas would result to the observed picture.

Kinousa orebody and Uncle Charles do not provide any additional evidence on the problem. The latter was discovered directly beneath scree so that the originally overlying rocks are missing. Kinousa, on the other hand, was located directly beneath the sediments of the Perapedhi and Kannaviou formations and no lavas covered the deposit, although a considerable thickness of unmineralized Upper Pillow Lavas was deposited beyond the hanging wall fault. The conclusion regarding the deposit is that movements along the hanging wall fault were taking place directly after ore deposition so that accumulations of thick lavas were solely confined in the downthrow side.

Critical evidence on the horizon of the mineralization, however, is provided from the study of the Evloimeni mine which, although located within the Lower Pillow Lavas, as mapped on the basis of alteration and field characteristics, shows primitive chemistry (chapter 2) similar to the Upper Pillow Lavas. This places the period of mineralization at the onset of this primitive volcanism but prior to the extrusion of the limburgites and olivine basalts which, on the basis of field evidence, are free of the influence of the mineralizing fluids.

5.1.6. Conclusions from the study of the Limni deposits.

The following conclusions are justified from the preceding:

The sulphide deposits of the Limni mining district are controlled in their localisation by major northwesterly faults which were aligned parallel to the dykes of the Sheeted Complex. In light of the plate tectonic setting of the Troodos ophiolite on a spreading axis, such faults may be considered as parallel to this axis. No interference of transverse structures is evident in ore localisation. It is envisaged that the ore fluids gained access to higher levels through these major faults, widening them in some cases by processes of hydraulic fracturing.

Ore deposition has been found to be temporally related to the initial stages of primitive volcanism, typically represented by the Upper Pillow Lavas, but the main representatives of this formation, i.e. the limburgites and olivine basalts, are later than the main period of hydrothermal activity which resulted to the formation of the sulphide deposits.

5.2. The Kalavassos mining district.

5.2.1. Introduction

The Kalavassos mining district, situated in southeastern Cyprus (Fig. 1.1), has been an important mining centre in ancient times. This is suggested by the presence of major slag accumulations in the vicinity of the mines and the abundance of ancient workings discovered during recent mining operations.

Recently interest was aroused in 1927, probably stemmed by the publication of the report on the sulphide deposits of Cyprus by Cullis and Edge. These authors (Cullis and Edge, 1927)

reported favourably on the area as possibly containing deposits of the 'Skouriotissa type'. Exploration and exploitation for the next 50 years resulted in the discovery of a large number of deposits of variable sizes (Table 5.1), the most recent being Mousoulos orebody, which was exhausted in 1976. Mining has at present temporarily ceased in the area.

A detailed account of previous geological work has been presented by Constantinou (1972) who summarised the literature up to that date. The present author mapped the area in detail between 1975-1978 and presented the results in a series of private company reports. Some of the results were described in a recent publication (Adamides, 1980).

The purpose of this section is to describe the geology and structure of the sulphide deposits in relation to the volcanic stratigraphy and regional setting. Particular emphasis is placed on plate tectonic setting and controls of ore localisation.

5.2.2. Geological framework.

The area is situated in the tectonically disturbed region of southern Cyprus and only 5 km south of the major easterly-trending Arakapas Fault Belt (Fig. 5.7), which is almost universally regarded as a fossil transform structure (Moore and Vine, 1971, Simonian, 1975). This major tectonic feature has significant effects on the geology of the area and the mode of occurrence of the deposits.

Fig. 5.8 shows the stratigraphy and pertinent lithological details. The geology of the area is shown in fig.

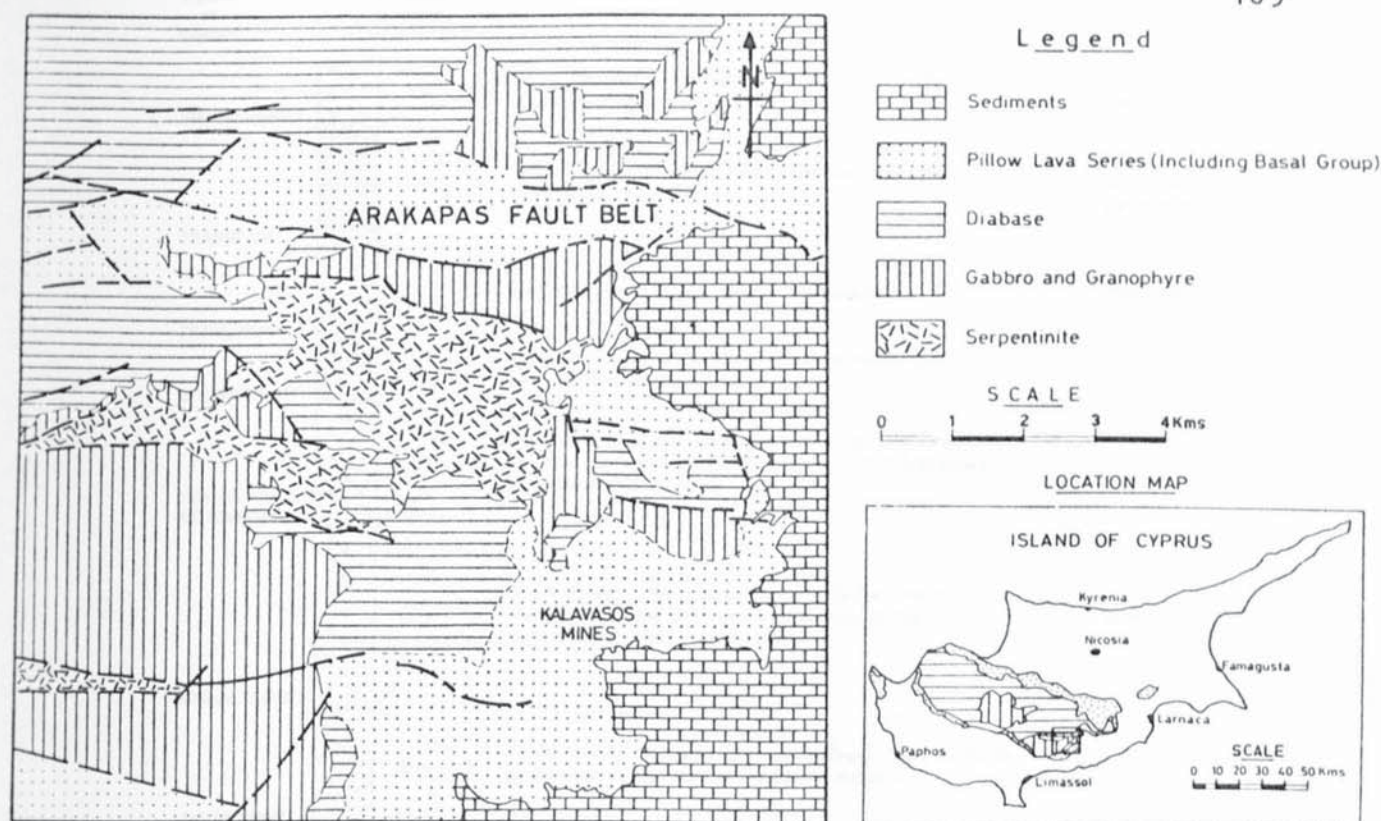


FIG. 5.7. Location map of the Kalavasos mining district with relation to the Arakapas fault belt. Map redrawn after Pantazis (1967).

TABLE 5.1. Production data for the mines of Kalavasos. Mainly after Bear (1963) and Pantazis (1967), updated by the author.

Mine	Years of operation	Method of mining	Ore mined (metric tons)	Remaining reserves (metric tons)
Kalavasos A,B,C,D,D',D'',E,E'	1937-1939 1941-1956	Underground (sub-level caving)	1,910,000	—
Petra	1953-1957	Underground (sub-level caving)	226,000	300,000
Mavri Sykia underground	1954-1962	Underground (sub-level caving)	269,000	—
Mavri Sykia opencast	Intermittently between 1970-1977	Opencast	107,000	590,000
Landaria	1963-1964	Underground (sub-level caving)	65,500	250,000
Platies	1955-1958	Glory-hole	43,900	—
Mousoulos	1964-1976	Underground (top-slicing)	1,660,000	940,000 (mostly sulphur ore)
Mavridia	Intermittently between 1971-1977	Opencast	400,000	200,000

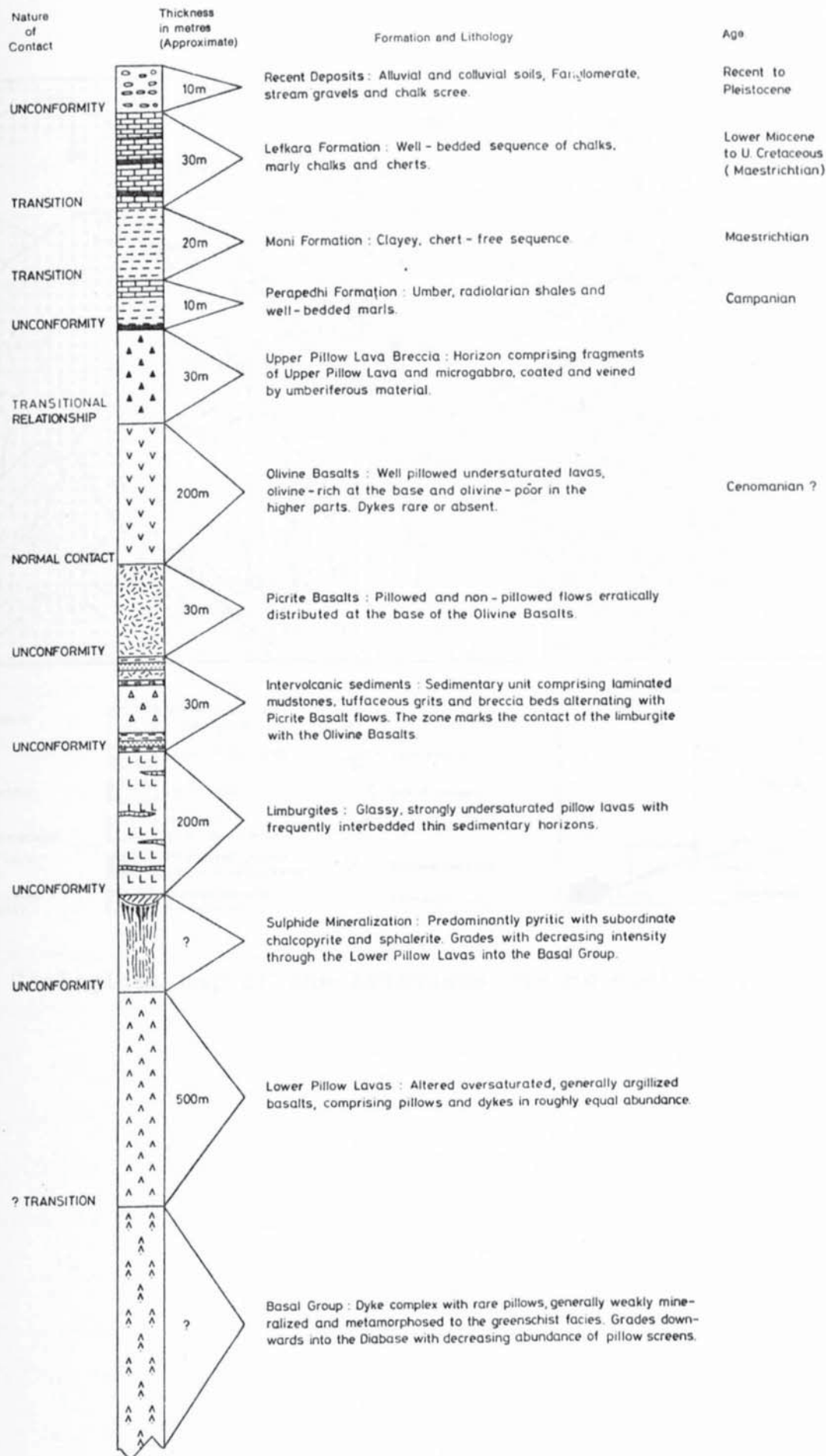


FIG. 5.8. The stratigraphic sequence in the Kalavassos mining district.

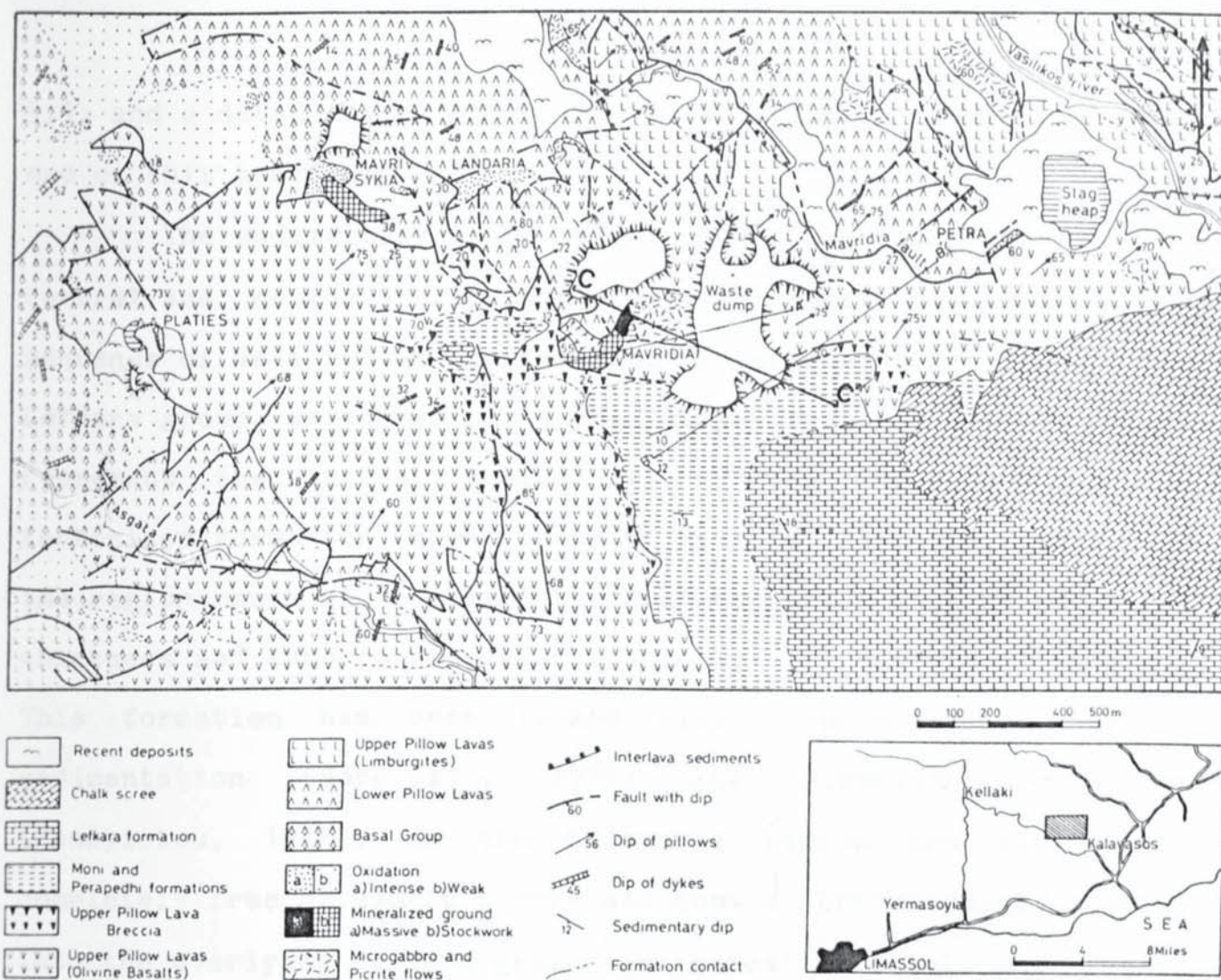


FIG. 5.9. Geological map of the Kalavasos mining district.

5.9. and a detailed geological map is enclosed in pocket at the end of this book (Map 2).

The sedimentary rocks (Fig. 5.9) are confined to the central and southeasterly parts of the area and comprise a sequence of well bedded chalks and interbedded cherts of the Lefkara group, which rest on a thin clayey sequence. These clays represent the lateral equivalents of the thick and highly tectonised formation termed the Moni Melange (Pantazis, 1967). In the region south of Kalavassos the Moni Formation attains a great thickness and incorporates exotic blocks of Mamonia lithology. This formation has been linked with processes of trench sedimentation (Robertson, 1977) and subsequent obduction (Panayiotou, 1977). In the Kalavassos region the clays are completely free of exotic blocks and show a transitional passage into the overlying Lefkara group, an indication that the region was rather removed from the source of disturbances which gave rise to the melange.

The Moni clays rest unconformably on the thin umbers and radiolarites of the Perapedhi Formation which form the base of the sedimentary sequence. In view of the small thickness and impersistent nature of these rocks, they are grouped together with the Moni clays on the geological map. Their genesis and significance is, however, quite distinct.

The contact of the sediments with the lavas is marked by a sequence of breccia comprising mostly olivine basalts and microgabbro fragments, both apparently derived from the Upper Pillow Lavas, welded together by umberous material. These breccia

have been the subject of some controversy in the past and have been variously termed volcanic agglomerate (Mousoulos, 1957), the tectonic breccia along thrust planes (Searle, 1967), olisthostromes (Constantinou, 1972), detrital (Searle and Panayiotou, 1980) or breccia formed concomittantly with the deposition of the umber (Robertson, 1975). The author tends to favour the last hypothesis in view of the following:

a. There is a close spatial relationship between the breccia and the umbers with the breccia invariably underlying the umbers.

b. The welding material between the fragments is not lava or volcanic glass which tends to rule out the 'agglomerate' hypothesis.

c. The contact of the breccia with the underlying olivine basalts is gradational and therefore neither the 'thrust' nor the 'detrital' alternative can be sustained. A vertical passage is frequently observed in the field from the thoroughly brecciated rocks through a zone of moderate brecciation into undisturbed pillows veined by umberous material.

The Upper Pillow Lavas are the most extensive formation in the Kalavassos mining district and are present in a complete sequence from the limburgites at the base, to the olivine basalts which form the upper parts of the formation. The contact of the limburgites with the underlying Lower Pillow Lavas is defined in some cases by a thin discontinuous band of finely laminated umberous sediment or, locally, as in the area close to the mine offices, pure umber indistinguishable from the stratigraphically

higher number of the Perapedhi formation. Elsewhere a concordant intrusive marks the contact.

Extrusion of the limburgites was accompanied by minor but widespread sedimentation, especially evident in the area north of Petra locality, where thin zones of finely laminated clayey, sandy or gritty sediments are continuously interbedded with lava flows. Intervolcanic sedimentation reaches a climax at the contact of the limburgites with the olivine basalts where a thick zone of fine sediments and breccia beds are associated with basaltic and picritic flows (Plate 5.4). The details of this sedimentary zone as observed in the area directly north of Petra are shown in fig. 5.10.

It must be emphasised that this type of intervolcanic sedimentation is not characteristic of the whole of the Kalavassos mining district. These sediments are most strongly developed in the region north of Vasilikos stream, increasing in intensity northwards, as indicated by reconnaissance mapping. Intervolcanic sedimentation reaches a maximum in the Arakapas fault belt (Simonian, 1975, Searle and Panayiotou, 1980). There, conglomerates up to 100 metres in thickness occur interbedded with the lavas. South of Vasilikos stream, the intervolcanic sediments become scarcer and to the north of Landaria locality the equivalent of the 30 metre band of sediments is only 2 metres thick. Farther south, such sediments are completely absent from the volcanic formations.

Picritic intrusives and pillowed flows are another characteristic feature of the area and these are frequently



PLATE 5.4. Detail of the coarse fraction of the intervalcanic sediments as exposed in the region north of Vasilikos stream. Note the presence of oxidised blocks of diabase.



PLATE 5.5. Low angle gravity fault west of Mavridia opencast. Fault plane of clay gouge marks the boundary between Upper Pillow Lava Breccia (above) and Lower Pillow Lavas.

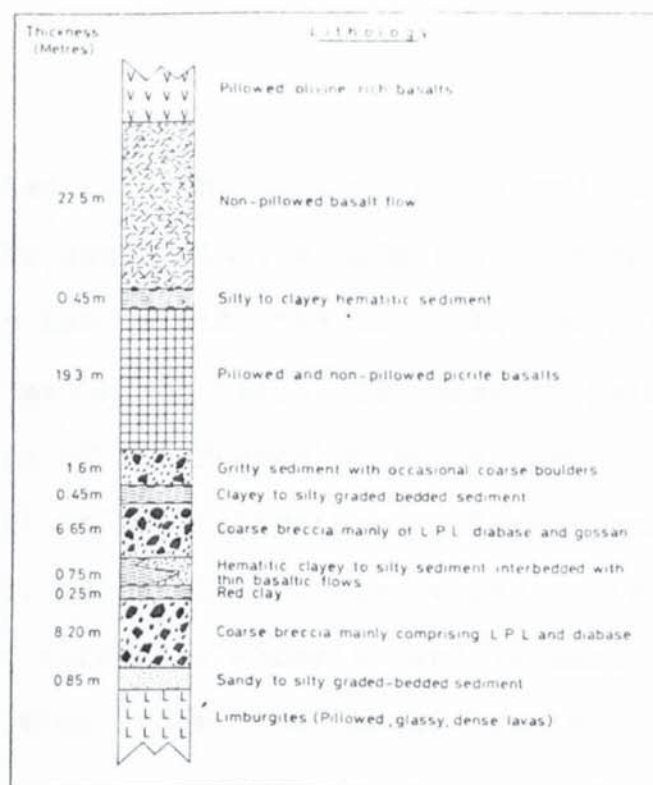


FIG. 5.10. Lithological details of the intervolcanic sediments as observed in the region north of Vasilikos stream.

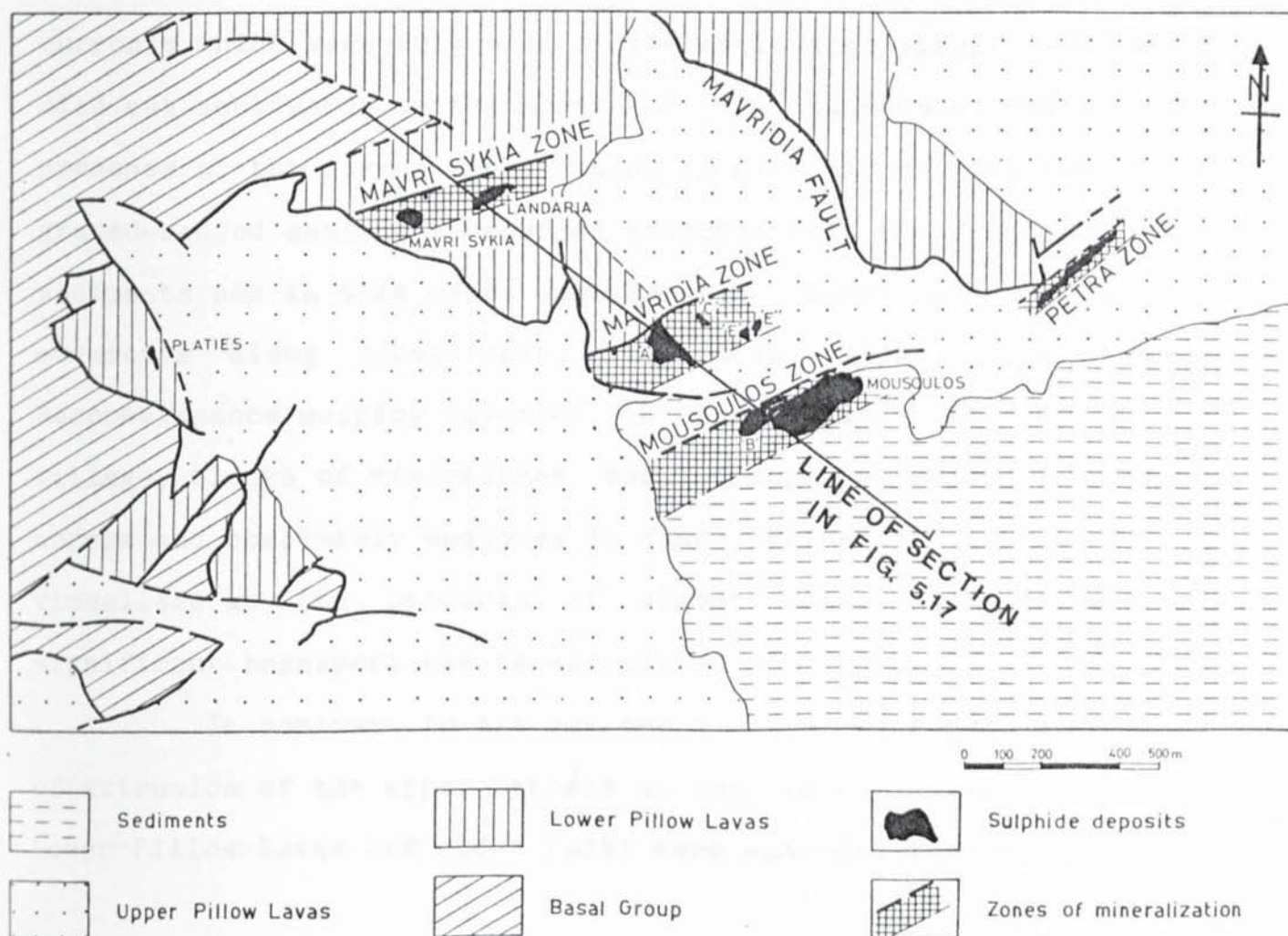


FIG. 5.11. Map showing the disposition of the Kalavassos deposits below the post-mineralization cover.

spatially associated with the intervalvolcanic sediments. They also occur deeper in the succession, within the limburgites, while at the contact of the latter with the Lower Pillow Lavas, to the north of Landaria, a major picritic columnarly-jointed sill is developed. The mode of occurrence of these rocks has already been described in detail in the literature (Searle and Constantinou, 1967; Constantinou, 1972) while their petrographic characteristics have been detailed elsewhere (Searle and Vokes, 1969). In the Kalavassos region they form the basal facies of the olivine basalts.

It is suggested here that there is a close relationship between intervalvolcanic sediments and the Arakapas Fault Belt. It is possible to visualise the sediments as the products of turbidity currents which were triggered in the fault zone itself and which died out southwards to the north of the Kalavassos region. The presence of the coarse breccia beds in alternation with the finer graded-bedded sediments provides evidence that the source of the sediments was in some cases considerably closer and related to movements along subsidiaries to this major fault zone. Reconnaissance mapping revealed, in the region east of Drapia village, blocks of mineralized Basal Group measuring 15 metres across and completely enclosed in finer sediments. Such blocks are visualised as the products of almost local slumping and no significant transport can be associated with them.

In contrast to the extremely active tectonic conditions of extrusion of the upper members of the volcanic sequence, the Lower Pillow Lavas and older rocks were extruded in conditions of

relative quiescence and no sedimentary breaks have been noted throughout the sequence. Moreover, no distinct angular unconformity is apparent between the Upper Pillow Lavas and the older formations. The uppermost part of the Lower Pillow Lavas, directly beneath the sedimentary horizon which separates them from the limburgites, is characterised by intense veining by ochreous matter which decreases gradually in intensity as deeper parts of the succession are reached and the more typical Lower Pillow Lavas with their characteristic alteration assemblages are developed.

The Basal Group, represented by the sheeted diabase dykes with rare pillow screens, which is usually characteristic of the deeper parts of the formation, is exposed in the western parts of the area and occurs in generally faulted contact with the younger formations. Isolated outcrops of oxidised Basal Group are also present in the Kokkinokremos area to the southwest of the Mavridia deposits.

5.2.3. The tectonic situation.

The complex relationships between the volcanic formations are further complicated by the fact that the rocks have been affected by severe tectonic movements which resulted to a steep northeasterly regional dip. The tilting has preceded sedimentary deposition and the members of the Perapedhi formation rest almost horizontally on the tilted volcanics.

A consequence of the bodily rotation of the lavas is the development of a series of low-angle gravity faults (Plate 5.5) which represent an attempt at tectonic re-adjustment. The net

result of this type of faulting is repetition of geological features and, in many cases, the masking of the underlying geology by a cover of younger pillow lavas. An example of the former situation is observed northeast of Petra, where basaltic flows and associated intervalcanic sediments are repeated by such faults. These tectonic features are clearly later in age than the mineralization and have, therefore, played a determining role in the fragmentation and dislocation of the sulphide deposits.

Undoubtedly the most important fault in the area is the Mavridia fault (Fig. 5.9) which extends northwestwards from the neighbourhood of Petra, forming to a large extent the boundary between the Upper Pillow Lavas and the Lower Pillow Lavas. This fault, which trends at 100° and dips 25° to the south, is clearly a very early structure as judged from the following:

a. There is propylitisation and sporadic patches of oxidation on the fault plane, indicating that it is to some extent mineralized. Borehole evidence indicates that, at depth, it is defined by a thickness of propylitic alteration with widespread pyritic impregnations.

b. All the orebodies are located in the hanging wall side of the fault and there is no correlation between the geology on the footwall and hanging wall, indicating that the fault was an important controlling structure during ore deposition.

c. The Upper Pillow Lavas are disposed in the form of a basin in the hanging wall side of the fault so that the structure may have also acted as control during lava extrusion.

All the above evidence suggests that the Mavridia fault

is a very early structure and quite distinct from the similarly dipping low-angle gravity faults. Re-tilting of the lavas to their horizontal attitude brings the fault to an almost vertical attitude with an easterly strike. It is here considered as a subsidiary fracture to the major Arakapas transform. This is supported by the evidence already presented in previous paragraphs (cf. intervolcanic sediments) on the effects of this structure on the geology of the area.

A most important series of faults trends to the northeast and may be clearly correlated with the trend of the dykes both in the Basal Group and Lower Pillow Lavas. These faults are exposed in the southwesterly parts of the area where they continuously form the boundary between the Basal Group and Lower Pillow Lavas but they are also especially evident in the region of the mines where their role in localisation of ore is particularly well shown.

5.2.4. The sulphide deposits.

It is clear from the brief description of the structure of the area that severe tectonic re-adjustments have taken place after extrusion of the volcanic rocks, these being evident in the steep tilt of the lavas and the resultant low angle faults. It is to be expected that these movements would also affect the enclosed orebodies resulting in some cases to the complete disruption of originally continuous bodies of ore. Nevertheless the original situation may be reconstructed, despite the structural complexity, and the essential features of the orebodies at the time of

formation envisaged. A most important point, however, to be kept in mind in the following discussion, is that, as a result of the tilting, the original upper levels of the deposits will be located to the northeast of the stockwork zone and not vertically above as would be the normal situation.

The orebodies, totalling 13 major and minor ones (Table 5.1) , may be classified into three groups on purely structural grounds:

a. The Petra group, comprising only one deposit bearing this name,

b. The Mavridia group, which includes the major deposits of Mousoulos, 'A', 'B' and the smaller concentrations called 'C', 'D', 'D'', 'D'''', 'E' and 'E'' located in the general area to the northeast of 'A' orebody.

c. The Mavri Sykia group which includes the deposits of Mavri Sykia (Underground and Opencast) and Landaria Underground.

The three groups occur in a belt which is roughly parallel to the strike of the Mavridia fault. The location of the orebodies beneath the cover of pillow lavas and sediments is shown in fig. 5.11.

5.2.4.1. The Petra orebody.

The orebody occurs in the form of a narrow pipe, 300 metres in length and 35 metres in maximum width (Fig. 5.12) and is localised at the intersection between the Mavridia fault and a northeasterly fault, termed the Petra fault, the mineralization following the latter structure. To the northwest, unmineralized

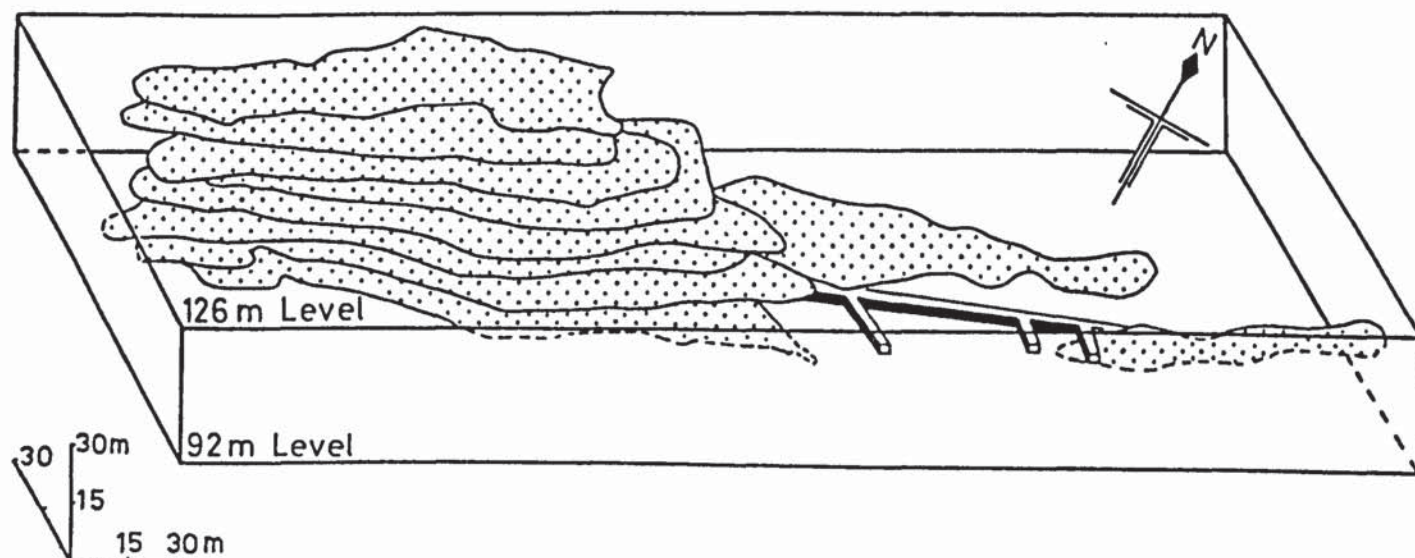


FIG. 5.12. Isometric projection of levels of the Petra orebody illustrating the narrow pipe-like nature of the deposit.

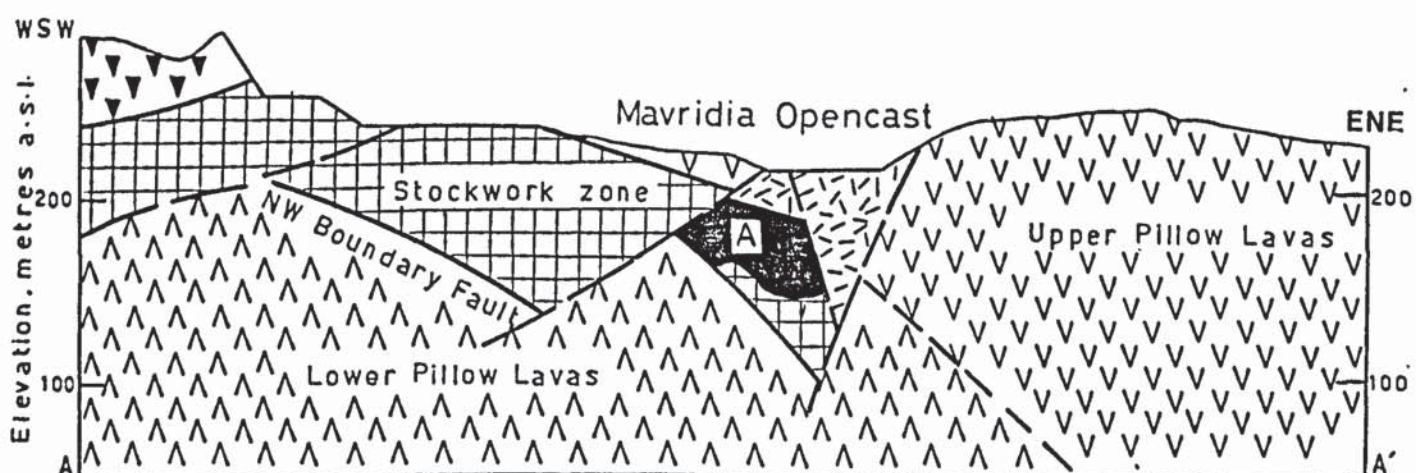


FIG. 5.13. Longitudinal section across 'A' orebody and the Mavridia opencast.

Lower Pillow Lavas are exposed, which are overlain by the limburgites in a normal sedimentary contact. To the southeast, the area is completely covered by unmineralized olivine basalts. The fault plane is marked by a zone of red hematitic gouge and gypsum (satin spar) veining and no trace of mineralization is detected beyond the boundary.

The grade of mineralization is very uniform throughout the length of the deposit and generally lies between 20 and 30 % S, richer mineralization and some massive concentrations only being encountered at the extreme northeasterly extensions, in its original higher parts. Study of assay plans suggests that copper was similarly regularly distributed within the ore zone.

The extensions of the mineralization towards the southwest are dislocated by a fault and the recently detected continuations of the zone are clearly of much lower grade than the main deposit.

The contacts of the mineralization with the surrounding rocks are described as gradational with a zone of propylitic alteration intervening between the mineralized ground and the unmineralized country rocks (Gordon-Smith, 1963). This feature provides indication that the present shape of the deposit is original and not the result of faulting. Formation of this narrow pipe is envisaged to have taken place by the sharp localisation of the ore fluids in the intersection between the Mavridia fault and the Petra fault, ore deposition taking place in these thoroughly fractured rocks. The description provided by previous workers of the ore as being composed of 'subangular fragments of mineralized

lava showing concentric and cross-cutting banding, enclosed in a fine sugary matrix' (Gordon-Smith, 1963) is consistent with the conditions of formation within a narrow tectonic zone.

5.2.4.2. The Mavridia group.

5.2.4.2.1 'A' orebody.

This is the most northwesterly of the group. The massive mineralization was located beneath a major microgabbroic flow (Fig.5.13 and Plate 5.6) and was bounded to the northwest by a steeply dipping northeasterly fault which defined the contact with unmineralized Lower Pillow Lavas. The fault, similarly to the previously described Petra fault, was marked by a zone of hematitic gouge and gypsum veining. Fractures subsidiary to the main fault were occasionally mineralized, otherwise the rocks on the footwall side of the fault were devoid of mineralization. This structure was termed the Northwestern Boundary fault (Adamides, 1980) in view of its role as a footwall to the mineralization in that direction.

To the southwest of the massive ore, and in the hanging wall side of the Northwestern Boundary fault, stockwork mineralization was located, occasionally traversed by unmineralized dykes feeders to Upper Pillow Lava flows. This mineralization was mined under the name 'Mavridia opencast' and the details of the geology and structure were brought to light during the mining operations (Fig. 5.14).

Low-angle faults dislocate the mineralization in its



PLATE 5.6. Mavridia opencast looking north. Note the major microgabbroic flow (top right) which overlay the massive pyrite of 'A' orebody (relic seen at bottom) and the exposed plane of the Northwestern Boundary Fault (left).
Length of field of view 50 metres.

topographically higher continuations but borehole evidence indicates that both the controlling structure and the mineralization continue uninterrupted beneath these faults. The grade continuously diminishes in this direction until both the footwall and hanging wall merge into weakly mineralized and strongly epidotised Basal Group rocks.

To the southeast the contacts between the mineralized ground and the dark unmineralized Lower Pillow Lavas are apparently gradational and roughly follow the dip of the Northwestern Boundary fault.

The essential features of 'A' orebody, therefore, are a northeasterly trending ore zone, exhibiting a massive upper part and stockwork mineralization beneath, now situated to the southwest as a result of the tilting, a controlling fault to the northwest, bounding the ore zone from the unmineralized Lower Pillow Lavas in that direction, and transitional contacts to the southeast. Re-tilting of the rocks to the horizontal will not much modify the situation since the controlling structure strikes parallel to the direction of dip of the formations. The most significant change will be the positioning of the stockwork zone directly beneath the massive pyrite in conformity with the situation in typical Cyprus sulphide deposits.

In light of the above, the smaller deposits each amounting to approximately 50 000 tons and situated directly northeast of 'A' orebody, may be either viewed as parts of this deposit, dislocated by faulting, or, more probably, as individual pockets of massive pyrite deposited within the fault zone and left

behind when the main body of the mineralization slid further down dip along the Northwestern Boundary fault. The lack of associated stockwork and the fact that these pockets of ore are completely enclosed within the fault zone provide further support to the inference.

5.2.4.2.2. The Mousoulos and 'B' orebodies.

After the detailed description of 'A' orebody, a recounting of the situation at the Mousoulos orebody would be in most part repetitive. A northeasterly structure, although much steeper than the Northwestern Boundary fault and almost vertical in attitude, forms the northwestern boundary of the deposits with the unmineralized lavas (Fig. 5.15). The massive pyrite is again located to the northeast as a result of tilting and a zone of ochreous sediment formed the boundary between this and unmineralized Upper Pillow Lavas. This zone was interpreted as evidence of submarine weathering of part of the massive pyrite prior to the extrusion of the Upper Pillow Lavas (Constantinou, 1972). To the southeast the contact is faulted with Upper Pillow Lavas in the hanging wall side, while in the southwesterly direction, parallel to the localising structure, the mineralization passes from massive to stockwork and the grade gradually diminishes.

The relationship between Mousoulos orebody and 'B' is illustrated in fig. 5.16. As this diagram suggests, 'B' orebody represents a fragment of the Mousoulos deposit disconnected by one of the low-angle faults described in previous paragraphs, while it

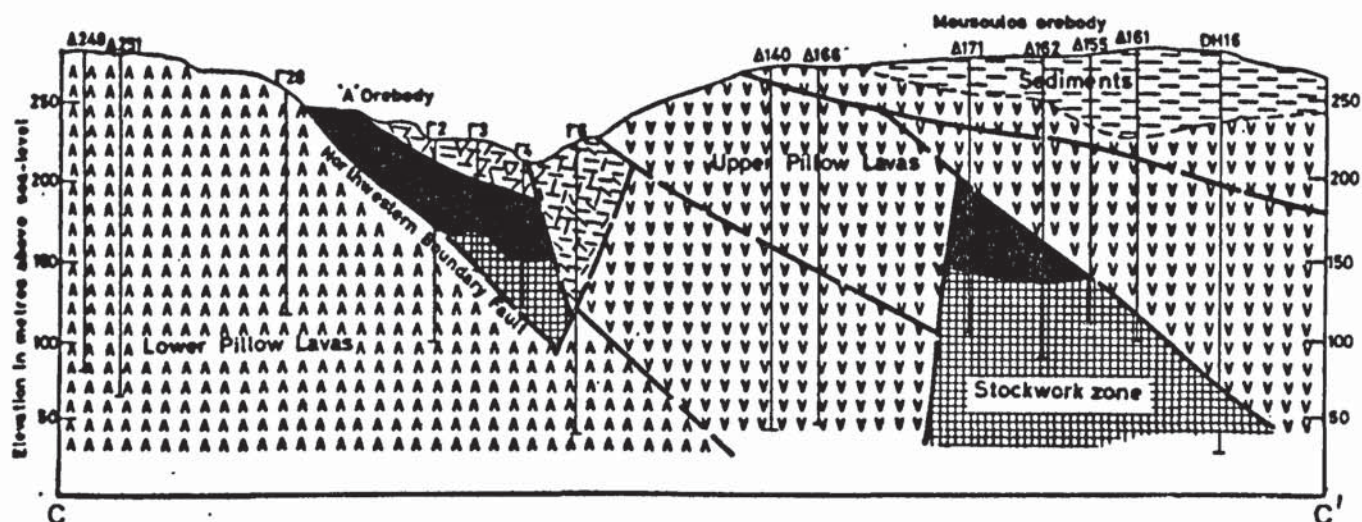


FIG. 5.15. Transverse geological section through 'A' and Mousoulos orebodies.

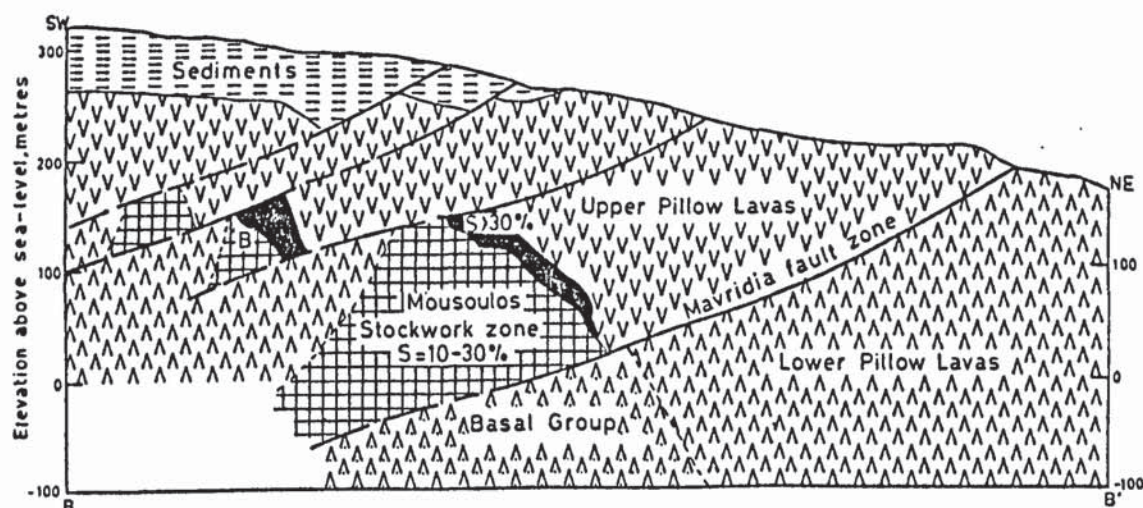


FIG. 5.16. Longitudinal geological section through Mousoulos and 'B' orebodies.

itself is similarly affected by another low-angle fault and the situation repeated. On the same section (Fig. 5.16) the function of the Mavridia fault is clearly shown: It formed a definite footwall for the mineralization in the northeasterly direction, although the structures which acted as controls in ore localisation were clearly the northeasterly faults as the morphology of the deposits indicates.

5.2.4.3. The Landaria and Mavri Sykia deposits.

The control imposed by the northeasterly structures on the deposition of the mineralization is even more indisputably apparent in the case of the Landaria-Mavri Sykia ore zone than in the deposits previously described.

The presence of ore is reflected on the surface by a linear zone of oxidation completely enclosed within Lower Pillow Lavas. This zone terminates to the northeast in a gradational manner even before the contact with the overlying limburgites is encountered. Examination of borehole evidence suggests that both Landaria and Mavri Sykia represent richer concentrations of mineralization within the ore zone and they are surrounded by a halo of weaker mineralization.

Observation of the differences between the lavas on either side of the mineralized zone indicates that it defines a fault, with Lower Pillow Lavas characteristic of the lower part of the formation developed to the northwest and brecciated lavas typical of the uppermost parts of the Lower Pillow Lavas being dominant to the southeast. Furthermore, detailed examination of

the gossan indicates that a zone of propylitic alteration defining the footwall to the northwest passes into intense gossanisation in the central parts of the zone and thence through iron stained lavas into the unmineralized rocks to the southeast. These features, together with the envelop of propylite which reputedly surrounded the mineralization underground (Pantazis, 1966) are taken as evidence that, similarly to Petra, the deposits are found together with their associated rocks and exhibit gradational boundaries with the surrounding lavas. These may have been later modified by slippage as a result of the difference in competence between the mineralized and unmineralized rocks, with the envelop of propylite acting as the slip surface, but the original rock relationships were not significantly modified.

A noteworthy feature of the Landaria-Mavri Sykia ore zone is the lack of evidence that the solutions ever reached the surface of the lavas. The zone itself terminates within the Lower Pillow Lavas whereas the orebodies are in the form of richer concentrations within the ore zone. As such they may be termed replacement deposits as contrasted to the truly exhalative character which may be postulated for 'A', 'B' and Mousoulos as well as, probably, for the massive pyrite at the extreme northeast of Petra, in its original uppermost parts.

5.2.5. Stratigraphic position of the orebodies.

The first piece of evidence to suggest that mineralization was intervalcanic rather than post-volcanic relates to the presence of blocks of oxidised ground in the coarse

fraction of the intervalcanic sediments.

Both 'A' orebody and Mousoulos orebody are located at the boundary between the limburgitic lavas and the Lower Pillow lavas and the ochreous band occurring between the massive pyrite and the overlying lavas suggests a stratigraphic break.

The evidence from the Petra orebody is inconclusive: Extrapolation of the sedimentary boundary between the limburgites and the Lower Pillow Lavas intersects the orebody and this implies that the higher parts (northeasterly extensions) are located within the limburgites. The lack of exposure, however, does not permit the evaluation of this inference.

The most significant conclusion on the stratigraphic position of the deposits is derived from the chemical data on the Mavri Sykia lavas which were described in chapter 2 as the EMS lavas. These suggest that no chemical break exists between rocks which are mapped as Lower Pillow Lavas on the basis of lithology and alteration, and the overlying limburgites, included in the Upper Pillow Lavas. The ensuing paradox results to the deposits being localised at the contact between the Lower Pillow Lavas and the Upper Pillow Lavas on the basis of field geology and within the Upper Pillow Lavas on the basis of chemistry. The implication of this is that hydrothermal deposition is genetically linked to the early stages of extrusion of chemically primitive lavas whose main representatives are the limburgites and olivine basalts of the Upper Pillow Lavas.

5.2.6. The Kalavastos deposits in relation to their setting.

It is interesting and informative to speculate on the morphological and tectonic features of the Kalavastos orebodies as interpreted in the light of the tectonic environment of their formation. The area provides an opportunity, unique on the island, of studying the interaction in ore genesis between a spreading axis and a transform fault.

A most important conclusion derived from the study of the deposits is the strict structural control imposed on the deposition of the mineralization by northeasterly structures. The tectonic analysis presented indicates that such structures are parallel to the dykes of the Sheeted Complex and Lower Pillow Lavas and, in the light of the tectonic environment of formation of the ophiolite in a spreading axis, the direction of the dykes in these formations, and particularly in the former, defines the direction of the spreading axis. It is therefore evident that the Kalavastos deposits are localised by faults which were parallel to this axis.

It has also been conclusively proved that the Mavridia fault is a subsidiary of the Arakapas fault belt. Its main function, however, lay in the creation of a basin of lava extrusion and, although its fault plane shows evidence of the effects of the mineralizing solutions, it has not localised any orebodies. The Mousoulos orebody is the only deposit which is bounded by the Mavridia fault to the northeast, so that it was deposited in close juxtaposition with this structure, but the deposit was clearly localised by a northeasterly fault as

previously concluded.

The above evidence indicates that transform structures and their subsidiaries are not favourable hosts for the deposition of mineralization and that, even in environments where such faults play a dominant role, orebodies are localised by axis-related structures. The reason probably lies in the fact that such faults are essentially closed structures and mainly transcurrent in nature. A broader relationship may, however, exist between transform faulting and ore deposition in the creation of a much dissected terrain where ore solutions may find amenable ground for deposition. In special situations, as at Petra, such faults may act in conjunction with axial faults in localising mineralization.

A corollary of the intense tectonism characterising areas of transform faulting is the size of the resultant orebodies. The Kalavassos mining district is characterised by generally small deposits as a result of the multitude of favourable structures developed. It is interesting to note that the 'A' ore zone and the Mousoulos-'B' ore zone, although clearly coalescing in their stratigraphically deeper extensions, are localised by separate structures on the surface, even despite the fact that the intervening barren ground may be measured in tens of metres. In the absence of this intense structural disturbance, the solutions would tend to follow one major structure, widening it by hydraulic fracturing and depositing their burden in a single large deposit.

A further implication of the interaction of transform faulting in metallogenesis is the absence of major sulphide deposits in the fault trough of the Arakapas transform. Robertson

(1978), on the basis of this fact, concluded that transform faulting bears little relationship to the sulphide mineralization. Evidence from Kalavassos indicates that the function of transform-related features lies more in ground preparation rather than ore localisation. This conclusion may be taken to the extreme situation of sulphide mineralization being deposited in the fault trough: The intense tectonism would result to a multitude of favourable structures and the consequent dissipation of ore solutions into small concentrations, while continued disturbance would further brecciate these and vulcanicity in the fault trough would almost completely obliterate any trace of a sizeable deposit. This conclusion is verified in the field by examination of the evidence of mineralization in the region of Ephtagonia village, in the valley of the Arakapas fault belt. This evidence is in the form of small pockets of oxidation, not exceeding a few metres in dimensions, erratically interspersed in terrain comprising mostly unmineralized lavas.

A final feature of the Kalavassos deposits relates to the nature of their localising structures. They are by no means major faults and they become completely inconspicuous away from the orebodies although they were instrumental in the channeling of the hydrothermal fluids. The implication of this feature is that the faults have only acted as the passive recipients of the ore solutions in higher levels, their role largely diminishing in the deeper parts of the volcanic pile. This is in complete agreement with the theory of seawater circulation in the formation of Cyprus sulphide deposits. The ore solutions, diffuse in their nature in

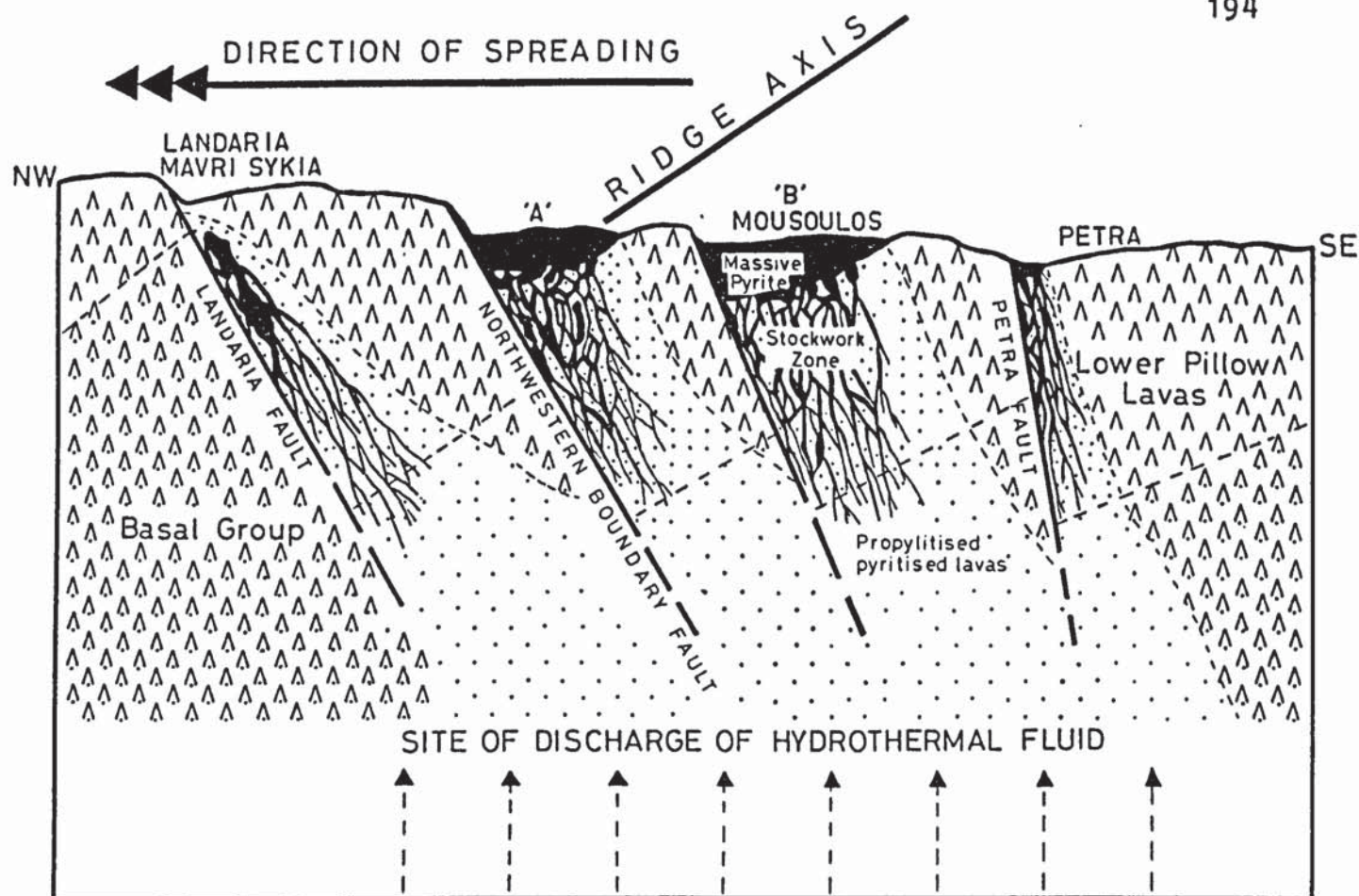


FIG. 5.17. Diagrammatic illustration of the regime of formation of the Kalavassos deposits. The diagram highlights the role of axis-related tectonic features in the localisation of hydrothermal fluids and interprets the widespread pyritic mineralization observed at low stratigraphic levels below the deposits as the result of the delocalised upward movement of hydrothermal fluids prior to reaching the sea floor.

the Sheeted Complex, are sharply localised in the upper parts of the volcanic sequence by open structures created at the axis of spreading. Formation of 'A', Mousoulos, 'B' and, probably, Petra orebodies was associated with exhalative processes. By contrast, Landaria and Mavri Sykia show evidence that the solutions never reached the surface and deposited their burden within favourable horizons in the Lower Pillow Lavas. Fig. 5.17 shows the mode of formation of the deposits in relation to the axis of spreading and according to the theory of seawater circulation.

5.2.7. Conclusions from the study of the Kalavassos deposits.

The detailed study of the mode of occurrence of the sulphide deposits of Kalavassos with relation to the situation of the area close to a transform structure leads to the following conclusions:

Close structural control is exercised in ore deposition by axial faults as opposed to transform-related features. The effect of the latter structures lies more in ground preparation than ore localisation.

The deposits are predominantly exhalative and comparatively small as a result of the abundance of structures available for the percolation of ore fluids.

The localising structures are relatively minor features, inconspicuous away from mineralization. This suggests that they were not themselves the cause for the uprise of the ore fluids. Deep-seated causes are envisaged, with the faults acting as the passive recipients of the ore bearing fluids.

5.3. The Mangaleni orebody, Parekklishia area: An unusual deposit.

5.3.1. Introduction.

The Parekklishia area is situated in the southern part of Cyprus (Fig. 1.1) and close to the Limassol Forest Plutonic Complex.

Evidence of mineralization is relatively limited and was originally in the form of narrow zones of oxidation in tectonic relationship with unmineralized lavas and sediments. The oxidation was locally intense and highly auriferous, and has been the subject of small scale exploitation in the past. It is reputed that this is the site of the richest sample of gold ore in Cyprus, assaying 1500 grams of gold per ton (Ch. Marangos, pers. com. 1980).

Drilling in the area in the 1970s revealed the presence of locally rich mineralization which was mined in a small opencast between the years 1976-1977. The total ore mined was 100 000 tons, assaying 1.8 % Cu and 3 % S.

The author mapped the area initially in a scale 1:1000 and later, when it became evident that regional mapping was required for the unravelling of the structural complexity, in a scale 1:5000. The opencast workings were mapped in two phases of the mining operations.

The area is described in the following paragraphs mainly in view of the peculiar mode of occurrence of the mineralization and the evidence of intense tectonism as indicated in both the regional structure and the microscopic characteristics of the ore.

5.3.2. Geological framework.

The stratigraphic sequence in the area is shown in fig. 5.18 and the geology of the area surrounding the mineralized occurrence is shown in Map 3 (Enclosed in pocket).

Beneath the massive or bedded reef limestone there is developed in the area a thick sequence of clays with occasional interbedded chalks and cherts and a variety of incorporated exotic blocks of sandstones, alkaline lavas and, elsewhere, serpentinites. The formation is strongly tectonised and attains a great thickness. It is the lateral equivalent of the autochthonous Moni clays which in the Kalavassos mining district do not exceed 10 metres in thickness and are completely free of exotic blocks. Similarly it is the lateral equivalent of the Kannaviou Formation described in the Limni area. It has been termed 'the Moni Melange' (Pantazis, 1967) and has been interpreted as the product of trench sedimentation (Panayiotou, 1977, Robertson, 1977).

The Moni melange rests on the Perapedhi Formation represented by the normal sequence of well-bedded radiolarites and a thick sequence of bedded and delicately-banded umbers in hues of orange and dark brown which, in the basal parts, are massive and unbedded. The contact of the umbers with the Upper Pillow Lavas is marked by a zone of brecciated, umberiferous lavas.

Beneath the sedimentary cover, the sequence of Upper Pillow Lavas comprises olivine basalts in the higher levels and limburgitic lavas in the basal section. Picritic flows are absent, the closest approach to the latter rock type being represented by

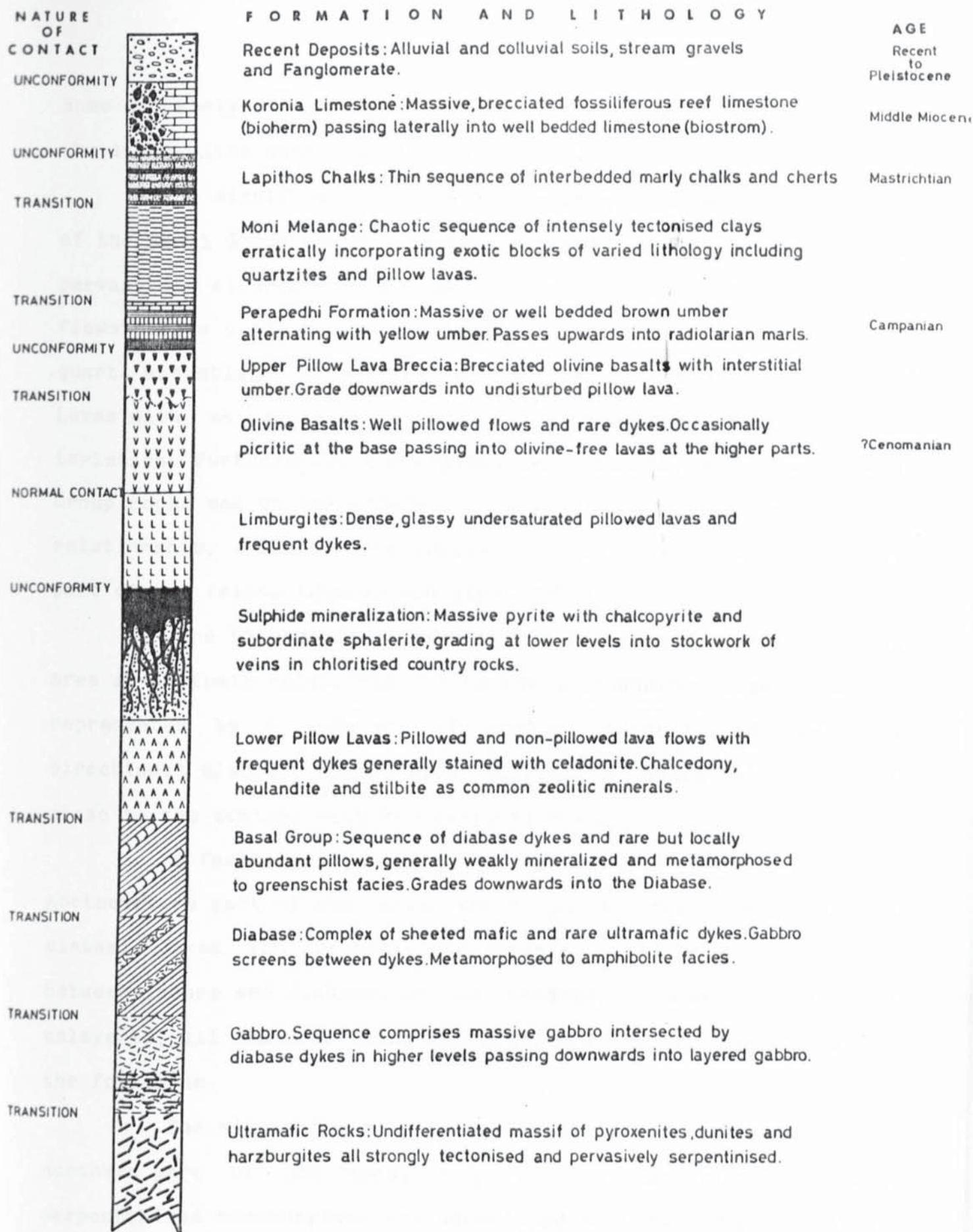


FIG. 5.18. The stratigraphic sequence in the Parekklishia area.

some extremely olivine-rich basaltic flows close to the contact of the limburgites with the olivine basalts.

A significant feature of the area relates to the nature of the Basal Group which is mostly represented by a sequence of pervasively altered and frequently weakly mineralized pillowed flows (Plate 5.7) characteristically containing an epidote and quartz assemblage but passing transitionally into Lower Pillow Lavas with no apparent change in lithological field characteristics. Furthermore, limburgites rest directly on these Basal Group rocks and on the adjacent Lower Pillow Lavas in overlap relationship, a feature previously noted by other workers in this part of the island (Moores and Vine, 1971).

The Diabase is exposed in the northwestern part of the area in tectonic relationship with the surrounding rocks and is represented by a sequence of mostly unmineralized and unidirectional diabasic dykes, with ultramafic dykes also present close to the contact with the serpentinites.

A fault-bounded block of gabbro is present in the northeastern part of the area where it is much traversed by diabasic dykes and probably represents a transitional facies between gabbro and Diabase. It is massive, coarse grained and unlayered, all features being characteristic of the upper part of the formation.

The ultramafic massif, occupying a large portion of the northern part of the area, comprises in the main intensely serpentinitised harzburgites and associated dunites and pyroxenites. This serpentinite is in tectonic relationship with the volcanic



PLATE 5.7. Chloritised and epidotised pillowed flows of the Basal Group as exposed in the region west of Mangaleni opencast. Such flows comprise the larger part of the outcrop almost to the exclusion of dykes.



PLATE 5.8. Strongly folded umbers exposed in the Mangaleni opencast.

rocks and has not been mapped in any detail.

5.3.3. Structure of the area.

The tectonic relationships between the igneous and sedimentary rocks are complicated as a result of the upheavals which culminated in the emplacement of the ultramafic massif. The tectonic complexity is especially evident in the more plastic rocks of the Moni Melange, resulting in complex folding and a generally chaotic situation in this formation. The umbers, and, to a much greater extent, the igneous rocks are much more competent in their behaviour, yielding to stress either by a combination of folding and faulting (umbers) or simply by fracturing and shearing (igneous rocks).

The contact of the Diabase with the ultramafic rocks is marked by a zone of intense mylonitisation and shearing, witness to the magnitude of the forces which operated in order to bring the two into structural juxtaposition. This major fault, which in the mapped area is dipping steeply towards the north, and is thus high angle reverse in nature, gradually changes in dip westwards and in the region of Akrounda village is a typical low-angle thrust bringing the serpentinites to rest over sediments of the Perapedhi formation (Panayiotou, 1977).

A similar function is played by the fault defining the contact of the Basal Group with the Diabase and this high-angle reverse fault is almost the exact replica of the previously described structure. The fact that the diabase dykes are predominantly oriented parallel to these faults while their

direction of dip changes in a northerly traverse from southerly to northerly may be the result of the couple operating during the thrust movements.

The two reverse faults described above, are dislocated in their southerly continuations by a steep northeasterly trending fault which dominates the central part of the area. In the hanging wall side of this normal structure the continuation of the reverse fault which bounds the Basal Group from the Diabase may be traced continuously towards the southeast, forming the boundary between Lower Pillow Lavas, Basal Group or limburgites in the footwall side and olivine basalts and sediments in the hanging wall. The reverse fault which formed the contact between the Diabase and the serpentinites is extrapolated to extend through the Mangaleni opencast.

5.3.4. Mode of occurrence of the Mangaleni mineralization.

The mineralization was originally evident on the surface by a series of linear, thin, zones of oxidation, occasionally intense but mostly in the form of moderate iron staining in fractured lavas. The slices of oxidised lava were generally enclosed in unmineralized Upper Pillow Lavas and in other cases at the contact between umber and pillow lavas, all contacts being clearly tectonic.

The geology of the mine, as exposed after the cessation of mining operations is shown in fig. 5.19. In the field the pillow lavas are deformed by intense shearing which locally results to the complete obliteration of pillow structure, while

Legend

- Lapithos cherts and cherts
- Moni clays
- Pink marls
- Brown umber
- Interbedded yellow and brown umber
- Upper Pillow Lava Breccia
- Upper Pillow Lavas
- Iron stained lavas
- White propylitic ore type
- Black cupriferous ore type
- Massive pyrite
- Fault with dip
- Dip of sediments
- Dip of pillows
- Mine bench
- Exploration borehole
- Elevation contour (metres)

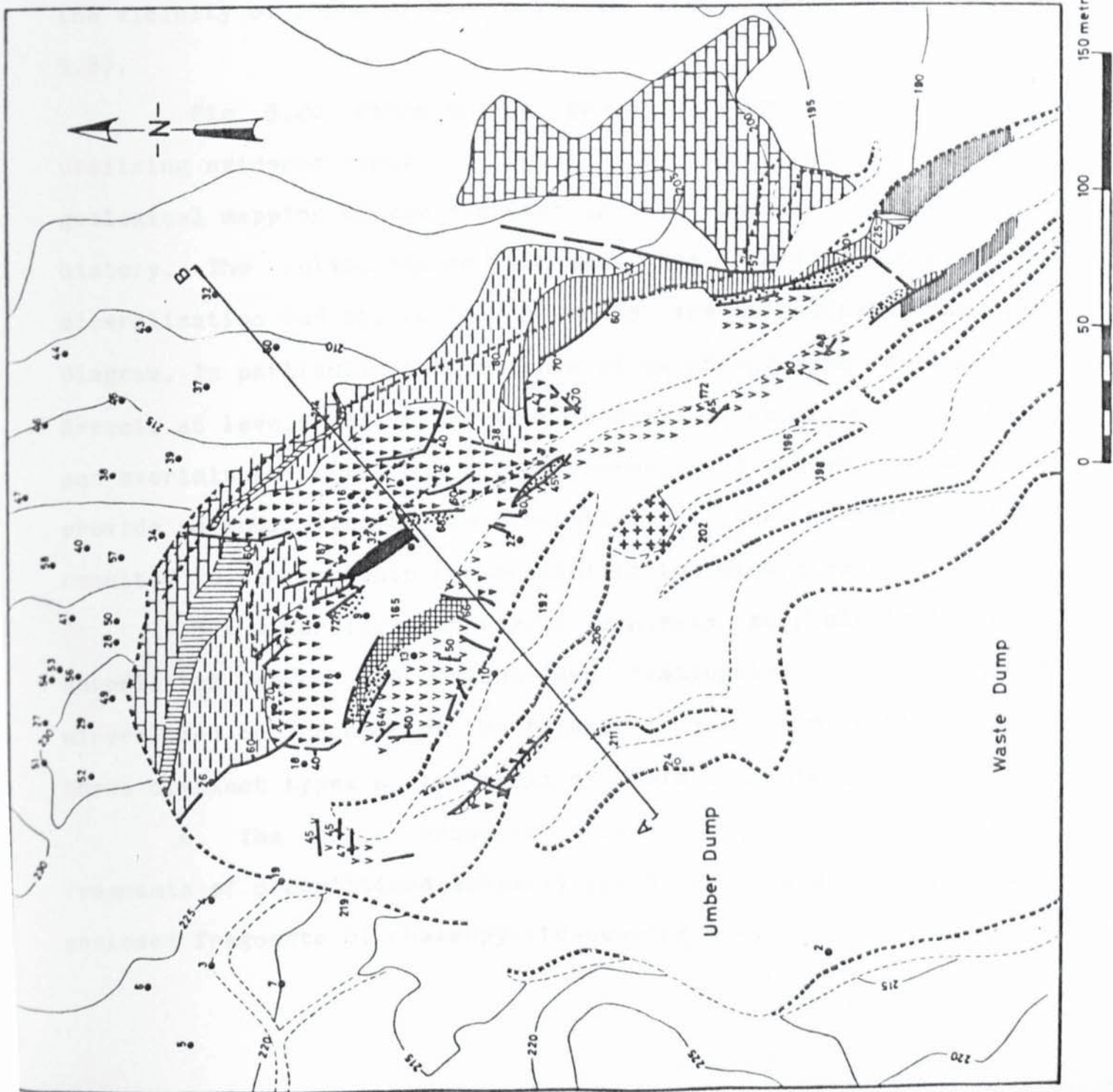


FIG. 5.19.

Geological map of Mangaleni mine.

the slices of mineralized ground are always bounded by faults from the unmineralized rocks. Faults are numerous in the opencast and show a dominant northwesterly orientation, which is also the direction of the major reverse structure of which they are components. Each individual fracture, even where it traverses unmineralized lavas, is marked by a zone of propylitic alteration with pyrite disseminations, bearing every indication of having been squeezed into position by tectonic movements. The umbers in the vicinity of the mine are deformed into tight folds (Plate 5.8).

Fig. 5.20 represents a geological section constructed utilising evidence provided both from the boreholes and the geological mapping of the opencast in two phases of its brief history. The relationships between the various types of mineralization and the enclosing rocks are illustrated in the diagram. In particular the presence of umber and Upper Pillow Lava Breccia at levels well below their normal stratigraphic position and overlain by rocks which are normally situated below them provide an indication of the complexity of the movements which resulted to the tectonic emplacement of the mineralization.

The mineralization itself exhibits morphological characteristics which are unique and distinguish it from other mineralized occurrences on the island. It has been divided into three distinct types on the basis of field character.

a. The white propylitic ore type, comprising mostly fragments of propylitised sparsely pyritised lava with very rare enclosed fragments of chalcopyrite-bearing ore.

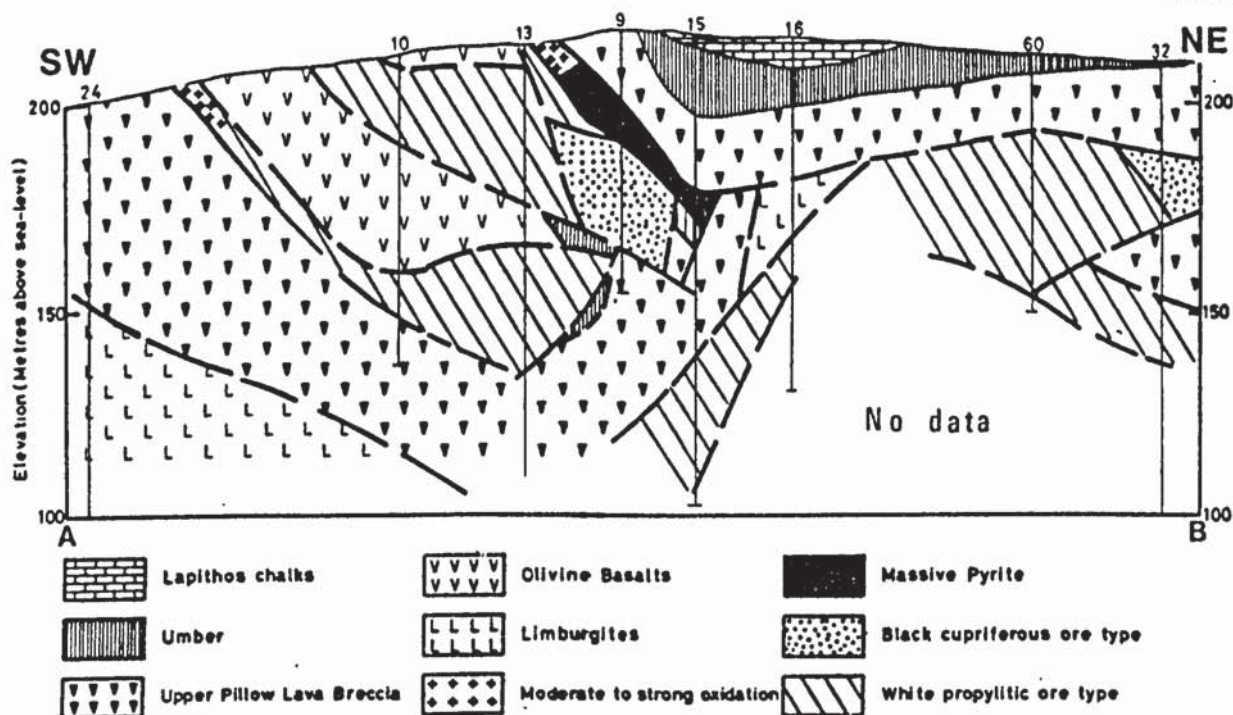


FIG. 5.20. Geological section through the Mangaleni mineralization. The diagram was constructed utilising data from two phases of mapping and from boreholes and emphasises the intense structural complexity of this occurrence. Note in particular the presence of umber at levels far below its normal stratigraphic position.

b. The black cupriferous ore type, which consists of intensely sheared lava with veins and concretions of chalcopyrite. This type occurs in some cases in association with the first type and the boundary between the two is marked both by the change in colour as well as by the concomittant change in grade since the latter is generally associated with much higher copper content.

c. The massive pyrite which is similar in all respects to the massive pyrite associated with typical Cyprus type deposits and comprises black, sandy-textured cupriferous pyrite occasionally enclosing blocks of chalcopyrite-sphalerite-rich ore, intensely sheared and rounded by tectonic movements.

An important feature of the detected mineralization is the absence of typical stockwork. No blocks or siliceous, sulphide-veined ore was detected in any part of the opencast. With the exception of the massive sulphide blocks, the rest of the mineralization is represented by pervasively chloritised but otherwise very weakly mineralized lava.

It is difficult to reconstruct the morphology and original rock relationships of the parent body of which this mineralization is a part, or the exact provenance of the deposit. The geological section shown in fig. 5.20 indicates clearly that all mineralization encountered is in the form of disconnected slices over a zone which, on the basis of additional borehole evidence, exceeds 300 metres in horizontal width and, through this zone, the ore blocks are erratically interspersed and tectonically interbedded with unmineralized lavas and sediments. The presumed parent body has not yet been located.

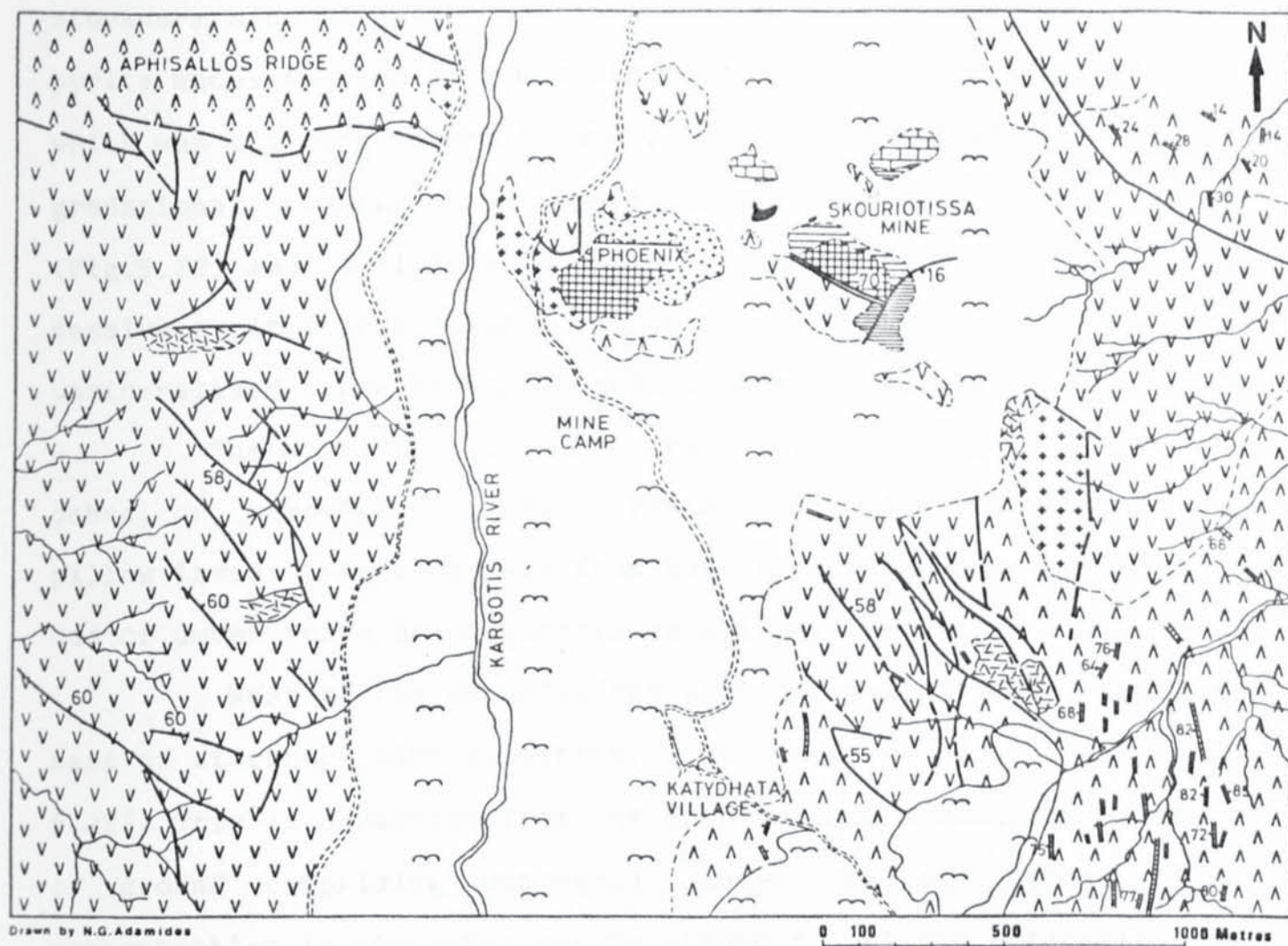
It may be inferred from the above that the mineralization at Mangaleni has been affected by the severe tectonic movements which resulted to the emplacement of the ultramafic rocks of the Limassol Forest and these movements have disconnected the original mineralization from its locus of deposition and have tectonically transported it in the form of a series of slices towards higher levels. The large width of the zone of disturbance is considered to be the result of the degeneration of the original clearly-defined thrust faults on encountering the much more incompetent sediments and lavas, so that they are now apparent in the form of a series of anastomosing shears. The net sense of movement is not expected to have changed and this is indicated by the fact that intense shearing characterises the tectonism in the opencast as opposed to the open structures created by normal faulting.

5.4. Skouriotissa and Phoenix.

The Skouriotissa orebody, on the northern flanks of Troodos (Fig. 1.1), is one of the largest deposits on the island, having yielded 6 million tons of massive pyrite. The geology of the area surrounding the mineralization is shown in fig. 5.21.

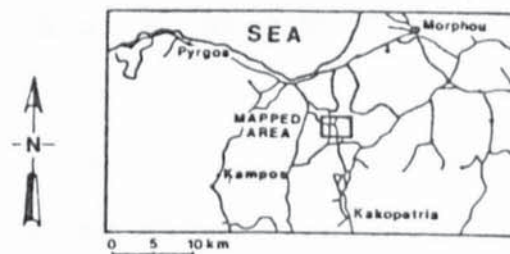
Geological studies (Adamides, 1981) suggest that localisation of the mineralization was effected by the interaction of northerly structures, which reflect the structural grain of the Lower Pillow Lavas in the area, and a major easterly-trending structure which is indicated on the surface by a ridge of hydrothermally altered lavas (Fig. 5.21).

The deposit is characterised by a central pipe of



LEGEND

	Drift and dump cover		Massive pyrite
	Reef Limestone		Stockwork mineralization
	Marls, clays and umber		Altered lavas
	Upper Pillow Lavas		Leached lava
	Lower Pillow Lavas		Oxidised lava
	Basal Group		Intrusive



Geologically surveyed by N.G. Adamides

FIG. 5.21. Geological map of the Skouriotissa area.

stockwork mineralization and an extensive flat lens of massive pyrite whose thicker part was directly located above the pipe and which was thinning laterally away. The stockwork pipe exhibits a gradational passage into unmineralized Lower Pillow Lavas (Fig.5.22) and is limited in extent compared to the overlying massive pyritic lens so that the latter is resting on completely unmineralized lavas in its lateral extensions (Plate 5.9).

The massive pyrite is covered locally by a layer of ochre, or, elsewhere, by umber (Plate 5.10), with no intervening pillow lavas. Laterally away from the deposit the same continuous bed of umber rests on unmineralized olivine basalts.

West of the Skouriotissa orebody is located an extensive mass of stockwork mineralization, the Phoenix occurrence (Fig. 5.22). This is separated from the Skouriotissa orebody by a tract of ground comprising unaltered Lower Pillow Lavas. This concentration is characterised by strong propylitic alteration in the upper parts, passing in deeper levels into a stockwork of sulphide veins.

Constantinou (1972, 1980) considered the lavas underlying the massive pyrite as belonging to the olivine basalts and the Phoenix mineralization as the stockwork zone of the Skouriotissa orebody, invoking faulting and tilting to account for the observed picture. The present study suggests that the two occurrences are distinct concentrations of ore, although partly localised by similar structures. Borehole evidence indicates that the pipe of stockwork mineralization underlying the massive Skouriotissa deposit extends to considerable depths and no



PLATE 5.9. Skouriotissa opencast. Massive pyrite (indicated by arrow) resting on unmineralized Lower Pillow Lavas. Length of field of view 60 metres.



PLATE 5.10. Well bedded umber resting on massive pyrite. Skouriotissa opencast. Length of field of view 30 metres.

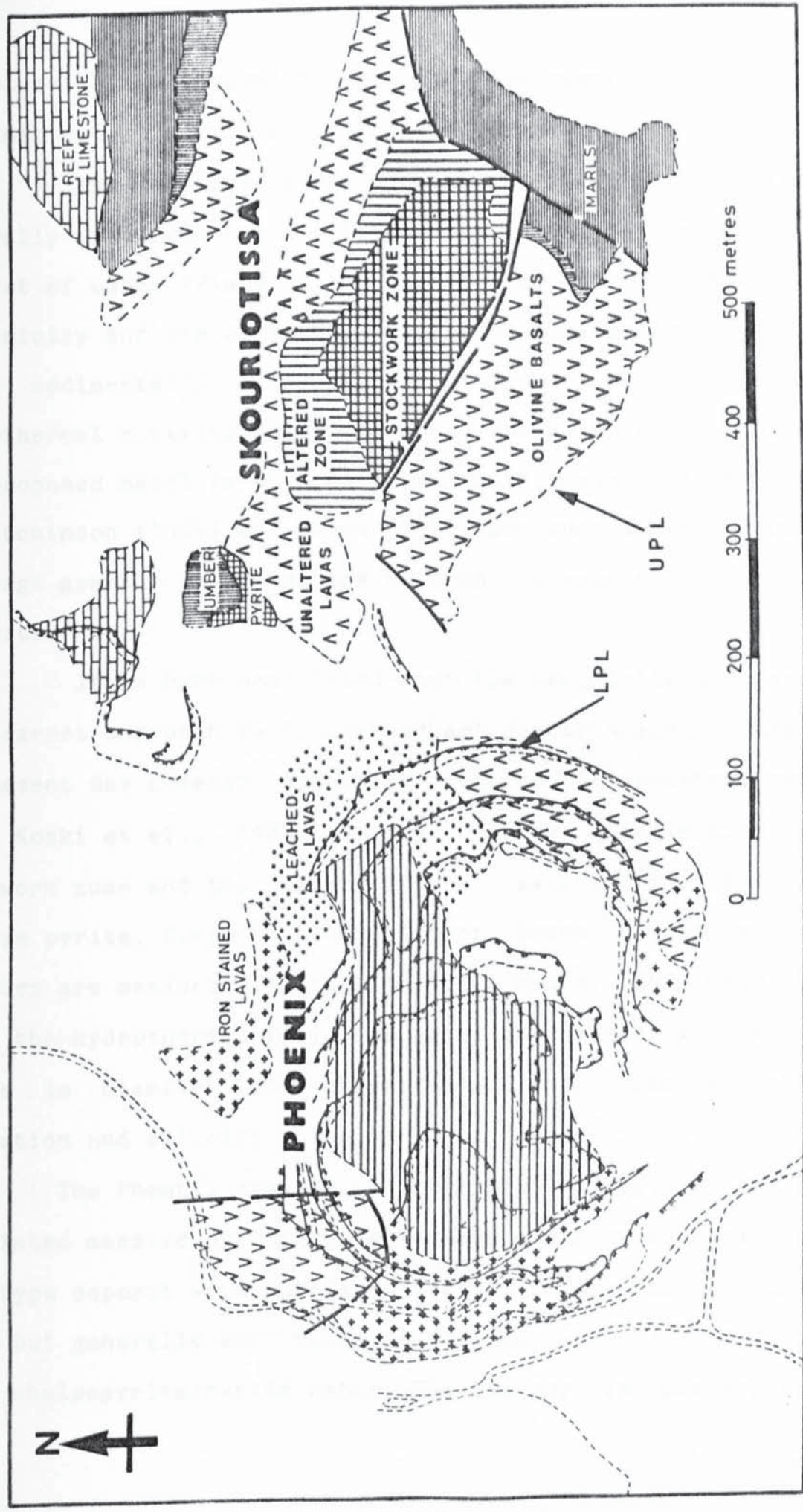


FIG. 5.22. Detailed geological map of Skouriotissa and Phoenix.

structure may be invoked to transport the massive pyrite from an original situation above the Phoenix orebody.

The development of thick Upper Pillow Lavas in the area laterally away from the massive pyrite and the cover by a common blanket of umber (Plate 5.10) testifies to penecontemporaneous vulcanicity and ore deposition, followed by a prolonged period of umber sedimentation probably related to the same cycle of hydrothermal activity which deposited the sulphide mineralization. The proposed model is thus in accord with ideas earlier proposed by Hutchinson (1965) and Clark (1971) who were among the first to envisage genetic relationships between the umbers and the sulphide deposits.

It is here postulated that the Skouriotissa orebody is the nearest approach to 'black smoker' deposits such as are found on present day oceanic spreading centres (Francheteau et al., 1979, Koski et al., 1982) in the narrow localisation of its stockwork zone and the large lateral extent of the overlying massive pyrite. Compared to the latter deposits, however, whose orifices are measured in fractions of a metre, the pipe through which the hydrothermal fluids ascended to higher levels is 300 metres in diameter and characterised by intense chloritic alteration and silicification.

The Phoenix orebody, in most probability, never had an associated massive pyritic zone and bears all characteristics of a vein-type deposit with intense chloritic alteration of the host rocks but generally weak sulphide veining and disproportionately large chalcopyrite:pyrite ratio. The orebody is envisaged as a

linear broad zone of sulphide veining and propylitisation with ore deposition taking place within the lava pile and probably not having reached the surface except in limited areas. Rock relationships in the opencast suggest that propylitised but otherwise unmineralized lavas in the upper parts of the ore zone pass gradually in deeper levels into sulphide-impregnated ground.

5.5. The deposits of the Tamasos area

5.5.1. Agrokipia

Geological mapping in the Tamasos area (Adamides, 1983) suggests a marked absence of strong tectonism which could provide the necessary structural control for ore deposition and a predominance of concordant sills and flows which would tend to dam the solutions and lead to the formation of deposits within the lavas as opposed to exhalative ones.

The Agrokipia 'B' orebody (Fig. 5.23) provides an example of sulphide mineralization completely enclosed within the Lower Pillow Lavas. The orebody has been studied by Constantinou (1972), who, in disagreement with Searle (Searle and Constantinou, 1968), who postulated that the deposit was formed at the boundary between the Basal Group and Lower Pillow Lavas, considered that the horizon of the mineralization was the boundary between the Lower and Upper Pillow Lavas. The present investigation indicates that, not only the Lower Pillow Lava-Upper Pillow Lava boundary is completely unmineralized, but a considerable thickness of unmineralized Lower Pillow Lavas is penetrated before the



FIG. 5.23. Isometric projection of the Agrokipia deposits.

mineralization is encountered (Fig. 5.23). The passage from unmineralized to mineralized lavas is effected gradually through a zone of sulphide veining in otherwise very little altered lavas. A large thickness of glassy lavas is present in the close proximity to the mineralization and these thin considerably above the orebody, probably indicating that they preferentially provided the host for the deposition of the mineralization.

The isometric projection suggests that the Agrokipia 'B' deposit deviates markedly from the typical Cyprus-type sulphide deposits in the absence of a well-defined massive pyritic zone and a regular decrease in grade with depth. It shows every indication of having formed entirely within the Lower Pillow Lavas and is characterised by frequent alternations in lithology between massive flows and glassy lavas, a feature which has been recently brought to light as a result of drilling by the Crustal Study Project (Robinson and Gibson, 1983).

In contrast to Agrokipia 'B' deposit the neighbouring Agrokipia 'A' orebody is localised at the contact between Lower and Upper Pillow Lavas and the original massive mineralization was concentrated at this boundary. The stockwork zone of Agrokipia 'A' deposit, however, is generally diffuse and characterised by frequent gradations into weakly altered and little mineralized lava. This is probably indication of the marked absence of a strong structural control which would strongly focus the ore fluids. Fig. 5.24 represents a geological section showing the relationships between the two deposits. It is envisaged from the section that the same ore fluids which were responsible for the

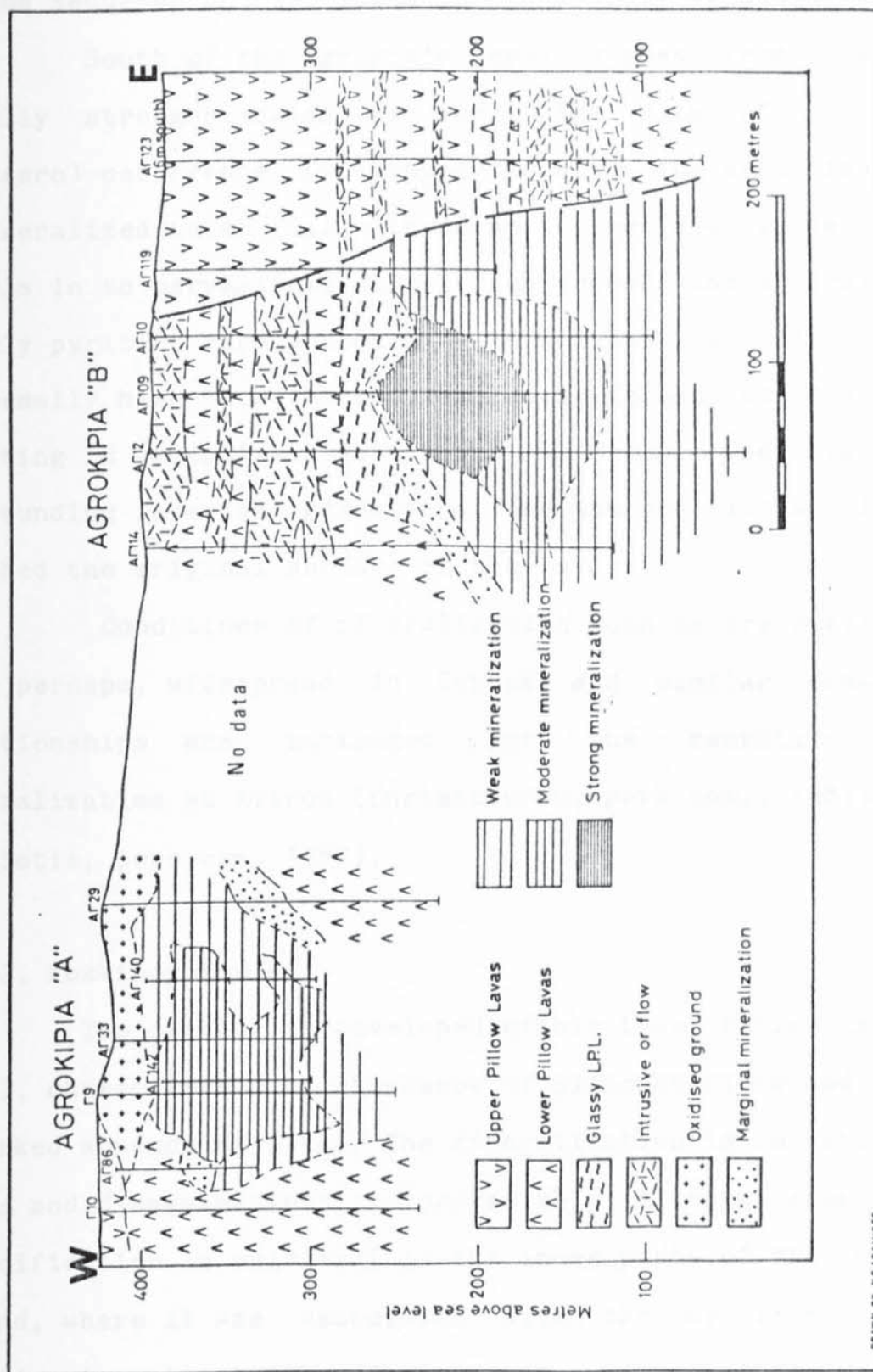


FIG. 5.24. Detailed geological section through the Agrokopia deposits.

deposition of Agrokippa 'B' followed a fracture to higher levels in the sequence and deposited 'A' as a truly exhalative deposit.

South of the Agrokippa deposits weak iron staining and locally stronger oxidation marks the site of the Mathiatis (Mitsero) occurrence. Drilling evidence in the area discloses that unmineralized Lower Pillow Lavas at the surface grade in deeper levels in to pervasively chloritised ground. The mineralization is weakly pyritic, rarely exceeding 10 % S but is characterised by abnormally high zinc content, exceeding in many cases 1 % Zn and reaching in exceptional situations 15 % Zn. Contacts with the surrounding lavas are gradational and the ore fluids only locally reached the original surface of the lavas.

Conditions of mineralization such as are outlined above are, perhaps, widespread in Cyprus and similar ore-host rock relationships are envisaged for the recently discovered mineralization at Klirou (Christoforou, pers.com., 1981) and Sha (Maliotis, pers.com. 1982).

5.5.2. Kokkinopezoula

The orebody is developed within Lower Pillow Lavas (Fig. 5.25), characterised by abundance of pillowed flows and sills with a marked absence of dykes. The mineralization is in the form of veins and disseminations in pervasively altered country rocks. Silicification is universal in the inner parts of the mineralized ground, where it was associated with the development of rich pyritic mineralization, and passes in a gradational manner into propylitised but generally unmineralized ground and thence into

GEOLOGICAL MAP OF KOKKINOPEZOULA OPENCAST

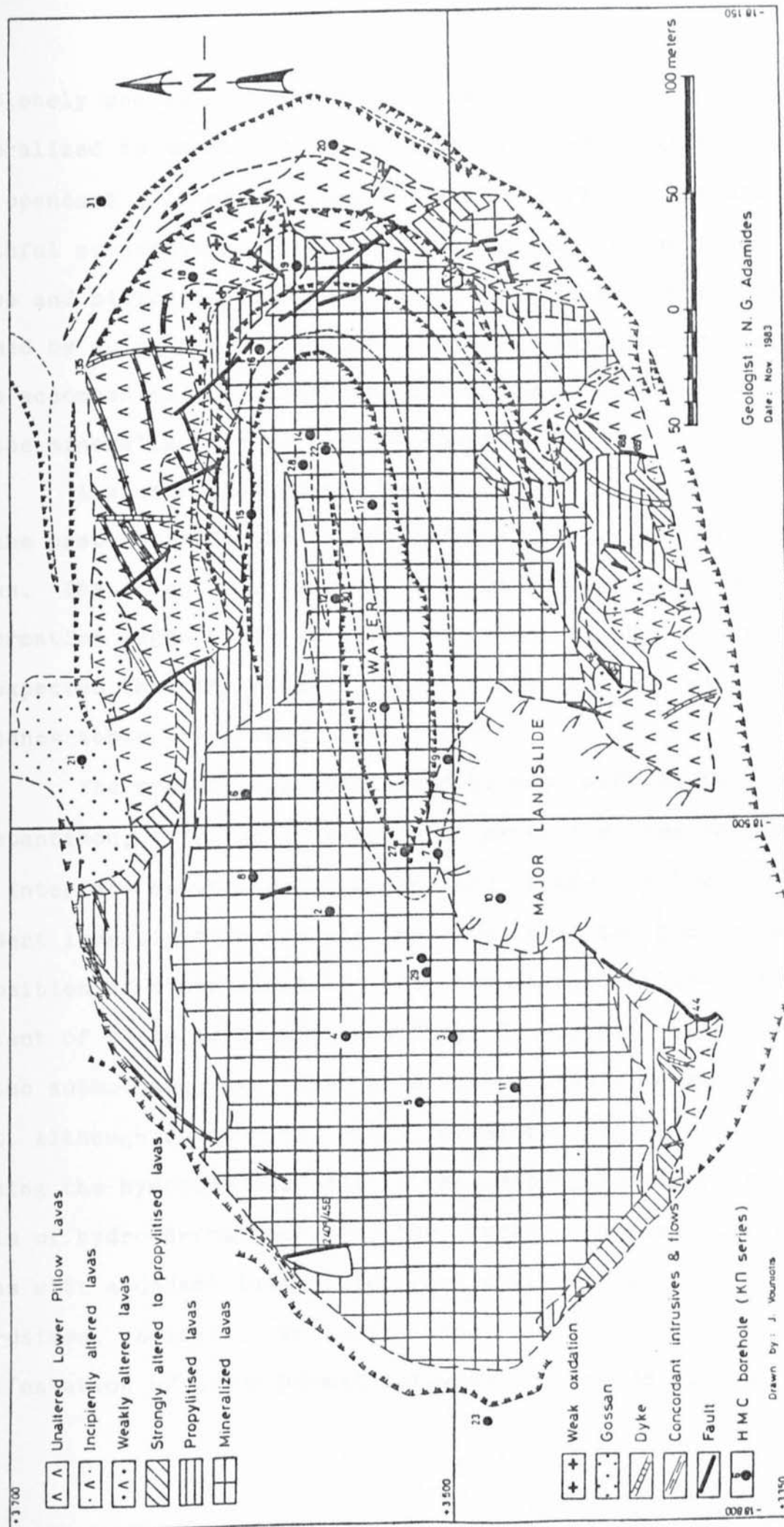


FIG. 5.25. Geological map of the Kokkinopezoula opencast.

completely unaltered Lower Pillow Lavas. Such transitions from mineralized to unaltered pillow lavas are universally present in the opencast (Plates 5.11 and 5.12). A remarkable feature is the faithful preservation of original structures in the lavas, such as flows and pillows, replaced by quartz-chlorite assemblages and veined by sulphides. No severe tectonic brecciation appears to have accompanied the mineralization process, at least in the parts of the mineralization at present observable.

A spectacular gossan marked the site of rich sulphide ore in the past, so that the higher extents of the ore zone are not known. The richer parts of the exploited ore, as borehole information suggests (Fig. 5.26) comprised siliceous pyrite and it is expected that the massive zone, if one existed, was at no great distance above the present surface.

The orebody was considered by past workers (Vokes, 1965, Constantinou, 1972) as an example of exhalative ore deposition at the interface between Basal Group and Lower Pillow Lavas. The present investigation clearly indicates that the host rock for the deposition of mineralization are the Lower Pillow Lavas. The contact of these lavas with the Basal Group, as regional mapping by the author suggests, lies at a considerable distance to the west. Although epidote is locally developed in propylitic lavas forming the hydrothermal halo of the mineralization, beyond the realm of hydrothermal activity the rocks comprise Lower Pillow Lavas with abundant laumontite, rare dykes and dominant concordant intrusives. Epidote, in this case, is thought to be a manifestation of hydrothermal activity as opposed to a regional



PLATE 5.11. Kokkinopezoula opencast looking north. Lower Pillow Lavas (top part of photograph), comprising concordant intrusives and pillowed flows, grade at lower levels into mineralized lavas (grey orange stained).



PLATE 5.12. Kokkinopezoula opencast. Transitional passage from unaltered Lower Pillow Lavas (left) to mineralized lavas (right) through a zone of weak propylitic alteration. Note complete preservation of original structures.

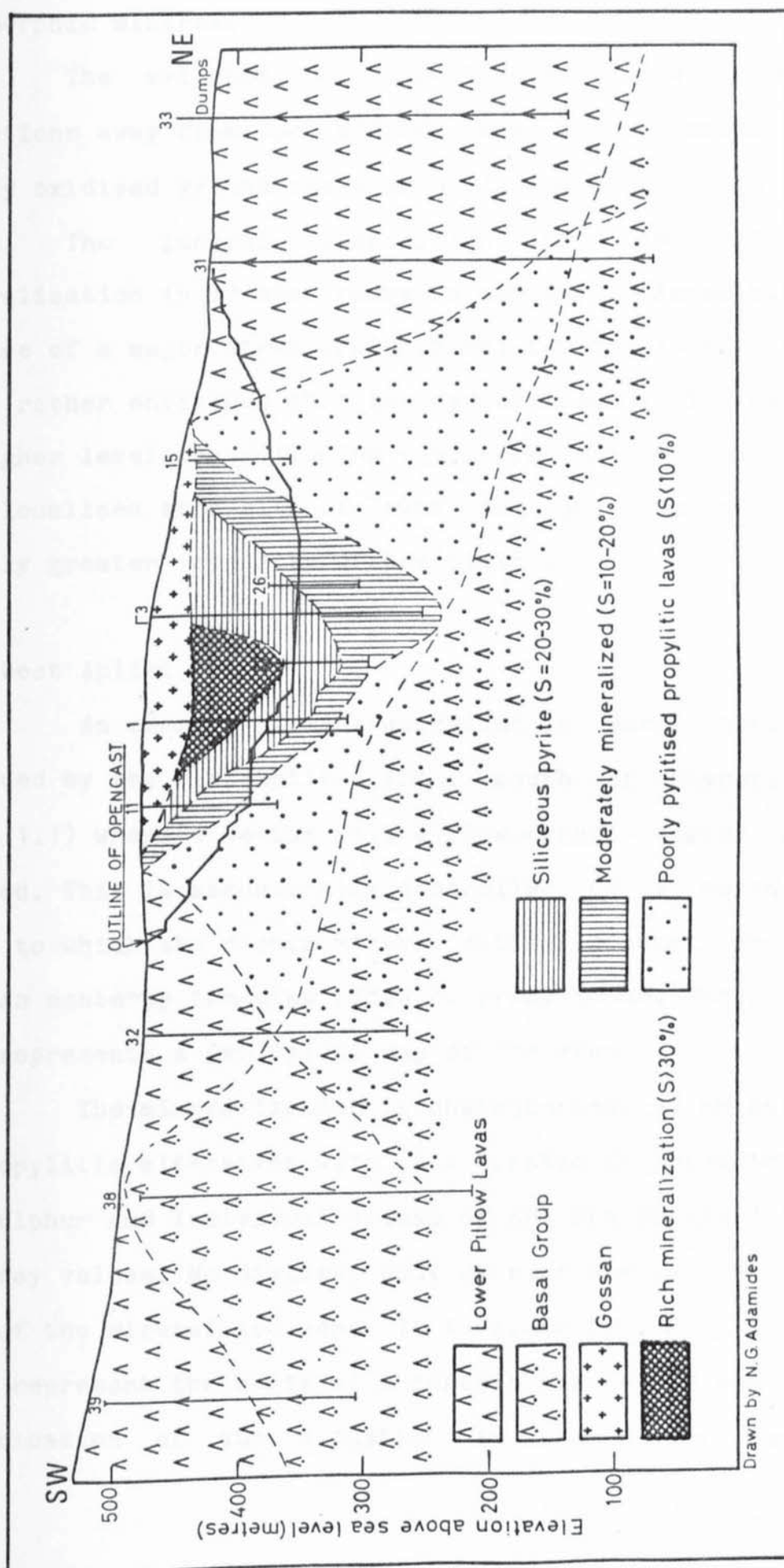


FIG. 5.26. Geological section through the Kokkinopezoula orebody.

metamorphic mineral.

The evidence of mineralization diminishes in all directions away from the orebody and only limited patches of weakly oxidised ground are present in the surrounding Lower Pillow Lavas. The general disposition of the Kokkinopezoula mineralization is in many respects similar to Agrokipia 'B' in the absence of a major structural control for the localisation of ore. It is rather envisaged that the hydrothermal fluids gained access to higher levels by following minor structures in the lavas and were localised at a site of lower pressure and temperature and locally greater intensity of brecciation.

5.6. West Apliki.

An example of mineralization in Basal Group rocks is provided by the West Apliki area, south of Mavrovouni orebody (Fig. 1.1) where a medium sized low-grade copper orebody was located. This is structurally controlled by a northerly fault, close to which the richer mineralization occurs, in association with an easterly trending ridge of propylitised Basal Group. Fig. 5.27 represents a geological map of the area.

The mineralization is characterised by an extensive zone of propylitic alteration with very erratic distribution of copper and sulphur and individual blocks of ore are outlined on the basis of assay values. No distinct body of rich ore is located in any part of the mineralized zone. It is clear that such mineralization could represent the roots of a deposit now eroded and it provides an indication of the situation in the deeper parts of the

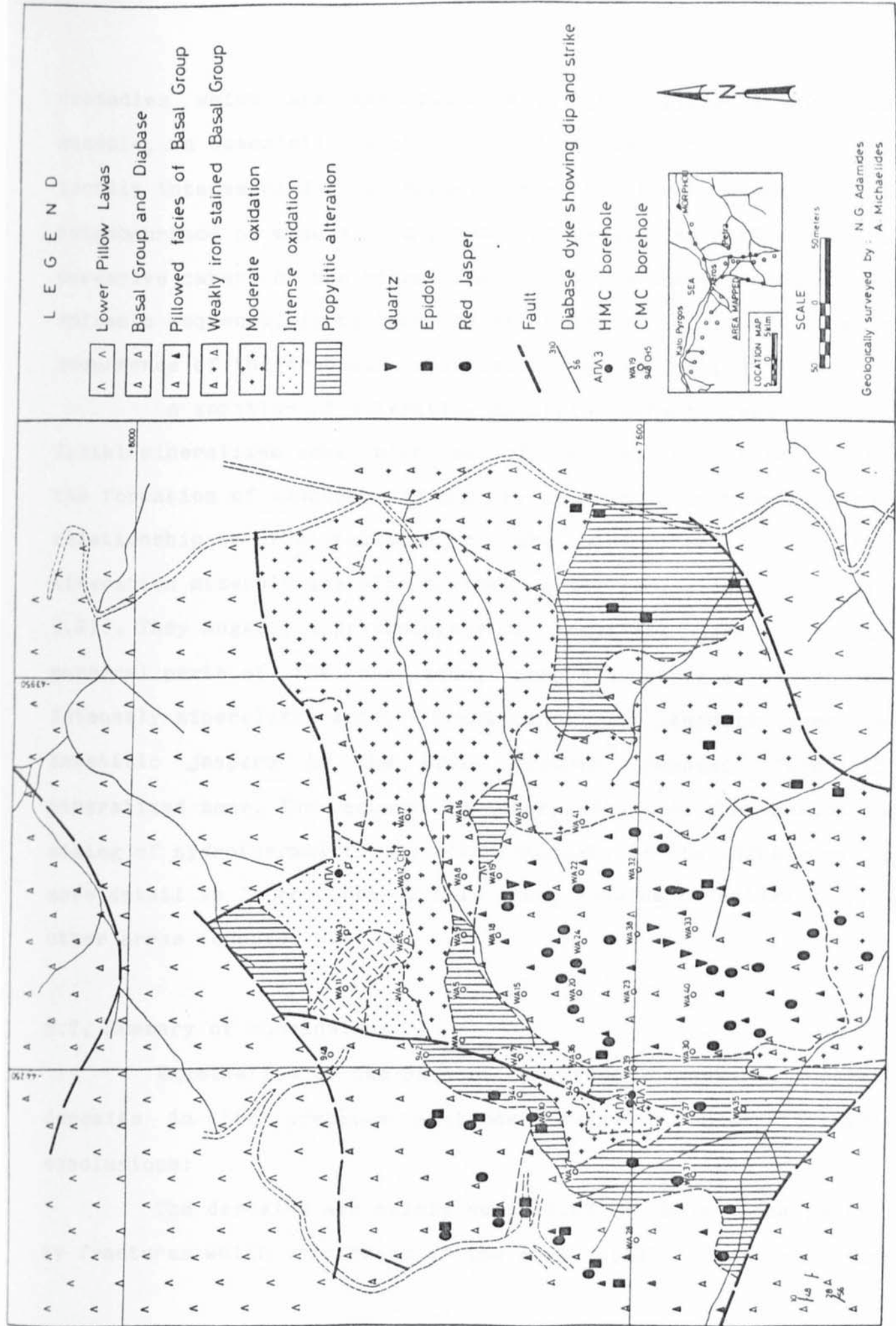


FIG. 5.27. Geological map of West Apliki mineralized occurrence.

orebodies which are associated with the pillow lavas. This example, in association with the widespread iron staining and locally intense oxidation characterising the Basal Group in the neighbourhood of mineralized areas, provides indication of the pervasive nature of the mineralization in the deeper parts of the volcanic sequence, in contrast to the sharply localised mode of occurrence of the orebodies associated with the pillow lavas.

A zonation of alteration minerals characterises the West Apliki mineralized zone, with silicification, epidotisation and the formation of abundant red jasper, apparently bearing a direct relationship to the position of the mineralized zone. These alteration minerals are also plotted on the geological map (Fig. 5.27). They suggest a predominance of hematitic jaspers in the marginal parts of the ore zone, complete absence within the intensely mineralized zone, and dominance of epidote over the hematitic jaspers in the areas farther removed from the mineralized zone. The sequence is interpreted as the result of mixing of hydrothermal fluids with seawater. It is discussed in more detail in later parts of this work, drawing on evidence from other areas (chapter 6).

5.7. Summary of conclusions

Examination of the mode of occurrence of several sulphide deposits in the previous sections suggests the following conclusions:

The deposits are mainly controlled in their localisation by fractures which originated at the early stages of oceanic crust

formation. The abundance of structures determines the size of the resultant orebodies, smaller deposits favoured in intensely tectonised terrains. Fracture intensity favours, in addition, the formation of exhalative deposits, while in the absence of major tectonism ore localisation within the lava pile takes place. This is interpreted as implying that the role of faulting lay mainly in the localisation of hydrothermal fluids which were triggered by deep seated causes, such as the presence of a heat source.

There was only one period of ore-producing hydrothermal circulation. This is temporally placed at the boundary between the Upper and Lower Pillow Lavas. No exhalative deposits formed at any time prior to this. The presence of deposits within the Lower Pillow Lavas is interpreted as the result of lithological factors, probably associated with the absence of strong structural control for the percolation of fluids to higher levels. Similarly, the presence of deposits directly covered by umbers without intervening Upper Pillow Lavas (cf. Skouriotissa and Kinousa) is thought to be the result of non-deposition of these lavas over the mineralization. An implicit conclusion is that the time interval between sulphide mineralization, Upper Pillow Lava extrusion and umber deposition was very brief, otherwise the sulphides would have been removed by erosion. This, further, indirectly implies that the umbers are the products of the same phase of hydrothermal circulation which produced the sulphide deposits.

CHAPTER 6
Mineralogical and chemical characteristics
of
Cyprus sulphide deposits

6.1. Introduction

The deductions made in chapter 3 suggest that enough metal is leached from the Sheeted Complex by a process of seawater circulation to account for the metal content of the sulphide deposits. Since the sites of ore deposition are presumed to mark loci of exit of these fluids the study of the mineralogical and chemical characteristics of the deposits and the enclosing and surrounding wall rocks provide clues on the behaviour of the hydrothermal fluids at discharge sites.

Mineral precipitation and wall rock alteration are processes directly linked with changes in the original character of the hydrothermal fluids and wall rocks as a result of mutual interaction. An additional variable is interaction of the fluids with ambient seawater, a process resulting to drastic changes in the properties of the fluids. Depending on the nature of the interaction, varying mineral assemblages are produced. Directly relevant to this is the formation of copper- rich and copper- poor orebodies and the presence or absence of zinc from the deposits.

The purpose of the present chapter is to discuss the mineralogical and chemical characteristics of some of the deposits and to interpret these as a function of the nature of the processes active at discharge sites.

A complete description of the detailed mineralogy of any specific deposit is hindered by the fact that none is present in its original complete form. At the time of the present work all deposits were either exhausted or at an advanced stage of exploitation. Mineralogical studies were, therefore, confined to the description of limited samples, mainly from the lower parts of the stockwork zones. The mineralogical characteristics of the deposits have been summarised in chapter 4. Exhaustive accounts of the mineralogies of several deposits were presented in the past (Constantinou, 1972; Johnson, 1970).

6.2. Descriptive mineralogy

6.2.1. The Limni orebody

The Limni orebody was characterised by a high copper content as compared with other deposits of similar pyrite content. This high copper was reflected in the abundance of chalcopyrite which, in the higher parts of the orebody, was extensively altered to secondary sulphides and sulphates as a result of ancient mining (Gordon-Smith, 1959). In the examined deeper parts of the deposit the secondary minerals are extremely scarce and chalcopyrite is usually free of alteration.

Pyrite is the commonest ore mineral. It is universally present in the form of veins or disseminations in the altered country rocks. The mineral is mostly unaltered and chemically stoichiometric (Table 6.1) and contains variable amounts of copper and zinc reflecting minute inclusions of chalcopyrite and

TABLE 6.1. Electron microprobe analyses of pyrites, Limni mine.

Wt. %	FR3	FR6	FR8	FR21	FR26	FR10
S	53.89	54.16	54.53	54.45	53.92	54.70
Fe	44.36	45.19	45.96	45.83	45.64	45.60
Cu	0.48	0.33	N.D.	0.13	0.45	0.29
Zn	0.28	0.10	0.13	0.32	0.24	0.23
Total	99.01	99.78	100.62	100.73	100.25	100.82
F o r m u l a						
S	2.000	2.000	2.000	2.000	2.000	2.000
Fe	0.958	0.958	0.968	0.966	0.972	0.957
Cu	0.009	0.006	0.000	0.002	0.008	0.005
Zn	0.005	0.002	0.002	0.006	0.004	0.004

N.D. : Not detected.

TABLE 6.2. Electron microprobe analyses of chalcopyrites, Limni.

Wt. %	LC2	LC18	LC29	LC25	LC31	LC23
S	35.61	35.48	34.62	35.45	35.15	35.59
Fe	30.23	30.47	30.24	30.74	30.59	31.75
Cu	33.99	34.26	34.10	33.93	33.37	32.51
Zn	0.17	N.D.	0.63	0.40	0.68	0.25
Total	100.00	100.21	99.59	100.52	99.74	100.10
F o r m u l a						
S	2.000	2.000	2.000	2.000	2.000	2.000
Fe	0.975	0.986	1.003	0.995	0.999	1.024
Cu	0.963	0.974	0.994	0.966	0.958	0.922
Zn	0.005	0.000	0.018	0.011	0.019	0.007

sphalerite. In the paragenetic sequence pyrite is one of the earlier minerals and is often brecciated and healed by quartz or chalcopyrite. The partial replacement of pyrite by quartz bears testimony of periods of silicification post-dating the deposition of the pyrite. In many cases the healing of fractures in pyrite by quartz is not accompanied by noticeable replacement and adjacent fragments may be frequently envisaged to fit back to the original crystal, in contrast to the strong reaction relationship exhibited between pyrite and chalcopyrite (Plate 6.1).

Chalcopyrite is the second most abundant ore mineral and post-dates pyrite in the paragenesis, infilling the intespaces between pyrite crystals in veins. Commonly in those cases it also post-dates associated quartz. Veining of chalcopyrite by quartz is, however, also documented while the formation of pyrite along veinlets in the chalcopyrite is observed in rare cases, probably related to late stage processes. The chalcopyrite is most commonly devoid of any sign of alteration but, in view of its late position in the paragenesis, it frequently contains numerous inclusions of gangue and pyrite. Chemically it is very close to stoichiometric (Table 6.2) with very small amounts of zinc almost universally present. Cobalt and nickel are in most cases completely absent.

Sphalerite is very rare in the examined assemblages and has only been found in some instances replacing chalcopyrite. As a result of its scarcity it is not possible to discuss its detailed relationships with the rest of the ore and gangue minerals.

An assemblage highly significant from the viewpoint of the chemical environment of ore deposition relates to the

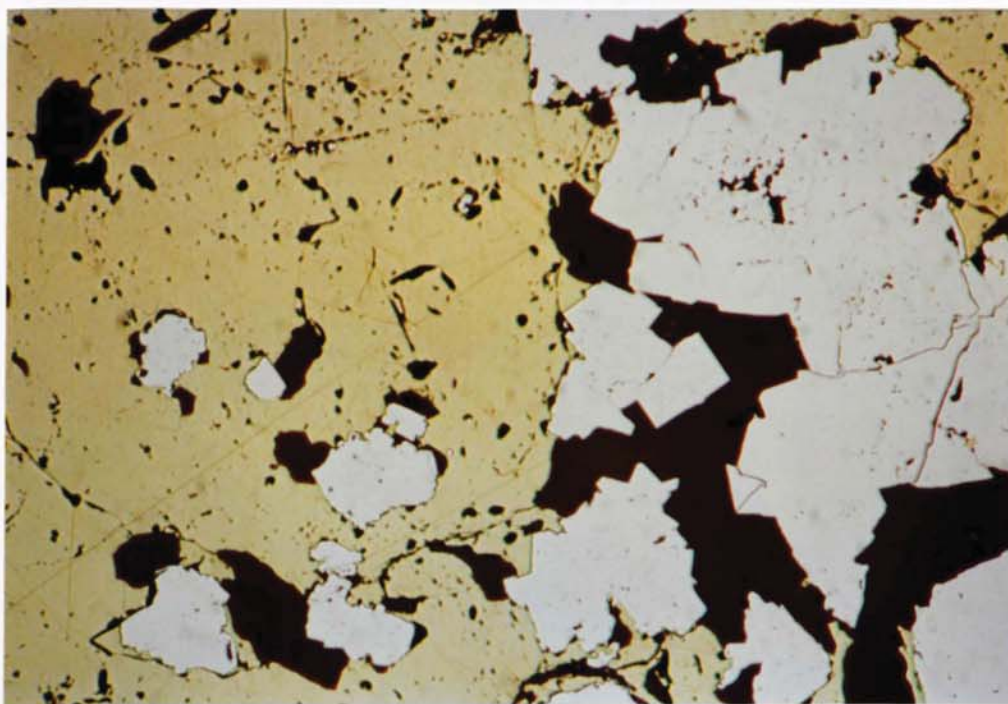


PLATE 6.1. Pyrite, partly enclosed in quartz (black) is replaced by anhedral chalcopyrite. Limni orebody. Parallel polars, X100.

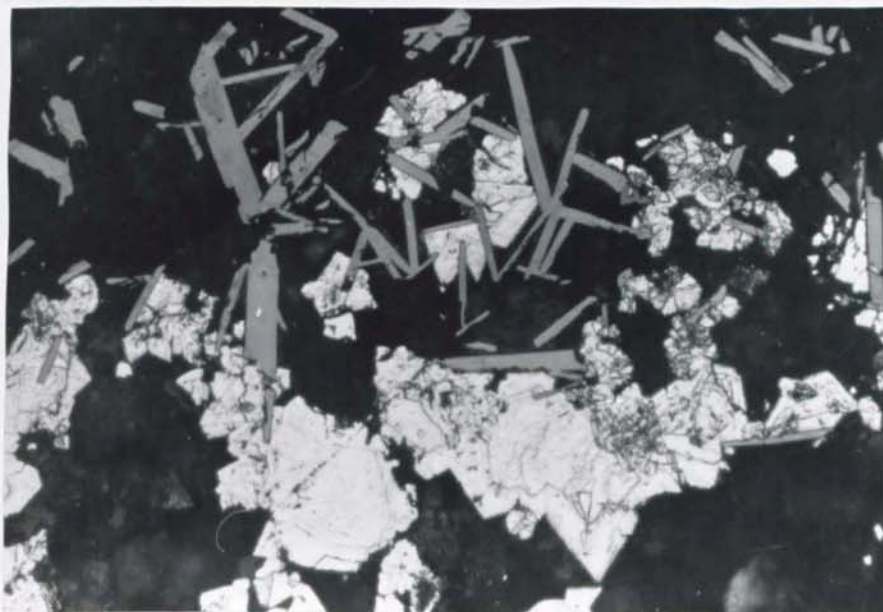


PLATE 6.2. Euhedral hematite (grey) associated with corroded pyrite in gangue. Oil, X256, Parallel polars.



PLATE 6.3. Crystallographically-guided replacement of chalcopyrite (white) by bornite (grey) and subsequent replacement of bornite by covellite (dark grey) along fractures. Parallel polars, X156.

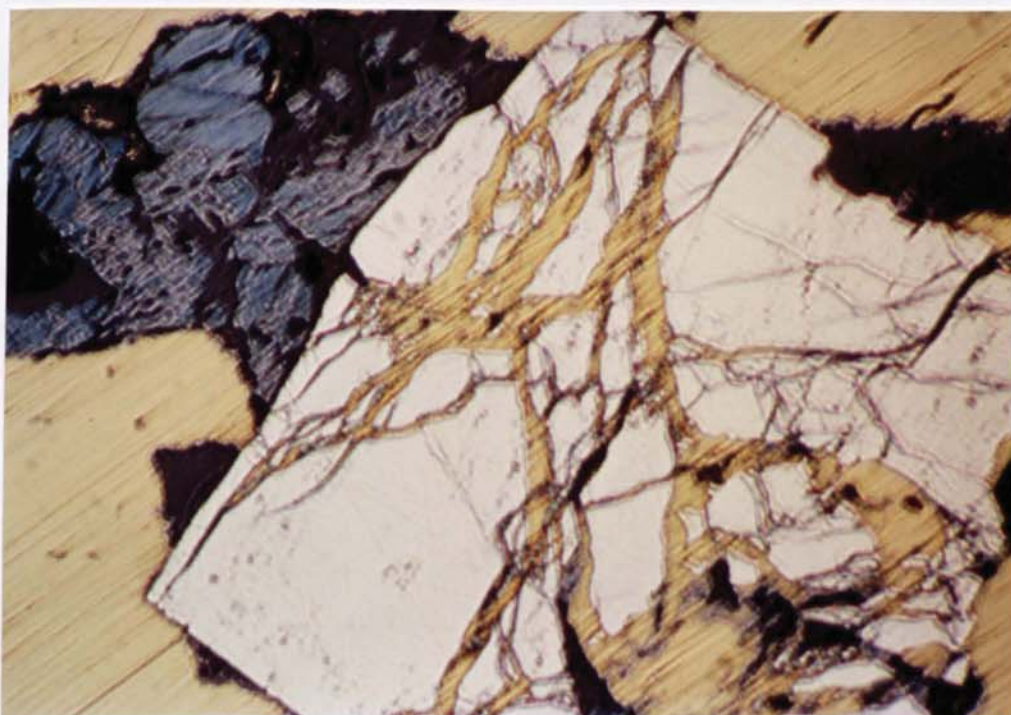


PLATE 6.4. Euhedral pyrite, healed along fractures and partly replaced by chalcopyrite. Cuprian sphalerite (reddish grey) occupies cavity and is partly replaced by covellite (blue). Parallel polars, X200.

association observed in some instances of simultaneous crystallisation of pyrite and hematite. The latter forms oriented acicular crystals in the pyrite, frequently showing a zonary arrangement while the quartz adjacent to the pyrite also shows abundant inclusions of hematite. Partial dissolution of the hematite and the infilling of the resultant empty space by chalcopryrite provide clear evidence that the hematite is related to the main period of the mineralization and is not the result of a later period of oxidation (Plate 6.2).

The commonest products of the supergene alteration of the chalcopryrite are bornite, covellite and chalcocite. Alteration of the chalcopryrite to bornite (Plate 6.3) results in the formation of textures similar in all respects to exsolution intergrowths produced experimentally (Brett, 1964), with flames and spindles of chalcopryrite following crystallographic directions in bornite.

Cuprian sphalerite was detected in one sample, infilling cavities in chalcopryrite. The mineral is partly replaced by covellite, along crystallographic directions, and is associated with brecciated pyrite healed by chalcopryrite (Plate 6.4).

It is not clear whether the formation of the cuprian sphalerite is related to purely supergene processes or is formed in a late stage hypogene period of mineralization. It is in many cases related to fractures in the chalcopryrite but also occurs in the form of euhedral crystals in cavities, almost universally partly replaced along cleavages by covellite. The chemical analyses of the mineral (Table 6.3) are in this sense composite and include a certain amount of covellite but are generally

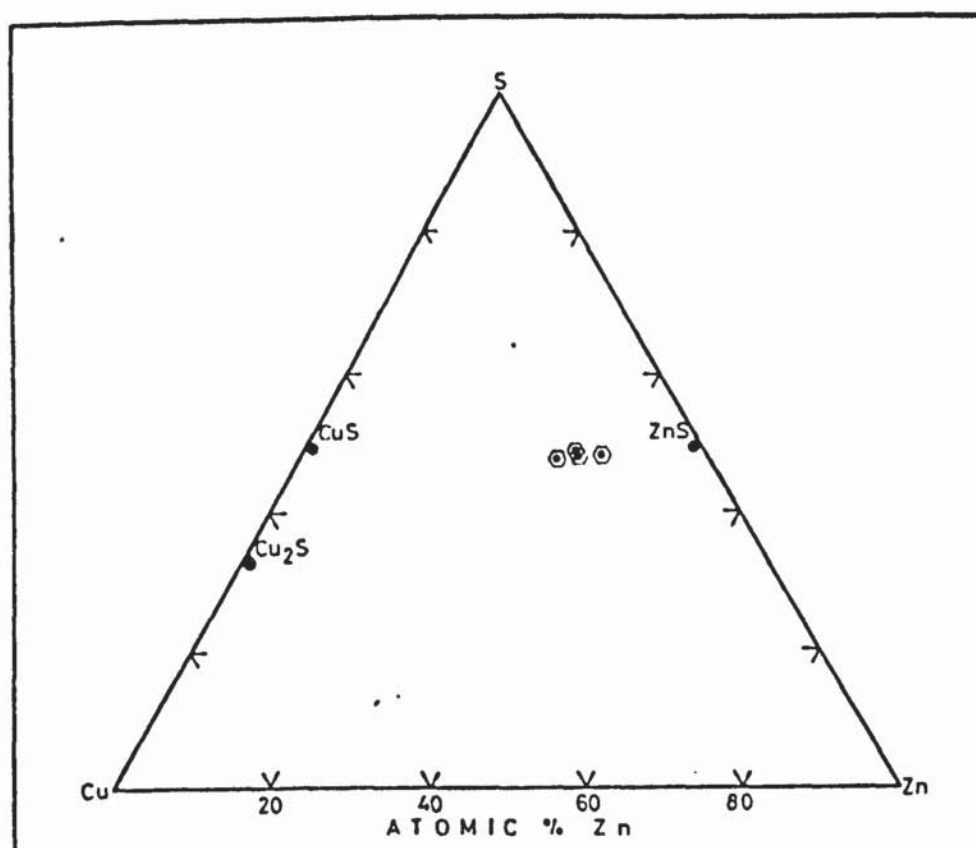


FIG. 6.1. Electron microprobe (EDS) analyses of cuprian sphalerite from Limni mine plotted on the Cu-Zn-S diagram.

TABLE 6.3. Electron microprobe analyses of cuprian sphalerite from Limni mine.

Wt.%	1	2	3	4	5
S	30.05	28.62	30.44	30.05	29.91
Fe	1.30	0.49	1.25	3.38	0.68
Ni	0.07	N.D*	N.D	0.13	0.27
Co	0.04	0.11	0.04	N.D	N.D
Cu	16.60	39.02	20.79	19.89	24.05
Zn	46.98	28.19	45.58	43.09	41.86
Total	95.04	96.43	98.10	96.54	96.77
Formula					
S	1.000	1.000	1.000	1.000	1.000
Fe	0.025	0.010	0.024	0.045	0.013
Ni	0.001	0.000	0.000	0.002	0.005
Co	0.000	0.002	0.001	0.000	0.000
Cu	0.279	0.688	0.344	0.334	0.406
Zn	0.767	0.483	0.734	0.703	0.686

* N.D. : Not detected.

closely comparable with reported compositions (Clark and Sillitoe, 1970). The electron microprobe analyses as plotted on the Cu-Zn-S diagram are shown in fig. 6.1.

Formation of the cuprian sphalerite has been related to supergene processes as an intermediate stage in the replacement of iron-free sphalerite by djurleite (Clark and Sillitoe, 1970). In the present situation no associated sphalerite, or evidence of pre-existing sphalerite is observed and the supergene mode of genesis is difficult to sustain. The mineral is probably late stage hypogene in genesis and relates to the interaction of zinc-rich solutions with chalcopyrite. Its conditions of formation, however, are unknown since work on the system Cu-Zn-S failed to detect any ternary phases throughout the interval ranging between 100^o-1050^oC (Craig and Kullerud, 1973).

6.2.2. The mineralogy of the Mangaleni ore.

Detailed investigations of a series of samples from the mineralized ground reveal a complexity of textures hitherto unrecorded in any of the Cyprus sulphide deposits and as such warrant a detailed description.

The main components of the Parekklishia ore are pyrite, marcasite, chalcopyrite and sphalerite with a variety of secondary minerals resultant upon supergene alteration of the ore. The nature and relationships of the ore minerals and an attempt at interpretation of the assemblages will be the subject of the next paragraphs.

6.2.2.1 The massive sulphide.

Pyrite, in intimate association with marcasite are the predominant sulphides in the massive friable ore and occur in a variety of intricate crystal forms which without exception are skeletal in nature and resultant from rapid growth (Plate 6.5). The commonest crystal exhibits a lath-like shape with empty interiors and the outline made up of smaller marcasite crystals showing different orientation. Circular and elongated shapes and intermediate shapes are also present. Lamellar twinning is also documented but rather uncommon.

Chalcopyrite is the second most abundant mineral of the massive friable ore. It occurs in the form of irregular fragments of variable size mainly disconnected from the iron sulphide and exhibits a peculiar mode of alteration. This alteration results to breakdown of the mineral into a light brown aggregate along fractures and veinlets (Plate 6.6). In more advanced stages, transformation of the whole of the mineral into a grey fine-grained aggregate commonly associated with reticulate veining of iron sulphide takes place. Replacement of the chalcopyrite by bornite and subsequent replacement of the latter by covellite are also documented and are clearly related to supergene processes (Plate 6.7).

The alteration of the chalcopyrite to the brown and grey aggregate has not been previously recorded in the literature. Electron probe analyses (Table 6.4) suggest that the two represent different stages of the same process probably related to the interaction of chalcopyrite and zinc-rich solutions, the grey

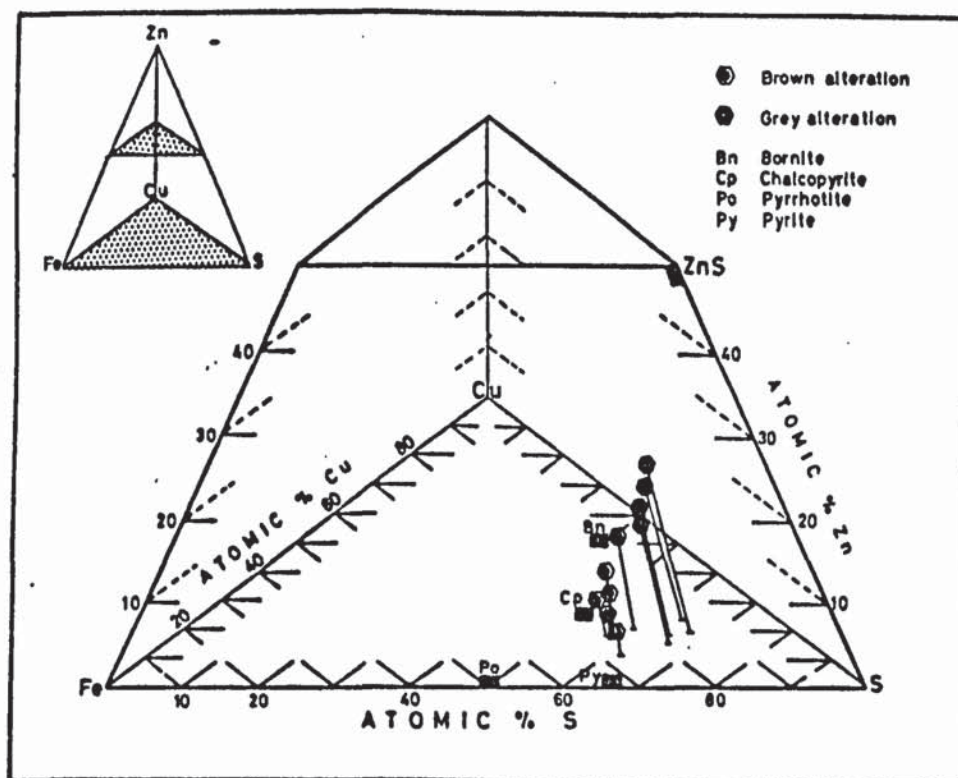


FIG. 6.2. Plot of analyses of brown and grey alteration of Parekklishia chalcopyrite on the Cu-Fe-Zn-S tetrahedron.

TABLE 6.4. Electron microprobe analyses of brown and grey alterations of the chalcopyrite-Parekklishia.

Wt. %	B19	B27	B26	B17	B10	B13
S	35.92	34.13	32.20	35.89	33.04	32.79
Fe	27.40	24.90	20.07	18.45	11.95	12.18
Ni	N.D.*	0.04	0.10	0.07	0.02	0.11
Co	N.D.	N.D.	N.D.	N.D.	N.D.	0.05
Cu	21.63	27.53	21.82	16.48	23.06	18.93
Zn	7.51	9.03	15.15	19.72	21.80	27.06
Total	92.46	95.63	89.34	90.61	89.87	91.12
Formula						
S	2.000	2.000	2.000	2.000	2.000	2.000
Fe	0.878	0.837	0.715	0.584	0.415	0.426
Ni	0.000	0.001	0.003	0.002	0.001	0.004
Co	0.000	0.000	0.000	0.000	0.000	0.002
Cu	0.607	0.814	0.684	0.463	0.704	0.582
Zn	0.205	0.260	0.461	0.539	0.647	0.809

* N.D. : Not detected.



PLATE 6.5. Skeletal pyrite and fragmental chalcopyrite in massive ore of Parekklishia. Parallel polars, X100.

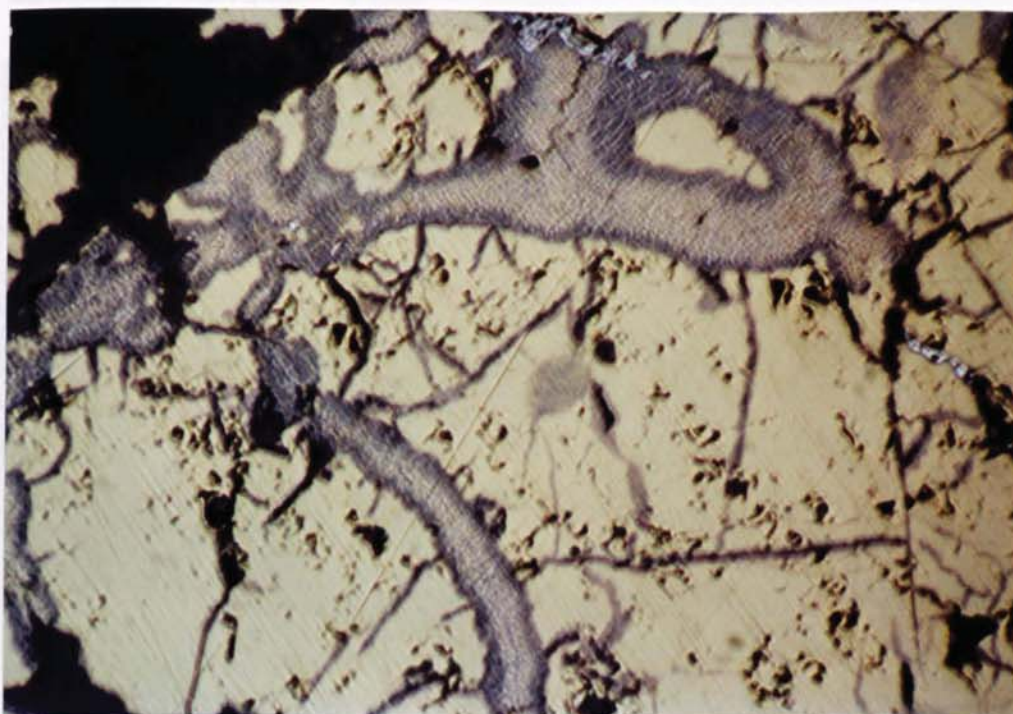


PLATE 6.6. Fracture-guided replacement of chalcopyrite by the brown alteration product. Parallel polars, X500, Oil.

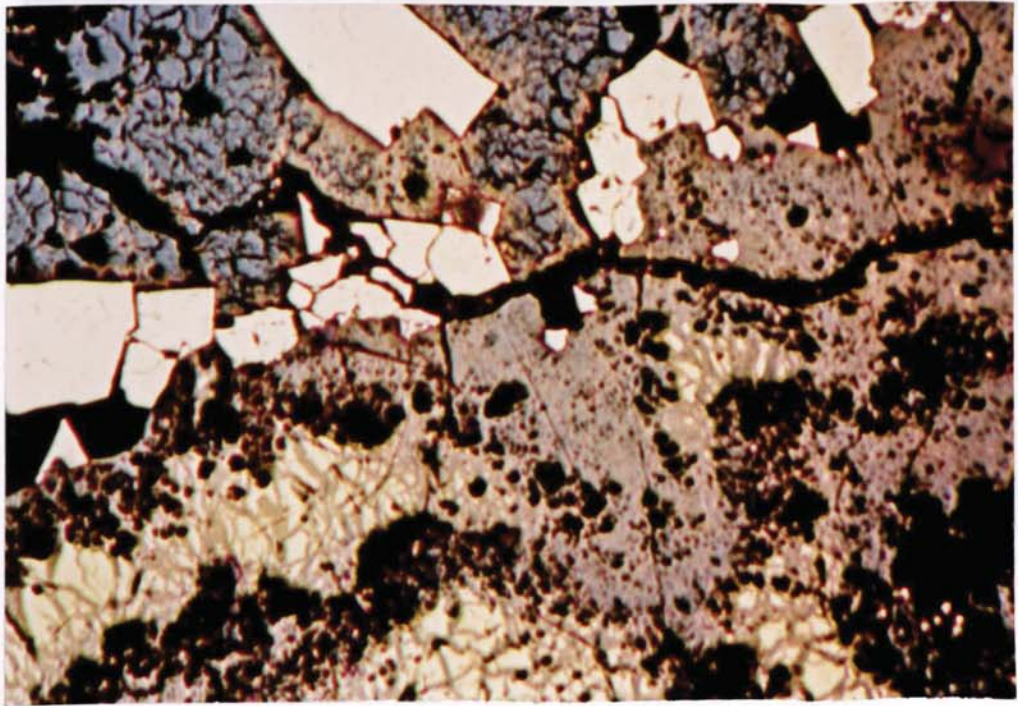


PLATE 6.7. Chalcopyrite (creamy yellow) replaced along fractures by bornite (brown) and subsequently by covellite (blue). Note complete preservation of pyrite through the alteration. Parallel polars, X100.

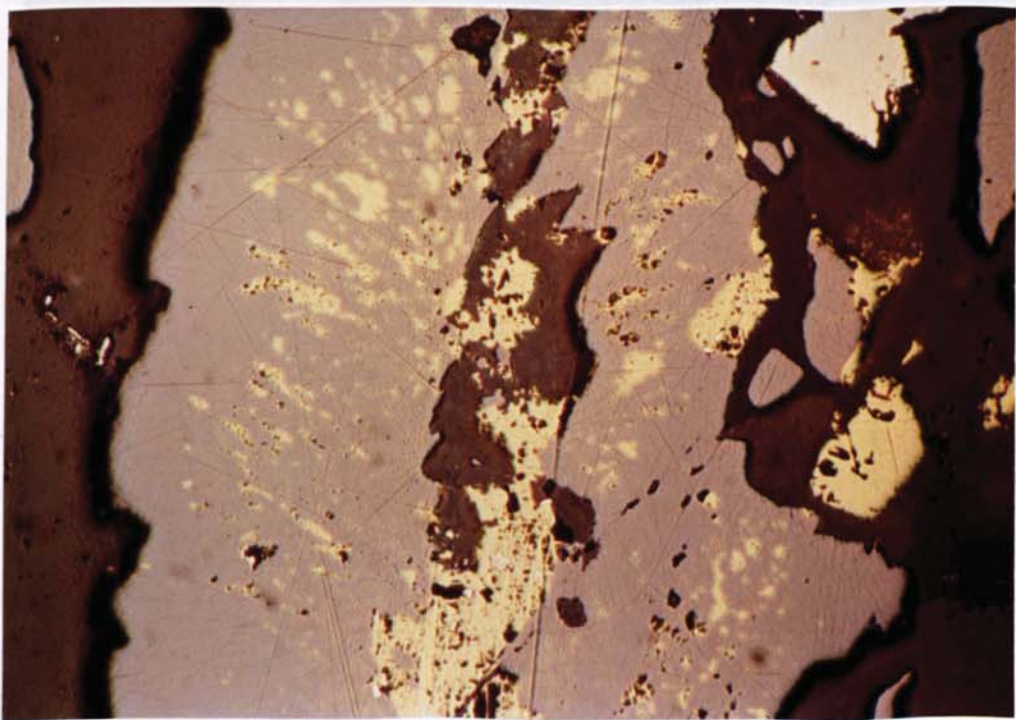


PLATE 6.8. Ghost chalcopyrite (yellow) almost totally replaced by sphalerite (grey). Parallel polars, X100.

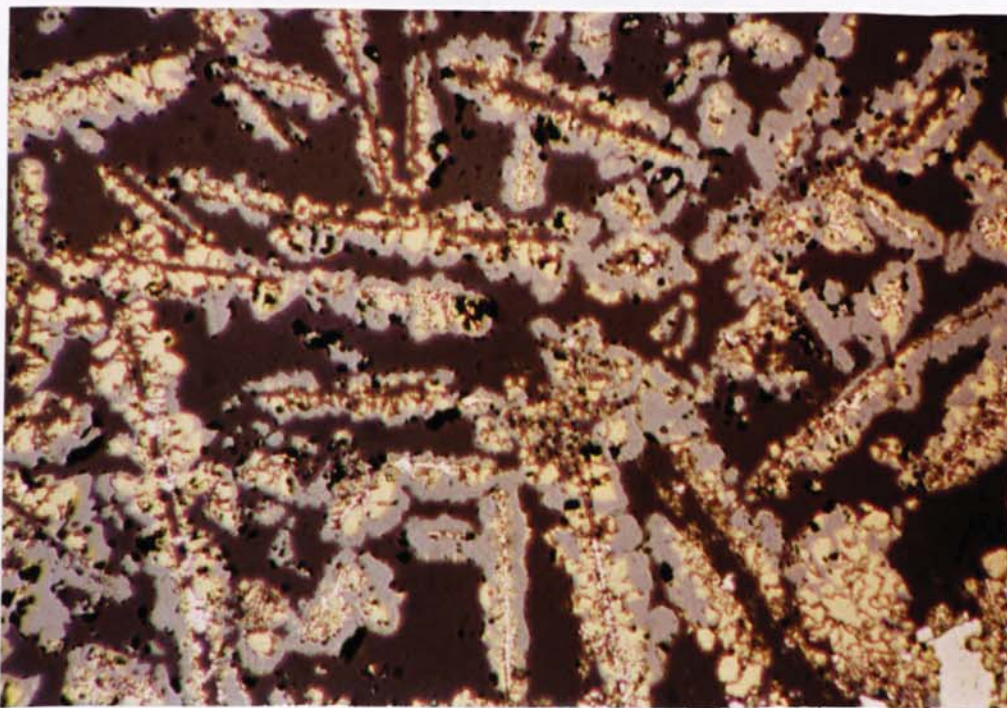


PLATE 6.9. Delicate growths of pyrite (central rods) overgrown by chalcopyrite (yellow) and sphalerite (grey) in quartz gangue. Parallel polars, X100.

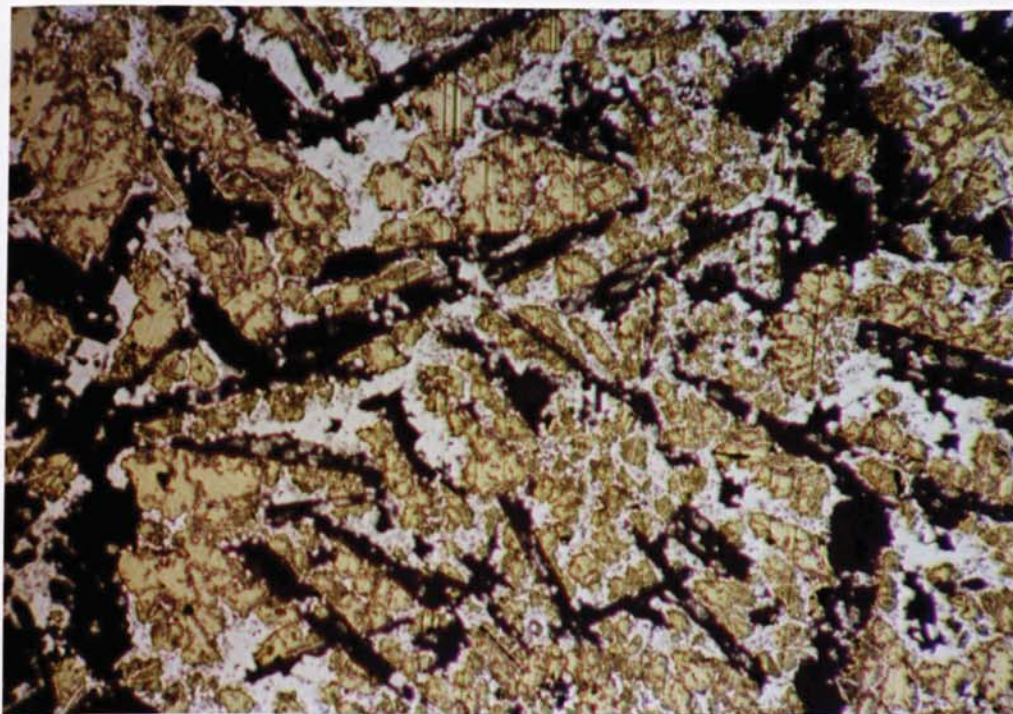


PLATE 6.10. Epitaxial growth of pyrite on chalcopyrite in banded chalcopyrite-pyrite-sphalerite zone. Black is gangue. Parallel polars, X100.

alteration representing a more advanced stage of the process. Fig. 6.2 shows a plot of the two types of alteration on the Cu-Fe-Zn-S tetrahedron.

The relationship between chalcopyrite and sphalerite is commonly one of clear-cut replacement, the latter mineral being in most examined situations paragenetically later than chalcopyrite (Plate 6.8). The preservation of delicate dendritic crystals, however, involving epitaxial growth of sphalerite on chalcopyrite (Plate 6.9), or pyrite on chalcopyrite (Plate 6.10), suggests alternating precipitation of these minerals as a function of changing physicochemical parameters and a periodicity in hydrothermal activity which is contrary to the application of strict rules in the order of mineral paragenesis.

6.2.2.2. The hard sulphide blocks.

The mineralogy of the sulphide blocks frequently enclosed in the friable pyrite is characterised by extreme complexity testifying to several periods of precipitation, brecciation and recurrence of mineralization. The typical texture involves large fragments of chalcopyrite and colloform pyrite and marcasite, enclosed in a fine matrix comprising skeletal crystals of iron sulphide, single framboids and small fragments of sphalerite and chalcopyrite.

The large chalcopyrite fragments are frequently completely unaltered or partly veined by the brown alteration and show evidence of brecciation and healing of fractures by quartz accompanied by partial replacement. This period of silicification

pre-dates the later period of mineralization associated with the finer matrix.

Coarse fragments of framboidal iron sulphide, occasionally enclosing chalcopyrite, are also widespread in the matrix and are observed in detail to comprise either alternating zones of marcasite and pyrite, or uniformly either of the two minerals, while in other situations framboidal marcasite is overgrown by coarsely-crystalline pyrite.

There does not appear to exist a specific rule in the transformation of pyrite to marcasite but in general the latter is dominant in the more porous colloform sulphide and pyrite predominates in the well crystalline material. Fracture-guided transformation of pyrite to marcasite is documented, while the complete transformation of apparently euhedral pyrite into a mosaïque of smaller marcasite crystals is a common occurrence.

The fine matrix into which the coarser fragments are embedded comprises an intimate mixture of skeletal, micro-crystalline and framboidal iron sulphide, with varying amounts of sphalerite and chalcopyrite. The size of the fragments varies widely from a fraction of a mm to single framboïds measuring .25 microns in diameter, while the skeletal pyrite and marcasite frequently enclose fresh or variously altered chalcopyrite.

The chalcopyrite, similarly to the iron sulphide, occurs in fragments of varying sizes in the fine matrix and individual fragments vary widely in the degree of alteration from the completely fresh to the thoroughly altered state. The alteration ranges from the faint brown colouration to the complete trans-

formation of the mineral into the grey alteration product. The occurrence side by side of completely fresh and thoroughly altered fragments indicates that the alteration has preceded the consolidation of the ore and its cementation by the gangue and is probably related to the incoming of zinc-rich hydrothermal solutions under late hypogene conditions.

6.2.2.3. The effects of tectonism on the ores.

The involvement of the Parekklishia ore in the severe tectonic movements which resulted to the emplacement of the blocks of mineralization in their present position (chapter 5) played a determining role in the modification of original textures and the formation of new textures indicative of deformation. Examination of samples which have been severely affected by the tectonic movements indicates the following characteristics:

Chalcopyrite yields to stress by plastic deformation and commonly infills interstices between fragments of the more competent pyrite. The latter is frequently cataclastically brecciated but increased abundance of marcasite along shear planes and the apparent growth of new marcasite suggest transformation of pyrite into marcasite by the tectonic movements (Plate 6.11).

Tectonic effects on the chalcopyrite, in addition to the flow textures described above, relate to the formation of a regular intergrowth involving fine chalcopyrite lamellae, oriented parallel to crystallographic directions (Plate 6.12). The interspace between the lamellae is made up of a fine grained aggregate of a brownish color with abundant blebs of iron sulphide in the

form of sweats accompanying the transformation.

The transformation of the chalcopyrite to the lamellar intergrowth is observed in some cases to be accompanied by the development of a 'ridged' pattern in the mineral (Plate 6.13). These are observed at high magnifications to result from incipient development of the lamellar intergrowth.

Recurrence of the period of deformation after formation of the lamellar intergrowth results to deformation by kinking and bending of the lamellae (Plate 6.14) and the exsolution of iron sulphide in minute blebs. Formation of new chalcopyrite along fractures is interpreted as resultant upon post-deformation re-establishment of equilibrium.

6.2.2.4. Discussion of the lamellar intergrowth in chalcopyrite.

The lamellar intergrowth is in all respects similar to that experimentally produced by Brett (1964) during cooling experiments in the system chalcopyrite-bornite; however, in the present case no trace of bornite is detected.

Electron microprobe analyses of the lamellar intergrowth, the compositionally similar 'ridged' chalcopyrite (Table 6.5), and unaltered chalcopyrite (Table 6.6), reveal that the formerly stoichiometric chalcopyrite changes in composition along the chalcopyrite-pyrite join (Fig. 6.3.) suggesting that the process involved the release of copper from the original chalcopyrite, resulting to the release of excess iron sulphide in the form of sweats associated with the lamellar intergrowth. The presence of abundant native copper in botryoidal masses associated

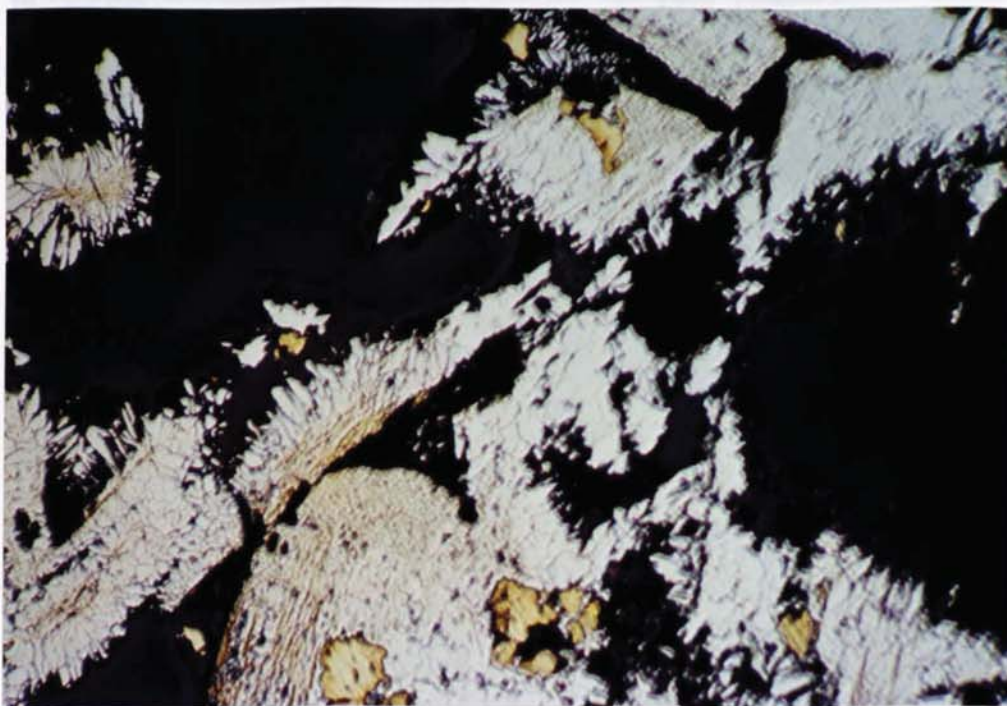


PLATE 6.11. Cataclastic brecciation of pyrite, associated with formation of marcasite (laths projecting into gangue). Note yield of chalcopyrite to deformation by flow.

Oil, Parallel polars, X500.

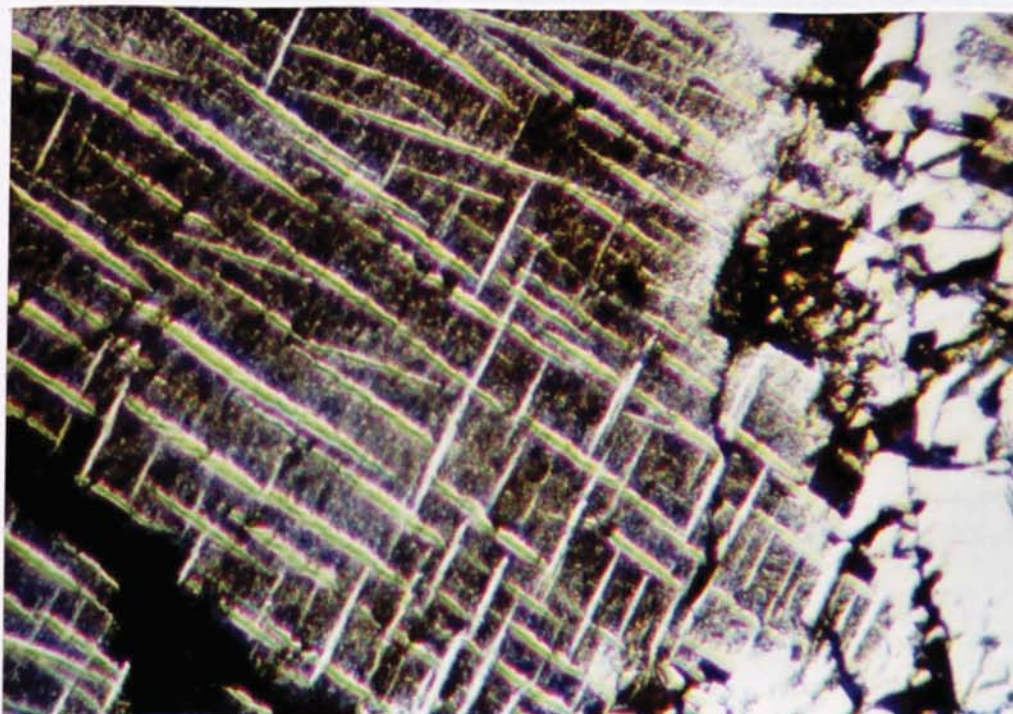


PLATE 6.12. Detail of the exsolution lamellae of chalcopyrite (rod-like structures) in matrix of copper-deficient chalcopyrite (brown). Bright white at left is stoichiometric chalcopyrite.

Oil, Parallel polars, X500.



PLATE 6.13. The 'ridge' pattern in Parekklishia chalcopyrite, the result of incipient development of the lamellar intergrowth. Parallel polars, X50.

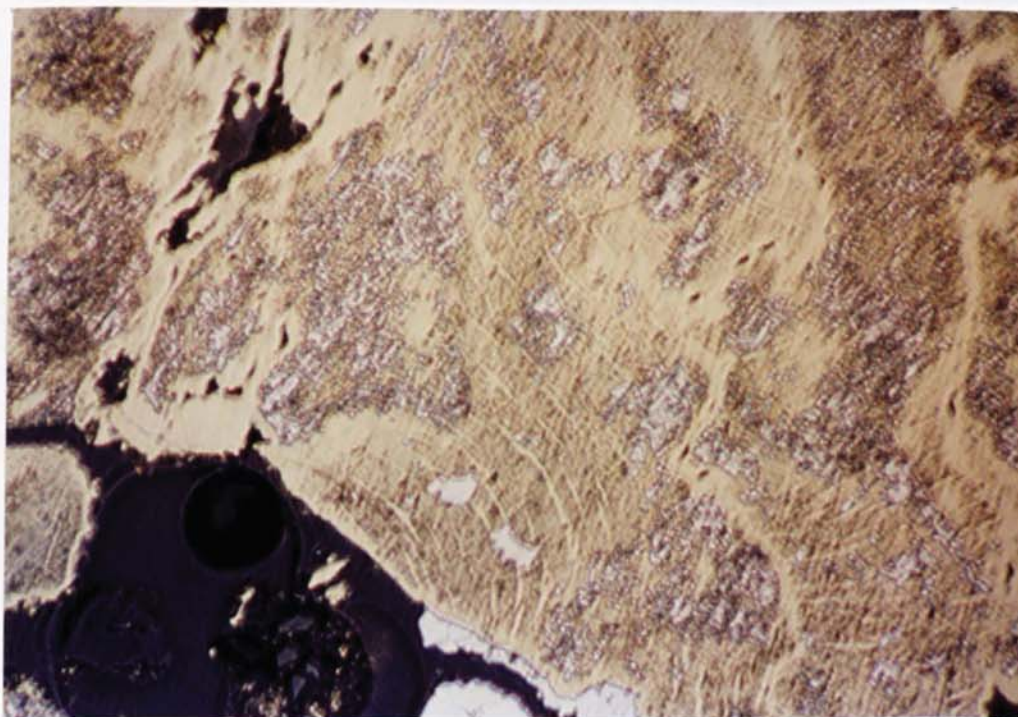


PLATE 6.14. Deformation of lamellae in chalcopyrite, and formation of stoichiometric chalcopyrite along fractures. Note the abundant presence of 'sweats' of iron sulphide. Parallel polars, X50.

TABLE 6.5. Electron microprobe analyses of lamellar and 'ridged' chalcopyrite, Parekklishia mine.

L A M E L L A R C H A L C O P Y R I T E					
Wt.%	C1	C13	C14	C18	C16
S	36.70	35.51	41.00	35.67	34.83
Fe	31.95	31.11	34.42	30.82	30.11
Ni	N.D.*	N.D.	N.D.	0.05	N.D.
Co	0.16	0.05	0.22	0.23	N.D.
Cu	24.98	28.13	19.31	22.00	26.09
Zn	0.82	0.19	0.59	0.28	0.27
Total	94.61	94.99	95.54	89.05	91.30
F o r m u l a					
S	2.000	2.000	2.000	2.000	2.000
Fe	0.999	1.005	0.963	0.992	0.993
Ni	0.000	0.000	0.000	0.002	0.000
Co	0.005	0.002	0.006	0.007	0.000
Cu	0.686	0.798	0.475	0.622	0.755
Zn	0.023	0.005	0.014	0.007	0.007

R I D G E D C H A L C O P Y R I T E					
Wt.%	RV.1	RV.3	RV.4	RV.5	RT.1
S	36.00	36.03	36.34	35.90	39.95
Fe	30.44	30.49	30.47	30.69	34.08
Ni	N.D.	N.D.	0.05	N.D.	N.D.
Co	0.14	N.D.	N.D.	0.23	0.26
Cu	25.39	25.70	26.68	26.32	21.41
Zn	0.15	0.92	N.D.	N.D.	0.54
Total	92.12	93.14	93.54	93.14	96.24
F o r m u l a					
S	2.000	2.000	2.000	2.000	2.000
Fe	0.970	0.972	0.963	0.981	0.980
Ni	0.000	0.000	0.002	0.000	0.000
Co	0.004	0.000	0.000	0.007	0.007
Cu	0.712	0.720	0.741	0.740	0.541
Zn	0.004	0.025	0.000	0.000	0.013

* N.D. : Not detected.

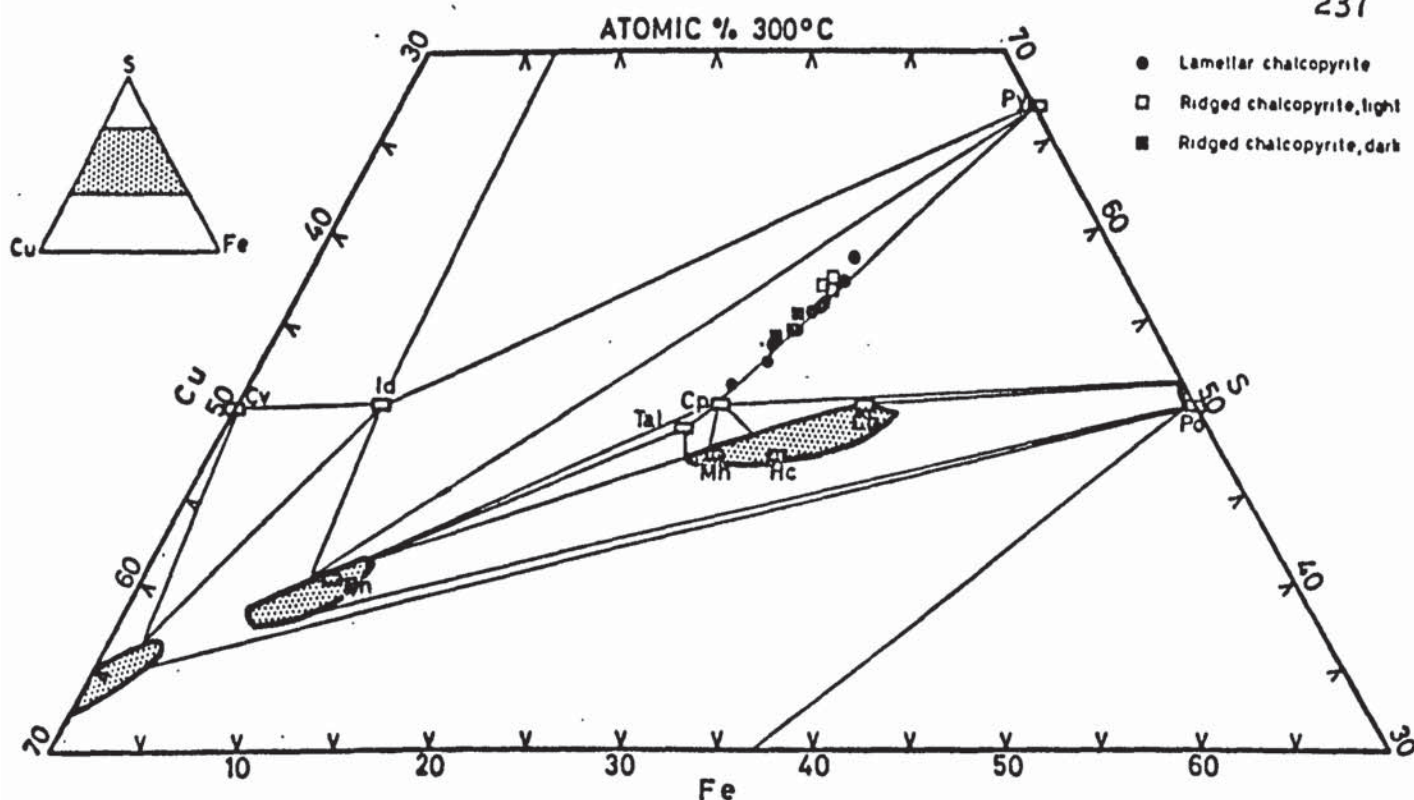


FIG. 6.3. Plot of lamellar and 'ridged' chalcopyrites on the Cu-Fe-S diagram. Phase relations at 300° C from Craig and Scott (1974).

Cp: Chalcopyrite; Py: Pyrite; Po: Pyrrhotite; Cb: Cubanite;
Hc: Haycockite; Mh: Mooihoekite; Tal: Talnakhite; Bn: Bornite;
Id: Idaite; Cv: Covellite; Dg: Digenite.

TABLE 6.6. Electron probe analyses of unaltered chalcopyrites from Parekklishia.

Wt. %	PCP-1	PCP-2	PCP-3	PCP-4	PCP-5
S	35.12	34.94	34.83	33.92	34.81
Fe	30.52	30.75	30.41	30.31	29.50
Ni	N.D.*	0.14	N.D.	N.D.	0.17
Co	N.D.	N.D.	N.D.	N.D.	N.D.
Cu	34.52	34.46	35.29	34.39	34.25
Zn	0.76	0.11	0.17	0.18	0.60
Total	100.92	100.40	100.70	98.80	99.33
F o r m u l a					
S	2.000	2.000	2.000	2.000	2.000
Fe	0.998	1.011	1.002	1.026	0.973
Ni	0.000	0.004	0.000	0.000	0.005
Co	0.000	0.000	0.000	0.000	0.000
Cu	0.992	0.995	1.023	1.023	0.993
Zn	0.021	0.003	0.005	0.005	0.017

* N.D. : Not detected.

with the sheared host rocks in the mine is in favour of the inference.

The features of deformation of the chalcopyrite are not documented in the literature. Deformation studies of sulphide minerals (Clark and Kelly, 1973; Roscoe, 1975; Kelly and Clark, 1975) produce textures which are similar in appearance to the regular intergrowth observed in the Parekklishia ores but differ in the fact that individual lamellae show no evidence of thinning at the intersections with transverse sets and are clearly deformation twins. In the case under consideration, however, the texture is identical to that produced by exsolution in the sense that individual lamellae do not transect transverse sets of lamellae. Friedrich (pers.com. 1982) suggested that the textures are probably indicative of high temperature bornite with twin lamellae of chalcopyrite decomposed to newly formed Cu-Fe minerals with a deficit in copper. No evidence, however, of a solid solution of bornite and chalcopyrite is found in any of the analysed samples of the unaltered chalcopyrite.

Ramdohr (1980) suggests that the formation of twins of even the thinly lamellar type in the chalcopyrite can take place during crystal growth. Furthermore, a texture similar in all respects to the one presently reported is described by Short (1964) as resulting from growth twinning. It is therefore probable that the lamellar intergrowth is a texture inherent in the mineral during crystallisation, represents growth twinning and the role of tectonism was to destroy the interstitial chalcopyrite with the formation of an aggregate of copper-deficient chalcopyrite and the

release of iron sulphide in the process. It is significant to point out that situations are observed where the unaltered chalcopyrite shows evidence of the existence of faint lamellae, even though its composition does not deviate from stoichiometry.

A more likely explanation of the lamellar chalcopyrite may be found in the study of phase relations in the Cu-Fe-S system. These suggest that, at temperatures above 500° C the dominant ternary phase is intermediate solid solution (iss) which at lower temperatures inverts to a primitive cubic phase which persists down to 20-200°C. Natural intergrowths of chalcopyrite and cubanite probably form as decomposition products of initially deposited iss (Craig and Scott, 1974). Iss has been identified as a common phase in black smoker deposits and normally occurs in the form of a lamellar intergrowth made up of light and dark lamellae of mixed chalcopyrite-iss (Haymon, 1982). The appearance under the microscope of these intergrowths is identical to the lamellar textures of the Parekklishia. It may be inferred that the latter textures are the result of relic preservation of original iss, later equilibrated to chalcopyrite. This pattern is revealed by partial breakdown of the chalcopyrite into pyrite and the copper-deficient phase.

6.2.2.5. Sphalerite compositions and their implications.

Electron microprobe analyses of sphalerites from Parekklishia and the East Pacific Rise (Haymon, 1982) are shown in Table 6.7. These are compared with sphalerites from Mathiatis (Mitsero), and from Agrokippia 'B' deposit (Botros, 1982) (Table

TABLE 6.7. Electron microprobe analyses of sphalerites from Parekklishia and the East Pacific Rise.

Wt. %	1	2	3	4	5	6
S	32.74	32.92	32.34	33.16	33.02	33.31
Fe	7.84	7.60	6.05	16.61	11.75	16.71
Ni	0.10	0.11	0.23	0.01	N.A.*	N.A.
Co	0.14	N.D.	N.D.	0.01	N.A.	N.A.
Cu	2.08	1.57	3.42	1.98	0.92	0.49
Zn	58.07	57.92	57.57	46.98	54.64	49.22
Total	100.97	100.12	99.61	98.75	100.33	99.73

1=SPD20, 2= SPD19, 3= SPD21, 4= SPD15, Parekklishia sphalerites.
 5= 914 R-3B, 6= 914 S-4, Sphalerites from the East Pacific Rise (Haymon, 1982).

* N.A. : Not analysed
 N.D. : Not detected.

TABLE 6.8. Electron microprobe analyses of sphalerites from Mathiatis (Mitsero) and Agrokipia 'B' orebody.

Wt. %	1	2	3	4	5	6
S	33.08	32.73	33.39	32.71	32.86	33.09
Fe	2.14	2.67	0.42	2.11	1.83	4.03
Mn	n.d.	0.07	n.d.*	n.a.	n.a.	n.a.
Ni	0.07	n.d.	0.09	n.a.	n.a.	n.a.
Cu	0.17	0.05	0.11	n.a.	n.a.	n.a.
Zn	65.25	64.37	66.93	65.25	65.42	63.21
Total	100.71	99.89	100.94	100.07	100.11	100.33

n.a = Not analysed.

1, 2, 3 = Sphalerites from Mathiatis, sample KN-5.
 4= Sphalerite in matrix of CY-2A, 153.25 m.
 5= Sphalerite in veins of CY-2A, 153.25 m.
 6= Zoned sphalerite in vesicles, CY-2A, 153.25 m.
 Analyses of CY-2A sphalerites from Botros (1982).

* n.d. : Not detected
 n.a. : Not analysed.

6.8) . The assemblages of Parekklishia co-exist with pyrite (or marcasite) and chalcopyrite. The sphalerites from the East Pacific Rise co-exist with a complex assemblage of pyrite, pyrrhotite, chalcopyrite (or iss), wurtzite and , sometimes, bornite. Sphalerites from Mathiatis and Agrokipia 'B' co-exist with pyrite and chalcopyrite but represent stockwork assemblages in contrast to the first two which are associated with massive mineralization.

The iron-rich nature of some of the Parekklishia sphalerites contrasts strongly with the iron-poor sphalerites from Agrokipia and Mathiatis and shows similarities to the sphalerites of the East Pacific Rise black smokers (Fig. 6.4).

Experimental studies on the Fe-Zn-S system (Barton and Toulmin, 1966, Boorman, 1967) suggest that the iron content of sphalerite in equilibrium with pyrite and pyrrhotite is buffered at 20.7 mole per cent FeS in the temperature range 300-600° C. Higher FeS contents in this range are found in sphalerites co-existing with pyrrhotite alone; lower contents characterise sphalerites co-existing with pyrite. Relationships below 250°C (Scott and Kissin, 1973) suggest that the iron content of sphalerite co-existing with pyrite and pyrrhotite is in the region of 10-12 mole per cent FeS. Sphalerites lower in FeS content co-exist with pyrite alone.

Assemblages of high sulphidation state as e.g. the chalcopyrite-pyrite-bornite fS_2 buffer (Czamanske, 1974), are characterised by very low iron contents of associated sphalerites (between 0.1 and 1.0 mole per cent FeS).

The above relationships, defined experimentally, have

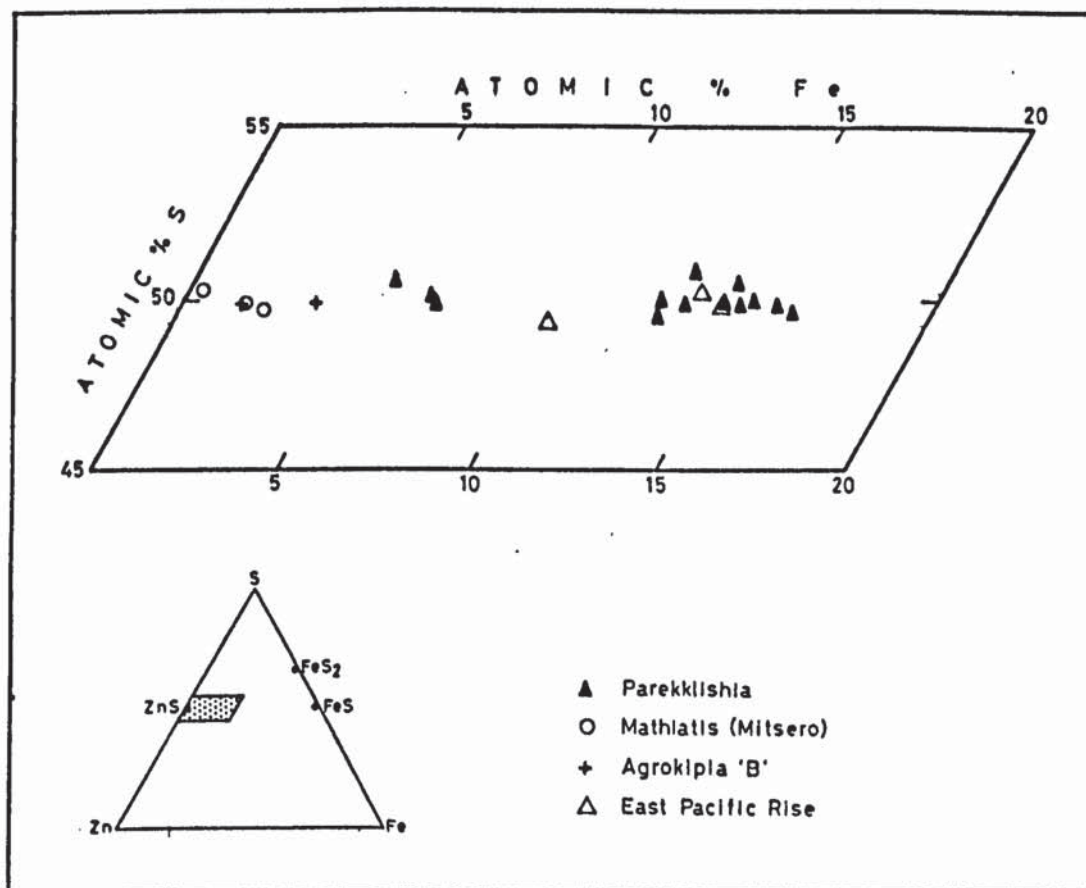


FIG. 6.4. Plot of sphalerite compositions from various environments of the Fe-Zn-S diagram. Note the contrast in iron content between sphalerites of Parekklisshia and the East Pacific Rise and sphalerites from Agrokipia 'B' deposit and Mathiatis (Mitsero).

been applied to natural assemblages. Sphalerites from the Salton Sea geothermal brines (Skinner et al., 1967) are characterised by FeS contents varying between 3-16 mole per cent, in agreement with their co-existence with pyrite. The sphalerites in the Broadlands geothermal field (Browne and Lovering, 1973) show variable FeS contents when in co-existence with pyrite, attributed to fS_2 fluctuations, and constant compositions when buffered by pyrrhotite.

It is clear from the above that the assemblages of Agrokípia and Mathiatis are in equilibrium with pyrite, while those of Parekklíshia and the East Pacific Rise were in equilibrium with pyrrhotite at the time of their formation. The absence of pyrrhotite from the Parekklíshia assemblages is interpreted as due to equilibration to pyrite, a conclusion substantiated by the abundant presence of pyrrhotite in the crystallising phases of recent oceanic sulphide deposits and its absence from the older mounds (Haymon and Kastner, 1981).

6.2.3. Petrography of mineralized lavas

The petrographic changes in the mineralized lavas, as exemplified by the examination of a number of samples from the stockwork zones of Limni and Mavri Sykia mines suggest a complete destruction of original mineralogy and textures with only rare preservation of phenocryst outlines and vesicles.

The groundmass is generally altered to a fine-grained intimate mixture of quartz and chlorite, the latter frequently brownish-tinted, in contrast to vein chlorite which is

inclusion-free and strongly pleochroic.

In vesicle associations the chlorite occupies the marginal parts and generally pre-dates quartz which is concentrated at the centres (Plate.6.15).

Original clinopyroxene microphenocrysts are universally replaced by a mixture of quartz and chlorite. Plagioclase is replaced by microcrystalline quartz.

Chlorite compositions, as determined from limited electron microprobe analyses and numerous X-ray diffraction patterns lie close to ripidolite (Table 6.9).

Smectite is present in small amounts in the central parts of the Limni ore zone, associated with hydrothermal quartz and chlorite. Vesicle relationships suggest that it is paragenetically later than chlorite but pre-dates quartz. It forms a major proportion of the clays in the marginal parts of the ore zone (Table 6.10), and in the hydrothermally altered Basal Group of the Athkijatjia ridge, where it is associated with quartz and chlorite.

6.2.4. Paragenetic relationships

Detailed examination of numerous thin and polished sections suggests a sequence of mineral deposition which, although commonly reversed, is indicative of the behaviour of the hydrothermal fluids with changing physicochemical parameters.

Chloritisation of the matrix and formation of disseminated pyrite in the groundmass of lavas appears to be the earliest manifestation of interaction of hydrothermal fluids with the wall rocks. This is suggested by the common occurrence of

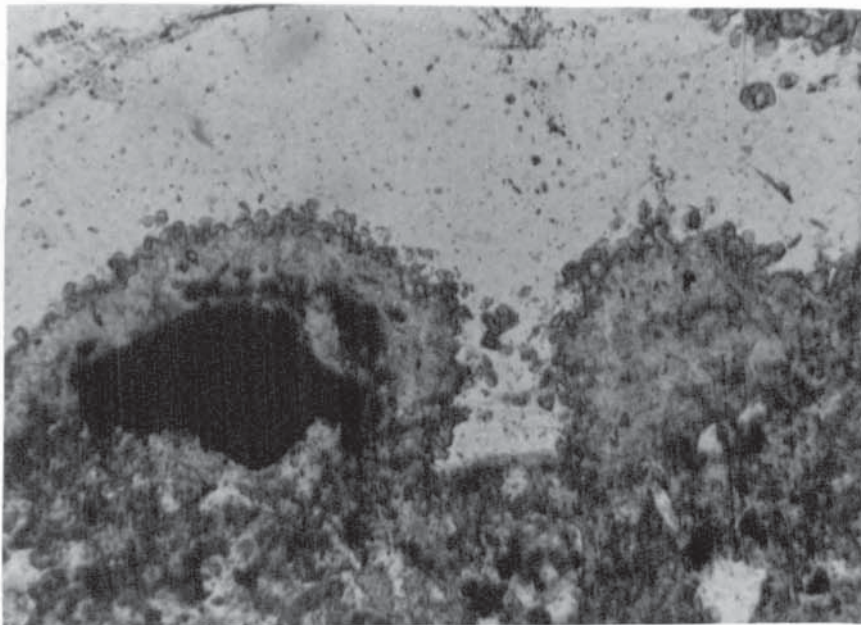


PLATE 6.15. Chlorite platelets associated with quartz (white) in vesicle.
Parallel polars, X100.

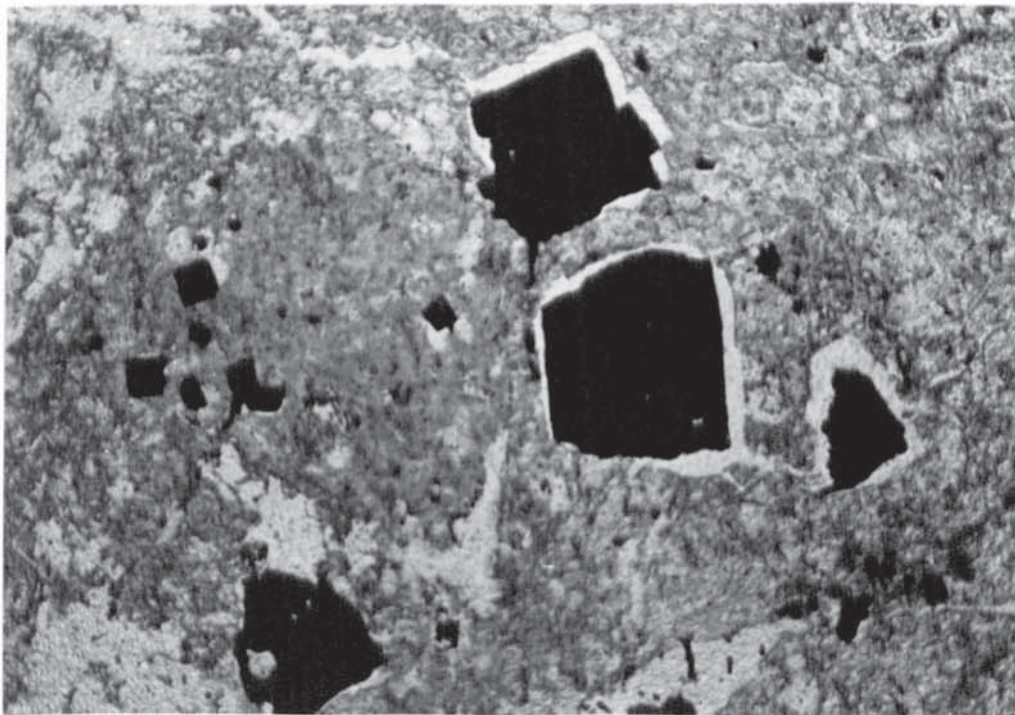


PLATE 6.16. Texture of mineralized lava showing intense chloritisation of groundmass and partial rimming and replacement of pyrite by quartz.
Parallel polars, X25.

TABLE 6.9. Electron microprobe analyses of chlorites from Limni mine compared with chlorites from Agrokippia.

Ox. %	1	2	3	4	5
SiO ₂	27.84	24.71	28.22	27.59	27.13
TiO ₂	0.12	0.01	----*	----	----
Al ₂ O ₃	18.76	20.52	16.28	19.32	21.95
FeO	25.74	25.63	27.03	26.08	16.59
MgO	14.12	13.05	10.64	15.65	19.67
Cr ₂ O ₃	0.05	0.35	N.D.	N.D.	N.D.
MnO	0.01	0.21	5.64	0.97	1.52
CaO	0.01	0.13	0.30	N.D.	N.D.
Na ₂ O	0.28	0.01	N.D.	N.D.	N.D.
K ₂ O	0.02	N.D.	N.D.	0.06	N.D.
Total	86.95	84.62	88.11	89.67	86.86

1, 2 = Chlorite from vesicles, Limni Mine (LI-6M).
 3 = Chlorite in vesicles, CY-2, 92.85 m.
 4 = Chlorite in vesicles, CY-2A, 173.66 m.
 5 = Chlorite in vesicles, CY-2A, 285.05 m.

* N.D. : Not detected , --- : Not analysed.

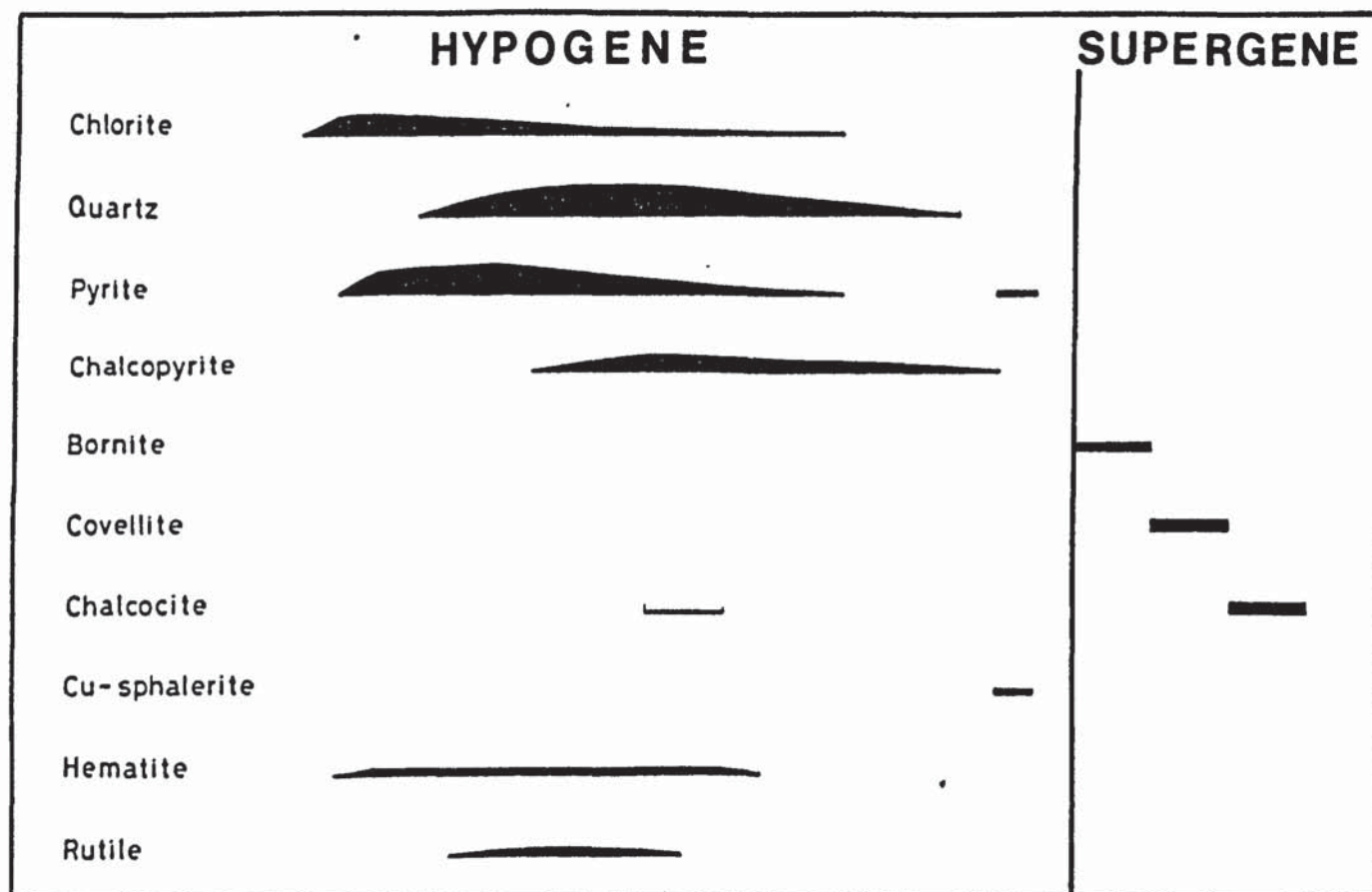


FIG. 6.5. Paragenetic relationships in the stockwork zone of the Limni orebody.

TABLE 6.10. Summary of X-ray diffraction data for mineralized and unmineralized lavas within and around the Limni orebody.

Refer to Appendix 3 for location of collection of samples.

Sample	SMECT.	MONTM. SYN AL.	CALC.	ANALC.	CHLOR.	QUARTZ	ACTIN.	ALB.
MINERALIZED BASAL GROUP OF ATHKIATJIA RIDGE =====								
LI-12M	T				A	A		C
LI-13M	C				A	A	T	C
LI-14M	A	A			A	T		
LI-15M	C				C	T		
LI-16M	A				A		T	
LI-17M	A	A			A	T		
LI-19M	A	A			A	A		
LATERAL EXTENSIONS OF THE ORE ZONE. =====								
LI-6M	A	C			C			
LI-7M	C	C			A			
LI-8M	A	A			A	T		
LI-9M	C				A			
LI-10M	A	A			A	T		
MINERALIZED LAVAS WITHIN THE LIMNI ORE ZONE. =====								
LI-1M	T				A	T		
LI-2M					A	T		
LI-3M					A			
LI-4M	T				A			
LI-5M	T				A	C		
LI-4	T				A	C		
LI-10-2	T				A	C		
LI-5a	T				A	T		
LI-11	C				A	C		
LI-1	T				C	A		
LI-2	C				A	T		
LI-6-1					A			
LI-3					A	T		
LI-11	C				A	C		
LI-7	C				C	A		
LI-6					A	T		
LI-8					A	A		
L109-100					A	C		
L109-180					A	A		
L115-300	T				A	A		
UNMINERALIZED LAVAS SURROUNDING THE OREBODY. =====								
L115-60	C		A	A				
L115-180	A		A	C				
LI-15R	C		C	T				
LI-16R	A							
LI-13R	A							
LI-11R	A							

A= Abundant, C= Considerable, T= Trace.

SMECT= Smectite, MONTM= Montmorillonite, CALC= Calcite, ANALC= Analcite, CHLOR= Chlorite, ACTIN.= Actinolite, ALB= Albite.

chlorite at the margins of walls of veins and vesicles, and the common replacement of early disseminated pyrite by later quartz (Plate 6.16).

Of the sulphides, pyrite is always the earliest mineral to be precipitated in veins in the form of euhedral crystals, commonly fractured and replaced by later quartz and chalcopyrite.

Chalcopyrite, although in rare cases occupying growth zones in pyrite, suggesting contemporaneous precipitation, is most commonly found in the form of anhedral concentrations between pyrite crystals, or healing fractures in brecciated pyrite.

Sphalerite appears to be always the last of the common sulphides to be precipitated in the stockwork zones, its commonest occurrence being as anhedral replacements of chalcopyrite.

The period of maximum quartz deposition appears to be before chalcopyrite and after deposition of pyrite, but quartz deposition persists after chalcopyrite in many cases and late stage quartz is common in the stockwork zones, coating vugs and fractures in mineralized lava (Plate 6.17).

The generalized paragenesis described above is shown in fig. 6.5, which, although specifically reflecting mineralogical associations in the stockwork zone of Limni orebody, is generally applicable to the majority of deposits in Cyprus (cf. Bear (1963); Christoforou (1975)).

In contrast to the generally simple relationships observed in veins, conditions of mineral precipitation in the massive zones are suggestive of several periods of precipitation, brecciation and recurrence of the mineralization. Mineralogical



PLATE 6.17. Euhedral quartz coating fracture in mineralized lava. Limni stockwork.

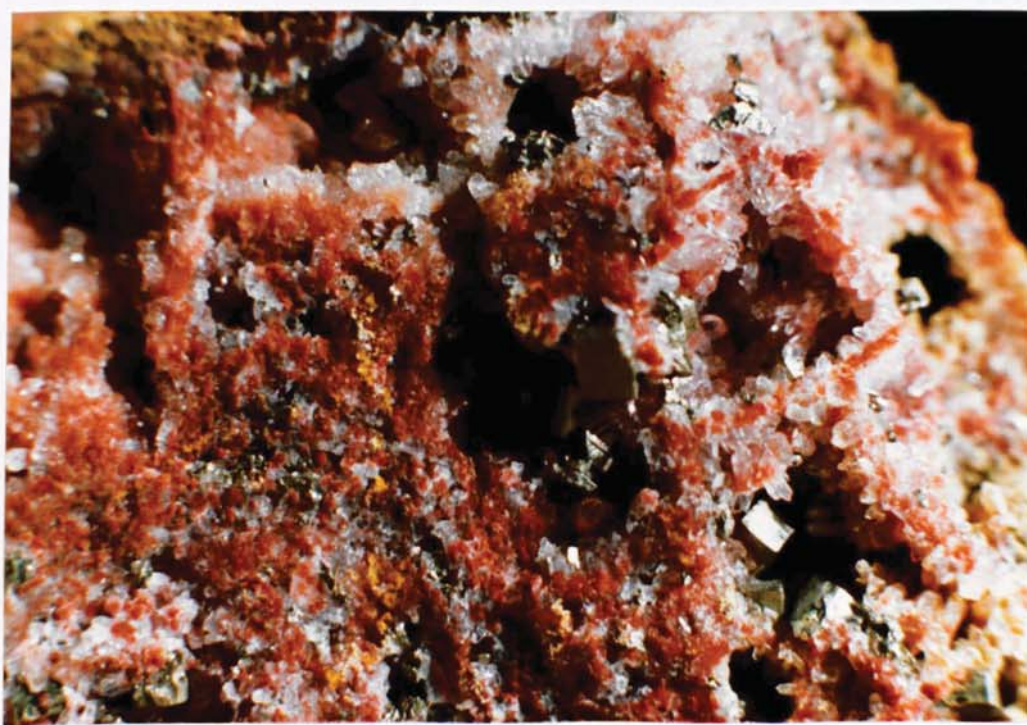


PLATE 6.18. Quartz enclosing hematite is overgrown by clear quartz and finally pyrite. Kokkinopezoula opencast.

Horizontal field of view is 3 cm.

relationships, as exemplified by the description of mineralogy of the Mangaleni massive ore, are interpreted, in the light of similar assemblages from modern spreading centres (Spiess et al., 1979; Oudin et al., 1981; Haymon and Kastner, 1981; Koski et al., 1982), as consistent with the build-up and subsequent collapse of sulphide mounds; and their burial by fine colloform sulphides which represent the products of crystallisation of fluids exiting from later forming vents.

6.3. The transition between mineralized and unmineralized ground

6.3.1. Field and mineralogical evidence

6.3.1.1. Skouriotissa

The stockwork pipe of Skouriotissa orebody (chapter 5), which marks the channelway of access of the mineralizing fluids for the deposition of the massive ore, is characterised by intense silicification, chloritisation and pyritisation, with complete obliteration of pillow structures. The lateral passage into the unaltered lavas, on which the massive lens was deposited, is accompanied by decreasing silicification, decrease in pyrite content of the lavas and gradual emergence of pillow outlines. The well pillowed unmineralized lavas beyond the transition zone are devoid of any sign of pervasive alteration.

The clay mineralogy of all three zones, and, in addition, of the unmineralized olivine basalts beyond the boundary fault (Fig.5.22, chapter 5) was examined by H. Elsbree as part of her M. Sc. dissertation, from samples collected in collaboration with the author. The main conclusions (Elsbree, pers. com., 1983) suggest

that:

The dominant clay mineral within the alteration pipe is chlorite, judged from diffraction peaks to belong to a mixed Mg-Fe species close to ripidolite in composition. Only subordinate amounts of smectite were detected.

The zone of transition from stockwork mineralization to the fresh lavas, evident in the field by propylitic alteration, is dominated by mixed layer clays, particularly regular chlorite-smectite and an unidentified mixed layer clay mineral. Little chlorite and traces of smectite are present in the transition zone.

The Lower Pillow Lavas further removed from the stockwork pipe show dominant smectite, as do the olivine basalts in the southwestern boundary of the mineralization.

It is significant of the temperature gradients obtaining around the alteration pipe that, although massive pyrite rests on the unmineralized Lower Pillow Lavas, the alteration minerals are indistinguishable from those characteristic of lavas unrelated to mineralization.

6.3.1.2. Limni

The dominant mineralogical assemblages in the Limni ore zone and the surrounding unmineralized olivine basalts were examined by X-ray diffraction methods, using samples of boreholes. Analyses were carried out courtesy of J. Lydon, Geological Survey of Canada.

The central parts of the ore zone are characterised by a

vertical downward passage from quartz-sulphide dominated into quartz-chlorite dominated sequence. The pyrite content steadily decreases, while the amount of silica shows a gradual decrease with depth. At the margins of the ore zone, the unmineralized olivine basalts are characterised, in addition to the primary augite and plagioclase, by abundant calcite and analcite and minor smectite. As the mineralization is approached, analcite disappears completely and the dominant assemblage comprises calcite and regularly interlayered chlorite-smectite. This is followed by chlorite, quartz and, finally, pyrite as the central parts of the ore zone are approached.

All the above assemblages are illustrated in fig. 6.6. They are consistent with a pattern of massive precipitation of quartz and sulphides at the higher levels of the ore zone, as the rock-seawater interface is approached, and a gradual lateral decrease in silicification. Magnesium metasomatism, as suggested from the distribution of chlorite and smectite persists to a greater lateral extent than silicification. The introduction of sodium and calcium into the surrounding unmineralized lavas is suggested from the distribution of calcite and analcite and their spatial relationship to the mineralization.

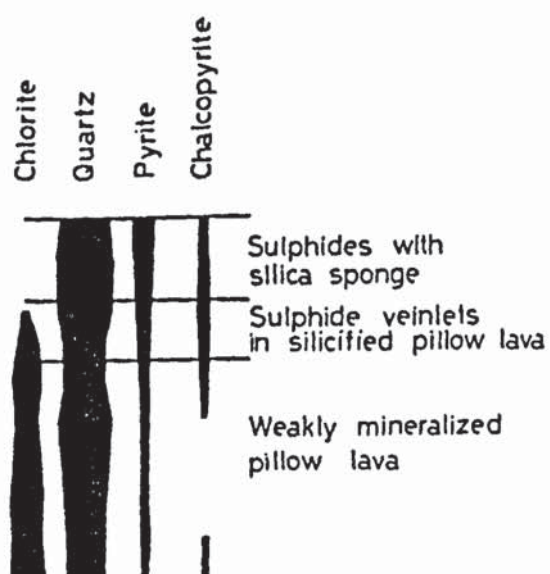
6.3.1.3. Kokkinopezoula

Geological mapping by the author at the Kokkinopezoula opencast (Fig. 5.25, chapter 5) suggests that ore deposition has taken place within the Lower Pillow Lavas. With the exception of the central parts of the ore zone, where steep gradients resulting

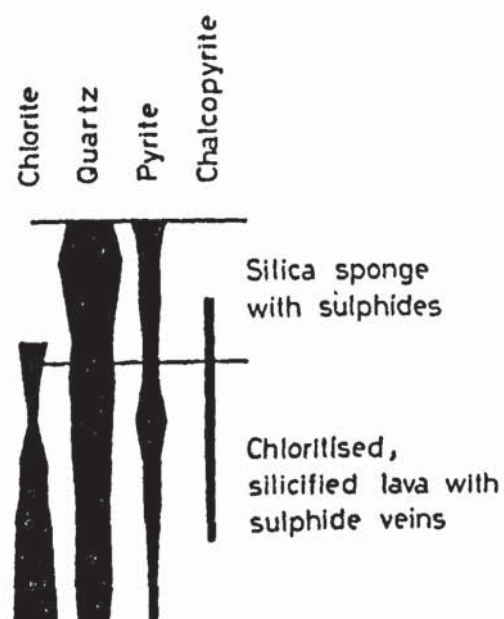
FIG. 6.6. X-ray diffraction results for three boreholes through the Limni orebody. Boreholes L109 and L118 are located in the central parts of the ore zone. Borehole L115 is located in the marginal parts and illustrates relationships at the transition from the barren cover of olivine basalts into the mineralized ground. Note in particular the successive disappearance of analcite and calcite, increase in smectite and finally the incoming of quartz-chlorite assemblage in the mineralized lavas. In boreholes L118 and L109 note the dominance of quartz and pyrite at higher levels and the increasing importance of chlorite at low levels in the ore zone.

Lithological descriptions of samples are from original borehole logging by Gordon-Smith.

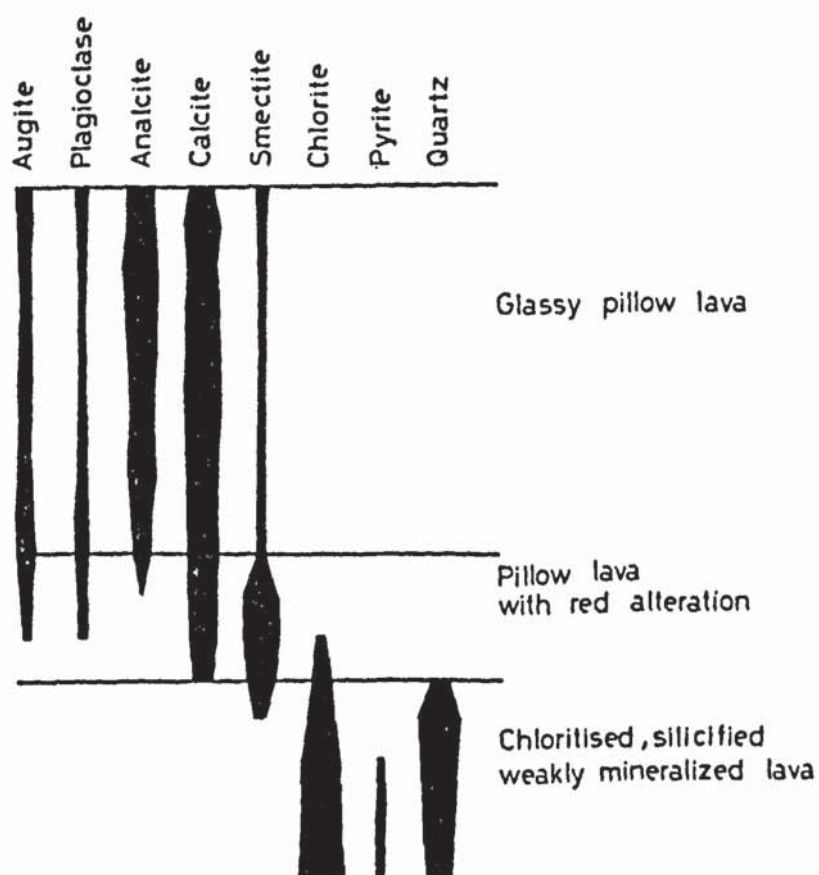
L118



L109



L115



50 metres
25
0

from structural factors caused massive precipitation of sulphides, conditions of mineralization in the marginal areas are characterised by preservation of original structures and universal transitions into unmineralized lavas through an intermediate zone of propylitised lavas.

Vesicle filling minerals in the mineralized lavas are mainly quartz and pyrite, commonly associated with hematite (Plate 6.18). The unmineralized Lower Pillow Lavas show typical cavity filling minerals of celadonite and heulandite. The altered, weakly propylitised lavas bounding the mineralization show complex assemblages of calcite, analcite, smectite, quartz and pyrite. Paragenetic relationships in these transitional lavas suggest early precipitation of smectite, followed by successive deposition of calcite-pyrite-smectite and finally a quartz-pyrite assemblage (Plate 6.19). These relationships are suggestive of early introduction of magnesium into the rocks, followed by calcium and finally silica with progressive alteration.

6.3.1.4. Memi- Alestos ore zone

Field mapping and borehole investigations at the area of Memi- Alestos ore zone (Plate 6.20) revealed the following relationships:

Pillowed flows are dominant in both areas, particularly at Alestos where dykes are almost completely absent. Sulphide mineralization, dominated by pyrite and chalcopyrite, is located in the central parts of the ore zone, associated with intense silicification and chloritic alteration. Silicification, in the



PLATE 6.19. Sequential infilling of vesicle by smectite-quartz-pyrite assemblage (lower part of photograph), followed by calcite (large euhedral crystals). Deposition of quartz-pyrite assemblage on calcite also observed but not shown on photograph. Horizontal field of view is 6 cm.



PLATE 6.20. General view, looking west, of Memi opencast in foreground and Alestos hill in the background. Red colouration at top of Alestos marks site of sulphide mineralization.

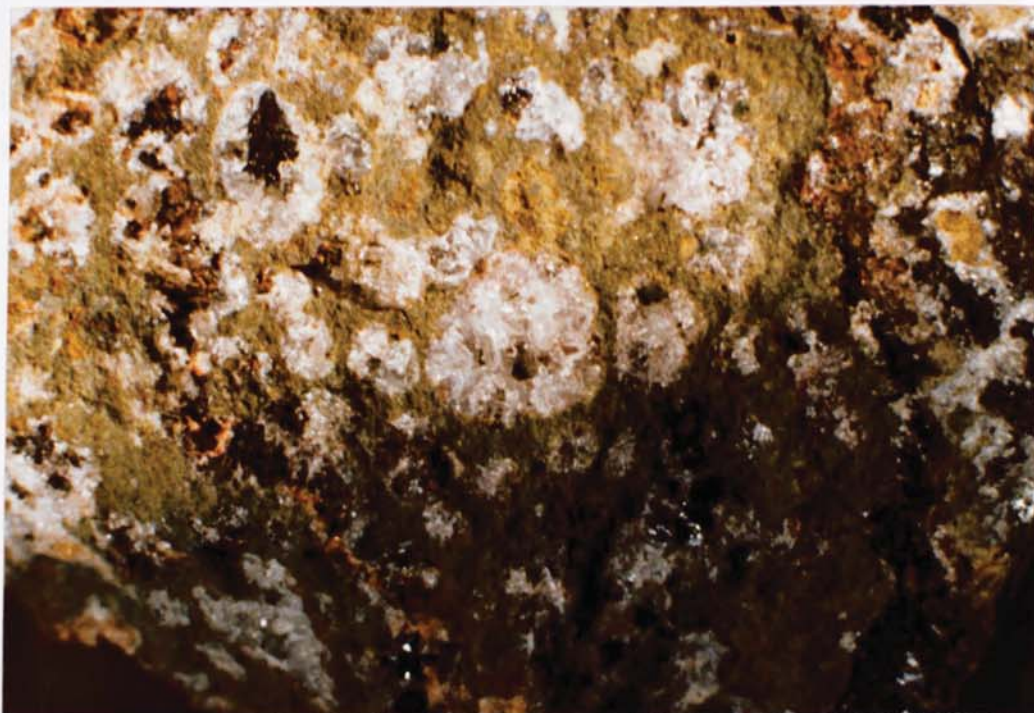


PLATE 6.21. Association of quartz and micaceous hematite (black) in veins and vesicles of chloritised lava. Alestos-Memi area.

Horizontal field of view is 7 cm.

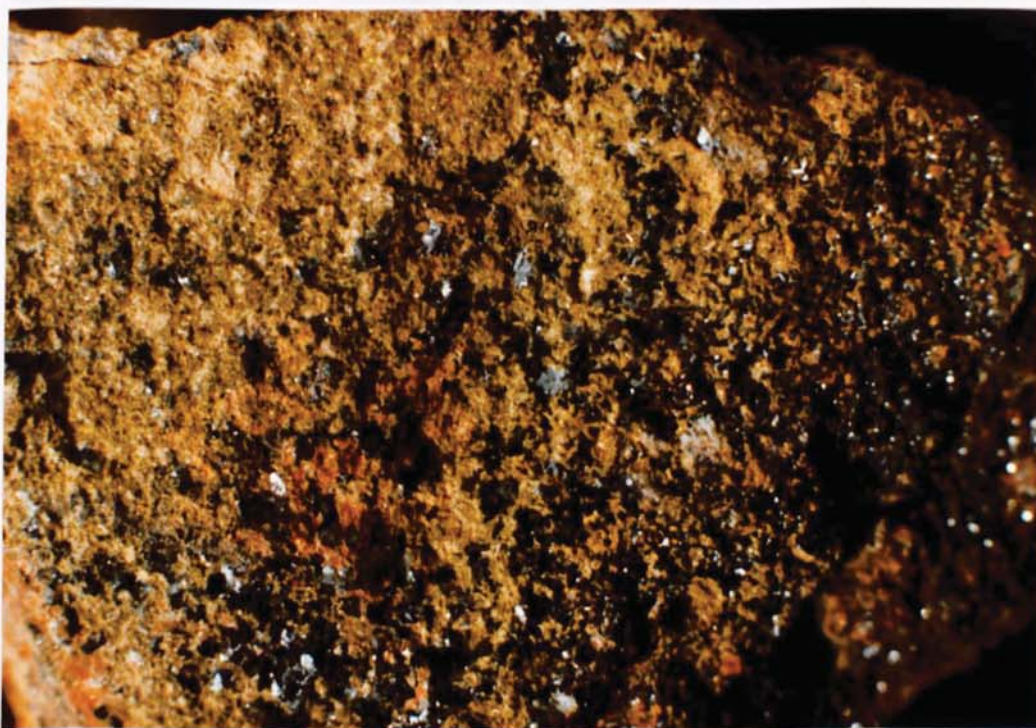


PLATE 6.22. Association of epidote (yellowish green) and micaceous hematite (black) in interpillow material of chloritised lava. Alestos-Memi area.

Horizontal field of view is 4 cm.



PLATE 6.23. Memi opencast. Pillows showing quartz-chlorite alteration of pillow margins.



PLATE 6.24. Memi opencast. Transitional passage from altered pillowed flows with chloritic rims (left) to mineralized lavas (partly oxidised).

form of intense veining and vesicle-filling of the pillow lavas by quartz, persists to great distances away from the areas of sulphide concentration as also does chloritisation.

The outward passage from sulphide-dominated to silicified and chloritised assemblages is associated with a parallel passage into hematitic mineralization. The hematite occurs both as disseminations within the lavas and as pseudomorphous replacements of original sulphides and is commonly associated with breakdown of chalcopyrite into secondary copper minerals. That the hematite is primary and not the result of secondary oxidation is suggested by its persistence at depth to more than 150 metres below surface and the absence of oxidation of associated rocks.

Hematite, in association with quartz and epidote, characterises the pervasively chloritised lavas which surround the zone of sulphide mineralization (Plates 6.21, 6.22).

The Memi mineralization (Fig. 6.7), representing the northeasterly extensions of the Alestos zone, is enclosed within Lower Pillow Lavas. These show a unique form of alteration associated with intensely chloritised pillow margins and dark interiors (Plate 6.23). Microscopic investigations reveal that the pillow margins are converted into a quartz-chlorite assemblage. Narrow elongated vesicles at the marginal parts of pillows are uniformly filled by smectite and quartz, and the glassy groundmass almost wholly converted to acicular birefringent smectite. Alteration minerals are abundantly associated with these lavas and include, apart from smectite and quartz, also epidote, micaceous hematite, pyrite, calcite and analcite. These pillows grade into mineralized lavas (Plate 6.24).

Legend

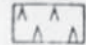
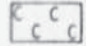
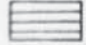
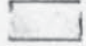






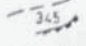
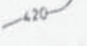
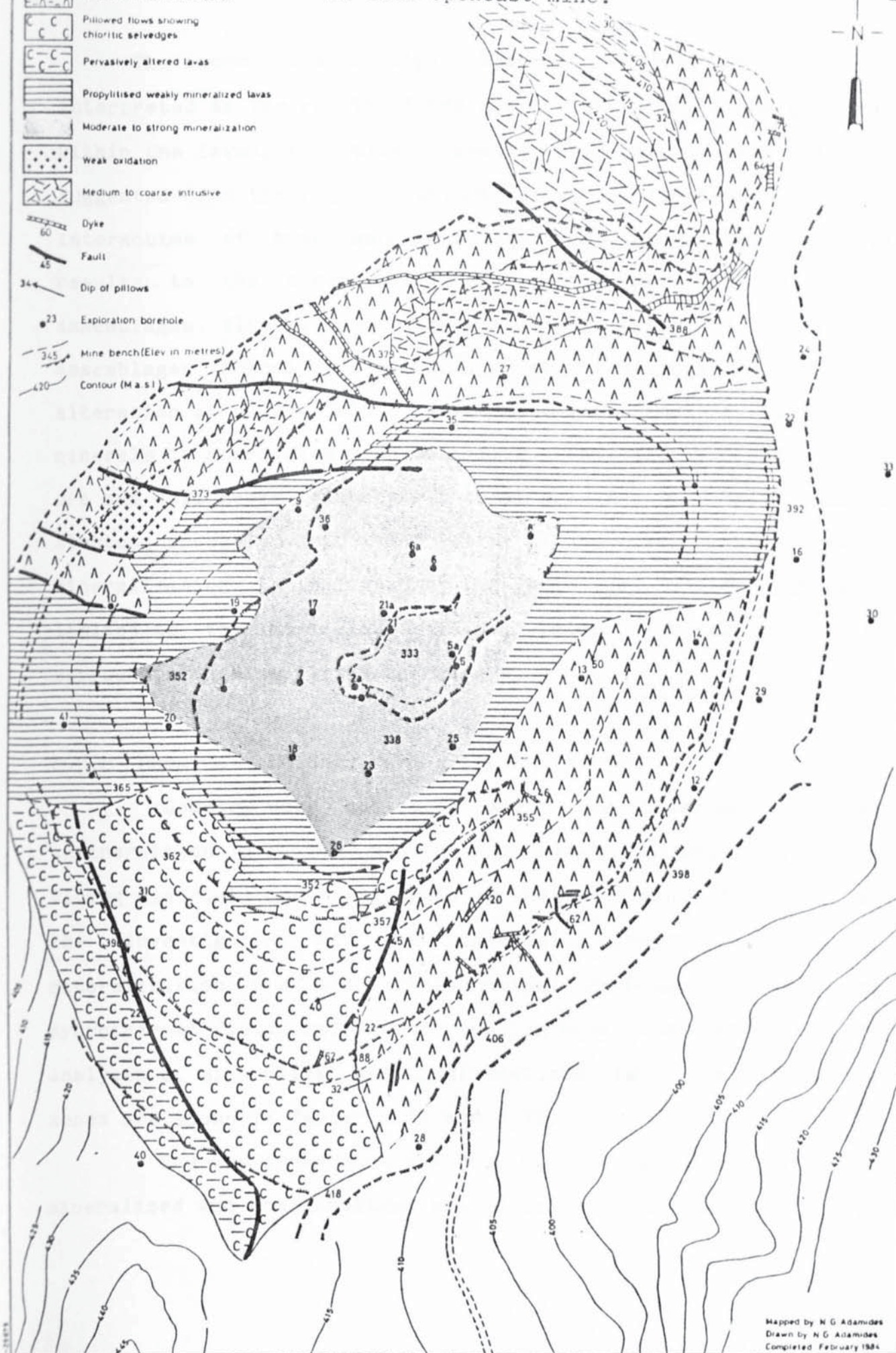
-  Unmineralized Lower Pillow Lavas
-  Siliceous Lower Pillow Lavas
-  Pillow flows showing chloritic selvages
-  Pervasively altered lavas
-  Propylitised weakly mineralized lavas
-  Moderate to strong mineralization
-  Weak oxidation
-  Medium to coarse intrusive
-  Dyke
-  Fault
-  Dip of pillows
-  Exploration borehole
-  Mine bench (Elev in metres)
-  Contour (M a s l)

FIG. 6.7. Geological map of Memi opencast mine.

255



Mapped by N.G. Adamides
 Drawn by N.G. Adamides
 Completed February 1984

0 50 100 150 metres

The above relationships, both at Alestos and Memi are interpreted as the result of ore deposition taking place at depth within the lavas, resulting to gentle temperature gradients, as suggested from the regional extent of silicification. Extensive interaction of hydrothermal fluids with oxygenated seawater results to the overprinting of earlier pyritic by oxidic assemblages. Alteration at high water:rock ratios is implied by assemblages at Memi, in particular the dominance of chloritic alteration at pillow rims, while the abundance of alteration minerals is associated with extensive chemical exchange between ore and wall rocks. A steeper thermal gradient at Memi than at Alestos, probably associated with a shallower environment of mineralization, is indicated by the fact that silicification is limited to the mineralized lavas, being only slight in the surrounding unmineralized formations.

6.3.2. Chemical exchange during mineralization

Samples were collected along two traverses from the unmineralized into the mineralized lavas at Evloimeni (Limni mining district) and Mavri Sykia (Kalavassos mining district) for the investigation of the chemical changes accompanying mineralization and also the chemical exchange between the hydrothermal fluids and the surrounding wall rocks. Representative analyses of mineralized and unmineralized lavas from both ore zones are shown in Tables 6.11 and 6.12.

The two areas show contrasting relationships between the mineralized and unmineralized ground in so far as Mavri Sykia

TABLE 6.11. Major and trace element analyses of mineralized and unmineralized lavas from the Evloimeni ore zone¹.

Ox. %	Major Elements					
	EV-1CHR	EV-2CHR	EV-3CHR	EV-18CHM	EV-19CHM	EV-21CHM
S102	52.30	53.85	52.70	54.75	53.25	59.55
T102	0.42	0.40	0.42	0.48	0.43	0.34
Al2O3	16.15	14.85	15.15	15.60	16.25	16.20
Fe2O3	8.95	9.37	9.03	9.35	9.83	7.04
MnO	0.10	0.14	0.08	0.17	0.15	0.02
MgO	7.60	9.95	12.10	8.00	11.65	2.50
CaO	7.58	5.19	5.80	8.52	6.34	2.55
Na2O	3.42	0.44	1.90	1.14	0.76	3.71
K2O	1.54	0.16	0.98	1.26	0.99	3.37
P2O5	0.05	0.03	0.02	0.04	0.03	0.03
Total	98.11	94.38	98.18	99.31	99.68	95.31
Total Iron as Fe2O3.						
	Trace Elements					
	EV-1CHR	EV-2CHR	EV-3CHR	EV-18CHM	EV-19CHM	EV-21CHM
Nb	2.1	1.4	2.0	2.0	1.7	2.3
Zr	14	20	22	26	24	21
Y	13.0	8.5	4.9	10.5	10.5	3.5
Sr	413	152	118	61	56	114
Rb	26.8	18.6	10.2	8.0	8.0	15.9
Ga	12.0	13.0	12.3	15.1	14.4	11.0
Zn	64	64	72	198	179	167
Cr	77	84	99	87	119	127
V	276	253	280	328	341	136
La	0	0	0	0	0	0
Ce	3.2	2.7	3.4	0.9	1.3	21.0
Nd	2.0	1.6	0.3	3.0	1.8	2.1
Ba	71	59	27	185	114	298

¹ Prefix CHR refers to unmineralized lavas, CHM to mineralized.

TABLE 6.12. Major and trace element analyses of mineralized and unmineralized lavas from the Mavri Sykia ore zone¹.

Ox. %	Major Elements					
	MS-4CHM	MS-5CHM	MS-6CHM	MS-7CHM	MS-8CHM	MS-9CHM
SiO ₂	51.00	49.55	50.60	45.55	49.30	51.60
TiO ₂	0.23	0.22	0.21	0.24	0.45	0.45
Al ₂ O ₃	12.40	12.30	11.85	13.25	16.20	16.30
Fe ₂ O ₃	17.70	19.94	20.53	19.79	16.81	16.43
MnO	0.19	0.12	0.13	0.16	0.07	0.07
MgO	13.20	11.50	9.45	15.50	11.75	10.65
CaO	0.07	0.09	0.07	0.11	0.20	0.06
Na ₂ O	0.03	0.05	0.05	0.05	0.04	0.07
K ₂ O	0.00	0.01	0.00	0.00	0.00	0.00
P ₂ O ₅	0.02	0.03	0.03	0.03	0.03	0.03
Total	94.84	93.81	92.92	94.68	94.85	95.66
Total Iron as Fe ₂ O ₃ .						
	Trace Elements					
Nb	2.5	2.5	1.9	2.6	2.3	2.3
Zr	18	17	19	18	41	43
Y	4.5	5.9	4.8	4.0	9.8	8.3
Sr	1	2	3	3	6	2
Rb	1.4	1.1	1.1	1.4	1.6	0.7
Ga	10.8	10.2	11.2	12.2	13.8	14.5
Zn	758	386	362	616	459	147
Cr	535	546	521	586	112	87
V	306	315	300	333	245	249
La	0	0	0	0	0.4	0
Ce	5.0	2.5	3.4	5.5	9.2	8.7
Nd	0	0	0	0.9	4.4	3.6
Ba	0	0	0	0	0	0

¹ Prefix CHR refers to unmineralized lavas, CHM to mineralized.

represents deep parts of the ore zone and a close structural control, while Evloimeni is characterized by general gradations from the mineralized to the unmineralized lavas.

Enrichments and depletions in the various elements were derived by utilising the method outlined in chapter 3, i.e. element- zirconium variations. The results for various elements are shown on figures 6.8 and 6.9. They suggest that:

Zinc is strongly enriched in the marginal parts of the Mavri Sykia ore zone but falls to background values in the unmineralized lavas. Zinc enrichment in the Evloimeni ore zone extends into the unmineralized lavas, suggesting introduction of zinc by the hydrothermal fluids.

Calcium is quantitatively removed from the Mavri Sykia ore zone and also depleted in the unmineralized lavas relative to the unaltered equivalents. In the Evloimeni ore zone calcium shows a depleted pattern which also persists into the unmineralized lavas.

Magnesium is introduced into both the mineralized and the surrounding unmineralized lavas in both areas. The pattern of magnesium enrichment in the unmineralized lavas coincides with the pattern of calcium depletion.

Sodium is quantitatively removed from the Mavri Sykia ore zone and erratically enriched in the unmineralized lavas. Local enrichment is observed in the mineralized lavas of Evloimeni and the surrounding unmineralized lavas.

The distributions of barium and potassium around the two ore zones are shown in figures 6.10 and 6.11. Both elements are

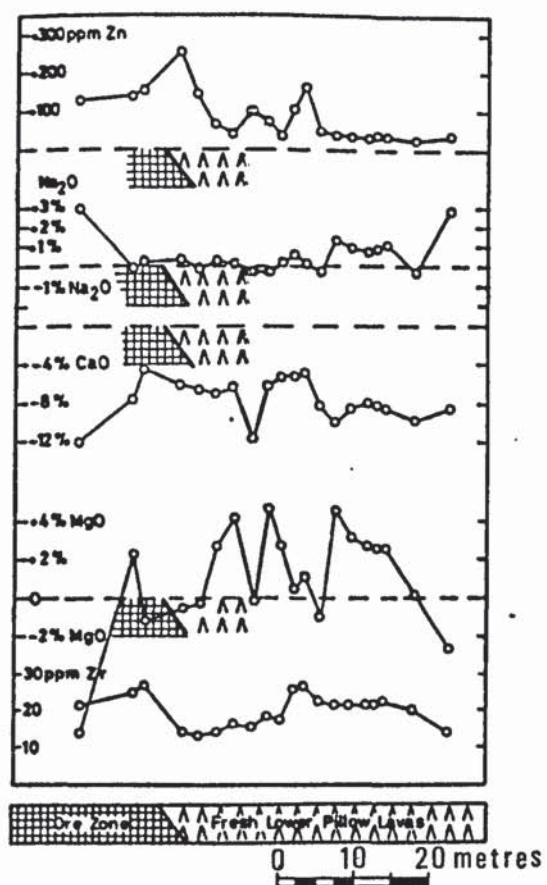


FIG. 6.8. Chemical variations at Evloimeni ore zone.

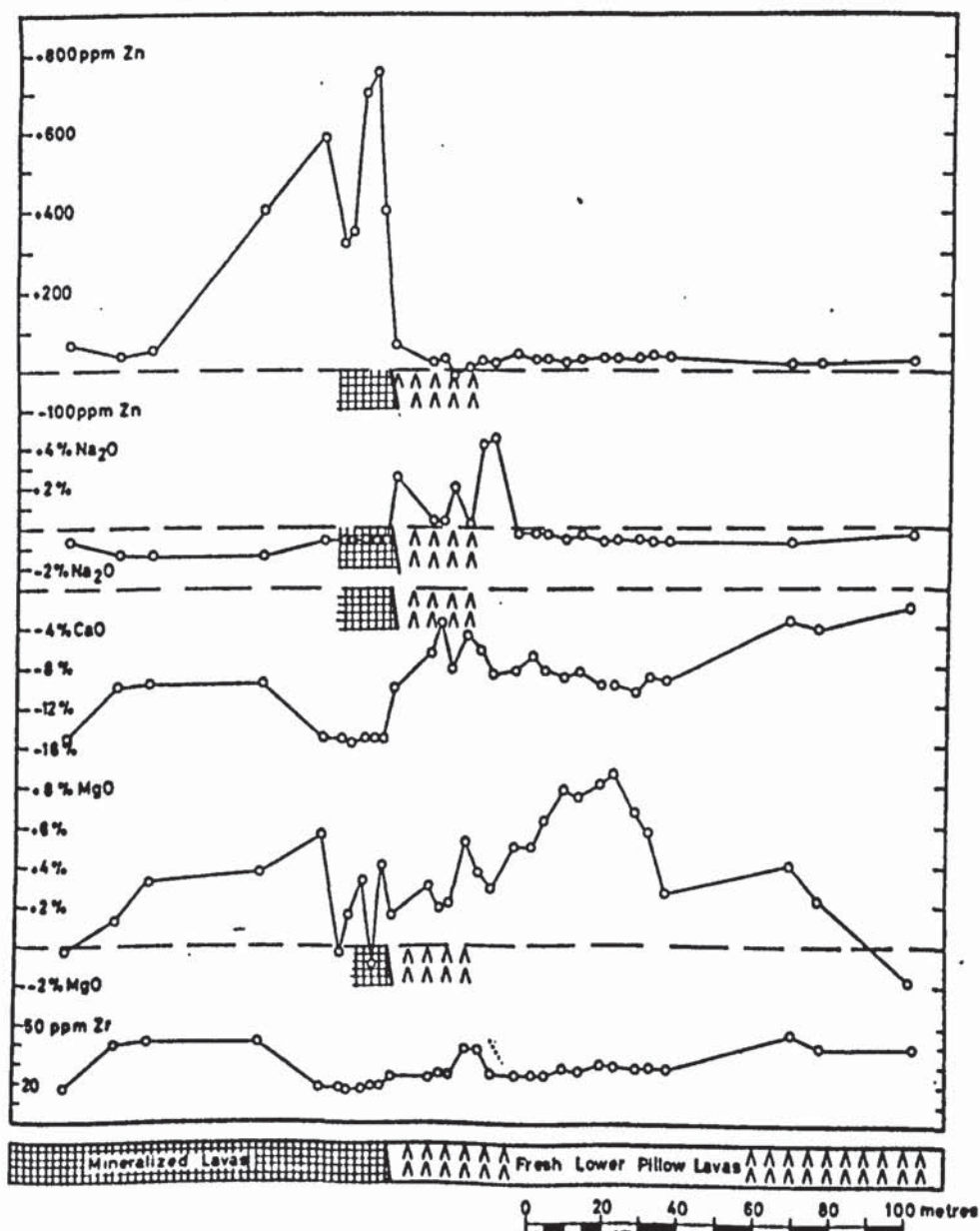


FIG. 6.9. Chemical variations in the Mavri Sykia ore zone.

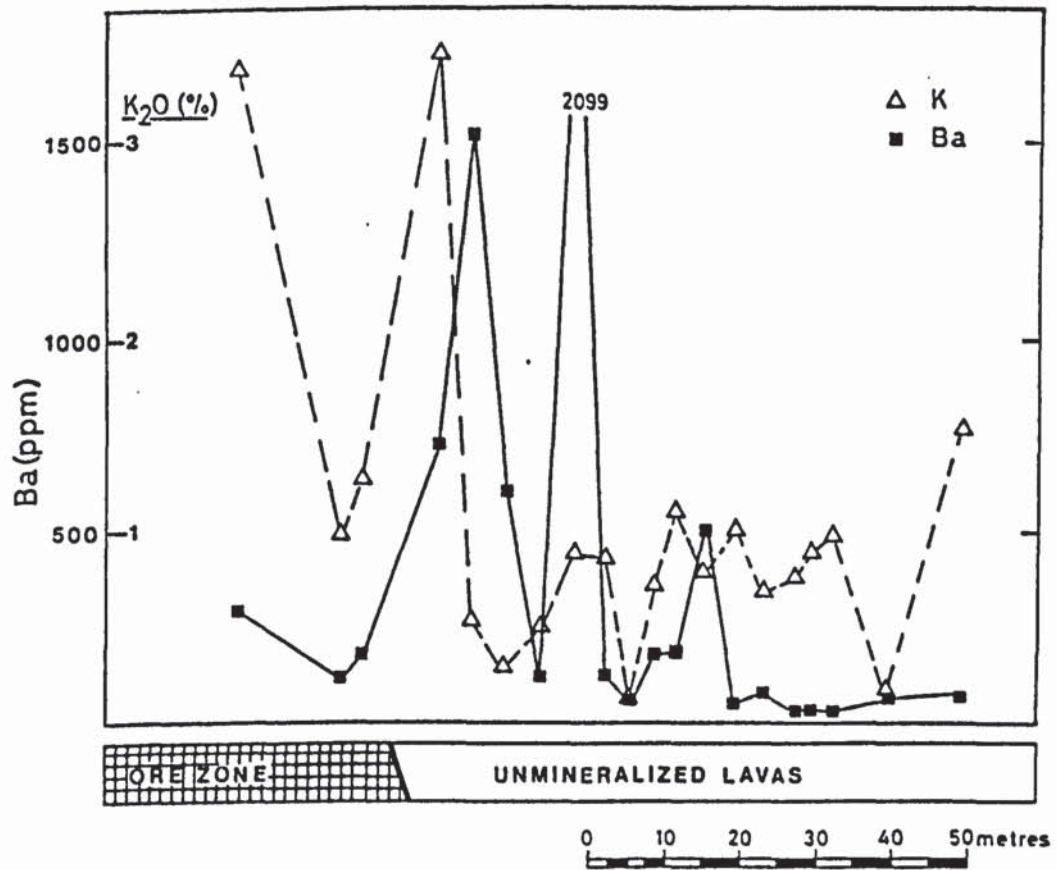


FIG. 6.10. Distribution of barium and potassium within and around the Evloimeni ore zone.

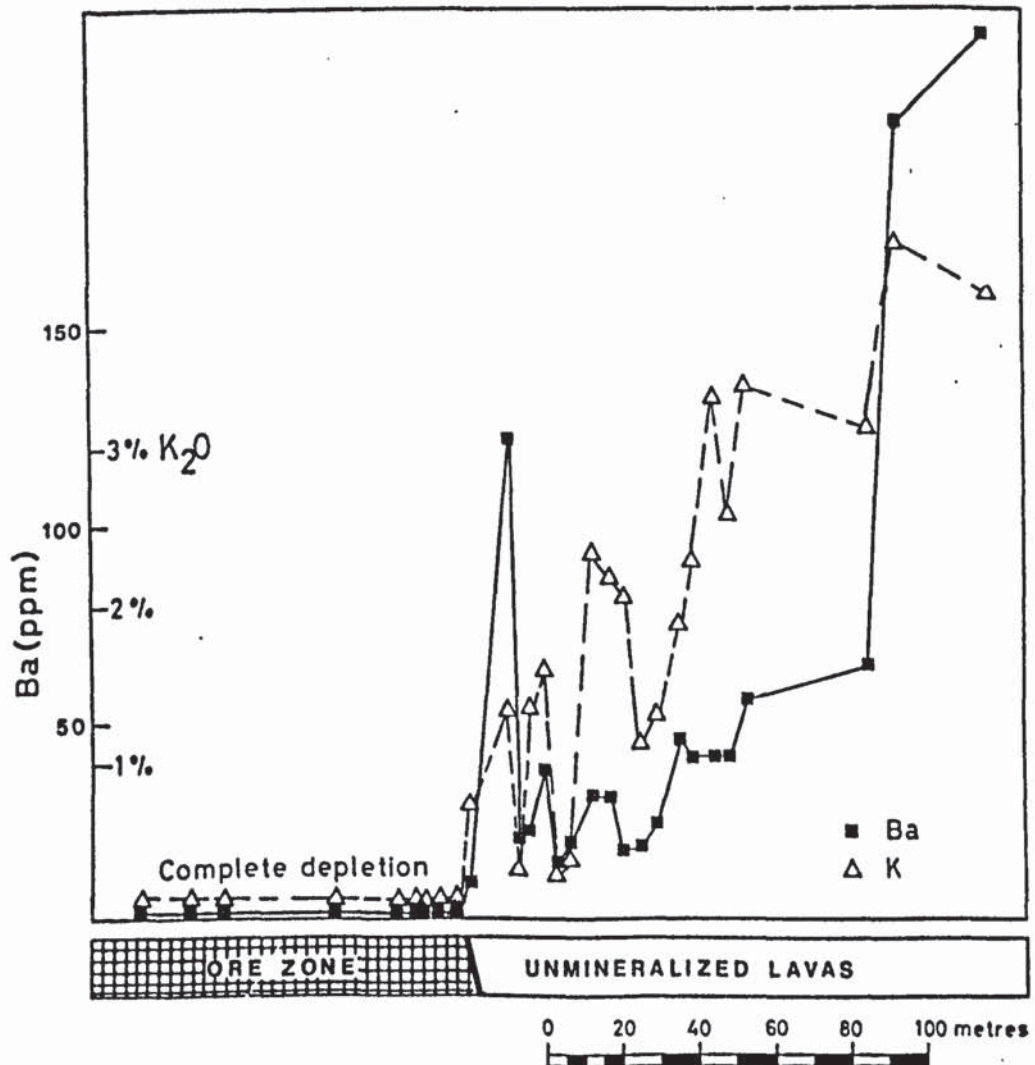


FIG. 6.11. Distribution of barium and potassium within and around the Mavri Sykia ore zone.

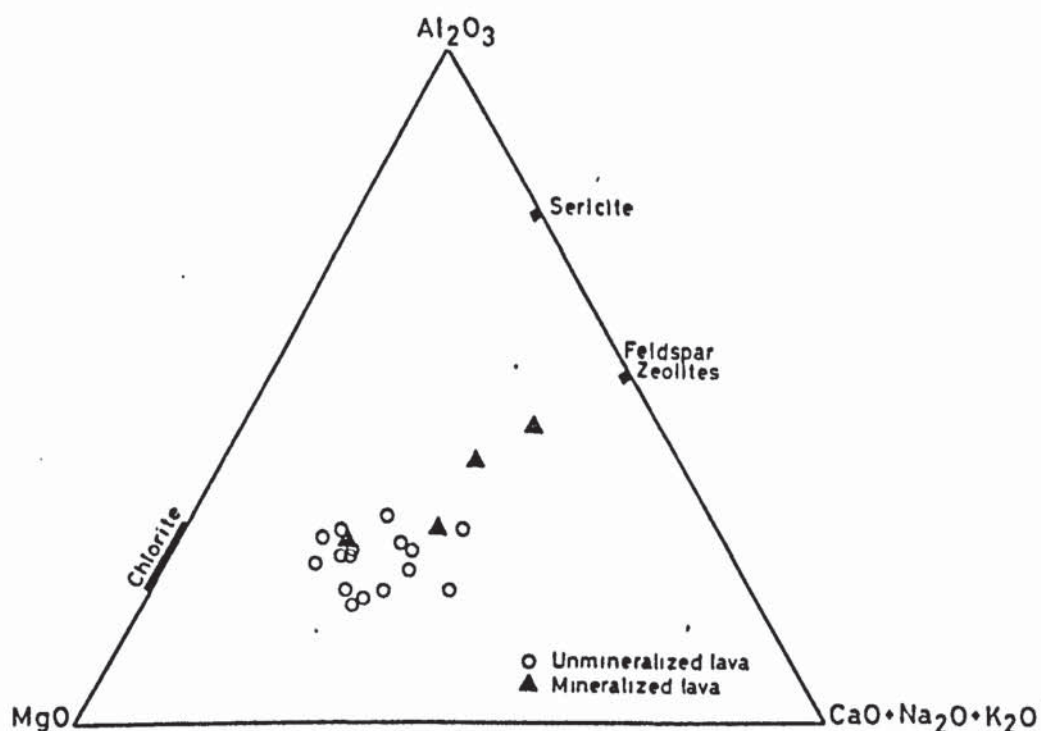


FIG. 6.12. Plot of assemblages from Evloimeni ore zone on the $\text{MgO-Al}_2\text{O}_3$ -Alkalis diagram (Izawa et al., 1978). Note trend towards zeolitic assemblages exhibited by the mineralized lavas, a reflection of alkali enrichment.

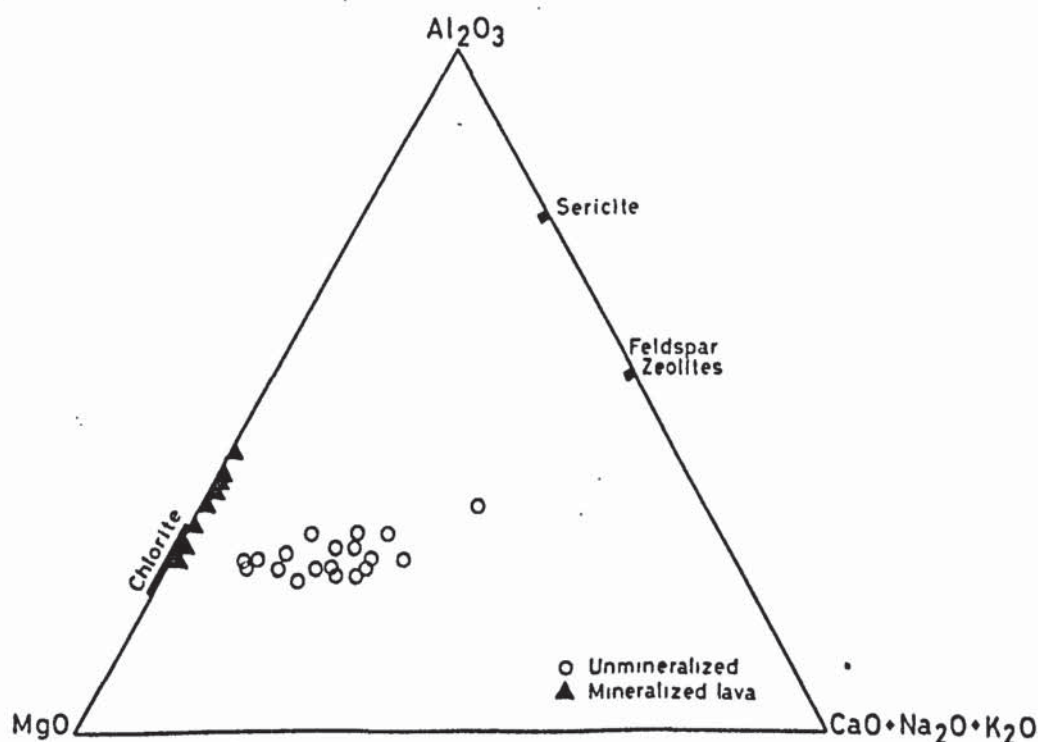


FIG. 6.13. Plot of mineralized and unmineralized lavas from Mavri Sykia on the $\text{MgO-Al}_2\text{O}_3$ -Alkalis diagram. Complete leaching of alkalis in the mineralized lavas is evident in the dominance of chlorite.

completely leached from the Mavri Sykia ore zone and enriched in the unmineralized lavas. The Evloimeni ore zone is locally enriched, with much greater enrichments in the unmineralized lavas.

The contrasting mineralogies of the two areas are shown on the Al_2O_3 - MgO - Alkalies diagrams (Figs. 6.12 and 6.13). A trend towards zeolitic assemblages at Evloimeni contrasts strongly with the strong alkali depletion at Mavri Sykia which results to the development of chloritic assemblages in the ore zone. Mavri Sykia may be considered as a typical representative of the situation at deep levels of ore zones (cf. earlier descriptions of petrographic characteristics of Limni mineralized lavas); Evloimeni typifies the chemical changes in the uppermost levels of ore zones as the hydrothermal fluids cool by mixing with seawater and by interaction with the wall rocks. Patterns of chemical exchange similar to Evloimeni are envisaged for such deposits as Agrokippia 'B' and the marginal parts of Kokkinopezoula orebody.

6.4. Metal zonations

The behaviour of hydrothermal fluids at discharge sites is directly linked to their original character and the changes in this character at the site of ore deposition. Depending on these changes, the metals contained in solution may be precipitated or dissipated into the surroundings without leaving any trace of their existence. The distribution of metals in ore deposits and variations within and between deposits provide evidence for the formulation of the laws which control the final mineralogical

composition of the deposits.

The Kinousa- Uncle Charles ore zone was chosen for detailed study of metal zonations mainly as a result of the presence of detailed plans of workings and the contrasting mineralogies between the two concentrations (Kinousa underground and Uncle Charles). Further data were obtained from boreholes in other deposits.

The overall distribution of copper and zinc in two of the uppermost levels of the Kinousa orebody (Figures 6.14- 6.17) is not suggestive of any distinct pattern. The variation of $\text{Cu}/\text{Cu}+\text{Zn}$ ratio, however, (Figures 6.18- 6.19) suggest a regularity determined by the arrangement of fractures parallel to the Kinousa fault (chapter 5), the controlling structure for the deposition of the orebody. This points to the conclusion that the pattern is the result of the paragenetically late introduction of copper- and zinc-rich fluids overprinting earlier assemblages.

Enrichment in both copper and zinc in the upper levels of the deposit and enrichment of zinc relative to copper also in the higher levels is suggested from Table 6.13 and interpretable as due to a temperature control, with copper being deposited at lower, hotter levels than zinc.

The strong fractionation of both copper and zinc relative to sulphur in the higher levels of the deposit is further illustrated in fig. 6.20, which represents an oblique section through the orebody. Since successively higher levels in the massive deposit define a time stratigraphic sequence related to the building up of a sulphide mound, the figure illustrates the

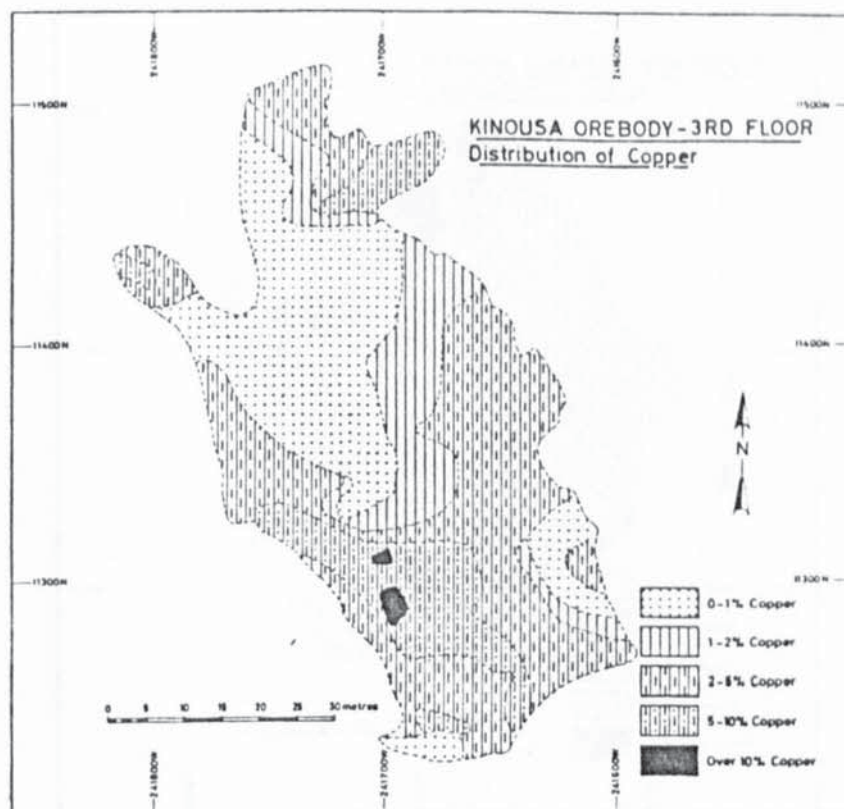


FIG. 6.14. Distribution of copper in the third floor of the Kinoussa underground deposit.

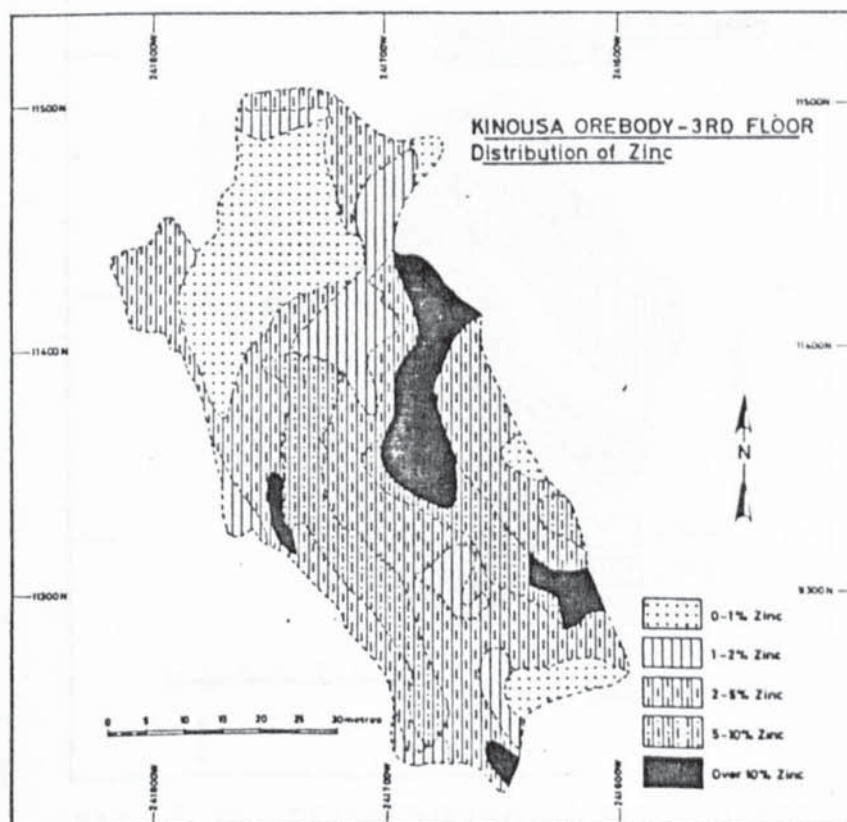


FIG. 6.15. Distribution of zinc in the third floor of the Kinoussa underground deposit.

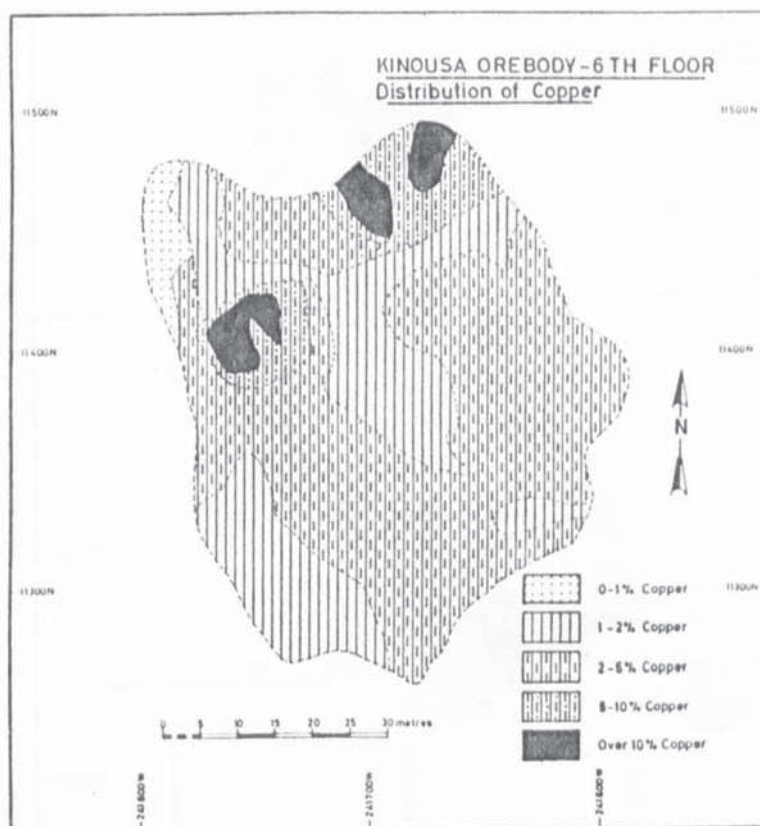


FIG. 6.16. Distribution of copper in the sixth floor of Kinousa underground deposit.

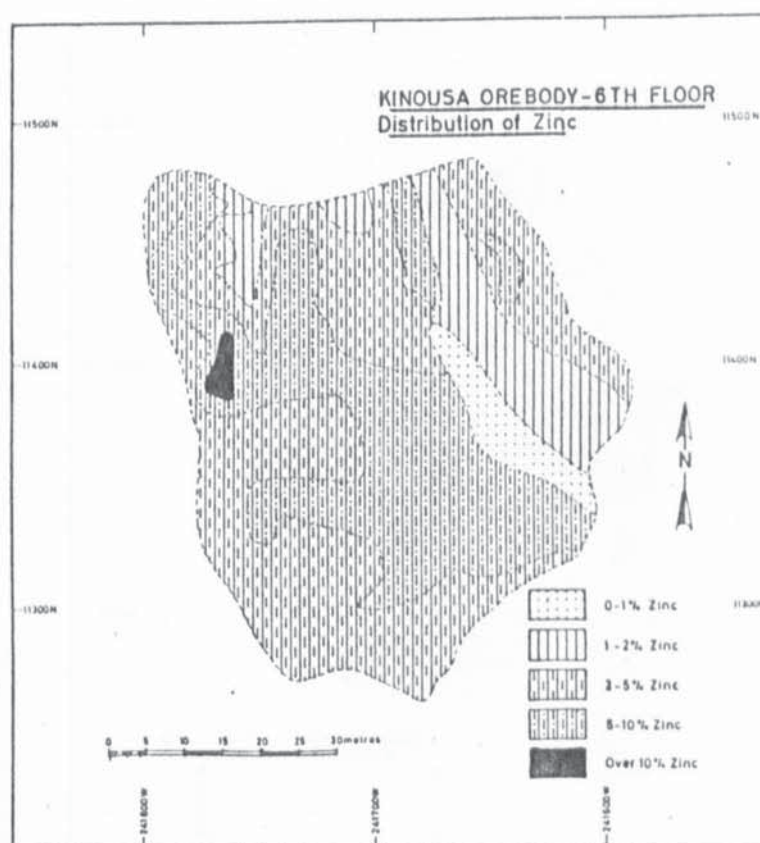


FIG. 6.17. Distribution of zinc in the sixth floor of Kinousa underground deposit.

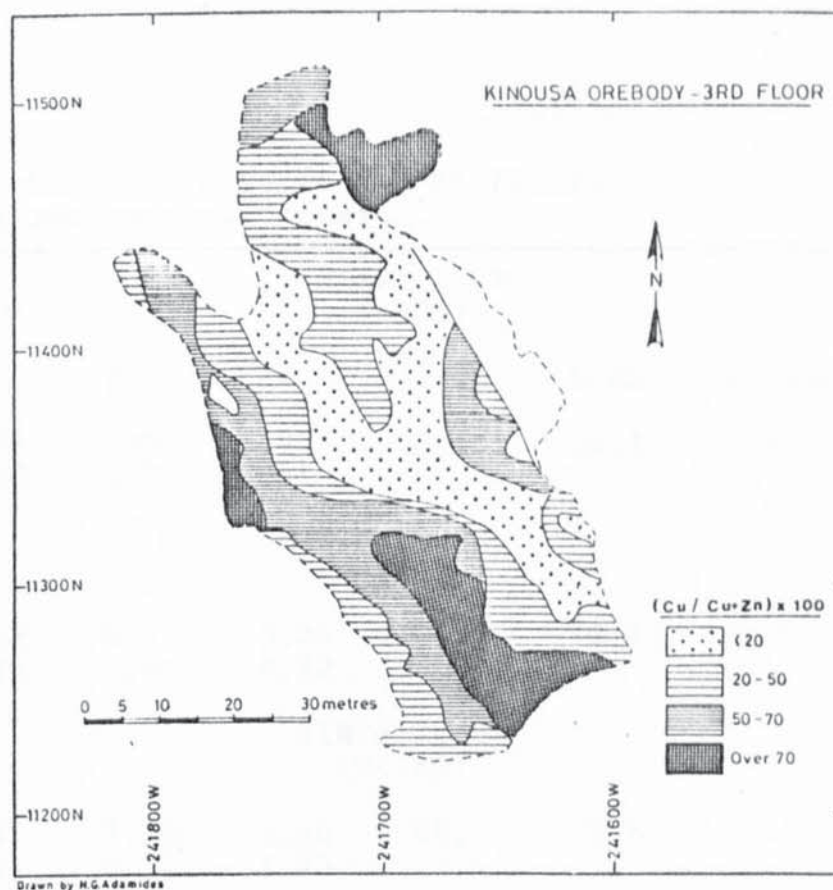


FIG. 6.18. Distribution of the ratio $\text{Cu}/\text{Cu}+\text{Zn}$ in the third floor of Kinoussa underground deposit.

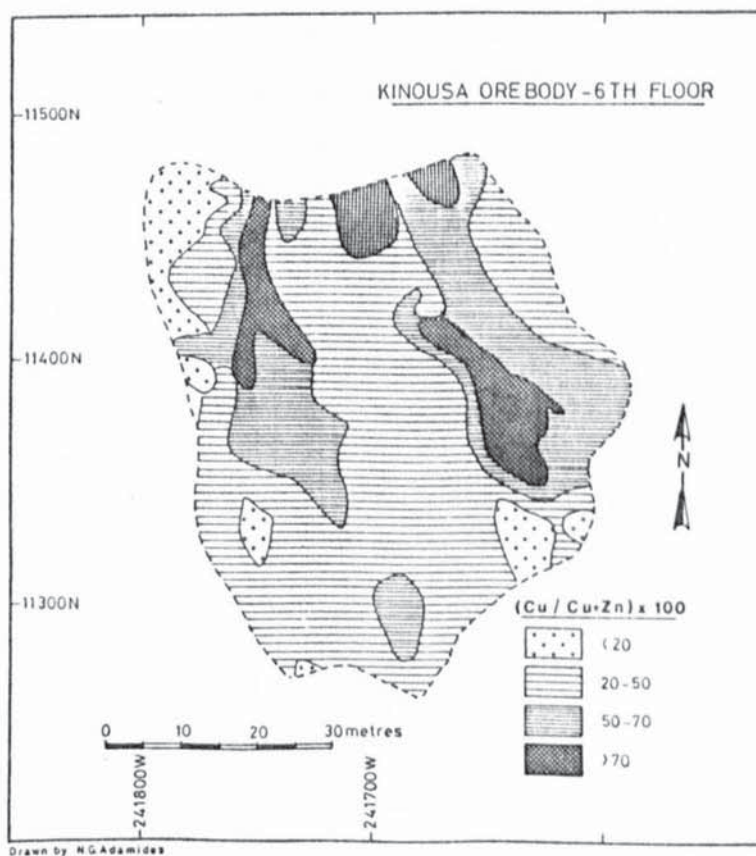


FIG. 6.19. Distribution of the ratio $\text{Cu}/\text{Cu}+\text{Zn}$ in the sixth floor of Kinoussa underground deposit.

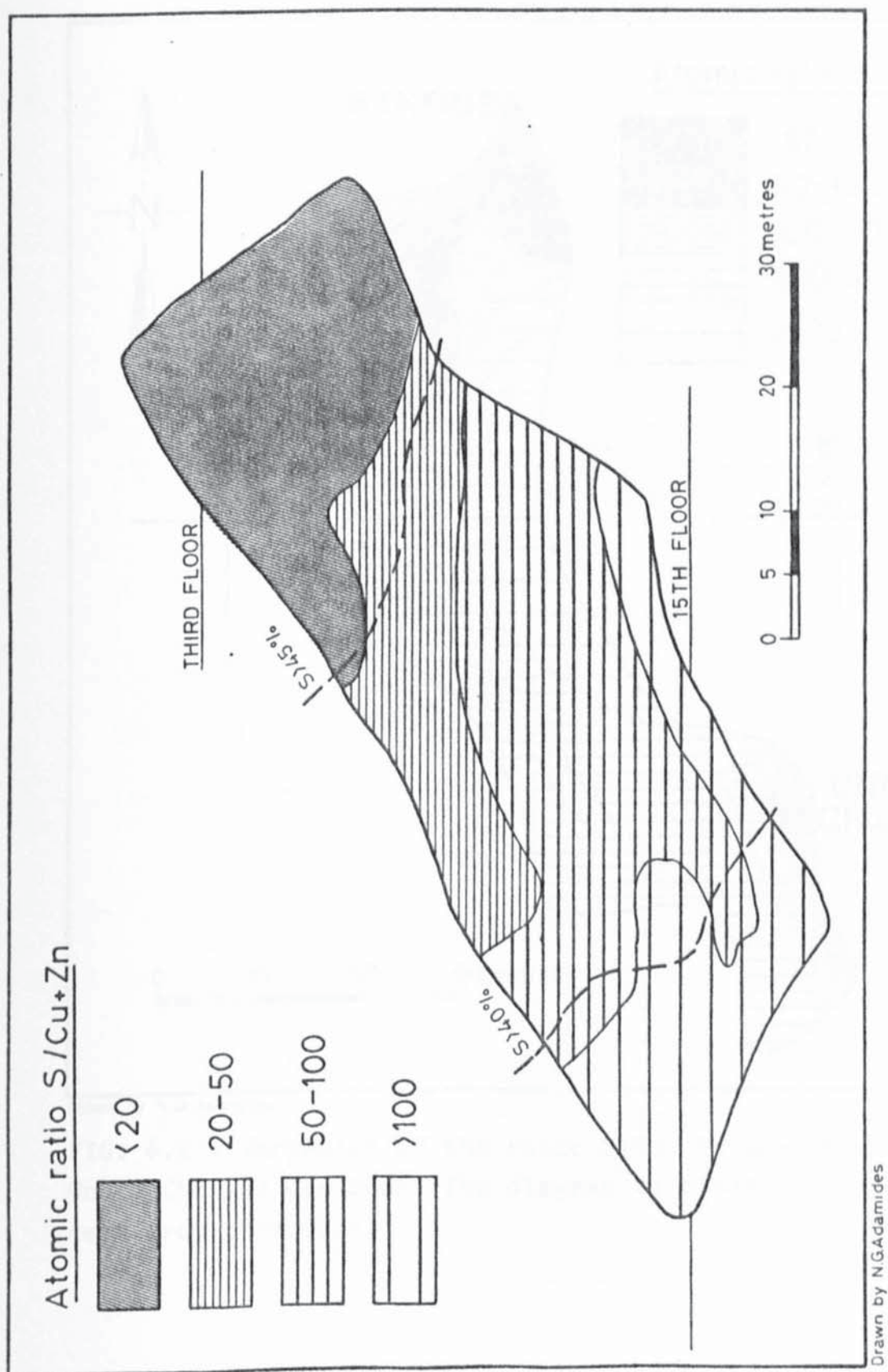
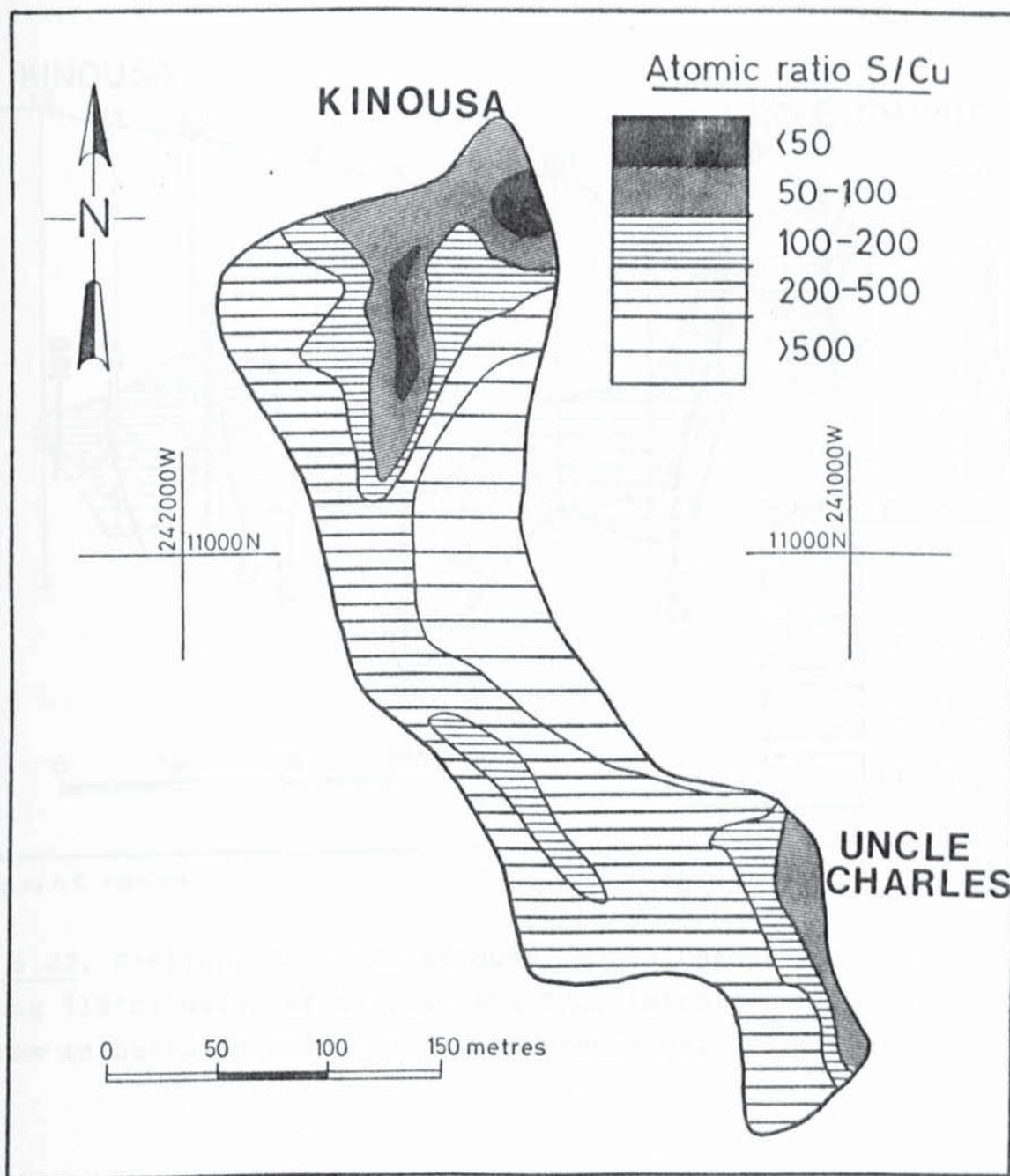
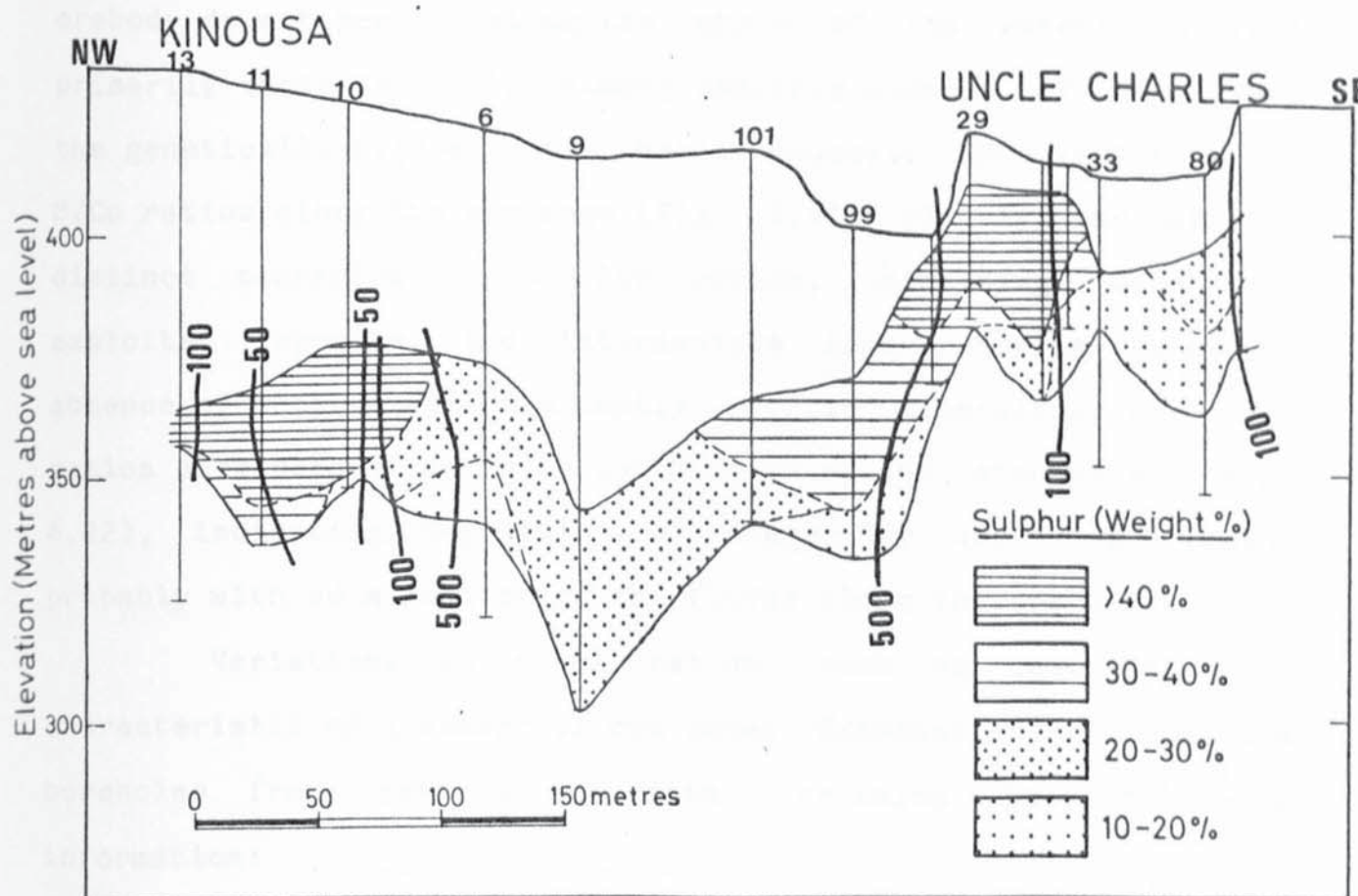


FIG. 6.20. Section through the Kinoussa underground deposit illustrating variation in the ratio $S/Cu+Zn$ and total sulphur.



Drawn by N.G. Adamides

FIG. 6.21. Variation of the ratio S/Cu in the Kinousa-Uncle Charles ore zone. The diagram is based on assay data from boreholes.



Drawn by N.G. Adamides

FIG. 6.22. Section along the Kinoussa- Uncle Charles ore zone showing distribution of sulphur and S/Cu (atomic) ratio. The diagram is based on assay data from boreholes.

late introduction of copper and zinc by the hydrothermal fluids.

The above mineralogical characteristics of the Kinousa orebody do not persist along the whole of its extent, a fact primarily indicated by the almost complete absence of zinc from the genetically related Uncle Charles deposit. The variation of S/Cu ratios along the ore zone (Fig. 6.21) clearly indicates a distinct concentration of low ratios, coinciding with the exploited deposits, the intermediate space showing complete absence of copper and dominantly pyritic mineralization. S/Cu ratios show persistence with depth within the stockworks (Fig. 6.22), indicating deposition of copper by ascending fluids probably with no migration of the fluids along the ore zones.

Variations in metal ratios, such as described, are characteristic of a number of ore zones. Examination of numerous boreholes from several deposits, revealed the following information:

The Mavridia opencast shows a distinct copper enrichment in the stockwork zone relative to the overlying massive 'A' orebody and preferential concentration of copper close to the Northwestern Boundary fault, the controlling structure for the deposition of mineralization (chapter 5), relative to areas remote from this structure. This suggests the late introduction of copper-rich fluids, which preferentially utilised this structure during ascent to higher levels.

Extremely uniform ratios obtain throughout the Limni ore zone, S/Cu generally lying between 20-50 and the average for the orebody being 28. By contrast, generally high ratios (> 100)

characterise the Evloimeni orebody which may be considered as the extreme extensions of the Limni ore zone.

The Petra orebody (Kalavassos), similarly to Limni, shows remarkably uniform ratios throughout its 300 metre length with mean S/Cu of 50 (St. Dev. 15). Mousoulos orebody shows mean S/Cu ratio of 64 (St. Dev. 24), being therefore correspondingly poorer in copper than Petra.

Alestos- Memi represent extreme examples of fractionation within ore zones. Alestos is characterised by extremely low and uniform ratios (Mean 9 and St. Dev. 3). By contrast, Memi is characterised by very erratic ratios, in general higher than 100 and commonly reaching 250.

6.5. Discussion of the mineralogical characteristics of the sulphide deposits

The mineralogical characteristics of the sulphide deposits suggest that pyrite, chalcopyrite and sphalerite were the dominant sulphide phases, with hematite being a common additional phase, in association with pyrite, particularly in the marginal parts of ore zones. The only exception is Alestos, where the dominance of hematite and its paragenesis as a replacement product of earlier sulphides suggest the ingress of large amounts of oxygenated fluids at the last stages of hydrothermal activity. This is consistent with the deduced formation of this deposit at depth within the lava pile, as suggested by the regional extent of silicification and chloritic alteration.

The absence of pyrrhotite as a stable phase within the

stockworks places constraints on the thermodynamic character of the fluids, as does the presence of hematite. Pyrrhotite has been deduced to have been an additional phase at the zone of massive sulphide precipitation, based on the compositions of sphalerites, so that its absence from the assemblages is attributable to later equilibration to sphalerite. The evidence is, however, unequivocal that, within the stockworks, pyrite was the stable iron sulphide.

Based on the above deductions and on evidence provided from fluid inclusions (Spooner and Bray, 1977) and isotope studies (Heaton and Sheppard, 1977) of temperatures of at least 300° C during mineralization, the fields of fS_2 and fO_2 within which pyrite, chalcopyrite, sphalerite and hematite are stable (Figures 6.23- 6.24) suggest fS_2 in the range of 10^{-10} atmospheres and fO_2 in the range of 10^{-30} atmospheres.

The dominance of pyrite in the Sheeted Complex, generally to the exclusion of both magnetite and pyrrhotite, indicates that the pyrite stability field was not transgressed at any stage during the upward path of the hydrothermal fluids to the discharge sites. The only exception may have been isolated occurrences of ore within the gabbros, such as at Ayios Ioannis (Agros), where fracture- guided sulphide mineralization exhibits a complex paragenesis of dominant pyrrhotite- chalcopyrite, with subordinate sphalerite, pyrite and marcasite (Constantinou, 1980). Such occurrences may be interpreted as resulting from the higher temperatures obtaining in the gabbros, and the transcendence of the pyrite- pyrrhotite solvus at, probably, constant fS_2 (Barton, 1967). Evidence provided in chapter 3, however, suggests that the

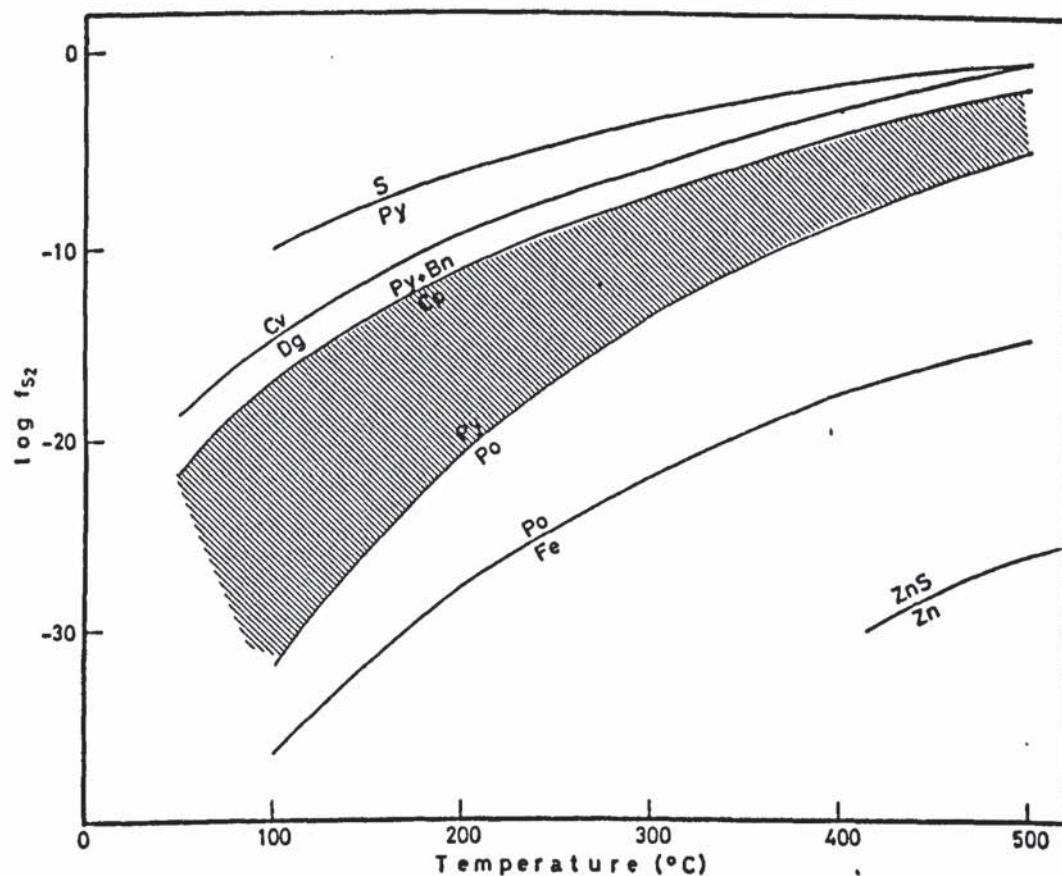


FIG. 6.23. FS_2 -Temperature diagram (after Kajiwara, 1971). Shaded field represents the range of fS_2 at which Cyprus assemblages are stable.

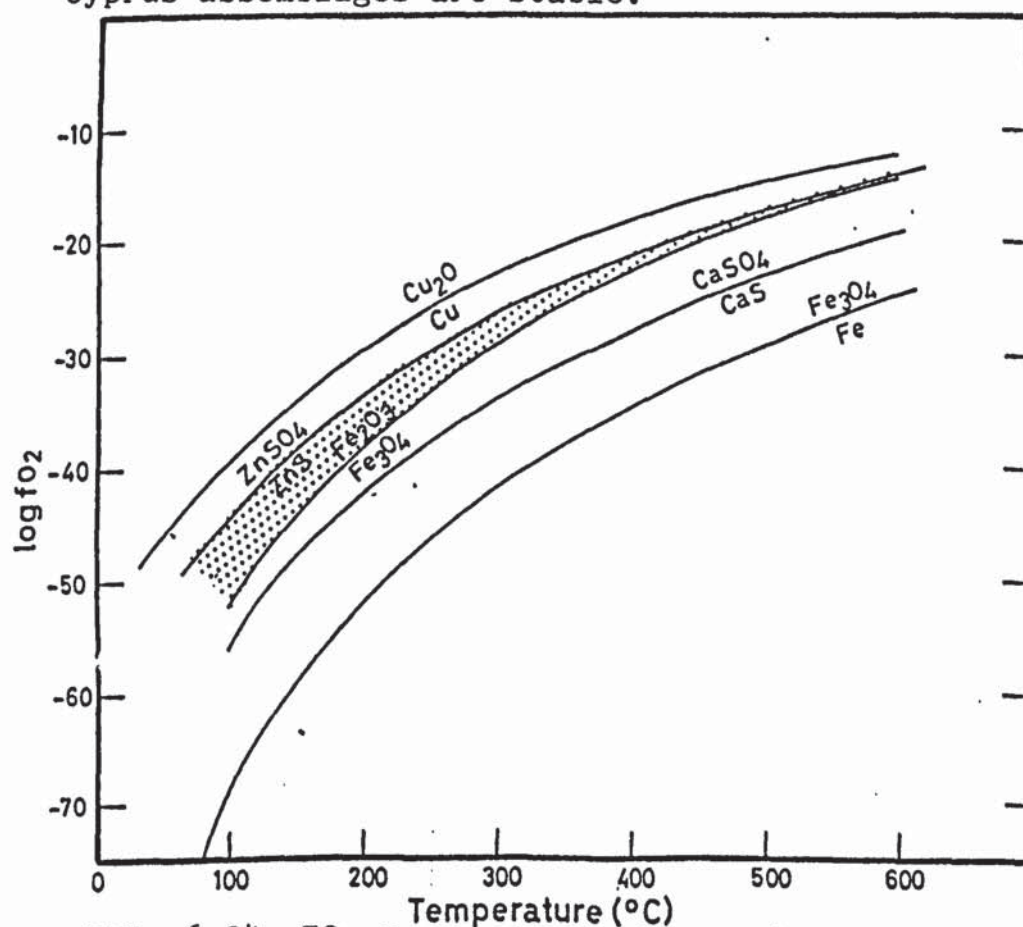


FIG. 6.24. FO_2 -Temperature diagram (after Kajiwara, 1971), illustrating probable range of fO_2 during formation of Cyprus deposits.

involvement of the gabbroic sequence in hydrothermal metamorphism was limited.

Based on inferences made in chapter 3, the hydrothermal fluids are enriched in calcium, barium, silica, copper, zinc, iron, manganese, rubidium and potassium. Although evidence of leaching of magnesium is present in the deeper parts of the Sheeted Complex, the strong partitioning of this element into solid phases, particularly chlorite, suggests that it is removed from the fluids on reaching higher levels, probably partly accounting for the chloritic alteration at deep levels in the stockworks. The evidence, both for enrichment of the fluids in the described elements and the depletion in magnesium is substantiated by studies of similarly derived fluids from modern spreading centres (Edmond et al., 1979; Edmond, 1982). Silica is partly deposited during ascent as a result of supersaturation induced by cooling (Holland, 1967) as also does iron, by saturation with respect to pyrite (Lydon, 1983). Additional factors inducing precipitation of minerals, in addition to temperature are structure and the extent of mixing of the fluids with seawater.

The prime example on the role of structure on the extent of interaction of the hydrothermal fluids with the wall rocks is provided by Skouriotissa: Intense quartz-chlorite alteration within the central vent which exhaled enough fluid to form at least 6 million tons of massive pyrite, passes within the space of a few tens of metres, into lavas indistinguishable from similar lavas unrelated to mineralization. Gradients of the order of 15°C / metre may be inferred for this deposit. Away from the pipe the

pyrite rests on completely unaltered lavas. The pattern of deposition of the orebody is inferred to be identical to similar deposits forming at the East Pacific Rise, where sulphides are described as resting on completely unaltered basalts (Hekinian, 1979).

Similar gradients to those described at Skouriotissa may be inferred from closely structure-controlled orebodies such as Limni, Mavri Sykia, Petra and the Mavridia group where ore precipitation takes place within narrow tectonic zones. Gentler gradients are inferred for deposits forming partly within the lavas, such as Evloimeni, Agrokipia 'B' and Kokkinopezoula. Such deposits are characterised by a gradual passage from chloritic alteration in the cores to zeolitic alteration at the marginal parts with ill-defined boundaries between the zone of dominant sulphide precipitation and the surrounding unaltered lavas. The extensive formation of zeolitic minerals in the weakly altered zone of such deposits is attributed to fixation of elements which are removed from the zone of intense mineralization or transferred from deeper levels by the hydrothermal fluids.

The imposition of a high temperature regime along the structures which control the flow of hydrothermal fluids may be thought of as inducing a convection cell resulting to the ingress of water from the surroundings into the zone of hydrothermal activity and mixing with the fluids. Such influx from the sides has been inferred for the formative processes of similar deposits as the Mattagami Lake massive sulphide deposit (Roberts and Reardon, 1978), the deposits of the East Pacific Rise (Haymon,

1982) and the diverse and temperature-dependent chemistry of the Galapagos hot springs (Edmond, 1982).

Evidence for similar processes in Cyprus is provided from several lines. The petrographic examination of samples from the stockwork zones suggests that chlorite is the dominant product of alteration by the hydrothermal fluids. Formation of chlorite pre-supposes the introduction of magnesium and/ or iron into the altered zones (Meyer and Hemley, 1967) as also does formation of interlayered chlorite- smectite at the margins. This is in conflict with the deduced magnesium-poor nature of the fluids. Introduction of magnesium into the ore zones is similarly suggested from the chemical changes in mineralized and unmineralized lavas both at Evloimeni and Mavri Sykia ore zones. A readily available source of magnesium is seawater. Introduction into the rocks surrounding the mineralized zones appears to be balanced by depletion of calcium and the reactions may be related to base exchange in smectites. Calcium is locally deposited, in association with zeolites, in veins and vesicles in the lavas close to the deposits.

In addition to the evidence provided by magnesium, similar evidence is provided by the abundance of hematitic jaspers within ore zones. The presence of these in association with the sulphides is in conflict with the reduced nature of the fluids at deeper levels of the ore zones and suggestive of interaction with oxygenated fluids. The extent of the interaction is directly linked with the depth of ore formation, resulting to higher pressures of the fluids surrounding the ore zones, finally culminating in the

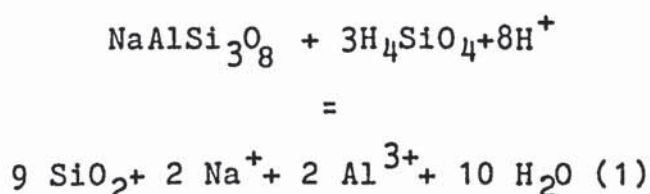
overprinting of earlier sulphidic by oxidic assemblages. The extreme of this situation is observed at Alestos where hematite replaces earlier sulphides. A similar zonation of minerals from central sulphides to marginal hematite- epidote is also present at West Apliki (chapter 5).

Probably the best evidence of the temperature gradients which obtain at ore zones and the surroundings and the association of these gradients to the alteration minerals produced, is provided by quartz. The solubility of quartz is strongly temperature dependent and unaffected by other dissolved components (Holland, 1967). In closely structure- controlled deposits, such as Skouriotissa and Limni, quartz is limited within the ore zone and, in association with sulphides, dominates the paragenesis at higher levels of the stockwork zones. The formation of zone 'B' in massive sulphide deposits, which is overlain by a zone of pure sulphide (Hutchinson and Searle, 1971; Constantinou, 1972) may be the result of temperature-controlled drop in quartz solubility close to the lava- seawater interface. A temperature drop, e.g. from 250°C to 50°C is accompanied by a change in the solubility of quartz from 0.4 g/kg of solution to 0.025 g/kg, suggesting that, below 50°C only a very small amount of silica remains in the fluids. In deposits forming at deeper levels, a gentler temperature gradient results to extensive introduction of silica into the surrounding rocks, as exemplified by the Alestos ore zone.

Directly linked with the regime of interaction of the hydrothermal fluids with the wall rocks and seawater are the

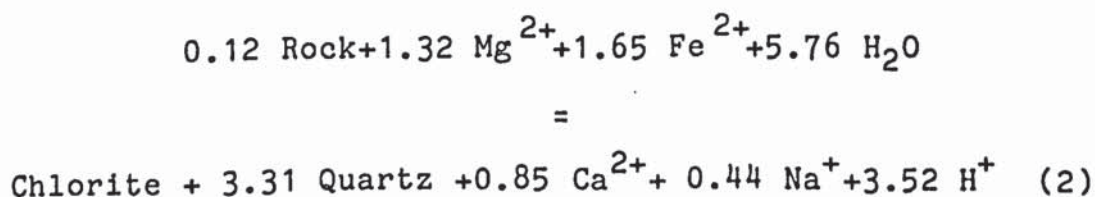
examined changes, both chemical and mineralogical, partly described above. These will be discussed in detail in this section.

The conversion of the wall rocks in stockwork zones into a quartz-chlorite assemblage, accompanied by intense leaching of alkalis are characteristic features of the sulphide deposits in Cyprus and also in similar deposits elsewhere, as e.g. at Millenbach, Noranda district (Knuckey et al., 1982), Whalesback, Newfoundland (Bachinski, 1977) and the Brunswick No. 12 deposit (Goodfellow, 1975). Such changes are consistent with petrographic characteristics described in chapter 3 and relevant reactions may be written as:



The reaction results to the liberation of sodium and alumina, the latter presumably fixed in chlorite, and is consistent with the relatively acid, silica-rich fluids.

The transformation of basalt to quartz and chlorite has been described in chapter 3 as probably effected by the reaction:



The above reaction is consistent with conservation of alumina and results to the liberation of calcium and sodium and drop in pH.

The alkalis liberated from the above reactions are either fixed in zeolites and smectites around the ore zones or are removed by the hydrothermal fluids and dispersed into seawater. Alkali enrichment is directly related to the nature of the fluid-wall rock interaction, and this, in turn, to the reactivity of the rocks and the structural characteristics of the deposits. Relevant to this is the fact that Evloimeni ore zone shows enrichment in alkalis in the upper parts of the mineralization and the surrounding pre-mineralization lavas, while the Mavri Sykia ore zone, a closely structure-controlled deposit, is completely depleted in alkalis by the processes of intense chloritisation throughout its width, alkali enrichment being only apparent in the surrounding unmineralized lavas.

It is inferred from the above that marginal potassium enrichment and central magnesium enrichment, supposed characteristic of several volcanogenic sulphide deposits (Franklin et al., 1981; Lydon, 1983) is directly related to the detailed mode of occurrence of the deposits and the gradients obtaining during hydrothermal ore deposition. It may be speculated that Agrokipia 'B' deposit will exhibit a well defined pattern of alkali enrichment in the marginal, weakly mineralized areas, the alkalis being removed from the central parts by magnesium fixation due to chloritisation. This pattern will gradually merge into the zones of strong chloritic alteration and will be in direct contrast with

more closely structure-controlled deposits such as Mavri Sykia.

The above conclusions are in disagreement with earlier studies (Constantinou, 1972) which suggest that potassium enrichment is characteristic of the intensely mineralized lavas, reflected in the dominance of illite over chlorite in such lavas. Formation of illite, favoured by high K/H ratios, is precluded by the evidence of complete leaching of potassium in the intensely mineralized lavas. X-ray diffraction examination of such samples, collected from the underground workings of the Kokkinoyia ore zone, in contact with massive pyrite, indicated a quartz-chlorite-pyrite assemblage, corroborating the results of similar studies in the Limni ore zone presented in earlier paragraphs. On the other hand, illite was found to be a significant phase in a recent study of Agrokipia 'B' deposit (Botros, 1982) where plagioclase was also partly preserved, suggestive of relatively weak hydrothermal processes.

It may be concluded from the above that alkali depletion and magnesium enrichment are characteristic features of hydrothermal alteration of the Cyprus sulphide deposits. At the sites of ore deposition, the hydrothermal processes result to the further enrichment of the hydrothermal fluids in calcium, potassium, strontium, barium and sodium. Part of these elements are used in the enrichment of marginal parts of the ore zones and the surrounding unmineralized lavas, the remainder being dispersed into seawater. Subsequent precipitation of these elements as chemical precipitates is governed by their behaviour on entering the SO_4^{2-} -rich, high pH environment. Directly relevant to this is

the absence of barytes as a gangue mineral in the massive zones of the deposits. The solubility of barytes is strongly dependent on concentration of NaCl in the hydrothermal fluids (high concentration favouring abundant precipitation of barytes). Solubility is also temperature-dependent, barytes being deposited by simple cooling from solutions saturated with respect to barytes, maximum precipitation occurring at SO_4 concentrations of $10^{-3.5} \text{ mSO}_4$ (Holland, 1967). Simple mixing of hydrothermal fluid ($\text{mSO}_4=0$), with seawater ($\text{mSO}_4=10^{-1.55}$, $\text{mNaCl}=0.5$ (Haymon, 1982)) should result to the precipitation of barytes, if the fluids were saturated with respect to barytes. Its general absence as a gangue mineral in the massive zone, therefore, suggests undersaturation of the hydrothermal fluids. The enrichment of barium in the umbers and radiolarites is consistent with non-precipitation at discharge sites and later scavenging in the latter precipitates.

The abundance of barytes as a gangue mineral in Japanese Kuroko deposits (Kajiwara, 1971) is consistent with the high barium content of the source rocks, generally in the range of 1000 ppm (Jakes and White, 1972; Wood et al., 1980) as compared to the mean barium content of 30 ppm for the Troodos source rocks.

Following similar reasoning as above, it may be argued that the absence of abundant anhydrite in the massive zones of the sulphide deposits may be interpreted as the result of instability at discharge sites. The solubility of anhydrite is strongly temperature dependent, decreasing with increasing temperature (Holland, 1967). Formation of anhydrite by mixing of the Ca^{2+} -rich fluids with ambient seawater, in a manner presently observed

at the exteriors of active black smoker chimneys (Haymon, 1982), is followed by re-dissolution on cooling as a result of enhanced solubility. The presence of late-stage gypsum in the massive sulphide zones is probably related to the decrease in solubility at temperatures lower than 40° C.

Zonations in gangue minerals and wall rock alteration associated with the sulphide deposits have been described and interpreted in previous paragraphs in light of the physical and chemical gradients pertaining at discharge sites. These mainly related to dominance of chloritic assemblages at marginal parts of ore zones, merging into a zone of alkali enrichment, commonly confined to the surrounding unmineralized lavas; dominance of quartz in the central and higher levels of the stockwork pipes; and, finally, dominance of sulphides at the uppermost levels in keeping with the idealised model of volcanogenic sulphide deposits. Such zonations of alteration mineralogy and chemistry around discharge sites is, in other similar deposits, emphasised by a zonation of sulphide mineralogy. E.g. at Millenbach (Knuckey et al., 1982) the passage from central chloritic alteration to marginal sericitic assemblages is accompanied by a parallel passage from dominant pyrrhotitic to increasingly pyritic mineralogy. This zonation is also accompanied by a similar zonation of copper and zinc, with copper being dominant in the central parts of the massive lenses and zinc being enriched in the marginal parts.

Similar zoning, on a smaller scale, is observed at black smoker chimneys, from a central chalcopyrite-rich zone to

sphalerite-rich assemblages at the margins (Haymon and Kastner, 1981).

Although the larger-scale processes of the Cyprus examples mask the details of mineralogical zonations in individual conduits, paragenetic relationships between sulphide minerals are suggestive of a sequence of mineral precipitation: Chalcopyrite is generally paragenetically later than pyrite and sphalerite follows chalcopyrite. This sequence is suggested from ore microscopy and is further supported by the metal zonations described at the Kinousa deposit. Contemporaneous and, sometimes, simultaneous precipitation of all three minerals, suggested on a local scale, does not modify the general pattern of higher copper and zinc at higher levels of the deposits. Overriding, however, this general zonation is the fact that, with the exception of some deposits such as Kinousa, most orebodies are devoid of significant zinc and a great number are devoid of copper. It has been suggested in the past (Vokes, 1965) that there are two horizons of mineralization, the one at the base of the Lower Pillow Lavas and the other at the base of the Upper Pillow Lavas, giving copper-poor and copper-rich deposits respectively. Evidence based on field and stratigraphic relations of the deposits (chapter 5) suggests that there was only one period of mineralization, temporally and genetically associated with the boundary between the Upper Pillow Lavas and the Lower Pillow Lavas. Furthermore, a broad spectrum of metal ratios within a single ore zone is suggested by Kinousa, clearly located on a single stratigraphic horizon, while higher copper characterises the Alestos ore zone, located at a deeper level than

the associated copper-poor Memi mineralization.

A similar reasoning to that applied for copper may be used for the discussion of the zinc content of the deposits. It is not possible to attribute the absence of zinc from some deposits and its presence in others to differences in the chemistry of the source rocks. The chemistry of the Sheeted Complex, established in chapter 3 as the source of the zinc in the hydrothermal fluids, does not suggest any major variations in initial content and evidence of leaching of the element is relatively uniform. It may, therefore, be inferred that the initial composition of the hydrothermal fluids was essentially similar. Fractionation of copper and zinc is concluded to be the result of processes at discharge sites, or en route, and not a function of the initial composition of the fluids.

A process of mixing of hydrothermal fluids with seawater (Large, 1977) may be one of the most important controls in the development of mineralogical zonations and the formation of copper-rich and copper-poor deposits. Supporting evidence is provided by:

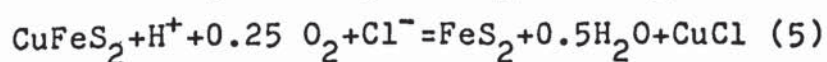
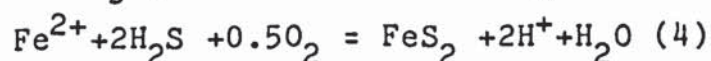
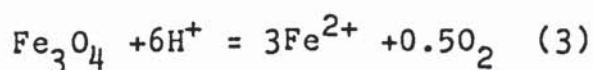
1. The dominance of chalcopyrite close to the Northwestern Boundary fault at the Mavridia opencast, relative to areas further removed from the structure.

2. The high copper content of the Alestos ore zone where oxidic assemblages suggest a history of thorough mixing of hydrothermal fluids with seawater at depth. The similar association of copper-rich deposits such as Limni and Petra with narrow permeable tectonic zones favouring ingress of seawater to

deep levels within the ore zones.

The effect of mixing of the hydrothermal fluids with seawater is mainly the increase in SO_4 and pH. $f\text{O}_2$ of present day seawater varies widely from 10^{-10} - 10^{-70} atmospheres (Large, op. cit.). The dominance of hematite in interpillow sediments (cf. the Kalavassos intervalcanic sediments, chapter 5) suggests oxygenated conditions so that mixing will be expected to lead to $f\text{O}_2$ increase. The concentration of NaCl in the hydrothermal fluids (mNaCl) was probably close to 0.5 and comparable to present day seawater (Spooner and Bray, 1977). The hydrothermal fluids are considered here to have lain well within the pyrite stability field and not in the pyrrhotite field as previously suggested (Large, op. cit.).

In deposits forming within the lavas, such as Kokkinopezoula, or generally by replacement processes, wall rock alteration may be the dominant control in the chemical modifications leading to ore precipitation. Critical reactions at these levels may be:



Reaction (4) leads to decrease in pH, probably prohibiting chalcopyrite precipitation, as indicated by reaction (5), and leading to copper-poor deposits within the lavas. Reaction (5) is reversible and suggests that increasing pH by interaction of fluids with seawater will lead to chalcopyrite precipitation by pyrite replacement if copper is present in the

fluids.

With prolonged passage of the fluids through the channelways the effect of wall rock alteration diminishes and later fluids will precipitate ore mainly under the influence of dropping temperature and mixing, resulting to copper-rich ores at higher levels. It is possible to speculate that the originally slightly acid fluids (by chloritisation) were progressively tending towards alkaline chemistry, favouring chalcopyrite deposition.

Precipitation of sphalerite from relatively acid, chloride-rich solutions may be effected by dilution (Barnes and Czamanske, 1967), cooling, and increase in pH towards neutrality (Large, 1977). Marginal zinc enrichment in the channelways of the hydrothermal fluids may be interpreted as the result of neutralisation and cooling by wall rock alteration. In the zone of massive ore deposition, increase in pH and cooling are the result of the mixing with seawater.

The trends of mixing and massive sulphide deposition are illustrated in fig. 6.25. Parameters chosen are in agreement with deductions made above. Total S of 10^{-2} was chosen in agreement with mineralogically analogous deposits at the East Pacific Rise (Haymon, 1982). The trends are also consistent with the absence of pyrrhotite and magnetite as associates of the ore minerals, indicating that the fluids remained within the pyrite field throughout their history, passing into the hematite field only after leaving the immediate environment of the vents. Well-zoned deposits, such as Kinousa, traverse the pyrite field and enter in

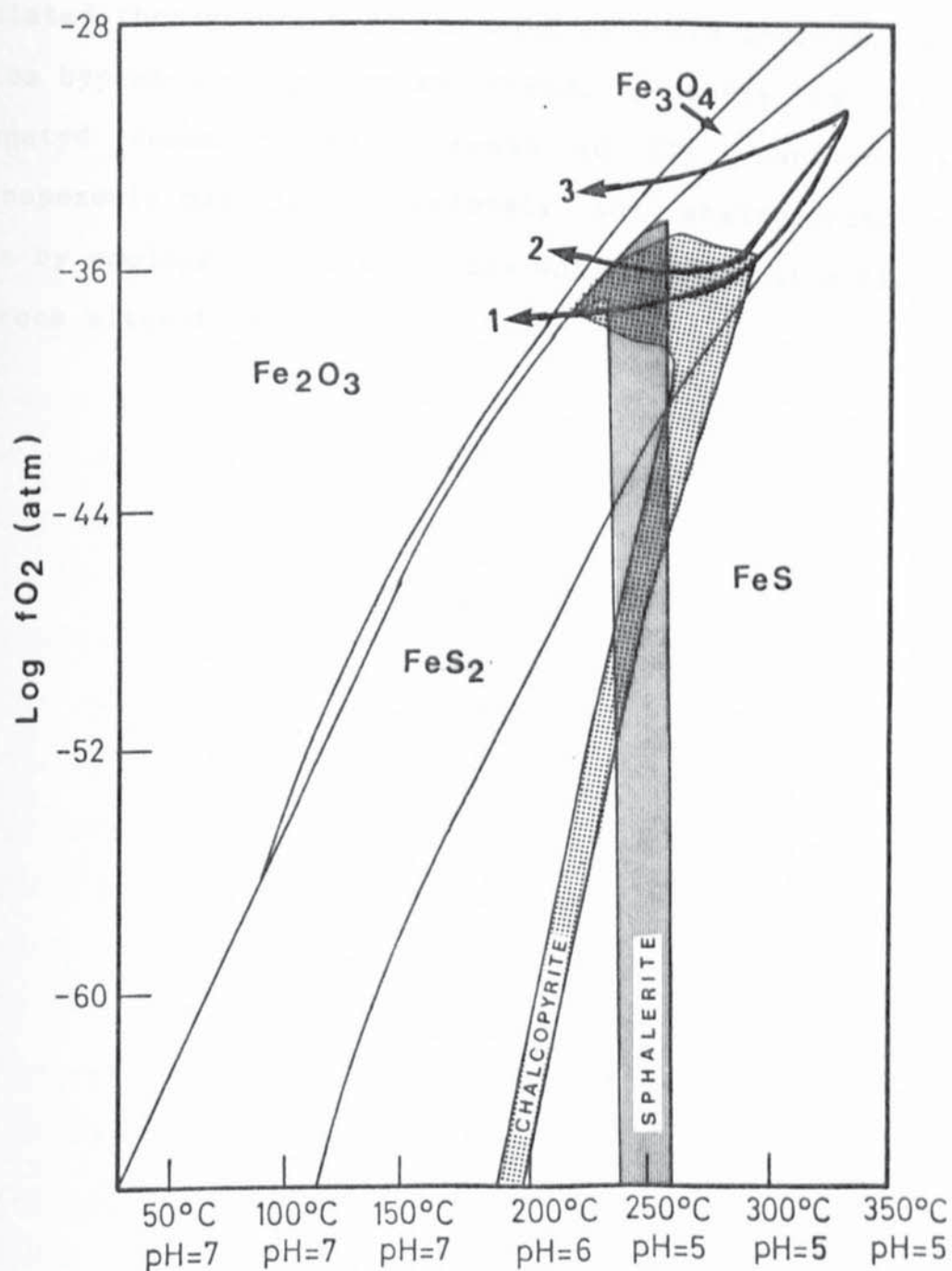


FIG. 6.25. $\text{Log } f\text{O}_2$ Temperature diagram (after Large, 1977) assuming $S=10^{-2}\text{M}$ and 1 M NaCl with variable pH. Possible trends for some Cyprus deposits also shown. See text for discussion.

1: Kinousa, 2: Limni, 3: Kokkinopezoula.

sequence the chalcopryrite and sphalerite fields. Pyrite is associated throughout. Deposits such as Uncle Charles, Limni and Alestos bypass the sphalerite field, probably by mixing with oxygenated seawater and increase in fO_2 . Deposits such as Kokkinopezoula may bypass completely the chalcopryrite-sphalerite fields by cooling within the rocks while maintaining high fO_2 by wall rock alteration.

CHAPTER 7

Summary and conclusions

7.1. Summary

Data presented in this thesis suggest that formation of the Troodos ophiolite has taken place by spreading processes above a subduction zone. This is particularly indicated by the enrichment of the primary magmas in silica and the large ion lithophile elements and the strongly depleted nature of the source as indicated by the low initial abundances of the high field strength elements (Zr, Y, Ti, P). Contribution from the subducted slab is commonly suggested as the process responsible for LILE and silica enrichment, while dehydration of the slab is thought to promote more intense partial melting of the source. Processes of formation are suggested to have been similar to those operating at present day marginal basins, as indicated by the similarity in geochemical patterns to the West Mariana Ridge.

Formation of the Sheeted Complex and Lower Pillow Lavas is interpreted to have taken place close to the axis of spreading from subaxial chambers which exhibited both open and closed system fractionation. The inference is supported from the geochemical data which suggest a progressive change from less fractionated to more fractionated lavas in the transition from the sheeted dykes to the pillow lavas. A model proposed for the interpretation of similar characteristics in Chilean ophiolites (Stern and De Wit, 1980) presupposes the presence of magma cells distributed in a gaussian fashion around the axis of spreading, with the centrally

located chambers being frequently tapped and essentially behaving as open systems, and the marginal chambers behaving as closed systems, being less commonly tapped and producing more fractionated lavas. A similar model, applicable to the Cyprus situation, explains the statistically more fractionated nature of the later intrusives and extrusives (Basal Group and Lower Pillow Lavas) as compared to the Diabase.

Extrusion of the EMS lavas (chapter 2) and the genetically related Upper Pillow Lavas, is envisaged to have taken place at the flanks of the spreading axis. Although these lavas have been interpreted as the result of more intense melting of the source which generated the older members of the ophiolite, the available geochemical data are compatible with a model whereby both suites are related by fractional crystallisation. The absence of well defined structural or stratigraphic break, the continuity of alteration mineralogy and the presence of interdigitation relationships between the two suites (Malpas, pers. com., 1983) are suggestive of close environmental relationships which are difficult to explain by a model of two stage melting. It is suggested here that the chemical discontinuity is a result of the diapiric uprise of unfractionated magma, identical in composition to the magmas which generated the Diabase- Lower Pillow Lavas, resulting from the off-axis regime of extrusion and probably related to, as yet, unfathomed tectonic causes. Intrusion of high level chambers responsible for the chemically primitive lavas is suggested to be the cause of intense circulation of fluids, leaching of ore metals from the Sheeted Complex and the formation

of the sulphide deposits.

Examination of the evidence of hydrothermal alteration in the ophiolite indicates that the Lower Pillow Lavas and gabbros have, in most part, retained original geochemical and petrographic characteristics, with alteration and elemental mobility being only evident along fractures and open spaces. In contrast, alteration in the Sheeted Complex is pervasive, with chlorite-albite being dominant at high levels and actinolite-oligoclase at lower levels. Geochemical patterns of enrichment and depletion in various elements are consistent with a model of seawater-rock interaction in the derivation of the hydrothermal fluids. Magnesium is dominantly enriched at higher levels, by fixation in chlorite and smectite. Silica and calcium are leached from this zone and also from lower levels, but silica is locally deposited in zones of upwelling fluids as a result of decreasing solubility with decreasing temperature. Barium is generally leached from lower levels in the Sheeted Complex by feldspar destruction and locally deposited at higher levels, although most of the barium is lost into seawater and fixed in the umbers and radiolarites which overlie the last extrusives of the ophiolite. Zinc is leached from the Sheeted Complex, particularly from lower levels, and partly deposited during ascent of the hydrothermal fluids or at discharge sites.

The derived patterns of hydrothermal circulation are consistent with a model whereby seawater, originally trapped within the rocks by secondary mineral formation, is gradually heated under the influence of the geothermal gradient.

Hydrothermal metamorphism results to the enrichment of these fluids in elements originally contained in the component minerals of the lavas. The intrusion of magma at high levels creates a low-pressure, high-temperature region and causes the movement of the metal enriched fluids to higher levels. Two such major chambers are envisaged to exist in the examined area, each being responsible for the formation of the Skouriotissa and Tamasos groups of deposits respectively. These chambers are inferred to have been oriented parallel to the spreading axis, and spaced approximately 25 km apart, as suggested by the reflection of their presence in the Diabase farther removed from the region of the deposits.

The postulated hydrothermal model suggests that all deposits in a single mining district are genetically related and of contemporaneous formation and precludes earlier suggestions (Spooner, 1977) which necessitated the existence of a specific circulation cell for each deposit.

The initial movement of the hydrothermal fluids was probably aided by the presence of deep fractures, either related to the spreading axis regime, or to the intrusion of the main chamber. Localisation of the deposits within the mining districts was mostly controlled by the local structure. The behaviour of the hydrothermal fluids at the discharge sites was examined from two angles:

1. Relationships of mineralization to structure and stratigraphy of the area,
2. The interaction of the hydrothermal fluids with the

host rocks, as indicated by the mineralogical characteristics of the deposits and the chemical changes accompanying mineralization.

Examination of the mode of occurrence of the deposits at the Limni mining district suggests a close relationship to the structure of the area, with all orebodies being located along major faults which, on the basis of their parallelism with the dykes of the Sheeted Complex, are inferred to have been oriented parallel to the spreading axis. The Limni orebody is overlain by olivine basalts and is deduced to have been localised within the Lower Pillow Lavas. Absence of limburgitic lavas at the vicinity of the deposit is attributed to the positive relief of the area and resultant non-deposition above the mineralization. A similar explanation is given for the absence of lava cover over the Kinousa deposits. The Evloimeni orebody was localised within the Lower Pillow Lavas by relatively weak hydrothermal fluids.

The deposits of the Kalavassos mining district were formed in an area tectonically disturbed by synvolcanic faulting as a result of proximity to the Arakapas fault belt. As a result of tectonism, and the abundance of favourable structures, the orebodies are typically small, with well developed zonation of massive and stockwork mineralization due to the strong focusing of the fluids. The stratigraphic horizon of the mineralization, similarly to Limni, is deduced to have been the contact between the Lower Pillow Lavas and the limburgites (basal facies of the Upper Pillow Lavas). The deposits were preferentially localised by structures which were parallel to the sheeted dykes and, therefore, also parallel to the palaeospreading axis.

Examination of the geology in the region of Skouriotissa deposit indicates that the mineralization was localised at the intersection between axial and transverse structures. The hydrothermal fluids ascended to higher levels along a pipe-like structure created by this structural intersection, and deposited massive mineralization, in the form of a major extensive lens, directly above the pipe. This lens is locally overlain by amber. Stratigraphic relationships are interpreted as implying that a very small time interval separated hydrothermal ore deposition, Upper Pillow Lava volcanicity and amber deposition. This conclusion is also supported by the chemistry of the mineralized lavas both at Evloimeni and Mavri Sykia which is identical to the chemistry of typical Upper Pillow Lavas. Based on this evidence it is suggested that the hydrothermal activity is genetically linked to the earliest phase of extrusion of the Upper Pillow Lavas. A consequence of this is that rapid extrusion of later flows of these lavas was responsible for the preservation of the orebodies and their spatial separation from the genetically related ambers. Where little or no lavas were deposited, as at Skouriotissa and Kinousa, the orebodies were preserved under a cover of amber.

Although structures are concluded to have been essential in the formation of rich deposits, their absence does not preclude the presence of mineralization. This conclusion is particularly suggested from the study of the deposits at the Tamasos mining district. Agrokippia 'B' orebody is deduced to have been localised within Lower Pillow Lavas by replacement of favourable horizons. Kokkinopezoula, similarly located within the Lower Pillow Lavas,

was characterised by poor pyritic mineralization, only locally, in the central parts, being deposition of massive pyrite evident.

The main implications on the structural and stratigraphic controls of all examined deposits are that faulting, although instrumental in the formation of strongly focused, rich deposits, was not itself the cause of movement of the hydrothermal fluids. The role of faults lay mainly in the localisation of the hydrothermal fluids which were initially triggered in their circulation by deep-seated causes such as the presence of a heat source to promote circulation. Secondly, there was only one period of mineralization, temporally related to the early stages of Upper Pillow Lava volcanicity. No exhalative deposits are formed in deep levels and none formed after the extrusion of the Upper Pillow Lavas. In view of the regime of formation of these lavas at the flanks of the spreading axis, formation of the sulphide deposits in a similar environment is envisaged. Analogies are, therefore, suggested with the deposits of the Oman ophiolite (Alabaster, 1982) but, in contrast to the latter situation where individual magma cupolas responsible for the deposits are recognised, no such evidence is present in Cyprus.

Examination of the mineralogical characteristics of a number of orebodies suggests a complex history of interaction of hydrothermal fluids with the wall rocks and seawater during ore deposition, depending on the depth of ore formation, the structural control and the extent of mixing of the fluids with seawater. The hydrothermal fluids, at the beginning of their ascent to higher levels, are essentially seawater enriched in S,

Si, Cu, Zn, Ca, Ba, Fe, Mn and strongly depleted in magnesium relative to unreacted seawater. The dominance of pyrite relative to either hematite, pyrrhotite or magnetite as the main iron-bearing phase throughout the Sheeted Complex suggests that the thermodynamic parameters of the fluids lay within the pyrite stability field. The dominance of pyrite as the main sulphide in all deposits suggests that this stability field was not transcended at the site of ore deposition, although formation of pyrrhotite as a result of strong disequilibrium during exit from the vents may have taken place, the pyrrhotite later reverting to pyrite.

At the site of ore formation, the dominant petrographic changes in the lavas is the extensive transformation into a quartz-chlorite assemblage, with chloritisation persisting to the margins of the ore zones and silicification occupying the inner and higher levels, in association with the sulphides. Chlorite passes marginally into smectite, characteristic of unmineralized lavas, through an intermediate zone of interlayered chlorite-smectite. The pattern is suggestive of magnesium metasomatism, weak at the margins and stronger in the interiors of the ore zones, the magnesium being presumably derived from interaction with cold seawater. Deposition of quartz is correlated with the strong temperature and pressure gradients developed at discharge sites and resultant drop in solubility. Active replacement of the wall rocks and earlier sulphides by silica, resulting to the formation of zone 'B' (Hutchinson and Searle, 1971) characteristic of many exhalative deposits, is envisaged to be the result of high silica activity in the hydrothermal fluids

and the effects of rapidly decreasing temperature.

In addition to the enrichment in magnesium, related to extensive chloritisation in the stockwork zones, leaching of alkalis (K, Ca, Na, Ba) is characteristic of inner parts of ore zones, and these elements are enriched in the surrounding lavas, mainly in the form of extensive zeolitisation and smectitisation. Such zeolitic alteration may extend into the mineralized lavas, particularly in deposits formed by relatively weak hydrothermal fluids, as at Evloimeni, or where the role of structure in the focusing of the fluids is minimised, as at the marginal parts of the Kokkinopezoula orebody. By contrast, where strong structural control was present, as at Skouriotissa, a rapid transition from mineralized to unmineralized lavas takes place over very short distances. The extreme of interaction of hydrothermal fluids with the wall rocks is observed in deposits formed at deep levels within the lavas, such as Alestos and West Apliki. These, and particularly the former, are associated with extensive zones of silicic and chloritic alteration, spatially associated with centrally located sulphides, and extensive overprinting of sulphidic by oxidic assemblages as seawater enters the ore zones at the final stages of hydrothermal activity. The formation of complex alteration zones around such deposits is indicative of the exchange between the hydrothermal fluids, the wall rocks and seawater.

Based on the evidence of wall rock alteration and mixing with seawater, the main mineralogical characteristics of the orebodies, i.e. copper and zinc enrichment at higher levels,

absence of copper from some deposits and the scarcity of zinc in the majority of deposits are discussed. It is concluded that extensive interaction with the wall rocks may be responsible for the loss of copper into seawater, resulting to copper-poor deposits within the lavas. Similarly, changes in pH of the fluids by interaction with seawater may be the main cause of precipitation of chalcopyrite and sphalerite at sites of massive ore deposition and the typical enrichment of these elements at higher, relative to lower, levels of the deposits.

In addition to the elements deposited at discharge sites, the fate of other elements leached from the Sheeted Complex is discussed, with particular emphasis on the enrichment of umbers and radiolarites in elements which are not deposited at sites of ore deposition. It is concluded that the source of the umber constituents is the same as that for the sulphide deposits.

7.2. Remarks on future work

Several conclusions regarding the trend of future exploration for volcanogenic sulphide deposits are derived from the data presented in the preceding chapters. At the same time a number of questions await resolution by future work. It is the purpose of the closing paragraphs to highlight points requiring further investigation and to assess the possibility for the discovery of new deposits on the basis of conclusions derived from the available data.

The geochemical study of hydrothermal circulation in the ophiolite and the interpretation of patterns of chemical changes

suggests that it is possible to trace zones of upwelling metal-enriched fluids by examination of the pervasively metamorphosed rocks of the Sheeted Complex. The position of the major mining districts may be predicted by such studies and barren areas broadly outlined, as e.g. the interspace between Memi and the Skouriotissa district where both sulphide deposits and strong indications for the presence of major orebodies are completely absent. It may be speculated that such geochemically oriented studies may be used to delineate the pathways of the fluids for the formation of individual deposits. However, pervasive mineralization in the higher levels of the Sheeted Complex in the region of the mining districts, probably related to the development of secondary circulation cells (Solomon, 1976) may effectively mask individual channelways, resulting to anomalies too broad for accurate definition of targets. This suggests that regional investigations are of limited value in exploration for individual orebodies. Detailed studies of potentially mineralized areas are required and these may take two forms:

1. Structural-stratigraphic studies based on field work,
2. Chemical investigations.

It has been established from the descriptions of the controls of localisation of specific deposits that faulting plays a dominant role in the formation of rich deposits. This role is envisaged to be twofold:

- a. Through major faults hydrothermal fluids gain access to higher levels, where strong gradients may result to precipitation of massive mineralization.

b. Faulting permits ingress of seawater and mixing with the hydrothermal fluids, a potentially powerful way for copper precipitation.

Mapping, therefore, of structure in the volcanic rocks, in association with the evidence of mineralization, assists in the delineation of potential targets. A necessary pre-requisite is knowledge of the stratigraphic horizon of the mineralization. Clearly, faulting in post-mineralization lavas neither precludes nor necessitates the presence of ore at depth; faulting in pre-mineralization lavas, on the other hand, not associated with significant surface evidence of mineralization, generally precludes the presence of an important deposit: Either the fluids were too weak to reach the surface, precipitating disseminated mineralization at depth, or no hydrothermal fluids were available.

It has been demonstrated, e.g. at Agrokippia 'B', that ore localisation may, in the absence of strong tectonism, take place within the lava pile. It is speculated that such deposits will be characterised by lower grades as a result of extensive interaction of the fluids with the wall rocks and the absence of strong temperature and pressure gradients. However, lithological factors, such as the presence of glassy horizons within the lavas, may, in exceptional situations, cause the precipitation of richer mineralization by replacement.

It is deduced from the above that knowledge of the boundary between pre- and post-mineralization lavas is essential in the assessment of surface indications of mineralization and the significance of structural disturbance in the area. This boundary

has been inferred from field studies to coincide with the Upper Pillow Lava- Lower Pillow Lava boundary as presently mapped. However, as described in text, the mapped boundary is not coincident with the chemical boundary between evolved and primitive members of the extrusive sequence. The postulated model for the formation of the sulphide deposits involves initial extrusion of the earliest flows of chemically primitive lavas, formation of the deposits and covering of these deposits by later flows of such lavas which, with progressive fractionation of clinopyroxene and olivine, are represented mainly by the limburgites, olivine-phyric and olivine-free basalts. Clearly, contemporaneous vulcanicity and ore deposition results to a relatively confused situation at the boundary between pre- and post-mineralization lavas. It has been postulated (Henley and Thornley, 1979) that hydrothermal discharge continues for several thousands of years at low power after the main period of sulphide mineralization ceases, maintaining a heat flow anomaly which may be reflected in the imprint of lower temperature alteration mineralogy on volcanics overlying the hydrothermal system. The presence of abundant calcite and analcite in the unmineralized olivine basalts which overlie the Limni orebody may be related to this cause, since these lavas definitely post-date the period of sulphide mineralization.

The above comments bring forth the possibility of applying alteration and chemical methods in exploration for sulphide deposits. Such methods are used in the search for Kuroko deposits in Japan (Utada et al., 1974), where analcite has been

determined to exhibit a close spatial relationship to the position of deposits. Evidence presented in this thesis suggests extensive formation of zeolites around the ore zones, particularly where ore deposition took place within the lavas. It rests within the scope of future investigations to examine whether the distribution of zeolites around individual deposits may be used as an exploration tool. A major difference between alteration associated with Kuroko deposits and the Cyprus examples relates to the nature of the enclosing rocks: The former are enclosed in highly reactive volcanogenic tuffs; Cyprus deposits, enclosed or overlain by lavas, commonly massive, are expected to show mainly fracture-guided zeolitisation as well as highly variable intensity due to lithological factors. Detailed studies, taking into consideration the above, are required in order to clarify the potential use of alteration studies.

Similar caution applies in the use of chemical methods in exploration. Enrichment in magnesium and alkalis in the lavas close to mineralization has been demonstrated in the ore zones of Evloimeni and Mavri Sykia. Investigations were confined to the lavas enclosing mineralization and were not extended in post mineralization lavas overlying sulphide deposits. Such studies are, however, essential if geochemical methods are to be used in exploration. They will also be limited by the same constraints as those discussed with reference to zeolitic alteration, i.e. lithological factors and the superimposed effects of cold seawater- rock interaction.

It may be concluded that, as the impressive surface

indications of mineralization which spurned exploration in the beginning of this century are thoroughly explored, sophisticated methods are required for the assessment of the potentialities of unknown areas and the detection of new, presently concealed deposits.

LIST OF REFERENCES.

- Adamides, N. G., Geological history of the Limni concession, Cyprus, in the light of the plate tectonics hypothesis. Trans. Inst. Min. Metal. 84, 17-23, 1975.
- Adamides, N. G. The form and environment of formation of the Kalavassos ore deposits-Cyprus. Proc. Intern. Ophiol. Symp., Cyprus, 117-127, 1980.
- Adamides, N. G., Introductory report on the Skouriotissa area. Unpubl. Rep. Hellenic Mining Co., 1981.
- Adamides, N. G., Report on the geology of the Tamasos mining district. Unpubl. Rep. Hellenic Mining Co., 1983.
- Alabaster, T., Pearce, J. A., Mallick, D. I. J. and Elboushi, I. M. The volcanic stratigraphy and location of massive sulphide deposits in the Oman ophiolite. Proc. Intern. Ophiol. Sympos., Cyprus, 751-757, 1980.
- Alabaster, T., The interrelationship between volcanic and hydrothermal processes in the Oman ophiolite. Unpubl. Ph. D. thesis, Open University, 408 pp, 1982.
- Allen, C. R., The petrology of a portion of the Troodos Plutonic Complex, Cyprus. Unpubl. Ph. D. Thesis, Cambridge, 161 p, 1975.
- Anderson, C. A. Massive sulphide deposits and volcanism, Econ. Geol., 64, 129-146, 1969.
- Andrews, A. J. and Fyfe, W. S., Metamorphism and massive sulphide generation in oceanic crust. Geoscience Canada, 3, No. 2, 84-94, 1976.
- Aumento, F., The oceanic crust of the mid-Atlantic Ridge at 45° N. The ancient oceanic lithosphere. Canadian contribution No. 2 to the geodynamics project, 49-52, 1972.
- Bachinski, D.J., Metamorphism of cupriferous iron sulfide deposits, Notre Dame Bay, Newfoundland. Econ. Geol. 71, 443-452, 1976.
- Bachinski, D. J., Sulfur isotopic composition of ophiolitic cupriferous iron sulfide deposits, Notre Dame Bay, Newfoundland. Econ. Geol., 72, 243-257, 1977.
- Bachinski, D. J., Alteration associated with metamorphosed ophiolitic cupriferous iron sulphide deposits: Whaleback mine, Notre Dame Bay, Newfoundland. Mineral. Deposita, 12, 48-63, 1977.
- Bagnall, P. S., The geology of the Pano Lefkara-Larnaca area. Geol. Surv. Dept. Cyprus, Mem. No. 5, 116 p, 1960.

Ballard, R. D. and van Andel, T. H. Morphology and tectonics of the inner rift valley at lat 36° 50' N on the mid- Atlantic Ridge. *Geol. Soc. Amer. Bull.*, 507-530, 1977.

Barton, P. B. Jr. and Skinner, B. J., Sulphide mineral stabilities. In Barnes, H. L., Ed., *Geochemistry of hydrothermal ore deposits*. Holt, Rinehart and Winston, 236-333, 1967.

Barton, P.B., Jr. and Toulmin, P., III, The electrum tarnish method for the determination of the fugacity of sulfur in laboratory sulfide systems. *Geoch. Cosmoch. Acta*, 28, 619-640, 1964.

Barton, P. B. Jr. and Toulmin, P., III., Phase relations involving sphalerite in the Fe-Zn-S system. *Econ. Geol.*, 61, 815-849, 1966.

Bastin, E. S., Interpretation of ore textures. *Geol. Soc. Am. Memoir* 45, 101 p, 1960.

Bear, L.M., Annual Rep. *Geol. Surv. Dept. Cyprus*, 1959.

Bear, L. M., The mineral resources and mining industry of Cyprus. *Geol. Surv. Dept., Cyprus, Bull. No. 1*, 208p, 1963.

Beccaluva, L., Piccardo, G. B. and Serri, G., Petrology of northern Apennine ophiolites and comparison with other Tethyan ophiolites. *Proc. Intern. Ophiol. Symp. Cyprus*, 314-331, 1980.

Bignell, R. D., Cronan, D. S. and Tooms, J. S., Red Sea metalliferous brine precipitates. *Geol. Assoc. Canada Spec. Pap. No. 14*, 147-178, 1976.

Bischoff, J. L. and Dickson, F. W., Seawater-basalt interaction at 200° C and 500 bars: Implications for origin of seawater heavy metal deposits and regulation of seawater chemistry. *Earth Planet. Sci. Lett.*, 25, 385-397, 1975.

Bohlke, J. K., Honnorez, J. and Guerstein, B. M. H., Alteration of basalts from site 396B, D. S. D. P.: Petrographic and mineralogic studies. *Contr. Miner. Petrol.*, 73, 341-364, 1980.

Bonatti, E., Zerbi, M., Kay, R. and Rydell, H., Metalliferous deposits from the Apennine ophiolites: Mesozoic equivalents of modern deposits from oceanic spreading centres. *Geol. Soc. Amer. Bull.*, 87, 83-94, 1976.

Bonatti, E., Vertical tectonism in oceanic fracture zones. *Earth Planet. Sci. Lett.*, 37, 369-379, 1978.

Bonatti, E., Guerstein, H.M.B. and Honnorez, J., Hydrothermal pyrite concretions from the Romanche trench (Equatorial Atlantic): Metallogenesis in oceanic fracture zones. *Earth Planet. Sci. Lett.*, 32, 1-10, 1976.

Boorman, R. S., Subsolidus studies in the ZnS-FeS-FeS₂ system. *Econ. Geol.*, 62, 614-631, 1967.

Bostrom, K. and Peterson, M. N. A., Precipitates from hydrothermal exhalations on the East Pacific Rise. *Econ. Geol.*, 61, 1258-1265, 1966.

Brett, R. Experimental data from the system Cu-Fe-S and their bearing on exsolution textures in ores. *Econ. Geol.* 59, 1241-1269, 1964.

Brevart, O., Dupre, B. and Allegre, C. J., Metallogenesis at spreading centres: Lead isotope systematics for sulfides, manganese-rich crusts, basalts, and sediments from the Cyamex and Alvin areas (East Pacific Rise). *Econ. Geol.*, 76, 1205-1210, 1981.

Brown, P.R.L. and Lovering, J.F. Compositions of sphalerites from the Broadlands geothermal field and their significance to sphalerite geothermometry and geobarometry. *Econ. Geol.* 68, 381-387, 1973.

Bryan, W. B. and Moore, J. G., Compositional variations of young basalts in the mid-Atlantic Ridge rift valley near lat 36° 49' N. *Bul. Geol. Soc. Am.*, 88, 556-570, 1977.

Burnham, C. W., Facies and types of hydrothermal alteration. *Econ. Geol.*, 57, 768-784, 1962.

Busenberg, E., The products of the interaction of feldspars with aqueous solutions at 250 C. *Geochem. Cosmochem. Acta*, 42, 1679-1686, 1978.

Cameron, W. E., Nisbet, E. G. and Dietrich, V. J., Petrographic dissimilarities between ophiolitic and ocean-floor basalts. *Proc. Intern. Ophiol. Symp. Cyprus*, 182-192, 1980.

Cameron, W. E., Nisbet, E. G. and Dietrich, V. J., Boninites, komatiites and ophiolitic basalts. *Nature*, 280, 550-553, 1979.

Cann, J. R., Rb, Sr, Y, Zr and Nb in some ocean floor basaltic rocks. *Earth Planet. Sci. Lett.*, 10, 7-11, 1970.

Cann, J. R., Geological processes at mid-ocean ridge crests. *Geophys. J. R. Astr. Soc.*, 15, 331-341, 1968.

Cann, J. R., Metamorphism in the ocean crust. In "Deep drilling results in the Atlantic ocean crust". Eds Talwani, M; Harrison, C. G. and Hayes, D. E. Maurice Ewing Series 2. A. G. U., Washington, Geodynamics Project: Scientific report, 48, 230-238, 1979.

Cann, J. R. and Strens, M. R., Black smokers fuelled by freezing magma. *Nature*, 298, 147-149, 1982.

Capedri, S. and Venturelli, G., Clinopyroxene composition of

ophiolitic metabasalts in the Mediterranean area. *Earth Planet. Sci. Lett.*, 43, 61-73, 1979.

Chapman, H. J. and Spooner, E. T. C., ^{87}Sr enrichment of ophiolitic sulphide deposits in Cyprus confirms ore formation by circulating seawater. *Earth Planet. Sci. Lett.*, 35, 71-78, 1977.

Chazen, S. I. and Vogel, T. A. Distribution of Ti and P in basalts as a test of origin. *Contr. Mineral. Petrol.*, 43, 307-316, 1974.

Christoforou, Y. N. Cupriferous sulphide mineralization of the Kokkinoyia mine. Unpubl. M. Sc. Thesis, Cardiff, 169p, 1975.

Church, W. R. and Coish, R. A., Oceanic versus island arc origin of ophiolites. *Earth Planet. Sci. Lett.*, 31, 8-14, 1976.

Clark, L. A., Volcanogenic ores: Comparison of cupriferous pyrite deposits of Cyprus and Japanese Kuroko deposits. *Soc. Min. Geol. Japan, Spec. Issue 3*, 206-215, 1971.

Clark, B. R. and Kelly, W. C. Sulfide deformation studies. I. Experimental deformation of pyrrhotite and sphalerite to 2000 bars and 500°C. *Econ. Geol.* 68, 332-352, 1973.

Clark, A. H. and Sillitoe, R. H., Cuprian sphalerite and a probable copper-zinc sulphide, Chile. *Amer. Mineral.*, 55, 1021-1025, 1970.

Coish, R. A. Ocean floor metamorphism in the Betts Cove ophiolite, Newfoundland. *Contr. Mineral. Petrol.*, 60, 255-270, 1977.

Coleman, R. G. and Peterman, Z. E., Oceanic Plagiogranite. *Journ. Geoph. Res.*, 80, 1099-1108, 1975.

Constantinou, G., The geology and genesis of the sulphide ores of Cyprus. Unpubl. Ph. D. Thesis, University of London, 275 p, 1972.

Constantinou, G. and Govett, G. J. S., Geology, geochemistry and genesis of Cyprus sulfide deposits. *Econ. Geol.*, 68, 843-858, 1973.

Constantinou, G., Hydrothermal alteration of the basaltic lavas of the Troodos ophiolite complex associated with the formation of the massive sulphide deposits (Summary). In volcanic processes in ore genesis (Institution of Mining and Metallurgy and Geological Society, London), p77, 1977.

Constantinou, G. Metallogenesis associated with Troodos ophiolite. *Proc. Intern. Ophiol. Sympos.*, Cyprus, 663-674, 1980.

Corliss, J. B., The origin of metal bearing submarine hydrothermal solutions. *J. Geophys. Res.*, 76, No. 33, 8128-8138, 1971.

Corliss, J. B., Dymond, J., Gordon, L. I., Edmond, J. M., Herzen,

R. P., Ballard, R. D., Green, K., Williams, D., Bainbridge, A., Crane, K. and van Andel, T. H., Submarine thermal springs on the Galapagos rift. *Science*, 203, 1073-1083, 1979.

Craig, J. R. and Kullerud, G., The Cu-Zn-S system. *Mineral. Deposita*, 8, 81-91, 1973.

Crane, K. and Normark, W.R., Hydrothermal activity and crestal structure of the East Pacific Rise at 21° N. *J. Geophys. Res.*, 82, No. 33, 5336-5348, 1977.

Crawford, A. J., Beccaluva, L. and Serri, G., Tectonomagmatic evolution of the West Philippine Mariana region and the origin of boninites. *Earth Planet. Sci. Lett.* 54, 346-356, 1981.

Cronan, D. S., Metallogenesis at oceanic spreading centres. *J. Geol. Soc. London*, 136, 621-626, 1979.

Cullis, C. G. and Edge, A. B., Report on the cupriferous deposits of Cyprus. London (Crown Agents for Overseas Governments and Administrations), 1927.

Czamanske, G. K., The FeS content of sphalerite along the chalcopyrite-pyrite-bornite sulphur fugacity buffer. *Econ. Geol.*, 69, 1328-1334, 1974.

Deer, W. A., Howie, R. A. and Zussman, J., An introduction to the rock-forming minerals. Longmans, Green and Co., 528 p, 1966.

Desmet, A. P., Evidence of co-genesis of the Troodos lavas, Cyprus. *Geol. Mag.*, 113, 165-168, 1976.

Dietrich, V., Emmermann, R. Oberhansli, R. and Puchelt, H., Geochemistry of basaltic and gabbroic rocks from the west Mariana basin and the Mariana trench. *Earth Planet. Sci. Lett.*, 39, 127-144, 1978.

Dick, H. J. B., Marsh, N. G. and Bullen, T. D., Deep sea drilling project LEG 58 abyssal basalts from the Shikoku Basin: Their petrology and major element geochemistry. Initial Reports D. S. D. P., 58, 843-872.

Edmond, J. M., Measures, C., McDuff, R. E., Chan, L. H., Collier, R. and Grant, B., Ridge crest hydrothermal activity and the balances of the major and minor elements in the ocean: The Galapagos data. *Earth Planet. Sci. Lett.*, 46, 1-18, 1979.

Edmond, L., The chemistry of ridge crest hot springs. *MTS Journal*, 16, 23-31, 1982.

Edwards, A. B., Textures of the ore minerals and their significance. *Australasian Inst. Mining Metall.*, 242p, 1974.

Elder, J. W., Physical processes in geothermal areas. In

'Terrestrial heat flow', Amer. Geophys. Union, Geoph. Monogr. 8, 211-239, 1965.

Elder, J. W., Model of hydrothermal ore genesis. In 'Volcanic processes in ore genesis', Institution of Mining and Metallurgy and Geological Society of London, 14-24, 1977.

Elderfield, H., Gass, I. G., Hammond, A. and Bear, L. M., The origin of ferromanganese sediments associated with the Troodos Massif of Cyprus. *Sedimentology*, 19, 1-19, 1971.

Erlank, A. J. and Kable, E. J. D., The significance of incompatible elements in mid-Atlantic ridge basalts from 45°N with particular reference to the Zr:Nb ratio. *Contr. Miner. Petrol.*, 54, 281-291, 1976.

Francheteau, J. and 15 others, Massive deep-sea sulphide ore deposits discovered on the East Pacific Rise. *Nature*, 277, 523-528, 1979.

Franklin, J. M., Kasarda, J. and Poulsen, K. H., Petrology and chemistry of the alteration zone of the Mattabi massive sulfide deposit. *Econ. Geol.*, 70, 63-79, 1975.

Franklin, J. M., Lydon, J. W. and Sangster, D. F., Volcanic-associated massive sulfide deposits. *Econ. Geol.* 75th anniv. volume, 485-627, 1981.

Frey, F. A., Bryan, W. B. and Thompson, G., Atlantic ocean floor: Geochemistry and petrology of basalts from Legs 2 and 3 of the deep sea drilling project. *J. Geophys. Res.*, 79, 5507-5527, 1974.

Gale, G. H., Palaeozoic basaltic komatiite and ocean-floor type basalts from northeastern Newfoundland. *Earth Planet. Sci. Lett.*, 18, 22-28, 1973.

Gale, N. H., Spooner, E. T. C. and Potts, P. J., The lead and strontium isotope geochemistry of metalliferous sediments associated with Upper Cretaceous ophiolitic rocks in Cyprus, Syria and the sultanate of Oman. *Can. J. Earth Sci.*, 18, 1290-1302, 1981.

Gale, G.H. and Roberts, D., Trace element geochemistry of Norwegian lower palaeozoic basic volcanics and its tectonic implications. *Earth Planet. Sci. Lett.*, 22, 380-390, 1974.

Garson, M.S. and Shalaby, I.M., Precambrian- Lower Palaeozoic plate tectonics and metallogenesis in the Red Sea region. *Geol. Ass. Canada, Spec. Paper No. 14*, 573-595, 1976.

Gass, I. G., The Troodos Massif: Its role in the unravelling of the ophiolite problem and its significance in the understanding of constructive margin processes. *Proc. Intern. Ophiol. Symp. Cyprus*, 23-35, 1980.

Gass, I. G. and Masson-Smith, D., The geology and gravity anomalies of the Troodos Massif. Phil. Trans. Roy. Soc. London, A255, 417-467, 1963.

Gass, I.G. and Smewing, J. D., Intrusion, extrusion and metamorphism at constructive margins: Evidence from the Troodos Massif, Cyprus. Nature, 243, 26-29, 1973.

George, R. P. Jr., Structural petrology of the Olympus ultramafic complex in the Troodos ophiolite, Cyprus. Geol. Soc. Am. Bull., 89, 845-865, 1978.

Gibson, H. L. and Watkinson, D. H., Silicification in the Amulet 'rhyolite' formation, Turcotte Lake section, Noranda area, Quebec. Current Research, Geol. Surv. Canada, Paper 79-1B, 111-120, 1979.

Gibson, H. L., Watkinson, D. H. and Comba, C. D. A., Silicification, hydrothermal alteration in an Archaean geothermal system within the Amulet Rhyolite formation, Noranda, Quebec. Econ. Geol. 78, 954-971, 1983.

Goldie, R. and Bottrill, T.J., Seminar on sea-floor hydrothermal systems. Geoscience Canada, 8, No. 3, 93-104, 1981.

Goldschmidt, V. M., Geochemistry, Oxford Univ. Press, 730p, 1954.

Goodfellow, W.D., Major and minor element haloes in volcanic rocks at Brunswick No. 12 sulphide deposit, N. B., Canada. Geochem. Explor. 1974, Amsterdam, Elsevier, 279-295, 1975.

Gordon-Smith, J., The Limni orebody, an interim report. Unpub. Rep. Cyprus Sulphur and Copper Co., 1959.

Gordon-Smith, J., Kalavassos, an interim report on the mining area. Priv. Rep. Hellenic Mining Co., 1963.

Greenbaum, D., Magmatic processes at oceanic ridges: Evidence from the Troodos Massif, Cyprus. Nature, 238, 18-21, 1972.

Griffiths, W.R., Albers, J.P. and Oner, O., Massive sulfide copper deposits of the Ergani-Maden area southeastern Turkey. Econ. Geol. 67, 701-716, 1972.

Groves, D. I., Binns, R. A., Barrett, F. M. and McQueen, K. G., Sphalerite compositions from Western Australian nickel deposits, a guide to equilibria below 300°C. Econ. Geol. 70, 391-395, 1975.

Haas, J. L., Jr., The effect of salinity on the maximum thermal gradient of a hydrothermal system at hydrostatic pressures. Econ. Geol. 66, 940-946, 1971.

Hajash, A., Hydrothermal processes along mid-ocean ridges: An

experimental investigation. *Contr. Miner. Petrol.*, 53, 205-226, 1975.

Harrigan, D.B. and MacLean, W.H., Petrography and geochemistry of epidote alteration patches in gabbro dykes at Matagami, Quebec. *Can. J. Earth Sci.*, 13, 500-511, 1976.

Hart, R. A., Chemical exchange between seawater and deep ocean basalts. *Earth Planet. Sci. Lett.*, 9, 269-279, 1970.

Hart, R. A., A model for chemical exchange in the basalt-seawater system of oceanic layer II. *Can. Journ. Earth Sci.*, 10, 799-816, 1973.

Hart, S. R., Glassley, W. E. and Karig, D. E., Basalts and seafloor spreading behind the Mariana island arc. *Earth Planet. Sci. Lett.*, 15, 12-18, 1972.

Hatch, F. H., Wells, A. K. and Wells, M. K., Petrology of the igneous rocks. Thomas Murby and Co., 515 p, 1965.

Hawkins, D. B. and Roy, R., Experimental hydrothermal studies on rock alteration and clay mineral formation. *Geoch. Cosmoch. Acta*, 27, 1047-1054, 1963.

Hay, D. E., Theory of origin of massive sulphide deposits supported by their mineralogical character. Unpubl. Thesis for Independent Study, Wooster, 229p, 1979.

Haymon, R. M., Hydrothermal deposition on the East Pacific Rise at 21° N. Unpubl. Ph. D. thesis, University of California, 266 p, 1982.

Haymon, R. M. and Kastner, M., Hot spring deposits on the East Pacific Rise at 21° N: Preliminary description of mineralogy and genesis. *Earth Planet. Sci. Lett.*, 53, 363-381, 1981.

Heaton, T. H. E. and Sheppard, S. M. F., Hydrogen and oxygen isotope evidence for sea-water-hydrothermal alteration and ore deposition, Troodos complex, Cyprus. In 'Volcanic processes in ore genesis', Institution of Mining and Metallurgy and Geological Society of London, 58-71, 1977.

Hekinian, R., Moore, J. G. and Bryan, W. B., Volcanic rocks and processes of the mid-Atlantic Ridge rift valley near 36° 49' N. *Contr. Mineral. Petrol.*, 58, 83-110, 1976.

Hekinian, R., Fevrier, M., Bischoff, J. L., Picot, P. and Shanks, W. C., Sulphide deposits from the East Pacific Rise near 21° N. *Science*, 207, 1433-1444, 1980.

Helgeson, H. C. A., A chemical and thermodynamic model for ore deposition in hydrothermal systems. *Miner. Soc. America Spec. Paper* 3, 155-186, 1970.

Hemley, J. J., Montoya, J. W., Merinenko, J. W. and Luce, R. W., General equilibria in the system $\text{Al}_2\text{O}_3\text{-SiO}_2\text{-H}_2\text{O}$ and some implications for alteration mineralization processes. *Econ. Geol.*, 75, 210-228, 1980.

Henley, R. W. and Thornley, P., Some geothermal aspects of massive sulfide formation. *Econ. Geol.*, 74, 1600-1612, 1979.

Holland, H. D., Some applications of thermochemical data to problems of ore deposits. I. Stability relations among the oxides, sulfides, sulfates and carbonates of ore and gangue minerals. *Econ. Geol.* 54, 184-233, 1959.

Holland, H. D., Gangue minerals in hydrothermal deposits. In Barnes H. L. (Ed.) *Geochemistry of hydrothermal ore deposits*. Holt, Rinehart and Winston, 382-436, 1967.

Holland, H. D. Some applications of thermochemical data to problems of ore deposits. II: Mineral assemblages and the compositions of ore forming fluids. *Econ. Geol.* 60, 1101-1164, 1965.

Honnorez, J., Bohlke, J. K., Guernstein, H. B. M., Petrographical and geochemical study of the low temperature submarine alteration of basalt from hole 396B, LEG 46. Initial Reports D. S. D. P., 46, 299-318, 1978.

Humphris, S. E. and Thompson, G., Trace element mobility during hydrothermal alteration of oceanic basalts. *Geoch. Cosmoch. Acta*, 42, 127-136, 1978.

Hutchinson, R. W., Genesis of Canadian massive sulphides reconsidered by comparison to Cyprus deposits. *Can. Inst. Min. Metal. Trans.*, 68, 286-300, 1965.

Hutchinson, R. W. and Searle, D. L., Stratabound pyrite deposits in Cyprus and relations to other sulphide ores. *Soc. Min. Geol. Japan, Spec. Issue* 3, 198-205, 1971.

Hynes, A., Comment on 'The Troodos ophiolite complex was probably formed in an island arc' by Akiho Miyashiro. *Earth Planet. Sci. Lett.*, 25, 213-216, 1975.

Hynes, A., Magmatic affinity of Ordovician volcanic rocks in northern Maine and their tectonic significance. *Amer. J. Sci.*, 276, 1208-1224, 1976.

Iijima, A., Clay and zeolitic alteration zones surrounding Kuroko deposits in the Hokuroku district, Northern Akita, as submarine hydrothermal-diagenetic alteration products. *Mining Geology, special issue No. 6*, 267-289, 1974.

Irvine, T. N., Chromian spinel as a petrogenetic indicator. Part

2. Petrologic applications. Can. J. Earth Sci., 4, 71-103, 1967.

Ishikawa, H., Kuroda, R. and Sudo, T., Minor elements in some altered zones of 'Kuroko' (black ore) deposits of Japan. Econ. Geol. 57, 785-789, 1962.

Izawa, E., Yoshida, T. and Saito, R., Geochemical characteristics of hydrothermal alteration around the Fukazawa Kuroko deposit, Akita, Japan. Mining Geology, 28, 325-335, 1978.

Jacobsen, J. B. E., Copper deposits in time and space. Miner. Sci. Engng. 7, No. 4, 337-371, 1975.

Jakes, P. and White, A. J. R., Major and trace element abundances in volcanic rocks of orogenic areas. Geol. Soc. Amer. Bull. 83, 29-39, 1972.

Johnson, A. E., Textural and geochemical investigations of Cyprus pyrite deposits. Unpubl. Ph. D. Thesis, University of W. Ontario, 1970.

Johnson, A. E., Origin of Cyprus pyrite deposits. 24th Intern. Geol. Cong., sect. 4, 291-298, 1972.

Jorgensen, K. A. and Brooks, C. K., The Troodos ophiolite: Petrology of a fresh glassy basalt. Bul. Geol. Soc. Denmark, 30, 43-50, 1981.

Kajiwarra, Y., Chemical composition of ore forming solution responsible for the Kuroko type mineralization in Japan. Geoch. J., 6, 141-149, 1973.

Kajiwarra, Y., Some limitations on the physico-chemical environment of deposition of the Kuroko ore. In 'Volcanism and ore genesis', Tokyo, University of Tokyo press, 367-380, 1970.

Kanehira, K. and Bachinski, D. J., Framboidal pyrite and concentric textures in ores of the Tilt Cove mine, northeastern Newfoundland. Can. Mineral., 9, 124-127, 1967.

Karig, D. E., Origin and development of marginal basins in the Western Pacific. Journ. Geoph. Res., 76, 2542-2561, 1971.

Kay, R. W. and Hubbard, N. J., Trace elements in oceanic ridge basalts. Earth Planet. Sci. Lett., 38, 95-116, 1978.

Kay, R., Hubbard, N. J. and Gast, R. W., Chemical characteristics and origin of oceanic ridge volcanic rocks. J. Geoph. Res., 75, 1585-1613, 1970.

Kay, R. W. and Senechal, R. G., The rare earth geochemistry of the Troodos ophiolite complex. Journ. Geoph. Res., 81, No. 5, 964-970, 1976.

Kelly, W. C. and Clark, B. R., Sulfide deformation studies. III. Experimental deformation of chalcopyrite to 2000 bars and 5000 C. *Econ. Geol.*, 70, 431-453, 1975.

Kidd, R. G. W. and Cann, J. R., Chilling statistics indicate an ocean-floor spreading origin for the Troodos Complex, Cyprus. *Earth Planet. Sci. Lett.*, 24, 151-155, 1974.

Knuckey, M. J., Comba, C. D. A. and Riverin, G., Structure, metal zoning and alteration at the Millenbach deposit, Noranda, Quebec. In *Precambrian sulphide deposits*, H. S. Robinson Memorial Vol., *Geol. Ass. Canada spec. paper* 25, 255-295, 1982.

Koski, R. A., Normark, W. R., Morton, J. L. and Delaney, J. R., Metal sulfide deposits on the Juan de Fuca ridge. *Oceanus*, 25, 42-48, 1982.

Krauskopf, K., *Introduction to geochemistry*. McGraw Hill, 721 p, 1967.

Kullerud, G., Sulfide systems as geological thermometers. *Researches in geochemistry*, Abelson, P. H. (Editor), 2, 301-335, 1967.

Kushiro, I., Si-Al relations in clinopyroxenes from igneous rocks. *Am. J. Sci.*, 258, 548-554, 1960.

Langdon, G., The Troodos Upper Pillow Lavas. M. Sc. Thesis, Memorial University of Newfoundland, 130 p, (Unpublished), 1982.

Large, R. R., Chemical evolution and zonation of massive sulfide deposits in volcanic terrains. *Econ. Geol.*, 72, 549-572, 1977.

Laurent, R., Delaloye, M., Vuagnat, M. and Wagner, J. J., Composition of parental basaltic magma in ophiolites. *Proc. Intern. Ophiol. Sympos. Cyprus*, 172-181, 1980.

Le Bas, M. J., The role of aluminum in igneous clinopyroxenes with relation to their parentage. *Am. J. Sci.*, 260, 267-288, 1962.

Le Pichon, X., Francheteau, J. and Bonnin, J., *Plate tectonics*. Elsevier, 213p, 1973.

Liou, J. G., Synthesis and stability relations of epidote. *Jour. Petrol.*, 14, 381-413, 1973.

Lydon, J. W., Chemical parameters of stratiform lead-zinc deposits. In Sangster, D. F. (Ed.), *Sediment-hosted stratiform lead-zinc deposits*. *Miner. Ass. Canada, Short Course Handbook*, 9, 1983.

Lydon, J. W., Some observations on the morphology and ore textures of volcanogenic sulphide deposits of Cyprus. In *Current Research, Part A*, *Geol. Surv. Canada, Paper* 84-1A, 601-610, 1984.

Lydon, J. W., Some observations on the mineralogical and chemical zonation patterns of volcanogenic sulphide deposits of Cyprus. In Current Research, Part A, Geol. Surv. Canada, Paper 84-1A, 611-616, 1984a.

Lydon, J. W. and Jamieson, H. E., The generation of ore forming hydrothermal solutions in the Troodos ophiolite complex. In Current Research, Part A, Geol. Surv. Canada, Paper 84-1A, 617-625, 1984.

Maaloe, S., Compositional range of primary tholeiitic magmas evaluated from major element trends. Lithos, 12, 59-72, 1979.

MacGeehan, P. J., The geochemistry of altered volcanic rocks at Matagami, Quebec: a geothermal model form massive sulphide genesis. Canadian Journ. Earth Sci., 15, 551-570, 1978.

Malahoff, A., A comparison of the massive polymetallic sulfides of the Galapagos Rift with some continental deposits. MTS Journal, 16, 39-45, 1982.

Mantis, M., Palaeontological evidence defining the age of the Troodos pillow lava series of Cyprus. Kypriakos Logos, 3, 202-208, 1971.

Marsh, B. D. and Carmichael, S. E., Benioff zone magmatism. Jour. Geoph. Res., 79, No. 8, 1196-1206, 1974.

Marsh, N. G., Saunders, A. D., Tarney, J. and Dick, H. J. B., Geochemistry of basalts from the Shikoku and Daito basins, Deep Sea Drilling Project LEG 58. Initial Reports, D. S. D. P., 58, 805-842, 1980.

Mastushima, S., Kennedy, G. C., Akella, J. and Haygarth, J., A study of equilibrium relations in the systems $Al_2O_3-SiO_2-H_2O$ and $Al_2O_3-H_2O$. Amer. J. Sci., 265, 28-44, 1967.

Mattey, D. P., Marsh, N. G. and Tarney, J., The geochemistry, mineralogy and petrology of basalts from the West Philippine and Papece Vela Basins and from the Palau-Kyushu and West Mariana Ridges, Deep Sea Drilling Project LEG 59. Init. Rep. D. S. D. P., 59, 753-800, 1980.

Meyer, C. and Hemley, J. J., Wall rock alteration. In Barnes, H. L. (Ed.), Geochemistry of hydrothermal ore deposits. Holt, Rinehart and Winston, 166-235, 1967.

Mitchell, A. H. and Bell, J. D., Island arc evolution and related mineral deposits. J. Geol., 81, 381-405, 1973.

Miyashiro, A., The Troodos ophiolite complex was probably formed in an island arc. Earth Planet. Sci. Lett., 19, 218-224, 1973.

Miyashiro, A., Origin of the Troodos and other ophiolites: A reply to Hynes. *Earth Planet. Sci. Lett.*, 25, 217-222, 1975.

Miyashiro, A., Origin of the Troodos and other ophiolites: A reply to Moores. *Earth Planet. Sci. Lett.*, 25, 227-235, 1975.

Miyashiro, A. and Shido, F., Tholeiitic and calc-alkaline series in relation to the behavior of titanium, vanadium, chromium and nickel. *Am. J. Sci.* 275, 265-277, 1975.

Miyashiro, A., Shido, F. and Ewing, M., Metamorphism at the mid-Atlantic ridge near 24° N and 30° N. *Phil. Trans. Roy. Soc. London*, A268, 589-603, 1971.

Miyashiro, A., Origin of the Troodos and other ophiolites: A reply to Moores. *Earth Planet. Sci. Lett.*, 25, 227-235, 1975.

Moore, J. G., Fleming, H. S. and Phillips, J. D., Preliminary model for extrusion and rifting at the axis of the mid-Atlantic Ridge 36° 48' N. *Geology*, 437-440, 1974.

Moores, E. M., Discussion of 'origin of the Troodos and other ophiolites: A reply to Hynes' by Akiho Miyashiro. *Earth Planet. Sci. Lett.*, 25, 223-226, 1975.

Moores, E. M. and Vine, F. J., Troodos Massif, Cyprus and other ophiolites as oceanic crust: Evaluation and implications. *Phil. Trans. Roy. Soc. London*, A268, 443-466, 1971.

Mousoulos, L., Contribution to the study of cupriferous pyrite deposits of the island of Cyprus. *Ann. Geol. Pays Hellen.*, 8, 269-320, 1957.

Mottl, M. J., Chemical exchange during hydrothermal alteration of basalt by seawater. I: Experimental results for major and minor components of seawater. *Geoch. Cosmoch. Acta*, 42, 1103-1115, 1978.

Mottl, M. J. and Holland, H. D., Chemical exchange during hydrothermal alteration of basalt by seawater-II. Experimental results for Fe, Mn and sulfur species. *Geoch. Cosmoch. Acta*, 43, 869-884, 1979.

Mottl, M. J., Metabasalts, axial hot springs and the structure of hydrothermal systems at mid-ocean ridges. *Bull. Geol. Soc. Amer.* 94, 161-180, 1983.

Nisbet, E. and Pearce, J. A., TiO_2 and a possible guide to past oceanic spreading rates. *Nature*, 246, 468-469, 1973.

Nisbet, E. G. and Pearce, J. A., Clinopyroxene composition in mafic lavas from different tectonic settings. *Contr. Miner. Petrol.*, 63, 149-160, 1977.

Normark, W. R., Lupton, J. E., Murrey, J. W., Delaney, J. R.,

Johnson, H. P., Koski, R. A., Clague, D. A. and Morton, J. L., Polymetallic sulphide deposits and water column of active hydrothermal vents on the southern Juan de Fuca Ridge. *MTS Journal*, 16, 46-53, 1982.

O'Hara, M. J., Geochemical evolution during fractional crystallisation of a periodically refilled magma chamber. *Nature*, 266, 503-508, 1977.

O'Nions, R. K. and Pankhurst, R. J., Petrogenetic significance of isotope and trace element variations in volcanic rocks from the mid-Atlantic. *J. Petrol.*, 15, 603-634, 1974.

Oudin, E., Picot, P. and Pouit, G., Comparison of sulphide deposits from the East Pacific Rise and Cyprus. *Nature*, 291, 404-407, 1981.

Oxburgh, E. R. and Turcotte, D. L., Mid-ocean ridges and geotherm distribution during mantle convection. *J. Geoph. Res.*, 73, 2643-2661, 1968.

Pallister, J. S. and Hopson, C. A., Samail ophiolite plutonic suite: Field relations, phase variation, cryptic variation and layering, and a model of a spreading ridge magma chamber. *Jour. Geoph. Res.*, 86, No. B4, 2593-2644, 1981.

Panayiotou, A., Geology and geochemistry of the Limassol Forest Plutonic Complex and the associated sulphide and chromite deposits, Cyprus. Ph. D. Thesis, University of New Brunswick, Canada (Unpublished), 1977.

Pantazis, Th., Contribution to the economic geology of the Kalavassos mine. Priv. Report Geol. Surv. Dept. Cyprus (Unpublished), 1966.

Pantazis, Th., The geology of the Pharmakas-Kalavassos area. *Geol. Surv. Dept. Cyprus, Mem. Mo.8*, 1967.

Pantazis, Th., Major oxide geochemistry and origin of the Troodos ophiolite complex. *Bull. Mineral.*, 103, 59-65, 1980.

Pearce, J. A., Basalt geochemistry used to investigate past tectonic environments on Cyprus. *Tectonophysics*, 25, 41-67, 1975.

Pearce, J. A. and Cann, J. R., Tectonic setting of basic volcanic rocks determined using trace element analyses. *Earth Planet. Sci. Lett.*, 19, 290-300, 1973.

Pearce, J. A. and Norry, M. J., Petrogenetic implications of Ti, Zr, Y and Nb variations in volcanic rocks. *Contr. Miner. Petrol.*, 69, 33-47, 1979.

Phillips, W. J., Hydraulic fracturing and mineralization. *J. Geol. Soc. London*, 128, 337-359, 1972.

Rankama, K. and Sahama, T. G., Geochemistry. University of Chicago press, 911p, 1949.

Ridge, J. D., Volcanic exhalations and ore deposition in the vicinity of the sea floor. Miner. Deposita, 8, 332-348, 1973.

Riverin, G. and Hodgson, C. J., Wall-rock alteration at the Millenbach Cu-Zn mine, Noranda, Quebec. Econ. Geol., 75, 424-444, 1980.

Roberts, R. G. and Reardon, E. J., Alteration and ore forming processes at Mattagami Lake Mine, Quebec. Canadian Journ. Earth Sci., 15, 1-21, 1978.

Robertson, A. H. F., Cyprus umbers: Basalt-sediment relationships on a mesozoic ocean ridge. Jour. Geol. Soc. London, 131, 511-531, 1975.

Robertson, A. H. F., The Moni Melange, Cyprus: An olisthostrome formed at a destructive plate margin. Jour. Geol. Soc. London, 133, 447-466, 1977.

Robertson, A. H. F., Metallogenesis along a fossil oceanic fracture zone: Arakapas fault belt, Troodos Massif, Cyprus. Earth Planet. Sci. Lett., 41, 317-329, 1978.

Robertson, A. H. F. and Fleet, A. J., Rare earth evidence for the genesis of the metalliferous sediments of Troodos, Cyprus. In 'Volcanic processes in ore genesis', Institution of Mining and Metallurgy and Geological Society, London, 78-79, 1977.

Robertson, A. H. F. and Hudson, J. D., Pelagic sediments in the Cretaceous and Tertiary history of the Troodos Massif, Cyprus. Spec. Publ. Int. Ass. Sediment., 1, 403-436, 1974.

Robertson, A. H. F. and Woodcock, N. H., Tectonic setting of the Troodos massif in the east Mediterranean. Proc. Intern. Ophiol. Sympos. Cyprus, 36-49, 1980.

Robinson, P. T., Flower, M. F. J., Schmincke, H. and Ohnmacht, W., Low temperature alteration of oceanic basalts, D. S. D. P. LEG 37. Initial Reports, D. S. D.P, 37, 775-789, 1977.

Robinson, P. T., Melson, W. G., O'Hearn, T. and Schmincke, H., Volcanic glass compositions of the Troodos ophiolite, Cyprus. Geology, 11, 400-404, 1983.

Roscoe, W. E., Experimental deformation of natural chalcopyrite at temperatures up to 300°C over the strain rate range 10^{-2} to 10^{-6} Sec $^{-1}$. Econ. Geol., 70, 454-472, 1975.

Sato, T., Kuroko deposits: Their geology, geochemistry and origin. In 'Volcanic processes in ore genesis', Institution of

mining and Metallurgy and Geological Society, London, 153-161, 1977.

Saunders, A. D., Tarney, J., Marsh, N. G. and Wood, D. A., Ophiolites as ocean crust or marginal basin crust: A geochemical approach. Proc. Intern. Ophiol. Sympos. Cyprus, 193-204, 1980.

Scott, S. D., Experimental calibration of the sphalerite geobarometer. Econ. Geol. 68, 466-474, 1973.

Scott, S. D. and Barnes, H. L., Sphalerite geothermometry and geobarometry. Econ. Geol. 66, 653-669, 1971.

Scott, S. D. and Kissin, S. A., Sphalerite composition in the Zn-Fe-S system below 300o C. Econ. Geol., 68, 475-479, 1973.

Searle, D. L., The geology of the Limni opencast mine. Unpubl. United Nations report, 1964.

Searle, D. L., The geology of the Kalavassos mining district. Priv. Report Geol. Surv. Dept., Cyprus, 66 p, 1967.

Searle, D. L. and Constantinou, G., The geology of the Asgata-Drapia-Vasa area. Priv. Report, Geol. Surv. Dept. Cyprus (Unpublished), 23 p, 1967.

Searle, D. L. and Panayiotou, A., Structural implications in the evolution of the Troodos Massif. Proc. Intern. Ophiol. Sympos. Cyprus, 51-60, 1980.

Searle, D. L. and Vokes, F. M., Layered ultrabasic lavas from Cyprus. Geol. Mag. 106, No. 6, 515-530, 1969.

Seyfried, W. and Bischoff, J. L., Hydrothermal transport of heavy metals by seawater: The role of the seawater/basalt ratio. Earth Planet. Sci. Lett., 34, 71-77, 1977.

Seyfried, W. and Bischoff, J. L., Low temperature alteration by seawater: An experimental study at 70o C and 150o C. Geoch. Cosmoch. Acta, 43, 1937-1947, 1979.

Seyfried, W. E., Jr. and Bischoff, J. L., Experimental seawater-basalt interaction at 300o C, 500 bars, chemical exchange, secondary mineral formation and implications for the transport of heavy metals. Geochimica Cosmoch. Acta, 45, 135-147, 1981.

Sharaskin, A. Y., Dobretsov, N. L. and Sobolev, N. V., Marianites: The clinoenstatite-bearing pillow lavas associated with the ophiolite assemblage of Mariana trench. Proc. Intern. Ophiol. Sympos. Cyprus, 473-479, 1980.

Shelton, A. W. and Gass, I. G., Rotation of the Troodos microplate. Proc. Intern. Ophiol. Sympos. Cyprus, 61-65, 1980.

Short, M. N., Microscopic determination of the ore minerals. U. S. Geological Survey Bull. 14, 314 p, 1940.

Simonian, K. O., The geology of the Arakapas fault belt area, Troodos Massif, Cyprus. Ph. D. Thesis, Open University (Unpublished), 1975.

Skinner, B. J., White, D. E., Rose, H. J. and Mays, R. E., Sulfides associated with the Salton Sea geothermal brine. Econ. Geol., 62, 316-330, 1967.

Smewing, J. D., Metamorphism of the Troodos Massif, Cyprus. Ph. D. Thesis, Open University (Unpublished), 1975.

Smewing, J. D. and Potts, P. J., Rare earth abundances in basalts and metabasalts from the Troodos Massif, Cyprus. Contr. Miner. Petrol., 57, 245-258, 1976.

Smewing, J. D., Simonian, K. O. and Gass, I. G., Metabasalts from the Troodos Massif, Cyprus: Genetic implications deduced from petrography and trace element geochemistry. Contr. Miner. Petrol. 51, 49-64, 1975.

Smirnov, V. I., Borodayev, Y. S. and Starostin, V. I., Pyritic ores and deposits of Japan. Intern. Geol. Rev., 11, No. 8, 845-856, 1969.

Solomon, M., "Volcanic" massive sulphide deposits and their host rocks- a review and an explanation, in Wolf, K. A., ed., Handbook of stratabound and stratiform ore deposits, II Regional studies and specific deposits: Amsterdam, Elsevier, 21-50, 1976.

Solomon, M. and Walshe, J. L., The formation of massive sulfide deposits on the sea floor. Econ. Geol., 74, 797-813, 1979.

Spooner, E. T. C., Hydrodynamic model for the origin of the ophiolitic cupriferous pyrite deposits of Cyprus. In 'volcanic processes in ore genesis', Institution of Mining and Metallurgy and Geological Society of London, 58-71, 1977.

Spooner, E. T. C. and Bray, C. J., Hydrothermal fluids of seawater salinity in ophiolitic sulphide ore deposits in Cyprus. Nature, 266, 808-812, 1977.

Spooner, E. T. C. and Fyfe, W. S., Sub-sea-floor metamorphism, heat and mass transfer. Contr. Miner. Petrol., 42, 287-304, 1973.

Stakes, D. S. and O'Neal, J. R., Mineralogy and stable isotope geochemistry of hydrothermally altered oceanic rocks. Earth Planet. Sci. Lett., 57, 285-304, 1982.

Stern, C. and de Wit, M. J., The role of spreading centre magma chambers in the formation of phanerozoic oceanic crust: Evidence from Chilean ophiolites. Proc. Intern. Ophiol. Sympos. Cyprus,

497-506, 1980.

Suffel, G. G., Remarks on some sulphide deposits in volcanic extrusives. *Trans. Can. Inst. Min. Metal.*, 68, 301-307, 1965.

Sun, S. S. and Nesbitt, R. W., Geochemical regularities and genetic significance of ophiolitic basalts. *Geology*, 6, 689-693, 1978.

Swarbrick, R. E., The Mamonia complex of S.W. Cyprus: A mesozoic continental margin and its relationship to the Troodos complex. *Proc. Intern. Ophiol. Sympos. Cyprus*, 86-92, 1980.

Tarney, J., Saunders, A. D., Matthey, D. P., Wood, D. A. and Marsh, N. G., Geochemical aspects of back-arc spreading in the Scotia Sea and western Pacific. *Phil. Trans. Roy. Soc. London*, A300, 263-285, 1981.

Tarney, J., Saunders, A. D., Weaver, S. D., Donellan, N. C. B. and Hendry, G. L., Minor element geochemistry of basalts from LEG 49, North Atlantic Ocean. *Initial Reports D. S. D. P.*, 49, 657-691, 1978.

Tarney, J. and Windley, B. F., Marginal basins through geological time. *Phil. Trans. Roy. Soc. London*, A301, 217-232, 1981.

Thompson, A. B., PCO_2 in low grade metamorphism; zeolite, carbonate, clay mineral, prehnite relations in the system $CaO-Al_2O_3-SiO_2-CO_2-H_2O$. *Contr. Miner. Petrol.*, 33, 145-161, 1971.

Tomasson, J. and Kristmannsdottir, H., High temperature alteration minerals and thermal brines, Reykjanes, Iceland. *Contr. Miner. Petrol.* 36, 123-134, 1972.

Spooner, E. T. C., Chapman, H. J. and Smewing, J. D., Strontium isotope contamination and oxidation during ocean floor hydrothermal metamorphism of the ophiolitic rocks of the Troodos massif, Cyprus. *Geoch. Cosmoch. Acta*, 41, 873-890, 1977.

Upadhyay, H. D. and Strong, D. F., Geological setting of the Betts Cove copper deposits, Newfoundland: An example of ophiolite sulphide mineralization. *Econ. Geol.*, 68, 161-167, 1973.

Utada, M., Minato, H., Ishikawa, T. and Yoshizaki, Y., The alteration zones surrounding Kuroko-type deposits in Nishi-Aizu district, Fukushima Prefecture, with emphasis on the analcime zone as an indicator in exploration for ore deposits. *Mining Geology*, Special issue No. 6, 291-302, 1974.

Uytendogaardt, W. and Burke, E. A. J., Tables for microscopic identifications of pre minerals. Elsevier, 430 p, 1971.

Vokes, F. M. and Gale, G. H., Metallogeny relatable to global tectonics in southern Scandinavia. *Geol. Assoc. Canada Spec. Pap.*

No. 14, 413-441, 1976.

Vokes, F.M., Remarks on the origin of the Cyprus pyritic ores. Can. Min. Metal. Bull., 59, No. 647, 388-391, 1966.

Weaver, C. E. and Pollard, L. D., The chemistry of clay minerals. Developments in sedimentology, 15, Elsevier, 213 p, 1973.

White, W. M. and Bryan, W. B., Sr-isotope, K, Rb, Cs, Sr, Ba, and rare-earth geochemistry of basalts from the FAMOUS area. Geol. Soc. Amer. Bull., 88, 571-576, 1977.

Whitmarsh, R. B. and Laughton, A. S., The fault pattern of a slow spreading ridge near a fracture zone. Nature, 258, 509-510, 1975.

Wiggins, L. B. and Craig, J. R., Reconnaissance of the Cu-Fe-Zn-S system: Sphalerite phase relations. Econ. Geol., 75, 741-751, 1980.

Winchester, J. A. and Floyd, P. A., Geochemical discrimination of different magma series and their differentiation products using immobile elements. Chemical Geology, 20, 325-343, 1977.

Wilson, R. A. M., The geology of the Xeros-Troodos area. Geol. Surv. Dept. Cyprus, Memoir No.1, 184 p, 1959.

Wood, D. A., Gibson, I. L. and Thompson, R. N., Elemental mobility during zeolite facies alteration of the tertiary basalts of Eastern Iceland. Contr. Miner. Petrol., 55, 241-254, 1976.

Wood, D. A., Joron, J. L., Treuil, M., Norry, M. and Tarney, J., Elemental and Sr isotope variations in basic lavas from Iceland and the surrounding ocean floor. Contr. Mineral. Petrol., 70, 319-339, 1979.

Wood, D. A., Matthey, D. P., Joron, J. L., Marsh, N. G., Tarney, J. and Treuil, M. A., A geochemical study of 17 selected samples from basement cores recovered at sites 447, 448, 449, 450 and 451, deep sea drilling project LEG 59. Initial Reports D. S. D. P., 59, 743-752, 1980.

Wood, D. A., Joron, J. L., Marsh, N. G., Tarney, J. and Treuil, M., Major and trace element variations in basalts from the North Philippine sea drilled during deep sea drilling project LEG 58: A comparative study of back-arc basin basalts with lava series from Japan and mid-ocean ridges. Initial Reports, D. S. D. P., 58, 873-894, 1980a.

Woolery, T. J. and Sleep, N. H., Hydrothermal circulation and geochemical flux at mid-ocean ridges. Jour. Geol., 84, No. 3, 249-275, 1976.

APPENDIX 1.

Major and trace element (XRF) analyses of samples collected along nine traverses over northern Troodos.

Refer to section 3.4.2 (page 83) for location of sample points and analytical techniques.

Major Elements

Ox. %	TR1-1	TR1-2	TR1-3	TR1-4	TR1-5FL	TR1-5DY
SiO ₂	52.65	57.25	59.20	56.75	71.75	63.65
TiO ₂	0.62	0.64	1.16	1.33	1.19	1.41
Al ₂ O ₃	15.10	13.90	13.30	12.20	11.35	13.50
Fe ₂ O ₃	10.12	9.68	10.49	11.54	7.09	8.20
MnO	0.12	0.10	0.14	0.17	0.08	0.17
MgO	7.55	6.60	5.10	5.10	1.50	3.10
CaO	10.13	10.00	7.56	8.89	5.54	5.21
Na ₂ O	1.42	1.53	2.50	2.19	2.24	3.58
K ₂ O	1.10	0.49	0.54	0.95	0.60	0.28
P ₂ O ₅	0.06	0.06	0.10	0.11	0.11	0.15
Total	98.87	100.25	100.09	99.23	101.45	99.25

Total Iron as Fe₂O₃.

Trace Elements

Nb	1.5	1.6	1.7	1.7	1.3	2.0
Zr	41	44	81	85	68	125
Y	13.1	14.2	26.8	27.9	27.1	39.7
Sr	71	76	101	98	82	109
Rb	54.5	12.5	33.0	20.1	16.1	4.2
Ga	15	15.2	17.3	17.8	14.9	18.8
Zn	84	79	70	74	53	97
Cr	180	38	13	11	12	8
V	246	274	325	367	418	130
La	0.5	0.3	1.7	2.6	2.6	4.7
Ce	5.1	5.6	9.8	9.5	7.4	16.1
Nd	4.4	3.8	8.5	9.6	7.7	13.6
Ba	27	30	38	41	35	62

Selected Trace Element Ratios

Zr:Nb	27	27	48	50	52	63
Zr:Y	3.1	3.1	3.0	3.0	2.5	3.1
Y:Nb	8.7	8.9	15.8	16.4	20.8	19.9
Ti:Zr	91	87	86	94	105	68

- TR1-1: Massive Upper Pillow Lava flow.
 TR1-2: Central parts of non pillowed flow in Lower Pillow Lava.
 TR1-3: Celadonite stained, vesicular, dyke in Lower Pillow Lava.
 TR1-4: Columnar jointed celadonite stained, slightly vesicular massive flow in LPL.
 TR1-5FL: Lower margin of non pillowed flow (1 metre) in LPL.
 TR1-5DY: Central parts of celadonite stained dyke in LPL.

Major Elements

Ox. %	TR1-6	TR1-7	TR1-8	TR1-9CH	TR1-9M	TR1-10
SiO ₂	59.55	52.20	57.15	51.90	51.65	57.15
TiO ₂	1.30	1.60	1.30	1.59	1.42	1.62
Al ₂ O ₃	13.20	13.70	13.70	15.00	14.70	13.55
Fe ₂ O ₃	9.34	13.27	11.37	14.41	13.52	10.89
MnO	0.18	0.23	0.17	0.25	0.27	0.17
MgO	4.20	10.90	5.00	10.00	10.70	5.40
CaO	5.50	3.23	3.49	2.29	2.18	2.52
Na ₂ O	3.33	3.62	5.05	3.70	3.27	5.21
K ₂ O	0.18	0.34	0.60	0.33	0.41	0.03
P ₂ O ₅	0.23	0.11	0.14	0.12	0.11	0.21
Total	97.01	99.20	97.97	99.59	98.23	96.75

*Total Iron as Fe₂O₃.

Trace Elements

Nb	2.5	1.8	2.3	1.5	1.9	3.5
Zr	132	92	106	94	86	179
Y	44.5	32.6	33.9	29.1	27.1	55.9
Sr	98	90	137	106	101	94
Rb	2.4	1.6	2.7	2.5	2.5	0.5
Ga	19.4	18.3	19.2	18.4	19.5	18.0
Zn	85	179	101	134	147	96
Cr	10	12	7	11	15	287
V	51	566	299	598	565	234
La	5.2	2.4	2.6	2.9	1.3	4.7
Ce	18.1	9.6	11.2	11.4	10.3	13.8
Nd	15.1	8.9	10.6	8.4	7.9	10.9
Ba	48	39	45	37	38	56

Selected Trace Element Ratios

Zr:Nb	53	51	46	63	45	51
Zr:Y	3.0	2.8	3.1	3.2	3.2	3.2
Y:Nb	17.8	18.1	14.7	19.4	14.3	16.0
Ti:Zr	59	104	74	101	99	54

TR1-6: Central part of dyke close to BG/LPL boundary.
 TR1-7: Thick (2m) dyke in BG. Sparse pyrite disseminations.
 TR1-8: Coarse grained dyke in BG.
 TR1-9M: Middle parts of diabase dyke (0.75 m thick).
 TR1-9CH: Chilled margin of previous dyke.
 TR1-10: Diabase dyke, 1.5 m. thick.

Major Elements

Ox. %	TR1-11	TR1-12	TR1-13	TR1-14	TR1-15	TR1-16
SiO ₂	54.15	54.85	52.40	55.10	60.60	54.75
TiO ₂	1.14	1.14	1.46	1.30	1.05	0.92
Al ₂ O ₃	14.00	14.00	13.70	12.10	12.40	13.80
Fe ₂ O ₃	11.69	11.18	12.47	12.07	10.01	11.72
MnO	0.18	0.34	0.24	0.17	0.15	0.20
MgO	8.40	6.55	8.55	5.25	2.40	8.20
CaO	2.98	2.77	4.09	6.51	8.46	6.22
Na ₂ O	3.58	4.23	3.06	3.34	2.27	2.87
K ₂ O	0.62	0.01	0.01	0.00	0.00	0.33
P ₂ O ₅	0.10	0.14	0.12	0.09	0.30	0.09
Total	96.84	95.21	96.10	95.93	97.64	99.10

*Total Iron as Fe₂O₃.

Trace Elements

Nb	1.2	1.6	1.4	1.5	2.2	1.9
Zr	72	104	92	71	119	75
Y	28.4	32.8	30.2	22.9	43.0	24.4
Sr	41	52	77	116	164	108
Rb	4.2	0.9	1.5	0.2	0.9	2.7
Ga	19.6	20.8	18.6	18.6	22.5	16.6
Zn	92	912	141	81	35	41
Cr	10	12	11	10	7	33
V	277	261	382	348	45	311
La	1.2	2.7	1.3	0.6	2.5	1.4
Ce	11.0	14.1	10.0	6.2	13.1	10.2
Nd	9.2	11.2	8.6	7.4	12.2	8.8
Ba	36	21	24	18	16	38

Selected Trace Element Ratios

Zr:Nb	60	65	66	47	54	40
Zr:Y	2.5	3.2	3.0	3.1	2.8	3.1
Y:Nb	23.7	20.5	21.6	15.3	19.5	12.8
Ti:Zr	95	66	95	110	53	74

All samples from the Sheeted Complex.

- TR1-11: Middle of diabase dyke, 1 m thick.
 TR1-12: Medium grained weakly iron stained diabase dyke.
 TR1-13: Medium grained doleritic dyke from general environment of weak iron stain and epidotisation.
 TR1-14: Green doleritic dyke, 1 m thick. Rare pyrite.
 TR1-15: Weakly iron stained diabasic dyke.
 TR1-16: Tough, medium to fine grained diabase dyke.

Major Elements

Ox. %	TR1-17	TR1-18	TR1-19	TR1-21	TR1-22	TR1-23
SiO ₂	50.70	51.15	52.90	49.20	53.45	53.40
TiO ₂	0.32	0.52	1.28	0.29	1.48	1.38
Al ₂ O ₃	13.80	14.60	12.90	19.55	14.65	13.30
Fe ₂ O ₃	8.93	9.06	12.01	5.91	10.81	9.94
MnO	0.15	0.18	0.16	0.09	0.08	0.09
MgO	9.95	13.75	6.35	6.95	5.70	5.70
CaO	11.91	7.74	7.42	14.37	10.33	9.03
Na ₂ O	1.39	1.41	4.36	1.69	2.29	3.17
K ₂ O	0.08	0.54	0.13	0.09	0.04	0.10
P ₂ O ₅	0.04	0.04	0.11	0.04	0.12	0.14
Total	97.27	98.99	97.62	98.18	98.95	96.25

Total Iron as Fe₂O₃.

Trace Elements

Nb	0.7	0.9	1.6	0.8	1.7	1.7
Zr	29	44	92	29	71	87
Y	6.9	10.3	29.2	3.5	26.3	29.6
Sr	75	134	104	119	121	124
Rb	1.2	3.2	0.6	1.2	1.8	1.7
Ga	13.2	13.4	18.9	15.3	20.8	19.2
Zn	46	71	46	29	19	18
Cr	236	223	10	259	17	20
V	216	236	398	140	445	422
La	0	0	1.5	0	1.4	2.0
Ce	3.5	4.8	7.5	3.2	6.0	10.5
Nd	1.5	3.3	6.9	3.2	6.1	9.8
Ba	15	11	27	9	31	30

Selected Trace Element Ratios

Zr:Nb	41	49	58	36	42	51
Zr:Y	4.2	4.3	3.2	8.3	2.7	2.9
Y:Nb	9.9	11.4	18.3	4.4	15.5	17.4
Ti:Zr	66	71	83	60	125	95

TR1-17: Massive coarse gabbro.

TR1-18: Massive friable gabbro.

TR1-19: Thin (25 cm) fine grained diabase dyke.

TR1-21: Fresh, melanocratic gabbro.

TR1-22: Gabbro from main body. Tough, microgabbroic-grained.

TR1-23: Fresh doleritic dyke in diabase.

Major Elements

Ox. %	TR2-1	TR2-CHM	TR2-2A	TR2-2B	TR2-3	TR2-4
SiO ₂	71.35	56.70	56.50	67.10	62.05	61.55
TiO ₂	0.63	0.62	1.49	0.79	1.26	1.57
Al ₂ O ₃	13.55	13.90	12.90	12.70	13.55	13.35
Fe ₂ O ₃	5.84	11.49	10.33	7.40	9.54	10.21
MnO	0.05	0.15	0.13	0.12	0.08	0.17
MgO	1.10	7.50	6.00	3.00	4.80	4.00
CaO	3.35	9.36	9.40	3.46	5.71	5.75
Na ₂ O	4.51	1.41	2.76	3.70	2.82	2.91
K ₂ O	0.32	0.44	0.12	0.35	0.21	0.21
P ₂ O ₅	0.14	0.04	0.13	0.12	0.11	0.14
Total	100.84	101.61	99.76	98.74	100.13	99.86

*Total Iron as Fe₂O₃.

Trace Elements

Nb	2.8	1.4	1.8	2.4	2.1	2.0
Zr	146	44	102	149	102	106
Y	44.6	14.8	32.1	45.8	34.1	41.6
Sr	93	65	108	88	98	108
Rb	0.9	11.2	1.3	2.9	2.7	4.7
Ga	17.3	13.2	17.1	17.6	18.1	19.1
Zn	90	9	104	90	88	97
Cr	11	36	24	9	8	8
V	14	264	329	57	288	331
La	4.3	0	2.7	5.1	3.0	2.3
Ce	13.0	2.1	13.1	14.7	11.3	13.1
Nd	16.9	3.6	11.6	16.1	11.7	11.0
Ba	54	23	43	56	50	51

Selected Trace Element Ratios

Zr:Nb	52	31	57	62	49	53
Zr:Y	3.3	3.0	3.2	3.3	3.0	2.5
Y:Nb	15.9	10.6	17.8	19.1	16.2	20.8
Ti:Zr	26	85	88	32	74	89

TR2-1 : Flow in LPL.

TR2-CHM: Chilled margin of dyke in LPL.

TR2-2A: Fresh dyke in LPL.

TR2-2B: Central parts of thick, weakly iron stained dyke in LPL.

TR2-3: Massive dyke in LPL. General environment of weak iron staining.

TR2-4: Dyke in LPL. Area celadonite patchily gossanised.

Major Elements

Ox. %	TR2-5A	TR2-5B	TR2-6	TR2-7	TR2-8	TR2-9
SiO ₂	65.00	73.90	55.15	64.95	56.30	52.50
TiO ₂	0.82	0.82	1.69	1.58	1.26	1.50
Al ₂ O ₃	12.95	12.40	14.70	14.25	13.75	14.00
Fe ₂ O ₃	8.79	5.12	11.19	7.91	11.70	12.93
MnO	0.16	0.06	0.18	0.10	0.19	0.22
MgO	0.80	1.90	7.70	3.35	6.80	10.00
CaO	4.26	3.42	4.39	5.43	3.71	3.39
Na ₂ O	4.20	3.92	2.46	3.14	3.49	3.42
K ₂ O	0.61	0.45	0.58	0.22	1.15	0.55
P ₂ O ₅	0.16	0.18	0.11	0.14	0.12	0.11
Total	97.75	102.17	98.15	101.07	98.47	98.62

Total Iron as Fe₂O₃.

Trace Elements

Nb	3.5	2.7	1.8	2.4	1.5	1.8
Zr	172	163	101	113	95	92
Y	60.8	52.4	34.8	34.4	34.3	31.2
Sr	91	89	80	110	75	73
Rb	8.7	10.4	3.6	2.0	5.5	2.5
Ga	18.6	16.9	17.1	20.0	17.2	17.8
Zn	101	80	100	97	48	141
Cr	9	8	6	7	7	12
V	0	0	161	228	273	495
La	4.5	4.9	4.4	2.4	2.9	1.1
Ce	20.4	20.0	13.8	16.1	10.3	8.1
Nd	18.8	19.3	12.0	12.6	10.6	9.0
Ba	63	58	87	56	52	48

Selected Trace Element Ratios

Zr:Nb	49	60	56	47	63	51
Zr:Y	2.8	3.1	2.9	3.3	2.8	2.9
Y:Nb	17.4	19.4	19.3	14.3	22.9	17.3
Ti:Zr	29	30	100	84	80	98

TR2-5A: Fresh glassy lava (LPL).

TR2-5B: From dyke cutting 5A.

TR2-6: Massive dyke in Sheeted Complex.

TR2-7: Dyke in LPL. General area weakly iron stained.

TR2-8: Massive dyke in slightly iron stained Sheeted Complex.

TR2-9: Massive dyke in Sheeted Complex. Rare sulphide crystals.

Major Elements

Ox. %	TR2-10	TR2-11	TR2-12	TR2-13	TR2-14	TR2-15
SiO ₂	55.05	50.40	53.55	69.35	58.05	54.05
TiO ₂	1.46	0.84	1.37	0.77	0.80	1.28
Al ₂ O ₃	13.20	14.30	13.60	13.75	15.00	14.45
Fe ₂ O ₃	11.87	14.62	12.71	7.32	12.00	13.24
MnO	0.18	0.36	0.17	0.04	0.08	0.13
MgO	6.20	9.90	6.80	1.80	7.15	7.10
CaO	3.99	5.44	5.20	4.53	5.84	5.40
Na ₂ O	4.89	1.35	3.78	3.00	3.43	3.85
K ₂ O	0.02	0.54	0.01	1.04	0.17	0.25
P ₂ O ₅	0.11	0.06	0.10	0.12	0.06	0.09
Total	96.97	97.81	97.29	101.72	102.58	99.84

*Total Iron as Fe₂O₃.

Trace Elements

Nb	1.1	1.1	2.3	2.3	1.6	1.8
Zr	92	56	81	146	51	74
Y	34.1	18.2	26.8	53.2	19.2	23.2
Sr	48	67	78	114	112	108
Rb	0.6	4.2	1.2	3.1	1.7	2.2
Ga	16.8	17.8	18.6	15.2	16.0	17.9
Zn	117	66	81	20	26	33
Cr	5	39	9	12	13	15
V	408	382	476	32	356	496
La	2.6	0.1	1.7	3.9	0	1.4
Ce	10.3	6.6	11.8	19.1	3.7	7.3
Nd	10.1	4.5	8.7	14.9	3.7	7.0
Ba	27	33	22	16	23	33

Selected Trace Element Ratios

Zr:Nb	84	51	35	64	32	41
Zr:Y	2.7	3.1	3.0	2.7	2.7	3.2
Y:Nb	31.0	16.5	11.6	23.1	12.0	12.9
Ti:Zr	95	90	101	32	94	104

TR2-10: Dyke in generally unmineralized Sheeted Complex.
 TR2-11: Dyke in superficially iron stained Sheeted Complex.
 TR2-12: Dyke in weakly iron stained Sheeted Complex.
 TR2-13: Leucocratic coarse intrusive in Diabase.
 TR2-14: Diabase dyke.
 TR2-15: Diabase dyke. General area superficially iron stained.

Major Elements

Ox. %	TR2-16	TR2-17	TR2-18	TR2-19	TR2-20	TR2-21
SiO ₂	59.70	55.85	52.10	68.90	58.40	62.85
TiO ₂	1.50	0.62	0.63	1.27	1.68	1.51
Al ₂ O ₃	12.80	14.55	14.35	12.40	11.60	14.85
Fe ₂ O ₃ *	11.25	9.53	10.86	8.23	11.99	8.05
MnO	0.12	0.12	0.13	0.08	0.31	0.26
MgO	4.40	6.00	8.15	0.85	3.35	3.70
CaO	6.45	11.85	11.21	5.06	7.71	6.42
Na ₂ O	2.60	1.62	1.31	2.93	2.50	3.54
K ₂ O	0.98	0.94	0.10	0.45	1.24	0.27
P ₂ O ₅	0.11	0.05	0.06	0.15	0.16	0.14
Total	99.91	101.13	98.90	100.32	98.94	101.59

*Total Iron as Fe₂O₃.

Trace Elements

Nb	1.6	0.5	1.0	2.6	2.0	1.9
Zr	87	38	42	101	101	100
Y	28.7	12.4	10.2	34.5	36.0	33.3
Sr	100	74	82	104	99	109
Rb	21.6	30.0	1.8	10.9	32.5	5.4
Ga	18.2	14.3	15.2	17.6	18.6	19.7
Zn	98	53	68	84	97	101
Cr	5	85	237	8	13	6
V	410	245	255	234	298	212
La	2.7	0	0	2.7	3.0	4.2
Ce	11.8	4.2	8.2	10.8	12.9	14.0
Nd	9.3	4.1	3.8	12.5	10.3	10.8
Ba	47	21	14	50	54	56

Selected Trace Element Ratios

Zr:Nb	54	76	42	39	51	53
Zr:Y	3.0	3.1	4.1	2.9	2.8	3.0
Y:Nb	17.9	24.8	10.2	13.3	18.0	17.5
Ti:Zr	103.4	98	90	75	100	91

TR2-16: Celadonite stained dyke in LPL. Highly vesicular.

TR2-17: Medium grained dyke in LPL.

TR2-18: Dark, massive, medium grained intrusive in LPL.

TR2-19: Chilled wall of dyke in LPL. Chalcedony, celadonite and smectite in vesicles.

TR2-20: Central parts of concordant intrusive in LPL.

TR2-21: Chilled wall of dyke in LPL.

Major Elements

Ox. %	TR3-1	TR3-2	TR3-3	TR3-4	TR3-5	TR3-6
SiO ₂	62.00	64.15	64.10	62.15	54.85	54.65
TiO ₂	1.31	1.23	0.92	1.65	1.11	1.46
Al ₂ O ₃	14.05	13.20	13.70	13.65	14.10	19.00
Fe ₂ O ₃	9.04	8.01	8.27	9.09	11.49	10.40
MnO	0.11	0.09	0.11	0.07	0.06	0.03
MgO	4.20	4.10	2.50	1.40	8.95	12.40
CaO	4.52	4.23	2.14	6.96	5.56	0.66
Na ₂ O	3.15	3.36	5.56	2.93	1.59	0.18
K ₂ O	0.32	0.24	0.24	0.63	0.43	0.23
P ₂ O ₅	0.13	0.13	0.16	0.16	0.17	0.17
Total	98.83	98.74	97.70	98.69	98.31	99.18

*Total Iron as Fe₂O₃.

Trace Elements

Nb	2.5	2.4	2.4	1.5	1.9	2.4
Zr	113	122	127	105	85	98
Y	38.1	40.4	48.0	33.5	43.4	23.6
Sr	86	95	101	107	50	14
Rb	4.7	2.0	1.4	13.8	2.6	1.1
Ga	17.4	16.5	17.2	19.4	15.5	15.5
Zn	103	88	88	134	35	26
Cr	6	10	7	21	8	17
V	72	53	56	319	142	131
La	3.3	4.3	3.2	3.5	5.0	2.0
Ce	13.2	15.3	15.4	13.4	19.9	9.5
Nd	12.0	14.2	15.0	12.3	16.0	10.0
Ba	58	49	46	56	25	25

Selected Trace Element Ratios

Zr:Nb	45	51	53	70	45	41
Zr:Y	3.0	3.0	2.6	3.1	2.0	4.1
Y:Nb	15.2	16.8	20.0	22.3	22.8	9.8
Ti:Zr	70	60.4	43	94	78	89

TR3-1: Central parts of dyke in LPL.

TR3-2: Chilled margin of thick dyke in iron stained LPL.

TR3-3: Dyke in generally iron stained LPL.

TR3-4: Central parts of flow in LPL.

TR3-5: Upper part of pillow in regionally propylitised LPL.

TR3-6: Large dyke in same area as 3-5.

Major Elements

Ox. %	TR3-7	TR3-8	TR3-9	TR3-10	TR3-11	TR3-12
SiO ₂	59.30	54.15	71.90	53.55	74.85	56.60
TiO ₂	1.20	1.52	0.53	0.48	0.40	0.60
Al ₂ O ₃	14.30	13.80	12.60	14.30	13.55	15.40
Fe ₂ O ₃	10.09	12.87	6.92	9.88	5.40	9.02
MnO	0.17	0.19	0.04	0.16	0.01	0.10
MgO	5.00	8.40	1.10	10.90	1.00	8.10
CaO	2.06	3.92	1.60	9.38	4.74	8.76
Na ₂ O	4.01	3.68	7.14	2.18	2.66	2.49
K ₂ O	0.58	0.22	0.05	0.53	1.42	0.25
P ₂ O ₅	0.18	0.12	0.11	0.04	0.11	0.06
Total	96.89	98.87	101.99	101.40	104.14	101.38

*Total Iron as Fe₂O₃.

Trace Elements

Nb	2.4	2.0	3.0	1.1	2.6	1.4
Zr	127	98	192	36	93	51
Y	44.1	33.1	62.5	9.6	37.4	14.2
Sr	91	102	68	94	167	141
Rb	3.7	1.5	0.5	2.5	6.2	0.9
Ga	18.2	18.9	15.5	14.3	16.4	16.4
Zn	109	76	22	61	10	17
Cr	9	8	39	200	16	26
V	34	442	3	266	0	265
La	3.7	2.2	5.0	0.5	2.1	0.9
Ce	18.2	11.8	25.0	3.8	7.5	6.4
Nd	14.6	9.5	20.7	3.1	9.8	4.2
Ba	46	45	10	17	11	20

Selected Trace Element Ratios

Zr:Nb	53	49	64	33	36	36
Zr:Y	2.9	3.0	3.1	3.8	2.5	3.6
Y:Nb	18.4	16.6	20.8	8.7	14.4	10.1
Ti:Zr	57	93	17	80	26	71

TR3-7: Central parts of dyke in LPL.

TR3-8: Diabase dyke, fresh, from area of weak propylitisation.

TR3-9: Siliceous, fine, diabase dyke.

TR3-10: Middle part of coarse grained dyke in Sheeted Complex.

TR3-11: Central part of leucocratic, epidotised dyke.

TR3-12: Gabbro.

Major Elements

Ox. %	TR3-13	TR3-14	TR3-15	TR3-16	TR3-17	TR3-18
SiO ₂	53.05	53.00	70.90	55.40	61.95	76.75
TiO ₂	0.38	0.32	0.65	1.30	1.28	0.25
Al ₂ O ₃	15.50	15.40	14.35	14.40	13.60	12.40
Fe ₂ O ₃	10.28	8.05	5.84	12.61	9.55	5.15
MnO	0.17	0.12	0.03	0.10	0.06	0.02
MgO	9.90	13.05	1.50	7.70	3.15	0.40
CaO	12.04	13.37	3.55	6.34	11.70	2.72
Na ₂ O	1.31	0.89	5.27	2.94	0.08	4.22
K ₂ O	0.09	0.10	0.26	0.41	0.01	0.18
P ₂ O ₅	0.04	0.03	0.14	0.10	0.21	0.06
Total	102.76	104.33	102.49	101.30	101.59	102.15

*Total Iron as Fe₂O₃.

Trace Elements

Nb	1.1	1.0	1.6	1.7	1.7	4.2
Zr	33	25	98	83	102	70
Y	9.1	4.7	40.9	26.8	35.5	40.5
Sr	80	61	109	113	203	84
Rb	1.1	0.9	1.5	2.5	0.4	0.5
Ga	14.2	11.9	15.2	16.7	14.4	11.5
Zn	43	33	17	28	17	19
Cr	43	374	11	9	11	14
V	198	176	40	457	115	0
La	0.6	0	1.4	1.7	3.2	1.4
Ce	1.1	1.7	12.1	7.9	10.1	5.9
Nd	3.3	1.4	11.1	8.7	9.1	6.8
Ba	12	10	22	28	16	21

Selected Trace Element Ratios

Zr:Nb	30	25	61	49	60	17
Zr:Y	3.6	5.3	2.4	3.1	2.9	1.7
Y:Nb	8.3	4.7	25.6	15.8	20.9	9.6
Ti:Zr	69	77	40	94	75	21

TR3-13: Gabbro.

TR3-14: Massive gabbro.

TR3-15: From granophyric mass associated with gabbro.

TR3-16: Diabase dyke.

TR3-17: Medium grained diabase dyke.

TR3-18: Weakly altered granophyre.

Major Elements

Ox. %	TR4-1	TR4-2	TR4-3	TR4-4	TR4-5	TR4-6
SiO ₂	61.80	56.95	54.45	61.70	54.35	55.35
TiO ₂	1.28	1.48	1.26	1.08	1.05	0.91
Al ₂ O ₃	13.50	13.80	14.60	13.05	13.20	14.20
Fe ₂ O ₃	9.17	11.24	12.93	10.69	11.76	10.85
MnO	0.09	0.11	0.13	0.14	0.17	0.14
MgO	4.00	5.75	8.20	3.05	8.60	6.90
CaO	5.05	6.95	4.85	3.18	6.46	5.68
Na ₂ O	3.45	2.90	3.14	6.33	2.92	4.53
K ₂ O	0.80	0.49	0.30	0.06	0.30	0.40
P ₂ O ₅	0.15	0.11	0.10	0.26	0.93	0.08
Total	99.29	99.78	99.96	99.54	99.74	99.04

*Total Iron as Fe₂O₃.

Trace Elements

Nb	2.7	1.2	1.8	2.5	1.6	0.8
Zr	113	84	79	124	80	65
Y	36.6	24.0	25.3	47.5	25.2	20.2
Sr	107	105	94	80	97	149
Rb	16.8	8.6	1.2	0.5	3.0	3.2
Ga	18.5	18.2	19.4	16.6	16.8	14.8
Zn	100	82	20	53	43	28
Cr	20	25	8	9	50	26
V	81	453	498	86	360	340
La	3.5	1.1	2.1	2.8	1.2	0.8
Ce	15.1	7.0	10.5	20.5	10.6	5.7
Nd	13.1	7.7	7.5	15.5	7.2	7.0
Ba	52	42	35	20	32	29

Selected Trace Element Ratios

Zr:Nb	42	70	44	50	50	81
Zr:Y	3.1	3.5	3.1	2.6	3.2	3.2
Y:Nb	13.6	20.0	14.0	19.0	15.8	25.3
Ti:Zr	68	106	96	52	79	84

TR4-1: Massive flow in LPL.

TR4-2: Massive dyke in LPL.

TR4-3: Medium grained dyke in Sheeted Complex.

TR4-4: Fine grained diabase dyke in very weakly iron stained Sheeted Complex.

TR4-5: Medium to fine grained dyke in Sheeted Complex.

TR4-6: Medium grained dyke in Sheeted Complex.

Major Elements

Ox. %	TR4-7	TR4-8	TR4-9	TR4-10	TR4-11	TR4-11DY
SiO ₂	55.60	63.45	67.80	69.25	55.10	52.25
TiO ₂	1.11	0.93	0.68	0.44	1.33	0.93
Al ₂ O ₃	12.90	13.05	12.90	12.10	15.55	13.20
Fe ₂ O ₃ [*]	12.18	9.16	7.12	6.54	10.73	11.39
MnO	0.15	0.09	0.08	0.11	0.18	0.17
MgO	6.40	2.60	1.50	1.05	7.20	10.90
CaO	3.40	2.75	3.59	0.83	6.59	9.17
Na ₂ O	4.35	6.27	4.97	6.39	3.19	2.18
K ₂ O	0.24	0.20	0.14	0.09	0.52	0.43
P ₂ O ₅	0.10	0.15	0.17	0.09	0.19	0.07
Total	96.43	98.65	98.95	96.89	100.58	100.69

*Total Iron as Fe₂O₃.

Trace Elements

Nb	1.7	2.0	2.3	2.9	1.8	1.3
Zr	78	112	131	157	68	56
Y	26.5	40.2	45.6	53.3	24.6	21.8
Sr	122	80	101	57	106	69
Rb	1.3	0.9	1.0	0.9	4.9	3.7
Ga	17.2	17.5	16.9	17.0	17.8	17.5
Zn	40	25	21	44	67	62
Cr	8	13	14	14	16	90
V	440	196	21	0	283	306
La	2.1	2.1	3.2	4.1	1.9	0
Ce	10.1	11.4	17.6	17.7	11.3	6.0
Nd	8.2	12.3	15.3	15.9	8.1	5.8
Ba	35	30	34	11	45	23

Selected Trace Element Ratios

Zr:Nb	46	56	57	54	38	43
Zr:Y	2.9	2.8	2.9	2.9	2.8	2.6
Y:Nb	15.6	20.1	19.8	18.4	13.7	16.8
Ti:Zr	85	50	31	17	117	100

TR4-7: Medium grained dyke in Sheeted Complex. Some weathering.

TR4-8: Weakly iron stained dyke in Sheeted Complex.

TR4-9: Fine grained diabase dyke.

TR4-10: Medium grained dyke in Sheeted Complex.

TR4-11: Coarse melanocratic gabbro.

TR4-11DY: Fine melanocratic dyke cutting the gabbro of 4-11.

Major Elements

Ox. %	TR4-12	TR4-13	TR4-14	TR4-15	TR4-16	TR4-17
SiO ₂	51.55	52.25	73.30	71.95	53.20	51.70
TiO ₂	0.71	0.64	0.34	0.29	0.87	0.49
Al ₂ O ₃	15.05	14.60	11.80	11.00	13.20	15.90
Fe ₂ O ₃ *	10.56	10.13	4.66	4.12	12.43	9.75
MnO	0.12	0.16	0.05	0.01	0.16	0.16
MgO	11.90	11.00	0.60	0.40	6.90	9.95
CaO	5.76	11.46	1.71	1.59	10.11	9.08
Na ₂ O	3.67	1.29	6.24	6.22	0.14	2.11
K ₂ O	0.45	0.18	0.03	0.07	0.00	0.38
P ₂ O ₅	0.05	0.05	0.08	0.06	0.07	0.04
Total	99.82	101.76	98.81	95.71	97.08	99.56

*Total Iron as Fe₂O₃.

Trace Elements

Nb	1.1	0.6	3.0	3.8	1.1	1.2
Zr	45	42	147	230	54	37
Y	13.4	10.6	51.5	74.9	15.8	9.5
Sr	107	77	50	85	156	100
Rb	2.1	1.6	0.7	0.00	1.4	2.8
Ga	13.3	14.6	14.1	15.8	16.0	14.5
Zn	29	41	25	12	71	76
Cr	117	107	11	10	44	85
V	322	314	4	3	341	257
La	0.3	0.4	3.9	1.3	0	0.1
Ce	5.1	8.2	13.6	9.5	4.1	5.3
Nd	4.2	4.8	15.6	12.2	4.3	3.2
Ba	30	17	4	10	11	12

Selected Trace Element Ratios

Zr:Nb	41	70	49	61	49	31
Zr:Y	3.4	4.0	2.8	3.1	3.4	3.9
Y:Nb	12.2	17.7	17.2	19.7	14.4	7.9
Ti:Zr	95	91	14	8	97	79

TR4-12: Medium grained diabase dyke.

TR4-13: Medium grained gabbro.

TR4-14: Epidotised plagiogranite.

TR4-15: Plagiogranite intrusive in diabase.

TR4-16: Altered iron stained medium grained intrusive. Sheeted Complex.

TR4-17: Melanocratic gabbro, fresh to weakly altered.

Major Elements

Ox. %	TR4-18	TR4-19	TR4-20	TR5-1	TR5-2	TR5-3
SiO ₂	52.45	51.50	49.30	49.20	48.75	48.40
TiO ₂	0.41	0.51	0.27	0.13	0.11	0.12
Al ₂ O ₃	13.80	15.20	15.60	19.30	20.20	22.20
Fe ₂ O ₃	9.84	9.54	8.78	5.59	6.08	5.64
MnO	0.16	0.16	0.15	0.11	0.12	0.11
MgO	11.35	7.80	10.00	8.90	9.55	8.00
CaO	11.33	11.69	14.58	18.40	15.57	15.80
Na ₂ O	1.21	1.58	0.86	0.70	0.85	0.96
K ₂ O	0.23	0.10	0.03	0.00	0.01	0.02
P ₂ O ₅	0.04	0.05	0.03	0.02	0.02	0.02
Total	100.82	98.13	99.60	102.35	101.26	101.27

*Total Iron as Fe₂O₃.

Trace Elements

Nb	0.9	1.0	1.4	0.7	1.0	0.4
Zr	34	37	23	17	17	19
Y	8.8	9.4	4.1	0	0	0
Sr	99	83	64	62	69	69
Rb	1.3	1.7	0.9	0.6	0.5	1.3
Ga	13.1	14.4	12.5	11.5	12.8	13.6
Zn	62	84	49	27	31	29
Cr	262	235	461	771	200	121
V	244	272	204	129	104	101
La	0.4	0	0	0	0	0
Ce	0	4.4	0	0.4	1.0	0
Nd	1.1	4.2	2.9	1.5	2.0	1.0
Ba	13	18	7	5	4	5

Selected Trace Element Ratios

Zr:Nb	38	37	16	24	17	48
Zr:Y	3.9	3.9	5.6	--	--	--
Y:Nb	9.8	5.6	2.9	0	0	0
Ti:Zr	72	83	70	46	39	38

TR4-18: Fresh gabbro.

TR4-19: Fresh tough melanocratic gabbro.

TR4-20: Weakly altered coarse grained melanocratic gabbro.

TR5-1: Massive gabbro.

TR5-2: Massive, unlayered gabbro.

TR5-3: Massive gabbro.

Major Elements

Ox. %	TR5-4	TR5-5	TR5-6	TR5-7	TR5-8	TR5-9
SiO ₂	50.90	51.70	54.05	64.85	51.35	52.50
TiO ₂	0.24	0.45	0.68	0.78	0.63	0.87
Al ₂ O ₃	17.80	15.40	13.90	13.70	14.50	14.20
Fe ₂ O ₃	9.28	10.12	11.02	9.02	10.31	10.81
MnO	0.18	0.16	0.17	0.06	0.15	0.16
MgO	9.10	8.50	7.60	2.50	13.80	11.55
CaO	13.36	10.95	6.34	4.82	4.78	4.71
Na ₂ O	1.11	2.26	3.50	4.18	2.05	2.73
K ₂ O	0.10	0.21	0.55	0.17	1.08	0.09
P ₂ O ₅	0.03	0.04	0.06	0.11	0.06	0.07
Total	102.10	99.79	97.87	100.19	98.71	97.69

*Total Iron as Fe₂O₃.

Trace Elements

Nb	0.9	0.8	1.7	2.4	1.4	1.6
Zr	26	33	52	82	47	64
Y	4.5	8.6	16.5	30.2	12.8	18.7
Sr	76	120	113	108	91	79
Rb	3.0	2.2	3.5	2.6	7.0	1.5
Ga	14.9	13.7	16.4	17.9	15.4	16.5
Zn	91	30	54	22	94	67
Cr	64	28	19	11	72	31
V	157	296	338	68	309	355
La	0	0.3	0.2	2.1	1.0	1.8
Ce	0	6.0	8.7	8.9	6.4	5.8
Nd	2.8	4.5	5.6	8.2	4.8	6.8
Ba	16	16	22	31	29	26

Selected Trace Element Ratios

Zr:Nb	29	41	31	34	34	40
Zr:Y	5.8	3.8	3.2	2.7	3.7	3.4
Y:Nb	5.0	10.8	9.7	12.6	9.1	11.7
Ti:Zr	55	82	78	57	80	82

TR5-4: Gabbro, from main body.

TR5-5: Gabbro.

TR5-6: Medium grained diabase dyke.

TR5-7: Fine grained massive diabase dyke.

TR5-8: Diabase dyke, friable, somewhat altered.

TR5-9: Medium grained dyke in Sheeted Complex. Area moderately iron stained.

Major Elements

Ox. %	TR5-10	TR5-11	TR5-12	TR5-13	TR5-14	TR5-15
SiO ₂	59.40	51.10	54.35	51.40	52.90	55.60
TiO ₂	0.97	0.97	1.09	1.41	1.17	1.38
Al ₂ O ₃	13.30	13.30	14.30	14.10	13.55	13.20
Fe ₂ O ₃	9.24	12.21	10.58	13.12	12.60	11.87
MnO	0.08	0.17	0.14	0.15	0.18	0.11
MgO	6.60	11.50	8.20	9.70	8.70	9.20
CaO	6.66	4.39	4.09	3.35	4.47	5.96
Na ₂ O	2.47	2.50	2.46	2.44	3.62	2.31
K ₂ O	0.55	0.97	1.20	0.50	0.07	0.08
P ₂ O ₅	0.08	0.07	0.13	0.10	0.09	0.10
Total	99.35	97.18	96.54	96.27	97.35	99.81

*Total Iron as Fe₂O₃.

Trace Elements

Nb	1.5	0.8	1.9	1.5	1.2	1.6
Zr	71	59	97	88	75	83
Y	24.2	18.9	30.2	22.9	23.1	25.9
Sr	98	84	105	88	97	112
Rb	7.0	5.0	4.9	2.8	1.0	1.0
Ga	14.7	17.1	17.4	18.6	17.9	17.7
Zn	58	74	93	342	83	99
Cr	15	21	33	20	10	9
V	270	476	293	520	497	460
La	1.2	0.1	3.4	2.9	2.0	1.4
Ce	6.6	7.3	7.8	10.1	11.8	8.6
Nd	7.3	6.7	9.1	10.0	8.0	8.9
Ba	28	59	51	38	30	43

Selected Trace Element Ratios

Zr:Nb	47	74	51	59	63	52
Zr:Y	2.9	3.1	3.2	3.8	3.2	3.2
Y:Nb	16.1	23.6	15.9	15.3	19.3	16.2
Ti:Zr	82	99	67	96	94	100

TR5-10: Margin of dyke in LPL.

TR5-11: Medium grained diabase dyke.

TR5-12: Weakly iron stained dyke in Sheeted Complex.

TR5-13: Medium grained weakly iron stained dyke. Sheeted Complex.

TR5-14: Weakly iron stained pyritised dyke in Sheeted Complex.

TR5-15: Fine, vesicular dyke in iron stained Sheeted Complex.

Major Elements

Ox. %	TR5-16	TR5-17	TR5-18	TR5-19	TR5-20	TR5-20A
SiO ₂	54.80	61.10	53.05	58.55	52.55	50.90
TiO ₂	1.62	1.10	1.18	1.45	0.61	0.70
Al ₂ O ₃	13.15	13.25	13.60	13.05	13.45	13.35
Fe ₂ O ₃ *	13.02	9.27	12.18	11.15	8.72	10.14
MnO	0.14	0.11	0.18	0.14	0.16	0.23
MgO	5.95	5.75	8.30	4.35	11.75	8.45
CaO	6.86	6.68	5.45	6.56	10.17	13.14
Na ₂ O	1.84	1.95	2.59	2.92	1.35	1.58
K ₂ O	0.06	0.12	0.15	1.30	0.10	0.66
P ₂ O ₅	0.11	0.08	0.10	0.12	0.06	0.07
Total	97.55	99.41	96.78	99.59	98.92	99.22

*Total Iron as Fe₂O₃.

Trace Elements

Nb	1.9	1.3	1.6	2.0	1.6	1.1
Zr	82	67	81	90	44	51
Y	20.6	16.8	23.9	30.8	11.8	14.6
Sr	115	101	101	112	92	95
Rb	1.6	1.6	1.0	31.1	1.1	12.0
Ga	18.8	16.8	18.4	19.3	14.7	14.4
Zn	99	84	114	91	56	63
Cr	14	20	15	13	236	182
V	465	323	450	301	220	225
La	1.0	0.1	2.0	3.6	1.2	1.3
Ce	8.9	8.6	11.6	9.5	4.9	6.2
Nd	8.3	8.7	7.9	8.9	4.4	6.5
Ba	35	34	31	53	19	24

Selected Trace Element Ratios

Zr:Nb	43	52	51	45	28	46
Zr:Y	4.0	4.0	3.4	2.9	3.7	3.5
Y:Nb	10.8	12.9	14.9	15.4	7.4	13.3
Ti:Zr	118	98	87	97	83	82

TR5-16: Centre of pillow in celadonite stained LPL.

TR5-17: Edge of thin dyke in LPL.

TR5-18: Weakly iron stained dyke in Sheeted Complex.

TR5-19: Edge of celadonite stained dyke in LPL.

TR5-20: Central parts of dyke in LPL.

TR5-20A: Edge of dyke in 5-20.

Major Elements

Ox. %	TR6-1	TR6-2	TR6-3	TR6-4	TR6-5	TR6-6
SiO ₂	50.55	52.80	61.40	68.35	58.45	61.15
TiO ₂	0.89	0.33	1.09	0.82	1.23	1.08
Al ₂ O ₃	17.00	16.00	14.80	13.30	14.30	12.50
Fe ₂ O ₃	12.87	9.88	10.17	8.75	12.28	11.53
MnO	0.16	0.17	0.12	0.07	0.12	0.16
MgO	9.35	10.20	4.10	1.60	5.20	5.80
CaO	13.25	12.86	6.61	3.83	3.54	9.13
Na ₂ O	1.13	1.12	3.40	5.63	4.74	0.07
K ₂ O	0.07	0.06	0.22	0.00	0.00	0.00
P ₂ O ₅	0.03	0.03	0.08	0.10	0.13	0.08
Total	105.30	103.45	101.99	102.45	99.99	101.50

*Total Iron as Fe₂O₃.

Trace Elements

Nb	0.9	1.1	1.8	2.0	1.5	1.3
Zr	23	28	63	75	96	68
Y	4.7	7.3	20.7	33.4	33.5	20.8
Sr	68	68	91	85	57	145
Rb	2.6	2.0	2.6	0.6	0.7	0.8
Ga	16.9	14.0	17.9	16.4	16.9	15.3
Zn	69	61	25	21	37	22
Cr	77	131	11	9	8	16
V	718	184	230	41	372	372
La	0	0	0	0.8	3.0	1.8
Ce	0.5	4.8	7.0	12.3	14.3	6.0
Nd	1.5	3.6	4.6	9.8	10.5	6.4
Ba	17	9	32	10	20	13

Selected Trace Element Ratios

Zr:Nb	26	26	35	38	64	52
Zr:Y	4.9	3.8	3.0	2.2	2.9	3.3
Y:Nb	5.2	6.6	11.5	16.7	22.3	16.0
Ti:Zr	232	71	104	66	77	95

TR6-1: Massive, coarse, melanocratic gabbro.

TR6-2: Massive, medium grained gabbro.

TR6-3: Medium grained diabase dyke.

TR6-4: Massive, fine grained diabase dyke.

TR6-5: Medium grained diabase dyke.

TR6-6: Medium grained diabase dyke.

Major Elements

Ox. %	TR6-7	TR6-8	TR6-9	TR6-10	TR6-11	TR6-12
SiO ₂	59.75	61.05	57.50	58.15	53.45	56.55
TiO ₂	0.90	1.09	0.96	0.98	0.97	1.06
Al ₂ O ₃	14.00	14.70	14.10	13.80	14.80	12.85
Fe ₂ O ₃	12.06	11.32	9.61	12.45	12.95	15.30
MnO	0.07	0.09	0.13	0.12	0.18	0.13
MgO	6.15	3.60	7.00	4.35	4.40	7.90
CaO	10.25	5.15	6.05	5.64	11.97	6.99
Na ₂ O	0.07	4.61	4.74	4.45	3.12	0.24
K ₂ O	0.08	0.40	0.22	0.03	0.01	0.00
P ₂ O ₅	0.06	0.10	0.08	0.09	0.08	0.07
Total	103.39	102.11	100.39	100.06	101.93	101.09

*Total Iron as Fe₂O₃.

Trace Elements

Nb	1.6	1.7	1.2	1.0	1.4	1.9
Zr	57	77	69	67	57	57
Y	19.4	25.2	22.3	23.2	22.7	27.5
Sr	159	113	96	85	222	121
Rb	2.1	2.3	1.3	0.8	1.6	2.1
Ga	17.7	15.1	13.5	18.1	23.5	15.9
Zn	15	23	29	23	34	25
Cr	13	7	11	8	7	11
V	453	163	281	358	551	412
La	0.4	1.8	1.2	1.6	0.7	0
Ce	5.4	5.4	6.9	8.2	4.9	9.5
Nd	4.7	6.9	7.5	6.9	6.1	5.3
Ba	10	22	16	14	17	9

Selected Trace Element Ratios

Zr:Nb	36	45	58	67	41	30
Zr:Y	2.9	3.1	3.1	2.9	2.5	2.1
Y:Nb	12.1	14.8	18.6	23.2	16.2	14.5
Ti:Zr	95	85	83	88	102	111

TR6-7: Medium grained diabase dyke.

TR6-8: Medium grained diabase dyke.

TR6-9: Medium grained diabase dyke.

TR6-10: Medium grained, epidotised diabase dyke.

TR6-11: Slightly altered diabase dyke.

TR6-12: Much altered, epidotised, sheared, friable intrusive.

Major Elements

Ox. %	TR6-13	TR6-14	TR6-15	TR6-17	TR6-18	TR6-19
SiO ₂	55.05	55.70	56.40	47.30	60.90	63.20
TiO ₂	0.85	0.81	0.99	0.56	0.85	1.16
Al ₂ O ₃	14.55	13.80	13.65	17.60	13.90	14.10
Fe ₂ O ₃	13.97	15.82	12.77	17.44	10.17	9.20
MnO	0.41	0.24	0.11	0.06	0.21	0.10
MgO	8.20	7.00	7.70	14.60	5.35	4.45
CaO	1.75	1.43	9.40	0.79	5.39	5.31
Na ₂ O	1.80	1.65	0.15	1.13	2.61	2.82
K ₂ O	0.25	0.02	0.00	1.22	0.27	0.55
P ₂ O ₅	0.07	0.07	0.09	0.04	0.09	0.10
Total	96.90	96.54	101.26	100.74	99.74	100.99

*Total Iron as Fe₂O₃.

Trace Elements

Nb	1.7	1.7	1.7	1.8	2.6	2.3
Zr	55	56	59	36	73	75
Y	52.9	20.7	23.8	11.4	26.3	29.7
Sr	33	34	150	53	89	85
Rb	3.1	1.2	2.1	7.0	4.4	12.8
Ga	15.9	15.6	17.0	12.5	17.2	17.8
Zn	175	74	19	22	180	105
Cr	15	12	21	60	12	7
V	396	395	352	317	193	244
La	2.5	0	1.2	0	2.1	2.0
Ce	9.7	9.8	8.2	7.3	10.6	10.3
Nd	9.2	3.3	5.0	0.7	8.1	8.3
Ba	34	7	14	16	38	42

Selected Trace Element Ratios

Zr:Nb	32	33	35	20	28	33
Zr:Y	1.0	2.7	2.5	3.2	2.8	2.5
Y:Nb	31.1	12.2	14.0	6.3	10.1	12.9
Ti:Zr	93	87	101	93	70	93

TR6-13: Altered, epidotised, friable intrusive. Sheeted Complex.
 TR6-14: Strongly mineralized dyke in Sheeted Complex.
 TR6-15: Densely impregnated dyke in Sheeted Complex.
 TR6-17: Intensely propylitised, epidotised Sheeted Complex.
 TR6-18: Vesicular, weakly iron stained concordant intrusive. LPL.
 TR6-19: Green stained concordant intrusive in LPL.

Major Elements

Ox. %	TR7-1A	TR7-1B	TR7-2	TR7-3	TR7-4	TR7-5
SiO ₂	55.20	59.05	54.90	59.20	68.75	64.45
TiO ₂	0.86	0.98	0.77	0.92	0.60	0.67
Al ₂ O ₃	15.40	13.70	13.20	14.20	12.90	14.70
Fe ₂ O ₃	11.97	11.50	12.31	10.66	6.97	7.60
MnO	0.19	0.16	0.19	0.16	0.10	0.09
MgO	7.20	3.55	6.50	4.20	2.00	3.60
CaO	9.24	4.02	4.57	4.16	2.10	4.53
Na ₂ O	1.80	6.55	4.16	5.67	5.68	4.02
K ₂ O	0.06	0.02	0.12	0.01	0.06	0.06
P ₂ O ₅	0.06	0.08	0.07	0.08	0.11	0.10
Total	101.98	99.61	96.79	99.26	99.27	99.82

*Total Iron as Fe₂O₃.

Trace Elements

Nb	1.7	1.9	1.4	2.2	2.7	1.7
Zr	41	57	49	60	81	67
Y	17.5	23.8	19.3	24.5	29.5	28.2
Sr	84	54	94	65	81	37
Rb	1.3	0.4	2.0	0.7	0.3	0.7
Ga	17.7	16.9	15.4	17.7	13.2	16.4
Zn	59	92	53	121	42	403
Cr	15	11	22	8	8	8
V	389	324	398	310	45	143
La	0.1	1.8	0.8	0.9	1.9	1.6
Ce	7.2	5.5	4.0	5.1	11.4	6.4
Nd	5.5	6.0	5.4	5.7	9.5	7.6
Ba	14	18	18	15	8	12

Selected Trace Element Ratios

Zr:Nb	24	30	35	27	30	39
Zr:Y	2.3	2.4	2.5	2.4	2.7	2.4
Y:Nb	10.3	12.5	13.8	11.1	10.8	16.6
Ti:Zr	126	103	94	92	44	60

TR7-1A: Fresh doleritic dyke in Sheeted Complex.

TR7-1B: Diabase dyke from area of 7-1A.

TR7-2: Central parts of diabase dyke.

TR7-3: Medium grained dyke in Sheeted Complex.

TR7-4: Fine grained, weakly pyritised diabase dyke.

TR7-5: Medium grained diabase dyke. Area weakly mineralized.

Major Elements

Ox. %	TR7-6	TR7-7	TR7-8	TR7-9	TR7-10	TR7-11
SiO ₂	58.95	59.00	57.80	54.40	52.35	51.65
TiO ₂	1.05	1.05	1.03	1.10	0.66	0.59
Al ₂ O ₃	14.30	14.50	14.00	13.90	15.70	15.35
Fe ₂ O ₃	11.95	11.31	11.09	12.53	11.77	10.88
MnO	0.31	0.26	0.19	0.17	0.19	0.22
MgO	5.50	6.00	6.15	5.10	9.10	9.90
CaO	4.14	2.56	3.32	7.38	8.46	7.01
Na ₂ O	4.39	5.20	4.99	2.90	2.94	2.68
K ₂ O	0.14	0.00	0.01	0.03	0.16	0.16
P ₂ O ₅	0.08	0.08	0.08	0.08	0.04	0.05
Total	100.81	99.96	98.66	97.59	101.37	98.49

*Total Iron as Fe₂O₃.

Trace Elements

Nb	2.6	2.2	1.2	1.2	1.4	1.6
Zr	59	64	61	60	33	41
Y	22.9	24.7	21.9	25.0	10.3	12.6
Sr	119	64	44	29	185	113
Rb	2.0	0.8	1.1	1.2	2.7	2.1
Ga	17.2	15.2	14.3	16.4	15.0	13.7
Zn	163	463	117	89	78	64
Cr	9	8	10	11	42	103
V	488	387	341	459	397	268
La	1.1	1.0	1.4	2.2	0	0.1
Ce	7.8	9.1	7.3	8.7	4.9	4.9
Nd	5.9	6.1	6.9	8.5	3.5	3.5
Ba	22	14	21	13	34	32

Selected Trace Element Ratios

Zr:Nb	23	29	51	50	24	26
Zr:Y	2.6	2.6	2.8	2.4	3.2	3.2
Y:Nb	8.8	11.2	18.2	20.8	7.4	7.9
Ti:Zr	107	98	101	110	120	86

TR7-6: Medium grained diabase dyke.

TR7-7: Medium grained fairly friable,
weakly epidotised dyke in Sheeted Complex.

TR7-8: Fine, strongly chloritised, epidotised diabase dyke.

TR7-9: Superficially iron stained, medium to fine grained,
zeolitised dyke in Sheeted Complex.

TR7-10: Coarse grained gabbroic intrusive in Sheeted Complex.

TR7-11: Medium to fine grained diabase dyke.

Major Elements

Ox. %	TR7-12	TR7-13	TR7-14	TR7-15	TR8-1	TR8-2
SiO ₂	57.90	55.40	56.75	63.50	57.95	59.10
TiO ₂	0.75	0.74	0.91	0.81	0.72	1.31
Al ₂ O ₃	15.10	14.00	11.90	14.00	14.20	13.70
Fe ₂ O ₃ *	10.47	10.48	10.73	8.39	10.31	11.08
MnO	0.16	0.20	0.14	0.14	0.23	0.14
MgO	6.40	7.20	3.80	3.40	7.90	5.50
CaO	6.47	9.31	5.41	3.39	6.47	5.03
Na ₂ O	4.72	2.99	4.16	5.76	1.65	3.94
K ₂ O	0.21	0.00	0.00	0.01	1.92	0.59
P ₂ O ₅	0.06	0.06	0.09	0.09	0.06	0.12
Total	102.24	100.38	93.89	99.49	101.41	100.51

*Total Iron as Fe₂O₃.

Trace Elements

Nb	1.4	1.9	1.7	2.5	2.0	2.3
Zr	46	47	66	76	46	85
Y	17.4	16.8	22.3	24.6	17.2	34.2
Sr	135	123	122	85	93	84
Rb	1.8	1.4	1.1	0.5	11.1	4.0
Ga	14.9	17.4	14.2	16.8	15.2	18.7
Zn	65	127	27	96	67	66
Cr	26	29	8	15	8	8
V	364	312	344	142	342	315
La	1.2	0.4	0	1.0	2.1	2.3
Ce	7.3	6.7	11.6	11.1	7.5	10.9
Nd	5.8	6.0	9.0	9.1	5.7	9.6
Ba	28	11	18	12	87	58

Selected Trace Element Ratios

Zr:Nb	33	25	39	30	23	37
Zr:Y	2.6	2.8	3.0	3.1	2.7	2.5
Y:Nb	12.4	8.8	13.1	9.8	8.6	14.9
Ti:Zr	98	94	83	64	94	92

TR7-12: Fine grained, weakly pyritised diabase dyke.

TR7-13: Medium grained epidotised intrusive in Sheeted Complex.

TR7-14: Fine grained diabase dyke. Some malachite staining.

TR7-15: Epidotised, medium grained dyke in Sheeted Complex.

TR8-1: Central parts of dyke in LPL.

TR8-2: Central parts of concordant intrusive in LPL.

Major Elements

Ox. %	TR8-3	TR8-4	TR8-5	TR8-6	TR8-7	TR8-8
SiO ₂	59.70	58.60	55.60	51.85	59.55	52.25
TiO ₂	1.31	1.27	1.37	0.73	1.47	0.63
Al ₂ O ₃	14.65	14.15	13.55	14.75	13.50	15.50
Fe ₂ O ₃	9.98	10.35	12.36	9.66	10.80	9.24
MnO	0.16	0.11	0.15	0.17	0.15	0.19
MgO	5.10	6.20	6.80	11.05	4.55	10.70
CaO	5.81	4.90	5.52	8.02	2.45	8.43
Na ₂ O	2.96	3.04	3.29	2.72	5.76	3.01
K ₂ O	0.22	0.20	0.19	0.57	0.10	0.74
P ₂ O ₅	0.10	0.12	0.09	0.06	0.15	0.05
Total	99.99	98.94	98.92	99.58	98.48	100.74

Total Iron as Fe₂O₃.

Trace Elements

Nb	2.4	2.1	2.0	1.7	2.5	1.4
Zr	72	97	67	50	107	38
Y	26.8	34.1	27.1	17.4	39.7	13.0
Sr	90	92	86	116	69	126
Rb	2.7	2.2	2.8	4.5	1.4	4.7
Ga	17.3	18.2	17.8	15.5	16.0	14.1
Zn	100	83	80	72	86	87
Cr	20	8	10	67	6	280
V	234	197	386	256	82	265
La	2.4	3.0	1.6	1.2	4.4	0.9
Ce	10.5	13.7	10.0	5.1	14.0	0.7
Nd	9.4	10.5	7.7	5.7	12.3	4.8
Ba	48	50	42	30	23	36

Selected Trace Element Ratios

Zr:Nb	30	46	34	29.4	43	27
Zr:Y	2.7	2.8	2.5	2.9	2.7	2.9
Y:Nb	11.2	16.2	13.6	10.2	15.9	9.3
Ti:Zr	109	79	123	88	82	99

TR8-3: Central parts of dyke in LPL.

TR8-4: Central parts of dyke in weakly iron stained LPL.

TR8-5: Inner parts of dyke in LPL,
transitional to Sheeted Complex.

TR8-6: Central parts of medium grained dyke in Sheeted Complex.

TR8-7: Inner parts of diabase dyke. Weak pyritic disseminations.

TR8-8: Inner parts of weakly pyritised diabase dyke.

Major Elements

Ox. %	TR8-9	TR8-10	TR8-11	TR8-12	TR8-13	TR8-14
SiO ₂	54.80	52.45	54.60	54.65	54.25	54.90
TiO ₂	1.36	0.91	1.10	1.11	1.24	0.99
Al ₂ O ₃	13.70	15.30	14.55	15.40	14.20	15.15
Fe ₂ O ₃ *	12.91	11.06	12.25	11.98	13.12	11.58
MnO	0.17	0.19	0.21	0.21	0.19	0.12
MgO	7.50	7.90	6.15	5.80	7.55	9.90
CaO	3.31	9.15	5.50	7.82	6.76	7.85
Na ₂ O	4.28	3.17	4.64	3.79	3.26	2.14
K ₂ O	0.11	0.30	0.28	0.14	0.33	0.20
P ₂ O ₅	0.09	0.08	0.08	0.09	0.09	0.07
Total	98.23	100.51	99.36	100.99	100.99	102.90

*Total Iron as Fe₂O₃.

Trace Elements

Nb	2.4	1.3	1.7	2.3	1.5	1.0
Zr	76	53	54	67	68	60
Y	29.5	20.7	21.9	25.3	25.0	21.9
Sr	43	118	52	116	108	107
Rb	0.9	2.5	3.1	1.7	3.2	1.7
Ga	17.0	17.1	17.1	18.0	19.1	16.6
Zn	78	86	111	133	126	30
Cr	14	23	16	24	12	22
V	554	326	440	381	556	403
La	1.6	1.1	0.6	1.0	1.7	1.7
Ce	11.5	9.0	8.9	7.3	8.9	7.9
Nd	9.5	7.4	5.3	7.7	7.4	7.5
Ba	21	26	30	23	29	13

Selected Trace Element Ratios

Zr:Nb	32	41	32	29	45	60
Zr:Y	2.6	2.6	2.5	2.6	2.7	2.7
Y:Nb	12.3	15.9	12.9	11.0	16.7	21.9
Ti:Zr	107	103	122	99	109	99

TR8-9: Inner parts of diabase dyke.

TR8-10: Inner parts of diabase dyke.

TR8-11: Inner parts of diabase dyke.

TR8-12: Medium grained, weakly pyritised diabase dyke.

TR8-13: Central parts of diabase dyke.

TR8-14: Fresh doleritic dyke in Sheeted Complex.

Major Elements

Ox. %	TR8-15	TR8-16	TR8-17	TR8-18	TR8-19	TR8-20
SiO ₂	52.40	56.30	63.30	57.10	53.85	53.15
TiO ₂	0.77	1.30	0.72	0.67	1.36	0.50
Al ₂ O ₃	15.65	14.80	14.10	15.10	14.60	14.20
Fe ₂ O ₃ *	10.56	11.99	10.01	10.30	13.13	10.53
MnO	0.17	0.17	0.08	0.13	0.14	0.15
MgO	7.50	5.65	3.70	6.35	8.20	9.95
CaO	8.05	6.67	4.25	9.13	7.54	6.54
Na ₂ O	4.21	3.34	3.79	2.96	2.51	3.49
K ₂ O	0.29	0.25	0.22	0.21	0.62	0.29
P ₂ O ₅	0.06	0.11	0.14	0.06	0.11	0.04
Total	99.66	100.58	100.31	102.01	102.06	98.84

*Total Iron as Fe₂O₃.

Trace Elements

Nb	1.5	2.7	2.4	1.9	2.1	2.3
Zr	49	82	65	43	94	29
Y	16.4	30.7	29.2	16.9	31.4	12.5
Sr	101	131	101	95	103	176
Rb	2.2	2.6	2.0	2.8	4.6	2.1
Ga	16.3	17.5	15.5	15.1	16.1	14.3
Zn	73	98	20	32	29	40
Cr	56	14	12	31	33	147
V	314	418	77	294	430	309
La	0.3	1.5	1.6	0	1.8	0
Ce	4.6	11.8	7.6	7.3	11.1	2.5
Nd	5.7	9.0	6.5	4.6	9.7	1.8
Ba	22	29	10	15	24	25

Selected Trace Element Ratios

Zr:Nb	33	30	27	23	45	13
Zr:Y	3.0	2.7	2.2	2.5	3.0	2.3
Y:Nb	10.9	11.4	12.2	8.9	14.9	5.4
Ti:Zr	94	95	66	93	87	103

TR8-15: Inner parts of diabase dyke.

TR8-16: Medium grained dyke in Sheeted Complex.

TR8-17: Epidotised diabase dyke.

TR8-18: Diabase dyke.

TR8-19: Weakly epidotised diabase dyke.

TR8-20: Diabase dyke.

Major Elements

Ox. %	TR9-1	TR9-2	TR9-3	TR9-4	TR9-5	TR9-6B
SiO ₂	58.80	50.90	49.10	50.00	54.15	51.55
TiO ₂	1.32	0.63	0.82	0.59	0.76	0.91
Al ₂ O ₃	12.80	14.10	13.40	15.10	14.05	15.00
Fe ₂ O ₃	11.01	10.83	11.06	10.43	11.15	11.26
MnO	0.10	0.22	0.20	0.17	0.18	0.17
MgO	4.00	11.00	9.50	7.50	8.20	8.25
CaO	5.66	7.31	6.25	8.10	6.01	8.30
Na ₂ O	2.73	2.01	3.61	3.10	2.97	4.71
K ₂ O	1.02	0.94	0.34	0.38	0.80	0.11
P ₂ O ₅	0.11	0.07	0.08	0.06	0.07	0.06
Total	97.55	98.01	94.36	95.43	98.34	100.32

*Total Iron as Fe₂O₃.

Trace Elements

Nb	1.5	1.4	1.3	1.8	2.1	1.4
Zr	79	45	49	37	44	49
Y	40.9	19.0	18.5	15.6	19.2	18.8
Sr	96	92	45	100	154	223
Rb	26.7	6.8	1.9	3.4	5.1	1.8
Ga	16.7	15.6	16.2	14.0	15.5	15.9
Zn	86	47	64	66	68	36
Cr	6	37	29	32	11	44
V	282	294	340	287	366	343
La	2.1	0	0.8	0	0.9	0.4
Ce	9.8	6.8	6.0	3.5	5.5	4.2
Nd	8.5	5.1	4.1	3.5	4.6	5.2
Ba	38	42	13	20	24	17

Selected Trace Element Ratios

Zr:Nb	53	32	38	21	21	35
Zr:Y	1.9	2.4	2.6	2.4	2.3	2.6
Y:Nb	27.3	13.6	14.2	8.7	9.1	13.4
Ti:Zr	100	84	100	96	104	111

TR9-1: Upper middle parts of concordant intrusive in LPL.

TR9-2: Diabase dyke.

TR9-3: Medium grained diabase dyke.

TR9-4: Diabase dyke.

TR9-5: Inner parts of diabase dyke.

TR9-6B: Inner parts of diabase dyke.

Major Elements

Ox. %	TR9-7	TR9-8	TR9-9	TR9-10	TR9-11	TR9-12
SiO ₂	57.35	57.60	54.80	54.50	55.65	53.30
TiO ₂	1.23	0.96	0.66	1.03	1.08	1.07
Al ₂ O ₃	14.00	14.40	12.65	12.30	13.40	13.60
Fe ₂ O ₃ *	11.50	10.56	9.61	11.51	11.94	11.60
MnO	0.11	0.13	0.13	0.22	0.14	0.20
MgO	5.50	6.70	9.45	7.80	5.90	8.40
CaO	5.83	6.47	6.31	5.20	5.82	3.50
Na ₂ O	4.09	3.43	4.12	3.78	3.67	4.56
K ₂ O	1.29	0.25	0.17	0.36	0.22	0.11
P ₂ O ₅	0.10	0.09	0.06	0.12	0.12	0.13
Total	101.00	100.59	97.96	96.82	97.94	96.47

*Total Iron as Fe₂O₃.

Trace Elements

Nb	1.8	2.5	1.8	2.0	2.2	2.1
Zr	78	71	46	76	84	86
Y	29.8	27.3	16.2	28.7	33.6	31.5
Sr	123	113	128	115	118	65
Rb	4.9	2.8	1.1	3.3	2.4	1.8
Ga	16.1	17.2	17.0	17.2	18.0	17.6
Zn	25	38	41	82	67	240
Cr	6	28	13	15	9	9
V	459	310	354	381	404	376
La	1.6	1.5	0.9	1.0	1.7	0.3
Ce	10.0	7.2	6.4	10.2	10.4	12.4
Nd	7.8	6.3	4.4	7.1	9.2	8.8
Ba	70	39	17	42	27	15

Selected Trace Element Ratios

Zr:Nb	43	28	26	38	38	41
Zr:Y	2.6	2.6	2.8	2.6	2.5	2.7
Y:Nb	16.6	10.9	9.0	14.4	15.3	15.0
Ti:Zr	95	81	86	81	77	75

TR9-7: Medium grained diabase dyke.

TR9-8: Diabase dyke.

TR9-9: Diabase dyke.

TR9-10: Medium to fine grained diabase dyke.

TR9-11: Inner parts of diabase dyke.

TR9-12: Medium to fine grained diabase dyke.

Major Elements

Ox. %	TR9-13	TR9-14	TR9-15	TR9-16	TR9-17	TR9-18
SiO ₂	54.60	53.05	52.50	51.85	51.95	54.85
TiO ₂	0.83	1.06	0.99	0.73	0.73	0.97
Al ₂ O ₃	14.30	13.90	14.20	15.25	15.60	13.00
Fe ₂ O ₃	11.22	11.92	11.87	10.45	10.98	10.61
MnO	0.16	0.19	0.20	0.17	0.17	0.15
MgO	6.45	7.80	6.90	7.00	8.60	6.50
CaO	8.02	4.56	6.72	7.30	7.97	5.34
Na ₂ O	3.01	3.79	3.99	5.03	3.52	4.71
K ₂ O	0.07	0.33	0.12	0.20	0.27	0.23
P ₂ O ₅	0.08	0.10	0.08	0.08	0.06	0.11
Total	98.74	96.70	97.57	98.06	99.85	96.47

*Total Iron as Fe₂O₃.

Trace Elements

Nb	1.8	1.4	1.0	1.0	1.5	2.2
Zr	64	53	60	52	41	75
Y	25.4	21.4	22.3	18.7	17.1	26.9
Sr	56	120	92	136	104	68
Rb	2.4	1.1	2.0	2.3	2.8	2.2
Ga	18.6	15.2	16.4	15.3	15.0	15.5
Zn	154	50	170	91	71	40
Cr	11	25	22	52	50	13
V	435	341	386	269	315	393
La	2.0	0.7	0.5	0.3	0.2	1.2
Ce	8.3	6.1	5.6	6.6	6.5	8.0
Nd	6.8	6.4	7.2	6.0	4.3	8.6
Ba	31	25	22	26	28	20

Selected Trace Element Ratios

Zr:Nb	36	38	60	52	27	34
Zr:Y	2.5	2.5	2.7	2.8	2.4	2.8
Y:Nb	14.1	15.3	22.3	18.7	11.4	12.2
Ti:Zr	78	120	99	84	107	78

TR9-13: Inner parts of diabase dyke.

TR9-14: Diabase dyke.

TR9-15: Diabase dyke.

TR9-16: Medium grained diabase dyke.

TR9-17: Fine grained diabase dyke.

TR9-18: Diabase dyke.

APPENDIX 2

Major and trace element (XRF) analyses of samples collected from the region of Evloimeni mine (Limni mining district) and Mavri Sykia mine (Kalavassos mining district).

All samples are from pillowed flows. Refer to Appendix 3 for location of collection.

Prefix CHR refers to samples of unmineralized lavas, CHM to mineralized.

Major Elements

Ox. %	EV-1CHR	EV-2CHR	EV-3CHR	EV-4CHR	EV-5CHR	EV-6CHR
SiO ₂	52.30	53.85	52.70	50.90	49.75	50.30
TiO ₂	0.42	0.40	0.42	0.43	0.42	0.44
Al ₂ O ₃	16.15	14.85	15.15	16.15	16.50	15.70
Fe ₂ O ₃	8.95	9.37	9.03	9.58	9.73	9.56
MnO	0.10	0.14	0.08	0.10	0.08	0.06
MgO	7.60	9.95	12.10	12.20	12.30	12.75
CaO	7.58	5.19	5.80	6.40	6.57	5.98
Na ₂ O	3.42	0.44	1.90	1.62	1.50	1.70
K ₂ O	1.54	0.16	0.98	0.90	0.77	0.69
P ₂ O ₅	0.05	0.03	0.02	0.02	0.02	0.02
Total	98.11	94.38	98.18	98.30	97.64	97.20

*Total Iron as Fe₂O₃.

Trace Elements

Nb	2.1	1.4	2.0	1.6	1.7	1.1
Zr	14	20	22	21	21	21
Y	13.0	8.5	4.9	4.2	5.2	3.8
Sr	413	152	118	142	148	172
Rb	26.8	18.6	10.2	10.0	5.8	7.2
Ga	12.0	13.0	12.3	13.9	15.5	15.2
Zn	64	64	72	75	70	73
Cr	77	84	99	97	110	97
V	276	253	280	345	350	321
La	0	0	0	0	0	0
Ce	3.2	2.7	3.4	0.2	0	1.9
Nd	2.0	1.6	0.3	1.6	1.3	1.7
Ba	71	59	27	25	26	79

Selected Trace Element Ratios

Zr:Nb	7	14	11	13	12	19
Zr:Y	1.1	2.4	4.5	5.0	4.0	5.5
Y:Nb	6.2	6.1	2.5	2.6	3.1	3.5
Ti:Zr	180	120	114	123	120	126

Major Elements

Ox. %	EV-7CHR	EV-8CHR	EV-9CHR	EV-10CHR	EV-11CHR	EV-12CHR
SiO ₂	51.70	54.10	54.50	56.25	53.35	53.10
TiO ₂	0.42	0.44	0.48	0.45	0.27	0.32
Al ₂ O ₃	15.05	15.75	16.25	14.80	12.95	13.85
Fe ₂ O ₃	8.63	9.80	7.90	7.93	10.00	9.09
MnO	0.04	0.11	0.07	0.08	0.13	0.07
MgO	14.10	8.50	10.25	9.75	12.65	14.40
CaO	4.48	6.09	8.32	8.24	10.33	9.04
Na ₂ O	2.12	0.54	1.02	1.48	0.82	0.42
K ₂ O	1.01	0.80	1.11	0.73	0.13	0.87
P ₂ O ₅	0.02	0.03	0.04	0.04	0.03	0.02
Total	97.57	96.16	99.94	99.75	100.66	101.18

*Total Iron as Fe₂O₃.

Trace Elements

Nb	1.0	1.3	1.5	2.0	1.4	1.3
Zr	21	22	26	25	17	18
Y	6.0	8.5	4.5	9.6	7.7	2.0
Sr	109	99	44	77	24	23
Rb	8.4	14.4	16.4	5.5	2.3	8.5
Ga	13.4	11.6	14.7	14.7	13.4	11.8
Zn	79	89	207	150	70	110
Cr	112	72	85	56	699	663
V	369	346	282	319	280	341
La	0	0.2	0	0.2	0	0
Ce	4.6	2.9	1.2	1.3	0.7	0.3
Nd	1.4	2.0	2.9	0.9	0.4	0.8
Ba	44	508	183	175	44	127

Selected Trace Element Ratios

Zr:Nb	21	17	17	13	12	14
Zr:Y	3.5	2.6	5.8	2.6	2.2	9.0
Y:Nb	6.0	6.5	3.0	4.8	5.5	1.5
Ti:Zr	120	120	111	108	95	107

Major Elements

Ox. %	EV-12CHM	EV-13CHR	EV-14CHR	EV-15CHR	EV-16CHR	EV-17CHR
SiO ₂	56.10	53.70	52.15	54.00	53.50	52.25
TiO ₂	0.28	0.30	0.29	0.26	0.28	0.27
Al ₂ O ₃	13.55	13.40	12.10	12.35	13.10	12.15
Fe ₂ O ₃	7.38	10.63	8.83	9.08	9.12	9.87
MnO	0.02	0.12	0.15	0.17	0.15	0.14
MgO	3.65	10.00	14.15	12.95	10.05	9.65
CaO	2.38	4.31	9.48	9.26	9.76	10.22
Na ₂ O	2.66	0.33	0.72	0.82	0.40	0.90
K ₂ O	2.95	0.89	0.51	0.30	0.54	3.45
P ₂ O ₅	0.03	0.02	0.03	0.03	0.02	0.03
Total	89.00	93.70	98.41	99.22	96.92	98.93

*Total Iron as Fe₂O₃.

Trace Elements

Nb	1.2	1.1	1.3	0.9	1.7	1.4
Zr	20	15	16	14	13	14
Y	5.7	5.2	5.1	6.8	8.6	8.4
Sr	114	60	29	72	98	135
Rb	14.3	21.5	2.8	2.9	11.3	44.6
Ga	8.8	9.3	12.1	10.5	8.6	10.6
Zn	399	130	73	92	172	284
Cr	110	572	390	637	628	557
V	37	347	300	280	411	268
La	0	0	0	0	0	0.5
Ce	5.5	0	1.6	0	0	0
Nd	1.9	0	1.0	0.8	0	1.0
Ba	226	2099	102	584	1534	716

Selected Trace Element Ratios

Zr:Nb	17	14	12	16	8	10
Zr:Y	3.5	2.9	3.1	2.1	1.5	1.7
Y:Nb	4.8	4.7	3.9	7.5	5.0	6.0
Ti:Zr	84	120	109	111	129	116

Major Elements

Ox. %	EV-18CHM	EV-19CHM	EV-21CHM	MS-1CHR	MS-2CHM	MS-3CHM
SiO ₂	54.75	53.25	59.55	50.95	45.90	47.85
TiO ₂	0.48	0.43	0.34	0.41	0.24	0.22
Al ₂ O ₃	15.60	16.25	16.20	14.75	13.35	12.35
Fe ₂ O ₃	9.35	9.83	7.04	10.16	20.99	23.36
MnO	0.17	0.15	0.02	0.12	0.17	0.06
MgO	8.00	11.65	2.50	10.85	13.85	8.90
CaO	8.52	6.34	2.55	3.80	0.16	0.13
Na ₂ O	1.14	0.76	3.71	3.39	0.04	0.04
K ₂ O	1.26	0.99	3.37	0.72	0.02	0.00
P ₂ O ₅	0.04	0.03	0.03	0.03	0.03	0.02
Total	99.31	99.68	95.31	95.18	94.75	92.93

Total Iron as Fe₂O₃.

Trace Elements

Nb	2.0	1.7	2.3	1.6	2.6	1.4
Zr	26	24	21	24	19	19
Y	10.5	10.5	3.5	8.6	4.5	2.5
Sr	61	56	114	55	3	1
Rb	8.0	8.0	15.9	10.2	2.7	2.3
Ga	15.1	14.4	11.0	13.5	12.1	13.3
Zn	198	179	167	105	451	800
Cr	87	119	127	67	604	557
V	328	341	136	279	342	312
La	0	0	0	0	0	0
Ce	0.9	1.3	21.0	6.9	3.6	6.6
Nd	3.0	1.8	2.1	3.0	0	1.1
Ba	185	114	298	29	0	0

Selected Trace Element Ratios

Zr:Nb	13	14	9	15	7	14
Zr:Y	2.5	2.3	6.0	2.8	4.2	7.6
Y:Nb	5.3	6.2	1.5	5.4	1.7	1.8
Ti:Zr	111	107	97	102	76	69

Major Elements

Ox. %	MS-4CHM	MS-5CHM	MS-6CHM	MS-7CHM	MS-8CHM	MS-9CHM
SiO ₂	51.00	49.55	50.60	45.55	49.30	51.60
TiO ₂	0.23	0.22	0.21	0.24	0.45	0.45
Al ₂ O ₃	12.40	12.30	11.85	13.25	16.20	16.30
Fe ₂ O ₃	17.70	19.94	20.53	19.79	16.81	16.43
MnO	0.19	0.12	0.13	0.16	0.07	0.07
MgO	13.20	11.50	9.45	15.50	11.75	10.65
CaO	0.07	0.09	0.07	0.11	0.20	0.06
Na ₂ O	0.03	0.05	0.05	0.05	0.04	0.07
K ₂ O	0.00	0.01	0.00	0.00	0.00	0.00
P ₂ O ₅	0.02	0.03	0.03	0.03	0.03	0.03
Total	94.84	93.81	92.92	94.68	94.85	95.66

Total Iron as Fe₂O₃.

Trace Elements

Nb	2.5	2.5	1.9	2.6	2.3	2.3
Zr	18	17	19	18	41	43
Y	4.5	5.9	4.8	4.0	9.8	8.3
Sr	1	2	3	3	6	2
Rb	1.4	1.1	1.1	1.4	1.6	0.7
Ga	10.8	10.2	11.2	12.2	13.8	14.5
Zn	758	386	362	616	459	147
Cr	535	546	521	586	112	87
V	306	315	300	333	245	249
La	0	0	0	0	0.4	0
Ce	5.0	2.5	3.4	5.5	9.2	8.7
Nd	0	0	0	0.9	4.4	3.6
Ba	0	0	0	0	0	0

Selected Trace Element Ratios

Zr:Nb	7	7	10	7	18	19
Zr:Y	4.0	2.9	4.0	4.5	4.2	5.2
Y:Nb	1.8	2.4	2.5	1.5	4.3	3.6
Ti:Zr	77	78	66	80	66	63

Major Elements

Ox. %	MS-10CHM	MS-11CHM	MS-12CHM	MS-13CHR	MS-14CHR	MS-15CHR
SiO ₂	51.45	52.70	50.35	53.15	51.40	54.60
TiO ₂	0.44	0.40	0.20	0.46	0.44	0.40
Al ₂ O ₃	16.75	16.60	12.40	14.30	16.25	14.70
Fe ₂ O ₃ [*]	15.64	16.19	20.15	10.47	10.69	9.21
MnO	0.18	0.07	0.09	0.23	0.12	0.10
MgO	11.25	9.40	9.55	12.35	11.10	11.40
CaO	0.05	0.02	0.11	7.16	9.46	5.43
Na ₂ O	0.06	0.07	0.04	1.17	1.30	2.92
K ₂ O	0.00	0.00	0.00	1.32	0.30	1.33
P ₂ O ₅	0.02	0.02	0.02	0.03	0.03	0.03
Total	95.84	95.47	92.91	100.64	101.09	100.12

*Total Iron as Fe₂O₃.

Trace Elements

Nb	2.2	2.1	2.3	2.5	2.3	2.8
Zr	42	40	18	24	26	25
Y	7.5	6.2	2.8	9.8	5.5	7.6
Sr	2	2	2	160	76	71
Rb	0.8	2.8	2.1	13.1	3.7	5.7
Ga	14.3	13.4	14.0	12.4	15.4	13.0
Zn	113	74	100	59	70	27
Cr	91	85	483	210	70	63
V	256	223	282	280	291	270
La	0.1	0	0	0	0	0
Ce	7.7	7.0	4.5	2.2	3.8	3.0
Nd	2.6	1.2	0.9	2.5	2.0	1.8
Ba	0	0	0	122	20	22

Selected Trace Element Ratios

Zr:Nb	19	19	8	10	11	9
Zr:Y	5.6	6.4	6.4	2.4	4.7	3.3
Y:Nb	3.4	2.9	1.2	3.9	2.4	2.7
Ti:Zr	63	60	67	115	102	96

Major Elements

Ox. %	MS-16CHR	MS-17CHR	MS-18CHR	MS-19CHR	MS-20CHR	MS-21CHR
SiO ₂	52.85	50.40	49.95	52.20	52.10	51.00
TiO ₂	0.62	0.61	0.46	0.51	0.50	0.45
Al ₂ O ₃	15.50	14.95	15.10	15.35	15.45	14.65
Fe ₂ O ₃	9.43	9.48	10.01	9.68	8.99	10.47
MnO	0.18	0.19	0.16	0.12	0.12	0.15
MgO	13.50	11.95	12.10	14.30	14.30	15.60
CaO	5.53	4.09	4.40	5.26	6.69	5.08
Na ₂ O	1.50	5.44	5.34	0.62	0.58	0.53
K ₂ O	1.57	0.27	0.36	2.31	2.15	2.02
P ₂ O ₅	0.04	0.04	0.03	0.03	0.02	0.02
Total	100.72	97.42	97.91	100.38	100.90	99.97

*Total Iron as Fe₂O₃.

Trace Elements

Nb	2.5	2.0	2.5	2.9	2.6	2.2
Zr	38	38	26	25	25	25
Y	13.3	13.3	7.6	7.8	4.3	5.1
Sr	84	58	78	116	106	91
Rb	7.5	2.8	3.3	14.5	12.7	12.8
Ga	14.6	12.3	12.3	12.6	13.4	13.9
Zn	64	81	65	85	70	72
Cr	390	353	279	240	263	273
V	254	245	284	317	307	277
La	0.7	2.2	0	0.4	0	0
Ce	5.1	7.1	3.6	1.9	3.5	3.6
Nd	4.8	5.8	2.4	2.6	2.1	2.4
Ba	38	14	19	31	31	17

Selected Trace Element Ratios

Zr:Nb	15	19	10	9	10	11
Zr:Y	2.9	2.9	3.4	3.2	5.8	4.9
Y:Nb	5.3	6.6	3.0	2.7	1.6	2.3
Ti:Zr	98	96	106	122	120	108

Major Elements

Ox. %	MS-22CHR	MS-23CHR	MS-24CHR	MS-25CHR	MS-26CHR	MS-27CHR
SiO ₂	49.40	49.75	48.50	49.30	50.00	49.60
TiO ₂	0.53	0.52	0.57	0.53	0.54	0.54
Al ₂ O ₃	17.10	16.05	16.75	16.55	15.60	16.50
Fe ₂ O ₃	9.69	10.09	9.93	10.07	10.23	10.55
MnO	0.19	0.21	0.24	0.22	0.23	0.21
MgO	16.80	16.55	17.00	17.50	15.70	14.60
CaO	3.59	4.40	2.34	2.42	1.98	3.16
Na ₂ O	0.37	0.59	0.36	0.37	0.37	0.32
K ₂ O	1.10	1.28	1.86	2.26	3.27	2.55
P ₂ O ₅	0.03	0.02	0.02	0.02	0.02	0.03
Total	98.80	99.46	97.57	99.24	97.94	98.06

*Total Iron as Fe₂O₃.

Trace Elements

Nb	2.2	2.7	2.8	2.8	2.1	2.6
Zr	28	27	30	29	28	29
Y	8.9	5.0	4.0	4.8	2.9	5.2
Sr	89	118	73	96	89	78
Rb	8.1	8.7	11.9	12.9	17.8	18.0
Ga	15.6	15.8	14.9	14.2	12.7	13.4
Zn	66	74	80	75	79	83
Cr	196	162	185	187	188	175
V	362	342	378	361	341	304
La	0.7	0	0	0	0.2	0.8
Ce	3.2	4.7	3.0	2.3	1.8	5.0
Nd	1.7	1.9	2.4	2.4	2.1	3.2
Ba	18	24	45	41	41	41

Selected Trace Element Ratios

Zr:Nb	13	10	11	10	13	11
Zr:Y	3.1	5.4	7.5	6.0	9.7	5.6
Y:Nb	4.0	1.8	1.4	1.7	1.4	2.0
Ti:Zr	114	116	114	110	116	112

Major Elements

Ox. %	MS-28CHR	MS-29CHR	MS-30CHR	MS-31CHR	MS-32CHR
SiO ₂	51.60	50.90	52.60	51.85	49.85
TiO ₂	0.53	0.61	0.55	0.56	0.56
Al ₂ O ₃	16.05	18.15	17.35	18.30	17.95
Fe ₂ O ₃	10.76	7.96	7.40	8.72	8.14
MnO	0.21	0.15	0.19	0.10	0.27
MgO	11.60	11.85	10.55	6.45	13.70
CaO	2.91	5.51	5.76	8.03	5.41
Na ₂ O	0.29	0.82	0.72	0.92	0.62
K ₂ O	3.35	3.08	4.26	3.94	3.10
P ₂ O ₅	0.03	0.03	0.07	0.07	0.07
Total	97.33	99.06	99.45	98.94	99.67

*Total Iron as Fe₂O₃.

Trace Elements

Nb	2.4	2.0	2.3	2.2	2.3
Zr	28	46	39	39	38
Y	4.5	5.7	9.7	10.5	8.1
Sr	80	125	131	148	115
Rb	25.2	20.0	24.5	29.5	19.2
Ga	13.2	14.0	12.6	15.2	15.2
Zn	78	78	73	81	75
Cr	172	95	274	323	301
V	300	275	162	151	191
La	1.9	0.5	2.3	1.2	1.3
Ce	4.9	5.5	5.3	3.9	8.1
Nd	3.7	4.1	6.0	3.5	5.6
Ba	55	64	203	223	76

Selected Trace Element Ratios

Zr:Nb	12	23	17	18	17
Zr:Y	6.2	8.1	4.0	3.7	4.7
Y:Nb	1.9	2.9	4.2	4.8	3.5
Ti:Zr	114	80	85	86	88

APPENDIX 3.

Location of samples collected for the purpose of examining petrographic and mineralogical changes in the region of ore zones.

Location of samples of unmineralized pillow lavas (-CHR) and mineralized lavas (-CHM) from Evloimeni mine.

Sample No.	Coordinates		Elev. (mt.)	Sample No.	Coordinates		Elev. (mt.)
	W	N			W	N	
EV-1CHR	75468	2522	182	EV-2CHR	75460	2517	182
EV-3CHR	75453	2517	182	EV-4CHR	75450	2518	182
EV-5CHR	75448	2518	182	EV-6CHR	75444	2519	182
EV-7CHR	75440	2520	182	EV-8CHR	75436	2520	182
EV-9CHR	75432	2522	182	EV-10CHR	75430	2523	182
EV-11CHR	75427	2524	182	EV-12CHR	75424	2525	182
EV-12CHM	75424	2525	182	EV-13CHR	75420	2526	182
EV-14CHR	75416	2527	182	EV-15CHR	75411	2529	182
EV-16CHR	75407	2530	182	EV-17CHR	75403	2531	182
EV-18CHM	75394	2535	182	EV-19CHR	75391	2537	182
EV-20CHM	75383	2540	182	EV-21CHM	75379	2542	182

Coordinates of samples of mineralized lavas (-CHM) and unmineralized lavas (-CHR) from the region of Mavri Sykia mine, Kalavassos mining district.

Sample No.	Coordinates		Sample No.	Coordinates	
	W	N		W	N
MS-1CHR	-23150	-6218	MS-2CHM	-23148	-6220
MS-3CHM	-23147	-6221	MS-4CHM	-23145	-6224
MS-5CHM	-23143	-6227	MS-6CHM	-23142	-6229
MS-7CHM	-23139	-6233	MS-8CHM	-23130	-6247
MS-9CHM	-23125	-6268	MS-10CHM	-23120	-6274
MS-11CHM	-23115	-6280	MS-12CHM	-23113	-6293
MS-13CHR	-23155	-6209	MS-14CHR	-23156	-6207
MS-15CHR	-23158	-6204	MS-16CHR	-23160	-6201
MS-17CHR	-23162	-6198	MS-18CHR	-23163	-6195
MS-19CHR	-23167	-6190	MS-20CHR	-23169	-6186
MS-21CHR	-23171	-6184	MS-22CHR	-23169	-6179
MS-23CHR	-23170	-6176	MS-24CHR	-23172	-6171
MS-25CHR	-23174	-6167	MS-26CHR	-23179	-6164
MS-27CHR	-23181	-6162	MS-28CHR	-23185	-6159
MS-29CHR	-23205	-6134	MS-30CHR	-23208	-6126
MS-31CHR	-23224	-6105	MS-32CHR	-23203	-6118

Coordinates of samples of mineralized lava
(LI-1 to LI-10 and LI-1M to LI-10M inclusive)
and mineralized sheeted dykes (LI-11M to LI-19M)
from Limni opencast mine.

Sample No.	Coordinates		Elev. (mt.)	Sample No.	Coordinates		Elev. (mt.)
	W	N			W	N	
LI-1	75886	3856	96	LI-2	75876	3810	96
LI-3	75853	3745	92	LI-4	75878	3711	92
LI-5	75918	3706	90	LI-7	75942	3766	82
LI-8	75951	3758	82	LI-9	75953	3979	100
LI-10	75997	3981	100	LI-1M	76062	3990	108
LI-2M	76040	3951	102	LI-3M	76029	3865	93
LI-4M	75981	3904	88	LI-5M	76164	4274	179
LI-6M	76189	4262	179	LI-7M	76194	4240	179
LI-8M	76202	4217	179	LI-9M	76202	4196	179
LI-10M	76203	4181	179	LI-11M	75718	3858	204
LI-12M	75713	3843	204	LI-13M	75703	3799	204
LI-14M	75699	3785	204	LI-15M	75696	3762	204
LI-16M	75697	3739	204	LI-17M	75703	3686	204
LI-18M	75713	3652	204	LI-19M	75722	3646	204

Coordinates of samples of unmineralized olivine basalts
from Limni mine.

Sample No.	Coordinates		Elev. (Mt.)	Sample No.	Coordinates		Elev. (Mt.)
	W	N			W	N	
LI-10R	76021	3656	138	LI-11R	76033	3639	138
LI-12R	76033	3639	138	LI-12R	76040	3622	138
LI-13R	76051	3604	138	LI-14R	76059	3588	138
LI-15R	76072	3562	138	LI-16R	75870	3649	131
LI-17R	75892	3644	131	LI-18R	75917	3638	131
LI-19R	75976	3651	136	LI-20R	75987	3652	138

Location of samples of mineralized lava (MS-1 to MS-6)
and unmineralized lavas (MS-1R to MS-7R) from the
region of Mavri Sykia mine, Kalavassos mining district.

Sample No.	Coordinates		Sample No.	Coordinates	
	W	N		W	N
MS-1	-23048	-6374	MS-2	-23080	-6350
MS-3	-23084	-6346	MS-4	-23100	-6334
MS-5	-23112	-6316	MS-6	-23122	-6308
MS-1R	-23155	-6208	MS-2R	-23157	-6204
MS-3R	-23158	-6201	MS-4R	-23162	-6192
MS-5R	-23165	-6185	MS-6R	-23169	-6175
MS-7R	-23173	-6167			

APPENDIX 4

Electron microprobe (Energy Dispersive) analyses of pyroxenes from the Troodos ophiolite. Refer to Appendix 1 for sample descriptions.

Ox. %	1	2	3	4	5	6
SiO ₂	49.94	50.44	49.88	51.88	49.74	49.73
Al ₂ O ₃	2.06	1.97	2.17	1.48	2.11	2.04
MgO	13.02	13.07	12.99	14.72	13.51	13.09
CaO	19.60	19.70	17.74	18.61	17.76	19.36
TiO ₂	0.58	0.80	0.63	0.41	0.49	0.59
Cr ₂ O ₃	0.03	0.17	0.06	0.12	0.12	0.26
FeO	11.84	12.34	14.82	13.42	14.07	12.81
Na ₂ O	0.24	0.03	0.35	0.52	0.43	0.22
K ₂ O	0.01	0.00	0.05	0.00	0.15	0.00
MnO	0.21	0.23	0.21	0.31	0.20	0.40
Total	97.53	98.75	98.90	101.47	98.58	98.50

Formula based on 6 O

Si	1.931	1.929	1.919	1.933	1.917	1.915
Al _{iv}	0.069	0.071	0.081	0.065	0.083	0.085
<hr/>						
Al _{vi}	0.025	0.018	0.017	0.000	0.013	0.008
Ti	0.017	0.023	0.018	0.012	0.014	0.017
Fe	0.383	0.395	0.477	0.416	0.454	0.413
Cr	0.001	0.005	0.002	0.003	0.004	0.008
Mn	0.007	0.008	0.007	0.010	0.006	0.013
Mg	0.581	0.554	0.504	0.598	0.549	0.567
<hr/>						
Mg	0.169	0.191	0.241	0.220	0.227	0.184
Ca	0.812	0.807	0.731	0.743	0.733	0.799
Na	0.018	0.002	0.026	0.037	0.032	0.017
K	0.001	0.000	0.002	0.000	0.008	0.000
Al ₂	3.45	3.55	4.05	3.25	4.15	4.25
Ca	42	41	38	39	38	41
Mg	38	38	38	40	39	38
Fe	20	21	24	21	23	21

All analyses of microphenocrysts in TR1-11. 37, 31, 29, 45, 42, 47.

Ox. %	1	2	3	4	5	6
SiO ₂	50.29	50.42	50.66	50.33	50.70	49.28
Al ₂ O ₃	1.85	2.19	1.92	1.59	1.92	3.11
MgO	13.40	13.55	13.92	13.85	13.75	13.39
CaO	18.08	20.02	17.56	17.80	17.92	19.50
TiO ₂	0.70	0.66	0.61	0.61	0.51	0.60
Cr ₂ O ₃	0.10	0.00	0.00	0.17	0.11	0.16
FeO	14.41	12.24	14.51	14.79	14.88	12.88
Na ₂ O	0.29	0.30	0.28	0.38	0.39	0.62
K ₂ O	0.03	0.00	0.03	0.00	0.01	0.00
MnO	0.40	0.27	0.51	0.37	0.33	0.26
Total	99.55	99.65	100.00	99.89	100.52	99.80

Formula based on 6 O

Si	1.921	1.913	1.923	1.919	1.919	1.876
Al _{iv}	0.079	0.087	0.077	0.072	0.081	0.124
<hr/>						
Al _{vi}	0.004	0.011	0.009	0.000	0.005	0.016
Ti	0.020	0.019	0.017	0.017	0.015	0.017
Fe	0.460	0.388	0.461	0.463	0.471	0.410
Cr	0.003	0.000	0.000	0.005	0.003	0.005
Mn	0.013	0.009	0.016	0.012	0.011	0.008
Mg	0.525	0.603	0.525	0.542	0.533	0.602
<hr/>						
Mg	0.238	0.164	0.263	0.245	0.243	0.158
Ca	0.740	0.814	0.714	0.727	0.727	0.796
Na	0.021	0.022	0.021	0.028	0.029	0.046
K	0.001	0.000	0.002	0.000	0.001	0.000
Al ₂	3.95	4.35	3.85	3.6	4.05	6.20
Ca	38	42	37	37	38	42
Mg	38	38	39	39	38	37
Fe	24	20	24	24	24	21

All analyses of microphenocrysts in TR1-11. 48, 43, 49, 30, 44, 32.

Ox. %	1	2	3	4	5	6
SiO ₂	51.78	51.45	51.94	51.11	52.21	51.37
Al ₂ O ₃	2.19	2.00	1.88	2.14	2.75	1.83
MgO	16.89	16.37	17.56	16.69	16.84	16.44
CaO	21.13	20.81	17.86	20.29	21.11	20.91
TiO ₂	0.22	0.39	0.38	0.30	0.27	0.22
Cr ₂ O ₃	0.27	0.25	0.13	0.44	0.21	0.35
FeO	5.73	6.60	8.29	6.25	6.90	6.20
Na ₂ O	0.38	0.29	0.32	0.25	0.37	0.19
K ₂ O	0.07	0.00	0.06	0.08	0.00	0.08
MnO	0.17	0.32	0.30	0.23	0.20	0.06
Total	98.83	98.48	98.72	97.78	100.86	97.65

Formula based on 6 O

Si	1.927	1.928	1.938	1.925	1.911	1.937
Al _{iv}	0.073	0.072	0.062	0.075	0.089	0.063
<hr/>						
Al _{vi}	0.023	0.016	0.021	0.020	0.029	0.018
Ti	0.006	0.011	0.011	0.009	0.008	0.006
Fe	0.178	0.207	0.259	0.197	0.211	0.195
Cr	0.008	0.007	0.004	0.013	0.006	0.010
Mn	0.005	0.010	0.009	0.007	0.006	0.002
Mg	0.810	0.772	0.717	0.779	0.773	0.787
<hr/>						
Mg	0.127	0.143	0.260	0.158	0.146	0.137
Ca	0.843	0.836	0.714	0.819	0.828	0.845
Na	0.027	0.021	0.023	0.019	0.026	0.014
K	0.003	0.000	0.003	0.004	0.000	0.004
Al _z	3.65	3.60	3.10	3.75	4.45	3.15
Ca	44	43	37	43	43	43
Mg	47	46	49	47	46	47
Fe	9	11	14	10	11	10

All analyses from TR9-16. 50, 52, 53, 26, 27, 28.

Ox. %	1	2	3	4	5	6
SiO ₂	52.36	51.48	52.15	51.45	50.86	51.29
Al ₂ O ₃	1.25	1.75	0.45	0.43	1.98	0.39
MgO	13.00	13.77	12.89	11.01	13.57	12.25
CaO	19.94	21.03	22.06	20.84	21.08	21.76
TiO ₂	0.17	0.31	0.30	0.12	0.60	0.27
Cr ₂ O ₃	0.04	0.05	0.10	0.05	0.01	0.00
FeO	13.57	10.92	10.86	15.09	10.65	12.52
Na ₂ O	0.60	0.65	0.18	0.67	0.36	0.47
K ₂ O	0.00	0.07	0.07	0.00	0.00	0.00
MnO	0.24	0.32	0.40	0.30	0.34	0.45
Total	101.17	100.35	99.46	99.96	99.45	99.40

Formula based on 6 O

Si	1.962	1.934	1.978	1.977	1.925	1.966
Al _{iv}	0.038	0.066	0.020	0.020	0.075	0.018
Fe	0.000	0.000	0.002	0.003	0.000	0.016
<hr/>						
Al _{vi}	0.017	0.012	0.000	0.000	0.014	0.000
Ti	0.005	0.009	0.009	0.003	0.017	0.008
Fe	0.425	0.343	0.345	0.485	0.337	0.385
Cr	0.001	0.002	0.003	0.001	0.000	0.000
Mn	0.007	0.010	0.013	0.010	0.011	0.015
Mg	0.571	0.667	0.642	0.539	0.648	0.628
<hr/>						
Mg	0.155	0.104	0.087	0.092	0.118	0.072
Ca	0.801	0.846	0.897	0.858	0.855	0.893
Na	0.044	0.047	0.013	0.050	0.027	0.035
K	0.000	0.003	0.003	0.000	0.000	0.000
<hr/>						
Al _z	1.90	3.30	1.0	1.0	3.75	0.90
<hr/>						
Ca	42	44	46	45	44	45
Mg	37	38	36	31	38	34
Fe	21	18	18	24	18	21

All pyroxenes from TR4-11. 10, 56, 57, 9, 11, 55.

Ox. %	1	2	3	4	5	6
SiO ₂	50.34	51.03	51.14	51.51	52.08	52.49
Al ₂ O ₃	2.60	3.01	2.97	2.90	2.06	1.48
MgO	15.57	15.82	16.42	16.05	18.02	17.21
CaO	17.92	20.30	20.64	21.36	15.26	20.65
TiO ₂	0.53	0.42	0.37	0.34	0.28	0.25
Cr ₂ O ₃	0.00	0.12	0.20	0.00	0.06	0.03
FeO	11.12	8.24	6.32	6.74	11.83	5.77
Na ₂ O	0.27	0.30	0.17	0.49	0.07	0.20
K ₂ O	0.01	0.00	0.00	0.01	0.00	0.03
MnO	0.29	0.29	0.15	0.15	0.28	0.16
Total	98.65	99.53	98.38	99.55	99.94	98.27

Formula based on 6 O

Si	1.908	1.903	1.912	1.911	1.932	1.957
Aliv	0.092	0.097	0.088	0.089	0.068	0.043
<hr/>						
Alvi	0.024	0.035	0.043	0.038	0.022	0.022
Ti	0.015	0.012	0.010	0.009	0.008	0.007
Fe	0.353	0.257	0.198	0.209	0.367	0.180
Cr	0.000	0.003	0.006	0.000	0.002	0.001
Mn	0.009	0.009	0.005	0.005	0.009	0.005
Mg	0.628	0.711	0.754	0.772	0.609	0.796
<hr/>						
Mg	0.251	0.168	0.161	0.116	0.388	0.160
Ca	0.728	0.811	0.827	0.849	0.607	0.825
Na	0.020	0.021	0.012	0.035	0.005	0.014
K	0.001	0.000	0.000	0.000	0.000	0.001
<hr/>						
Alz	4.60	4.85	4.40	4.45	3.40	2.15
Ca	38	42	43	44	31	43
Mg	44	45	47	45	50	48
Fe	18	13	10	11	19	9

All pyroxenes from TR9-4. 36, 35, 41, 40, 34, 33a.

Ox. %	1	2	3	4	5	6
SiO ₂	53.81	53.93	53.95	52.80	52.45	52.35
Al ₂ O ₃	1.07	1.37	1.50	1.11	0.94	0.91
MgO	26.36	26.40	25.95	23.82	22.48	22.41
CaO	1.75	1.67	1.61	1.60	1.62	1.70
TiO ₂	0.12	0.00	0.20	0.16	0.12	0.12
Cr ₂ O ₃	0.01	0.00	0.00	0.07	0.05	0.06
FeO	14.75	15.31	16.35	19.31	21.09	21.27
Na ₂ O	0.00	0.10	0.22	0.47	0.09	0.25
K ₂ O	0.00	0.00	0.00	0.01	0.00	0.00
MnO	0.25	0.42	0.50	0.41	0.53	0.30
Total	98.12	99.20	100.28	99.76	99.37	99.37

Formula based on 6 O

Si	1.976	1.965	1.955	1.955	1.964	1.962
Al _{iv}	0.024	0.035	0.045	0.045	0.036	0.038
<hr/>						
Al _{vi}	0.022	0.024	0.019	0.003	0.005	0.002
Ti	0.003	0.000	0.005	0.004	0.003	0.003
Fe	0.453	0.467	0.495	0.598	0.661	0.667
Cr	0.000	0.000	0.000	0.002	0.002	0.002
Mn	0.008	0.013	0.015	0.013	0.017	0.009
Mg	0.512	0.506	0.480	0.413	0.326	0.338
<hr/>						
Mg	0.931	0.928	0.922	0.902	0.929	0.914
Ca	0.069	0.065	0.063	0.063	0.065	0.068
Na	0.000	0.000	0.015	0.034	0.006	0.018
K	0.000	0.000	0.000	0.001	0.000	0.000
<hr/>						
Al ₂	1.20	1.75	2.25	2.25	1.80	1.90
Ca	4	4	4	5	3	4
Mg	73	72	70	65	63	62
Fe	23	24	26	30	34	34

All analyses are orthopyroxenes from TR6-1, arranged in order of increasing iron content (19, 5, 6, 21, 7, 22).

Ox. %	1	2	3	4	5
SiO ₂	51.24	51.51	51.62	51.91	52.07
Al ₂ O ₃	1.74	1.45	4.21	1.60	2.28
MgO	14.02	14.77	16.16	16.29	14.60
CaO	21.01	22.12	11.70	20.17	22.33
TiO ₂	0.34	0.37	0.24	0.32	0.43
Cr ₂ O ₃	0.18	0.02	0.15	0.00	0.05
FeO	9.09	7.73	12.91	8.36	8.71
Na ₂ O	0.17	0.10	1.02	0.30	0.56
K ₂ O	0.07	0.00	0.11	0.00	0.00
MnO	0.30	0.32	0.25	0.20	0.16
Total	98.16	98.39	98.37	99.15	101.19

Formula based on 6 O

Si	1.949	1.947	1.937	1.941	1.922
Al _{iv}	0.051	0.053	0.063	0.059	0.078
<hr/>					
Al _{vi}	0.027	0.012	0.123	0.012	0.021
Ti	0.010	0.011	0.007	0.009	0.012
Fe	0.289	0.244	0.405	0.261	0.269
Cr	0.005	0.001	0.004	0.000	0.002
Mn	0.010	0.010	0.008	0.006	0.005
Mg	0.667	0.735	0.453	0.738	0.726
<hr/>					
Mg	0.128	0.097	0.451	0.170	0.077
Ca	0.856	0.896	0.470	0.808	0.883
Na	0.013	0.007	0.074	0.022	0.040
K	0.003	0.000	0.005	0.000	0.000
Al ₂	2.55	2.65	3.15	2.95	3.90
Ca	45	45	30	42	46
Mg	40	42	48	45	40
Fe	15	13	22	13	14

All clinopyroxenes from TR6-1. 15, 14, 16, 23, 24.

Ox. %	1	2	3	4	5
SiO ₂	51.06	51.19	51.65	52.11	52.20
Al ₂ O ₃	1.78	1.71	1.67	1.56	1.70
MgO	13.58	15.59	13.63	15.08	14.66
CaO	20.44	18.96	19.63	19.37	18.50
TiO ₂	0.46	0.01	0.40	0.27	0.37
Cr ₂ O ₃	0.08	0.00	0.00	0.11	0.00
FeO	12.86	10.04	13.60	12.01	13.74
Na ₂ O	0.57	0.36	0.38	0.33	0.44
K ₂ O	0.02	0.07	0.01	0.02	0.00
MnO	0.34	0.33	0.22	0.14	0.26
Total	101.19	98.26	101.19	101.00	101.87

Formula based on 6 O

Si	1.917	1.937	1.935	1.939	1.936
Al _{iv}	0.079	0.063	0.065	0.061	0.063
Fe	0.004	0.000	0.000	0.000	0.000

Al _{vi}	0.000	0.013	0.009	0.007	0.011
Ti	0.013	0.011	0.011	0.007	0.010
Fe	0.400	0.318	0.426	0.374	0.426
Cr	0.003	0.000	0.000	0.003	0.000
Mn	0.011	0.011	0.007	0.004	0.008
Mg	0.624	0.675	0.577	0.634	0.577

Mg	0.136	0.204	0.184	0.203	0.223
Ca	0.822	0.769	0.788	0.772	0.735
Na	0.042	0.027	0.028	0.024	0.032
K	0.001	0.003	0.000	0.001	0.000
Al ₂	3.95	3.15	3.25	3.05	3.15
Ca	43	40	41	40	38
Mg	37	44	38	41	40
Fe	20	16	21	19	22

All clinopyroxenes from TR5-1. 4, 3, 18, 13, 2.

Ox. %	1	2	3	4	5
SiO ₂	51.27	51.44	51.65	51.86	52.30
Al ₂ O ₃	1.64	2.02	1.24	1.29	1.53
MgO	14.54	14.32	13.82	13.86	15.45
CaO	18.52	20.64	20.00	19.73	19.91
TiO ₂	0.39	0.32	0.28	0.34	0.29
Cr ₂ O ₃	0.00	0.14	0.14	0.17	0.00
FeO	12.90	10.89	12.63	12.62	10.71
Na ₂ O	0.42	0.20	0.36	0.53	0.16
K ₂ O	0.06	0.06	0.00	0.00	0.00
MnO	0.23	0.26	0.21	0.43	0.50
Total	99.97	100.29	100.33	100.83	100.85

Formula based on 6 O

Si	1.935	1.928	1.947	1.945	1.942
Al _{iv}	0.065	0.072	0.053	0.055	0.058
<hr/>					
Al _{vi}	0.008	0.017	0.002	0.002	0.009
Ti	0.011	0.009	0.008	0.010	0.008
Fe	0.407	0.341	0.398	0.396	0.332
Cr	0.000	0.004	0.004	0.005	0.000
Mn	0.007	0.008	0.007	0.014	0.016
Mg	0.601	0.646	0.611	0.606	0.658
<hr/>					
Mg	0.217	0.154	0.166	0.169	0.197
Ca	0.749	0.829	0.808	0.793	0.792
Na	0.031	0.014	0.026	0.038	0.011
K	0.003	0.003	0.000	0.000	0.000
<hr/>					
Al ₂	3.25	3.60	2.65	2.75	2.90
Ca	39	42	41	41	40
Mg	41	40	39	39	43
Fe	20	18	20	20	17

All clinopyroxenes from TR7-1A. 3A, 5A, 6A, 4A, 2A.

Ox. %	1	2	3	4	5	6
SiO ₂	51.64	52.43	52.97	50.64	50.66	50.86
Al ₂ O ₃	2.76	1.78	1.58	1.83	1.79	2.37
MgO	17.27	18.64	18.19	14.36	13.79	15.39
CaO	20.25	19.93	20.82	18.89	18.06	17.62
TiO ₂	0.34	0.21	0.15	0.62	0.45	0.58
Cr ₂ O ₃	0.15	0.36	0.26	0.07	0.10	0.00
FeO	5.95	4.86	4.49	12.08	13.66	11.75
Na ₂ O	0.51	0.07	0.38	0.47	0.49	0.59
K ₂ O	0.00	0.02	0.00	0.03	0.00	0.03
MnO	0.20	0.25	0.25	0.29	0.32	0.21
Total	99.07	98.55	99.09	99.28	99.32	99.40

Formula based on 6 O

Si	1.913	1.939	1.949	1.923	1.932	1.917
Aliv	0.087	0.061	0.051	0.077	0.068	0.083
<hr/>						
Alvi	0.034	0.017	0.018	0.005	0.012	0.022
Ti	0.009	0.006	0.004	0.018	0.013	0.016
Fe	0.184	0.150	0.138	0.384	0.436	0.370
Cr	0.004	0.010	0.007	0.002	0.003	0.000
Mn	0.006	0.008	0.008	0.009	0.010	0.007
Mg	0.795	0.824	0.846	0.617	0.558	0.621
<hr/>						
Mg	0.159	0.204	0.152	0.196	0.226	0.244
Ca	0.804	0.790	0.821	0.768	0.738	0.712
Na	0.037	0.005	0.027	0.034	0.036	0.043
K	0.000	0.001	0.000	0.002	0.000	0.001
<hr/>						
Alz	4.35	3.05	2.55	3.85	3.40	4.15
Ca	43	40	43	40	39	38
Mg	48	52	50	40	39	43
Fe	9	8	7	20	22	19

Analyses 1, 2 and 3 represent pyroxenes from TR7-11 (21A, 19A, 22A). Analyses 4, 5, and 6 represent pyroxenes from TR4-2 (29A, 28A, 30A).

Ox. %	1	2	3	4	5	6
SiO ₂	51.82	52.39	52.46	51.05	51.96	51.99
Al ₂ O ₃	0.81	0.89	0.63	2.49	1.39	2.26
MgO	14.88	15.02	14.77	15.40	16.68	16.42
CaO	22.14	21.90	21.90	19.81	19.28	19.01
TiO ₂	0.43	0.38	0.37	0.60	0.47	0.54
Cr ₂ O ₃	0.21	0.22	0.32	0.04	0.08	0.12
FeO	8.25	8.18	8.49	9.57	9.43	9.49
Na ₂ O	0.56	0.56	0.42	0.24	0.27	0.54
K ₂ O	0.03	0.09	0.08	0.06	0.06	0.02
MnO	0.13	0.10	0.20	0.40	0.15	0.26
Total	99.26	99.73	99.64	99.66	99.77	100.65

Formula based on 6 O

Si	1.950	1.958	1.965	1.911	1.936	1.919
Al _{iv}	0.036	0.039	0.028	0.089	0.061	0.081
Ti	0.012	0.003	0.007	0.000	0.003	0.000
Fe	0.002	0.000	0.000	0.000	0.000	0.000
<hr/>						
Al _{vi}	0.000	0.000	0.000	0.021	0.000	0.017
Ti	0.000	0.008	0.004	0.017	0.010	0.015
Fe	0.257	0.256	0.266	0.300	0.294	0.293
Cr	0.006	0.007	0.009	0.001	0.002	0.003
Mn	0.004	0.003	0.006	0.013	0.005	0.008
Mg	0.770	0.759	0.739	0.675	0.718	0.208
<hr/>						
Mg	0.065	0.078	0.086	0.184	0.208	0.208
Ca	0.893	0.877	0.879	0.795	0.770	0.752
Na	0.041	0.041	0.031	0.018	0.019	0.039
K	0.001	0.004	0.004	0.003	0.003	0.001
Al ₂	1.80	1.95	1.40	4.45	3.05	4.05
Ca	46	46	45	41	39	40
Mg	41	41	41	43	46	45
Fe	13	13	14	16	15	15

Analyses 1, 2, 3 represent clinopyroxenes from TR3-14 (10A, 8A, 7A). Analyses 4, 5, 6 are pyroxenes from TR1-3 (17A, 18A, 16A).

Ox. %	1	2	3	4	5	6
SiO ₂	51.07	53.41	53.80	51.77	52.42	52.64
Al ₂ O ₃	3.22	1.70	1.62	1.74	1.92	1.67
MgO	16.57	19.73	18.63	16.73	16.64	16.80
CaO	19.06	16.47	19.10	21.15	21.64	21.34
TiO ₂	0.41	0.16	0.05	0.18	0.10	0.40
Cr ₂ O ₃	0.20	0.21	0.16	0.00	0.10	0.07
FeO	7.85	7.94	6.62	6.82	6.50	6.42
Na ₂ O	0.27	0.23	0.32	0.50	0.51	0.53
K ₂ O	0.00	0.00	0.01	0.00	0.00	0.00
MnO	0.17	0.20	0.14	0.16	0.12	0.42
Total	98.82	100.05	100.45	99.05	99.95	100.29

Formula based on 6 O

Si	1.906	1.949	1.957	1.930	1.934	1.937
Aliv	0.094	0.051	0.043	0.070	0.066	0.063
<hr/>						
Alvi	0.048	0.022	0.026	0.006	0.018	0.009
Ti	0.012	0.004	0.001	0.005	0.003	0.011
Fe	0.245	0.242	0.201	0.213	0.201	0.197
Cr	0.006	0.006	0.005	0.000	0.003	0.002
Mn	0.005	0.006	0.004	0.005	0.004	0.013
Mg	0.704	0.733	0.776	0.811	0.808	0.802
<hr/>						
Mg	0.218	0.340	0.234	0.119	0.108	0.120
Ca	0.762	0.644	0.744	0.845	0.856	0.842
Na	0.020	0.016	0.022	0.036	0.036	0.038
K	0.000	0.000	0.000	0.000	0.000	0.000
Alz	4.70	2.55	2.15	3.50	3.30	3.15
Ca	40	33	39	43	44	44
Mg	47	54	51	46	46	46
Fe	13	13	10	11	10	10

Analyses 1, 2 and 3 represent pyroxenes from TR1-2 (1, 54, 1C).
 Analyses 4, 5, and 6 represent pyroxenes from TR5-3 (11A, 12A, 13A).

Ox. %	1	2	3	4	5
SiO ₂	49.88	50.24	50.82	51.98	52.06
Al ₂ O ₃	2.72	2.25	1.55	2.53	2.91
MgO	13.22	13.49	13.92	16.72	16.86
CaO	19.89	20.41	17.84	20.89	20.65
TiO ₂	0.75	0.74	0.67	0.29	0.26
Cr ₂ O ₃	0.10	0.12	0.06	0.31	0.11
FeO	12.54	11.83	14.05	6.12	5.98
Na ₂ O	0.43	0.53	0.27	0.34	0.51
K ₂ O	0.04	0.00	0.02	0.04	0.00
MnO	0.29	0.16	0.53	0.14	0.18
Total	99.86	99.77	99.73	99.36	99.52

Formula based on 6 O

Si	1.894	1.905	1.932	1.924	1.920
Aliv	0.106	0.095	0.068	0.076	0.080
<hr/>					
Alvi	0.016	0.006	0.002	0.034	0.047
Ti	0.021	0.021	0.019	0.008	0.007
Fe	0.398	0.375	0.447	0.189	0.184
Cr	0.003	0.004	0.002	0.009	0.003
Mn	0.009	0.005	0.017	0.004	0.006
Mg	0.592	0.630	0.537	0.777	0.779
<hr/>					
Mg	0.157	0.132	0.252	0.146	0.148
Ca	0.809	0.829	0.727	0.828	0.816
Na	0.032	0.039	0.020	0.024	0.036
K	0.002	0.000	0.001	0.002	0.000
Al ₂	5.30	4.75	3.50	3.80	4.00
Ca	42	43	37	43	43
Mg	38	38	39	47	47
Fe	20	19	23	10	10

Analyses 1, 2 and 3 represent pyroxenes from TR1-11 (39, 46, 38).

Ox. %	1	2	3	4	5	6
SiO ₂	51.90	51.94	50.02	50.82	50.34	52.83
Al ₂ O ₃	2.14	2.49	2.16	2.72	2.80	2.11
MgO	16.52	16.88	14.62	14.99	14.27	18.31
CaO	21.25	21.35	19.91	19.60	18.21	20.70
TiO ₂	0.32	0.22	0.57	0.62	0.73	0.32
Cr ₂ O ₃	0.15	0.33	0.00	0.05	0.00	0.29
FeO	6.66	6.38	9.36	9.38	12.19	4.32
Na ₂ O	0.33	0.31	0.60	0.47	0.37	0.42
K ₂ O	0.09	0.00	0.00	0.00	0.04	0.05
MnO	0.12	0.08	0.25	0.18	0.35	0.10
Total	99.48	99.98	97.49	98.83	99.30	99.45

Formula based on 6 O

Si	1.926	1.915	1.918	1.915	1.907	1.935
Aliv	0.074	0.085	0.082	0.085	0.093	0.065
<hr/>						
Alvi	0.020	0.023	0.015	0.036	0.032	0.026
Ti	0.009	0.006	0.016	0.018	0.021	0.009
Fe	0.207	0.197	0.300	0.296	0.386	0.132
Cr	0.004	0.010	0.000	0.001	0.000	0.008
Mn	0.004	0.002	0.008	0.006	0.011	0.003
Mg	0.787	0.793	0.698	0.667	0.574	0.845
<hr/>						
Mg	0.127	0.135	0.138	0.175	0.232	0.155
Ca	0.845	0.843	0.818	0.791	0.739	0.812
Na	0.024	0.022	0.044	0.034	0.027	0.030
K	0.004	0.000	0.000	0.000	0.002	0.003
Alz	3.70	4.25	4.10	4.25	4.65	3.25
Ca	44	43	43	42	39	43
Mg	46	47	42	43	41	50
Fe	10	10	15	15	20	7

Analyses 1 and 2 are clinopyroxenes from TR9-16 (51, 25). Analyses 3 and 4 are clinopyroxenes from TR1-4 (27A, 26A). Analysis 5 is from TR4-2(31A). Analysis 6 is from TR7-11 (20A).

GEOLOGICAL MAP OF THE LIMNI MINING AREA



Legend

SEDIMENTARY ROCKS

- Shale and siltstone
- Red Limestone
- Manganese-bearing conglomerate
- Silty sand
- Grey clay, Radiolarites and Limestone
- Reddish-brown and Limestone

IGNEOUS ROCKS

- Diorite Basalt
- Granite
- Lower Pluton (Leak)
- Basalt-Gabbro and Diabase

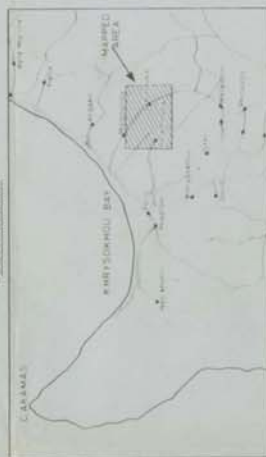
MINERALIZATION

- Exposed sulphide ore with Cu 0.6%
- Exposed low grade ore (0.3% Cu, 0.8% Pb)
- Exposed mineralization with Cu 0.3%
- Old lead sulphide mineralization (Gossan)

CONVENTIONAL SIGNS

- Hydrostatic pressure
- Fault showing amount of dip
- Dip at followed time
- Normal contact between formations
- Transition or obscured contact
- Lensoid
- Elevation contour or metres
- Metamorphic clay
- Dip of sediments and diagenetic
- Dike showing dip
- Open pit mine bench
- Waste dump
- Truck road

LOCATION MAP



Geologically surveyed by N. O. Adamides
Drawn by A. E. Louka

SCALE



Geological map of the Malayasag Mining Lease

This map displays the geological structure of the Malayasag Mining Lease. The central feature is a large, irregularly shaped area labeled 'WALIE DUM' with a cross symbol, representing a specific geological unit. Surrounding this are various other geological units, each color-coded and patterned according to the legend. The map includes a scale bar at the bottom left, indicating distances in kilometers (0, 1, 2, 3, 4, 5, 6, 7, 8, 9, 10). A north arrow is located at the bottom right. The legend, titled 'Legend', is positioned on the right side and lists various geological features and their corresponding symbols and colors. The map is oriented with North at the top.

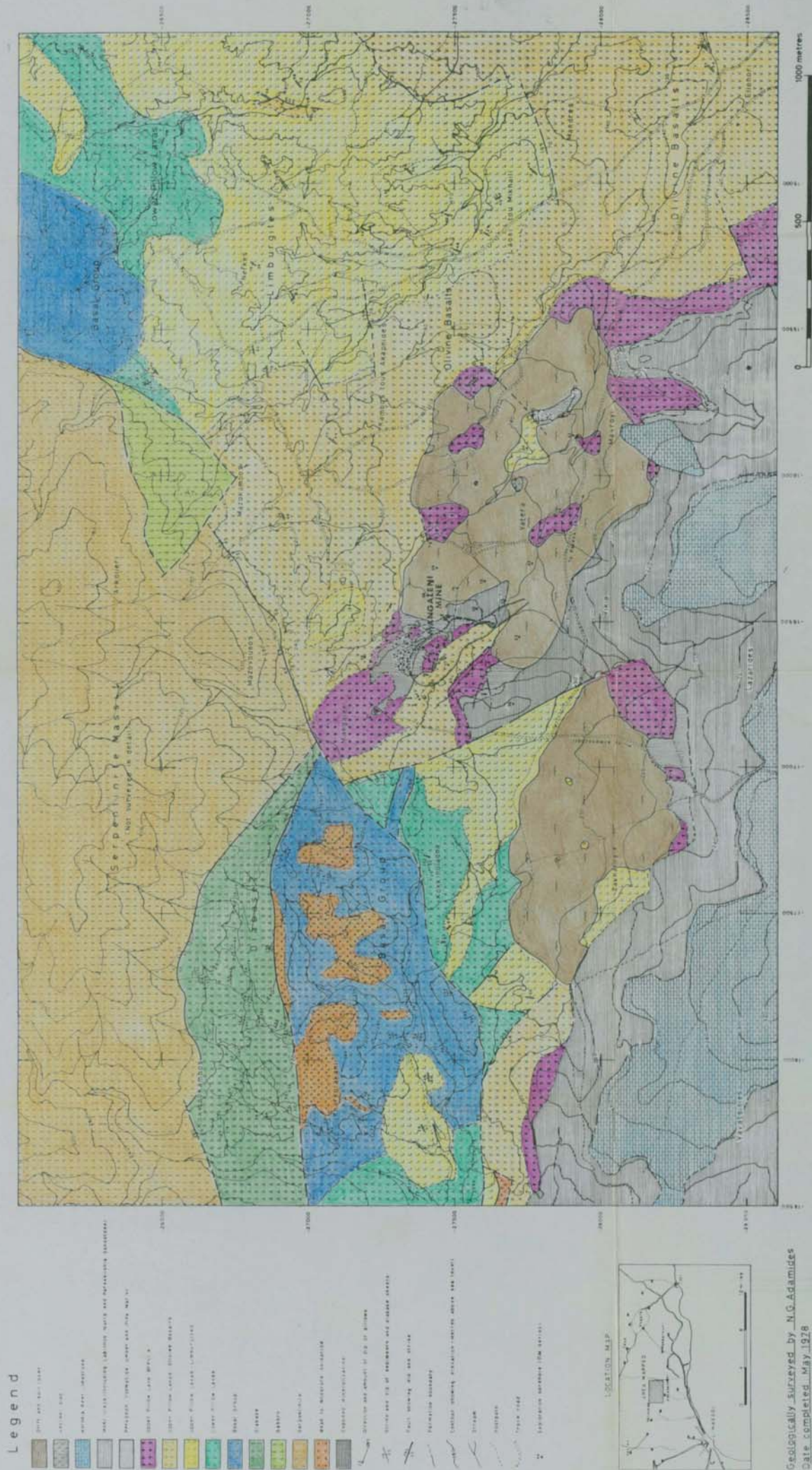
Legend

Symbol/Color	Description
Blue	Water bodies (rivers, lakes, etc.)
Green	Forest areas
Yellow	Barren land
Orange	Barren land (low altitude)
Red	Barren land (high altitude)
Purple	Barren land (very high altitude)
Black	Barren land (extremely high altitude)
White	Barren land (very low altitude)
Grey	Barren land (low altitude)
Light blue	Barren land (high altitude)
Light green	Barren land (very high altitude)
Light orange	Barren land (extremely high altitude)
Light purple	Barren land (very low altitude)
Light grey	Barren land (low altitude)
Light blue	Barren land (high altitude)
Light green	Barren land (very high altitude)
Light orange	Barren land (extremely high altitude)
Light purple	Barren land (very low altitude)
Light grey	Barren land (low altitude)
Light blue	Barren land (high altitude)
Light green	Barren land (very high altitude)
Light orange	Barren land (extremely high altitude)
Light purple	Barren land (very low altitude)
Light grey	Barren land (low altitude)
Light blue	Barren land (high altitude)
Light green	Barren land (very high altitude)
Light orange	Barren land (extremely high altitude)
Light purple	Barren land (very low altitude)
Light grey	Barren land (low altitude)
Light blue	Barren land (high altitude)
Light green	Barren land (very high altitude)
Light orange	Barren land (extremely high altitude)
Light purple	Barren land (very low altitude)
Light grey	Barren land (low altitude)
Light blue	Barren land (high altitude)
Light green	Barren land (very high altitude)
Light orange	Barren land (extremely high altitude)
Light purple	Barren land (very low altitude)
Light grey	Barren land (low altitude)
Light blue	Barren land (high altitude)
Light green	Barren land (very high altitude)
Light orange	Barren land (extremely high altitude)
Light purple	Barren land (very low altitude)
Light grey	Barren land (low altitude)
Light blue	Barren land (high altitude)
Light green	Barren land (very high altitude)
Light orange	Barren land (extremely high altitude)
Light purple	Barren land (very low altitude)
Light grey	Barren land (low altitude)
Light blue	Barren land (high altitude)
Light green	Barren land (very high altitude)
Light orange	Barren land (extremely high altitude)
Light purple	Barren land (very low altitude)
Light grey	Barren land (low altitude)
Light blue	Barren land (high altitude)
Light green	Barren land (very high altitude)
Light orange	Barren land (extremely high altitude)
Light purple	Barren land (very low altitude)
Light grey	Barren land (low altitude)
Light blue	Barren land (high altitude)
Light green	Barren land (very high altitude)
Light orange	Barren land (extremely high altitude)
Light purple	Barren land (very low altitude)
Light grey	Barren land (low altitude)
Light blue	Barren land (high altitude)
Light green	Barren land (very high altitude)
Light orange	Barren land (extremely high altitude)
Light purple	Barren land (very low altitude)
Light grey	Barren land (low altitude)
Light blue	Barren land (high altitude)
Light green	Barren land (very high altitude)
Light orange	Barren land (extremely high altitude)
Light purple	Barren land (very low altitude)
Light grey	Barren land (low altitude)
Light blue	Barren land (high altitude)
Light green	Barren land (very high altitude)
Light orange	Barren land (extremely high altitude)
Light purple	Barren land (very low altitude)
Light grey	Barren land (low altitude)
Light blue	Barren land (high altitude)
Light green	Barren land (very high altitude)
Light orange	Barren land (extremely high altitude)
Light purple	Barren land (very low altitude)
Light grey	Barren land (low altitude)
Light blue	Barren land (high altitude)
Light green	Barren land (very high altitude)
Light orange	Barren land (extremely high altitude)
Light purple	Barren land (very low altitude)
Light grey	Barren land (low altitude)
Light blue	Barren land (high altitude)
Light green	Barren land (very high altitude)
Light orange	Barren land (extremely high altitude)
Light purple	Barren land (very low altitude)
Light grey	Barren land (low altitude)
Light blue	Barren land (high altitude)
Light green	Barren land (very high altitude)
Light orange	Barren land (extremely high altitude)
Light purple	Barren land (very low altitude)
Light grey	Barren land (low altitude)
Light blue	Barren land (high altitude)
Light green	Barren land (very high altitude)
Light orange	Barren land (extremely high altitude)
Light purple	Barren land (very low altitude)
Light grey	Barren land (low altitude)
Light blue	Barren land (high altitude)
Light green	Barren land (very high altitude)
Light orange	Barren land (extremely high altitude)
Light purple	Barren land (very low altitude)
Light grey	Barren land (low altitude)
Light blue	Barren land (high altitude)
Light green	Barren land (very high altitude)
Light orange	Barren land (extremely high altitude)
Light purple	Barren land (very low altitude)
Light grey	Barren land (low altitude)
Light blue	Barren land (high altitude)
Light green	Barren land (very high altitude)
Light orange	Barren land (extremely high altitude)
Light purple	Barren land (very low altitude)
Light grey	Barren land (low altitude)
Light blue	Barren land (high altitude)
Light green	Barren land (very high altitude)
Light orange	Barren land (extremely high altitude)
Light purple	Barren land (very low altitude)
Light grey	Barren land (low altitude)
Light blue	Barren land (high altitude)
Light green	Barren land (very high altitude)
Light orange	Barren land (extremely high altitude)
Light purple	Barren land (very low altitude)
Light grey	Barren land (low altitude)
Light blue	Barren land (high altitude)
Light green	Barren land (very high altitude)
Light orange	Barren land (extremely high altitude)
Light purple	Barren land (very low altitude)
Light grey	Barren land (low altitude)
Light blue	Barren land (high altitude)
Light green	Barren land (very high altitude)
Light orange	Barren land (extremely high altitude)
Light purple	Barren land (very low altitude)
Light grey	Bar



Geologically surveyed by N.G. Adamides

GEOLOGICAL MAP OF THE AREA AROUND MANGALENI MINE



Geologically surveyed by N.G. Adamides
Date completed May 1978